# MEASUREMENT AND DETECTION OF RADIATION

Second Edition

# MEASUREMENT AND DETECTION OF RADIATION

Second Edition

**Nicholas Tsoulfanidis**
*University of Missouri-Rolla*

Taylor & Francis
*Publishers since 1798*

1995

| | | |
|---|---|---|
| USA | Publishing Office: | Taylor & Francis<br>1101 Vermont Avenue, N.W.<br>Suite 200<br>Washington, DC 200053521<br>Tel: (202) 289-2174<br>Fax: (202) 289-3665 |
| | Distribution Center: | Taylor & Francis<br>1900 Frost Road<br>Suite 101<br>Bristol, PA 19007-1598<br>Tel: (215) 7855800<br>Fax: (215) 785-5515 |
| UK | | Taylor & Francis Ltd.<br>4 John St.<br>London WC1N 2ET<br>Tel: 071405 2237<br>Fax: 071 8312035 |

**MEASUREMENT AND DETECTION OF RADIATION, Second Edition**

Copyright © 1995, 1983 Taylor & Francis. All rights reserved. Printed in the United States of America. Except as permitted under the United States Copyright Act of 1976, no part of this publication may be reproduced or distributed in any form or by any means, or stored in a database or retrieval system, without the prior written permission of the publisher.

12 3 4 5 6 7 8 9 0 BRBR 9 8 7 6 5

This book was set in Times Roman by Technical Typesetting Inc. The editors were Christine E. Williams and Carol Edwards. Cover design by Michelle M. Fleitz. Printing and binding by Braun-Brumfield, Inc.

A CIP catalog record for this book is available from the British Library.

∞ The paper in this publication meets the requirements of the ANSI Standard Z39.48-1984 (Permanence of Paper)

**Library of Congress Cataloging-in-Publication Data**

Tsoulfanidis, Nicholas
Measurement and detection of radiation/Nicholas Tsoulfanidis.—
2nd ed.
p. cm.

1. Radiation-Measurement. 2. Nuclear counters. I. Title.
QC795.42.T78 1995
539.7'7—dc20 94-24270
CIP

ISBN 1-56032-317-5

To Zizeta

# CONTENTS


| | | |
|---|---|---|
| | Preface to the First Edition | xvii |
| | Preface to the Second Edition | xxi |
| **1** | INTRODUCTION TO RADIATION MEASUREMENTS | 1 |
| 1.1 | What is Meant by Radiation? | 1 |
| 1.2 | Statistical Nature of Radiation Emission | 2 |
| 1.3 | The Errors and Accuracy and Precision of Measurements | 3 |
| 1.4 | Types of Errors | 5 |
| 1.5 | Nuclear Instrumentation | 6 |
| | 1.5.1 Introduction | 6 |
| | 1.5.2 The Detector | 7 |
| | 1.5.3 The NIM Concept | 9 |
| | 1.5.4 The High-Voltage Power Supply | 9 |
| | 1.5.5 The Preamplifier | 11 |
| | 1.5.6 The Amplifier | 14 |
| | 1.5.7 The Oscilloscope | 16 |
| | 1.5.8 The Discriminator or Single-Channel Analyzer (SCA) | 17 |
| | 1.5.9 The Scaler | 20 |
| | 1.5.10 The Timer | 21 |
| | 1.5.11 The Multichannel Analyzer | 21 |
| | Bibliography | 21 |
| | Reference | 21 |
| **2** | STATISTICAL ERRORS OF RADIATION COUNTING | 23 |
| 2.1 | Introduction | 23 |
| 2.2 | Definition of Probability | 23 |
| 2.3 | Basic Probability Theorems | 25 |
| 2.4 | Probability Distributions and Random Variables | 28 |

2.5 Location Indexes (Mode, Median, Mean) 30
2.6 Dispersion Indexes, Variance, and Standard Deviation 33
2.7 Covariance and Correlation 33
2.8 The Binomial Distribution 35
2.9 The Poisson Distribution 37
2.10 The Normal (Gaussian) Distribution 39
2.10.1 The Standard Normal Distribution 43
2.10.2 Importance of the Gaussian Distribution for Radiation Measurements 45
2.11 The Lorentzian Distribution 46
2.12 The Standard, Probable, and Other Errors 48
2.13 The Arithmetic Mean and Its Standard Error 49
2.14 Confidence Limits 52
2.15 Propagation of Errors 55
2.15.1 Calculation of the Average and Its Standard Deviation 55
2.15.2 Examples of Error Propagation—Uncorrelated Variables 56
2.16 Goodness of Data—$\chi^2$ Criterion—Rejection of Data 58
2.17 The Statistical Error of Radiation Measurements 62
2.18 The Standard Error of Counting Rates 64
2.18.1 Combining Counting Rates 67
2.19 Methods of Error Reduction 68
2.19.1 The Background Is Constant and There Is No Time Limit for Its Measurement 68
2.19.2 There Is a Fixed Time $T$ Available for Counting Both Background and Gross Count 69
2.19.3 Calculation of the Counting Time Necessary to Measure a Counting Rate with a Predetermined Statistical Error 69
2.19.4 Relative Importance of Error Components 70
2.20 Minimum Detectable Activity 71
2.21 Counter Dead-Time Correction and Measurement of Dead Time 73
Problems 76
Bibliography 78
References 78

3 REVIEW OF ATOMIC AND NUCLEAR PHYSICS 79

3.1 Introduction 79
3.2 Elements of Relativistic Kinematics 79
3.3 Atoms 83
3.4 Nuclei 86
3.5 Nuclear Binding Energy 88
3.6 Nuclear Energy Levels 91
3.7 Energetics of Nuclear Decays 92
3.7.1 Gamma Decay 94
3.7.2 Alpha Decay 96
3.7.3 Beta Decay 97
3.7.4 Particles, Antiparticles, and Electron-Positron Annihilation 102
3.7.5 Complex Decay Schemes 103
3.8 The Radioactive Decay Law 103

3.9 Nuclear Reactions 107
3.9.1 General Remarks 107
3.9.2 Kinematics of Nuclear Reactions 109
3.10 Fission 113
Problems 117
Bibliography 119
References 119

4 ENERGY LOSS AND PENETRATION OF RADIATION THROUGH MATTER 121

4.1 Introduction 121
4.2 Mechanisms of Charged-Particle Energy Loss 122
4.2.1 Coulomb Interactions 122
4.2.2 Emission of Electromagnetic Radiation (Bremsstrahlung) 123
4.3 Stopping Power Due to Ionization and Excitation 124
4.4 Energy Loss Due to Bremsstrahlung Emission 129
4.5 Calculation of $dE/dx$ for a Compound or Mixture 131
4.6 Range of Charged Particles 132
4.6.1 Range of Heavy Charged Particles ($p$, $d$, $t$, $\alpha$; $1 \leq A \leq 4$) 133
4.6.2 Range of Electrons and Positrons 138
4.6.3 Transmission of Beta Particles 142
4.6.4 Energy Loss after Traversing a Material of Thickness $t < R$ 143
4.7 Stopping Power and Range of Heavy Ions ($Z > 2$, $A > 4$) 144
4.7.1 Introduction 144
4.7.2 The $dE/dx$ Calculation 145
4.7.3 Range of Heavy Ions 149
4.8 Interactions of Photons with Matter 150
4.8.1 The Photoelectric Effect 153
4.8.2 Compton Scattering or Compton Effect 154
4.8.3 Pair Production 157
4.8.4 Total Photon Attenuation Coefficient 158
4.8.5 Photon Energy Absorption Coefficient 161
4.8.6 Buildup Factors 162
4.9 Interactions of Neutrons with Matter 166
4.9.1 Types of Neutron Interactions 166
4.9.2 Neutron Reaction Cross Sections 166
4.9.3 The Neutron Flux 171
4.9.4 Interaction Rates of Polyenergetic Neutrons 172
Problems 173
Bibliography 174
References 175

5 GAS-FILLED DETECTORS 177

5.1 Introduction 177
5.2 Relationship Between High Voltage and Charge Collected 179
5.3 Different Types of Gas-Filled Detectors 180

5.4 Ionization Chambers 183
5.4.1 Pulse Formation in an Ionization Chamber 183
5.4.2 Current Ionization Chambers 187
5.5 Proportional Counters 189
5.5.1 Gas Multiplication in Proportional Counters 189
5.5.2 The Pulse Shape of a Proportional Counter 194
5.5.3 The Change of Counting Rate with High Voltage—The High-Voltage Plateau 195
5.6 Geiger-Müller Counters 199
5.6.1 Operation of a GM Counter and Quenching of the Discharge 199
5.6.2 The Pulse Shape and the Dead Time of a GM Counter 200
5.7 Gas-Flow Counters 201
5.7.1 The Long-Range Alpha Detector (LRAD) 204
5.7.2 Internal Gas Counting 205
5.8 Rate Meters 206
5.9 General Comments about Construction of Gas-Filled Detectors 208
Problems 209
Bibliography 209
References 210

**6 SCINTILLATION DETECTORS 211**

6.1 Introduction 211
6.2 Inorganic (Crystal) Scintillators 212
6.2.1 The Mechanism of the Scintillation Process 212
6.2.2 Time Dependence of Photon Emission 215
6.2.3 Important Properties of Certain Inorganic Scintillators 216
6.3 Organic Scintillators 218
6.3.1 The Mechanism of the Scintillation Process 218
6.3.2 Organic Crystal Scintillators 220
6.3.3 Organic Liquid Scintillators 220
6.3.4 Plastic Scintillators 221
6.4 Gaseous Scintillators 222
6.5 The Relationship Between Pulse Height and Energy and Type of Incident Particle 222
6.5.1 The Response of Inorganic Scintillators 222
6.5.2 The Response of Organic Scintillators 223
6.6 The Photomultiplier Tube 224
6.6.1 General Description 224
6.6.2 Electron Multiplication in a Photomultiplier 227
6.7 Assembly of a Scintillation Counter and the Role of Light Pipes 228
6.8 Dead Time of Scintillation Counters 230
6.9 Sources of Background in a Scintillation Counter 231
6.10 The Phoswich Detector 232
Problems 233
Bibliography 233
References 234

| | | |
|---|---|---|
| **7** | SEMICONDUCTOR DETECTORS | 235 |
| 7.1 | Introduction | 235 |
| 7.2 | Electrical Classification of Solids | 236 |
| | 7.2.1 Electronic States in Solids–The Fermi Distribution Function | 236 |
| | 7.2.2 Insulators | 238 |
| | 7.2.3 Conductors | 238 |
| 7.3 | Semiconductors | 239 |
| | 7.3.1 The Change of the Energy Gap with Temperature | 241 |
| | 7.3.2 Conductivity of Semiconductors | 243 |
| | 7.3.3 Extrinsic and Intrinsic Semiconductors—The Role of Impurities | 245 |
| 7.4 | The p-n Junction | 246 |
| | 7.4.1 The Formation of a p-n Junction | 246 |
| | 7.4.2 The p-n Junction Operating as a Detector | 250 |
| 7.5 | The Different Types of Semiconductor Detectors | 252 |
| | 7.5.1 Surface-Barrier Detectors | 252 |
| | 7.5.2 Diffused-Junction Detectors | 252 |
| | 7.5.3 Silicon Lithium-Drifted [Si(Li)] Detectors | 254 |
| | 7.5.4 Germanium Lithium-Drifted [Ge(Li)] Detectors | 258 |
| | 7.5.5 Germanium (Ge) Detectors | 258 |
| | 7.5.6 CdTe and $HgI_2$ Detectors | 259 |
| 7.6 | Radiation Damage to Semiconductor Detectors | 260 |
| | Problems | 261 |
| | Bibliography | 262 |
| | References | 262 |
| **8** | RELATIVE AND ABSOLUTE MEASUREMENTS | 265 |
| 8.1 | Introduction | 265 |
| 8.2 | Geometry Effects | 267 |
| | 8.2.1 The Effect of the Medium between Source and Detector | 267 |
| | 8.2.2 The Solid Angle—General Definition | 268 |
| | 8.2.3 The Solid Angle for a Point Isotropic Source and a Detector with a Circular Aperture | 269 |
| | 8.2.4 The Solid Angle for a Disk Source Parallel to a Detector with a Circular Aperture | 273 |
| | 8.2.5 The Solid Angle for a Point Isotropic Source and a Detector with a Rectangular Aperture | 274 |
| | 8.2.6 The Solid Angle for a Disk Source and a Detector with a Rectangular Aperture | 274 |
| | 8.2.7 The Use of the Monte Carlo Method for the Calculation of the Solid Angle | 276 |
| 8.3 | Source Effects | 277 |
| | 8.3.1 Source Self-Absorption Factor ($f_a$) | 277 |
| | 8.3.2 Source Backscattering Factor ($f_b$) | 279 |
| 8.4 | Detector Effects | 282 |
| | 8.4.1 Scattering and Absorption Due to the Window of the Detector | 282 |
| | 8.4.2 Detector Efficiency ($\epsilon$) | 283 |

| | | |
|---|---|---|
| | 8.4.3 Determination of Detector Efficiency | 285 |
| 8.5 | Relationship Between Counting Rate and Source Strength | 287 |
| | Problems | 289 |
| | References | 291 |
| **9** | INTRODUCTION TO SPECTROSCOPY | 293 |
| 9.1 | Introduction | 293 |
| 9.2 | Definition of Energy Spectra | 293 |
| 9.3 | Measurement of an Integral Spectrum with a Single-Channel Analyzer | 295 |
| 9.4 | Measurement of a Differential Spectrum with a Single-Channel Analyzer (SCA) | 296 |
| 9.5 | The Relationship Between Pulse-Height Distribution and Energy Spectrum | 298 |
| 9.6 | Energy Resolution of a Detection System | 300 |
| | 9.6.1 The Effect of Statistical Fluctuations: The Fano Factor | 301 |
| | 9.6.2 The Effect of Electronic Noise on Energy Resolution | 303 |
| | 9.6.3 The Effect of Incomplete Charge Collection | 303 |
| | 9.6.4 The Total Width $\Gamma$ | 304 |
| 9.7 | Determination of the Energy Resolution—The Response Function | 304 |
| 9.8 | The Importance of Good Energy Resolution | 305 |
| 9.9 | Brief Description of a Multichannel Analyzer (MCA) | 307 |
| 9.10 | Calibration of a Multichannel Analyzer | 310 |
| | Problems | 314 |
| | References | 315 |
| **10** | ELECTRONICS | 317 |
| 10.1 | Introduction | 317 |
| 10.2 | Resistance, Capacitance, Inductance, and Impedance | 317 |
| 10.3 | A Differentiating Circuit | 321 |
| 10.4 | An Integrating Circuit | 324 |
| 10.5 | Delay Lines | 325 |
| 10.6 | Pulse Shaping | 326 |
| 10.7 | Timing | 328 |
| | 10.7.1 The Leading-Edge Timing Method | 329 |
| | 10.7.2 The Zero-Crossing Timing Method | 330 |
| | 10.7.3 The Constant-Fraction Timing Method | 331 |
| 10.8 | Coincidence-Anticoincidence Measurements | 331 |
| 10.9 | Pulse-Shape Discrimination | 337 |
| 10.10 | Preamplifiers | 339 |
| 10.11 | Amplifiers | 342 |
| 10.12 | Analog-to-Digital Converters (ADC) | 344 |
| 10.13 | Multiparameter Analyzers | 347 |
| | Problems | 349 |
| | Bibliography | 350 |
| | References | 350 |

| | | |
|---|---|---|
| **11** | DATA ANALYSIS METHODS | 353 |
| 11.1 | Introduction | 353 |
| 11.2 | Curve Fitting | 353 |
| 11.3 | Interpolation Schemes | 355 |
| 11.4 | Least-Squares Fitting | 359 |
| | 11.4.1 Least-Squares Fit of a Straight Line | 360 |
| | 11.4.2 Least-Squares Fit of General Functions | 361 |
| 11.5 | Folding and Unfolding | 364 |
| | 11.5.1 Examples of Folding | 365 |
| | 11.5.2 The General Method of Unfolding | 368 |
| | 11.5.3 An Iteration Method of Unfolding | 371 |
| | 11.5.4 Least-Squares Unfolding | 372 |
| 11.6 | Data Smoothing | 373 |
| | Problems | 377 |
| | Bibliography | 378 |
| | References | 378 |
| **12** | PHOTON (GAMMA-RAY AND X-RAY) SPECTROSCOPY | 381 |
| 12.1 | Introduction | 381 |
| 12.2 | Modes of Energy Deposition in the Detector | 381 |
| | 12.2.1 Energy Deposition by Photons with $E < 1.022$ MeV | 382 |
| | 12.2.2 Energy Deposition by Photons with $E > 1.022$ MeV | 385 |
| 12.3 | Efficiency of X-Ray and Gamma-Ray Detectors: Definitions | 389 |
| 12.4 | Detection of Photons with NaI(Tl) Scintillation Counters | 392 |
| | 12.4.1 Efficiency of NaI(Tl) Detectors | 392 |
| | 12.4.2 Analysis of Scintillation Detector Energy Spectra | 395 |
| 12.5 | Detection of Gammas with an NE 213 Organic Scintillator | 398 |
| 12.6 | Detection of X-Rays with a Proportional Counter | 399 |
| 12.7 | Detection of Gammas with Ge Detectors | 400 |
| | 12.7.1 Efficiency of Ge Detectors | 401 |
| | 12.7.2 Energy Resolution of Ge Detectors | 411 |
| | 12.7.3 Analysis of Ge Detector Energy Spectra | 412 |
| | 12.7.4 Timing Characteristics of the Pulse | 418 |
| 12.8 | CdTe and $HgI_2$ Detectors as Gamma Spectrometers | 419 |
| 12.9 | Detection of X-Rays with a Si(Li) Detector | 420 |
| 12.10 | Detection of X-Rays with a Crystal Spectrometer | 421 |
| | 12.10.1 Types of Crystal Spectrometers | 426 |
| | 12.10.2 Energy Resolution of Crystal Spectrometers | 428 |
| | Problems | 430 |
| | Bibliography | 431 |
| | References | 431 |
| **13** | CHARGED-PARTICLE SPECTROSCOPY | 433 |
| 13.1 | Introduction | 433 |
| 13.2 | Energy Straggling | 434 |

13.3 Electron Spectroscopy 439
13.3.1 Electron Backscattering 439
13.3.2 Energy Resolution and Response Function of Electron Detectors 441
13.3.3 Energy Calibration of Electron Spectrometers 442
13.3.4 Electron Source Preparation 444
13.4 Alpha, Proton, Deuteron, and Triton Spectroscopy 445
13.4.1 Energy Resolution and Response Function of Alpha Detectors 446
13.4.2 Energy Calibration 446
13.4.3 Source Preparation 446
13.5 Heavy-Ion ($Z > 2$) Spectroscopy 447
13.5.1 The Pulse-Height Defect 447
13.5.2 Energy Calibration: The Schmitt Method 450
13.5.3 Calibration Sources 452
13.5.4 Fission Foil Preparation 452
13.6 The Time-of-Flight Spectrometer 453
13.7 Detector Telescopes ($E\,dE/dx$ Detectors) 455
13.8 Magnetic Spectrometers 456
13.9 Electrostatic Spectrometers 458
13.10 Position-Sensitive Detectors 459
13.10.1 Position-Sensitive Semiconductor Detectors 459
13.10.2 Multiwire Proportional Chambers 461
Problems 462
Bibliography 463
References 463

**14** NEUTRON DETECTION AND SPECTROSCOPY 467

14.1 Introduction 467
14.2 Neutron Detection by ($n$, Charged Particle) Reaction 468
14.2.1 The $BF_3$ Counter 469
14.2.2 Boron-Lined Counters 473
14.2.3 $^6$Li Counters 474
14.2.4 $^3$He Counters 475
14.3 Fission Chambers 476
14.4 Neutron Detection by Foil Activation 478
14.4.1 Basic Equations 478
14.4.2 Determination of the Neutron Flux by Counting the Foil Activity 482
14.5 Measurement of a Neutron Energy Spectrum by Proton Recoil 484
14.5.1 Differentiation Unfolding of Proton Recoil Spectra 487
14.5.2 The FERDOR Unfolding Method 488
14.5.3 Proportional Counters Used as Fast-Neutron Spectrometers 489
14.5.4 Organic Scintillators Used as Fast-Neutron Spectrometers 494
14.6 Detection of Fast Neutrons Using Threshold Activation Reactions 496
14.6.1 The Code SAND-II 501
14.6.2 The Code SPECTRA 502
14.6.3 The Relative Deviation Minimization Method (RDMM) 502
14.6.4 The LSL-M2 Unfolding Code 503
14.7 Neutron Energy Measurement with a Crystal Spectrometer 503

14.8 The Time-of-Flight Method 505
14.8.1 The Neutron Velocity Selector (Neutron Chopper) 508
14.8.2 Pulsed-Ion Beams 509
14.9 Compensated Ion Chambers 510
14.10 Self-Powered Neutron Detectors (SPND) 511
14.10.1 SPNDs with Delayed Response 512
14.10.2 SPNDs with Prompt Response 517
14.11 Concluding Remarks 518
Problems 519
Bibliography 520
References 520

**15** ACTIVATION ANALYSIS 523

15.1 Introduction 523
15.2 Selection of the Optimum Nuclear Reaction 524
15.3 Preparation of the Sample for Irradiation 526
15.4 Sources of Radiation 528
15.4.1 Sources of Neutrons 528
15.4.2 Sources of Charged Particles 529
15.4.3 Sources of Photons 529
15.5 Irradiation of the Sample 530
15.6 Counting of the Sample 531
15.7 Analysis of the Results 532
15.8 Sensitivity of Activation Analysis 534
15.9 Interference Reactions 536
15.10 Advantages and Disadvantages of the Activation Analysis Method 537
Problems 537
Bibliography 538
References 538

**16** HEALTH PHYSICS FUNDAMENTALS 541

16.1 Introduction 541
16.2 Units of Exposure and Absorbed Dose 542
16.3 The Relative Biological Effectiveness—The Dose Equivalent 544
16.4 Dosimetry for Radiation External to the Body 547
16.4.1 Dose Due to Charged Particles 547
16.4.2 Dose Due to Photons 549
16.4.3 Dose Due to Neutrons 552
16.5 Dosimetry for Radiation Inside the Body 555
16.5.1 Dose from a Source of Charged Particles Inside the Body 555
16.5.2 Dose from a Photon Source Inside the Body 556
16.6 Internal Dose Time Dependence—Biological Half-Life 558
16.7 Biological Effects of Radiation 562
16.7.1 Basic Description of the Human Cell 563
16.7.2 Stochastic and Nonstochastic Effects 564

16.8 Radiation Protection Guides and Exposure Limits 567
16.9 Health Physics Instruments 570
16.9.1 Survey Instruments 571
16.9.2 Thermoluminescent Dosimeters 572
16.9.3 Solid-State Track Recorders (SSTRs) 576
16.9.4 The Bonner Sphere (the Rem Ball) 579
16.9.5 The Neutron Bubble Detector 580
16.9.6 The Electronic Personal Dosimeter 581
16.9.7 Foil Activation Used for Neutron Dosimetry 582
16.10 Proper Use of Radiation 582
Problems 585
Bibliography 587
References 587

APPENDIXES 589

A Useful Constants and Conversion Factors 589
B Atomic Masses and Other Properties of Isotopes 591
C Alpha, Beta, and Gamma Sources Commonly Used 595
D Tables of Photon Attenuation Coefficients 599
E Table of Buildup Factor Constants 605

INDEX 607

# PREFACE TO THE FIRST EDITION

The material in this book, which is the result of a 10-year experience obtained in teaching courses related to radiation measurements at the University of Missouri-Rolla, is intended to provide an introductory text on the subject. It includes not only what I believe the beginner ought to be taught but also some of the background material that people involved in radiation measurements should have. The subject matter is addressed to upper-level undergraduates and first-year graduate students. It is assumed that the students have had courses in calculus and differential equations and in basic atomic and nuclear physics. The book should be useful to students in nuclear, mechanical, and electrical engineering, physics, chemistry (for radiochemistry), nuclear medicine, and health physics; to engineers and scientists in laboratories using radiation sources; and to personnel in nuclear power plants.

The structure and the contents of the book are such that the person who masters the material will be able to

1 Select the proper detector given the energy and type of particle to be counted and the purpose of the measurement.
2 Analyze the results of counting experiments, i.e., calculate errors, smooth results, unfold energy spectra, fit results with a function, etc.
3 Perform radiation measurements following proper health physics procedures.

The first chapter defines the energy range of the different types of radiation for which instruments and methods of measurement are considered; it gives a brief discussion of errors that emphasizes their importance; and, finally, it presents a very general description of the components of a counting system. This last part of the chapter is necessary because a course on radiation measurements involves laboratory work, and for this reason the students should be familiar from the very beginning with the general features and functions of radiation instruments.

The second chapter addresses the very important subject of errors. Since all experimental results have errors, and results reported without their corresponding errors are meaningless, this chapter is fundamental for a book such as this one. Further discussion of errors caused by the analysis of the results is presented in Chap. 11.

Chapters 3 and 4 constitute a quick review of material that should have been covered in previous courses. My experience has been that students need this review of atomic and nuclear physics and of penetration of radiation through matter. These two chapters can be omitted if the instructor feels that the students know the subject.

Chapters 5–7 describe the different types of radiation detectors. Full chapters have been devoted to gas-filled counters, scintillation detectors, and semiconductor detectors. Detectors with "special" functions are discussed in Chap. 17.

The subject of relative and absolute measurements is presented in Chap. 8. The solid angle (geometry factor) between source and detector and effects due to the source and the detector, such as efficiency, backscattering, and source self-absorption are all discussed in detail.

Chapter 9 is an introduction to spectroscopy. It introduces and defines the concepts used in the next four chapters. Chapter 10 discusses the features of the electronic components of a counting system that are important in spectroscopy. Its objective is not to make the reader an expert in electronics but to show how the characteristics of the instruments may influence the measurements.

Chapter 11 presents methods of analysis of experimental data. Methods of curve fitting, of interpolation, and of least-squares fitting are discussed concisely but clearly. A general discussion of folding, unfolding, and data smoothing, which are necessary tools in analysis of spectroscopic measurements, occupies the second half of this chapter. Special methods of unfolding for photons, charged particles, and neutrons are further discussed in Chaps. 12 through 14, which also cover spectroscopy. Individual chapters are devoted to photons, charged particles, and neutrons. All the factors that affect spectroscopic measurements and the methods of analysis of the results are discussed in detail.

Chapter 15 is devoted to activation analysis, a field with wide-ranging applications. Health physics is discussed in Chap. 16. I feel that every person who handles radiation should know at least something about the effects of radiation, radiation units, and regulations related to radiation protection. This chapter may be omitted if the reader has already studied the subject.

Chapter 17 deals with special detectors and spectrometers that have found applications in many different fields but do not fit in any of the previous chapters. Examples are the self-powered detectors, which may be gamma or neutron detectors, fission track detectors, thermoluminescent dosimeters, photographic emulsions, and others.

The problems at the end of each chapter should help the student understand the concepts presented in the text. They are arranged not according to

difficulty but in the order of presentation of the material needed for their solution.

The appendixes at the end of the book provide useful information to the reader.

I use the SI (metric) units with the exception of some well-established nonmetric units, which, it seems, are here to stay. Examples are MeV, keV, and eV for energy; the barn for cross sections; the curie; and the rem. These units are given in parentheses along with their SI counterparts.

Writing a book is a tremendous undertaking, a task too big for any single person. I was fortunate to have been helped by many individuals, and it gives me great pleasure to recognize them here. First and foremost, I thank all the former students who struggled through my typed notes when they took the radiation measurements course at the University of Missouri-Rolla. Their numerous critical comments are deeply appreciated. I thank my colleagues, Dr. D. Ray Edwards for his continuous support, Dr. G. E. Mueller for his many useful suggestions, and Drs. A. E. Bolon and T. J. Dolan for many helpful discussions over the last 10 years. I also thank Dr. R. H. Johnson of Purdue University for reviewing certain chapters. I especially thank my dear friend Professor B. W. Wehring of the University of Illinois for numerous lengthy discussions following his detailed critical review of most of the chapters. I am grateful to Mrs. Susan Elizagary for expertly typing most of the manuscript and to Mrs. Betty Volosin for helping in the final stages of typing.

No single word or expression of appreciation can adequately reflect my gratitude to my wife Zizeta for her moral support and understanding during the last three painstaking years, and to my children Steve and Lena for providing pleasant and comforting distraction.

*Nicholas Tsoulfanidis*

# PREFACE TO THE SECOND EDITION

For an author it is very gratifying to discover that a technical book is still relevant more than ten years after it was first published. This is the case with this book because it addresses the fundamentals of nuclear radiation counting, which have not significantly changed during that period of time. Like the first edition, this book is written for persons who have no prior knowledge of radiation counting. These include undergraduate students in nuclear science and engineering; first-year graduate students who enter this field from another discipline; health physicists and health physics technicians; nuclear medicine technical personnel; and scientists, engineers, and technicians in laboratories where atomic and nuclear radiation are used. In addition, according to comments from former students and colleagues, the book has proven to be an excellent reference.

The second edition follows the same guidelines as the first—namely simplicity in writing and use of many examples. The main structural change is the elimination of Chap. 17 (Special Detectors and Spectrometers) and the relocation of the material in appropriate chapters. For example, rate meters and gas-filled detectors are now discussed in Chap. 5. Self-powered detectors are now included in Chap. 14 along with other neutron detectors. Chapter 16 deals with solid-state track recorders and thermoluminescent dosimeters.

As should be expected, all chapters have been corrected for errors, revised for clarification, and new examples have been added as needed. The more substantive revisions were made in the following chapters: In Chap. 2 there is now a better explanation of the $\chi^2$ procedure and the minimum detectable activity (MDA). In Chap. 4, relative to the stopping power of charged particles, there is a more detailed discussion and presentation of the latest formulas of gamma-ray build-up factors. The Long Range Alpha Detector (LRAD), a clever new counter of alpha radiation, is introduced in Chap. 5. In Chap. 7, pure germanium detectors, which are prominent devices for the detection of gamma

rays, are introduced. In Chap. 12 the latest information about Ge detectors is presented. Magnetic and electrostatic spectrometers and the position-sensitive detectors are included in Chap. 13. In Chap. 14, the LSL-M2 unfolding code is introduced as well as compensated ion chambers and self-powered neutron detectors. Chapter 16 is almost completely rewritten. There is an improved presentation in the dose rate calculation, detailed discussion of the new protection guides and exposure limits, and an expanded list of dosimeters.

I am grateful to Dr. Eiji Sakai who translated the First Edition into Japanese and in doing so discovered several typos and, more importantly, offered many suggestions that are incorporated into the Second Edition and make it better.

*Nicholas Tsoulfanidis*

CHAPTER
# ONE

# INTRODUCTION TO RADIATION MEASUREMENTS

## 1.1 WHAT IS MEANT BY RADIATION?

The word *radiation* was used until about 1900 to describe electromagnetic waves. Around the turn of the century, electrons, X-rays, and natural radioactivity were discovered and were also included under the umbrella of the term radiation. The newly discovered radiation showed characteristics of particles, in contrast to the electromagnetic radiation, which was treated as a wave. In the 1920s, DeBroglie developed his theory of the duality of matter, which was soon afterward proved correct by electron diffraction experiments, and the distinction between particles and waves ceased to be important. Today, radiation refers to the whole electromagnetic spectrum as well as to all the atomic and subatomic particles that have been discovered.

One of the many ways in which different types of radiation are grouped together is in terms of ionizing and nonionizing radiation. The word *ionizing* refers to the ability of the radiation to ionize an atom or a molecule of the medium it traverses.

Nonionizing radiation is electromagnetic radiation with wavelength $\lambda$ of about 10 nm or longer. That part of the electromagnetic spectrum includes radiowaves, microwaves, visible light ($\lambda$ = 770–390 nm), and ultraviolet light ($\lambda$ = 390–10 nm).

Ionizing radiation includes the rest of the electromagnetic spectrum (X-rays, $\lambda \approx$ 0.01–10 nm) and $\gamma$-rays with wavelength shorter than that of X-rays. It also

includes all the atomic and subatomic particles, such as electrons, positrons, protons, alphas, neutrons, heavy ions, and mesons.

The material in this text refers only to ionizing radiation. Specifically, it deals with detection instruments and methods, experimental techniques, and analysis of results for radiation in the energy range shown in Table 1.1. Particles with energies listed in Table 1.1 are encountered around nuclear reactors, around installations involving production or use of natural or manufactured radioisotopes, and also around low-energy accelerators. Not included in Table 1.1 are cosmic rays and particles produced by high-energy accelerators (GeV energy range).

## 1.2 STATISTICAL NATURE OF RADIATION EMISSION

Radiation emission is nothing more than release of energy by a system as it moves from one state to another. According to classical physics, exchange or release of energy takes place on a continuous basis; i.e., any amount of energy, no matter how small, may be exchanged as long as the exchange is consistent with conservation laws. The fate of a system is exactly determined if initial conditions and forces acting upon it are given. One may say that classical physics prescribed a "deterministic" view of the world.

Quantum theory changed all that. According to quantum theory, energy can be exchanged only in discrete amounts when a system moves from one state to another. The fact that conservation laws are satisfied is a necessary but not a sufficient condition for the change of a system. The fate of the system is not determined exactly if initial conditions and forces are known. One can only talk about the probability that the system will do something or do nothing. Thus, with the introduction of quantum theory, the study of the physical world changed from "deterministic" to "probabilistic."

The emission of atomic and nuclear radiation obeys the rules of quantum theory. As a result of this, one can only talk about the probability that a reaction will take place or that a particle will be emitted. If one attempts to measure the number of particles emitted by a nuclear reaction, that number is not constant in time; it has a statistical uncertainty because of the probabilistic nature of the phenomenon under study.

**Table 1.1 Maximum Energy Considered**

| Particle | Energy (MeV) |
|---|---|
| $\alpha$ | 20 |
| $\beta$ | 10 |
| $\gamma$ | 20 |
| $n$ | 20 |
| Heavy ions | 100 |

Consider a radioactive source emitting electrons and assume that one attempts to measure the number of electrons per unit time emitted by the source. For every atom of the source there is a probability, not a certainty, that an electron will be emitted during the next unit of time. One can never measure the "exact" number. The number of particles emitted per unit time is different for successive units of time. Therefore, one can only determine the average number of particles emitted. That average, like any average, carries with it an uncertainty, an error. The determination of this error is an integral part of any radiation measurement.

## 1.3 THE ERRORS AND ACCURACY AND PRECISION OF MEASUREMENTS

A measurement is an attempt to determine the value of a certain parameter or quantity. Anyone attempting a measurement should keep in mind the following two axioms regarding the result of the measurement:

*Axiom 1* No measurement yields a result without an error.
*Axiom 2* The result of a measurement is almost worthless unless the error associated with that result is also reported.

The term *error* is used to define the following concept:

$$\text{Error} = (\text{measured or computed value of quantity } Q) - (\text{true value of } Q)$$

or

$$\text{Error} = \text{estimated uncertainty of the measured or computed value of } Q.$$

Related to the error of a measurement are the terms *accuracy* and *precision*. The dictionary gives essentially the same meaning for both accuracy and precision, but in experimental work they have different meanings.

The accuracy of an experiment tells us how close the result of the measurement is to the true value of the measured quantity. The precision of an experiment is a measure of the exactness of the result. As an example, consider the measurement of the speed of light, which is known, from measurements, to be equal to $2.997930 \times 10^8$ m/s.

Assume that a measurement gave the result $2.9998 \times 10^8$ m/s. The difference between these two numbers is an estimate of the accuracy of the measurement. On the other hand, the precision of the measurement is related to the number of significant figures[†] representing the result. The number $2.9998 \times 10^8$ indicates that the result has been determined to be between 2.9997 and 2.9999 or, equivalently, that it is known to 1 part in 30,000 (1/29998).

[†]As an example of the number of significant figures, each of the following numbers has five significant figures: 2.9998. 29998. 20009. .0029998, $2.9880 \times 10^8$.

If the measurement is repeated and the new result is $2.9999 \times 10^8$ m/s, the accuracy has changed but not the precision. If, on the other hand, the result of the measurement is $2.99985 \times 10^8$ m/s, both precision and accuracy have changed.

Another way to look at the accuracy and precision of a measurement is in terms of the distribution of the data obtained (Fig. 1.1). To improve the error of a measurement, the process is repeated many times, if practical. The results recorded, after repeated identical tries, are not identical. Instead, the data follow a distribution, almost Gaussian in most cases (see Chap. 2 for more details), and the measured value reported is an average based on the shape of the distribution of data. The width of the distribution of individual results is a measure of the precision of the measurement; the distance of the average of the

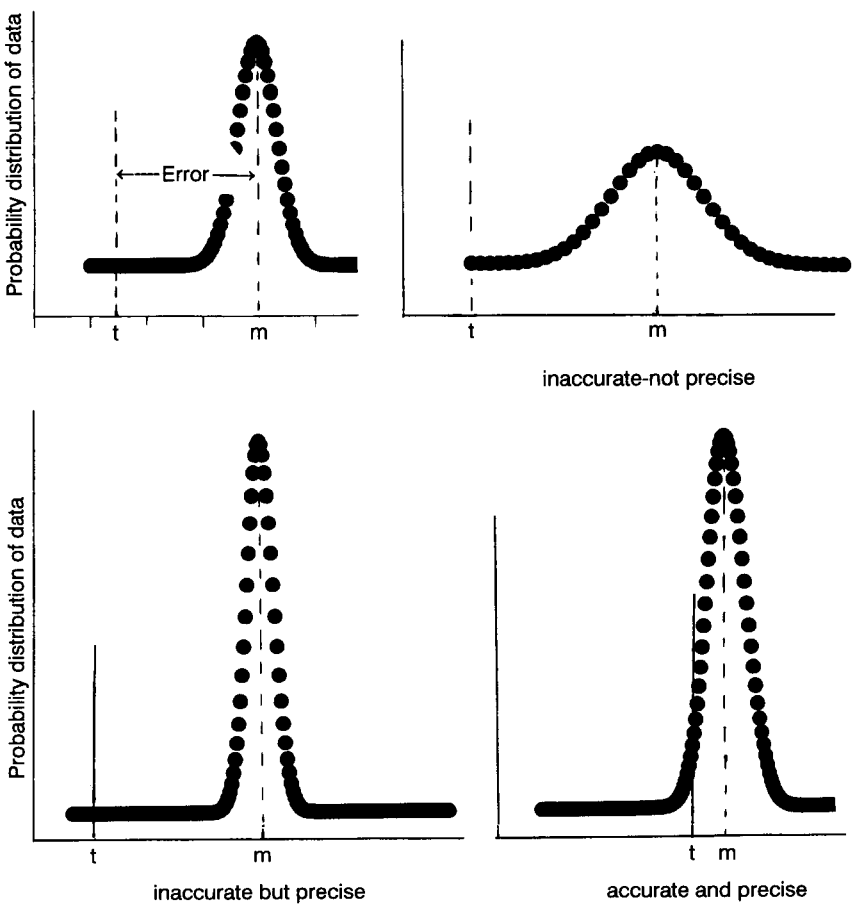


**Figure 1.1** Accuracy and precision of measurements; $t$, true value; $m$, measured value.

distribution from the true value is a measure of the accuracy of the measurement.

Every experimenter should consider accuracy and precision simultaneously. It would be a waste of effort to try to improve the precision of a measurement if it is known that the result is inaccurate. On the other hand, it is almost useless to try to achieve very high accuracy if the precision of the measurement is low.

Limitations in the accuracy and precision of measurements result from many causes. Among the most important are

1. Incorrectly calibrated instruments.
2. Algebraic or reading errors of the observer.
3. Uncontrolled changes in environmental conditions, such as temperature, pressure, and humidity.
4. Inability to construct arbitrarily small measuring meter-sticks, rods, pointers, clocks, apertures, lenses, etc.
5. A natural limit of sensitivity for any real measuring instrument detecting individual effects of atoms, electrons, molecules, and protons.
6. Imperfect method of measurement in most cases.
7. Unknown exact initial state of the system. Or, even if the initial state is known, it is impossible to follow the evolution of the system. For example, to determine the state of a gas in a container, one should know the exact position and velocity of every molecule at $t = 0$. Even if this is known, how practical is it to follow $10^{20}$ atoms or molecules moving in a box?
8. Statistical nature of some processes, e.g., radioactive decay. There is a probability that an atom of a radioactive isotope will decay in the next 10 s, and this is as much information as one can report on this matter. The probability can be calculated, but it is still a probability, never a certainty.

## 1.4 TYPES OF ERRORS

There are many types of errors, but they are usually grouped into two broad categories: systematic and random.

Systematic (or determinate) errors are those that affect all the results in the same way. Examples of systematic errors are

1. Errors from badly calibrated instruments
2. Personal errors (algebraic, wrong readings, etc.)
3. Imperfect technique

Systematic errors introduce uncertainties that do not obey a particular law and cannot be estimated by repeating the measurement. The experimenter should make every reasonable effort to minimize or, better yet, eliminate systematic errors. Once a systematic error is identified, all results are corrected appropriately. For example, if a measurement of temperature is made and it is

discovered that the thermocouple used overestimates the temperature by 10%, all temperatures measured are decreased by 10%.

Random (or statistical) errors can either decrease or increase the results of a measurement, but in a nonreproducible way. Most of the random errors cannot be eliminated. They can be reduced, however, by either improving the experimental apparatus, improving the technique, and/or repeating the experiment many times. Examples of random errors are

1. Errors resulting from experimental apparatus (reading of instruments, electronic noise, etc.)
2. Errors from uncontrolled change in condition such as voltage, temperature, or pressure
3. Probabilistic nature of the phenomenon under study

The determination of error associated with the measurement is a very important task. It is probably as important as the measurement. Technical journals and scientific reports never report results of experiments without the error corresponding to these results. A measurement reported without an error is almost worthless. For this reason, the study of errors is a topic of great importance for scientists and engineers.

This text does not give a complete theory of error. Only the fundamentals needed for a basic understanding of the statistical analysis of errors are presented. The objective is to present methods that provide an estimate of the error of a certain measurement or a series of measurements and procedures that minimize the error.

Only random errors are discussed from here on. In every measurement, systematic and random errors should be treated separately. Systematic and random errors should never be combined using the methods discussed in Chap. 2. Those methods apply to random errors only.

## 1.5 NUCLEAR INSTRUMENTATION

### 1.5.1 Introduction

This section is addressed to the person who has not seen or used radiation instruments.† Its purpose is to present a general description of the physical appearance and operation of the basic components of a radiation counting system. Every component is treated like a "black box," i.e., input and output are discussed without any details about how the output is obtained. Details about the construction and operation of individual units are given in later chapters.

†The term *radiation instruments* refers to instruments used for the detection of ionizing radiation as explained in Sec. 1.1

Detectors are discussed in Chaps. 5 through 7, and the rest of the electronics is discussed in Chap. 10.

Counting systems are classified into two types, according to the method of operation:

1. Pulse-type systems. The output consists of voltage pulses, one pulse per particle detected.
2. Current-type systems. The output is an average value, resulting from the detection of many particles.

A basic pulse-type system consists of the instruments shown in Fig. 1.2. The function of each component is discussed in later sections of this chapter.

A current-type system (e.g., an electrometer or a rate meter) is simpler than the pulse-type system. Such systems are discussed in Chap. 5. The remainder of this chapter concerns only pulse-type counting systems.

### 1.5.2 The Detector

The function of the detector is to produce a signal for every particle entering into it. Every detector works by using some interaction of particles with matter. Following is a list of the most common detector types.

1. Gas-filled counters (ionization, proportional, Geiger-Muller counters)
2. Scintillation detectors
3. Semiconductor detectors
4. Spark chambers (used with high energy particles)
5. Bubble chambers
6. Photographic emulsions
7. Thermoluminescent dosimeters (TLDs)
8. Cerenkov counters
9. Self-powered neutron detectors

The signal at the output of most detectors is a voltage pulse, such as the one

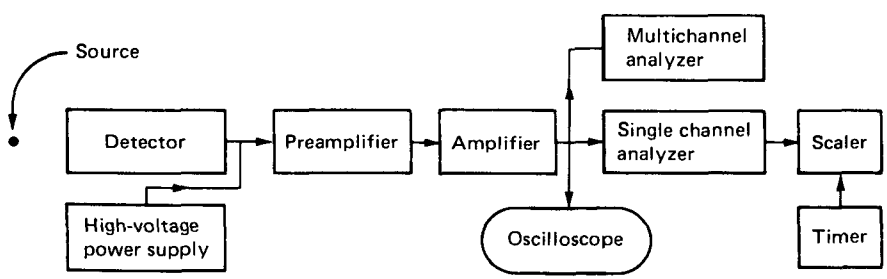


**Figure 1.2** A basic pulse-type detection system.

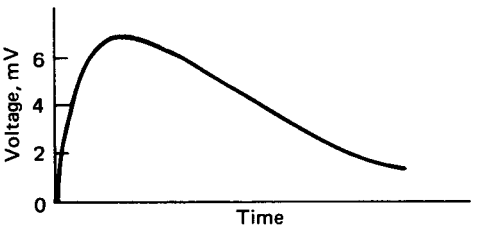


**Figure 1.3** A typical pulse-type detector signal.

shown in Fig. 1.3. For others, the signal may be a change in color (emulsions) or some trace that can be photographed (bubble or spark chambers)

The ideal pulse-type counter should satisfy the following requirements:

1. Every particle entering the detector should produce a pulse at the exit of the counter, which is higher than the electronic noise† level of the unit that accepts it (usually this unit is the preamplifier). In such a case, every particle entering the detector will be detected, and the detector efficiency, defined as the ratio of the number of particles detected to the number of particles entering the counter, will be equal to 100 percent (for more details on efficiency, see Chap. 8).
2. The duration of the pulse should be short, so that particles coming in one after the other in quick succession produce separate pulses. The duration of the pulse is a measure of the dead time of the counter (see Sec. 2.21) and may result in loss of counts in the case of high counting rates.
3. If the energy of the particle is to be measured, the height of the pulse should have some known fixed relationship to the energy of the particle. To achieve this, it is important that the size of the counter is such that the particle deposits all its energy (or a known fraction) in it.
4. If two or more particles deposit the same energy in the detector, the corresponding pulses should have the same height. This requirement is expressed in terms of the energy resolution of the detector (see Chap. 9). Good energy resolution is extremely important if the radiation field consists of particles with different energies and the objective of the measurement is to identify (resolve) these energies. Figure 1.4 shows an example of good and bad energy resolution.

There is no detector that satisfies all these requirements. Few detectors have 100 percent efficiency. In practice, it is not feasible for gamma and neutron detectors to have all the energy of the particle deposited in the counter. Because of statistical effects, there is no detector with ideal energy resolution. What should one do?

†Electronic noise is any type of interference that tends to "mask" the quantity to be observed. It is usually the result of the thermal motion of charge carriers in the components of the detection system (cables, resistors, the detector itself, etc.) and manifests itself as a large number of low-level pulses. Electronic noise should be distinguished from background pulses resulting from radiation sources that are always present, e.g., cosmic rays.

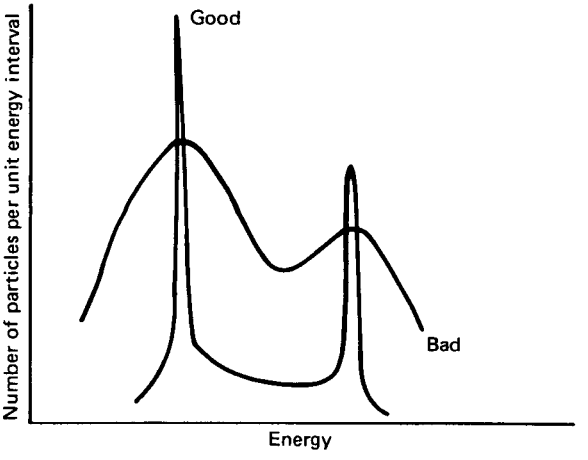


**Figure 1.4** Good and bad energy resolution.

In practice, the experimenter selects a detector that satisfies as many of these properties as possible to the highest degree possible and, depending on the objective of the measurement, applies appropriate corrections to the measured data.

### 1.5.3 The NIM Concept

Most of the commercially available instruments that are used in radiation measurements conform to the standards on nuclear instrument modules (NIM) developed by the U.S. Atomic Energy Commission (now the Nuclear Regulatory Commission) and now dictated by the Department of Energy.[1]

The objective of the NIM standard is the design of commercial modules that are interchangeable physically and electrically. The electrical interchangeability is confined to the supply of power to the modules and in general does not cover the design of the internal circuits.

The size of the smallest, called a single-width, NIM is 0.222 m × 0.035 m (8.71 in × 1.35 in). Multiple-width NIMs are also made. The standard NIM bin will accommodate 12 single-width NIMs or any combination of them having the same total equivalent width. Figure 1.5 is a photograph of the front and back sides of a commercial standard bin. Figure 1.6 is a photograph of the bin filled with NIMs of different widths, made by different manufacturers.

### 1.5.4 The High-Voltage Power Supply

The *high-voltage power supply* (HVPS) provides a positive or negative voltage necessary for the operation of the detector. Most detectors need positive high voltage (HV). Typical HVs for common detectors are given in Table 1.2. The HVPS is constructed in such a way that the HV at the output changes very little even though the input voltage (110 V, ac) may fluctuate.

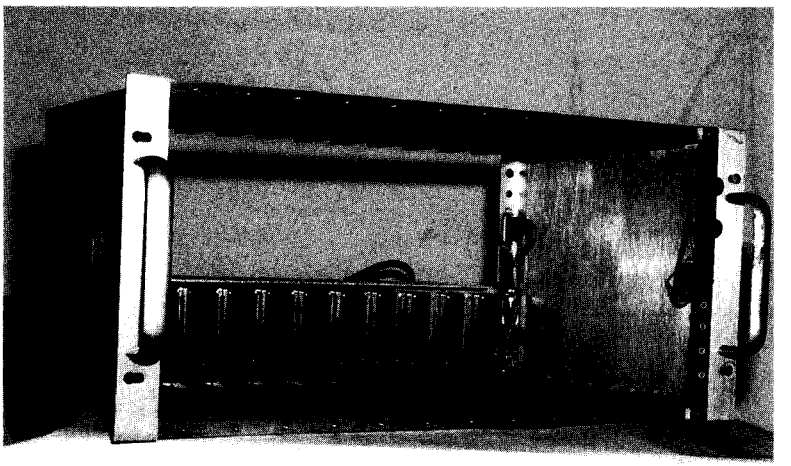

(*a*)

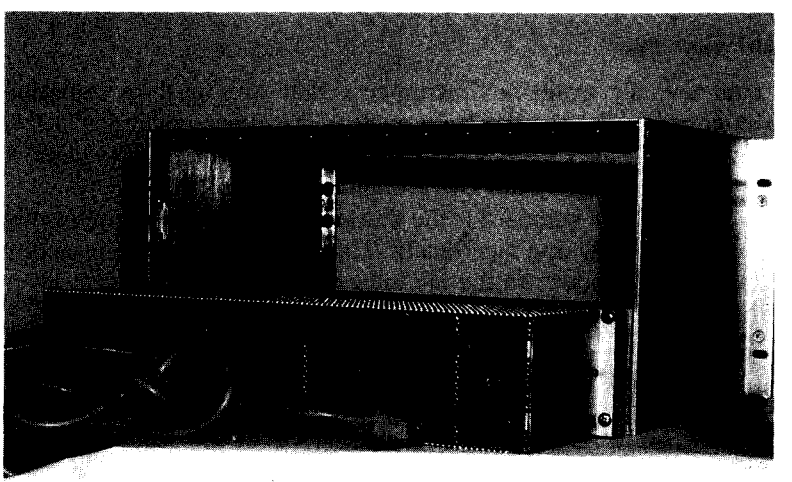

(*b*)

**Figure 1.5** Photographs of the (*a*) front and (*b*) back sides of a commercial NIM bin (from Canberra 1979–1980 catalog).

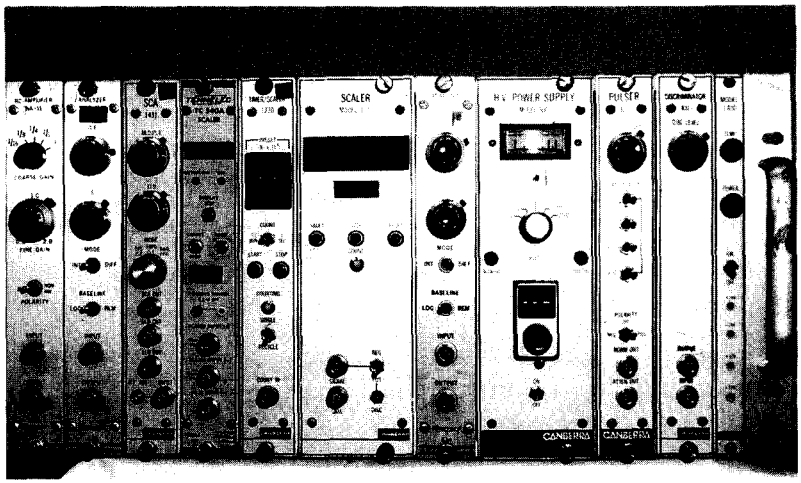


**Figure 1.6** A typical bin filled with a combination of NIMs made by different manufacturers.[1]

A typical commercial HVPS is shown in Fig. 1.7. The front panel has an indicator light that shows whether the unit is on or off and, if it is on, whether the output is positive or negative voltage. There are two knobs for voltage adjustment, one for coarse changes of 500-V intervals, the other for changes of 0.1 V. The output is at the rear of the unit.

### 1.5.5 The Preamplifier

The primary purpose of the preamplifier is to provide an optimized coupling between the output of the detector and the rest of the counting system. The preamplifier is also necessary to minimize any sources of noise that may change the signal.

**Table 1.2 High Voltage Needed for Certain Common Detectors**

| Detector | High voltage (V) |
|---|---|
| Ionization counters | HV < 1000 |
| Proportional counters | 500 < HV < 1500 |
| GM counters | 500 < HV < 1500 |
| Semiconductor detectors | |
| Surface-barrier | HV < 100 |
| Li-drifted | 100 < HV < 3000 |

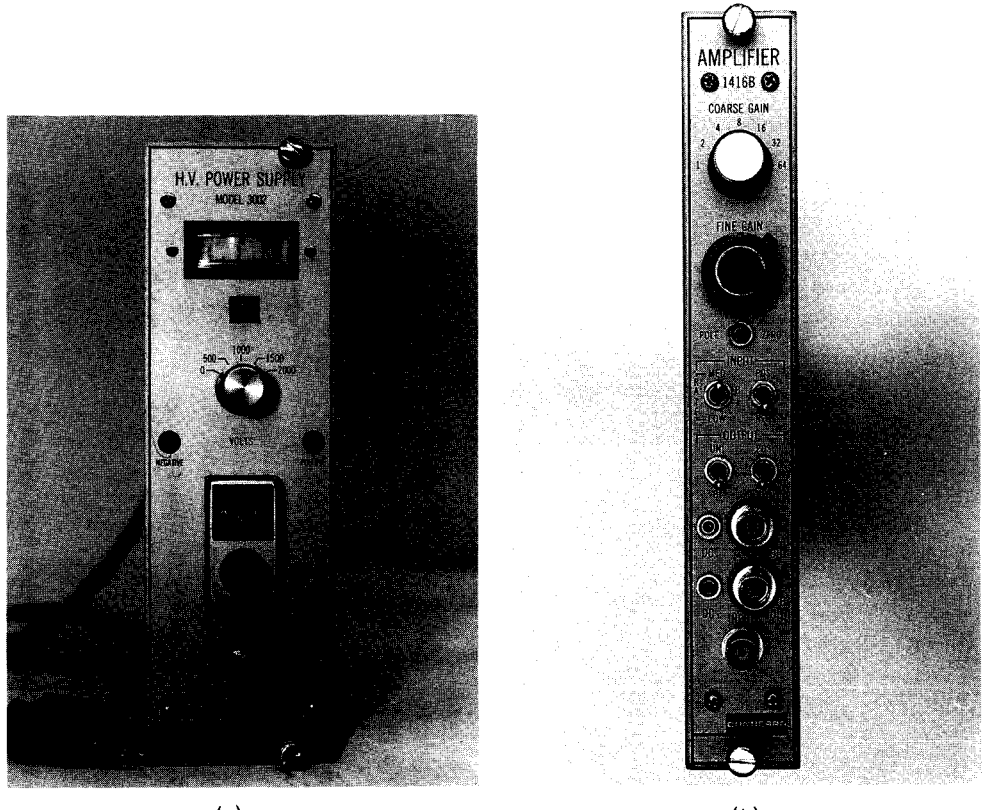


(a) (b)

**Figure 1.7** Typical commercial NIMs: (*a*) HV power supply, (*b*) amplifier (made by Canberra and Tennelec).

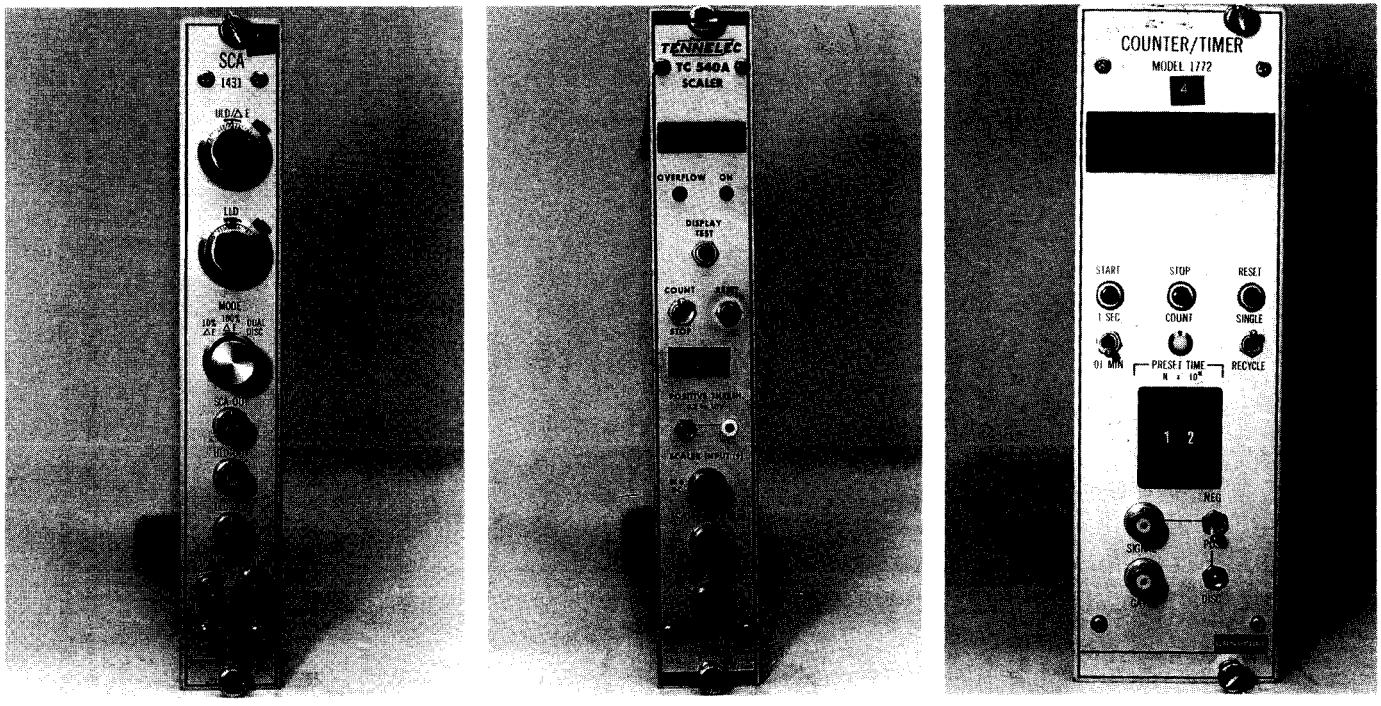


(a) (b) (c)

**Figure 1.7** Typical commercial NIMs *(Continued)*: (*c*) single-channel analyzer, (*d*) scaler, (*e*) timer (made by Canberra and Tennelec).

The signal that comes out of the detector is very weak, in the millivolt (mV) range (Fig. 1.3). Before it can be recorded, it will have to be amplified by a factor of a thousand or more. To achieve this, the signal will have to be transmitted through a cable to the next instrument of the counting system, which is the amplifier. Transmission of any signal through a cable attenuates it to a certain extent. If it is weak at the output of the detector, it might be lost in the electronic noise that accompanies the transmission. This is avoided by placing the preamplifier as close to the detector as possible. The preamplifier shapes the signal and reduces its attenuation by matching the impedance of the detector with that of the amplifier. After going through the preamplifier, the signal may be safely transmitted to the amplifier, which may be located at a considerable distance away. Although some preamplifiers amplify the signal slightly, their primary function is that of providing electronic matching between the output of the detector and the input of the amplifier.

There are many types of commercial preamplifiers, two of which are shown in Fig. 1.8. In most cases, the HV is fed to the detector through the preamplifier.

### 1.5.6 The Amplifier

The main amplification unit is the amplifier. It increases the signal by as many as 1000 times or more. Modern commercial amplifiers produce a maximum signal of 10 V, regardless of the input and the amplification. For example, consider a preamplifier that gives at its output three pulses with heights 50 mV, 100 mV, and 150 mV. Assume that the amplifier is set to 100. At the output of the unit, the three pulses will be

$$50 \times 10^{-3} \times 100 = 5 \text{ V}$$
$$100 \times 10^{-3} \times 100 = 10 \text{ V}$$
$$150 \times 10^{-3} \times 100 = 10 \text{ V}$$

Note that the third value should be 15 V, but since the amplifier produces a maximum signal of 10 V, the three different input pulses will show, erroneously, as two different pulses at the output. If only the number of particles is measured, there is no error introduced—but if the energy of the particles is measured, then the error is very serious. In the example given above, if gammas of three different energies produce the pulses at the output of the preamplifier, the pulses at the output of the amplifier will be attributed erroneously to gammas of two different energies. To avoid such an error, an observer should follow this rule:

> Before any measurement of particle energy, make certain that the highest pulse of the spectrum to be measured is less than *10 V* at the output of the amplifier.

In addition to signal amplification, an equally important function of the amplifier is to convert the signal at the output of the preamplifier into a form

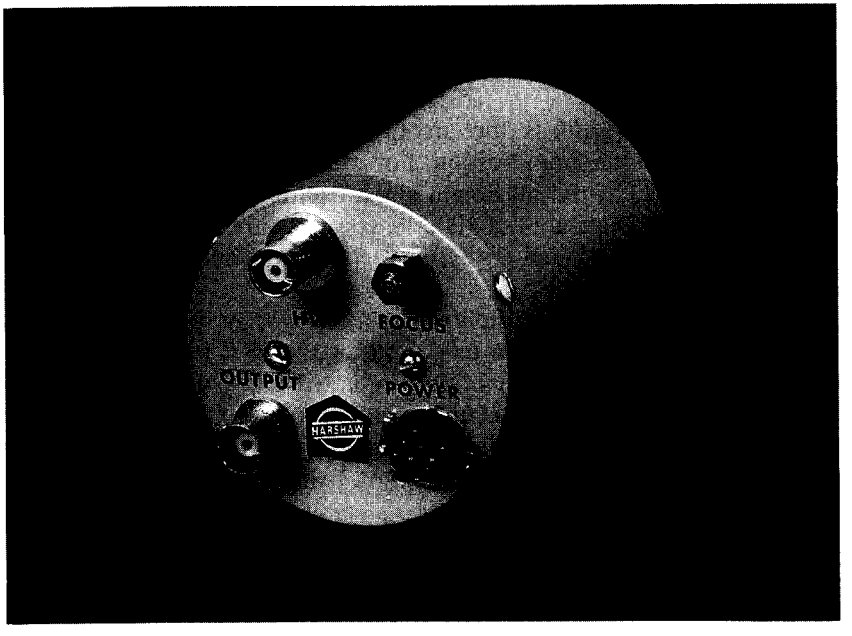


(a)

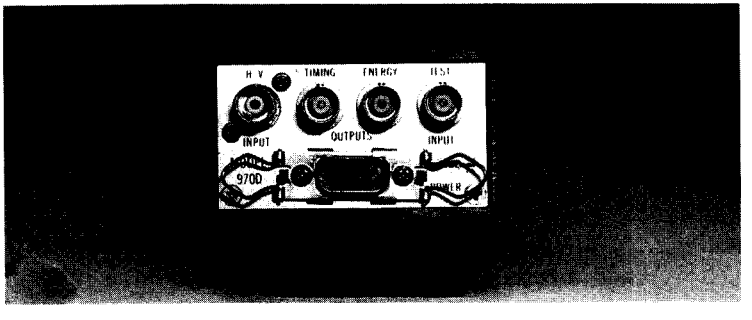


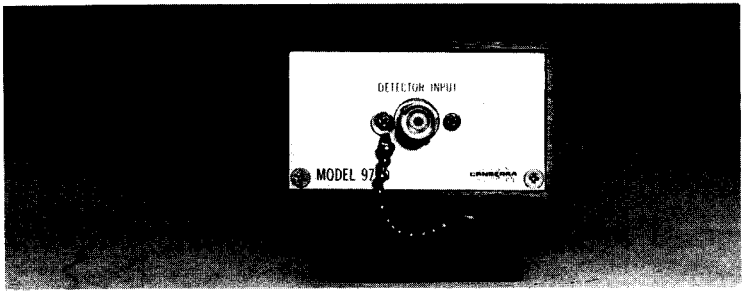


(b)

**Figure 1.8** Two typical commercial preamplifiers: (*a*) type used with a photomultiplier tube (made by Harshaw), and (*b*) type used with semiconductor detectors (made by Canberra).

suitable for the measurement desired. More details on this subject are given in Chap. 10. The front panel of a typical commercial amplifier is shown in Fig. 1.7.

Commercial amplifiers have two dials for adjusting the amplification.

1. *Coarse gain:* This dial adjusts the amplification in *steps*. Each step is a fraction of the maximum amplification. For example, the dial may show the numbers 1, 2, 4, 8, 16. If the maximum amplification is 100, then the coarse gain on 16 will give a maximum of 100, the coarse gain on 8 will give 50, etc. Some amplifiers have the numbers $\frac{1}{16}$, $\frac{1}{8}$, $\frac{1}{4}$, $\frac{1}{2}$, 1, and some newer ones have 1, 10, 100, 1000, etc.
2. *Fine gain:* This dial adjusts the amplification *continuously* within each step of the coarse gain. The numbers, in most units, go from 0 to 10. The highest number provides the maximum amplification indicated by the coarse gain. As an example, consider the maximum amplification to be 100. If the coarse gain is 8 (highest number 16) and the fine gain 5 (highest number 10), the amplification will be $100 \times \frac{1}{2}$ (coarse gain) $\times \frac{1}{2}$ (fine gain) = 25.

Most commercial amplifiers provide at the output two types of pulses, called unipolar and bipolar (Fig. 1.9).

### 1.5.7 The Oscilloscope

The oscilloscope is an instrument that permits the study of rapidly changing phenomena, such as a sinusoidal voltage or the pulse of a counter. The phenomenon is observed on a fluorescent screen as shown in Fig. 1.10. The horizontal axis of the screen measures time. The vertical axis gives volts.

In radiation measurements the oscilloscope is used to check the quality of the signal as well as the level and type of the electronic noise. It is always a good practice before any measurement is attempted to examine the signal at the output of the amplifier. A few examples of good and bad pulses are shown in Fig. 1.11. In Fig. 1.11, *a* and *b* represent good pulses, and Fig. 1.11*c* is probably

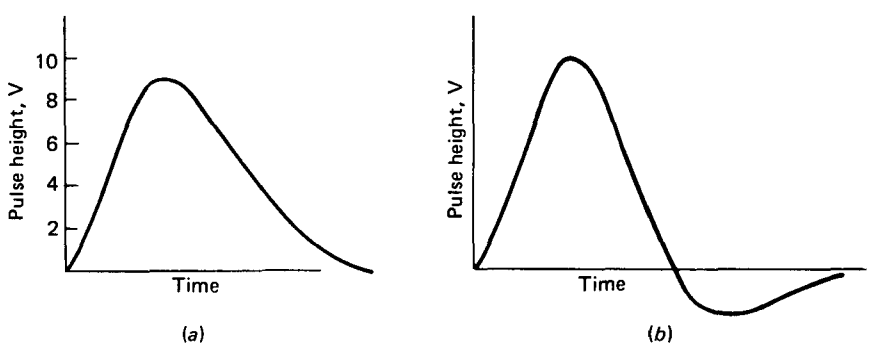


**Figure 1.9** The pulse at the output of the amplifier: (*a*) unipolar pulse and (*b*) bipolar pulse.

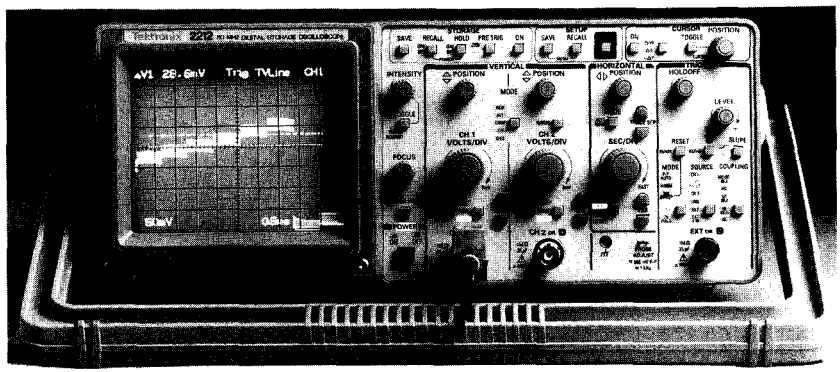

(a)

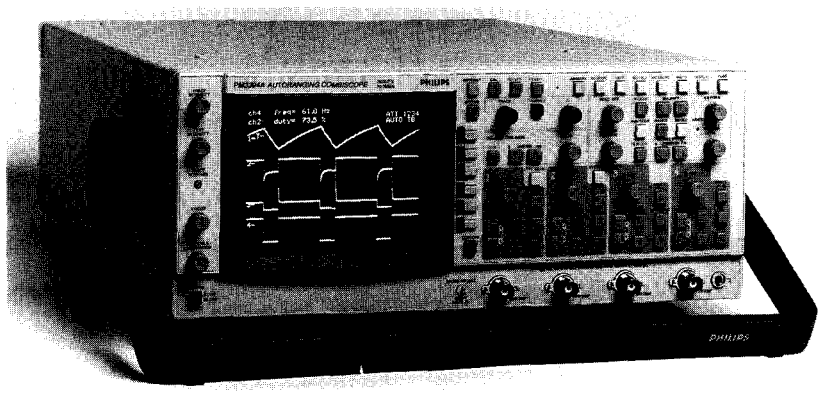

(b)

**Figure 1.10** Two commercial oscilloscopes: *a*) a Tektronix 2212 oscilloscope (Copyright © 1994 by Tektronix, Inc. All rights reserved. Reproduced by permission.); and *b*) a Philips PM3394A autoranging combiscope (Reproduced with permission).

an electrical discharge, not good for counting. Figure 1.11*d* is no good either, because a high-frequency signal is "riding" on the output of the preamplifier. If the pulse is not good, the observer should not proceed with the measurement unless the source of noise is identified and eliminated.

Modern oscilloscopes provide analog as well as digital signals.

### 1.5.8 The Discriminator or Single-Channel Analyzer (SCA)

The SCA is used to eliminate the electronic noise and, in general, to reject unwanted pulses. When a pulse is amplified, the electronic noise that is always present in a circuit is also amplified. If one attempts to count all the pulses present, the counting rate may be exceedingly high. But electronic noise is a nuisance and it should not be counted.

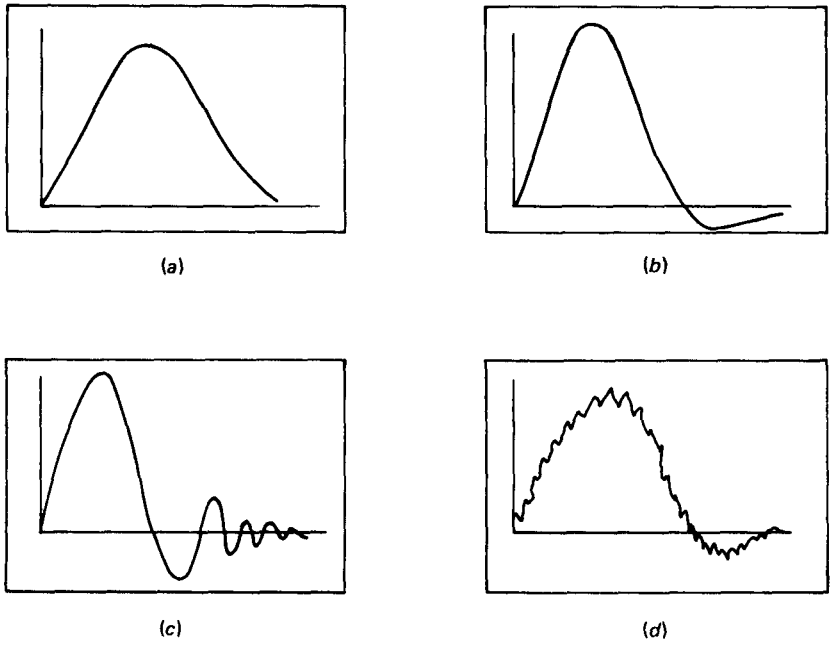


**Figure 1.11** Samples of good (*a* and *b*) and bad (*c* and *d*) pulses as seen on the screen of the oscilloscope.

In some cases, one may want to count only pulses above a certain height, i.e., particles with energy above certain threshold energy. Pulses lower than that height should be rejected. The discriminator or SCA is the unit that can make the selection of the desired pulses. Figure 1.7*c* shows the front panel of a typical commercial SCA. Modern SCAs work in the following way.

There are two dials on the front panel of the unit. One is marked E, for energy, or LLD, for lower-level dial; the other is marked $\Delta$E or ULD/$\Delta$E, for upper-level dial/$\Delta$E. There is also a two-position switch with INT (integral) and DIFF (differential) positions. In the INT position, only the E dial operates, and the unit functions as a *discriminator*. In the DIFF position, both E and $\Delta$E operate, and the unit is then a *single-channel analyzer*.

In some other commercial models, instead of INT and DIFF positions, the instrument has special connectors for the desired output.

**The discriminator (switch position: INT).** The dial E (for energy) may be changed continuously from 0 to 100. Of course, the discriminator works with voltage pulses, but there is a one-to-one correspondence between a pulse height and the energy of a particle. Assume that the discriminator is set to E = 2.00 V (the 2 V may also correspond to 2 MeV of energy). Only pulses with height greater than 2 V will pass through the discriminator. Pulses lower than 2 V will

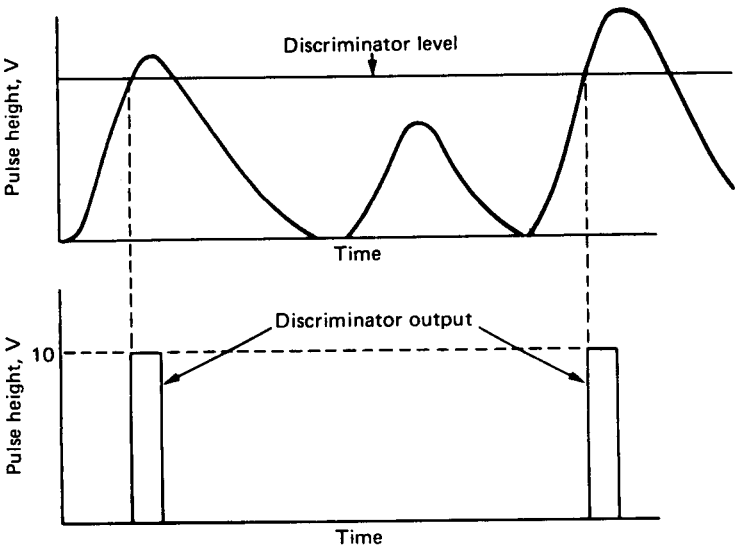


**Figure 1.12** The pulse at the output of a discriminator.

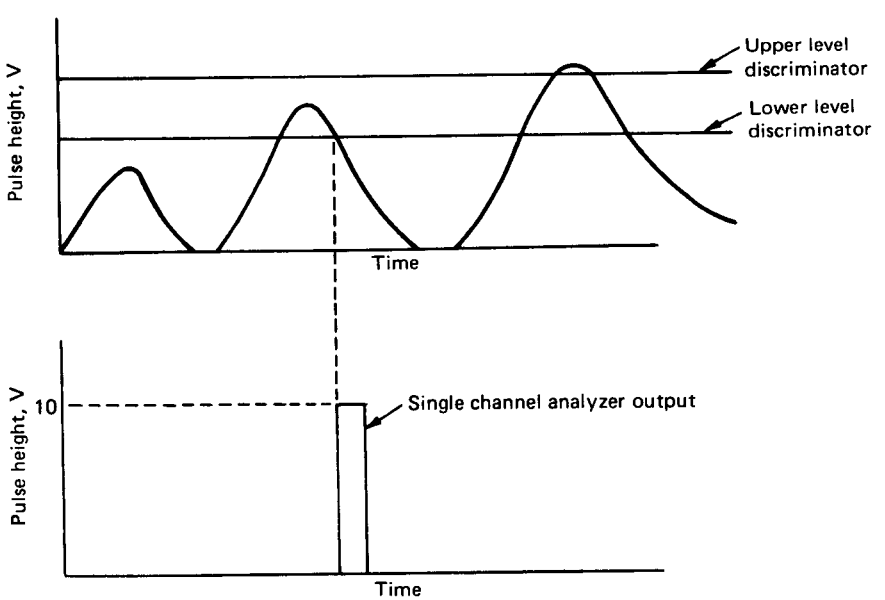


**Figure 1.13** The operation of a single-channel analyzer.

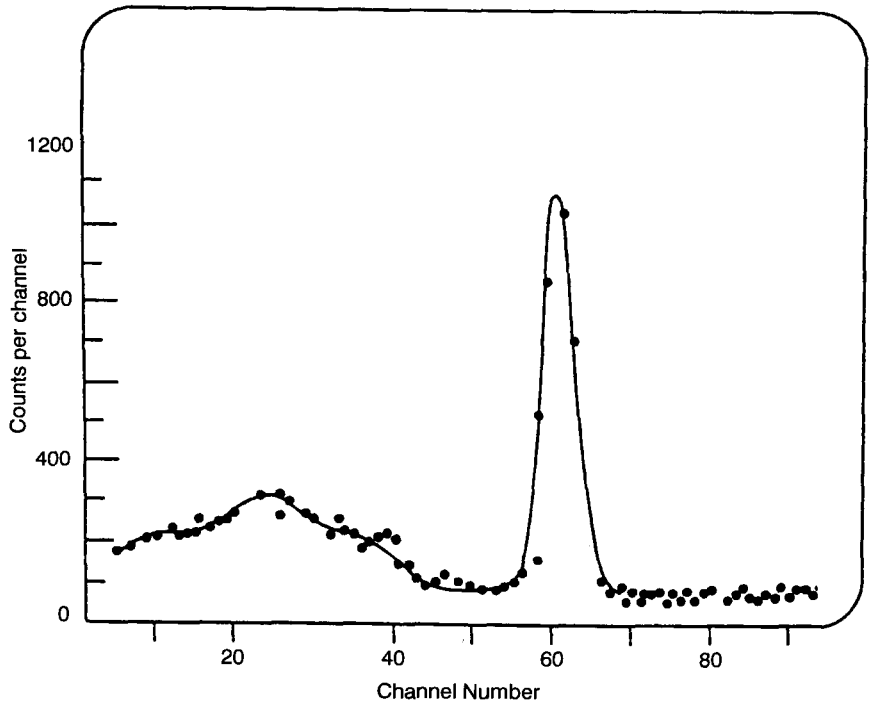


**Figure 1.14** An energy spectrum shown on the screen of an MCA.

be rejected. For every pulse that is larger than 2 V, the discriminator will provide at the output a rectangular pulse with height equal to 10 V (Fig. 1.12) regardless of the actual height of the input pulse. The output pulse of the discriminator is a pulse that triggers the unit (scaler), which counts individual pulses and tells it, "a pulse with height bigger than 2 V has arrived; count 1." Thus, the discriminator eliminates all pulses below E and allows only pulses that are higher than E to be counted.

**The single-channel analyzer (switch position: DIFF).** Both E and $\Delta E$ dials operate. Only pulses with heights between E and $E + \Delta E$ are counted (Fig. 1.13). The two dials form a "channel"; hence the name single-channel analyzer. If the E dial is changed to $E_1$, then pulses with heights between $E_1$ and $E_1 + \Delta E$ will be counted. In other words, the width $\Delta E$, or window, of the channel is always added to E.

### 1.5.9 The Scaler

The scaler is a recorder of pulses. For every pulse entering the scaler, a count of 1 is added to the previous total. At the end of the counting period, the total

number of pulses recorded is displayed. Figure 1.7*d* shows the front panel of a typical commercial scaler.

### 1.5.10 The Timer

The timer is connected to the scaler, and its purpose is to start and stop the scaler at desired counting time intervals. The front panel of a typical timer is shown in Fig. 1.7*e*. Some models combine the timer with the scaler in one module.

### 1.5.11 The Multichannel Analyzer

The multichannel analyzer (MCA) records and stores pulses according to their height. Each storage unit is called a channel.

The height of the pulse has some known relationship—usually proportional—to the energy of the particle that enters into the detector. Each pulse is in turn stored in a particular channel corresponding to a certain energy. The distribution of pulses in the channels is an image of the distribution of the energies of the particles. At the end of a counting period, the spectrum that was recorded may be displayed on the screen of the MCA (Fig. 1.14). The horizontal axis is a channel number, or particle energy. The vertical axis is a number of particles recorded per channel. More details about the MCA and its use are given in Chaps. 9 and 10.

## BIBLIOGRAPHY

Beers, Y., *Introduction to the Theory of Error*, Addison-Wesley, Reading, Mass., 1957.

Bevington, P. R., *Data Reduction and Error Analysis for the Physical Sciences*, McGraw-Hill, New York, 1969.

Jaech, J. L., "Statistical Methods in Nuclear Material Control," TID-26298, U.S. Atomic Energy Commission, 1973.

## REFERENCE

1. "Standard Nuclear Instrument Modules," TID-20893 (rev. 2), U.S. Atomic Energy Commission, 1968; now designated as DOE/ER-0457T.

CHAPTER
# TWO

# STATISTICAL ERRORS OF RADIATION COUNTING

## 2.1 INTRODUCTION

This chapter discusses statistics at the level needed for radiation measurements and analysis of their results. People who perform experiments need statistics for analysis of experiments that are statistical in nature, treatment of errors, and fitting a function to the experimental data. The first two uses are presented in this chapter. Data fitting is discussed in Chap. 11.

## 2.2 DEFINITION OF PROBABILITY

Assume that one repeats an experiment many times and observes whether or not a certain event x is the outcome. The event is a certain observable result defined by the experimenter. If the experiment was performed $N$ times, and $n$ results were of type x, the probability $P(\mathrm{x})$ that any single event will be of type x is equal to

$$P(\mathrm{x}) = \lim_{N \to \infty} \frac{n}{N} \tag{2.1}$$

The ratio $n/N$ is sometimes called the relative frequency of occurrence of x in the first $N$ trials.

There is an obvious difficulty with the definition given by Eq. 2.1—the requirement of an infinite number of trials. Clearly, it is impossible to perform an infinite number of experiments. Instead, the experiment is repeated $N$ times, and if the event x occurs $n$ times out of $N$, the probability $P(\mathrm{x})$ is

$$P(\mathrm{x}) = \frac{n}{N} \tag{2.2}$$

Equation 2.2 will not make a mathematician happy, but it is extensively used in practice because it is in accord with the idea behind Eq. 2.1 and gives useful results.

As an illustration of the use of Eq. 2.2, consider the experiment of tossing a coin 100 times and recording how many times the result is "heads" and how many it is "tails." Assume that the result is

Heads: 48 times
Tails: 52 times

On the basis of Eq. 2.2, the probability of getting heads or tails if the coin is tossed once more is

$$P(\text{heads}) = \frac{48}{100} = 0.48$$

$$P(\text{tails}) = \frac{52}{100} = 0.52$$

For this simple experiment, the correct result is known to be

$$P(\text{tails}) = P(\text{heads}) = 0.5$$

and one expects to approach the correct result as the number of trials increases. That is, Eq. 2.2 does not give the correct probability, but as $N \to \infty$, Eq. 2.2 approaches Eq. 2.1.

Since both $n$ and $N$ are positive numbers, $0 \le n/N \le 1$, therefore,

$$0 \le P(\mathrm{x}) \le 1$$

that is, the probability is measured on a scale from 0 to 1.

If the event x occurs every time the experiment is performed, then $n = N$ and $P(\mathrm{x}) = 1$. Thus the probability of a certain (sure) event is equal to 1.

If the event x never occurs, then $n = 0$ and $P(\mathrm{x}) = 0$. In this case the probability of an impossible event is 0.

If the result of a measurement has $N$ possible outcomes, each having equal probability, then the probability for the individual event $\mathrm{x}_i$ to occur is

$$P(\mathrm{x}_i) = \frac{1}{N} \qquad i = 1, \ldots, N$$

For example, in the case of coin tossing there are two events of equal probability; therefore

$$P(\text{heads}) = P(\text{tails}) = \frac{1}{2}$$

## 2.3 BASIC PROBABILITY THEOREMS

In the language of probability, an "event" is an outcome of one or more experiments or trials and is defined by the experimenter. Some examples of events are

1. Tossing a coin once
2. Tossing a coin twice and getting heads both times
3. Tossing a coin 10 times and getting heads for the first five times and tails for the other five
4. Picking up one card from a deck of cards and that card being red
5. Picking up 10 cards from a deck and all of them being hearts
6. Watching the street for 10 min and observing two cyclists pass by
7. Counting a radioactive sample for 10 s and recording 100 counts
8. Inspecting all the fuel rods in a nuclear reactor and finding faults in two of them.

Given enough information, one can calculate the probability that any one of these events will occur. In some cases, an event may consist of simpler components and one would like to know how to calculate the probability of the complex event from the probabilities of its components.

Consider two events x and y and a series of $N$ trials. The result of each trial will be only one of the following four possibilities:

1. x occurred but not y
2. y occurred but not x
3. Both x and y occurred
4. Neither x nor y occurred

Let $n_1$, $n_2$, $n_3$, $n_4$ be the number of times in the $N$ observations that the respective possibilities occurred. Then,

$$n_1 + n_2 + n_3 + n_4 = N \tag{2.3}$$

The following probabilities are defined with respect to the events x and y:

$P(\mathrm{x})$ = probability that x occurred

$P(\mathrm{y})$ = probability that y occurred

$P(\mathrm{x} + \mathrm{y})$ = probability that either x or y occurred

$P(\mathrm{xy})$ = probability that both x and y occurred

$P(\mathrm{x}|\mathrm{y})$ = conditional probability of x given y
= probability of x occurring given that y has occurred

$P(\mathrm{y}|\mathrm{x})$ = conditional probability of y given x
= probability of y occurring given that x has occurred

Using Eq. 2.2, these probabilities are

$$P(\mathrm{x}) = \frac{n_1 + n_3}{N} \tag{2.4}$$

$$P(\mathrm{y}) = \frac{n_2 + n_3}{N} \tag{2.5}$$

$$P(\mathrm{x} + \mathrm{y}) = \frac{n_1 + n_2 + n_3}{N} \tag{2.6}$$

$$P(\mathrm{xy}) = \frac{n_3}{N} \tag{2.7}$$

$$P(\mathrm{x}|\mathrm{y}) = \frac{n_3}{n_2 + n_3} \tag{2.8}$$

$$P(\mathrm{y}|\mathrm{x}) = \frac{n_3}{n_1 + n_3} \tag{2.9}$$

For the six probabilities given by Eqs. 2.4 to 2.9, the following two relations hold:

$$P(\mathrm{x} + \mathrm{y}) = P(\mathrm{x}) + P(\mathrm{y}) - P(\mathrm{xy}) \tag{2.10}$$

$$P(\mathrm{xy}) = P(\mathrm{x})P(\mathrm{y}|\mathrm{x}) = P(\mathrm{y})P(\mathrm{x}|\mathrm{y}) \tag{2.11}$$

Equation 2.10 is called the *addition law of probability.* Equation 2.11 is called the *multiplication law of probability.*

**Example 2.1** Consider two well-shuffled decks of cards. What is the probability of drawing one card from each deck with both of them being the ace of spades?

**Answer** The events of interest are

Event x = event y = (drawing one card and that card being ace of spades)

Since each deck has only one ace of spades,

$$P(\mathrm{x}) = P(\mathrm{y}) = P(\text{ace of spades}) = \tfrac{1}{52}$$

The conditional probability is

$$P(\mathrm{x}|\mathrm{y}) = P(\text{1st card ace of spades when 2nd card is ace of spades}) = \tfrac{1}{52}$$

In this case, $P(\mathrm{x}|\mathrm{y}) = P(\mathrm{x})$ because the two events are independent. The fact that the first card from the first deck is the ace of spades has no influence on what the first card from the second deck is going to be. Similarly, $P(\mathrm{y}|\mathrm{x}) = P(\mathrm{y})$.

Therefore, using Eq. 2.11, one has

$$P(\mathrm{xy}) = P(\mathrm{x})P(\mathrm{y}) = (\tfrac{1}{52})(\tfrac{1}{52}) = 0.00037$$

**Example 2.2** Consider two well-shuffled decks of cards and assume one card is drawn from each of them. What is the probability of one of the two cards being the ace of spades?

**Answer** Using Eq. 2.10,

$$P(x + y) = \tfrac{1}{52} + \tfrac{1}{52} - (\tfrac{1}{52})(\tfrac{1}{52}) = 0.038$$

Under certain conditions, the addition and multiplication laws expressed by Eqs. 2.10 and 2.11 are simplified.

If the events x and y are mutually exclusive—i.e., they cannot occur simultaneously—then $P(xy) = 0$ and the addition law becomes

$$P(x + y) = P(x) + P(y) \tag{2.12}$$

If the probability that x occurs is independent of whether or not y occurs, and vice versa, then as shown in Ex. 2.1,

$$P(y|x) = P(y)$$
$$P(x|y) = P(x)$$

In that case, the events x and y are called stochastically independent and the multiplication law takes the form

$$P(xy) = P(x)P(y) \tag{2.13}$$

Equations 2.12 and 2.13 are also known as the addition and multiplication laws of probability, but the reader should keep in mind that Eqs. 2.12 and 2.13 are special cases of Eqs. 2.10 and 2.11.

**Example 2.3** What is the probability that a single throw of a die will result in either 2 or 5?

**Answer**

$$P(2) = \tfrac{1}{6} \qquad P(5) = \tfrac{1}{6}$$
$$P(2 + 5) = P(2) + P(5) = \tfrac{1}{6} + \tfrac{1}{6} = \tfrac{1}{3}$$

**Example 2.4** Consider two well-shuffled decks of cards and assume one card is drawn from each deck. What is the probability of both cards being spades?

**Answer**

$$P(\text{one spade}) = \tfrac{13}{52}$$
$$P[(\text{spade})(\text{spade})] = (\tfrac{13}{52})(\tfrac{13}{52}) = \tfrac{1}{16}$$

Equations 2.12 and 2.13 hold for any number of events, provided the events are mutually exclusive or stochastically independent. Thus, if we have $N$ such events $x_{n|n=1,\ldots,N}$

$$P(\mathrm{x}_1 + \mathrm{x}_2 + \cdots + \mathrm{x}_N) = P(\mathrm{x}_1) + P(\mathrm{x}_2) + \cdots + P(\mathrm{x}_N) \tag{2.14}$$

$$P(\mathrm{x}_1\mathrm{x}_2 \cdots \mathrm{x}_N) = P(\mathrm{x}_1)P(\mathrm{x}_2) \cdots P(\mathrm{x}_N) \tag{2.15}$$

## 2.4 PROBABILITY DISTRIBUTIONS AND RANDOM VARIABLES

When an experiment is repeated many times under identical conditions, the results of the measurement will not necessarily be identical. In fact, as a rule rather than as an exception, the results will be different. Therefore, it is very desirable to know if there is a law that governs the individual outcomes of the experiment. Such a law, if it exists and is known, would be helpful in two ways. First, from a small number of measurements, the experimenter may obtain information about expected results of subsequent measurements. Second, a series of measurements may be checked for faults. If it is known that the results of an experiment obey a certain law and a given series of outcomes of such an experiment does not follow that law, then that series of outcomes is suspect and should be thoroughly investigated before it becomes acceptable.

There are many such laws governing different types of measurements. The three most frequently used will be discussed in later sections of this chapter, but first some general definitions and the concept of the random variable are introduced.

A quantity $x$ that can be determined quantitatively and that in successive but similar experiments can assume different values is called a random variable. Examples of random variables are the result of drawing one card from a deck of cards, the result of the throw of a die, the result of measuring the length of a nuclear fuel rod, and the result of counting the radioactivity of a sample. There are two types of random variables, discrete and continuous.

A discrete random variable takes one of a set of discrete values. Discrete random variables are especially useful in representing results that take integer values—for example, number of persons, number of defective batteries, or number of counts recorded in a scaler.

A continuous random variable can take any value within a certain interval —for example, weight or height of people, the length of a rod, or the temperature of the water coming out of a reactor.

For every random variable $x$, one may define a function $f(x)$ as follows:

**Discrete random variables**

$f(x_i)$ = probability that the value of the random variable is $x_i$ $\quad i = 1, 2, \ldots, N$

where $N$ = number of possible (discrete) values of $x$. Since $x$ takes only one

value at a time, the events represented by the probabilities $f(x_i)$ are mutually exclusive; therefore, using Eq. 2.14,

$$\sum_{i=1}^{N} f(x_i) = 1 \tag{2.16}$$

**Continuous random variables.** Assume that a random variable may take any value between $a$ and $b$ ($a \leq x \leq b$). Then

$$f(x)\,dx = \text{probability that the value of } x \text{ lies between } x \text{ and } x + dx$$

One should notice that for a continuous variable what is important is not the probability that $x$ will take a specific value, but only the probability that $x$ falls within an interval defined by two values of $x$. The equation corresponding to Eq. 2.16 is now

$$\int_a^b f(x)\,dx = 1 \tag{2.17}$$

Equations 2.16 and 2.17 give the probability of a sure event, because $x$ will certainly have one of the values $x_1, x_2, \ldots, x_N$ and will certainly have a value between $a$ and $b$.

The function $f(x)$ is called the probability density function† (pdf).

Consider now the following function:

$$F(x_j) = \int_a^{x_j} f(x')\,dx' \tag{2.18}$$

For a discrete variable,

$$F(x_j) = \sum_{i=1}^{j} f(x_i) \tag{2.19}$$

Thus,

$$F(x_j) = \text{probability that the value of } x \text{ is less than or equal to } x_j$$

The function $F(x)$ is called the cumulative distribution function‡ (cdf). The cdf has the following properties:

$$F(x_N) = 1 \tag{2.20}$$

$$F(a) = 0 \tag{2.21}$$

$$F(b) = 1 \tag{2.22}$$

The cdf is a positive monotonously increasing function, i.e., $F(b) > F(a)$, if $b > a$. There is a relationship between the cdf and the pdf obtained from Eq.

†It has also been called the frequency function.

‡It has also been called the integral or total distribution function.

2.18, namely,

$$f(x) = \frac{dF(x)}{dx} \tag{2.23}$$

## 2.5 LOCATION INDEXES (MODE, MEDIAN, MEAN)

If the distribution function $F(x)$ or $f(x)$ is known, a great deal of information can be obtained about the values of the random variable $x$. Conversely, if $F(x)$ or $f(x)$ is not completely known, certain values of $x$ provide valuable information about the distribution functions. In most practical applications the important values of $x$ are clustered within a relatively narrow interval. To obtain a rough idea about the whole distribution, it is often adequate to indicate the position of this interval by "location indexes" providing typical values of $x$.

In theory, an infinite number of location indexes† may be constructed, but in practice the following three are most frequently used: the mode, the median, and the mean of a distribution. Their definitions and physical meanings will be presented with the help of an example.

Consider the continuous pdf shown in Fig. 2.1. The function $f(x)$ satisfies Eq. 2.17, i.e., the total area under the curve of Fig. 2.1 is equal to 1, with $a = -\infty$ and $b = +\infty$.

The *mode* is defined as the most probable value of $x$. Therefore, the mode $x_1$ is that $x$ for which $f(x)$ is maximum and is obtained from

$$\frac{df(x)}{dx} = 0 \tag{2.24}$$

†Measure of location is another name for location indexes.

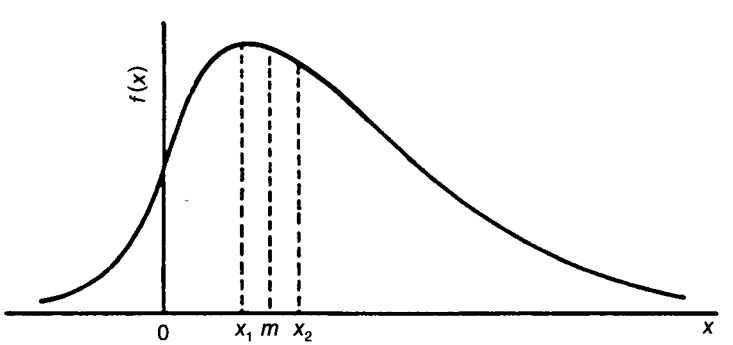


**Figure 2.1** The mode ($x_1$), the median ($x_2$), and the mean ($m$) for a continuous probability distribution function.

The *median* is the value $x_2$ for which

$$F(x_2) = \int_{-\infty}^{x_2} f(x)\,dx = \frac{1}{2} \tag{2.25}$$

i.e., the probability of $x$ taking a value less than $x_2$ is equal to the probability of $x$ taking a value greater than $x_2$.

The *mean*, also known as the "average" or the "expectation value" of $x$, is defined by the equation

$$\bar{x} = m = \int_{-\infty}^{\infty} xf(x)\,dx \tag{2.26}$$

An expression more general than Eq. 2.26 that gives the mean or average of any function $g(x)$, regardless of whether or not $f(x)$ satisfies Eq. 2.17, is

$$\overline{g(x)} = \frac{\int_{-\infty}^{\infty} g(x)f(x)\,dx}{\int_{+\infty}^{\infty} f(x)\,dx} \tag{2.27}$$

For a discontinuous pdf, the location indexes are defined in a similar way. If the pdf satisfies Eq. 2.16, the mean is given by

$$m = \bar{x} = \sum_{i=1}^{N} x_i f(x_i) \tag{2.28}$$

Equation 2.28 is an approximation because the true mean can only be determined with an infinite number of measurements. But, in practice, it is always a finite number of measurements that is available, and the average $\bar{x}$ instead of the true $m$ is determined. Equation 2.28 is analogous to Eq. 2.2, which defines the probability based on a finite number of events.

The general expression for the average of a discontinuous pdf, equivalent to Eq. 2.27, is

$$\overline{g(x)} = \frac{\sum_{i=1}^{N} g(x_i)f(x_i)}{\sum_{i=1}^{N} f(x_i)} \tag{2.29}$$

Which of these or some other location indexes one uses is a matter of personal choice and convenience, depending on the type of problem studied. The mean is by far the most frequently used index, and for this reason, only the mean will be discussed further.

Some elementary but useful properties of the mean that can be easily proven using Eqs. 2.26 or 2.28 are

$$\begin{aligned} \overline{ax} &= a\bar{x} = am \qquad a = \text{constant} \\ \overline{a + x} &= a + \bar{x} = a + m \\ \overline{g_1(x) + g_2(x) + \ldots + g_i(x)} &= \overline{g_1(x)} + \overline{g_2(x)} + \ldots + \overline{g_i(x)} \end{aligned} \tag{2.30}$$

**Example 2.5** Calculation of the mean. The probability that a radioactive nucleus will not decay for time $t$ is equal to

$$f(t) = \lambda e^{-\lambda t}$$

where $\lambda$ is a constant. What is the mean life of such a nucleus?

**Answer** Using Eq. 2.26, the mean life $\bar{t}$ is

$$\bar{t} = \int_0^\infty t\lambda e^{-\lambda t}\, dt = \frac{1}{\lambda}$$

**Example 2.6** Consider the throw of a die. The probability of getting any number between 1 and 6 is $\frac{1}{6}$. What is the average number?

**Answer** Using Eq. 2.29,

$$m = \bar{x} = \sum_{i=1}^{6} (i)\frac{1}{6} = \frac{1}{6}\sum_{i=1}^{6} i = \left(\frac{1}{6}\right)\frac{6(6+1)}{2} = 3.5$$

**Example 2.7** Consider an experiment repeated $N$ times giving the results $x_i|_{i=1,\ldots,N}$. What is the average of the results?

**Answer** Since the experiments were identical, all the results have the same probability of occurring, a probability that is equal to $1/N$. Therefore, the mean is

$$\bar{x} = \bar{m} = \sum_{i=1}^{N} x_i\left(\frac{1}{N}\right) \tag{2.31}$$

Equation 2.31 defines the so-called arithmetic mean of a series of $N$ random variables. It is used extensively when the results of several measurements of the same variable are combined.

An extension of Eq. 2.31 is the calculation of the "means of means." Assume that one has obtained the averages $\bar{x}_1, \bar{x}_2, \ldots, \bar{x}_M$ by performing a series of $M$ measurements, each involving $N_1, N_2, \ldots, N_M$ events, respectively.

The arithmetic mean of *all* the measurements, $\bar{X}$, is

$$\bar{X} = \frac{\bar{x}_1 + \bar{x}_2 + \cdots + \bar{x}_M}{M} \tag{2.32}$$

where

$$\bar{x}_j = \sum_{i=1}^{N_j} \frac{x_{ji}}{N_j} \qquad j = 1, \ldots, M$$

## 2.6 DISPERSION INDEXES, VARIANCE, AND STANDARD DEVIATION

A pdf or cdf is determined only approximately by any location index. For practical purposes it is sufficient to know the value of one location index—e.g., the mean—together with a measure indicating how the probability density is distributed around the chosen location index. There are several such measures called *dispersion indexes*. The dispersion index most commonly used and the only one to be discussed here is the variance $V(x)$ and its square root, which is called the standard deviation $\sigma$.

The variance of a pdf is defined as shown by Eqs. 2.33 and 2.34. For continuous distributions,

$$V(x) = \sigma^2 = \int_{-\infty}^{\infty} (x - m)^2 f(x)\, dx \tag{2.33}$$

For discrete distributions,

$$V(x) = \sigma^2 = \sum_{i=1}^{N} (x_i - m)^2 f(x_i) \tag{2.34}$$

It is assumed that $f(x)$ satisfies Eq. 2.16 or 2.17 and $N$ is a large number. It is worth noting that the variance is nothing more than the average of $(x - m)^2$. The variance of a linear function of $x$, $a + bx$, is

$$V(a + bx) = b^2 V(x) \tag{2.35}$$

where $a$ and $b$ are constants.

## 2.7 COVARIANCE AND CORRELATION

Consider the random variables $X_1, X_2, \ldots, X_M$ with means $m_1, m_2, \ldots, m_M$ and variances $\sigma_1^2, \sigma_2^2, \ldots, \sigma_M^2$. A question that arises frequently is, what is the average and the variance of the linear function

$$Q = a_1 X_1 + a_2 X_2 + \cdots + a_M X_M \tag{2.36a}$$

where the values of $a_i|_{i=1,\ldots,M}$ are constants?

The average is simply (using Eq. 2.28)

$$\overline{Q} = a_1 m_1 + a_2 m_2 + \cdots + a_M m_M = \sum_{i=1}^{M} a_i m_i \tag{2.36b}$$

The variance is

$$V(Q) = \sigma^2 = \overline{(Q - \overline{Q})^2} = \overline{\left[\sum_{i=1}^{M} a_i (X_i - m_i)\right]^2}$$

$$= \sum_{i=1}^{M} a_i^2 \sigma_i^2 + 2 \sum_{j>i}^{M} \sum^{M} a_i a_j \overline{(X_i - m_i)(X_j - m_j)} \tag{2.37}$$

The quantity $\overline{(X_i - m_i)(X_j - m_j)}$ is called the "covariance" between $X_i$ and $X_j$:

$$\text{cov}(X_i, X_j) = \overline{(X_i - m_i)(X_j - m_j)} \tag{2.38}$$

The covariance, as defined by Eq. 2.38, suffers from the serious drawback that its value changes with the units used for the measurement of $X_i, X_j$. To eliminate this effect, the covariance is divided by the product of the standard deviations $\sigma_i, \sigma_j$, and the resulting ratio is called the correlation coefficient $\rho(X_i, X_j)$. Thus,

$$\rho_{ij} = \rho(X_i, X_j) = \frac{\text{cov}(X_i, X_j)}{\sigma_i \sigma_j} \tag{2.39}$$

Using Eq. 2.39, the variance of $Q$ becomes

$$\sigma^2 = V(Q) = V\left(\sum_{i=1}^{M} a_i X_i\right) = \sum_{i=1}^{M} a_i^2 \sigma_i^2 + 2 \sum_{j>i}^{M} \sum^{M} a_i a_j \rho_{ij} \sigma_i \sigma_j \tag{2.40}$$

Random variables for which $\rho_{ij} = 0$ are said to be uncorrelated.

If the $X_i$'s are mutually uncorrelated, Eq. 2.40 takes the simpler form

$$\sigma^2 = V\left(\sum_{i=1}^{M} a_i X_i\right) = \sum_{i=1}^{M} a_i^2 \sigma_i^2 \tag{2.41}$$

Consider now a second linear function of the variables $X_1, X_2, X_3, \ldots, X_M$, namely, $R = b_1 X_1 + \cdots + b_M X_M$. The average of $R$ is

$$\overline{R} = b_1 m_1 + b_2 m_2 + \cdots + b_M m_M = \sum_{i=1}^{M} b_i m_i$$

The covariance of $Q$, $R$ is

$$\operatorname{cov}(Q, R) = \overline{\left[\sum_{i=1}^{M} a_i(X_i - m_i)\right]\left[\sum_{j=1}^{M} b_j(X_j - m_j)\right]}$$

$$= \sum_{i=1}^{M} a_i b_i \sigma_i^2 + \sum_{i \neq j}^{M} \sum^{M} a_i b_j \rho_{ij} \sigma_i \sigma_j \tag{2.42}$$

If all the $X$'s are mutually uncorrelated, then $\rho_{ij} = 0$ and

$$\operatorname{cov}(Q, R) = \sum_{i=1}^{M} a_i b_i \sigma_i^2 \tag{2.43}$$

If all the $X$'s have the same variance $\sigma^2$,

$$\operatorname{cov}(Q, R) = \sigma^2 \sum_{i=1}^{M} a_i b_i \tag{2.44}$$

Equations 2.40–2.44 will be applied in Sec. 2.15 for the calculation of the *propagation of errors*.

## 2.8 THE BINOMIAL DISTRIBUTION

The *binomial distribution* is a pdf that applies under the following conditions:

1. The experiment has two possible outcomes, A and B.
2. The probability that any given observation results in an outcome of type A or B is constant, independent of the number of observations.
3. The occurrence of a type A event in any given observation does not affect the probability that the event A or B will occur again in subsequent observations.

Examples of such experiments are tossing a coin (heads or tails is the outcome), inspecting a number of similar items for defects (items are defective or not), and picking up objects from a box containing two types of objects.

The binomial distribution will be introduced with the help of the following experiment.

Suppose that a box contains a large number of two types of objects, type A and type B. Let

$p$ = probability that an object selected at random from this box is type A

$1 - p$ = probability that the randomly selected object is type B

An experimenter selects $N$ objects at random.† The binomial distribution, giving the probability $P_n$ that $n$ out of the $N$ objects are of type A, is

$$P_n = \frac{N!}{(N-n)!n!} p^n (1-p)^{N-n} \tag{2.45}$$

**Example 2.8** A box contains a total of 10,000 small metallic spheres, of which 2000 are painted white and the rest are painted black. A person removes 100 spheres from the box one at a time at random. What is the probability that 10 of these spheres are white?

**Answer** The probability of picking one white sphere is

$$p = P(\text{white}) = \frac{2000}{10{,}000} = 0.2$$

The probability that 10 out of 100 selected spheres will be white is, according to Eq. 2.45,

$$P_{10} = \frac{100!}{(100-10)!10!} (0.2)^{10} (0.8)^{90} = 0.0034$$

**Example 2.9** A coin is tossed three times. What is the probability that the result will be heads in all three tosses?

**Answer** The probability of getting heads in one throw is 0.5. The probability of tossing the coin three times ($N = 3$) and getting heads in all three tosses ($n = 3$) is

$$P_3 = \frac{3!}{(3-3)!3!} (0.5)^3 (1-0.5)^{3-3} = 0.125$$

Of course, the same result could have been obtained in this simple case by using the multiplication law, Eq. 2.13:

$$P(\text{heads three times}) = (0.5)(0.5)(0.5) = 0.125$$

It is easy to show that the binomial distribution satisfies

$$\sum_{n=0}^{N} P_n = \sum_{n=0}^{N} \frac{N!}{(N-n)!n!} p^n (1-p)^{N-n} = 1 \tag{2.46}$$

The mean $m$ is equal to

$$m = \bar{n} = \sum_{n=0}^{N} nP_n = pN \tag{2.47}$$

†It is assumed that the box has an extremely large number of objects so that the removal of $N$ of them does not change their number appreciably, or, after an object is selected and its type recorded, it is thrown back into the box. If the total number of objects is small, instead of Eq. 2.45, the hypergeometric density function should be used (see Johnson & Leone and Jaech).

The variance $V(n)$ is

$$V(n) = \overline{(m-n)^2} = \sum_{n=0}^{N} (m-n)^2 P_n = m(1-p) = pN(1-p) \quad (2.48)$$

The standard deviation $\sigma$ is

$$\sigma = \sqrt{V(n)} = \sqrt{m(1-p)} = \sqrt{p(1-p)N} \quad (2.49)$$

Figure 2.2 shows three binomial distributions for $N = 10$ and $p = 0.1$, 0.4, and 0.8. Notice that as $p \to 0.5$, the distribution tends to be symmetric around the mean.

## 2.9 THE POISSON DISTRIBUTION

The Poisson distribution applies to events whose probability of occurrence is small and constant. It can be derived from the binomial distribution by letting

$$N \to \infty$$
$$p \to 0$$

in such a way that the value of the average $m = Np$ stays constant. It is left as an exercise for the reader to show that under the conditions mentioned above, the binomial distribution takes the form known as the Poisson distribution,

$$P_n = \frac{m^n}{n!} e^{-m} \quad (2.50)$$

where $P_n$ is the probability of observing the outcome $n$ when the average for a large number of trials is $m$.

The Poisson distribution has wide applications in many diverse fields, such as decay of nuclei, persons killed by lightning, number of telephone calls received in a switchboard, emission of photons by excited nuclei, and appearance of cosmic rays.

**Example 2.10** A radiation detector is used to count the particles emitted by a radioisotopic source. If it is known that the average counting rate is 20 counts/ min, what is the probability that the next trial will give 18 counts/min?

**Answer** The probability of decay of radioactive atoms follows the Poisson distribution. Therefore, using Eq. 2.50,

$$P_{18} = \frac{20^{18}}{18!} e^{-20} = 0.0844 \approx 8\%$$

That is, if one performs 10,000 measurements, 844 of them are expected to give the result 18 counts/min.

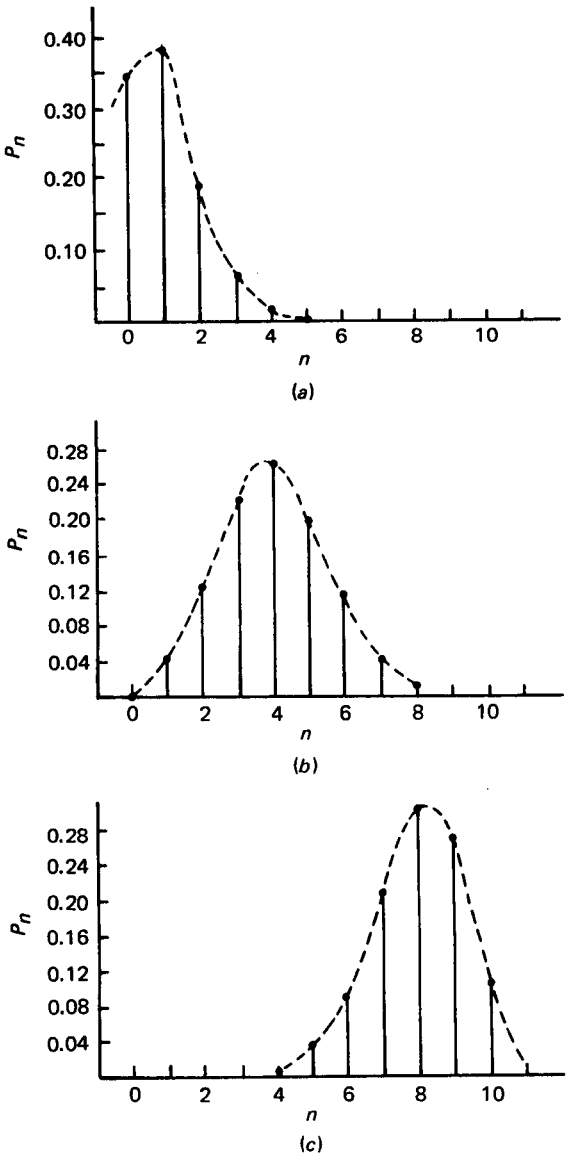


**Figure 2.2** Three binomial distributions with $N = 10$ and (*a*) $p = 0.1$, (*b*) $p = 0.4$, and (*c*) $p = 0.8$.

**Example 2.11** In a certain city with relatively constant population, the average number of people killed per year in automobile accidents is 75. What is the probability of having 80 auto-accident fatalities during the coming year?

**Answer** The Poisson distribution applies. Therefore, using Eq. 2.50,

$$P_{80} = \frac{75^{80}}{80!} e^{-75} = 0.038 \approx 4\%$$

The Poisson distribution satisfies

$$\sum_{n=0}^{\infty} P_n = 1 \tag{2.51}$$

The mean $m$ is equal to

$$m = \bar{n} = \sum_{n=0}^{\infty} nP_n = m \tag{2.52}$$

The variance is

$$V(n) = \overline{(m-n)^2} = \sum_{n=0}^{\infty} (m-n)^2 P_n = m \tag{2.53}$$

The standard deviation $\sigma$ is

$$\sigma = \sqrt{V(n)} = \sqrt{m} \tag{2.54}$$

Figure 2.3 shows the Poisson distribution for three different means. It should be pointed out that as the mean increases, the Poisson distribution becomes symmetric around the mean. For $m = 20$, the distribution is already for all practical purposes symmetric around the mean, and it resembles the normal distribution, which is discussed next.

## 2.10 THE NORMAL (GAUSSIAN) DISTRIBUTION

Both the binomial and Poisson distributions apply to discrete variables, whereas most of the random variables involved in experiments are continuous. In addition, the use of discrete distributions necessitates the use of long or infinite series for the calculation of such parameters as the mean and the standard deviation (see Eqs. 2.47, 2.48, 2.52, 2.53). It would be desirable, therefore, to have a pdf that applies to continuous variables. Such a distribution is the normal or Gaussian distribution.

The normal distribution $G(x)$ is given by

$$G(x)\,dx = \frac{1}{(\sqrt{2\pi})\sigma} \exp\left[-\frac{(x-m)^2}{2\sigma^2}\right] dx \tag{2.55}$$

where $G(x)\,dx$ = probability that the value of $x$ lies between $x$ and $x + dx$
$m$ = average of the distribution
$\sigma^2$ = variance of the distribution

Notice that this distribution, shown in Fig. 2.4, has a maximum at $x = m$, is symmetric around $m$, is defined uniquely by the two parameters $\sigma$ and $m$, and extends from $x = -\infty$ to $x = +\infty$. Equation 2.55 represents the shaded area under the curve of Fig. 2.4. In general, the probability of finding the value of $x$

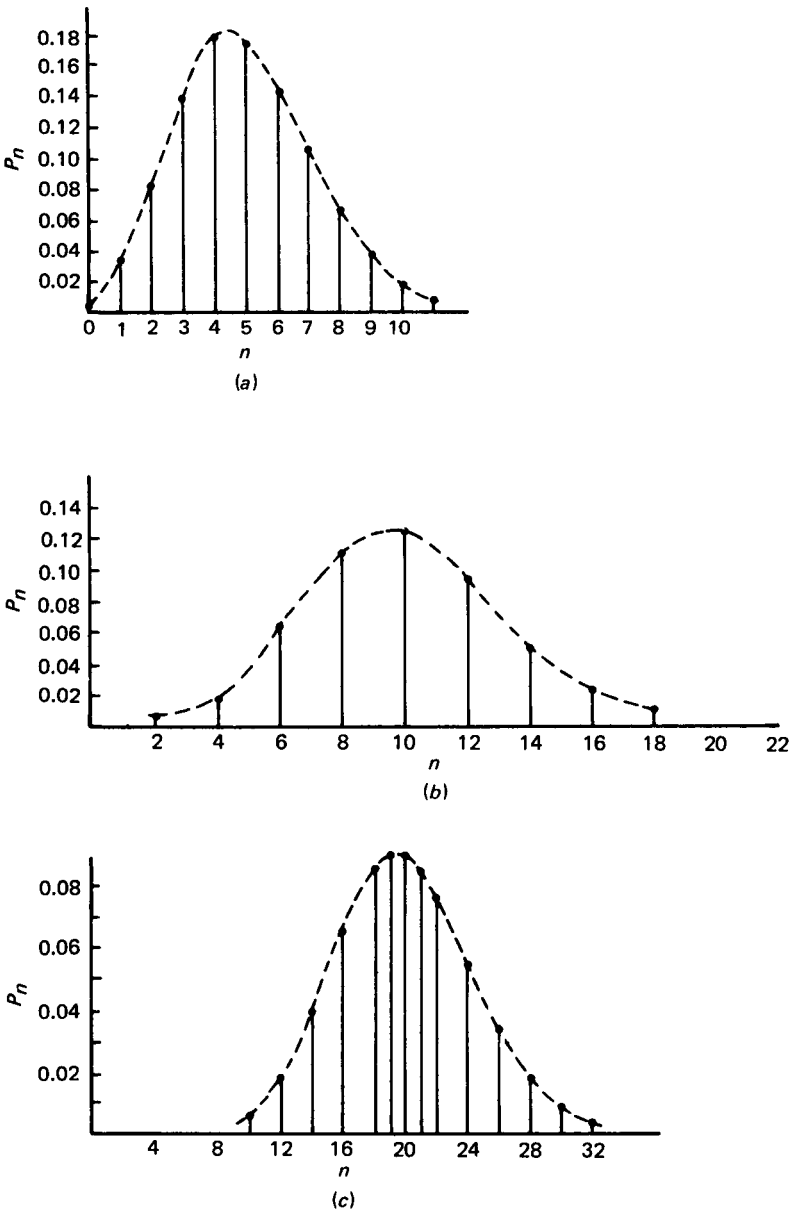


**Figure 2.3** Three Poisson distributions: (*a*) $m = 5$, (*b*) $m = 10$, (*c*) $m = 20$.

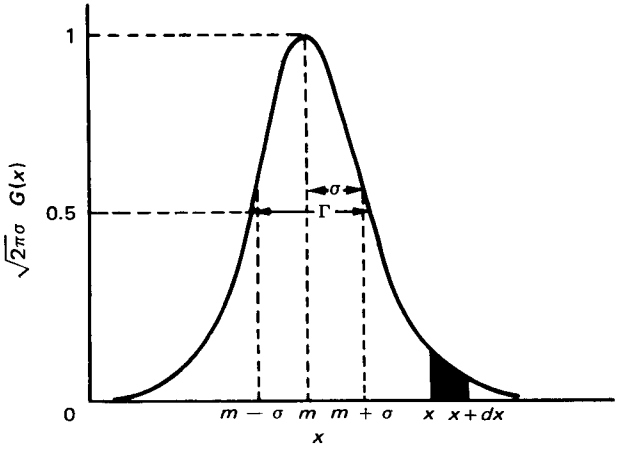


**Figure 2.4** A normal (Gaussian) distribution.

between any two limits $x_1$ and $x_2$ is given by

$$G(x_1 \le x \le x_2) = \int_{x_1}^{x_2} G(x)\,dx \tag{2.56}$$

The Gaussian given by Eq. 2.55 satisfies

$$\int_{-\infty}^{\infty} G(x)\,dx = 1 \tag{2.57}$$

The average of the distribution is

$$\bar{x} = m = \int_{-\infty}^{\infty} xG(x)\,dx = m \tag{2.58}$$

The variance is

$$V(x) = \int_{-\infty}^{\infty} (x-m)^2 G(x)\,dx = \sigma^2 \tag{2.59}$$

The standard deviation is

$$\sigma = \sqrt{V(x)} \tag{2.60}$$

Three very important items associated with the Gaussian distribution are the following.

1. The *cumulative normal distribution function*, defined by

$$E(x) = \int_{-\infty}^{x} G(x')\,dx' = \int_{-\infty}^{x} \frac{1}{(\sqrt{2\pi})\sigma} \exp\left[-\frac{(x'-m)^2}{2\sigma^2}\right] dx' \tag{2.61}$$

The function $E(x)$ is very useful and is generally known as the error function (see also Sec. 2.10.1). Graphically, the function $E(x)$ (Eq. 2.61) is equal to the shaded area of Fig. 2.5. The function is sketched in Fig. 2.6.

2. The *area under the curve of Fig. 2.4 from* $x = m - \sigma$ *to* $x = m + \sigma$, given by

$$A_\sigma = \int_{m-\sigma}^{m+\sigma} G(x)\,dx = 0.683 \tag{2.62}$$

Equation 2.62 indicates that 68.3 percent of the total area under the Gaussian is included between $m - \sigma$ and $m + \sigma$. Another way of expressing this statement is to say that if a series of events follows the normal distribution, then it should be expected that 68.3 percent of the events will be located between $m - \sigma$ and $m + \sigma$. As discussed later in Sec. 2.13, Eq. 2.62 is the basis for the definition of the "standard" error.

3. The *full width at half maximum (FWHM)*. The FWHM, usually denoted by the symbol $\Gamma$, is the width of the Gaussian distribution at the position of half of its maximum. The width $\Gamma$ is slightly wider than $2\sigma$ (Fig. 2.4). The correct

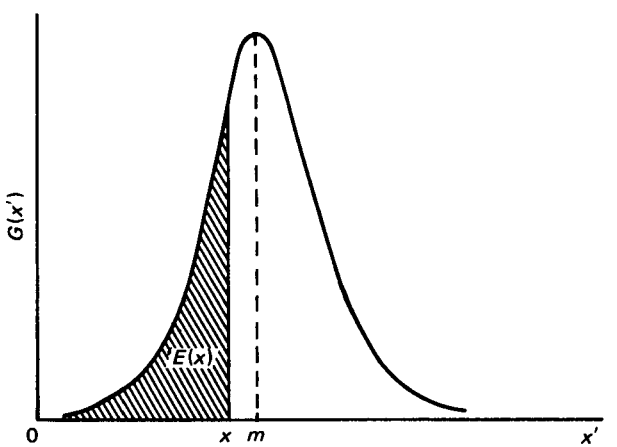


**Figure 2.5** The cumulative normal distribution is equal to the shaded area under the Gaussian curve.

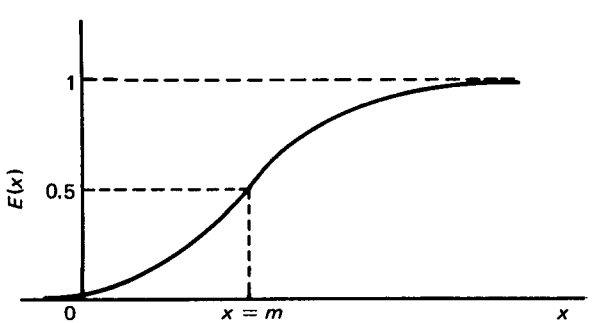


**Figure 2.6** The error function.

relationship between the two is obtained from Eq. 2.55 by writing

$$G\left(m - \frac{\Gamma}{2}\right) = G\left(m + \frac{\Gamma}{2}\right) = \frac{1}{2}G(m)$$

Solving this equation for $\Gamma$ gives

$$\Gamma = (2\sqrt{2\ln 2})\sigma \approx 2.35\sigma \tag{2.63}$$

The width $\Gamma$ is an extremely important parameter in measurements of the energy distribution of particles.

### 2.10.1 The Standard Normal Distribution

The evaluation of integrals involving the Gaussian distribution, such as those of Eqs. 2.56, 2.61, and 2.62, requires tedious numerical integration. The result of such integrations is a function of $m$ and $\sigma$. Therefore, the calculation should be repeated every time $m$ or $\sigma$ changes. To avoid this repetition, the normal distribution is rewritten in such as way that

$$m = 0 \quad \text{and} \quad \sigma = 1$$

The resulting function is called the *standard normal distribution.* Integrals involving the Gaussian distribution, such as that of Eq. 2.61, have been tabulated based on the standard normal distribution for a wide range of $x$ values. With the help of a simple transformation, it is very easy to obtain the integrals for any value of $m$ and $\sigma$.

The standard normal distribution is obtained by defining the new variable.

$$t = \frac{x - m}{\sigma} \tag{2.64}$$

Substituting into Eq. 2.55, one obtains

$$G(t)\,dt = \frac{1}{\sqrt{2\pi}}e^{-t^2/2}\,dt \tag{2.65}$$

It is very easy to show that the Gaussian given by Eq. 2.65 has mean

$$\bar{t} = m = \int_{-\infty}^{\infty} tG(t)\,dt = 0$$

and variance

$$V(t) = \sigma^2 = \int_{-\infty}^{\infty} t^2G(t)\,dt = 1$$

The cumulative standard normal distribution function, Eq. 2.61, is now written as

$$E(x) = \int_{-\infty}^{x} G(t)\,dt = \int_{-\infty}^{x} \frac{1}{\sqrt{2\pi}}e^{-t^2/2}\,dt \tag{2.66}$$

or, in terms of the error function that is tabulated

$$E(x) = \frac{1}{2}\left(1 + \operatorname{erf}\frac{x}{\sqrt{2}}\right)$$

where

$$\operatorname{erg}\frac{x}{\sqrt{2}} = \sqrt{\frac{2}{\pi}}\int_0^x e^{-t^2/2}\,dt$$

**Example 2.12** The uranium fuel of light-water reactors is enclosed in metallic tubes with an average outside diameter (OD) equal to 20 mm. It is assumed that the OD is normally distributed around this average with a standard deviation $\sigma = 0.5$ mm. For safety reasons, no tube should be used with OD > 21.5 mm or OD < 18.5 mm. If 10,000 tubes are manufactured, how many of them are expected to be discarded because they do not satisfy the requirements given above?

**Answer** The probability that the OD of a tube is going to be less than 18.5 mm or greater than 21.5 mm is

$$G(x < 18.5) + G(x > 21.5) = \int_{-\infty}^{18.5} \frac{dx}{\sqrt{2\pi}(0.5)} \exp\left[-\frac{(x-20)^2}{2(.05)^2}\right] + \int_{21.5}^{\infty} \frac{dx}{\sqrt{2\pi}(0.5)} \exp\left[-\frac{(x-20)^2}{2(0.5)^2}\right]$$

Graphically, the sum of these two probabilities is equal to the two shaded areas shown in Fig. 2.7.

In terms of the standard normal distribution and also because the two integrals are equal, one obtains

$$G(x < 18.5) + G(x > 21.5) = 2\left[1 - \int_{-\infty}^{3} \frac{1}{\sqrt{2\pi}} e^{-t^2/2}\,dt\right]$$

where

$$t = \frac{x - 20}{0.5}$$

This last integral is tabulated in many books, handbooks, and mathematical tables (see bibliography of this chapter). From such tables, one obtains

$$\int_{-\infty}^{3} \frac{1}{\sqrt{2\pi}} e^{-t^2/2}\,dt = 0.99865$$

which gives

$$G(x < 18.5) + G(x > 21.5) = 0.0027$$

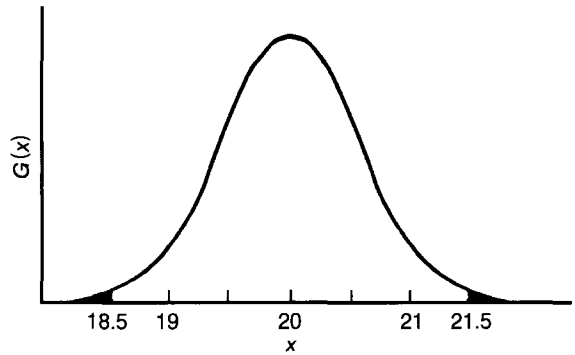


**Figure 2.7** The shaded areas represent the fraction of defective rods, Ex. 2.12.

Therefore, it should be expected that under the manufacturing conditions of this example, 27 tubes out of 10,000 would be rejected.

### 2.10.2 Importance of the Gaussian Distribution for Radiation Measurements

The normal distribution is the most important distribution for applications in measurements. It is extremely useful because for almost any type of measurement that has been taken many times, the frequency with which individual results occur forms, to a very good approximation, a Gaussian distribution centered around the average value of the results. The greater the number of trials, the better their representation by a Gaussian. Furthermore, statistical theory shows that even if the original population of the results under study does not follow a normal distribution, their average does. That is, if a series of measurements of the variable $x_i|_{i=1,\ldots,N}$ is repeated $M$ times, the average values $\bar{x}_N|_{N=1,\ldots,M}$ follow a normal distribution even though the $x_i$'s may not. This result is known as the *central limit theorem* and holds for any random sample of variables with finite standard deviation.

In reality, no distribution of experimental data can be exactly Gaussian, since the Gaussian extends from $-\infty$ to $+\infty$. But for all practical purposes, the approximation is good and it is widely used because it leads to excellent results.

It is worth reminding the reader that both the binomial (Fig. 2.2) and the Poisson (Fig. 2.3) distributions resemble a Gaussian under certain conditions. This observation is particularly important in radiation measurements.

The results of radiation measurements are, in most cases, expressed as the number of counts recorded in a scaler. These counts indicate that particles have interacted with a detector and produced a pulse that has been recorded. The particles, in turn, have been produced either by the decay of a radioisotope or as a result of a nuclear reaction. In either case, the emission of the particle is statistical in nature and follows the Poisson distribution. However, as indicated in Sec. 2.9, if the average of the number of counts involved is more than about 20, the Poisson approaches the Gaussian distribution. For this reason, the

individual results of such radiation measurements are treated as members of a normal distribution.

Consider now a Poisson and a Gaussian distribution having the same average, $m = 25$. Obviously, there is an infinite number of Gaussians with that average but with different standard deviations. The question one may ask is: "What is the standard deviation of the Gaussian that may represent the Poisson distribution with the same average?" The answer is that the Gaussian with $\sigma = \sqrt{m} = 5$ is almost identical with the Poisson. Table 2.1 presents values of the two distributions, and Fig. 2.8 shows them plotted.

The following very important conclusion is drawn from this result:

> The outcomes of a series of radiation measurements are members of a Poisson distribution. They may be treated as members of a Gaussian distribution if the average result is more than $m = 20$. The standard deviation of that Gaussian distribution is $\sigma = \sqrt{m}$.

Use of this conclusion is made in Sec. 2.17, which discusses statistics of radiation counting.

## 2.11 THE LORENTZIAN DISTRIBUTION

The Lorentzian distribution, which describes the resonances of nuclear reactions —in particular how the probability of interaction (cross section, see Chap. 4)

**Table 2.1 Comparison between a Poisson and a Gaussian Distribution Having the Same Mean ($m = 25$)**

| $n$ | $P_n$ (Poisson) | $G(n)$ (Gaussian) $\sigma = 5$ |
|---|---|---|
| 10 | 0.0004 | 0.0009 |
| 12 | 0.0017 | 0.0027 |
| 14 | 0.0059 | 0.0071 |
| 16 | 0.0154 | 0.0168 |
| 18 | 0.0316 | 0.0299 |
| 20 | 0.0519 | 0.0484 |
| 22 | 0.0702 | 0.0666 |
| 24 | 0.0795 | 0.0782 |
| 25 | 0.0795 | 0.0798 |
| 26 | 0.0765 | 0.0782 |
| 28 | 0.0632 | 0.0666 |
| 30 | 0.0454 | 0.0484 |
| 32 | 0.0286 | 0.0299 |
| 34 | 0.0159 | 0.0168 |
| 36 | 0.0079 | 0.0071 |
| 38 | 0.0035 | 0.0027 |

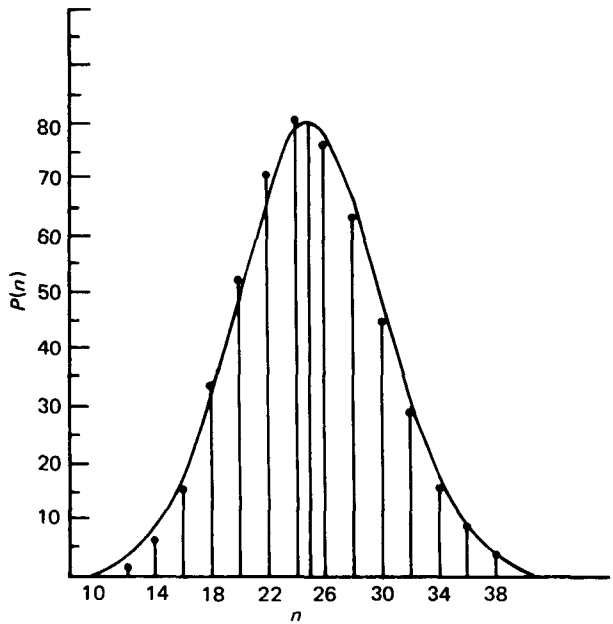


**Figure 2.8** Comparison between a Poisson distribution with $m = 25$ and a Gaussian distribution with the same average and standard deviation $\sigma = \sqrt{m} = 5$.

changes as a function of particle energy—is given by

$$L(x)\,dx = \frac{1}{\pi}\frac{\Gamma/2}{(x-m)^2 + \Gamma^2/4}\,dx \tag{2.67}$$

where $L(x)\,dx$ is the probability that the value of $x$ lies between $x$ and $x + dx$. The Lorentzian is a symmetric function (Fig. 2.9) centered around the value $x = m$. It can be easily shown that

$$\int_{-\infty}^{\infty} L(x)\,dx = 1$$

and that

$$\bar{x} = \int_{-\infty}^{\infty} xL(x)\,dx = m$$

Thus, the mean is given by the parameter $m$ as expected from the symmetry of the function. One peculiar characteristic of the Lorentzian is the fact that its variance cannot be calculated. Indeed, the integral

$$\sigma^2 = V(x) = \int_{-\infty}^{\infty} (x-m)^2 L(x)\,dx$$

does not converge, which is the result of the slow decrease of the function away from the peak.

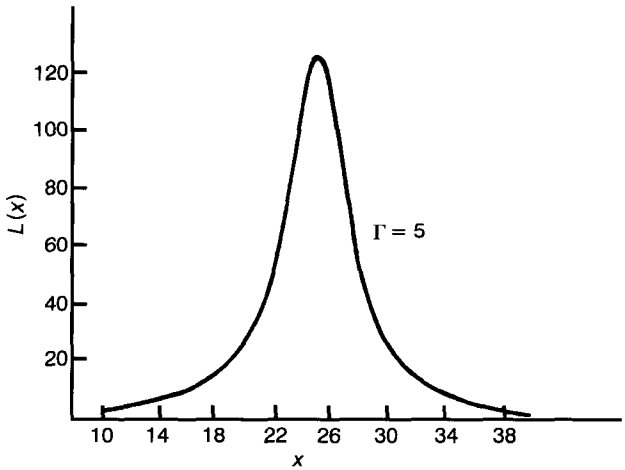


**Figure 2.9** A Lorentzian distribution peaking at $x = 25$ and having a FWHM at equal to 5.

In the absence of a standard deviation, the parameter $\Gamma$ is used for the description of the Lorentzian. The parameter $\Gamma$ is *equal to* the FWHM of the function.

## 2.12 THE STANDARD, PROBABLE, AND OTHER ERRORS

Consider a measurement or series of measurements that gave the result $R$ and its estimated error $E$. The experimenter reports the result as

$$R \pm E \tag{2.68}$$

in which case $E$ is the absolute error ($R$ and $E$ have the same units), or as

$$R \pm \epsilon\% \tag{2.69}$$

where $\epsilon = (E/R)100$ = relative error (dimensionless). In most cases, the relative rather than the absolute error is reported.

Whether either Eq. 2.68 or 2.69 is used, the important thing to understand is that $R \pm E$ *does not mean* that the correct result has been bracketed between $R - E$ and $R + E$. It means only that *there is a probability* that the correct result has a value between $R - E$ and $R + E$. What is the value of this probability? There is no unanimous agreement on this matter, and different people use different values. However, over the years, two probability values have been used more frequently than others and have led to the definition to two corresponding errors, the standard and the probable error.

**The standard error.** If the result of a measurement is reported as $R \pm E_s$ and $E_s$ is the standard error, then there is a 68.3 percent chance for the true result to have a value between $R - E_s$ and $R + E_s$.

**The probable error.** By definition, the probable error is equally likely to be exceeded or not. Therefore, if the result of a measurement is $R \pm E_p$ and $E_p$ is the probable error, then there is a 50 percent chance for the true result to have a value between $R - E_p$ and $R + E_p$.

Both standard and probable errors are based on a Gaussian distribution. That is, it is assumed that the result $R$ is the average of individual outcomes that belong to a normal distribution. This does not introduce any limitation in practice because, as stated in Sec. 2.10.2, the individual outcomes of a long series of any type of measurement are members of a Gaussian distribution.† With the Gaussian distribution in mind, it is obvious that the definition of the standard error is based on Eq. 2.62. If a result is $R$ and the standard error is $E_s$, then $E_s = \sigma$.

$$\int_{R-E_s}^{R+E_s} \frac{1}{(\sqrt{2\pi})\sigma} \exp\left[-\frac{(x-R)^2}{2\sigma^2}\right] dx = 0.683$$

Correspondingly, the probable error $E_p$ satisfies

$$\int_{R-E_p}^{R+E_p} \frac{1}{(\sqrt{2\pi})\sigma} \exp\left[-\frac{(x-R)^2}{2\sigma^2}\right] dx = 0.5$$

It can be shown that

$$E_p = 0.6745E_s \tag{2.70}$$

The standard and probable errors are the most commonly used in reporting experimental results. Individual researchers may define other errors that represent a different percentage of the Gaussian. For example, the 95 percent error, $E_{95}$, is that which gives a 95 percent chance to have the true result bracketed between $R - E_{95}$ and $R + E_{95}$. It turns out that $E_{95} = 1.645\sigma$ (see Table 2.2).

## 2.13 THE ARITHMETIC MEAN AND ITS STANDARD ERROR

Although the true value of a quantity can never be determined, the error of the measurement can be reduced if the experiment is repeated many times.

Consider an experiment that has been repeated $N$ times, where $N$ is a large number, and produced the individual outcomes $n_i|_{i=1,\ldots,N}$. Let the frequency of occurrence of $n_i$ be $P_{n_i}$.‡ If one plots $P_{n_i}$ versus $n_i$, the resulting curve

†Exception: Radiation counting measurements with $m < 20$ obey the Poisson distribution.
‡If $N = 1000$ and $n_i$ has occurred 15 times, $P_{n_i} = 15/1000$.

resembles a Gaussian distribution as shown in Fig. 2.10. The larger the value of $N$, the more the histogram of Fig. 2.10 coincides with a normal distribution. Assume that the dashed line of Fig. 2.10 is an acceptable representation of the experimental results. Under these circumstances, how should the result of the measurement be reported and what is its standard error?

The result of the measurement is reported as the arithmetic average defined by

$$\bar{n} = \frac{n_1 + n_2 + \cdots n_N}{N} = \sum_{i=1}^{N} \frac{n_i}{N} \tag{2.71}$$

This equation is the same as Eq. 2.31. As $N$ increases, a better estimate of the true value of $n$ is obtained—i.e., the error of the measurement becomes smaller. The true value of $n$, which is also called the true mean, can only be obtained with an infinite number of measurements. Since it is impossible to perform an infinite number of trials, $n$ is always calculated from Eq. 2.71.

The error of $\bar{n}$ depends on the way the individual measurements are distributed around $\bar{n}$—i.e., it depends on the width of the Gaussian of Fig. 2.10. As the width becomes smaller, the error gets smaller, and therefore the measurement is better. The standard error of $\bar{n}$ is defined in terms of the standard deviation of the distribution. Using Eq. 2.34 and setting $f(x_i) = 1/N$, the standard deviation of the distribution becomes

$$\sigma^2 = \sum_{i=1}^{N} \frac{(n_i - m)^2}{N} \tag{2.72}$$

With a finite number of measurements at our disposal, this equation for $\sigma$ has to be modified in two ways. First, because the true mean $m$ is never known, it is replaced by its best estimate, which is $\bar{n}$ (Eq. 2.71). Second, it can be generally

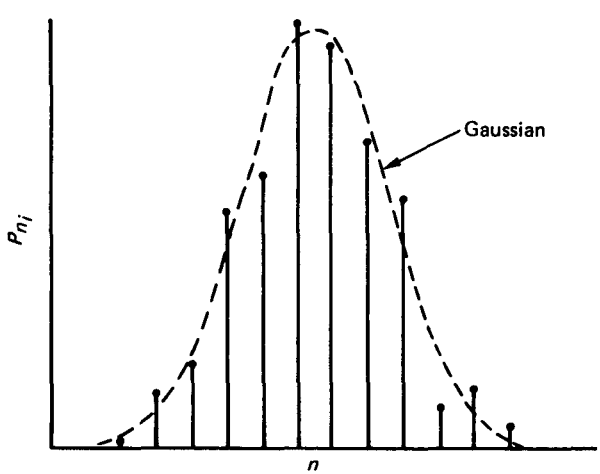


**Figure 2.10** The distribution of the frequency of occurrence of individual results of a series of identical measurements tends to follow a Gaussian distribution.

shown that the best estimate of the standard deviation of $N$ measurements is given by the following equation:

$$\sigma^2 = \frac{1}{N-1} \sum_{i=1}^{N} (n_i - \bar{n})^2 \tag{2.73}$$

The differences between Eq. 2.72 and Eq. 2.73 are the use of $\bar{n}$ instead of $m$ and the use of $N - 1$ in the denominator instead of $N$.† For a large number of measurements, it does not make any practical difference if one divides by $N$ or $N - 1$. But it makes a difference for small values of $N$. Using the extreme value of $N = 1$, one can show that division by $N$ gives the wrong result. Indeed, dividing by $N$, one obtains

$$\sigma^2 = \frac{1}{N} \sum (n_1 - \bar{n})^2 = \frac{1}{1} \sum (n_1 - n_1)^2 = \frac{0}{1} = 0$$

Zero $\sigma$ means zero error, which is obviously wrong. The error is never zero, certainly not in the case of one measurement. Division by $N - 1$, on the other hand, gives

$$\sigma^2 = \frac{1}{N-1} \sum (n_1 - n_1)^2 = \frac{0}{0}$$

which, being indeterminate, is a more realistic value of the error based on a single measurement.

Since the $N$ results are distributed as shown in Fig. 2.10, 68.3 percent of the outcomes fall between $\bar{n} - \sigma$ and $\bar{n} + \sigma$ (see Eq. 2.62). Therefore, one additional measurement has a 68.3 percent chance of providing a result within $\bar{n} \pm \sigma$. For this reason, $\sigma$ is called the standard deviation or *the standard error of a single measurement.* Is this equal to the standard error of $\bar{n}$? No, and here is why.

According to the definition of the standard error, if $\sigma_{\bar{n}}$ is the standard error of $\bar{n}$, it ought to have such a value that a new average $\bar{n}$ would have a 68.3 percent chance of falling between $\bar{n} - \sigma_{\bar{n}}$ and $\bar{n} + \sigma_{\bar{n}}$. To obtain the standard error of $\bar{n}$, consider Eq. 2.71 as a special case of Eq. 2.36*a*. The quantity $\bar{n}$ is a linear function of the uncorrelated random variables $n_1, n_2, \ldots, n_N$, each with standard deviation $\sigma$. Therefore

$$\bar{n} = \sum_{i=1}^{N} a_i n_i$$

†The factor $N - 1$ is equal to the "degrees of freedom" or the number of independent data or equations provided by the results. The $N$ independent outcomes constitute, originally, $N$ independent data. However, after $\bar{n}$ is calculated, only $N - 1$ independent data are left for the calculation of $\sigma$.

where $a_i = 1/N$. Using Eq. 2.41, the standard deviation of $\bar{n}$ is†

$$\sigma_{\bar{n}} = \sqrt{\sum_{i=1}^{N} a_i^2 \sigma_i^2} = \sqrt{\sum_{i=1}^{N} \frac{1}{N^2} \sigma^2} = \frac{\sigma}{\sqrt{N}} \tag{2.74}$$

If the series of $N$ measurements is repeated, the new average will probably be different from $\bar{n}$, but it has a 68.3 percent chance of having a value between $\bar{n} - \sigma_{\bar{n}}$ and $\bar{n} + \sigma_{\bar{n}}$. The result of the $N$ measurements is

$$\bar{n} \pm \sigma_{\bar{n}} = \bar{n} \pm \frac{\sigma}{\sqrt{N}} \tag{2.75}$$

When a series of measurements is performed, it would be desirable to calculate the result in such a way that the error is a minimum. It can be shown that the average $\bar{n}$ as defined by Eq. 2.71 minimizes the quantity

$$\sum_{i=1}^{N} (\bar{n} - n_i)^2$$

which is proportional to the standard error. Finally, Eq. 2.75 shows that the error is reduced if the number of trials increases. However, that reduction is proportional to $1/\sqrt{N}$, which means that the number of measurements should be increased by a factor of 100 to be able to reduce the error by a factor of 10.

## 2.14 CONFIDENCE LIMITS

Consider a variable $x_i$ that represents the value of the $i$th sample of a large population of specimens. The variable $x_i$ may be the diameter of a sphere or the thickness of the cladding of a fuel rod or the length of the fuel rod. A designer may desire a certain diameter of the sphere or a certain thickness of the fuel cladding or a certain length of the fuel rod. What happens during actual fabrication is that the individual units are not exactly the same. The person who examines individual units as they are constructed, machined, or fabricated will find that there is a distribution of values for the quantity being examined. The average value is equal to that specified in the blueprints and is called the nominal value. Individual specimens, however, have values of $x$ distributed around the nominal value $x_n$ according to a Gaussian distribution,

$$G(x) = \frac{1}{(\sqrt{2\pi})\sigma} \exp\left[-\frac{(x - x_n)^2}{2\sigma^2}\right]$$

where $x_n$ = nominal value of $x$ = average value of $x$
$\sigma$ = standard deviation of the distribution

†If the population of the events $n_i$ is finite in size, then it can be shown that $\sigma_{\bar{n}}^2 = [(M - N)/(M - 1)]\sigma^2/N$, where $M$ = total number of $n_i$'s (see Jaech).

The manufacturer of any product would like to know what the probability is that any one item will deviate from the nominal value by a certain amount. Or, setting some acceptable value of $x$, call it $x_a$, the manufacturer would like to know what is the probability that $x$ will be bigger than $x_a$. Questions of this type come under the subject of "quality control."

The probability that $x$ will exceed $x_a$ is given by

$$P(x > x_a) = \int_{x_a}^{\infty} \frac{dx}{(\sqrt{2\pi})\sigma} \exp\left[-\frac{(x - x_n)^2}{2\sigma^2}\right] \tag{2.76}$$

The acceptable value of $x$ is usually expressed as

$$x_a = x_n + k\sigma \tag{2.77}$$

i.e., the extreme acceptable vaue of $x$, $x_a$, is allowed to be $k$ standard deviations different from $x_n$.

In terms of the standard normal distribution, Eq. 2.76 takes the form

$$P(t > k) = \int_k^{\infty} \frac{1}{\sqrt{2\pi}} e^{-t^2/2}\, dt \tag{2.78}$$

where

$$t = \frac{x - x_n}{\sigma} \tag{2.79}$$

and

$P(t > k)$ = probability that $x$ will exceed $x_a$ by $k$ standard deviations

Table 2.2 gives values of $P(t > k)$ for several values of $k$. The values in Table 2.2 are interpreted as follows:

Consider $k = 1$. The probability that $x$ will exceed $x_a$ where $x_a = x_n + \sigma$ is 15.9 percent. If $x$ is some property of a manufactured product, it is said that the confidence limit is, in this case, $1 - 0.159 = 0.841$ or 84.1 percent, i.e., 84.1 percent of the specimens will have $x < x_a$ (Fig. 2.11). If $k = 2$, the probability

**Table 2.2 Probability Values and Confidence Limits**

| Number of standard deviations ($k$) | $P(x > x_a)$ | Confidence limit |
|---|---|---|
| 0 | 0.500 | 50.0 |
| 1.0 | 0.159 | 84.1 |
| 1.285 | 0.100 | 90.0 |
| 1.5 | 0.067 | 93.3 |
| 1.645 | 0.050 | 95.0 |
| 2.0 | 0.023 | 97.7 |
| 2.5 | 0.006 | 99.4 |
| 3.0 | 0.0013 | 99.87 |

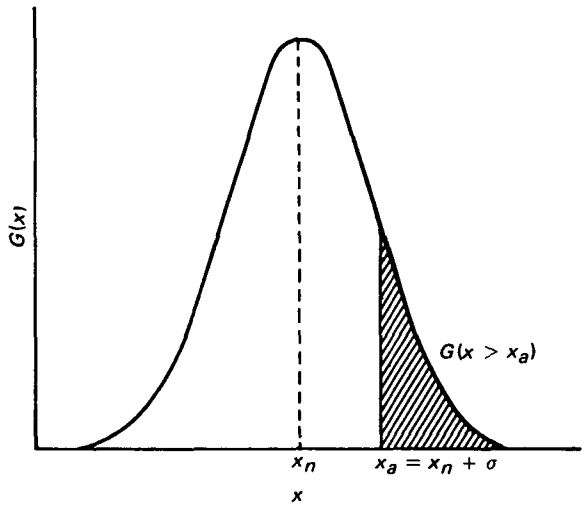


**Figure 2.11** The probability that $x$ will exceed $x_a$, where $x_a = x_n + \sigma$, is 15.9 percent (shaded area). The confidence limit is 1 − 0.159, or 84.1 percent.

that $x$ will exceed $x_a$ is equal to 2.3 percent; therefore, the confidence limit is 97.7 percent.

In actual construction or fabrication of an item, the Gaussian distribution is determined by checking the variable $x$ for a large number of specimens. An average value of $x$ is calculated,

$$\bar{x} = \frac{1}{N} \sum_{i=1}^{N} x_i$$

and a standard deviation

$$\sigma = \frac{1}{N-1} \sqrt{\sum_{i}^{N} (x_i - \bar{x})^2}$$

is obtained. The average $\bar{x}$ should be almost equal to the nominal value of $x$. A Gaussian distribution for this sample peaks at $\bar{x}$ and has a standard deviation $\sigma$. Knowing $\sigma$, the value of $x_a$ is calculated from Eq. 2.77 after the confidence limit—the value of $k$—has been decided upon.

The use of the concept of confidence limits is widespread in industry. As a specific example, let us assume that $x$ is the thickness of the cladding of a reactor fuel rod. The average (nominal) thickness is $x_n$. The reactor designer would like to be certain that a certain fraction of fuel rods will always have thickness within prescribed limits. Let us say that the designer desires a confidence limit of 99.87 percent. This means that no more than 13 rods out of 10,000 will be expected to have cladding thickness exceeding the nominal value by more than three standard deviations (Table 2.2).

## 2.15 PROPAGATION OF ERRORS

### 2.15.1 Calculation of the Average and Its Standard Deviation

Sometimes an investigator has to determine a quantity that is a function of more than one random variable. In such cases, it is very important to know how to calculate the error of the complex quantity in terms of the errors of the individual random variables. This procedure is generally known as propagation of errors and is described in this section.

Consider the function $f(x_1, x_2, \ldots, x_M)$, which depends on the random variables $x_1, x_2, \ldots, x_M$. Generally, the values of $x_1, x_2, \ldots, x_M$ are determined experimentally and then the value of $f(x_1, x_2, \ldots, x_M)$ is calculated. For example,

1. $f(x_1, x_2) = x_1 \pm x_2$
2. $f(x_1, x_2) = x_1 x_2$
3. $f(x_1, x_2) = x_1/x_2$
4. $f(x_1, x_2) = \ln(x_1 + x_2)$
5. $f(x) = x^2$
6. $f(x_1, x_2, x_3) = (x_1 + x_2)/x_3$

It has already been mentioned that the $x_i$'s are determined experimentally, which means that average values $\bar{x}_1, \bar{x}_2, \bar{x}_3, \ldots, \bar{x}_M$ are determined along with their standard errors $\sigma_1, \sigma_2, \ldots, \sigma_M$. Two questions arise:

1. What is the value of $f(x_1, \ldots, x_M)$ that should be reported?
2. What is the standard error of $f(x_1, \ldots, x_M)$?

It is assumed that the function $f(x_1, \ldots, x_M)$ can be expanded in a Taylor series around the averages $\bar{x}_i|_{i=1,\ldots,M}$:

$$f(x_1, x_2, \ldots, x_M) = f(\bar{x}_1, \bar{x}_2, \ldots, \bar{x}_M) + \sum_{i=1}^{M} (x_i - \bar{x}_i)\frac{\partial f}{\partial \bar{x}_i} + O(x_i - \bar{x}_i)^2$$

The notation used is that

$$\frac{\partial f}{\partial \bar{x}_i} = \left.\frac{\partial f}{\partial x_i}\right|_{x_i = \bar{x}_i}$$

The term $O(x_i - \bar{x}_i)^2$ includes all the terms of order higher than first, and it will be ignored. Thus, the function is written

$$f(x_1, x_2, \ldots, x_M) = f(\bar{x}_1, \bar{x}_2, \ldots, \bar{x}_m) + \sum_{i=1}^{M} (x_i - \bar{x}_i)\frac{\partial f}{\partial \bar{x}_i} \tag{2.80}$$

Equation 2.80 is a special case of Eq. 2.36*a*. The average value of $f(x_1, \ldots, x_M)$, which is the value to be reported, is

$$\bar{f} = f(\bar{x}_1, \bar{x}_2, \ldots, \bar{x}_M) \tag{2.81}$$

The variance of $f(x_1, \ldots, x_M)$ is given by Eq. 2.40:

$$\sigma_{\bar{f}}^2 = V(f) = \sum_{i=1}^{M} \left(\frac{\partial f}{\partial \bar{x}_i}\right)^2 \sigma_i^2 + 2 \sum_{j>i}^{M} \sum^{M} \left(\frac{\partial f}{\partial \bar{x}_i}\right)\left(\frac{\partial f}{\partial \bar{x}_j}\right) \rho_{ij} \sigma_i \sigma_j \tag{2.82}$$

where $\rho_{ij}$ is the correlation coefficient given by Eq. 2.39.

The standard error of $f(x_1, \ldots, x_M)$ is equal to the standard deviation

$$\sigma_{\bar{f}} = \sqrt{\sum_{i=1}^{M} \left(\frac{\partial f}{\partial \bar{x}_i}\right)^2 \sigma_i^2 + 2 \sum_{j>i}^{M} \sum^{M} \left(\frac{\partial f}{\partial \bar{x}_i}\right)\left(\frac{\partial f}{\partial \bar{x}_j}\right) \rho_{ij} \sigma_i \sigma_j} \tag{2.83}$$

Equations 2.81 and 2.83 are the answers to questions 1 and 2 stated previously. They indicate, first, that the average of the function is calculated using the average values of the random variables and, second, that its standard error is given by Eq. 2.83. Equation 2.83 looks complicated, but fortunately, in most practical cases, the random variables are uncorrelated—i.e., $\rho_{ij} = 0$, and Eq. 2.83 reduces to

$$\sigma_{\bar{f}} = \sqrt{\sum_{i=1}^{M} \left(\frac{\partial f}{\partial \bar{x}_i}\right)^2 \sigma_i^2} \tag{2.84}$$

Unless otherwise specified, the discussion in the rest of this chapter will concern *only uncorrelated variables*. Therefore, Eqs. 2.81 and 2.84 will be used. The reader, however, should always keep in mind the assumption under which Eq. 2.84 is valid.

### 2.15.2 Examples of Error Propagation—Uncorrelated Variables

Examples of error propagation formulas for many common functions are given in this section. In all cases, uncorrelated variables are assumed.

**Example 2.13** $f(x_1, x_2) = a_1 x_1 \pm a_2 x_2$, where $a_1$ and $a_2$ are constants

$$\bar{f} = a_1 \bar{x}_1 \pm a_2 \bar{x}_2$$

$$\sigma_{\bar{f}} = \sqrt{\left(\frac{\partial f}{\partial \bar{x}_1}\right)^2 \sigma_1^2 + \left(\frac{\partial f}{\partial \bar{x}_2}\right)^2 \sigma_2^2} = \sqrt{a_1^2 \sigma_1^2 + a_2^2 \sigma_2^2} \tag{2.85}$$

If $a_1 = a_2 = 1$, this example applies to the very common case of summation or difference of two variables.

**Example 2.14** $f(x_1, x_2) = a x_1 x_2$, where $a$ is a constant

$$\bar{f} = a \bar{x}_1 \bar{x}_2$$

$$\sigma_{\bar{f}} = a \sqrt{\bar{x}_2^2 \sigma_1^2 + \bar{x}_1^2 \sigma_2^2}$$

**Example 2.15** $f(x_1, x_2) = ax_1/x_2$

$$\bar{f} = a\frac{\bar{x}_1}{\bar{x}_2}$$

$$\sigma_{\bar{f}} = a\sqrt{\frac{1}{\bar{x}_2^2}\sigma_1^2 + \frac{\bar{x}_1^2}{\bar{x}_2^4}\sigma_2^2}$$

The standard error for Examples 2.14 and 2.15 takes a simpler and easy-to-remember form for both the product and the quotient if it is expressed as the relative error. It is trivial to show that

$$\frac{\sigma_{\bar{f}}}{\bar{f}} = \sqrt{\left(\frac{\sigma_1}{\bar{x}_1}\right)^2 + \left(\frac{\sigma_2}{\bar{x}_2}\right)^2} \tag{2.86}$$

Thus, the relative error of the product $ax_1x_2$ or the quotient $ax_1/x_2$ is equal to the square root of the sum of the squares of the relative errors of the variables $x_1$ and $x_2$.

**Example 2.16** $f(x) = x^m$, where $m$ is some real number

$$\bar{f} = (\bar{x})^m$$

$$\sigma_{\bar{f}} = \left(\frac{\partial f}{\partial \bar{x}}\right)\sigma_{\bar{x}} = m(\bar{x})^{m-1}\sigma_{\bar{x}}$$

or

$$\frac{\sigma_{\bar{f}}}{\bar{f}} = m\frac{\sigma_{\bar{x}}}{\bar{x}}$$

**Example 2.17** $f(x) = e^{ax}$

$$\bar{f} = c^{a\bar{x}}$$

$$\sigma_{\bar{f}} = \left(\frac{\partial f}{\partial \bar{x}}\right)\sigma_{\bar{x}} = ae^{a\bar{x}}\sigma_{\bar{x}}$$

or

$$\frac{\sigma_{\bar{f}}}{\bar{f}} = a\sigma_{\bar{x}}$$

There is another very important use of Eq. 2.84, which has to do with the calculation of the variation of a function in terms of changes of the independent variables. Consider again the function $f(x_1, x_2, \ldots, x_M)$ and assume that the variables $x_1, x_2, \ldots, x_M$ have changed by the amounts $\Delta x_1, \Delta x_2, \ldots, \Delta x_M$. The variation or change of $f(x_1, \ldots, x_M)$, $\Delta f$, is given by

$$\Delta f = \sqrt{\sum_{i=1}^{M}\left(\frac{\partial f}{\partial x_i}\right)^2 \Delta x_i^2} \tag{2.87}$$

Equation 2.87 should not be used if it is specified what the change of variable is, i.e., if the change is a decrease or an increase. If the change is known, one should calculate the function $f(x_1, x_2, \ldots, x_M)$ using the new values of the $x$'s and obtain $\Delta f$ by subtracting the new from the old value.

**Example 2.18** The speed of sound is obtained by measuring the time it takes for a certain sound signal to travel a certain distance. What is the speed of sound and its standard error if it takes the sound $2.5 \pm 0.125$ s to travel $850 \pm 5$ m?

**Answer**

$$f(x_1, x_2) = v = \frac{x}{t} = \frac{850}{2.5} = 340 \quad \text{m/s}$$

To calculate the error, use Eq. 2.86:

$$\frac{\sigma_v}{v} = \sqrt{\left(\frac{\sigma_x}{x}\right)^2 + \left(\frac{\sigma_t}{t}\right)^2} = \sqrt{\left(\frac{5}{850}\right)^2 + \left(\frac{0.125}{2.5}\right)^2} = 0.05 = 5\%$$

The result is $340 \pm 17$ m/s.

**Example 2.19** A beam of photons going through a material of thickness $x$ is attenuated in such a way that the fraction of photons traversing the material is $e^{-\mu x}$, where the constant $\mu$ is called the attenuation coefficient. If the thickness of the material changes by 10 percent, by how much will the emerging fraction of photons change? Take $x = 0.01$ m and $\mu = 15\ \text{m}^{-1}$.

**Answer** This is a case requiring the use of Eq. 2.87.

$$f(x) = e^{-\mu x}$$

$$\Delta f = \left(\frac{\partial f}{\partial x}\right)\Delta x = -\mu e^{-\mu x}\Delta x$$

$$\frac{\Delta f}{f} = -\mu\,\Delta x = -\mu x\left(\frac{\Delta x}{x}\right) = -(15)(0.01)(0.10) = -0.015$$

Therefore, if the thickness increases by 10 percent, the fraction of emerging photons decreases by 1.5 percent.

## 2.16 GOODNESS OF DATA—$\chi^2$ CRITERION—REJECTION OF DATA

It is desirable when data are obtained during an experiment to be able to determine if the recording system works well or not. The experimenter should

ask the question: Are all the obtained data true (due to the phenomenon studied), or are some or all due to extraneous disturbances that have nothing to do with the measurement? A number of tests have been devised for the purpose of checking how reliable the results are, i.e., checking the "goodness of data."

Before any tests are applied, an investigator should use common sense and try to avoid erroneous data. First of all, a good observer will never rely on a single measurement. He or she should repeat the experiment as many times as is feasible (but at least twice) and observe whether the results are reproducible or not. Second, the observer should check the results to see how they deviate from their average value. Too large or too small deviations are suspicious. The good investigator should be alert and should check such data very carefully. For example, if for identical, consecutive measurements one gets the following counts in a scaler:

10,000 10,000 10,000 10,002 9999 9998

the apparatus is not necessarily very accurate; it is probably faulty. In any event, a thorough check of the whole measuring setup should be performed.

The test that is used more frequently than any other to check the goodness of data is the $\chi^2$ criterion (chi square), or Pearson's $\chi^2$ test. The $\chi^2$ test is based on the quantity

$$\chi^2 = \frac{\sum_{i=1}^{N} (\bar{n} - n_i)^2}{\bar{n}} \tag{2.88}$$

where $n_i|_{i=1,\ldots,N}$ represents the results of $N$ measurements with $\bar{n}$ being the average.

To apply the $\chi^2$ test, one first calculates $\chi^2$ using Eq. 2.88. Then, using Table 2.3, the corresponding probability is obtained. The meaning of the probability values listed in Table 2.3 is the following. If the set of measurements is repeated, the value of $\chi^2$ gives the probability to obtain a new $\chi^2$ that is larger or smaller than the first value. For example, assume that $N = 15$ and $\chi^2 = 4.66$. From the table, the probability is 0.99, meaning that the probability for a new set of measurements to give a $\chi^2 < 4.66$ is less than $1 - 0.99$, i.e., less than 1%. What this implies is that the data are clustered around the mean much closer than one would expect. Assume next that $N = 15$ and $\chi^2 = 29.14$. Again, from the table, the probability to get $\chi^2 > 29.14$ is only 1% or less. In this case, the data are scattered in a pattern around the mean that is wider than one might expect. Finally, consider $N = 15$ and $\chi^2 = 13.34$. The probability is then 0.5, which means that, from a new set of measurements, it is equally probable to get a value of $\chi^2$ that is smaller or larger than 13.34. Notice that the probability is close to 0.5 when $\chi^2 \sim N - 1$. In practice, a range of acceptable $\chi^2$ values is selected in advance; then a set of data is accepted if $\chi^2$ falls within this preselected range. For more details about $\chi^2$, see Johnson & Leone, Jaech, and Smith.

**Table 2.3 Probability Table for $\chi^2$ Criterion†**

| Degrees of freedom‡ ($N-1$) | Probability | | | | | | |
|---|---|---|---|---|---|---|---|
| | 0.99 | 0.95 | 0.90 | 0.50 | 0.10 | 0.05 | 0.01 |
| 2 | 0.020 | 0.103 | 0.211 | 1.386 | 4.605 | 5.991 | 9.210 |
| 3 | 0.115 | 0.352 | 0.584 | 2.366 | 6.251 | 7.815 | 11.345 |
| 4 | 0.297 | 0.711 | 1.064 | 3.357 | 7.779 | 9.488 | 13.277 |
| 5 | 0.554 | 1.145 | 1.610 | 4.351 | 9.236 | 11.070 | 15.086 |
| 6 | 0.872 | 1.635 | 2.204 | 5.348 | 10.645 | 12.592 | 16.812 |
| 7 | 1.239 | 2.167 | 2.833 | 6.346 | 12.017 | 14.067 | 18.475 |
| 8 | 1.646 | 2.733 | 3.490 | 7.344 | 13.362 | 15.507 | 20.090 |
| 9 | 2.088 | 3.325 | 4.168 | 8.343 | 14.684 | 16.919 | 21.666 |
| 10 | 2.558 | 3.940 | 4.865 | 9.342 | 15.987 | 18.307 | 23.209 |
| 11 | 3.053 | 4.575 | 5.578 | 10.341 | 17.275 | 19.675 | 24.725 |
| 12 | 2.571 | 5.226 | 6.304 | 11.340 | 18.549 | 21.026 | 26.217 |
| 13 | 4.107 | 5.892 | 7.042 | 12.340 | 19.812 | 22.363 | 27.688 |
| 14 | 4.660 | 6.571 | 7.790 | 13.339 | 21.064 | 23.685 | 29.141 |
| 15 | 5.229 | 7.261 | 8.547 | 14.339 | 22.307 | 24.996 | 30.578 |
| 16 | 5.812 | 7.962 | 9.312 | 15.338 | 23.542 | 26.296 | 32.000 |
| 17 | 6.408 | 8.672 | 10.085 | 16.338 | 24.769 | 27.587 | 33.409 |
| 18 | 7.015 | 9.390 | 10.865 | 17.338 | 25.989 | 28.869 | 34.805 |
| 19 | 7.633 | 10.117 | 11.651 | 18.338 | 27.204 | 30.144 | 36.191 |
| 20 | 8.260 | 10.851 | 12.443 | 19.337 | 28.412 | 31.410 | 37.566 |
| 21 | 8.897 | 11.591 | 13.240 | 20.337 | 29.615 | 32.671 | 38.932 |
| 22 | 9.542 | 12.338 | 14.041 | 21.337 | 30.813 | 33.924 | 40.289 |
| 23 | 10.196 | 13.091 | 14.848 | 22.337 | 32.007 | 35.172 | 41.638 |
| 24 | 10.856 | 13.848 | 15.659 | 23.337 | 33.196 | 36.415 | 42.980 |
| 25 | 11.534 | 14.611 | 16.473 | 24.337 | 34.382 | 37.382 | 44.314 |
| 26 | 12.198 | 15.379 | 17.292 | 25.336 | 35.563 | 38.885 | 45.642 |
| 27 | 12.879 | 16.151 | 18.114 | 26.336 | 36.741 | 40.113 | 46.963 |
| 28 | 13.565 | 16.928 | 18.939 | 27.336 | 37.916 | 41.337 | 48.278 |
| 29 | 14.256 | 17.708 | 19.768 | 28.336 | 39.087 | 42.557 | 49.588 |

†Calculated values of $\chi^2$ will be equal to or greater than the values given in the table.
‡See footnote on p. 51.

What should one do if the data fail the test? Should all, some, or none of the data be rejected? The answer to these questions is not unique, but rather depends on the criteria set by the observer and the type of measurement. If the data fail the test, the experimenter should be on the lookout for trouble. Some possible reasons for trouble are the following:

1. Unstable equipment may give inconsistent results, e.g., spurious counts generated by a faulty component of an instrument.

2. External signals may be picked up by the apparatus and be "recorded." Sparks, radio signals, welding machines, etc., produce signals that may be recorded by a pulse-type counting system.
3. If a number of samples are involved, widely scattered results may be caused by lack of sample uniformity.
4. A large $\chi^2$ may result from one or two measurements that fall far away from the average. Such results are called the "outliers." Since the results are governed by the normal distribution, which extends from $-\infty$ to $+\infty$, in theory, at least, all results are possible. In practice, it is somewhat disturbing to have a few results that seem to be way out of line.

Should the outliers be rejected? And by what criterion? One should be conservative when rejecting data for three reasons:

1. The results are random variables following the Gaussian distribution. Therefore, outliers are possible.
2. As the number of measurements increases, the probability of an outlier increases.
3. In a large number of measurements, the rejection of an outlier has small effect on the average, although it makes the data look better by decreasing the dispersion.

One of the criteria used for data rejection is Chauvenet's criterion, stated as follows:

> A reading or outcome may be rejected if it has a deviation from the mean greater than that corresponding to the $1 - 1/2N$ error, where $N$ is the number of measurements.

Data used with Chauvenet's criterion are given in Table 2.4. For example, in a series of 10 measurements, $1 - 1/2N = 1 - 1/20 = 0.95$. If $n_i - \bar{n}$ exceeds the 95 percent error ($1.96\sigma$), then that reading could be rejected. In that case, a new mean should be calculated without this measurement and also a new standard deviation.

**Table 2.4 Data for Chauvenet's Criterion**

| Number of measurements | Number of standard deviations away from average |
|---|---|
| 2 | 1.15 |
| 3 | 1.38 |
| 4 | 1.54 |
| 5 | 1.65 |
| 10 | 1.96 |
| 15 | 2.13 |
| 25 | 2.33 |

The use of Chauvenet's, or any other, criterion is not mandatory. It is up to the observer to decide if a result should be rejected or not.

## 2.17 THE STATISTICAL ERROR OF RADIATION MEASUREMENTS

Radioactive decay is a truly random process that obeys the Poisson distribution, according to which the standard deviation of the true mean $m$ is $\sqrt{m}$. However, the true mean is never known and can never be found from a finite number of measurements. But is there a need for a large number of measurements?

Suppose one performs only one measurement and the result is $n$ counts. The best estimate of the true mean, as a result of this single measurement, is this number $n$. If one takes this to be the mean, its standard deviation will be $\sqrt{n}$.

Indeed, this is what is done in practice. The result of a single count $n$ is reported as $n \pm \sqrt{n}$, which implies that

1. The outcome $n$ is considered the true mean.
2. The standard deviation is reported as the standard error of $n$.

The relative standard error of the count $n$ is

$$\frac{\sigma_n}{n} = \frac{\sqrt{n}}{n} = \frac{1}{\sqrt{n}} \tag{2.89}$$

which shows that the relative error decreases if the number of counts obtained in the scaler increases. Table 2.5 gives several values of $n$ and the corresponding percent standard error. To increase the number $n$, one either counts for a long time or repeats the measurement many times and combines the results. Repetition of the measurement is preferable to one single long count because by performing the experiment many times, the reproducibility of the results is checked.

Consider now a series of $N$ counting measurements with the individual results $n_i|_{i=1,\ldots,N}$. It is assumed that the counts $n_i$ were obtained under

**Table 2.5 Percent Standard Error of $n$ Counts**

| $n$ | % Standard error of $n$ |
|---|---|
| 100 | 10 |
| 1,000 | 3.16 |
| 10,000 | 1 |
| 100,000 | 0.316 |
| 1,000,000 | 0.1 |

identical conditions and for the same counting time; thus, their differences are solely due to the statistical nature of radiation measurements. Each number $n_i$ has a standard deviation $\sigma_i = \sqrt{n_i}$. The average of this series of measurements is, using Eq. 2.31,

$$\bar{n} = \frac{1}{N}\sum_{i=1}^{N} n_i \tag{2.31'}$$

The standard error of $\bar{n}$ can be calculated in two ways:

1. The average $\bar{n}$ is the best estimate of a Poisson distribution of which the outcomes $n_i|_{i=1,\ldots,N}$ are members. The standard deviation of the Poisson distribution is (see Sec. 2.9) $\sigma = \sqrt{m} = \sqrt{\bar{n}}$. The standard error of the average is (see Eq. 2.75)

$$\sigma_{\bar{n}} = \frac{\sigma}{\sqrt{N}} = \sqrt{\frac{\bar{n}}{N}} \tag{2.90}$$

2. The average $\bar{n}$ may be considered a linear function of the independent variables $n_i$, each with standard error $\sqrt{n_i}$. Then, using Eq. 2.84, one obtains

$$\sigma_{\bar{n}} = \sqrt{\sum_{i=1}^{N}\left(\frac{\partial \bar{n}}{\partial n_i}\right)^2 \sigma_{n_i}^2} = \sqrt{\sum_{i=1}^{N}\frac{1}{N^2}\left(\sqrt{n_i}\right)^2} = \sqrt{\sum_{i=1}^{N}\frac{1}{N^2}n_i}$$
$$= \frac{1}{N}\sqrt{n_{\text{tot}}} \tag{2.91}$$

where

$$n_{\text{tot}} = n_1 + n_2 + \cdots + n_N = \text{total number of counts obtained from } N \text{ measurements}$$

It is not difficult to show that Eqs. 2.90 and 2.91 are identical.

In certain cases, the observer needs to combine results of counting experiments with quite different statistical uncertainties. For example, one may have to combine the results of a long and short counting measurement. Then the average should be calculated by weighting the individual results according to their standard deviations (see Bevington and Eadie et al.). The equation for the average is

$$\bar{n} = \frac{\sum_{i=1}^{N} n_i/\sigma_i^2}{\sum_{i=1}^{N} 1/\sigma_i^2} \tag{2.92}$$

**Example 2.20** Table 2.6 presents typical results of 10 counting measurements. Using these data, the average count and its standard error will be

**Table 2.6 Typical Results of a Counting Experiment†**

| Observation, $i$ | Number of counts obtained in the scaler, $n_i$ | Square of deviation, $(n_i - \bar{n})^2$ |
|---|---|---|
| 1 | 197 | 81 |
| 2 | 210 | 16 |
| 3 | 200 | 36 |
| 4 | 198 | 64 |
| 5 | 205 | 1 |
| 6 | 195 | 121 |
| 7 | 190 | 256 |
| 8 | 220 | 196 |
| 9 | 215 | 81 |
| 10 | 230 | 576 |
| Totals | 2060 | 1428 |

†One could use Eqs. 2.73 and 2.74 for the calculation of $\sigma$ and $\sigma_{\bar{n}}$. The result is

$$\sigma_{\bar{n}} = \sqrt{\frac{\sum_{i=1}^{N} (n_i - \bar{n})^2}{N(N-1)}} \equiv \sqrt{\frac{1428}{10(9)}} = 3.98 \approx 4$$

For radiation measurements, use of Eqs. 2.90 and 2.91 is preferred.

calculated using Eqs. 2.31, 2.90, and 2.91. The average is

$$\bar{n} = \frac{1}{N}\sum_{i=1}^{N} n_i = \frac{2060}{10} = 206$$

Using Eq. 2.90 or Eq. 2.91, the standard error of $\bar{n}$ is

$$\sigma_{\bar{n}} = \sqrt{\frac{206}{10}} = \frac{\sqrt{2060}}{10} = 4.5$$

## 2.18 THE STANDARD ERROR OF COUNTING RATES

In practice, the number of counts is usually recorded in a scaler, but what is reported is the counting rate, i.e., counts recorded per unit time. The following symbols and definitions will be used for counting rates.

$G$ = number of counts recorded by the scaler in time $t_G$ *with* the sample present
= gross count

$B$ = number of counts recorded by the scaler in time $t_B$ *without* the sample
= background count

$$g = \frac{G}{t_G} = \text{gross counting rate}$$

$$b = \frac{B}{t_B} = \text{background counting rate}$$

$$r = \text{net counting rate}^{\dagger} = \frac{G}{t_G} - \frac{B}{t_B} = g - b \tag{2.93}$$

The standard error of the net counting rate can be calculated based on Eq. 2.84 and by realizing that $r$ is a function of four independent variables $G$, $t_G$, $B$, and $t_B$:

$$\sigma_r = \sqrt{\left(\frac{\partial r}{\partial G}\right)^2 \sigma_G^2 + \left(\frac{\partial r}{\partial t_G}\right)^2 \sigma_{t_G}^2 + \left(\frac{\partial r}{\partial B}\right)^2 \sigma_B^2 + \left(\frac{\partial r}{\partial t_B}\right)^2 \sigma_{t_B}^2} \tag{2.94}$$

The electronic equipment available today is such that the error in the measurement of time is, in almost all practical cases, much smaller than the error in the measurement of $G$ and $B$.[‡] Unless otherwise specified, $\sigma_{tG}$ and $\sigma_{tB}$ will be taken as zero. Then Eq. 2.94 takes the form

$$\sigma_r = \sqrt{\left(\frac{\partial r}{\partial G}\right)^2 \sigma_G^2 + \left(\frac{\partial r}{\partial B}\right)^2 \sigma_B^2} \tag{2.95}$$

The standard errors of $G$ and $B$ are

$$\sigma_G = \sqrt{G} \qquad \sigma_B = \sqrt{B}$$

Using Eqs. 2.93 and 2.95, one obtains for the standard error of the net counting rate,

$$\sigma_r = \sqrt{\frac{G}{t_G^2} + \frac{B}{t_B^2}} \tag{2.96}$$

It is important to notice that in the equation for the net counting rate, the quantities $G$, $B$, $t_G$, and $t_B$ are the independent variables, not $g$ and $b$. The error of $r$ will be calculated from the error in $G$, $B$, $t_G$, and $t_B$. It is very helpful to remember the following rule: *The statistical error of a certain count is determined from the number recorded by the scaler. That number is G and B, not the rates g and b.*

**Example 2.21** A radioactive sample gave the following counts:

$$G = 1000 \qquad t_G = 2\,\text{min} \qquad B = 500 \qquad t_B = 10\,\text{min}$$

[†]When the counting rate is extremely high, the counter may be missing some counts. Then a "dead time" correction is necessary, in addition to background subtraction; see Sec. 2.21.

[‡]The errors $\sigma_{t_G}$ and $\sigma_{t_B}$ may become important in experiments where very accurate counting time is paramount for the measurement.

What is the net counting rate and its standard error?

**Answer**

$$r = \frac{G}{t_G} - \frac{B}{t_B} = \frac{1000}{2} - \frac{500}{10} = 500 - 50 = 450 \text{ counts/min}$$

$$\sigma_r = \sqrt{\frac{G}{t_G^2} + \frac{B}{t_B^2}} = \sqrt{\frac{1000}{2^2} + \frac{500}{10^2}} = \sqrt{250 + 5} = 16 \text{ counts/min}$$

$$r = 450 \pm 16 = 450 \pm 3.5\%$$

A common error is that, since $r = g - b$, one is tempted to write

$$\sigma_r = \sqrt{\sigma_g^2 + \sigma_b^2} = \sqrt{(\sqrt{g})^2 + (\sqrt{b})^2} = \sqrt{g + b} = \sqrt{500 + 50} = 23 \text{ counts/min}$$

This result, $\sigma_r = 23$, is wrong because

$$\sigma_g \neq \sqrt{g} \quad \text{and} \quad \sigma_b \neq \sqrt{b}$$

The correct way to calculate the standard error based on $g$ and $b$ is to use

$$\sigma_g = \frac{\sqrt{G}}{t_G} = \frac{\sqrt{1000}}{2} \qquad \sigma_b = \frac{\sqrt{B}}{t_B} = \frac{\sqrt{500}}{10}$$

Then

$$\sigma_r = \sqrt{\sigma_g^2 + \sigma_b^2} = \sqrt{\frac{G}{t_G^2} + \frac{B}{t_B^2}} = 16 \text{ counts/min}$$

Usually, one determines $G$ and $B$, in which case $\sigma_r$ is calculated from Eq. 2.96. However, sometimes the background counting rate and its error have been determined earlier. In such a case, $\sigma_r$ is calculated as shown in Ex. 2.22.

**Example 2.22** A radioactive sample gave $G = 1000$ counts in 2 min. The background rate of the counting system is known to be $b = 100 \pm 6$ counts/min. What is the net counting rate and its standard error?

**Answer**

$$r = \frac{G}{t_G} - b = \frac{1000}{2} - 100 = 400 \text{ counts/min}$$

$$\sigma_r = \sqrt{\left(\frac{\partial r}{\partial G}\right)^2 \sigma_G^2 + \left(\frac{\partial r}{\partial b}\right)^2 \sigma_b^2} = \sqrt{\frac{G}{t_G^2} + \sigma_b^2} = \sqrt{\frac{1000}{4} + 6^2} = \sqrt{286}$$

$$= 17 \text{ counts/min}$$

In this problem, $b$ and $\sigma_b$ are given, not $B$ and $t_B$. The standard error of the background rate has been determined by an earlier measurement. Obviously, $b$

was not determined by counting for 1 min, because in that case, one would have

$$B = 100 \qquad t_B = 1 \text{ min} \qquad b = 100 \text{ counts/min}$$

$$\sigma_b = \frac{\sqrt{B}}{t_B} = \frac{\sqrt{100}}{1} = 10$$

### 2.18.1 Combining Counting Rates

If the experiment is performed $N$ times with results

$$G_1, G_2, G_3, \ldots, G_N \qquad B_1, B_2, \ldots, B_N$$

for gross and background counts, the average net counting rate is

$$\bar{r} = \frac{1}{N}\sum_{i=1}^{N} r_i = \frac{1}{N}\sum_{i=1}^{N}\left(\frac{G_i}{t_{G_i}} - \frac{B_i}{t_{B_i}}\right)$$

In most cases, $t_{G_i}$ and $t_{B_i}$ are kept constant for all $N$ measurements. That is, $t_{G_i} = t_G$ and $t_{B_i} = t_B$. Then

$$\bar{r} = \frac{1}{N}\sum_{i=1}^{N}\left(\frac{G_i}{t_{B_i}} - \frac{B_i}{t_{B_i}}\right) = \frac{1}{N}\left(\frac{G}{t_G} - \frac{B}{t_B}\right) \tag{2.97}$$

where

$$G = \sum_{i=1}^{N} G_i \quad \text{and} \quad B = \sum_{i=1}^{N} B_i$$

The standard error of the average counting rate is, using Eqs. 2.84 and 2.96,

$$\sigma_{\bar{r}} = \frac{1}{N}\sqrt{\sum_{i=1}^{N}\sigma_{r_i}^2} = \frac{1}{N}\sqrt{\sum_{i=1}^{N}\left(\frac{G_i}{t_G^2} + \frac{B_i}{t_B^2}\right)} = \frac{1}{N}\sqrt{\frac{G}{t_G^2} + \frac{B}{t_B^2}} \tag{2.98}$$

**A special case.** Sometimes the background rate is negligible compared to the gross counting rate. Then, Eq. 2.98 becomes

$$\sigma_{\bar{r}} = \frac{1}{N}\frac{\sqrt{G}}{t_G}$$

The relative standard error is

$$\frac{\sigma_r}{\bar{r}} = \frac{(1/N)\sqrt{G}/t_G}{G/Nt_G} = \frac{1}{\sqrt{G}}$$

This is the same as Eq. 2.89. Therefore, if the background is negligible, the relative standard error is the same for either the total count or the counting rate.

## 2.19 METHODS OF ERROR REDUCTION

In every radiation measurement it is extremely important to perform it in such a way that the result is determined with the minimum possible error. In general, the first task of the investigator is to improve the counting apparatus by reducing the background as much as possible. Actually, the important quantity is the ratio $b/g$ or $b/r$ and not the absolute value of the background. Assuming that all possible improvements of background have been achieved, there is a procedure that, if followed, will result in a smaller error. Two such procedures will be discussed below. In addition, a method will be presented for the calculation of the counting time necessary to measure a counting rate with a desired degree of accuracy.

### 2.19.1 The Background Is Constant and There Is No Time Limit for Its Measurement

In this case, the background is measured for a long period of time to minimize the error introduced by it, i.e., $t_B$ is so long that

$$\sigma_r = \sqrt{\frac{G}{t_G^2} + \frac{B}{t_B^2}} \approx \sqrt{\frac{G}{t_G^2}}$$

**Example 2.23** Suppose one obtains the following data:

$$G = 400 \qquad t_G = 5 \text{ min}$$
$$B = 100 \qquad t_B = 2.5 \text{ min}$$

Then

$$r = \frac{400}{5} - \frac{100}{2.5} = 40 \text{ counts/min}$$

$$\sigma_r = \sqrt{\frac{400}{5^2} + \frac{100}{2.5^2}} = 5.65 \text{ counts/min}$$

$$\frac{\sigma_r}{r} = \frac{5.65}{40} = 0.14 = 14\%$$

If the background is constant, this result can be improved by counting background for a long period of time, e.g., 250 min. In that case, the result is

$$B = \frac{100}{2.5} \times 250 = 10{,}000 \text{ counts} \qquad t_B = 250 \text{ min}$$

$$r = \frac{400}{5} - \frac{10{,}000}{250} = 40 \text{ counts/min}$$

$$\sigma_r = \sqrt{\frac{400}{5^2} + \frac{10{,}000}{250^2}} = \sqrt{16 + 0.16} \approx 4$$

$$\frac{\sigma_r}{r} = \frac{4}{40} = 10\%$$

### 2.19.2 There Is a Fixed Time $T$ Available for Counting Both Background and Gross Count

In this case, the question is, What is the optimum time to be used for gross and background counting? Optimum time results in minimum statistical error for the net counting rate. The optimum time is determined as follows.

An estimate of the counting rates at the time of the measurement is obtained with a short count (not the final one). Assume that one obtained the approximate counting rates

$$g = \frac{G}{t_G} \quad b = \frac{B}{t_B}$$

Then, from Eq. 2.96 and also using $G = gt_G$, $B = bt_B$,

$$\sigma_r^2 = \frac{g}{t_G} + \frac{b}{t_B}$$

The best times $t_G$ and $t_B$ are those that minimize $\sigma_r$ or $(\sigma_r)^2$ subject to the constraint

$$t_B + t_G = T = \text{constant} \tag{2.99}$$

Considering $\sigma_r^2$ as a function of $t_B$ and $t_G$, the minimum will be found by differentiating $(\sigma_r)^2$ and setting the differential equal to zero:

$$d(\sigma_r)^2 = -\frac{g}{t_G^2}\,dt_G - \frac{b}{t_B^2}\,dt_B = 0$$

Differentiating the constraint, Eq. 2.99, one finds

$$dt_G = -dt_B$$

Substituting this value of $dt_G$ into $d(\sigma_r)^2$ gives

$$\frac{t_B}{t_G} = \sqrt{\frac{b}{g}}$$

Therefore, if there is a fixed time $T$ for the measurement, the optimum counting times are determined from the two equations

$$t_G + t_B = T$$

$$\frac{t_B}{t_G} = \sqrt{\frac{b}{g}} \tag{2.100}$$

### 2.19.3 Calculation of the Counting Time Necessary to Measure a Counting Rate with a Predetermined Statistical Error

Assume that the net counting rate of a radioactive sample should be measured with an accuracy of $a$ percent, i.e., $\sigma_r/r = a$ percent. Also assume that a counting system is provided with a background counting rate $b$ and standard

error $\sigma_b$. Both $b$ and $\sigma_b$ have been reduced as much as possible for this system and have been determined earlier. The task is to determine the counting time $t_G$ necessary to result in $a$ percent standard error for the net counting rate. The time $t_G$ is calculated as follows.

The net counting rate and its standard error are

$$r = \frac{G}{t_G} - b \qquad \sigma_r = \sqrt{\frac{G}{t_G^2} + \sigma_b^2} \tag{2.101}$$

Therefore

$$\frac{\sigma_r}{r} = \frac{a}{100} = \frac{\sqrt{G/t_G^2 + \sigma_b^2}}{G/t_G - b} = \frac{\sqrt{g/t_G + \sigma_b^2}}{g - b}$$

Equation 2.101 solved for $t_G$ gives

$$t_G = \frac{g}{(g - b)^2(a/100)^2 - \sigma_b^2} \tag{2.102}$$

It is assumed that an approximate gross counting rate is known.

**Example 2.24** How long should a sample be counted to obtain the net counting rate with an accuracy of 1 percent? It is given that the background for the counting system is $100 \pm 2$ counts/min.

**Answer** The first step is to obtain an approximate gross counting rate. Assume that the sample gave 800 counts in 2 min. Then $g = 800/2 = 400$ counts/ min and, using Eq. 2.102,

$$t_G = \frac{400}{(400 - 100)^2(0.01)^2 - 2^2} = 80 \text{ min}$$

Indeed, if one counts for 80 min, the error of $r$ is going to be

$$\sigma_r = \sqrt{\frac{g}{t_G} + \sigma_b^2} = \sqrt{\frac{400}{80} + 2^2} = 3$$

$$\frac{\sigma_r}{r} = \frac{3}{300} = 0.01 = 1\%$$

### 2.19.4 Relative Importance of Error Components

In every measurement, the observer tries to reduce the experimental error as much as possible. If the quantity of interest depends on many variables, each with its own error, the effort to reduce the error should be directed toward the variable with the largest contribution to the final error.

Consider the quantity $Q = x + y - z$ and assume $x = 3$, $y = 2$, and $z = 1$. Also assume that the corresponding standard errors are

$$\sigma_x = 0.1 \qquad \sigma_y = 0.23 \qquad \sigma_z = 0.05$$

The standard error of $Q$ is

$$\sigma_Q = \sqrt{\sigma_x^2 + \sigma_y^2 + \sigma_z^2} = \sqrt{0.1^2 + 0.23^2 + 0.05^2}$$
$$= \sqrt{0.01 + 0.0529 + 0.0025} = 0.26$$

From the relative magnitude of the errors, one can see that if it is necessary to reduce the error further, the effort should be directed toward reduction of $\sigma_y$ first, $\sigma_x$ second, and $\sigma_z$ third. In fact, there is no need to reduce $\sigma_z$ further before $\sigma_x$ and $\sigma_y$ reach the same magnitude as $\sigma_z$.

## 2.20 MINIMUM DETECTABLE ACTIVITY

The minimum detectable activity (MDA) is the smallest net count that can be reported with a certain degree of confidence that represents a true activity from a sample and is not a statistical variation of the background. The term MDA is not universally acceptable. In the general case, in measurements not necessarily involving radioactivity, other terms such as lowest detection limit have been used. Here, the notation and applications will be presented with the measurement of a radioactive sample in mind.

Obviously, MDA is related to low count rates. In such cases of low count rates, the person who performs the experiment faces two possible errors.

*TYPE I error*: To state that the true activity is greater than zero when, in fact, it is zero. If this is a suspected contaminated item, the person doing the measurement will report that the item is indeed contaminated when, in fact, it is not. This error is called *false positive*.

*TYPE II error*: To state that the true activity is zero when, in fact, it is not. Using the previous example, the person doing the measurement reports that the item is clean when, in fact, it is contaminated. This error is called *false negative*.

The outcomes of radiation measurements follow Poisson statistics, which become, essentially, Gaussian when the average is greater than about 20 (see Sec. 2.10.2). For this reason, the rest of this discussion will assume that the results of individual measurements follow a normal distribution and the confidence limits set will be interpreted with that distribution in mind. Following the

notation used earlier,

$B$ = background with standard deviation $\sigma_B$

$G$ = gross signal with standard deviation $\sigma_G$

$n = G - B$ = net signal with standard deviation $\sigma_n = (\sigma_G^2 + \sigma_B^2)^{1/2}$

When the net signal is zero (and has a standard deviation $\sigma_n = \sigma_0$), a critical detection limit (CDL) is defined in terms of $\sigma_0$ with the following meaning:

1. A signal lower than CDL is not worth reporting.
2. The decision that there is nothing to report has a confidence limit of $1 - \alpha$, where $\alpha$ is a certain fraction of the normalized Gaussian distribution (Fig. 2.12). Take as an example $\alpha = 0.05$. Then

$$\text{CDL} = k_\alpha \sigma_0 \tag{2.103}$$

with $k_\alpha = 1.645$ (see Table 2.2). If $n <$ CDL, one decides that the sample is not contaminated, and this decision has a 95% confidence limit.

The MDA should obviously be greater than the CDL. Keeping in mind that the possible MDA values also follow a normal distribution, a fraction $\beta$ is

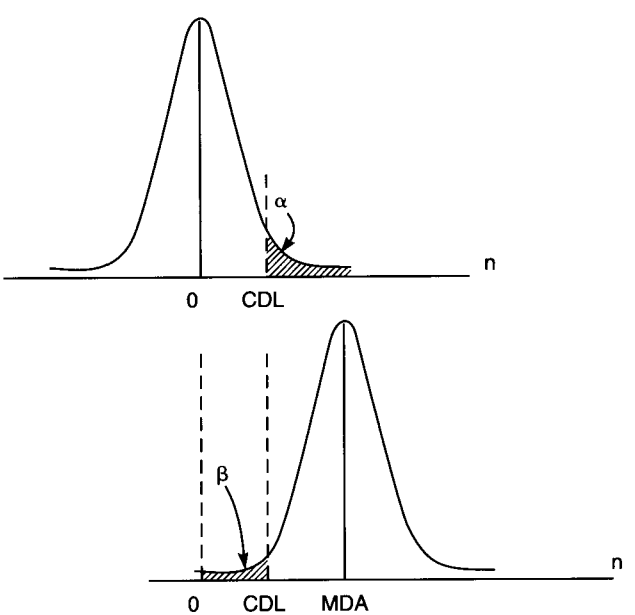


**Figure 2.12** The meaning of the critical detection limit (CDL) and minimum detectable activity (MDA) in terms of the confidence limits defined by $\alpha$ and $\beta$.

established, meaning that a signal equal to MDA is reported as a correct/true signal with a confidence limit $1 - \beta$. The value of MDA is given by

$$\text{MDA} = \text{CDL} + k_\beta \sigma_D \tag{2.104}$$

where $\sigma_D$ is the standard deviation of MDA (Fig. 2.12). Again, if $\beta = 0.05$, $k_\beta = 1.645$.

In most cases, in practice, $\alpha = \beta = 0.05$; then the CDL and MDA are defined with a 95% confidence limit. For radioactivity specifically, remember that

$$\sigma^2 = \sigma_G^2 + \sigma_B^2 = (\sigma_n^2 + \sigma_B^2) + \sigma_B^2 \tag{2.105}$$

and for $n = 0$, $\sigma_n = \sqrt{n} = 0$ and $\sigma = \sigma_0 = \sqrt{\sigma_B^2 + \sigma_B^2} = \sqrt{2}\,\sigma_B$. Then, if the 95% confidence limit is applied ($\alpha = \beta = 0.05$), CDL $= 1.645\sigma_0 = 2.326\sigma_B$. The value of MDA turns out to be (see Prob. 2.24)

$$\text{MDA} = k^2 + 2\text{CDL} = 2.71 + 4.653\sigma_B \tag{2.106}$$

**Example 2.25** Consider the data of a single measurement to be $G = 465$ counts/min, $B = 400$/min. Assume that from previous measurements in that counting system it has been determined that $\sigma_B = 10$/min. The assumption is made that the background is constant. What does one report in this case?

**Answer** The net count rate is $n = 465 - 400 = 65$ counts/min. The minimum detectable activity is, from Eq. 2.106, MDA $= 2.71 + 4.653 \times 10 = 49.2$. Since MDA $< 65$, one reports, with a 95% confidence limit, that this sample is radioactive.

In most cases, the second term of Eq. 2.106 is much larger than the first, and the MDA is taken as

$$\text{MDA} = 4.653\sigma_B \tag{2.107}$$

In using Eq. 2.106 or 2.107, the user should keep in mind the underlying assumption of the 95% confidence limit. The numerical factors will change if one chooses a different confidence limit.

## 2.21 COUNTER DEAD-TIME CORRECTION AND MEASUREMENT OF DEAD TIME

Dead time, or resolving time, of a counting system is defined as the minimum time that can elapse between the arrival of two successive particles at the detector and the recording of two distinct pulses. The components of dead time consist of the time it takes for the formation of the pulse in the detector itself and for the processing of the detector signal through the preamplifier-amplifier-discriminator-scaler (or preamplifier-amplifier-MCA). With modern electronics, the longest component of dead time is that of the detector, and for this

reason, the term "dead time" means the dead time of the detector. The dead-time component of the preamplifier-amplifier-discriminator-scaler can be ignored with any type of detector.

Because of counter dead time, the possibility exists that some particles will not be recorded since the counter will not produce pulses for them. Pulses will not be produced because the counter will be "occupied" with the formation of the signal generated by particles arriving earlier. The counting loss of particles is particularly important in the case of high counting rates. Obviously, the observed counting rate should be corrected for the loss of counts due to counter dead time. The rest of this section presents the method for correction as well as a method for the measurement of the dead time.

Suppose $\tau$ is the dead time of the system and $g$ the observed counting rate. The fraction of time during which the system is insensitive is $g\tau$. If $n$ is the true counting rate, the number of counts lost is $n(g\tau)$. Therefore

$$n = g + ng\tau$$

and

$$n = \frac{g}{1 - g\tau} \tag{2.108}$$

Equation 2.108 corrects the observed gross counting rate $g$ for the loss of counts due to the dead time of the counter.

**Example 2.26** Suppose $\tau = 200\ \mu$s and $g = 30{,}000$ counts/min. What fraction of counts is lost because of dead time? What is the true counting rate?

**Answer** The true counting rate is

$$n = \frac{g}{1 - g\tau} = \frac{30{,}000/60}{1 - (30{,}000/60)(200 \times 10^{-6})}$$

or

$$n = 555.5 \text{ counts/s}$$

Therefore, dead time is responsible for loss of

$$\frac{555 - 500}{555} = \frac{55}{555} = 10\% \text{ of the counts}$$

Notice that the product $g\tau = 0.10$, i.e., the product of the dead time and the gross counting rate, is a good indicator of the fraction of counts lost because of dead time.

The dead time is measured with the "two-source" method as follows. Let $n_1, n_2, n_{12}$ be the true gross counting rates from the first source only, from the second source only, and from both sources, respectively, and let $n_b$ be the true background rate. Let the corresponding observed counting rates be $g_1, g_2, g_{12}, b$.

The following equation holds:

$$\begin{pmatrix}\text{True net}\\ \text{counting rate}\end{pmatrix}_1 + \begin{pmatrix}\text{True net}\\ \text{counting rate}\end{pmatrix}_2 = \begin{pmatrix}\text{True net}\\ \text{counting rate}\end{pmatrix}_{1+2}$$

$$(n_1 - n_b) \quad + \quad (n_2 - n_b) \quad = \quad (n_{12} - n_b)$$

or

$$n_1 + n_2 = n_{12} + n_b$$

Using Eq. 2.108,

$$\frac{g_1}{1 - g_1\tau} + \frac{g_2}{1 - g_2\tau} = \frac{g_{12}}{1 - g_{12}\tau} + \frac{b}{1 - b\tau} \tag{2.109}$$

It will be assumed now that $b\tau \ll 1$, in which case,

$$\frac{b}{1 - b\tau} = b$$

(If $b\tau$ is not much less than 1, the instruments should be thoroughly checked for possible malfunction before proceeding with the measurement.)

The dead time $\tau$ can be determined from Eq. 2.109 after $g_1, g_2, g_{12}$, and $b$ are measured. This is achieved by counting radioactive source 1, then sources 1 and 2 together, then only source 2, and finally the background after removing both sources. Equation 2.109 can be rearranged to give:

$$\begin{aligned}(g_1g_2g_{12} + g_1g_2b - g_1g_{12}b - g_2g_{12}b)\tau^2 - 2(g_1g_2 - g_{12}b)\tau \\ + g_1 + g_2 - g_{12} - b = 0\end{aligned} \tag{2.110}$$

Equation 2.110 is a second-degree algebraic equation that can be solved for $\tau$. It was derived without any approximations.

If the background is negligible, Eq. 2.110 takes the form

$$g_1g_2g_{12}\tau^2 - 2g_1g_2\tau + g_1 + g_2 - g_{12} = 0 \tag{2.111}$$

Solving for $\tau$,

$$\tau = \frac{1}{g_{12}}\left[1 - \sqrt{\frac{g_{12}}{g_1g_2}(g_1 + g_2 - g_{12})}\right] \tag{2.112}$$

When dead-time correction is necessary, the net counting rate, called "true net counting rate," is given by

$$r = n - b = \frac{G/t_G}{1 - (G\tau/t_G)} - b \tag{2.113}$$

It is assumed that the true background rate has been determined earlier with the standard error $\sigma_b$. The standard error of $r$, $\sigma_r$, is calculated from Eq. 2.113 using Eq. 2.84. If the only sources of error are the gross count $G$ and the

background, the standard error of $r$ is

$$\sigma_r = \sqrt{\left(\frac{1}{1-(G/t_G)\tau}\right)^4 \frac{G}{t_G^2} + \sigma_b^2} \tag{2.114}$$

If there is an error due to dead-time determination, a third term consisting of that error will appear under the radical of Eq. 2.114.

## PROBLEMS

**2.1** What is the probability when throwing a die three times of getting a four in any of the throws?

**2.2** What is the probability when drawing one card from each of three decks of cards that all three cards will be diamonds?

**2.3** A box contains 2000 computer cards. If five faulty cards are expected to be found in the box, what is the probability of finding two faulty cards in a sample of 250?

**2.4** Calculate the average and the standard deviation of the probability density function $f(x) = 1/(b-a)$ when $a \le x \le b$. (This pdf is used for the calculation to round off errors.)

**2.5** The energy distribution of thermal (slow) neutrons in a light-wave reactor follows very closely the Maxwell-Boltzmann distribution:

$$N(E)\,dE = A\sqrt{E}\,e^{-E/kT}\,dE$$

where $N(E)\,dE$ = number of neutrons with kinetic energy between $E$ and $E + dE$
$k$ = Boltzmann constant = $1.380662 \times 10^{-23}$ J/° K
$T$ = temperature, K
$A$ = constant

Show that

(a) The mode of this distribution is $E = \frac{1}{2}kT$.
(b) The mean is $\bar{E} = \frac{3}{2}kT$.

**2.6** If the average for a large number of counting measurements is 15, what is the probability that a single measurement will produce the result 20?

**2.7** For the binomial distribution, prove

$$\text{(a)} \quad \sum_{n=0}^{N} P_{(N)}^{(n)} = 1 \qquad \text{(b)} \quad \bar{n} = pN \qquad \text{(c)} \quad \sigma^2 = m(1-p)$$

**2.8** For the Poisson distribution, prove

$$\text{(a)} \quad \sum_{n=0}^{\infty} P_n = 1 \qquad \text{(b)} \quad \bar{n} = m \qquad \text{(c)} \quad \sigma^2 = m$$

**2.9** For the normal distribution, show

$$\text{(a)} \quad \int_{-\infty}^{\infty} P(x)\,dx = 1 \qquad \text{(b)} \quad \bar{x} = m \qquad \text{(c)} \quad \text{the variance is } \sigma^2$$

**2.10** If $n_1, n_2, \ldots, n_N$ are mutually uncorrelated random variables with a common variance $\sigma^2$, show that

$$\overline{(n_i - \bar{n})^2} = \frac{N-1}{N}\sigma^2$$

**2.11** Show that in a series of $N$ measurements, the result $R$ that minimizes the quantity

$$Q = \sum_{i=1}^{N} (R - n_i)^2$$

is $R = \bar{n}$, where $\bar{n}$ is given by Eq. 2.31.

**2.12** Prove Eq. 2.62 using tables of the error function.

**2.13** As part of a quality control experiment, the lengths of 10 nuclear fuel rods have been measured with the following results in meters:

| | | | | |
|---|---|---|---|---|
| 2.60 | 2.62 | 2.65 | 2.58 | 2.61 |
| 2.62 | 2.59 | 2.59 | 2.60 | 2.63 |

What is the average length? What is the standard deviation of this series of measurements?

**2.14** At a uranium pellet fabrication plant the average pellet density is $17 \times 10^3$ kg/m$^3$ with a standard deviation equal to $10^3$ kg/m$^3$. What is the probability that a given pellet has a density less than $14 \times 10^3$ kg/m$^3$?

**2.15** A radioactive sample was counted once and gave 500 counts in 1 min. The corresponding number for the background is 480 counts. Is the sample radioactive or not? What should one report based on this measurement alone?

**2.16** A radioactive sample gave 750 counts in 5 min. When the sample was removed, the scaler recorded 1000 counts in 10 min. What is the net counting rate and its standard percent error?

**2.17** Calculate the average net counting rate and its standard error from the data given below:

| $G$ | $t_G$(min) | $B$ | $t_B$(min) |
|---|---|---|---|
| 355 | 5 | 120 | 10 |
| 385 | 5 | 130 | 10 |
| 365 | 5 | 132 | 10 |

**2.18** A counting experiment has to be performed in 5 min. The approximate gross and background counting rates are 200 counts/min and 50 counts/min, respectively.

(a) Determine the optimum gross and background counting times.

(b) Based on the times obtained in (a), what is the standard percent error of the net counting rate?

**2.19** The strength of a radioactive source was measured with a 2 percent standard error by taking a gross count for time $t$ min and a background for time $2t$ min. Calculate the time $t$ if it is given that the background is 300 counts/min and the gross count 45,000 counts/min.

**2.20** The strength of radioactive source is to be measured with a counter that has a background of $120 \pm 8$ counts/min. The approximate gross counting rate is 360 counts/min. How long should one count if the net counting rate is to be measured with an error of 2 percent?

**2.21** The buckling $B^2$ of a cylindrical reactor is given by

$$B^2 = \left(\frac{2.405}{R}\right)^2 + \left(\frac{\pi}{H}\right)^2$$

where $R$ = reactor radius

$H$ = reactor height

If the radius changes by 2 percent and the height by 8 percent, by what percent will $B^2$ change? Take $R = 1$ m, $H = 2$ m.

**2.22** Using Chauvenet's criterion, should any of the scaler readings listed below be rejected?

| | | | |
|---|---|---|---|
| 115 | 121 | 103 | 151 |
| 121 | 105 | 75 | 103 |
| 105 | 107 | 100 | 108 |
| 113 | 110 | 101 | 97 |
| 110 | 109 | 103 | 101 |

**2.23** Using the data of Prob. 2.13, what is the value of accepted length $x_a$ if the confidence limit is 99.4 percent?

**2.24** Prove that for radioactivity measurements the value of MDA is given by the equation $\text{MDA} = k^2 + 2\text{CDL}$, if $k_\alpha = k_\beta = k$. Hint: when $n = \text{MDA}$, the variance $\sigma^2 = \text{MDA} + \sigma_0^2$.

**2.25** A sample was counted for 5 min and gave 2250 counts; the background, also recorded for 5 min, gave 2050 counts. Is this sample radioactive? Assume confidence limits of both 95% and 90%.

**2.26** Determine the dead time of a counter based on the following data obtained with the two-source method:

$$g_1 = 14{,}000 \text{ counts/min} \qquad g_{12} = 26{,}000 \text{ counts/min}$$

$$g_2 = 15{,}000 \text{ counts/min} \qquad b = 50 \text{ counts/min}$$

**2.27** If the dead time of a counter is 100 $\mu$s, what is the observed counting rate if the loss of counts due to dead time is equal to 5 percent?

**2.28** Calculate the true net activity and its standard percent error for a sample that gave 70,000 counts in 2 min. The dead time of the counter is 200 $\mu$s. The background is known to be $100 \pm 1$ counts/min.

**2.29** Calculate the true net activity and its standard error based on the following data:

$G = 100{,}000$ counts obtained in 10 min

$B = 10{,}000$ counts obtained in 100 min

The dead time of the counter is 150 $\mu$s.

## BIBLIOGRAPHY


Arley, N., and Buck, K. R., *Introduction to the Theory of Probability and Statistics*, Wiley, New York, 1950.

Beers, Y., *Introduction to the Theory of Error*, Addison-Wesley, Reading, Mass., 1957.

Bevington, P. R., *Data Reduction and Error Analysis for the Physical Sciences*, McGraw-Hill, New York, 1969.

Chemical Rubber Company, *Handbook of Chemistry and Physics*, Cleveland, Ohio.

Chemical Rubber Company, *Standard Mathematical Tables*, Cleveland, Ohio.

Eadie, W. T., Dryard, D., James, F. E., Roos, M., and Sadoulet, B., *Statistical Methods in Experimental Physics*, North-Holland, Amsterdam, 1971.

Jaech, J. L., "Statistical Methods in Nuclear Material Control," TID-26298, U.S. Atomic Energy Commission, 1973.

Johnson, N. L., and Leone, F. C., *Statistics and Experimental Design*, Wiley, New York, 1964, Chaps. 1, 3, 4, and 5.

Smith, D. L., "Probability, Statistics, and Data Uncertainties in Nuclear Science and Technology," OECD/NEA, Vol. 4, American Nuclear Society, La Grange Park, Illinois, 1991.


## REFERENCES


1. Currie, L. A., *Anal. Chem.* 40(3):586 (1968).
2. Roberson, P. L., and Carlson, R. D., *Health Phys.* 62:2 (1992).
3. Flanigan, J. A., *Rad. Prot. Mgt.* Nov.-Dec.:37 (1993).

CHAPTER
# THREE

# REVIEW OF ATOMIC AND NUCLEAR PHYSICS

## 3.1 INTRODUCTION

This chapter reviews the concepts of atomic and nuclear physics relevant to radiation measurements. It should not be considered a comprehensive discussion of any of the subjects presented. For in-depth study, the reader should consult the references listed at the end of the chapter. If a person has studied and understood this material, this chapter could be skipped without loss of continuity.

This review is not presented from the historical point of view. Atomic and nuclear behavior and the theory and experiments backing it are discussed as we understand them today. Emphasis is given to the fact that the current "picture" of atoms, nuclei, and subatomic particles is only a model that represents our best current theoretical and experimental evidence. This model may change in the future if new evidence is obtained pointing to discrepancies between theory and experiment.

## 3.2 ELEMENTS OF RELATIVISTIC KINEMATICS

The special theory of relativity developed by Einstein in 1905 is based on two simple postulates.

*FIRST POSTULATE* The laws of nature and the results of all experiments performed in a given frame of reference (system of coordinates) are independent of the translational motion of the system as a whole.

*SECOND POSTULATE* The speed of light in vacuum is independent of the motion of its source.

These two postulates, simple as they are, predict consequences that were unthinkable at that time. The most famous predictions of the special theory of relativity are

1. The mass of a body changes when its speed changes.
2. Mass and energy are equivalent ($E = mc^2$).

Einstein's predictions were verified by experiment a few years later, and they are still believed to be correct today.

The main results of the special theory of relativity will be presented here without proof, using the following notations:

$M$ = rest mass of a particle (or body)
$M^*$ = mass of a particle in motion
$v$ = speed of the particle
$c$ = speed of light in vacuum = $3 \times 10^8$ m/s
$T$ = kinetic energy of the particle
$E$ = total energy of the particle

According to the theory of relativity, the mass of a moving particle (or body) changes with its speed according to the equation

$$M^* = \frac{M}{\sqrt{1 - (v/c)^2}} = \frac{M}{\sqrt{1 - \beta^2}} \tag{3.1}$$

or

$$M^* = \gamma M \tag{3.2}$$

where

$$\beta = \frac{v}{c} \tag{3.3}$$

and

$$\gamma = \frac{1}{\sqrt{1 - \beta^2}} \tag{3.4}$$

Equation 3.1 shows that

1. As the speed of a moving particle increases, its mass also increases, thus making additional increase of its speed more and more difficult.

2. It is impossible for any mass to reach a speed equal to or greater than the speed of light in vacuum.†

The total energy of a particle of mass $M^*$ is

$$E = M^*c^2 \tag{3.5}$$

Equation 3.5 expresses the very important concept of equivalence of mass and energy. Since the total energy $E$ consists of the rest mass energy plus the kinetic energy, Eq. 3.5 may be rewritten as

$$E = M^*c^2 = T + Mc^2 \tag{3.6}$$

Combining Eqs. 3.2 and 3.6, one obtains the relativistic equation for the kinetic energy

$$T = (\gamma - 1)Mc^2 \tag{3.7}$$

The quantity $\gamma$, which is defined by Eq. 3.4 ($\gamma = M^*c^2/Mc^2$), indicates how many times the mass of the particle has increased, relative to its rest mass, because of its motion. For large moving masses, the relativistic mass increase is too small to measure. Thus, without the availability of subatomic particles such as electrons and protons, it would be extremely difficult to verify this part of Einstein's theory.

The equation that relates the linear momentum and the total energy of a particle is

$$E^2 = (Mc^2) + (pc)^2 \tag{3.8}$$

where

$$\mathbf{p} = M^*\mathbf{v} = \gamma M\mathbf{v} \tag{3.9}$$

is the linear momentum. Combining Eqs. 3.6 and 3.8, one obtains

$$T = \sqrt{(Mc^2)^2 + (pc)^2} - Mc^2 \tag{3.10}$$

or

$$p = \frac{1}{c}\sqrt{T^2 + 2TMc^2} \tag{3.11}$$

Equation 3.10 is used for the determination of the kinetic energy if the momentum is known, while Eq. 3.11 gives the momentum if the kinetic energy is known.

For small values of $\beta$ (Eq. 3.3)—that is, for small speeds—the equations of relativity reduce to the equations of Newtonian (classical) mechanics. In classical mechanics, the mass is constant, and $T$ and $p$ are given by

$$T = \tfrac{1}{2}Mv^2 \tag{3.12}$$

$$\mathbf{p} = M\mathbf{v} \tag{3.13}$$

†The speed of light in a medium with index of refraction $n$ is $c/n$; thus, it is possible for particles to move faster than with $c/n$ in certain media (see Cerencov radiation, Evans).

If the kinetic energy of a particle is a considerable fraction of its rest mass energy, Eqs. 3.7 and 3.9 should be used for the determination of $T$ and **p**. Then the particle is *relativistic*. If, on the other hand, $\beta \ll 1$, the particle is *nonrelativistic*, and Eqs. 3.12 and 3.13 may be used.

**Example 3.1** What is the mass increase of a bullet weighing 0.010 kg and traveling at twice the speed of sound?

**Answer** The speed of the bullet is $v \approx 700$ m/s. Using Eqs. 3.2 and 3.4,

$$\frac{M^*}{M} = \gamma = \frac{1}{\sqrt{1-\beta^2}} \approx 1 + \frac{1}{2}\beta^2 = 1 + \frac{1}{2}\left(\frac{700}{3 \times 10^8}\right)^2 = 1 + 2.72 \times 10^{-12}$$

The mass increase is

$$M^* - M = 2.72 \times 10^{-12} M = 2.72 \times 10^{-14} \text{ kg}$$

which is almost impossible to detect.

**Example 3.2** An electron has a kinetic energy of 200 keV. (a) What is its speed? (b) What is its new mass relative to its rest mass?

**Answer** The rest mass energy of the electron is 511 keV. Since $T/mc^2 = 200/511 = 0.391$, relativistic equations should be used. (a) The speed of the electron is obtained with the help of Eqs. 3.7 and 3.4. Equation 3.7 gives

$$\gamma = 1 + \frac{T}{mc^2} = 1 + 0.391$$

and from Eq. 3.4 one obtains

$$\beta = \sqrt{1 - \frac{1}{\gamma^2}} = 0.695$$

Therefore

$$v = \beta c = (0.695)(3 \times 10^8 \text{ m/s}) = 2.085 \times 10^8 \text{ m/s}$$

(b) The new mass relative to the rest mass has already been determined because

$$\gamma = \frac{m^* c^2}{mc^2} = 1.391$$

i.e., the mass of this electron increased 39.1 percent.

It is instructive to calculate the speed of this electron using the classical method of Eq. 3.12 to see the difference:

$$v = \sqrt{\frac{2T}{m}} = \sqrt{\frac{2Tc^2}{mc^2}} = \left(\sqrt{\frac{2T}{mc^2}}\right)c = \left(\sqrt{\frac{2(200)}{511}}\right)c = 0.885c$$

Thus, the classical equation determines the speed with an error

$$\frac{v_{\text{cl}} - v_{\text{rel}}}{v_{\text{rel}}} = \frac{0.885c - 0.695c}{0.695c} = 27\%$$

**Example 3.3** What is the kinetic energy of a neutron with speed $6 \times 10^7$ m/s? What is its mass increase?

**Answer** For this particle,

$$\beta = \frac{v}{c} = \frac{6 \times 10^7}{3 \times 10^8} = 0.2$$

Using Eqs. 3.4 and 3.7,

$$T = (\gamma - 1)Mc^2 = \left(\frac{1}{\sqrt{1 - \beta^2}} - 1\right)Mc^2 = \left(\frac{1}{\sqrt{1 - 0.2^2}} - 1\right)Mc^2$$

$$= (1.021 - 1)Mc^2 = 0.021Mc^2 + (0.021)939.55 \text{ MeV} = 19.73 \text{ MeV}$$

$$= 3.16 \times 10^{-12} \text{ J}$$

The mass increase is $M^*/M = \gamma = 1.021$, i.e., a 2.1 percent mass increase.

## 3.3 ATOMS

To the best of our knowledge today, every atom consists of a central positively charged nucleus around which negative electrons revolve in stable orbits. Considered as a sphere, the atom has a radius of the order of $10^{-10}$ m and the nucleus has a radius of the order of $10^{-14}$ m. The number of electrons is equal to the number of positive charges of the nucleus; thus the atom is electrically neutral (in its normal state).

The number of positive elementary charges in the nucleus is called the *atomic number* and is indicated by $Z$. The atomic number identifies the chemical element. All atoms of an element have the same chemical properties.

The atomic electrons move around the nucleus as a result of the attractive electrostatic Coulomb force between the positive nucleus and the negative charge of the electron. According to classical electrodynamics, the revolving electrons ought to continuously radiate part of their energy, follow a spiral orbit, and eventually be captured by the nucleus. Obviously, this does not happen: atoms exist and are stable.

The available experimental evidence points toward the following facts regarding the motion of atomic electrons:

1. Bound atomic electrons revolve around the nucleus in stable orbits without radiating energy. Every orbit corresponds to a certain electron energy and is called an *energy state*.
2. Only certain orbits (only certain energies) are allowed. That is, the energy states of the bound electrons form a discrete spectrum, as shown in Fig. 3.1. This phenomenon is called *quantization.*
3. If an electron moves from an orbit (state) of energy $E_i$ to another of energy $E_f$, then (and only then) electromagnetic radiation, an X-ray, is emitted with frequency $\nu$ such that

$$\nu = \frac{E_i - E_f}{h} \tag{3.14}$$

where $h$ is Planck's constant.

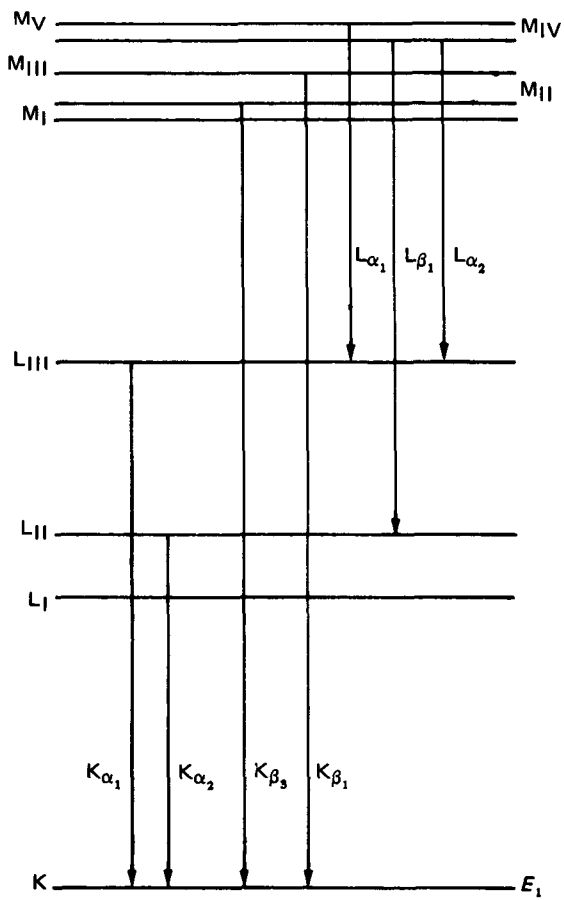


**Figure 3.1** An atomic energy level diagram showing X-ray nomenclature (not drawn to scale). $E_1$ = lowest energy state = ground state.

The energy of the X-ray depends on the atomic number:

$$E_x = h\nu = E_i - E_f = k(Z - a)^2 \tag{3.15}$$

where $k$ and $a$ are constants. X-ray energies range from a few eV for the light elements to a few hundreds of keV for the heaviest elements.

Every atom emits characteristic X-rays with discrete energies that identify the atom like fingerprints. For every atom, the, the X-rays are identified according to the final state of the electron transition that produced them. Historically, the energy states of atomic electrons are characterized by the letters K, L, M, N, etc. The K state or K orbit or K shell is the lowest energy state, also called the ground state. The X-rays that are emitted as a result of electronic transitions to the K state, from any other initial state, are called K X-rays (Fig. 3.1). Transitions to the L state give rise to L X-rays and so on. $K_\alpha$ and $K_\beta$ X-rays indicate transitions from L to K and M to K states, respectively.

A bound atomic electron may receive energy and move from a state of energy $E_1$ to another of higher energy $E_2$. This phenomenon is called excitation of the atom (Fig. 3.2). An excited atom moves preferentially to the lowest possible energy state. In times of the order of $10^{-8}$ s, the electron that jumped to $E_2$ or another from another state will fall to $E_1$ and an X-ray will be emitted.

An atomic electron may receive enough energy to leave the atom and become a free particle. This phenomenon is called *ionization*, and the positive entity left behind is called an ion. The energy necessary to cause ionization is the *ionization potential*. The ionization potential is not the same for all the electrons of the same atom because the electrons move at different distances from the nucleus. The closer the electron is to the nucleus, the more tightly bound it is and the greater its ionization potential becomes. Table 3.1 lists ionization potentials of the least bound electron for certain elements.

When two or more atoms join together and form a molecule, their common electrons are bound to the molecule. The energy spectrum of the molecule is also discrete, but more complicated than that shown in Fig. 3.1.

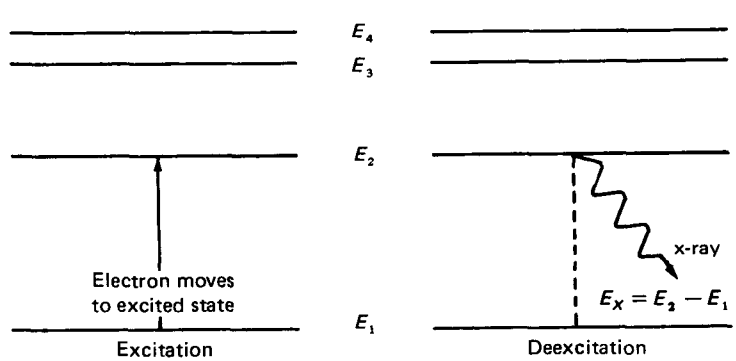


**Figure 3.2** Excitation and deexcitation of the atom.

**Table 3.1 Ionization Potential for the Least Bound Electron of Certain Elements**

| Element | Ionization potential (eV) | Element | Ionization potential (eV) |
|---|---|---|---|
| H | 13.6 | Ne | 21.56 |
| He | 24.56 | Na | 5.14 |
| Li | 5.4 | A | 15.76 |
| Be | 9.32 | Fe | 7.63 |
| B | 8.28 | Pb | 7.42 |
| C | 11.27 | U | 4.0 |

## 3.4 NUCLEI

At the present time, all experimental evidence indicates that nuclei consist of neutrons and protons, which are particles known as *nucleons*. Nuclei then consist of nucleons. Some of the properties of a neutron, a proton, and an electron, for comparison, are listed in Table 3.2. A free proton—outside the nucleus—will eventually pick up an electron and become a hydrogen atom, or it may be absorbed by a nucleus. A free neutron either will be absorbed by a nucleus or will decay according to the equation

$$n \rightarrow p^+ + e^- + \bar{\nu}$$

i.e., it will be transformed into a proton by emitting an electron and another particle called an *antineutrino*.

A nucleus consists of $A$ particles,

$$A = N + Z$$

where $A$ = mass number
$N$ = number of neutrons
$Z$ = number of protons = atomic number of the element

A nuclear species X is indicated as

$$^{A}_{Z}\mathrm{X}$$

where $X$ = chemical symbol of the element. For example,

$$^{16}_{8}\mathrm{O}$$

*Isobars* are nuclides that have the same $A$.

**Table 3.2 Neutron-Proton Properties**

| | Electron | Neutron | Proton |
|---|---|---|---|
| Rest mass | | | |
| kg | $9.109558 \times 10^{-31}$ | $1.674928 \times 10^{-27}$ | $1.672622 \times 10^{-27}$ |
| MeV | 0.511 | 939.552 | 938.258 |
| u | | 1.008665 | 1.007276 |
| Charge | $-e$ | 0 | $+e$ |

*Isotopes* are nuclides that have the same $Z$. They are nuclei of the same chemical element. They have the same chemical but slightly different physical properties, due to their difference in mass. The nuclear properties change drastically from isotope to isotope.

*Isotones* are nuclides that have the same $N$, i.e., the same number of neutrons.

*Isomers* are two different energy states of the same nucleus.

The different atomic species are the result of different combinations of one type of particle—the electron. There are 92 natural elements. Since 1940, 15 more have been artificially produced for a total of 107 elements. The different nuclides, on the other hand, are the result of different combinations of two kinds of particles, neutrons and protons, and so there are many more possibilities. There are more than 700 known nuclides.

Experiments have determined that nuclei are almost spherical, with a volume proportional to the mass number $A$ and a radius approximately equal to†

$$R = 1.3 \times 10^{-15} A^{1/3} \text{ in meters} \tag{3.16}$$

The mass of the nucleus with mass number $A$ and atomic number $Z$, indicated as $M_N(A, Z)$, is equal to

$$M_N(A, Z) = ZM_p + NM_n - B(A, Z)c^2 \tag{3.17}$$

where $M_p$ = mass of the proton
$M_n$ = mass of the neutron
$B(A, Z)$ = binding energy of the nucleus.

The binding energy is equal to the energy that was released when the $N$ neutrons and $Z$ protons formed the nucleus. More details about the binding energy are given in the next section.

The unit used for the measurement of nuclear mass is equal to $\frac{1}{12}$ of the mass of the isotope ${}^{13}_{6}\text{C}$. Its symbol is u (formerly amu for atomic mass unit):

$$1 \text{ u} = \tfrac{1}{12}\left(\text{mass of } {}^{12}_{6}\text{C}\right) = 1.660540 \times 10^{-27} \text{kg} = 931.481 \text{ MeV}$$

In many experiments, what is normally measured is the atomic, not the nuclear, mass. To obtain the atomic mass, one adds the mass of all the atomic electrons (see next section). A table of atomic masses of many isotopes is given in App. B. The mass may be given in any of the following three ways:

1. Units of u
2. Kilograms
3. Energy units (MeV or J), in view of the equivalence of mass and energy

†For nonspherical nuclei, the radius given by Eq. 3.16 is an average.

## 3.5 NUCLEAR BINDING ENERGY

The mass of a nucleus is given by Eq. 3.18 in terms of the masses of its constituents. That same equation also defines the binding energy of the nucleus:

$$B(A,Z) = \left[ZM_p + NM_n - M_N(A,Z)\right]c^2 \tag{3.18}$$

The factor $c^2$, which multiplies the mass to transform it into energy, will be omitted from now on. It will always be implied that multiplication or division by $c^2$ is necessary to obtain energy from mass or vice versa. Thus, Eq. 3.18 is rewritten as

$$B(A,Z) = ZM_p + NM_n - M_N(A,Z) \tag{3.19}$$

The meaning of $B(A,Z)$ may be expressed in two equivalent ways:

1. The binding energy $B(A,Z)$ of a nucleus is equal to the mass transformed into energy when the $Z$ protons and the $N = A - Z$ neutrons got together and formed the nucleus. An amount of energy equal to the binding energy was released when the nucleus was formed.
2. The binding energy $B(A,Z)$ is equal to the energy necessary to break the nucleus apart into its constituents, $Z$ free protons and $N$ free neutrons.

As mentioned in Section 3.4, atomic masses rather than nuclear masses are measured in most cases. For this reason, Eq. 3.19 will be expressed in terms of atomic masses by adding the appropriate masses of atomic electrons. If one adds and subtracts $Zm$ in Eq. 3.19,

$$\begin{aligned} B(A,Z) &= ZM_p + Zm + NM_n - M_N(A,Z) - Zm \\ &= Z(M_p + m) + NM_n - [M_N(A,Z) + Zm] \end{aligned} \tag{3.20}$$

Let

$M_H$ = mass of the hydrogen atom

$B_e$ = binding energy of the electron in the hydrogen atom

$B_e(A,Z)$ = binding energy of all the electrons of the atom whose nucleus has mass $M_N(A,Z)$

$M(A,Z)$ = mass of the atom with nuclear mass equal to $M_N(A,Z)$

Then

$$M_H = M_p + m - B_e \tag{3.21}$$

$$M(A,Z) = M_N(A,Z) + Zm - B_e(A,Z) \tag{3.22}$$

Combining Eqs. 3.20, 3.21, and 3.22, one obtains

$$B(A,Z) = ZM_H + NM_n - M(A,Z) - B_e(A,Z) + ZB_e \tag{3.23}$$

Unless extremely accurate calculations are involved, the last two terms of Eq. 3.23 are neglected. The error introduced by doing so is insignificant because $ZB_e$ and $B_e(A, Z)$ are less than a few keV and they tend to cancel each other, while $B(A, Z)$ is of the order of MeV. Equation 3.23 is, therefore, usually written as

$$B(A, Z) = ZM_H + NM_n - M(A, Z) \tag{3.24}$$

**Example 3.4** What is the total binding energy of ${}^{4}_{2}\mathrm{He}$?

**Answer** Using Eq. 3.24 and data from App. b,

$$\begin{aligned} B(4,2) &= 2M_H + 2M_n - M(4,2) \\ &= [2(1.00782522) + 2(1.00866544) - 4.00260361]\ \mathrm{u} \\ &= 0.03037771\ \mathrm{u} = (0.0303771\ \mathrm{u})931.478\ \mathrm{MeV/u} \\ &= 28.296\ \mathrm{MeV} = 4.53 \times 10^{-12}\ \mathrm{J} \end{aligned}$$

**Example 3.5** What is the binding energy of the nucleus ${}^{238}_{92}\mathrm{U}$?

**Answer**

$$\begin{aligned} B(238,92) &= [92(1.00782522) + 146(1.00866544) - 238.05076]\ \mathrm{u} \\ &= 1.93431448\ \mathrm{u} = (1.93431448\ \mathrm{u})931.478\ \mathrm{MeV/u} \\ &= 1801.771\ \mathrm{MeV} = 2.886 \times 10^{-10}\ \mathrm{J} \end{aligned}$$

The energy necessary to remove one particle from the nucleus is the *separation* or *binding energy* of that particle for that particular nuclide. A "particle" may be a neutron, a proton, an alpha particle, a deuteron, etc. The separation or binding energy of a nuclear particle is analogous to the ionization potential of an electron. If a particle enters the nucleus, an amount of energy equal to its separation energy is released.

The separation or binding energy of a neutron ($B_n$) is defined by the equation

$$B_n = M[(A - 1), Z] + M_n - M(A, Z) \tag{3.25}$$

Using Eq. 3.24, Eq. 3.25 is written

$$B_n = B(A, Z) - B[(A - 1), Z] \tag{3.26}$$

which shows that the binding energy of the last neutron is equal to the difference between the binding energies of the two nuclei involved. Typical values of $B_n$ are a few MeV (less than 10 MeV).

The separation or binding energy of a proton is

$$B_p = M(A - 1, Z - 1) + M_H - M(A, Z) \tag{3.27}$$

or, using Eq. 3.24,

$$B_p = B(A, Z) - B(A - 1, Z - 1) \tag{3.28}$$

The separation energy for an alpha particle is

$$B_\alpha = M(A-4, Z-2) + M_{\text{He}} - M(A, Z) \tag{3.29}$$

or, using Eq. 3.24,

$$B_\alpha = B(A, Z) - B(A-4, Z-2) - B(4, 2) \tag{3.30}$$

**Example 3.6** What is the separation energy of the last neutron of the ${}^4_2\text{He}$ nucleus?

**Answer** Using data from App. B and Eq. 3.25, one obtains

$$\begin{aligned} B_n &= M(3,2) + M_n - M(4,2) \\ &= [(3.016030 + 1.008665 - 4.002604)\ \text{u}]931.478\ \text{MeV/u} \\ &= 0.022091(931.478\ \text{MeV}) = 20.58\ \text{MeV} = 3.3 \times 10^{-12}\ \text{J} \end{aligned}$$

If the average binding energy per nucleon,

$$b(A, Z) = \frac{B(A, Z)}{A} \tag{3.31}$$

is plotted as a function of $A$, one obtains the result shown in Fig. 3.3. The

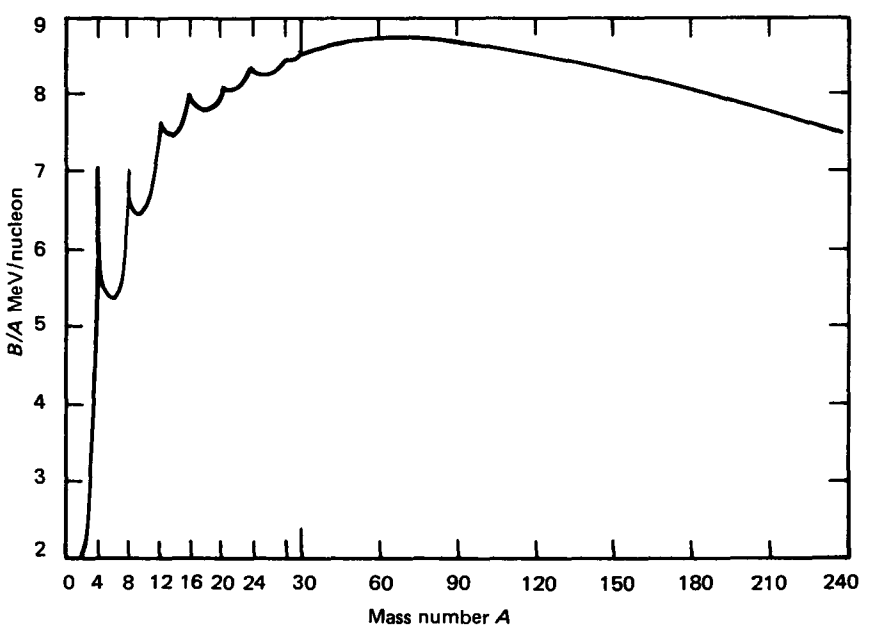


**Figure 3.3** The change of the average binding energy per nucleon with mass number $A$. Notice the change in scale after $A = 30$. (From *The Atomic Nucleus* by R. D. Evans. Copyright © 1972 by McGraw-Hill. Used with the permission of McGraw-Hill Book Company.)

average binding energy changes relatively little, especially for $A > 30$. Notice that Fig. 3.3 has a different scale for $A < 30$.

Figure 3.3 is very important because it reveals the processes by which energy may be released in nuclear reactions. If one starts with a very heavy nucleus ($A = 240$) and breaks it into two medium-size nuclei (fission), energy will be released because the average binding energy per nucleon is larger for nuclides in the middle of the periodic table than it is for heavy nuclides. On the other hand, if one takes two very small nuclei ($A = 2, 3$) and fuses them into a larger one, energy is again released due to similar increase in the average binding energy per nucleon.

## 3.6 NUCLEAR ENERGY LEVELS

Neutrons and protons are held together in the nucleus by nuclear forces. Although the exact nature of nuclear forces is not known, scientists have successfully predicted many characteristics of nuclear behavior by assuming a certain form for the force and constructing nuclear models based on that form. The success of these models is measured by how well their predicted results agree with the experiment. Many nuclear models have been proposed, each of them explaining certain features of the nucleus; but as of today, no model exists that explains all the facts about all the known nuclides.

All the nuclear models assume that the nucleus, like the atom, can exist only in certain discrete energy states. Depending on the model, the energy states may be assigned to the nucleons—neutrons and protons—or the nucleus as a whole. The present discussion of nuclear energy levels will be based on the second approach.

The lowest possible energy state of a nucleus is called the ground state (Fig. 3.4). In Fig. 3.4, the ground state is shown as having negative energy to indicate a bound state. The ground state and all the excited states below the zero energy level are called bound states. If the nucleus finds itself in any of the bound

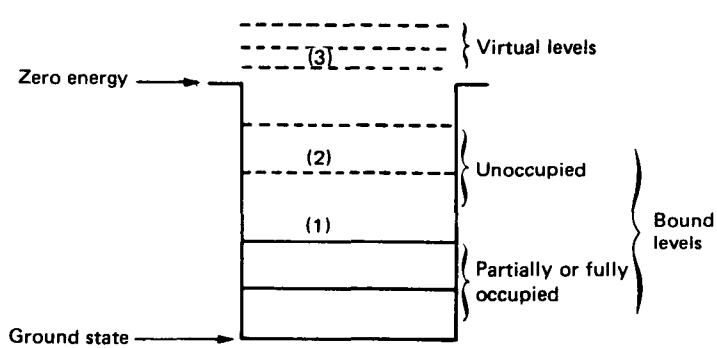


**Figure 3.4** Bound and virtual nuclear energy levels.

states, it deexcites after a time of the order of $10^{-12}$ to $10^{-10}$ s by dropping to a lower state. Deexcitation is accompanied by the emission of a photon with energy equal to the difference between the energies of the initial and final states. Energy states located above the zero energy level are called virtual energy levels. If the nucleus obtains enough energy to be raised to a virtual level, it may deexcite either by falling to one of the bound levels or by emitting a nucleon.

Studies of the energy levels of all the known nuclides reveal the following:

1. The distance between nuclear energy levels is of the order of keV to MeV. By contrast, the distance between atomic levels is of the order of eV.
2. The distance between levels decreases as the excitation energy increases (Fig. 3.5). For very high excitation energies, the density of levels becomes so high that it is difficult to distinguish individual energy levels.
3. As the mass number $A$ increases, the number of levels increases; i.e., heavier nuclei have more energy levels than lighter nuclei (in general—there may be exceptions).
4. As $A$ increases, the energy of the first excited state decreases (again, in general—exceptions exist). For example,

$^{9}$Be: first excited state is at 1.68 MeV

$^{56}$Fe: first excited state is at 0.847 MeV

$^{238}$U: first excited state is at 0.044 MeV

## 3.7 ENERGETICS OF NUCLEAR DECAYS

This section discusses the energetics of $\alpha$, $\beta$, and $\gamma$ decay, demonstrating how the kinetic energies of the products of the decay can be calculated from the masses of the particles involved. In all cases, it will be assumed that the original unstable nucleus is at rest—i.e., it has zero kinetic energy and linear momentum. This assumption is very realistic because the actual kinetic energies of nuclei due to thermal motion are of the order of $kT$ (of the order of eV), where $k$ is the Boltzmann constant and $T$ the temperature (Kelvin), while the energy released in most decays is of the order of MeV.

In writing the equation representing the decay, the following notation will be used:

$M$ = atomic mass (or $Mc^2$ = rest mass energy)

$E_\gamma$ = energy of a photon

$T_i$ = kinetic energy of a particle type $i$

$P_i$ = linear momentum of a particle type $i$

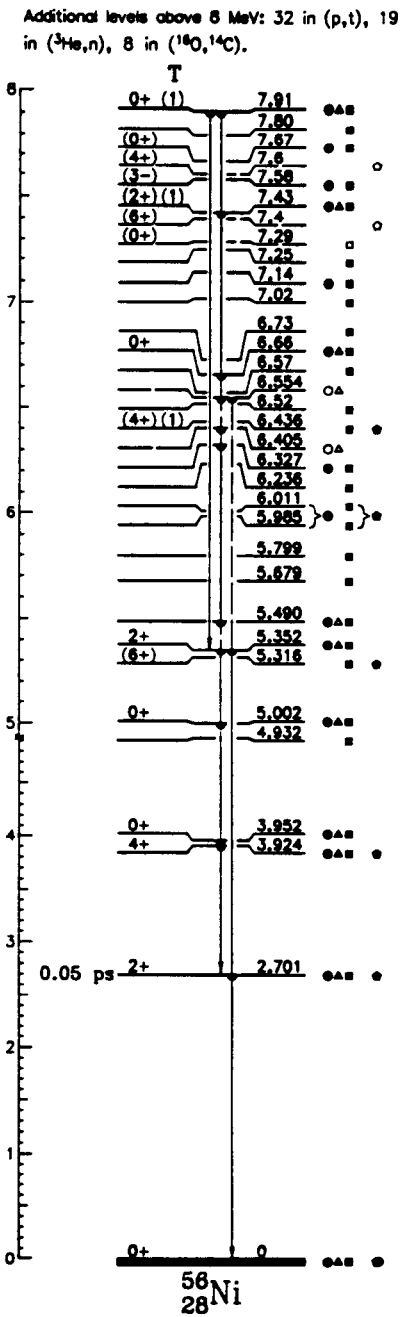


**Figure 3.5** The energy levels of $^{56}_{28}$Ni. In this diagram the zero energy has been switched to the ground state of the nucleus. The numbers on the right-hand column show the energy of each level in MeV (Ref. 4, p. 163).

### 3.7.1 Gamma Decay

In $\gamma$ decay, a nucleus goes from an excited state to a state of lower energy and the energy difference between the two states is released in the form of a photon. Gamma decay is represented by

$$ {}^{A}_{Z}\mathrm{X}^* \rightarrow {}^{A}_{Z}\mathrm{X} + \gamma $$

where ${}^{A}_{Z}\mathrm{X}^*$ indicates the excited nucleus.

Applying conservation of energy and momentum for the states before and after the decay, we have†

*Conservation of energy*:

$$ M^*(A, Z) = M(A, Z) + T_M + E_\gamma \tag{3.32} $$

*Conservation of momentum*:

$$ 0 = \mathbf{P}_M + \mathbf{P}\gamma \tag{3.33} $$

Using these two equations and the nonrelativistic form of the kinetic energy of the nucleus,

$$ T_M = \frac{1}{2}MV^2 = \frac{P_M^2}{2M} = \frac{P_\gamma^2}{2M} = \frac{E_\gamma^2}{2Mc^2} \tag{3.34} $$

Use has been made of the relationship $E_\gamma = P_\gamma c$ (the photon rest mass is zero). Equation 3.34 gives the kinetic energy of the nucleus after the emission of a photon of energy $E_\gamma$. This energy is called the *recoil energy*.

The recoil energy is small. Consider a typical photon of 1 MeV emitted by a nucleus with $A = 50$. Then, from Eq. 3.34,

$$ T_M \approx \frac{1^2\ (\mathrm{MeV})^2}{2(50)(932)(\mathrm{MeV})} \approx 11\ \mathrm{eV} $$

Most of the time, this energy is neglected and the gamma energy is written as

$$ E_\gamma = M^*(A, Z) - M(A, Z) $$

However, there are cases where the recoil energy may be important, e.g., in radiation damage studies.

Sometimes the excitation energy of the nucleus is given to an atomic electron instead of being released in the form of a photon. This type of nuclear transition is called internal conversion (IC), and the ejected atomic electron is called an internal conversion electron.

†Equations in this chapter are written in terms of atomic, not nuclear, masses. This notation introduces a slight error because the binding energy of the atomic electrons is not taken into account (see Sec. 3.5).

Let $T_i$ be the kinetic energy of an electron ejected from shell $i$ and $B_i$ be the binding energy of an electron in shell $i$. Equation 3.32 now takes the form

$$M^*(A, Z) = M(A, Z) + T_i + B_i + T_M \tag{3.35}$$

Even though the electron has some nonzero rest mass energy, it is so much lighter than the nucleus that $T_M \ll T_i$. Consequently, $T_M$ is neglected and Eq. 3.35 is written as

$$T_i = M^*(A, Z) - M(A, Z) - B_i \tag{3.36}$$

If $Q = M^*(A, Z) - M(A, Z) =$ energy released during the transition, then

$$T_i = Q - B_i$$

When internal conversion occurs, there is a probability than an electron from the K shell, L shell, or another shell, may be emitted. The corresponding equations for the electron kinetic energies are

$$\begin{aligned} T_{\mathrm{K}} &= Q - B_{\mathrm{K}} \\ T_{\mathrm{L}} &= Q - B_{\mathrm{L}} \\ T_{\mathrm{M}} &= Q - B_{\mathrm{M}} \quad \text{etc.} \end{aligned} \tag{3.37}$$

Therefore, a nucleus that undergoes internal conversion is a source of groups of monoenergetic electrons with energies given by Eqs. 3.37. A typical internal conversion electron spectrum is shown in Fig. 3.6. The two peaks correspond to K and L electrons. The diagram on the right (Fig. 3.6) shows the transition

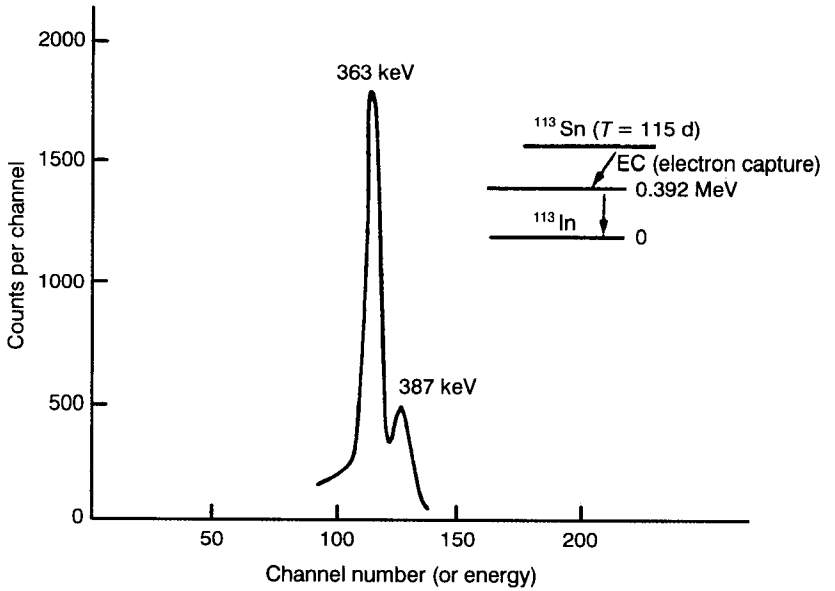


**Figure 3.6** The internal conversion spectrum of $^{113}$Sn. The two peaks correspond to K electrons (363 keV) and L electrons (387 keV).

energy to be 392 keV. The K-shell energy is then $B_K = 392 - 363 = 29$ keV and the L-shell binding energy is $B_L = 392 - 387 = 5$ keV. Let:

$\lambda_e$ = probability that internal conversion will occur

$\lambda_\gamma$ = probability that a photon will be emitted

$\lambda_i$ = probability that an electron from shell $i$ will be emitted

$\lambda$ = total probability for $\gamma$ decay

Then†

$$\lambda_e = \lambda_K + \lambda_L + \lambda_M + \cdots \tag{3.38}$$

and

$$\lambda = \lambda_\gamma + \lambda_e \tag{3.39}$$

For most nuclei, $\lambda_e = 0$, but there is no $\gamma$-decaying nucleus for which $\lambda_\gamma = 0$. This means radioisotopes that internally convert, emit gammas as well as electrons. After an atomic electron is emitted, the empty state that was created will quickly be filled by another electron that "falls in" from the outer shells. As a result of such a transition, an X-ray is emitted. Therefore, internally converting nuclei *emit $\gamma$-rays*, *electrons*, and *X-rays*.

Radioisotopes that undergo internal conversion are the only sources of monoenergetic electrons, except for accelerators. They are very useful as instrument calibration sources. Three isotopes frequently used are $^{113}$Sn, $^{137}$Cs, and $^{207}$Bi.

### 3.7.2 Alpha Decay

Alpha decay is represented by the equation

$$^{A}_{Z}\mathrm{X} \rightarrow {}^{A-4}_{Z-2}\mathrm{X} + {}^{4}_{2}\mathrm{He}$$

Applying conservation of energy and momentum,

$$M(A, Z) = M(A - 4, Z - 2) + M(4, 2) + T_M + T_\alpha \tag{3.40}$$

and

$$0 = \mathbf{P}_\alpha + \mathbf{P}_M \tag{3.41}$$

The energy that becomes available as a result of the emission of the alpha particle is called the *decay energy* $Q_\alpha$, defined by

$$\begin{aligned} Q_\alpha &= (\text{mass of parent}) - (\text{mass of decay products}) \\ Q_\alpha &= M(A, Z) - M(A - 4, Z - 2) - M(4, 2) \end{aligned} \tag{3.42}$$

†Tables of isotopes usually give, not the values of the different $\lambda$'s, but the so-called IC coefficients, which are the ratios $\lambda_K/\lambda_\gamma$, $\lambda_L/\lambda_\gamma$, etc. (see Ref. 4).

Obviously, for $\alpha$ decay to occur, $Q_\alpha$ should be greater than zero. Therefore, $\alpha$ decay is possible only when

$$M(A, Z) > M(A - 4, Z - 2) + M(4, 2) \tag{3.43}$$

If the daughter nucleus is left in its ground state, after the emission of the alpha, the kinetic energy of the two products is (from Eq. 3.40),

$$T_M + T_\alpha = Q_\alpha \tag{3.44}$$

In many cases, the daughter nucleus is left in an excited state of energy $E_i$, where $i$ indicates the energy level. Then, Eq. 3.44 becomes

$$T_M + T_\alpha = Q_\alpha - E_i \tag{3.45}$$

which shows that the available energy ($Q_\alpha$) is decreased by the amount $E_i$.

The kinetic energies $T_\alpha$ and $T_M$ can be calculated from Eqs. 3.41 and 3.44. The result is

$$T_\alpha = \frac{M(A - 4, Z - 2)}{M(A - 4, Z - 2) + M(4, 2)}(Q_\alpha - E_i) \approx \frac{A - 4}{A}(Q_\alpha - E_i) \tag{3.46}$$

$$T_M = \frac{M_\alpha}{M(A - 4, Z - 2) + M(4, 2)}(Q_\alpha - E_i) \approx \frac{4}{A}(Q_\alpha - E_i) \tag{3.47}$$

**Example 3.7** What are the kinetic energies of the alphas emitted by $^{238}$U?

**Answer** The decay scheme of $^{238}_{92}$U is shown in Fig. 3.7. After the alpha is emitted, the daughter nucleus, $^{234}_{90}$Th, may be left in one of the two excited states at 0.16 MeV and 0.048 MeV or go to the ground state.

The decay energy $Q_\alpha$ is (Eq. 3.42)

$$\begin{aligned} Q_\alpha &= M(238, 92) - M(234, 90) - M(4, 2) \\ &= 238.050786 - 234.043594 - 4.002603 \\ &= 0.004589 \text{ u} = 0.004589 \times 931.481 \text{ MeV} = 4.27 \text{ MeV} \end{aligned}$$

Depending on the final state of $^{234}_{90}$Th, the energy of the alpha particle is

$$T_\alpha = \tfrac{234}{238} Q_\alpha = 4.20 \text{ MeV}$$

$$T_\alpha = \tfrac{234}{238}(Q_\alpha - 0.048) = 4.15 \text{ MeV}$$

$$T_\alpha = \tfrac{234}{238}(Q_\alpha - 0.16) = 4.04 \text{ MeV}$$

### 3.7.3 Beta Decay

In $\beta$ decay, a nucleus emits an electron or a positron and is transformed into a new element. In addition to the electron or the positron, a neutral particle with rest mass zero is also emitted. There are two types of $\beta$ decay, $\beta^-$ and $\beta^+$.

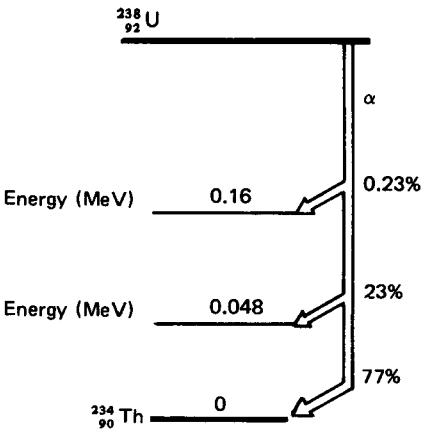


**Figure 3.7** The alpha decay scheme of $^{238}$U. The percentage values give the probability of decay through the corresponding level (from Ref. 4).

**β⁻ Decay.** This type of decay is represented by

$$ {}^{A}_{Z}\mathrm{X} \rightarrow {}_{Z+1}^{A}\mathrm{X} + \beta^- + \bar{\nu} $$

where $\beta^-$ = negative beta particle = electron
$\bar{\nu}$ = antineutrino

Historically, the name $\beta$ particle has been given to electrons that are emitted by nuclei undergoing beta decay. The antineutrino ($\bar{\nu}$) is a neutral particle with rest mass so small that it is taken equal to zero.

The energy equation of $\beta^-$ decay is

$$ M_N(A, Z) = M_N(A, Z + 1) + m + T_{\beta^-} + T_{\bar{\nu}} + T_M \tag{3.48} $$

where $M_N(A, Z)$ is the *nuclear* mass and $m$ is the electron rest mass. Using atomic masses, Eq. 3.48 becomes (see Sec. 3.5)

$$ M(A, Z) = M(A, Z + 1) + T_{\beta^-} + T_{\bar{\nu}} + T_M \tag{3.49} $$

The momentum equation is

$$ 0 = \mathbf{P}_M + \mathbf{P}_{\beta^-} + \mathbf{P}_{\bar{\nu}} \tag{3.50} $$

The $\beta^-$ decay energy, $Q_{\beta^-}$, is defined as

$$ Q_{\beta^-} = M(A, Z) - M(A, Z + 1) \tag{3.51} $$

The condition for $\beta^-$ decay to be possible is

$$ M(A, Z) - M(A, Z + 1) > 0 \tag{3.52} $$

In terms of $Q_{\beta^-}$, Eq. 3.49 is rewritten in the form

$$ T_{\beta^-} + T_{\bar{\nu}} + T_M = Q_{\beta^-} \tag{3.53} $$

Equations 3.50 and 3.53 show that three particles, the nucleus, the electron, and the antineutrino, share the energy $Q_{\beta^-}$, and their total momentum is zero.

There is an infinite number of combinations of kinetic energies and momenta that satisfy these two equations and as a result, the energy spectrum of the betas is continuous.

In Eq. 3.53, the energy of the nucleus, $T_M$, is much smaller than either $T_{\beta^-}$ or $T_{\bar{\nu}}$ because the nuclear mass is huge compared to that of the electron or the antineutrino. For all practical purposes, $T_M$ can be neglected and Eq. 3.53 takes the form

$$T_{\beta^-} + T_{\bar{\nu}} = Q_{\beta^-} \tag{3.54}$$

As in the case of $\alpha$ decay, the daughter nucleus may be left in an excited state after the emission of the $\beta^-$ particle. Then, the energy available to become kinetic energy of the emitted particles is less. If the nucleus is left in the $i$th excited state $E_i$, Eq. 3.54 takes the form

$$T_{\beta^-} + T_{\bar{\nu}} = Q_{\beta^-} - E_i = E_{\max} \tag{3.55}$$

According to Eq. 3.54, the electron and the antineutrino share the energy $Q_{\beta^-}$ (or $E_{\max}$) and there is a certain probability that either particle may have an energy within the limits

$$0 \leq T_{\beta^-} \leq E_{\max} \tag{3.56}$$

$$E_{\max} \geq T_{\bar{\nu}} \geq 0 \tag{3.57}$$

which means that the beta particles have a continuous energy spectrum. Let $\beta(T)\,dT$ be the number of beta particles with kinetic energy between $T$ and $T + dT$. The function $\beta(T)$ has the general shape shown in Fig. 3.8. The energy spectrum of the antineutrinos is the complement of that shown in Fig. 3.8, consistent with Eq. 3.57. The continuous energy spectrum of $\beta^-$ particles should be contrasted with the energy spectrum of internal conversion electrons shown by Fig. 3.6.

As stated earlier, beta particles are electrons. The practical difference between the terms *electrons* and *betas* is this: A beam of electrons of energy $T$ consists of electrons each of which has the kinetic energy $T$. A beam of beta particles with energy $E_{\max}$ consists of electrons that have a continuous energy spectrum (Fig 3.8) ranging from zero up to a maximum kinetic energy $E_{\max}$.

Figure 3.9 shows the $\beta^-$ decay scheme of the isotope ${}^{137}_{55}\text{Cs}$. For an example of a $Q_{\beta^-}$ calculation, consider the decay of ${}^{137}_{55}\text{Cs}$:

$$Q_{\beta^-} = M(55, 137) - M(56, 137) = (136.90682 - 136.90556\ \text{u} = 0.00126\ \text{u}$$

$$= 0.0012625(931.478\ \text{MeV}) = 1.1760\ \text{MeV} = 1.36 \times 10^{-13}\ \text{J}$$

If the ${}^{137}_{56}\text{Ba}$ is left in the 0.6616-MeV state (which happens 93.5 percent of the time), the available energy is

$$E_{\max} = 1.1760 - 0.6616 = 0.5144\ \text{MeV}$$

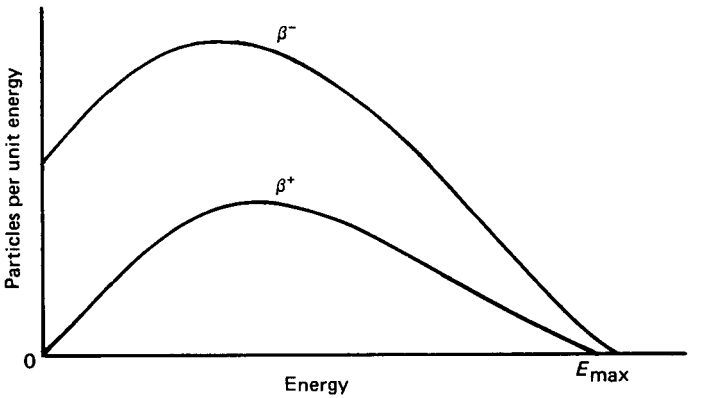


**Figure 3.8** A typical beta energy spectrum (shows shape only; does not mean that $\beta^-$ is more intense than $\beta^+$).

For many calculations it is necessary to use the average energy of the beta particles, $\bar{E}_{\beta^-}$. An accurate equation for $\bar{E}_{\beta^-}$ has been developed,[1] but in practice the average energy is taken to be

$$\bar{E}_{\beta^-} = \frac{E_{max}}{3}$$

**$\beta^+$ Decay.** The expression representing $\beta^+$ decay is

$$^{A}_{Z}X \rightarrow {}_{Z-1}^{A}X + \beta^+ + \nu$$

where $\beta^+$ = positron
$\nu$ = neutrino

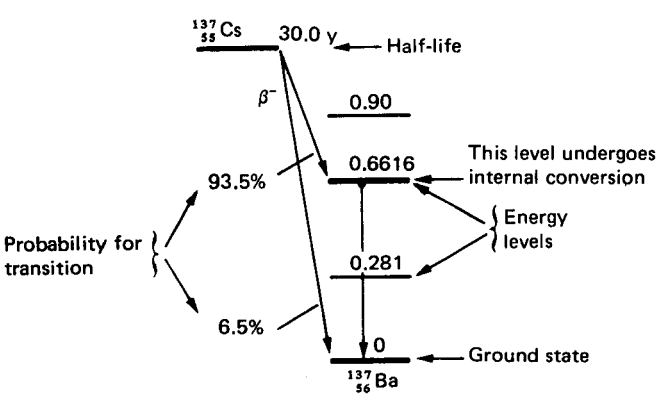


**Figure 3.9** The decay scheme of $^{137}$Cs. The $Q$ value of the $\beta^-$ decay is $-1.176$ MeV (from Ref. 4). Probability for each transition is given in percent.

The energy equation of $\beta^+$ decay is

$$M_N(A, Z) = M_N(A, Z - 1) + m + T_{\beta^+} + T_\nu + T_M \tag{3.58}$$

Using atomic masses, Eq. 3.58 becomes

$$M(A, Z) = M(A, Z - 1) + 2m + T_{\beta^+} + T_\nu + T_M \tag{3.59}$$

The momentum equation is

$$0 = \mathbf{P}_m + \mathbf{P}_{\beta^+} + \mathbf{P}_\nu \tag{3.60}$$

The $\beta^+$ decay energy is

$$Q_{\beta^+} = M(A, Z) - M(A, Z - 1) - 2m \tag{3.61}$$

The condition for $\beta^+$ decay to be possible is

$$M(A, Z) - M(A, Z - 1) - 2m > 0 \tag{3.62}$$

A comparison of Eqs. 3.52 and 3.62 shows that $\beta^-$ decay is possible if the mass of the parent is just bigger than the mass of the daughter nucleus, while $\beta^+$ decay is possible only if the parent and daughter nuclear masses differ by at least $2mc^2 = 1.022$ MeV.

The energy spectrum of $\beta^+$ particles is continuous, for the same reasons the $\beta^-$ spectrum is, and similar to that of $\beta^-$ decay (Fig. 3.8). The average energy of the positrons from $\beta^+$ decay, $\overline{E}_{\beta^+}$, is also taken to be equal to $E_{\max}/3$ unless extremely accurate values are needed, in which case the equation given in Ref. 1 should be used.

A typical $\beta^+$ decay scheme is shown in Fig. 3.10.

**Electron Capture.** In some cases, an atomic electron is captured by the nucleus and a neutrino is emitted according to the equation

$$M_N(A, Z) + m = M_N(A, Z - 1) + T_\nu + B_e \tag{3.63}$$

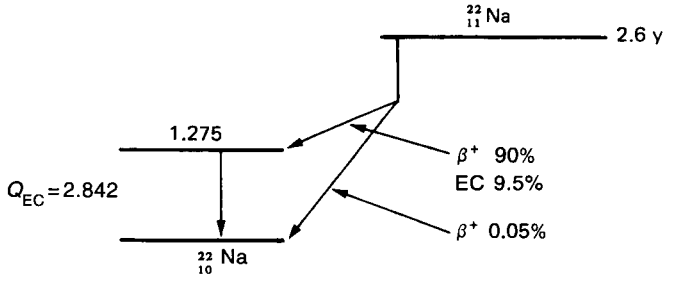


**Figure 3.10** The decay scheme of $^{22}$Na. Notice that it is $Q_{EC}$ that is plotted, not $Q_{\beta^+}$ (from Ref. 4).

In Eq. 3.63 all the symbols have been defined before except $B_e$, binding energy of the electron captured by the nucleus. This transformation is called *electron capture* (EC). In terms of atomic masses, Eq. 3.63 takes the form

$$M(A, Z) = M(A, Z - 1) + T_\nu \tag{3.64}$$

The energy $Q_{EC}$ released during EC is

$$Q_{EC} = M(A, Z) - M(A, Z - 1) \tag{3.65}$$

The condition for EC to be possible is

$$M(A, Z) - M(A, Z - 1) > 0 \tag{3.66}$$

Electron capture is an alternative to $\beta^+$ decay. Comparison of Eqs. 3.61 and 3.66 shows that nuclei that cannot experience $\beta^+$ decay can undergo EC, since a smaller mass difference is required for the latter process. Of course, EC is always possible if $\beta^+$ decay is. For example, $^{22}$Na (Fig. 3.10) decays both by $\beta^+$ and EC.

After EC, there is a vacancy left behind that is filled by an electron falling in from a higher orbit. Assuming that a K electron was captured, an L electron may fill the empty state left behind. When this happens, an energy approximately equal to $B_K - B_L$ becomes available (where $B_K$ and $B_L$ are the binding energy of a K or L electron, respectively). The energy $B_K - B_L$ may be emitted as a K X-ray called *fluorescent radiation*, or it may be given to another atomic electron. If this energy is given to an L electron, that particle will be emitted with kinetic energy equal to $(B_K - B_L) - B_L = B_K - 2B_L$. Atomic electrons emitted in this way are called *Auger electrons*.

Whenever an atomic electron is removed and the vacancy left behind is filled by an electron from a higher orbit, there is a competition between the emission of Auger electrons and fluorescent radiation. The number of X-rays emitted per vacancy in a given shell is the *fluorescent yield*. The fluorescent yield increases with atomic number.

### 3.7.4 Particles, Antiparticles, and Electron-Positron Annihilation

Every known subatomic particle has a counterpart called the *antiparticle*. A charged particle and an antiparticle have the same mass, and opposite charge. If a particle is neutral—for example, the neutron—its antiparticle is still neutral. Then their difference is due to some other property, such as magnetic moment. Some particles, like the photon, are identical with their own antiparticles. An antiparticle cannot exist together with the corresponding particle: when an antiparticle meets a particle, the two react and new particles appear.

Consider the example of the electron and the "antielectron," which is the positron. The electron and the positron are identical particles except for their charge, which is equal to $e$ but negative and positive, respectively. The rest mass of either particle is equal to 0.511 MeV. A positron moving in a medium loses

energy continuously, as a result of collisions with atomic electrons (see Chap. 4). Close to the end of its track, the positron combines with an atomic electron, the two annihilate, and photons appear with a total energy equal to $2mc^2$. At least two photons should be emitted for conservation of energy and momentum to be satisfied (Fig. 3.11). Most of the time, two photons, each with energy 0.511 MeV, are emitted. As a result, every positron emitter is also a source of 0.511-MeV annihilation gammas.

### 3.7.5 Complex Decay Schemes

For many nuclei, more than one mode of decay is positive. Users of radioisotopic sources need information about particles emitted, energies, and probabilities of emission. Many books on atomic and nuclear physics contain such information, and the most comprehensive collection of data on this subject can be found in the *Table of Isotopes* by Lederer and Shirley.[4] Figure 3.12 shows an example of a complex decay scheme taken from that book.

## 3.8 THE RADIOACTIVE DECAY LAW

Radioactive decay is spontaneous change of a nucleus. The change may result in a new nuclide or simply change the energy of the nucleus. If there is a certain amount of a radioisotope at hand, there is no certainty that in the next second "so many nuclei will decay" or "none will decay." One can talk of the probability that a nucleus will decay in a certain period of time.

The probability that a given nucleus will decay per unit time is called the *decay constant* and is indicated by the letter $\lambda$. For a certain species, $\lambda$ is

1. The same for all the nuclei
2. Constant, independent of the number of nuclei present
3. Independent of the age of the nucleus

Consider a certain mass $m$ of a certain radioisotope with decay constant $\lambda$. The number of atoms (or nuclei) in the mass $m$ is equal to

$$N = m\frac{N_A}{A} \tag{3.67}$$

where $N_A = 6.022 \times 10^{23}$ = Avogadro's number
$A$ = atomic weight of the isotope

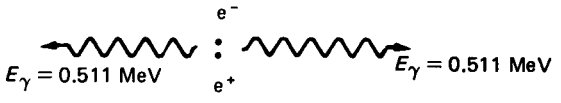


**Figure 3.11** Electron-positron annihilation.

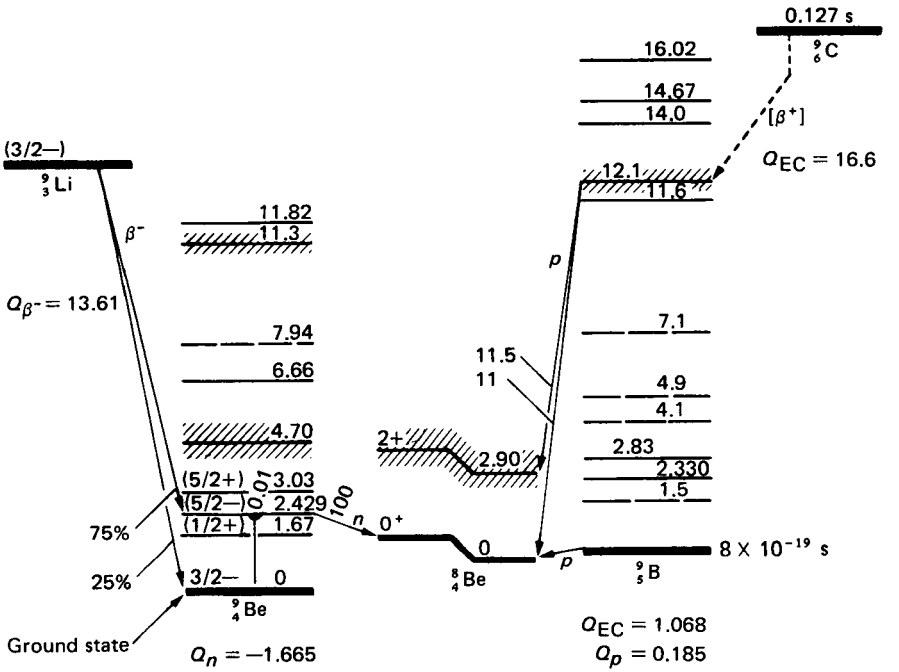


**Figure 3.12** A complex decay scheme. For complete explanation of all the symbols and numbers see Ref. 4. Half-life is given for each element's ground state, and energy of each level is given at intermediate states. $Q_n$ is the neutron separation energy. Transition probabilities are indicated as percentages (from Ref. 4).

This number of atoms decreases with time, due to the decay according to

$$\text{Decrease per unit time} = \text{decay per unit time}$$

or mathematically,

$$-\frac{dN(t)}{dt} = \lambda N(t) \tag{3.68}$$

The solution of this equation is

$$N(t) = N(0)e^{-\lambda t} \tag{3.69}$$

where $N(0)$ = number of atoms at $t = 0$.

The probability that a nucleus *will not decay* in time $t$—i.e., it will survive time $t$— is given by the ratio of

$$\frac{\text{atoms not decaying in time } t}{\text{atoms at } t = 0} = \frac{N(0)e^{-\lambda t}}{N(0)} = e^{-\lambda t} \tag{3.70}$$

The probability that the nucleus will decay between $t$ and $t + dt$ is

$p(t)\,dt$ = (probability to survive to time $t$)(probablility to decay in $dt$) $= e^{-\lambda t}\,\lambda\,dt$

The average lifetime $\bar{t}$ of the nucleus is given by

$$\bar{t} = \frac{\int_0^\infty tp(t)\,dt}{\int_0^\infty p(t)\,dt} = \frac{\int_0^\infty te^{-\lambda t}\,dt}{\int_0^\infty e^{-\lambda t}\,dt} = \frac{1}{\lambda} \tag{3.71}$$

One concept used extensively with radioisotopes in the *half-life* $T$, defined as the time it takes for half of a certain number of nuclei to decay. Thus, using Eq. 3.69,

$$\frac{N(T)}{N(0)} = \frac{1}{2} = e^{-\lambda T}$$

which then gives the relationship between $\lambda$ and $T$:

$$T = \frac{\ln 2}{\lambda} \tag{3.72}$$

For a sample of $N(t)$ nuclei at time $t$, each having decay constant $\lambda$, the expected number of nuclei decaying per unit time is

$$A(t) = \lambda N(t) \tag{3.73}$$

where $A(t)$ = activity of the sample at time $t$.

The units of activity are the Becquerel (Bq), equal to 1 decay/s, or the Curie (Ci) equal to $3.7 \times 10^{10}$ Bq. The Becquerel is the SI unit defined in 1977.

The term *specific activity* (SA) is used frequently. It may have one of the two following meanings:

1. For solids,

$$\text{SA} = \frac{\text{activity}}{\text{mass}}\ (\text{Bq/kg or Ci/g})$$

2. For gases or liquids,

$$\text{SA} = \frac{\text{activity}}{\text{volume}}\ (\text{Bq/m}^3 \text{ or Ci/cm}^3)$$

**Example 3.8** What is the SA of $^{60}$Co?

**Answer** The SA is

$$\text{SA} = \frac{A}{m} = \frac{\lambda N}{m} = \frac{\ln 2}{Tm} m \frac{N_A}{A} = \frac{(\ln 2)(6.022 \times 10^{23})}{(5.2\text{ y})(3.16 \times 10^7\text{ s/y})(0.060\text{ kg})}$$

$$= 4.23 \times 10^{16}\text{ Bq/kg} = 1.14 \times 10^3\text{ Ci/g}$$

**Example 3.9** What is the SA of a liquid sample of $10^{-3}$ m$^3$ containing $10^{-6}$ kg of $^{32}$P?

**Answer** The SA is

$$\mathrm{SA} = \frac{A}{V} = \frac{\lambda N}{V} = \frac{\ln 2}{VT} m \frac{N_A}{A} = \frac{(\ln 2)(10^{-6}\,\mathrm{kg})(6.022 \times 10^{23})}{(10^{-3}\,\mathrm{m}^3)(14.3\,\mathrm{d})(86400\,\mathrm{s/d})(0.032\,\mathrm{kg})}$$

$$= 1.05 \times 10^{16}\ \mathrm{Bq/m^3} = 0.285\ \mathrm{Ci/cm^3}$$

There are isotopes that decay by more than one mode. Consider such an isotope decaying by the modes $1, 2, 3, \ldots, i$ (e.g., alpha, beta, gamma, etc., decay), and let

$\lambda_i$ = probability per unit time that the nucleus will decay by the $i$th mode

The total probability of decay (total decay constant) is

$$\lambda = \lambda_1 + \lambda_2 + \cdots + \lambda_i + \cdots \tag{3.74}$$

If the sample contains $N(t)$ atoms at time $t$, the number of decays per unit time by the $i$th mode is

$$A_i(t) = \lambda_i N(t) = \lambda_i N(0) e^{-\lambda t} \tag{3.73a}$$

The term *partial half-life* is sometimes used to indicate a different decay mode. If $T_i$ is the partial half-life for the $i$th decay mode, using Eqs. 3.72 and 3.74, one obtains

$$\frac{1}{T} = \frac{1}{T_1} + \frac{1}{T_2} + \frac{1}{T_3} + \cdots + \frac{1}{T_i} + \cdots \tag{3.75}$$

It should be pointed out that it is the total decay constant that is used by Eqs. 3.69 and 3.73*a*, and not the partial decay constants.

**Example 3.10** The isotope $^{252}$Cf decays by alpha decay and by spontaneous fission. The total half-life is 2.646 years and the half-life for alpha decay is 2.731 years. What is the number of spontaneous fissions per second per $10^{-3}$ kg (1 g) of $^{252}$Cf?

**Answer** The spontaneous fission activity is

$$A_{\mathrm{sf}} = \lambda_{\mathrm{sf}} N = \frac{\ln 2}{T_{\mathrm{sf}}} m \frac{N_A}{A}$$

The spontaneous fission half-life is, using Eq. 3.75,

$$T_{\mathrm{sf}} = \frac{T_t T_\alpha}{T_\alpha - T_t} = \frac{(2.646 \times 2.731)}{2.731 - 2.646} = 85\mathrm{y} = 2.68 \times 10^9\ \mathrm{s}$$

Therefore,

$$A_{sf} = \frac{\ln 2}{2.68 \times 10^9 \text{ s}}(10^{-3} \text{ kg})\frac{6.022 \times 10^{22}}{252 \times 10^3} \text{ atoms/kg} = 6.17 \times 10^{11} \text{ sf/s}$$

Sometimes the daughter of a radioactive nucleus may also be radioactive and decay to a third radioactive nucleus. Thus, a radioactive chain

$$N_1 \rightarrow N_2 \rightarrow N_3 \rightarrow \text{etc.}$$

is generated. An example of a well-known series is that of $^{235}U$, which through combined $\alpha$ and $\beta^-$ decays ends up as an isotope of lead. The general equation giving the number of atoms of the $i$th isotope, at time $t$ in terms of the decay constants of all the other isotopes in the chain was developed by Bateman.[2] If $N_i(0)$ is the number of atoms of the $i$th isotope of the series at time $t = 0$ and

$$N_i(0) = 0 \qquad i > 1$$

then the Bateman equation takes the form

$$N_i(t) = \lambda_1 \lambda_2 \cdots \lambda_{i-1} N_1(0) \sum_{j=1}^{i} \frac{e^{-\lambda_j t}}{\prod_{k \neq j}(\lambda_k - \lambda_j)} \tag{3.76}$$

**Example 3.11** Apply the Bateman equation for the second and third isotope in a series.

**Answer**

(a) $$N_2(t) = \lambda_1 N_1(0)\left(\frac{e^{-\lambda_1 t}}{\lambda_2 - \lambda_1} + \frac{e^{-\lambda_2 t}}{\lambda_1 - \lambda_2}\right) = \frac{\lambda_1 N_1(0)}{(\lambda_2 - \lambda_1)}(e^{-\lambda_1 t} - e^{-\lambda_2 t})$$

(b) $$N_3(t) = \lambda_1 \lambda_2 N_1(0)\left[\frac{e^{-\lambda_1 t}}{(\lambda_2 - \lambda_1)(\lambda_3 - \lambda_1)} + \frac{e^{-\lambda_2 t}}{(\lambda_1 - \lambda_2)(\lambda_3 - \lambda_2)} + \frac{e^{-\lambda_3 t}}{(\lambda_1 - \lambda_3)(\lambda_2 - \lambda_3)}\right]$$

## 3.9 NUCLEAR REACTIONS

### 3.9.1 General Remarks

A *nuclear reaction* is an interaction between two particles, a fast bombarding particle, called the *projectile*, and a slower or stationary *target*. The products of the reaction may be two or more particles. For the energies considered here (< 20 MeV), the products are also two particles (with the exception of fission, which is discussed in the next section).

If $x_1, X_2$ are the colliding particles and $x_3, X_4$ are the products, the reaction is indicated as

$$ {}^{A_1}_{Z_1}x_1 + {}^{A_2}_{Z_2}X_2 \rightarrow {}^{A_3}_{Z_3}x_3 + {}^{A_4}_{Z_4}X_4 $$

or

$$ X_2(x_1, x_3)X_4 $$

The particles in parentheses are the light particles, $x_1$ being the projectile. Another representation for the reason is based on the light particles only, in which case the reaction shown above is indicated as an $(x_1, x_3)$ reaction. For example, the reaction

$$ {}^{1}_{0}n + {}^{10}_{5}B \rightarrow {}^{4}_{2}He + {}^{7}_{3}Li $$

may also be indicated as ${}^{10}_{5}B(n, \alpha){}^{7}_{3}Li$ or simply as an $(n, \alpha)$ reaction.

Certain quantities are conserved when a nuclear reaction takes place. Four are considered here. For the reaction shown above, the following quantities are conserved:

Charge:

$$ Z_1 + Z_2 = Z_3 + Z_4 $$

Mass number:

$$ A_1 + A_2 = A_3 + A_4 $$

Total energy:

$$ E_1 + E_2 = E_3 + E_4 \quad \text{(rest mass plus kinetic energy)} $$

Linear momentum:

$$ \mathbf{P}_1 + \mathbf{P}_2 = \mathbf{P}_3 + \mathbf{P}_4 $$

Many nuclear reactions proceed through the formation of a *compound nucleus*. The compound nucleus, formed after particle $x_1$ collides with $X_2$, is highly excited and lives for a time of the order of $10^{-12}$ to $10^{-14}$ s before it decays to $x_3$ and $X_4$. A compound nucleus may be formed in more than one way and may decay by more than one mode that does not depend on the mode of formation. Consider the example of the compound nucleus ${}^{14}_{7}N$:

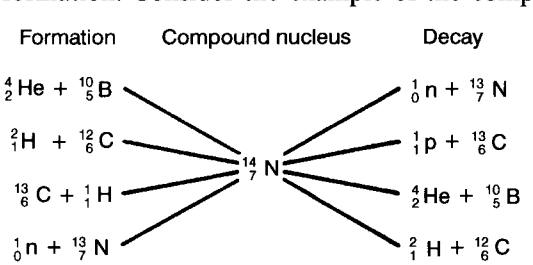


The modes of formation and decay of ${}^{14}N$ are shown in the form of an energy-level diagram in Fig. 3.13. No matter how the compound nucleus is

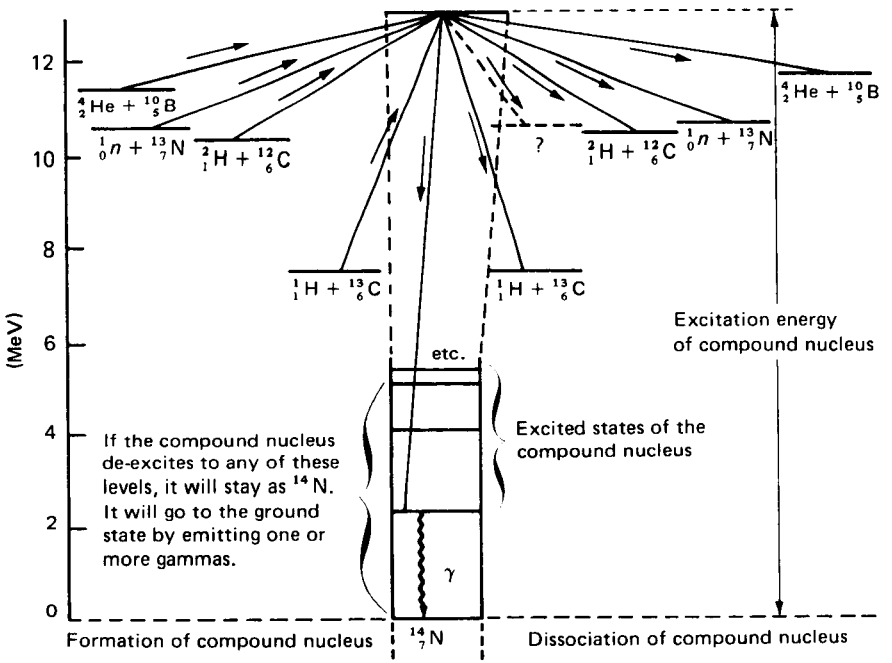


**Figure 3.13** Different modes of formation and decay of the component nucleus. For clarity, the diagram shows that the compound nucleus has the same excitation energy regardless of the way it is formed. This is not necessarily the case.

formed, it has an excitation energy equal to the separation energy of the projectile ($\alpha$, $n$, $p$, etc.) plus a fraction of the kinetic energy of the two particles. Since the separation energy is of the order of MeV, it is obvious that the compound nucleus has considerable excitation energy even if the projectile and the target have zero kinetic energy.

Exactly what happens inside the compound nucleus is not known. It is believed—and experiment does not contradict this idea—that the excitation energy of the compound nucleus is shared quickly by all the nucleons ($A_1 + A_2$). There is continuous exchange of energy among all the nucleons until one of them (or a cluster of them) obtains energy greater than its separation energy and is able to leave the compound nucleus, becoming a free particle.

### 3.9.2 Kinematics of Nuclear Reactions

In this section, two questions will be answered:

1. Given the masses $m_1$, $M_2$, $m_3$, $M_4$, and the kinetic energies of the projectile ($m_1$) and the target ($M_2$), how can one calculate the kinetic energies of the products with masses $m_3$ and $M_4$?

2. What is the minimum kinetic energy the particles with masses $m_1$, $M_2$ ought to have to be able to initiate the reaction?

The discussion will be limited to the case of a stationary target, the most commonly encountered in practice.

Consider a particle of mass $m_1$ having speed $v_1$ (kinetic energy $T_1$) hitting a stationary particle of Mass $M_2$. The particles $m_3$, $M_4$ are produced as a result of this reaction with speeds $v_3$, $v_4$ (kinetic energies $T_3$, $T_4$), as shown in Figure 3.14. Applying conservation of energy and linear momentum, one has

Energy:

$$m_1 + T_1 + M_2 = m_3 + T_3 + M_4 + T_4 \tag{3.77}$$

Momentum, $x$ axis:

$$m_1 v_1 = m_3 v_3 \cos\theta + M_4 v_4 \cos\phi \tag{3.78}$$

Momentum, $y$ axis:

$$m_3 v_3 \sin\theta = M_4 v_4 \sin\phi \tag{3.79}$$

The quantity

$$Q = m_1 + M_2 - m_3 - M_4 \tag{3.80}$$

is called the $Q$ value of the reaction. If $Q > 0$, the reaction is called *exothermic* or *exoergic*. If $Q < 0$, the reaction is called *endothermic* or *endoergic*.

Assuming nonrelativistic kinematics, in which case $T = \frac{1}{2}mv^2$, Eqs. 3.77 to 3.79 take the form

$$T_1 + Q = T_3 + T_4 \tag{3.81}$$

$$\sqrt{2m_1T_1} = \sqrt{2m_3T_3}\cos\theta + \sqrt{2M_4T_4}\cos\phi \tag{3.82}$$

$$\sqrt{2m_3T_3}\sin\theta = \sqrt{2M_4T_4}\sin\phi \tag{3.83}$$

Equations 3.81 to 3.83 have four unknowns $T_3$, $T_4$, $\phi$, and $\theta$, so they cannot be solved to give a unique answer for any single unknown. In practice, one expresses a single unknown in terms of a second one—e.g., $T_3$ as a function of

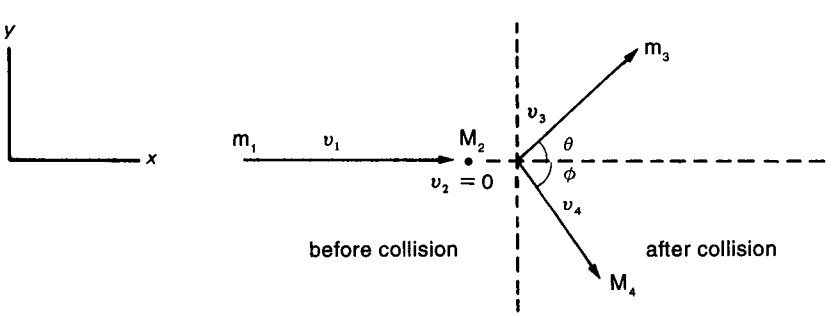


**Figure 3.14** The kinematics of the reaction $M_2(m_1, m_3)M_4$.

$\theta$, after eliminating $T_4$ and $\phi$. Such an expression, although straightforward, is complicated. Two cases of special interest are the following.

Case 1: $\theta = 0$, $\phi = 180°$. In this case, the particles $m_3$ and $M_4$ are emitted along the direction of motion of the bombarding particle (Fig. 3.15). Equations 3.81 and 3.82 take the form

$$T_1 + Q = T_3 + T_4 \tag{3.84}$$

$$\sqrt{m_1 T_1} = \sqrt{m_3 T_3} - \sqrt{M_4 T_4} \tag{3.85}$$

and they can be solved for $T_3$ and $T_4$. These values of $T_3$ and $T_4$ give the maximum and minimum kinetic energies of particles $m_3$ and $M_4$.

**Example 3.12** Consider the reaction

$$^{1}_{0}n + ^{14}_{7}\mathrm{N} \rightarrow ^{4}_{2}\mathrm{He} + ^{11}_{5}\mathrm{B}$$

with the nitrogen being at rest and the neutron having energy 2 MeV. What is the maximum kinetic energy of the alpha particle?

**Answer** The $Q$ value of the reaction is

$$\begin{aligned} Q &= (14.003074 + 1.008665 - 4.002603 - 11.009306) \times 931.481 \text{ MeV} \\ &= -0.158 \text{ MeV} \end{aligned}$$

Solving Eqs. 3.84 and 3.85 for $T_3$, one obtains a quadratic equation for $T_3$ ($T_3$ in MeV),

$$T_3^2 - 2.577 T_3 + 1.482 = 0$$

which gives two values of $T_3$:

$$T_{3,1} = 1.710 \text{ MeV} \qquad T_{3,2} = 0.866 \text{ MeV}$$

The corresponding values of $T_4$ are

$$T_{4,1} = 0.132 \text{ MeV} \qquad T_{4,2} = 0.976 \text{ MeV}$$

The two pairs of values correspond to the alpha being emitted at $\theta = 0$ ($T_3 = 1.709$ MeV = max. kin. energy) or $\theta = 180°$ ($T_2 = 0.865$ MeV = min. kin. energy). Correspondingly, the boron nucleus is emitted at $\phi = 180°$ or $\phi = 0°$. One can use the momentum balance equation (Eq. 3.85) to verify this conclusion.

Case 2: $\theta = 90°$. In this case, the reaction looks as shown in Fig. 3.16. The momentum vectors form a right triangle as shown on the right of Fig. 3.16.

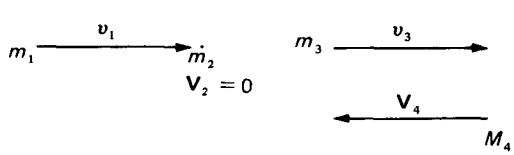


**Figure 3.15** A case where the reaction products are emitted 180° apart.

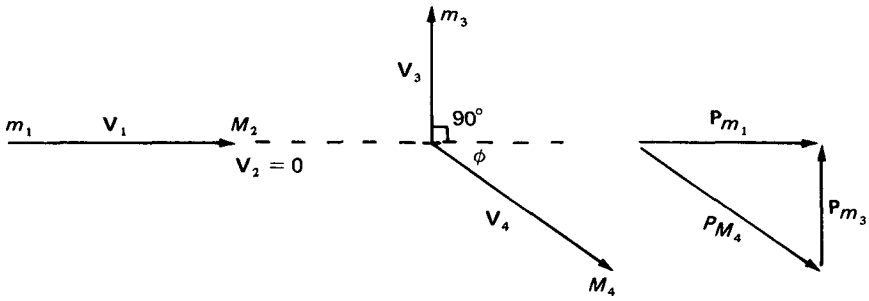


**Figure 3.16** A case where the reaction products are emitted 90° apart.

Therefore, Eqs. 3.81 and 3.82 take the form

$$T_1 + Q = T_3 + T_4 \tag{3.86}$$

$$m_1T_1 + m_3T_3 = M_4T_4 \tag{3.87}$$

Again, one can solve for $T_3$ and $T_4$. The value of $T_3$ is

$$T_3 = \frac{(M_4 - m_1)T_1 + M_4Q}{m_3 + M_4} \tag{3.88}$$

**Example 3.13** What is the energy of the alpha particle in the reaction

$${}^1_0n + {}^{14}_7\text{N} \rightarrow {}^4_2\text{He} + {}^{11}_5\text{B}$$

if it is emitted at 90°? Use $T_1 = 2$ MeV, the same as in Example 3.12.

**Answer** Using Eq. 3.88,

$$T_3 = \frac{(11 - 1)2 + 11(-0.163)}{15}\text{MeV} = 1.214\ \text{MeV}$$

The value of the minimum (threshold)energy necessary to initiate a reaction can be understood with the help of Fig. 3.17. When the particle $m_1$ enters the target nucleus $M_2$, a compound nucleus is formed with excitation energy equal to

$$B_{m_1} + \frac{M_2}{m_1 + M_2}T_1 \tag{3.89}$$

where $B_{m_1}$ = binding energy of particle $m_1$
$M_2T_1/(m_1 + M_2)$ = part of the incident particle kinetic energy available as excitation energy of the compound nucleus
Only a fraction of the kinetic energy $T_1$ is available as excitation energy,

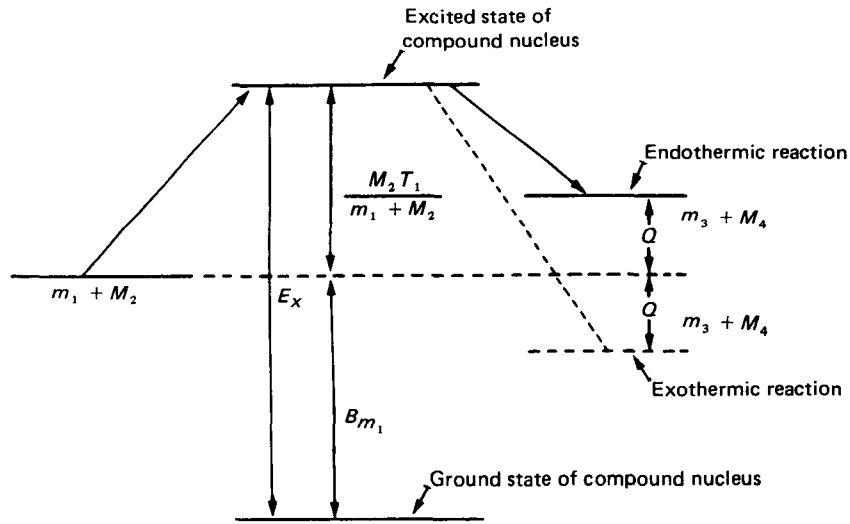


**Figure 3.17** Energy-level diagram for endothermic and exothermic reactions. For endothermic reactions, the threshold energy is equal to $[(m_1 + M_2)/M_2]|Q|$.

because the part

$$\left(\frac{m_1}{m_1 + M_2}\right)T_1$$

becomes kinetic energy of the compound nucleus (see Evans or any other book on nuclear physics), and as such is not available for excitation.

If the reaction is exothermic ($Q > 0$), it is energetically possible for the compound nucleus to deexcite by going to the state $(m_3 + M_4)$ (Fig. 3.17), even if $T_1 \approx 0$. For an endothermic reaction, however, energy at least equal to $|Q|$ should become available (from the kinetic energy of the projectile). Therefore, the kinetic energy $T_1$ should be such that

$$\frac{M_2}{m_1 + M_2}T_1 \geq |Q| \tag{3.90}$$

or the threshold kinetic energy for the reaction is

$$T_{1,\text{th}} = \frac{m_1 + M_2}{M_2}|Q| \tag{3.91}$$

## 3.10 FISSION

*Fission* is the reaction in which a heavy nucleus splits into two heavy fragments. In the fission process, net energy is released, because the heavy nucleus has less binding energy per nucleon that the fission fragments, which belong to the

middle of the periodic table. In fact, for $A > 85$ the binding energy per nucleon decreases (Fig. 3.3); therefore any nucleus with $A > 85$ would go to a more stable configuration by fissioning. Such "spontaneous" fission is possible but very improbable. Only very heavy nuclei ($Z > 92$) undergo spontaneous fission at a considerable rate.

For many heavy nuclei ($Z \geq 90$), fission takes place if an amount of energy at least equal to a critical energy $E_c$ is provided in some way, as by neutron or gamma absorption. Consider, as an example, the nucleus $^{235}$U (Fig. 3.18). If a neutron with kinetic energy $T_n$ is absorbed, the compound-nucleus $^{236}$U has excitation energy equal to (Eq. 3.89)

$$B_n + \frac{A}{A+1} T_n$$

If $B_n + AT_n/(A+1) \geq E_c$, fission may occur and the final state is the one shown as fission products in Fig. 3.18. For $^{236}$U, $E_c = 5.3$ MeV and $B_n = 6.4$ MeV. Therefore, even a neutron with zero kinetic energy may induce fission, if it is absorbed. For $^{239}$U, which is formed when a neutron is absorbed by $^{238}$U, $B_n = 4.9$ MeV and $E_c = 5.5$ MeV. Therefore, fission cannot take place unless the neutron kinetic energy satisfies

$$T_n > \frac{A+1}{A}(E_c - B_n) = \frac{239}{238}(5.5 - 4.9) \approx 0.6 \text{ MeV}$$

The fission fragments are nuclei in extremely excited states with mass numbers in the middle of the periodic system. They have a positive charge of about $20e$ and they are neutron-rich. This happens because the heavy nuclei have a much higher neutron-proton ratio than nuclei in the middle of the periodic table.

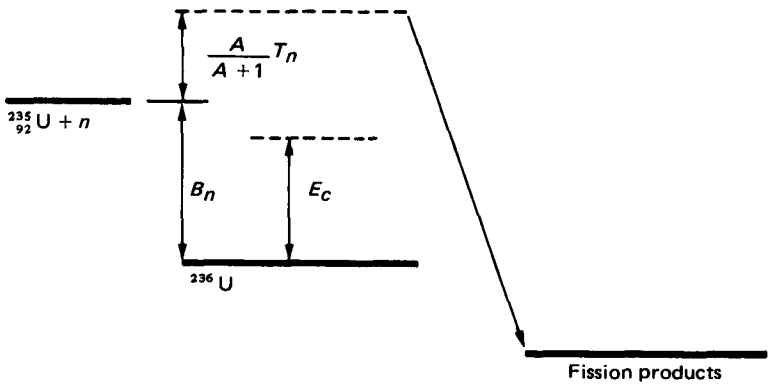


**Figure 3.18** The fission of $^{235}$U induced by neutron absorption.

Consider as an example $^{236}U$ (Fig. 3.19). Assume that it splits into two fragments as follows:

$$Z_1 = 48 \quad N_1 = 80 \quad A_1 = 128$$
$$Z_2 = 44 \quad N_2 = 64 \quad A_2 = 108$$

The two fission fragments have a neutron-proton ratio higher than what stability requires for their atomic mass. They get rid of the extra neutron either by directly emitting neutrons or by $\beta^-$ decay.

A nucleus does not always split in the same fashion. There is a probability that each fission fragment $(A, Z)$ will be emitted, a process called *fission yield*. Figure 3.20 shows the fission yield for $^{235}U$ fission. For thermal neutrons, the "asymmetric" fission is favored. It can be shown that asymmetric fission yields more energy. As the neutron energy increases, the excitation energy of the compound nucleus increases. The possibilities for fission are such that it does not make much difference, from an energy point of view, whether the fission is symmetric or asymmetric. Therefore, the probability of symmetric fission increases.

The fission fragments deexcite by emitting neutrons, betas, and gammas, and most of the fragments stay radioactive long after the fission takes place. The important characteristics of the particles emitted by fission fragments are:

1. Betas. About six $\beta^-$ particles are emitted per fission, carrying a total average energy of 7 MeV.
2. Gammas. About seven gammas are emitted at the time of fission. These are called *prompt gammas*. At later times, about seven to eight more gammas are released, called *delayed gammas*. Photons carry a total of about 15 MeV per fission.

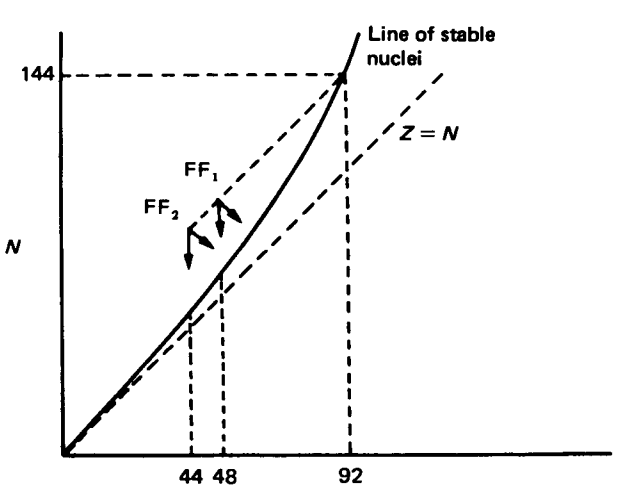


**Figure 3.19** The fission fragments $FF_1$ and $FF_2$ from $^{236}U$ fission are neutron-rich. They reduce their neutron number either by beta decay or by neutron emission.

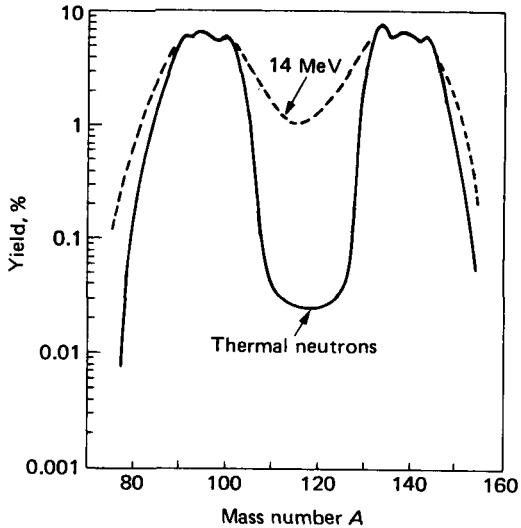


**Figure 3.20** $^{235}U$ fission yield for thermal neutron induced fission. Data from Ref. 3. The dashed line indicates the yield when the fission is induced by 14-MeV neutrons.

3. Neutrons. The number of neutrons per fission caused by thermal neutrons is between two and three. This number increases linearly with the kinetic energy of the neutron inducing the fission. The average energy of a neutron emitted in fission is about 2 MeV. More than 99 percent of the neutrons are emitted at the time of fission and are called *prompt neutrons*. A very small fraction is emitted as *delayed neutrons*. Delayed neutrons are very important for the control of nuclear reactors.
4. Neutrinos. About 11 MeV are taken away by neutrinos, which are also emitted during fission. This energy is the only part of the fission energy yield that completely escapes. It represents about 5 percent of the total fission energy.

Table 3.3 summarizes the particles and energies involved in fission.†

†Tritium is sometimes produced in fission. In reactors fueled with $^{235}U$, it is produced at the rate of $8.7 \times 10^{-6}$ tritons per fission. The most probable kinetic energy of the tritons is about 7.5 MeV.

**Table 3.3 Fission Products**

| Particle | Number/fission | MeV/fission |
|---|---|---|
| Fission fragments | 2 | 160 to 170 |
| Neutrons | 2 to 3 | 5 |
| Gammas (prompt) | 7 | 8 |
| Gammas (delayed) | 7 | 7 |
| Betas | 6 | 7 |
| Neutrinos | 6 | 11 |
| Total | | 198 to 208 |

## PROBLEMS

**3.1** What is the speed of a 10-MeV electron? What is its total mass, relative to its rest mass?

**3.2** What is the speed of a proton with a total mass equal to $2Mc^2$? ($M$ is the proton rest mass).

**3.3** What is the kinetic energy of a neutron that will result in 1 percent error difference between relativistic and classical calculation of its speed?

**3.4** What is the mass of an astronaut traveling with speed $v = 0.8c$? Mass at rest is 70 kg.

**3.5** What is the kinetic energy of an alpha particle with a total mass 10 percent greater than its rest mass?

**3.6** What would the density of graphite be if the atomic radius were $10^{-13}$ m? [Atomic radius (now) $10^{-10}$m; density of graphite (now) 1600 kg/m$^3$.]

**3.7** Calculate the binding energy of the deuteron. [$M(^1\text{H}) = 1.007825$ u; $M(^2\text{H}) = 2.01410$ u.]

**3.8** Calculate the separation energy of the last neutron of $^{241}$Pu. [$M(^{240}\text{Pu}) = 240.053809$ u; $M(^{241}\text{Pu}) = 241.056847$ u.]

**3.9** Assume that the average binding energy per nucleon (in some new galaxy) changes with $A$ as shown in the following figure:

(a) Would fission or fusion or both release energy in such a world?

(b) How much energy would be released if a tritium ($^3$H) nucleus and a helium ($^4$He) nucleus combined to form a lithium nucleus? [$M(^3\text{H}) = 3.016050$ u; $M(^4\text{He}) = 4.002603$ u; $M(^7\text{Li}) = 7.016004$ u.]

**3.10** A simplified diagram of the $^{137}$Cs decay is shown in the figure below. What is the recoil energy of the nucleus when the 0.6616-MeV gamma is emitted?

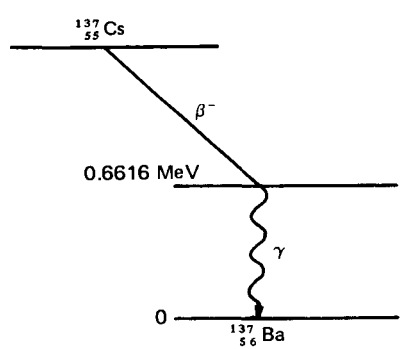


**3.11** The isotope $^{239}$Pu decays by alpha emissions to $^{235}$U as shown in the following figure.

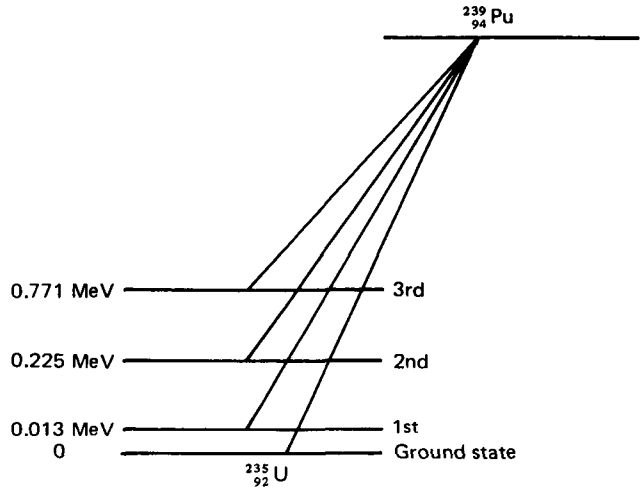


(a) What is $Q_\alpha$?

(b) What is the kinetic energy of the alphas if the $^{235}$U nucleus is left in the third excited state? What is the kinetic energy of the alphas if the $^{235}$U nucleus is left in the ground state? [$M(^{235}\text{U}) = 235.043926$ u; $M(^{239}\text{Pu}) = 239.052159$ u.]

**3.12** Consider the isotopes $^{63}$Zn and $^{63}$Cu. Is $\beta^+$ decay possible? Is EC possible? What is $Q_{\beta^+}$? What is $Q_{\text{EC}}$? [$M(^{63}\text{Cu}) = 62.929597$ u: $M(^{63}\text{Zn}) = 62.933212$ u.]

**3.13** The isotope $^{11}_{4}$Be decays to $^{11}_{5}$B. What are the maximum and average kinetic energy of the betas? [$M(^{11}\text{Be}) = 11.021658$ u; $M(^{11}\text{B}) = 11.009306$ u.]

**3.14** Natural uranium contains the isotopes $^{234}$U, $^{235}$U, and $^{238}$U, with abundances and half-lives as shown below:

| | Half-life (years) | Abundance (%) |
|---|---|---|
| $^{234}$U | $2.47 \times 10^5$ | 0.0057 |
| $^{235}$U | $7.10 \times 10^8$ | 0.71 |
| $^{238}$U | $4.51 \times 10^9$ | 99.284 |

(a) What is the alpha specific activity of natural uranium?

(b) What fraction of the activity is contributed by each isotope?

**3.15** The isotope $^{210}$Po generates 140,000 W/kg thermal power due to alpha decay. What is the energy of the alpha particle? ($T_\alpha = 138.4$ d.)

**3.16** How many years ago did the isotope $^{235}$U make up 3 percent of natural uranium?

**3.17** What is the specific alpha activity of $^{239}$Pu? (For $^{239}$Pu: $T_{\text{sf}} = 5.5 \times 10^{15}$ y, $T_{\text{tot}} = 2.44 \times 10^4$ y.)

**3.18** Consider the reaction $^{7}_{3}\text{Li}(p, n)^{7}_{4}\text{Be}$. What is the $Q$ value for this reaction? If a neutron is emitted at 90° (in LS) with kinetic energy 2 MeV, what is the energy of the incident proton? [$M(^7\text{Li}) = 7.016004$ u; $M(^7\text{Be}) = 7.016929$ u.]

**3.19** What is the necessary minimum kinetic energy of a proton to make the reaction $^{4}_{2}\text{He}(p, d)^{3}_{2}\text{H}$ possible? ($^4$He at rest.)

**3.20** A 1-MeV neutron collides with a stationary $^{13}_{7}$N nucleus. What is the maximum kinetic energy of the emerging proton?

**3.21** What is the threshold gamma energy for the reaction

$$\gamma + {}^{12}_{6}C \rightarrow 3\left({}^{4}_{2}\text{He}\right)$$

**3.22** What is the energy expected to be released as a result of a thermal neutron induced fission in $^{239}$Pu if the two fission fragments have masses $M_1 = 142$ u and $M_2 = 95$ u?

## BIBLIOGRAPHY

Born, M., *Atomic Physics*, Blackie & Son Limited, London, 1962.
Evans, R. D., *The Atomic Nucleus*, McGraw-Hill, New York, 1972.
Schiff, L. I., *Quantum Mechanics*, McGraw-Hill, New York, 1955.
Segre, E., *Nuclei and Particles*, Benjamin, New York, 1964.

## REFERENCES

1. Stamatelatos, M. G., and England, T. R., *Nucl. Sci. Eng.* **63**:304 (1977).
2. Bateman, H., *Proc. Cambridge Philos. Soc.* **15**:423 (1910).
3. DiIorio, G. J., "Direct Physical Measurement of Mass Yields in Thermal Fission of Uranium 235," Ph.D. thesis, University of Illinois at Urbana-Champaign, 1976.
4. Lederer, C. M., and Shirley, V. S. (eds.), *Table of Isotopes*, 7th ed., Wiley-Interscience, New York, 1978.

CHAPTER
# FOUR

# ENERGY LOSS AND PENETRATION OF RADIATION THROUGH MATTER

## 4.1 INTRODUCTION

This chapter discusses the mechanisms by which ionizing radiation interacts and loses energy as it moves through matter. The study of this subject is extremely important for radiation measurements because the detection of radiation is based on its interactions and the energy deposited in the material of which the detector is made. Therefore, to be able to build detectors and interpret the results of the measurement, we need to know how radiation interacts and what the consequences are of the various interactions.

The topics presented here should be considered only an introduction to this extensive subject. Emphasis is given to that material considered important for radiation measurements. The range of energies considered is shown in Table 1.1.

For the discussion that follows, ionizing radiation is divided into three groups:

1. Charges particles: electrons ($e^-$), positrons ($e^+$), protons ($p$), deuterons ($d$), alphas ($\alpha$), heavy ions ($A > 4$)
2. Photons: gammas ($\gamma$) or X-rays
3. Neutrons ($n$)

The division into three groups is convenient because each group has its own characteristic properties and can be studied separately.

A charged particle moving through a material interacts, primarily, through Coulomb forces, with the negative electrons and the positive nuclei that constitute the atoms of that material. As a result of these interactions, the charged particle loses energy continuously and finally stops after traversing a finite distance, called the *range*. The range depends on the type and energy of the particle and on the material through which the particle moves. The probability of a charged particle going through a piece of material without an interaction is practically zero. This fact is very important for the operation of charged-particle detectors.

Neutrons and gammas have no charge. They interact with matter in ways that will be discussed below, but there is a finite nonzero probability that a neutron or a $\gamma$-ray may go through any thickness of any material without having an interaction. As a result, no finite range can be defined for neutrons or gammas.

## 4.2 MECHANISMS OF CHARGED-PARTICLE ENERGY LOSS

Charged particles traveling through matter lose energy in the following ways:

1. In Coulomb interactions with electrons and nuclei
2. By emission of electromagnetic radiation (bremsstrahlung)
3. In nuclear interactions
4. By emission of Cerenkov radiation

For charged particles with kinetic energies considered here, nuclear interactions may be neglected, except for heavy ions ($A > 4$) (see Sec.4.7).

Cerenkov radiation constitutes a very small fraction of the energy loss. It is important only because it has a particle application in the operation of Cerenkov counters (see Evans). Cerenkov radiation is visible electromagnetic radiation emitted by particles traveling in a medium, with speed greater than the speed of light in that medium.

### 4.2.1. Coulomb Interactions

Consider a charged particle traveling through a certain material, and consider an atom of that material. As shown in Fig. 4.1, the fast charged particle may interact with the atomic electrons or the nucleus of the atom. Since the radius of the nucleus is approximately $10^{-14}$ m and the radius of the atom is $10^{-10}$ m, one might expect that

$$\frac{\text{Number of interactions with electrons}}{\text{number of interactions with nuclei}} = \frac{(R^2)\ \text{atom}}{(R^2)\ \text{nucleus}} = \frac{(10^{-10})^2}{(10^{-14})^2} \approx 10^8$$

This simplified argument indicates that collisions with atomic electrons are more important than with nuclei. Nuclear collisions will not be considered here.

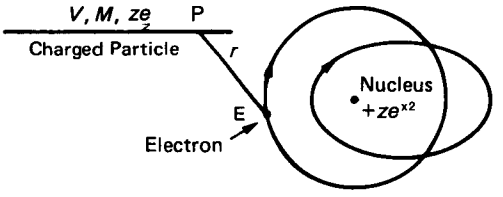


**Figure 4.1** A fast charged particle of mass $M$ and charge $ze$ interacts with the electrons of an atom.

Looking at Fig. 4.1, at a certain point in time the particle is at point P and the electron at E. If the distance between them is $r$, the coulomb force is $F = k(ze^2/r^2)$, where $ze$ is the charge of the particle and $k$ is a constant that depends on the units. The action of this force on the electron, over a period of time, may result in the transfer of energy from the moving charged particle to the bound electron. Since a bound atomic electron is in a quantized state, the result of the passage of the charged particle may be ionization or excitation.

*Ionization* occurs when the electron obtains enough energy to leave the atom and become a free particle with kinetic energy equal to

$$(\mathrm{KE})_e = (\text{energy given by particle}) - (\text{ionization potential})$$

The electron freed from the atom acts like any other moving charged particle. It may cause ionization of another atom if its energy is high enough. It will interact with matter, lose its kinetic energy, and finally stop. Fast electrons produced by ionizing collisions are called $\delta$ rays.

The ionization leaves behind a positive ion, which is a massive particle compared to an electron. If an ion and an electron move in a gas, the ion will move much slower than the electron. Eventually, the ion will pick up an electron from somewhere and will become a neutral atom again.

*Excitation* takes place when the electron acquires enough energy to move to an empty state in another orbit of higher energy. The electron is still bound, but it has moved from a state with energy $E_1$ to one with $E_2$, thus producing an excited atom. In a short period of time, of the order of $10^{-8}$ to $10^{-10}$ s, the electron will move to a lower energy state, provided there is one empty. If the electron falls from $E_2$ to $E_1$, the energy $E_2 - E_1$ is emitted in the form of an X-ray with frequency $\nu = (E_2 - E_1)/h$.

Collisions that result in ionization or excitation are called *inelastic collisions*. A charged particle moving through matter may also have elastic collisions with nuclei or atomic electrons. In such a case, the incident particle loses the energy required for conservation of kinetic energy and linear momentum. Elastic collisions are not important for charged-particle energy loss and detection.

### 4.2.2 Emission of Electromagnetic Radiation (Bremsstrahlung)

Every free charged particle that accelerates or decelerates loses part of its kinetic energy by emitting electromagnetic radiation. This radiation is called *bremsstrahlung*, which in German means braking radiation. Bremsstrahlung is

not a monoenergetic radiation. It consists of photons with energies from zero up to a maximum equal to the kinetic energy of the particle.

Emission of bremsstrahlung is predicted not only by quantum mechanics but also by classical physics. Theory predicts that a charge that is accelerated radiates energy with intensity proportional to the square of its acceleration. Consider a charged particle with charge $ze$ and mass $M$ moving in a certain material of atomic number $Z$. The Coulomb force between the particle and a nucleus of the material is $F \sim zeZe/r^2$, where $r$ = distance between the two charges. The acceleration of the incident charged particle is $a = F/M \sim zZe^2/M$. Therefore the intensity of the emitted radiation $I$ is

$$I \propto a^2 \sim \left(\frac{zZe^2}{M}\right)^2 \sim \frac{z^2Z^2}{M^2} \tag{4.1}$$

This expression indicates that

1. For two particles traveling in the same medium, the lighter particle will emit a much greater amount of bremsstrahlung than the heavier particle (other things being equal).
2. More bremsstrahlung is emitted if a particle travels in a medium with high atomic number $Z$ than in one with low atomic number.

For charged particles with energies considered here, the kinetic energy lost as bremsstrahlung might be important for electrons only. Even for electrons, it is important for high-$Z$ materials like lead ($Z = 82$). For more detailed treatment of the emission of bremsstrahlung, the reader should consult the references listed at the end of the chapter.

## 4.3 STOPPING POWER DUE TO IONIZATION AND EXCITATION

A charged particle moving through a material exerts Coulomb forces on many atoms simultaneously. Every atom has many electrons with different ionization and excitation potentials. As a result of this, the moving charged particle interacts with a tremendous number of electrons—millions. Each interaction has its own probability for occurrence and for a certain energy loss. It is impossible to calculate the energy loss by studying individual collisions. Instead, an average energy loss is calculated per unit distance traveled. The calculation is slightly different for electrons or positrons than for heavier charged particles like $p$, $d$, and $\alpha$, for the following reason.

It was mentioned earlier that most of the interactions of a charged particle involve the particle and atomic electrons. If the mass of the electron is taken as 1, then the masses of the other common heavy† charged particles are the

†In this discussion, "heavy" particles are all charged particles except electrons and positrons.

following:

$$\begin{aligned} \text{Electron mass} &= 1 \\ \text{Proton mass} &\approx 1840 \\ \text{Deuteron mass} &\approx 2(1840) \\ \text{Alpha mass} &\approx 4(1840) \end{aligned}$$

If the incoming charged particle is an electron or a positron, it may collide with an atomic electron and lose all its energy in a single collision because the collision involves two particles of the same mass. Hence, incident electrons or positrons may lose a large fraction of their kinetic energy in one collision. They may also be easily scattered to large angles, as a result of which their trajectory is zig-zag (Fig. 4.2). Heavy charged particles, on the other hand, behave differently. On the average, they lose smaller amounts of energy per collision. They are hardly deflected by atomic electrons, and their trajectory is almost a straight line.

Assuming that all the atoms and their atomic electrons act independently, and considering only energy lost to excitation and ionization, the average energy loss† per unit distance traveled by the particle is given by Eqs. 4.2, 4.3, and 4.4. (For their derivation, see the chapter bibliography: Evans, Segré, and Roy and Reed.)

**Stopping power due to ionization-excitation for $p, d, t, \alpha$.**

$$\frac{dE}{dx}(\text{MeV/m})^{\ddagger} = 4\pi r_0^2 z^2 \frac{mc^2}{\beta^2} NZ\left[\ln\left(\frac{2mc^2}{I}\beta^2\gamma^2\right) - \beta^2\right] \tag{4.2}$$

**Stopping power due to ionization-excitation for electrons.**

$$\frac{dE}{dx}(\text{MeV/m}) = 4\pi r_0^2 \frac{mc^2}{\beta^2} NZ\left\{\ln\left(\frac{\beta\gamma\sqrt{\gamma-1}}{I}mc^2\right) + \frac{1}{2\gamma^2}\left[\frac{(\gamma-1)^2}{8} + 1 - (\gamma^2 + 2\gamma - 1)\ln 2\right]\right\} \tag{4.3}$$

**Stopping power due to ionization-excitation for positrons.**

$$\frac{dE}{dx}(\text{MeV/m}) = 4\pi r_0^2 \frac{mc^2}{\beta^2} NZ\left\{\ln\left(\frac{\beta\gamma\sqrt{\gamma-1}}{I}mc^2\right) - \frac{\beta^2}{24}\left[23 + \frac{14}{\gamma+1} + \frac{10}{(\gamma+1)^2} + \frac{4}{(\gamma+1)^3}\right] + \frac{\ln 2}{2}\right\} \tag{4.4}$$

†Since $E = T + Mc^2$ and $Mc^2$ = constant, $dE/dx = dT/dx$; thus, Eqs. 4.2 to 4.4 express the kinetic as well as the total energy loss per unit distance.

‡In SI units, the result would be J/m; 1 MeV = $1.602 \times 10^{-13}$ J.

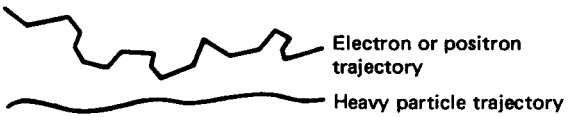


**Figure 4.2** Possible electron and heavy particle trajectories.

where $r_0 = e^2/mc^2 = 2.818 \times 10^{-15}$ m = classical electron radius
$4\pi r_0^2 = 9.98 \times 10^{-29}\ \text{m}^2 \approx 10^{-28}\ \text{m}^2 = 10^{-24}\ \text{cm}^2$
$mc^2$ = rest mass energy of the electron = 0.511 MeV
$\gamma = (T + Mc^2)/Mc^2 = 1/\sqrt{1-\beta^2}$
$T$ = kinetic energy = $(\gamma - 1)Mc^2$
$M$ = rest mass of the particle
$\beta = v/c$ $\quad c$ = speed of light in vacuum = $2.997930 \times 10^8$ m/s $\approx$ $3 \times 10^8$ m/s
$N$ = number of atoms/m$^3$ in the material through which the particle moves
$N = \rho(N_A/A)$ $\quad N_A$ = Avogadro's number = $6.022 \times 10^{23}$ atoms/mol
$A$ = atomic weight
$Z$ = atomic number of the material
$z$ = charge of the incident particle ($z = 1$ for $e^-, e^+, p, d$; $z = 2$ for $\alpha$)
$I$ = mean excitation potential of the material

An approximate equation for $I$, which gives good results for $Z > 12$,[1] is

$$I(\text{eV}) = (9.76 + 58.8Z^{-1.19})Z \tag{4.5}$$

Table 4.1 gives values of $I$ for many common elements.

Many different names have been used for the quantity $dE/dx$: names like energy loss, specific energy loss, differential energy loss, or stopping power. In

**Table 4.1 Values of Mean Excitation Potentials for Common Elements and Compounds**†

| Element | $I$ (eV) | Element | $I$ (eV) |
|---|---|---|---|
| H | 20.4 | Fe | 281* |
| He | 38.5 | Ni | 303* |
| Li | 57.2 | Cu | 321* |
| Be | 65.2 | Ge | 280.6 |
| B | 70.3 | Zr | 380.9 |
| C | 73.8 | I | 491 |
| N | 97.8 | Cs | 488 |
| O | 115.7 | Ag | 469* |
| Na | 149 | Au | 771* |
| Al | 160* | Pb | 818.8 |
| Si | 174.5 | U | 839* |

†Values of $I$ with * are from experimental results of refs. 2 and 3. Others are from refs. 4 and 5.

this text, the term *stopping power* will be used for $dE/dx$ given by Eq. 4.2 to 4.4, as well as for a similar equation for heavier charged particles presented in Sec. 4.7.2.

It should be noted that the stopping power

1. Is independent of the mass of the particle
2. Is proportional to $z^2$ [(charge)$^2$] of particle
3. Depends on the speed $v$ of particle
4. Is proportional to the density of the material ($N$)

For low kinetic energies, $dE/dx$ is almost proportional to $1/v^2$. For relativistic energies, the term in brackets predominates and $dE/dx$ increases with kinetic energy. Figure 4.3 shows the general behavior of $dE/dx$ as a function of kinetic energy. For all particles, $dE/dx$ exhibits a minimum that occurs approximately at $\gamma \approx 3$. For electrons, $\gamma = 3$ corresponds to $T = 1$ MeV; for alphas, $\gamma = 3$ corresponds to $T \simeq 7452$ MeV; for protons, $\gamma = 3$ corresponds to $T \cong 1876$ MeV. Therefore, for the energies considered here (see Table 1.1), the $dE/dx$ for protons and alphas will always increase, as the kinetic energy of the particle decreases (Fig. 4.3, always on the left of the curve minimum); for electrons, depending on the initial kinetic energy, $dE/dx$ may increase or decrease as the electron slows down.

Equations 4.3 and 4.4, giving the stopping power for electrons and positrons, respectively, are essentially the same. Their difference is due to the second term in the bracket, which is always much smaller than the logarithmic term. For an electron and positron with the same kinetic energy, Eqs. 4.3 and 4.4 provide results that are different by about 10 percent or less. For low kinetic energies, $dE/dx$ for positrons is larger than that for electrons; at about 2000 keV, the energy loss is the same; for higher kinetic energies, $dE/dx$ for positron is less than that for electrons.

As stated earlier, Eqs. 4.2 to 4.4 disregard the effect of forces between atoms and atomic electrons of the attenuating medium. A correction for this *density effect*[6,7] has been made, but it is small and it will be neglected here. The density effect reduces the stopping power slightly.

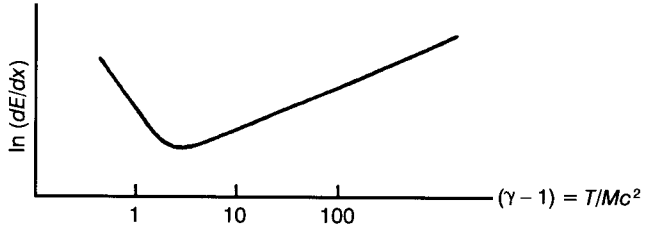


**Figure 4.3** Change of stopping power with the kinetic energy of the particle.

Equations 4.2–4.4 are not valid for very low energies. In the case of Eq. 4.2, a nuclear shell correction is applied (see Ziegler), which appears in the brackets as a negative term and becomes important at low energies ($T \leq 100$ keV). Even without this correction, the value in brackets takes a negative value when $(2mc^2\beta^2\gamma^2)/I \leq 1$. The value of this term depends on the medium because of the presence of the ionization potential $I$. As an example, for oxygen ($I = 89$ eV) this term becomes less than 1 for $T < 40$ keV.

For electrons of very low kinetic energy, Eq. 4.3, takes the form (see Roy & Reed)

$$\frac{dE}{dx} \approx 4\pi r_0^2 \frac{mc^2}{\beta^2} NZ \ln\left(\frac{mc^2\beta^2}{I}\sqrt{\frac{2.7182}{8}}\right) \qquad |\beta \ll 1 \qquad (4.5a)$$

Again for oxygen, the argument of the logarithm becomes less than 1 for electron kinetic energy $T < 76$ eV. For positrons, the low-energy limit of the validity of Eq. 4.4 is equal to the positron energy for which the whole value within brackets is less than zero.

**Example 4.1** What is the stopping power for a 5-MeV alpha particle moving in silicon?

**Answer** For silicon, $A = 28$, $Z = 14$, $\rho = 2.33$ kg/m$^3$,

$$\gamma = \frac{5 + 4(931.5)}{4(931.5)} = 1.00134 \qquad \beta^2 = 1 - \frac{1}{\gamma^2} = 0.00268$$

$$\frac{dE}{dx} = 10^{-28} \times 2^2 \frac{0.511}{0.00268} 2.33 \times 10^3 \frac{0.6022 \times 10^{24}}{28 \times 10^{-3}}$$

$$\times 14\left(\ln \frac{2(0.511)(0.00268)(1.00134)^2}{172 \times 10^{-6}} - 0.00268\right)$$

$$= 1.48 \times 10^5 \text{ MeV/m} = 2.37 \times 10^{-8} \text{ J/m} = 0.148 \text{ MeV}/\mu\text{m}$$

Or, in terms of MeV/(g/cm$^2$),

$$dE/dx = 1.48 \times 10^5 \text{ MeV/m} = 1480 \text{ MeV/cm}/(2.33\text{g/cm}^3)$$
$$= 635.2 \text{ MeV}/(\text{g/cm}^2)$$

**Example 4.2** What is the stopping power for a 5-MeV electron moving in silicon?

**Answer** For an electron,

$$\gamma = \frac{5 + 0.511}{0.511} = 10.785 \qquad \beta = \sqrt{1 - \frac{1}{\gamma^2}} = 0.9957 \qquad \beta^2 = 0.9914$$

$$\begin{aligned}\frac{dE}{dx} &= 10^{-28}\frac{0.511}{0.9914}2.33 \times 10^3\frac{0.6022 \times 10^{24}}{28 \times 10^{-3}} \\ &\quad \times 14\left[\ln \frac{0.9957(10.785)\sqrt{9.785}\,(0.511)}{172 \times 10^{-6}} + \frac{1}{2 \times 10.785^2}\right. \\ &\quad \left.\times\left(\frac{9.785^2}{8} + 1 - (10.785^2 + 2 \times 10.785 - 1)\ln 2\right)\right] \\ &= 403.5 \text{ MeV/m} = 4.035 \text{ MeV/cm} = 6.46 \times 10^{-11} \text{ J/m}\end{aligned}$$

In Ex. 4.2, the stopping power for the 5-MeV electron is, in terms of MeV/(g/cm$^2$),

$$\frac{4.035 \text{ MeV/cm}}{2.33 \text{ g/cm}^3} = 1.73 \text{ MeV/(g/cm}^2)$$

Notice the huge difference in the value of stopping power for an alpha versus an electron of the same kinetic energy traversing the same material.

Tables of $dE/dx$ values are usually given in units of MeV/(g/cm$^2$) [or in SI units of J/(kg/m$^2$)]. The advantage of giving the stopping power in these units is the elimination of the need to define the density of the stopping medium that is necessary, particularly for gases. The following simple equation gives the relationship between the two types of units:

$$\frac{1}{\rho(\text{g/cm}^3)}\frac{dE}{dx}(\text{MeV/cm}) = \frac{dE}{dx}[\text{MeV/(g/cm}^2)] \tag{4.6}$$

## 4.4 ENERGY LOSS DUE TO BREMSSTRAHLUNG EMISSION

The calculation of energy loss due to emission of bremsstrahlung is more involved than the calculation of energy loss due to ionization and excitation. Here, an approximate equation will be given for electrons or positrons only, because it is for these particles that energy loss due to emission of radiation may be important.

For electrons or positrons with kinetic energy $T$ (MeV) moving in a material with atomic number $Z$, the energy loss due to bremsstrahlung emission, $(dE/dx)_{\text{rad}}$, is given in terms of the ionization and excitation energy loss by Eq.

4.7 (see Evans).

$$\left(\frac{dE}{dx}\right)_{\text{rad}} = \frac{ZT\,(\text{MeV})}{750}\left(\frac{dE}{dx}\right)_{\text{ion}} \tag{4.7}$$

where $(dE/dx)_{\text{ion}}$ is the stopping power due to ionization-excitation (Eq. 4.3 or 4.4).

**Example 4.3** Consider an electron with $T = 5$ MeV. What fraction of its energy is lost as bremsstrahlung as it starts moving (a) in aluminum and (b) in lead?

**Answer** (a) If it travels in aluminum ($Z = 13$),

$$\left(\frac{dE}{dx}\right)_{\text{rad}} = \frac{13(5)}{750}\left(\frac{dE}{dx}\right)_{\text{ion}} = 0.09\left(\frac{dE}{dx}\right)_{\text{ion}}$$

That is, the rate of energy loss due to radiation is about 9 percent of $(dE/dx)_{\text{ion}}$.

(b) For the same electron moving in lead ($Z = 82$),

$$\left(\frac{dE}{dx}\right)_{\text{rad}} = \frac{82(5)}{750}\left(\frac{dE}{dx}\right)_{\text{ion}} = 0.55\left(\frac{dE}{dx}\right)_{\text{ion}}$$

In this case, the rate of radiation energy loss is 55 percent of $(dE/dx)_{\text{ion}}$.

Equation 4.7, relating radiation to ionization energy loss, is a function of the kinetic energy of the particle. As the particle slows down, $T$ decreases and $(dE/dx)_{\text{rad}}$ also decreases. The total energy radiated as bremsstrahlung is approximately equal in MeV to[†]

$$T_{\text{rad}} = 4.0 \times 10^{-4} ZT^2 \tag{4.8}$$

**Example 4.4** What is the total energy radiated by the electron of Ex. 4.3?

**Answer** Using Eq. 4.8,
(a) In aluminum: $T_{\text{rad}} = (4.0 \times 10^{-4})(13)5^2 = 0.130$ MeV
(b) In lead: $T_{\text{rad}} = (4.0 \times 10^{-4})(82)5^2 = 0.820$ MeV

The total stopping power for electrons or positrons is given by the sum of Eqs. 4.3 or 4.4 and 4.7:

$$\left(\frac{dE}{dx}\right)_{\text{tot}} = \left(\frac{dE}{dx}\right)_{\text{ion}} + \left(\frac{dE}{dx}\right)_{\text{rad}} = \left(1 + \frac{ZT}{750}\right)\left(\frac{dE}{dx}\right)_{\text{ion}} \tag{4.9}$$

If the particle moves in a compound or a mixture, instead of a pure element, an effective atomic number $Z_{\text{ef}}$ should be used in Eqs. 4.7 and 4.8. The value of

[†]The coefficient $4.0 \times 10^{-4}$ used in Eq. 4.8 is not universally accepted (see Evans).

$Z_{ef}$ is given by Eq. 4.10.

$$Z_{ef} = \frac{\sum_{i=1}^{L} (w_i/A_i)Z_i^2}{\sum_{i=1}^{L} (w_i/A_i)Z_i} \tag{4.10}$$

where $L$ = number of elements in the compound or mixture
$w_i$ = weight fraction of $i$th element
$A_i$ = atomic weight of $i$th element
$Z_i$ = atomic number of $i$th element

For a compound with molecular weight $M$, the weight fraction is given by

$$w_i = \frac{N_i A_i}{M} \tag{4.11}$$

where $N_i$ is the number of atoms of the $i$th element in the compound.

## 4.5 CALCULATION OF $dE/dx$ FOR A COMPOUND OR MIXTURE

Equations 4.2–4.4 give the result of the stopping power calculation if the particle moves in a pure element. If the particle travels in a compound or a mixture of several elements, the stopping power is given by

$$\left(\frac{1}{\rho}\frac{dE}{dx}\right)_{\text{compound}} = \sum_i w_i \frac{1}{\rho_i}\left(\frac{dE}{dx}\right)_i \tag{4.12}$$

where $\rho$ = density of compound or mixture
$\rho_i$ = density of the $i$th element
$1/\rho_i(dE/dx)_i$ = stopping power in MeV/(kg/m$^2$) for the $i$th element, as calculated using Eqs. 4.2–4.4 and 4.6.

**Example 4.5** What is the stopping power for a 10-MeV electron moving in air? Assume that air consists of 21 percent oxygen and 79 percent nitrogen.

**Answer** Equation 4.12 will be used, but first $dE/dx$ will have to be calculated for the two pure gases. Using Eq. 4.3,

$$\gamma = \frac{T + mc^2}{mc^2} = \frac{10 + 0.511}{0.511} = 20.569$$

$$\beta = \sqrt{\frac{\gamma^2 - 1}{\gamma^2}} = 0.9988 \qquad \beta = 0.9976$$

For oxygen,

$$\frac{1}{\rho}\left(\frac{dE}{dx}\right)_{\mathrm{O}} = 10^{-28}\left(\frac{0.511}{0.9976}\right)\frac{0.6022\times 10^{24}}{16\times 10^{-3}}(8)$$

$$\times\left[\ln\frac{0.9988(20.569)\sqrt{19.569}\,(0.511)}{115.7\times 10^{-6}} + \frac{1}{2(20.569)^2}\left(\frac{19.569^2}{8}\right.\right.$$

$$\left.\left. +1 - [(20.569)^2 + 2(20.569) - 1]\ln 2\right)\right] = 0.194\ \mathrm{MeV/(kg/m^2)}$$

$$= 3.10\times 10^{-14}\ \mathrm{J/(kg/m^2)} = 1.94\ \mathrm{MeV/(g/cm^2)}$$

For nitrogen,

$$\frac{1}{\rho}\left(\frac{dE}{dx}\right)_{\mathrm{N}} = 10^{-28}\left(\frac{0.511}{0.9976}\right)\frac{0.6022\times 10^{24}}{14\times 10^{-3}}(7)$$

$$\times\left[\ln\frac{0.9988(20.569)\sqrt{19.569}\,(0.511)}{97.8\times 10^{-6}} + \frac{1}{2(20.569)^2}\left(\frac{19.569^2}{8}\right.\right.$$

$$\left.\left. +1 - [(20.569)^2 + 2(20.569) - 1]\ln 2\right)\right] = 0.196\ \mathrm{MeV/(kg/m^2)}$$

$$= 3.14\times 10^{-14}\ \mathrm{J/(kg/m^2)} = 1.96\ \mathrm{MeV/(g/cm^2)}$$

For air,

$$\left(\frac{1}{\rho}\frac{dE}{dx}\right)_{\mathrm{air}} = 0.21\left(\frac{1}{\rho}\frac{dE}{dx}\right)_{\mathrm{O}} + 0.79\left(\frac{1}{\rho}\frac{dE}{dx}\right)_{\mathrm{N}}$$

$$= [0.21(3.10\times 10^{-14}) + 0.79(3.14\times 10^{-14})]\ \mathrm{J/(kg/m^2)}$$

$$= 3.14\times 10^{-14}\ \mathrm{J(kg/m^2)} = 1.96\ \mathrm{MeV/(g/cm^2)}$$

$$\left(\frac{dE}{dx}\right)_{\mathrm{air}} = 3.14\times 10^{-14}\ \mathrm{J/(kg/m^2)(1.29\ kg/m^3)}$$

$$= 4.05\times 10^{-14}\ \mathrm{J/m} = 0.253\ \mathrm{MeV/m}$$

## 4.6 RANGE OF CHARGED PARTICLES

A charged particle moving through a certain material loses its kinetic energy through interactions with the electrons and nuclei of the material. Eventually, the particle will stop, pick up the necessary number of electrons from the surrounding matter, and become neutral. For example,

$$p^+ + e^- \rightarrow \text{hydrogen atom}$$

$$\alpha^{2+} + 2e^- \rightarrow \text{He atom}$$

The total distance traveled by the particle is called the *pathlength*. The pathlength $S$, shown in Fig. 4.4, is equal to the sum of all the partial pathlengths $S_i$. The thickness of material that just stops a particle of kinetic energy $T$, mass $M$, and charge $z$ is called the *range* $R$ of the particle in that material. It is obvious that $R \leq S$. For electrons, which have a zig-zag path, $R < S$. For heavy charged particles, which are very slightly deflected, $R \approx S$.

Range is distance, and its basic dimension is length (m). In addition to meters, another common unit used for range is kg/m$^2$ (or g/cm$^2$). The relationship between the two is

$$R(\text{kg/m}^2) = [R(\text{m})][\rho(\text{kg/m}^3)] \tag{4.13}$$

where $\rho$ is the density of the material in which the particle travels. The range measured in kg/m$^2$ is independent of the state of matter. That is, a particle will have the same range in kg/m$^2$ whether it moves in ice, water, or stream. Of course, the range measured in meters will be different.

The range is an average quantity. Particles of the same type with the same kinetic energy moving in the same medium will not stop after traveling exactly the same thickness $R$. Their pathlength will not be the same either. What actually happens is that the end points of the pathlengths will be distributed around an average thickness called the range. To make this point more clear, two experiments will be discussed dealing with transmission of charged particles. Heavy particles and electrons-positrons will be treated separately.

### 4.6.1 Range of Heavy Charged Particles ($p, d, t, \alpha$; $1 \leq A \leq 4$)

Consider a parallel beam of heavy charged particles all having the same energy and impinging upon a certain material (Fig. 4.5). The thickness of the material may be changed at will. On the other side of the material, a detector records the particles that traverse it. It is assumed that the particle direction does not change and that the detector will record all particles that go through the material, no matter how low their energy is. The number of particles $N(t)$ traversing the thickness $t$ changes, as shown in Fig. 4.6.

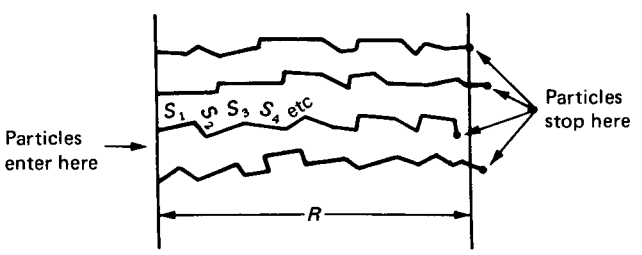


**Figure 4.4** Pathlength ($S$) and range ($R$). The end points of the pathlengths are distributed around an average thickness that is the range.

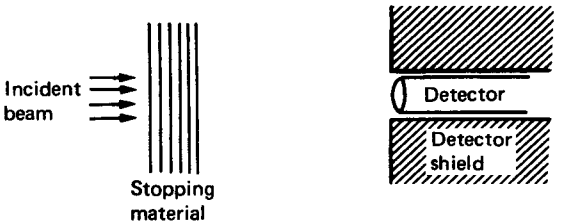


**Figure 4.5** Particle transmission experiment.

In the beginning, $N(t)$ stays constant, even though $t$ changes. Beyond a certain thickness, $N(t)$ starts decreasing and eventually goes to zero. The thickness for which $N(t)$ drops to half its initial value is called the *mean range* $R$. The thickness for which $N(t)$ is practically zero is called the *extrapolated range* $R_e$. The difference between $R$ and $R_e$ is about 5 percent or less. Unless otherwise specified, when range is used, it is the mean range $R$.

Semiempirical formulas have been developed that give the range as a function of particle kinetic energy. For alpha particles, the range in air at normal temperature and pressure is given by

$$\begin{aligned} R(\text{mm}) &= \exp\left[1.61\sqrt{T(\text{MeV})}\right] && 1 < T \leq 4 \text{ MeV} \\ R(\text{mm}) &= (0.05T + 2.85)T^{3/2} \text{ (MeV)} && 4 \leq T \leq 15 \text{ MeV} \end{aligned} \tag{4.14}$$

where $T$ = kinetic energy of the particle in MeV. Figure 4.7 gives the range of alphas in silicon.

If the range is known for one material, it can be determined for any other by applying the Bragg-Kleeman rule†:

$$\frac{R_1}{R_2} = \frac{\rho_2}{\rho_1}\sqrt{\frac{A_1}{A_2}} \tag{4.15}$$

where $\rho_i$ and $A_i$ are the density and atomic weight, respectively, of material $i$. For a compound or mixture, an effective molecular weight is used, obtained

†The Bragg-Kleeman rule does not hold for electron or positron ranges.

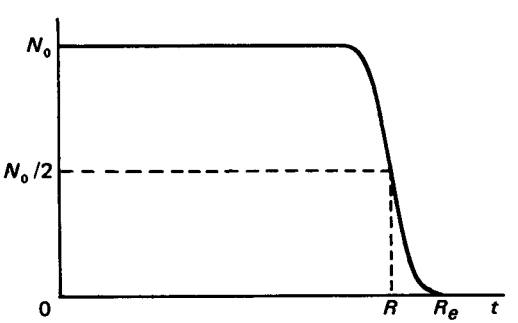


**Figure 4.6** The number of heavy charged particles $(\alpha, p, d, t)$ transmitted through thickness $t$.

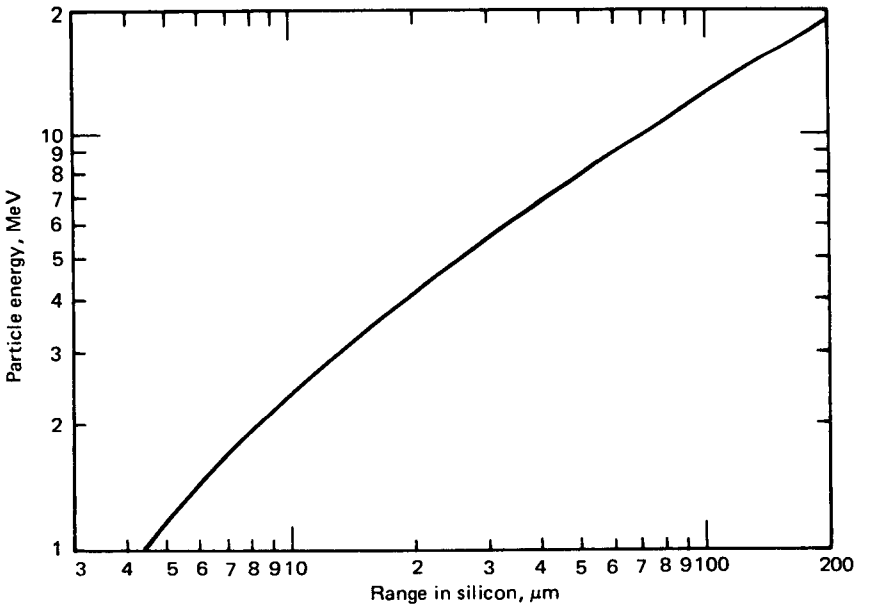


**Figure 4.7** Range-energy curve for alpha particles in silicon (Ref. 8).

from the equation

$$\sqrt{A_{\text{ef}}} = \left( \sum_{i=1}^{L} \frac{w_i}{\sqrt{A_i}} \right)^{-1} \tag{4.16}$$

where the quantities $w_i$, $A_i$, and $L$ have the same meaning as in Eq. 4.10.

**Example 4.6** What is the effective molecular weight for water? What is it for air?

**Answer** For $H_2O$ (11% H, 89% O),

$$\sqrt{A_{\text{ef}}} = \left( \frac{0.11}{\sqrt{1}} + \frac{0.89}{\sqrt{16}} \right)^{-1} = 3 \qquad A_{\text{ef}} = 9$$

For air (22.9% O, 74.5% N, 2.6% Ar),

$$\sqrt{A_{\text{ef}}} = \left( \frac{0.229}{\sqrt{16}} + \frac{0.745}{\sqrt{14}} + \frac{0.026}{\sqrt{40}} \right)^{-1} = 3.84 \qquad A_{\text{ef}} = 14.74$$

Using the Bragg-Kleeman rule (Eq. 4.15), with air at normal temperature and pressure as one of the materials ($\rho = 1.29$ kg/m$^3$, $\sqrt{A_{\text{ef}}} = 3.84$), one

obtains

$$R\ (\text{mm}) = (3.36 \times 10^{-1})\frac{\sqrt{A_{\text{ef}}}}{\rho\ (\text{kg/m}^3)}R_{\text{air}}\ (\text{mm}) \tag{4.17}$$

There are two ways to obtain the range of alphas in a material other than air and silicon:

1. The range in air should be obtained first, using Eq. 4.14, and then the range in the material of interest should be calculated using Eq. 4.17.
2. The range in silicon could be read from Fig. 4.7, and then the range in the material of interest should be calculated using Eq. 4.15.

**Example 4.7** What is the range of a 3-MeV alpha particle in gold?

**Answer** The range of this alpha in silicon is (Fig. 4.7) $R = 12.5\ \mu\text{m} = 12.5 \times 10^{-6}$ m. Using Eq. 4.15, the range in gold is

$$R_{\text{Au}} = (12.5 \times 10^{-6})\frac{2.33 \times 10^3}{19.32 \times 10^3}\sqrt{\frac{197}{28}} = 4 \times 10^{-6}\ \text{m} = 4\ \mu\text{m}$$

Or, using Eqs. 4.14 and 4.17,

$$R_{\text{Au}} = (3.2 \times 10^{-1})\frac{\sqrt{197}}{19.32 \times 10^3}\exp(1.61\sqrt{3}) = 3.8 \times 10^{-3}\ \text{mm} = 3.8\ \mu\text{m}$$

**Example 4.8** What is the range of a 10-MeV alpha particle in aluminum?

**Answer** From Fig. 4.7, the range in silicon is $R = 72\ \mu\text{m} = 7.2 \times 10^{-5}$ m. Using Eq. 4.15, the range in aluminum is

$$R_{\text{Al}} = (72\ \mu\text{m})\frac{2.33 \times 10^3}{2.7 \times 10^3}\sqrt{\frac{27}{28}} = 60.7\ \mu\text{m}$$

Or, using Eqs. 4.14 and 4.17,

$$\begin{aligned} R_{\text{Al}} &= (3.36 \times 10^{-1})\frac{\sqrt{27}}{2.7 \times 10^3}[0.05(10) + 2.85]10^{3/2}\ \text{mm} \\ &= 6.85 \times 10^{-5}\ \text{m} = 68.5\ \mu\text{m} \end{aligned}$$

The difference of 8 $\mu$m is within the range of accuracy of the Bragg-Kleeman rule and the ability to read a log-log graph.

The range of protons in *aluminum* has been measured by Bichsel.[9] His results are represented very well by the following two equations:

$$R(\mu\text{m}) = 14.21T^{1.5874} \qquad 1\ \text{MeV} < T \leq 2.7\ \text{MeV} \tag{4.18}$$

$$R(\mu\text{m}) = 10.5\frac{T^2}{0.68 + 0.434 \ln T} \qquad 2.7\ \text{MeV} \leq T < 20\ \text{MeV} \tag{4.19}$$

For other materials, Eq. 4.15 should be used after the range in aluminum is determined from Eqs. 4.18 and 4.19. A very comprehensive paper dealing with proton stopping power, as well as range, for many materials is that of Janni.[4]

The range of protons and deuterons can be calculated from the range of an alpha particle *of the same speed* using the formula

$$R(p,d) = 4\frac{M(p,d)}{M_\alpha}R_\alpha - 2\ (\text{mm, air}) \tag{4.20}$$

where $R_\alpha$ = range in air of an alpha particle having the same speed as the deuteron or the proton
$M$ = mass of the particle (1 for proton, 2 for deuteron)
$M_\alpha$ = mass of alpha particle = 4

For materials other than air, the Bragg-Kleeman rule (Eq. 4.17) should be used.

The fact that the alpha and proton or deuteron ranges are related by the same speed rather than the same kinetic energy is due to the dependence of $dE/dx$ on the speed of the particle.

**Example 4.9** What is the range of the 5-MeV deuteron in air?

**Answer** Equation 4.20 will be used, but first the range of an alpha particle with speed equal to that of a 5-MeV deuteron will have to be calculated. The kinetic energy of an alpha particle with the *same speed* as that of the deuteron will be found using the corresponding equations for the kinetic energy. Since $T = \frac{1}{2}MV^2$ for these nonrelativistic particles.

$$T_\alpha = \frac{M_\alpha}{M_d}T_d = 2T_d = 10\ \text{MeV}$$

The range of a 10-MeV alpha particle (in air) is (Eq. 4.14)

$$R_\alpha = (0.05T + 2.85)T^{3/2} = 106\ \text{mm} = 0.106\ \text{m}$$

The range of the 5-MeV deuteron (in air) is then (Eq. 4.20)

$$R_d = 2R_\alpha - 2 = 210 \text{ mm} = 0.21 \text{ m}$$

**Example 4.10** What is the range of a 5-MeV deuteron in aluminum?

**Answer** Using the Bragg-Kleeman rule (Eq. 4.17) and the result of the previous example,

$$R_d(\text{Al}) = (3.36 \times 10^{-1})\frac{\sqrt{27}}{2.7 \times 10^3} 210 \text{ mm} = 0.136 \text{ mm} = 136\ \mu\text{m}$$

### 4.6.2 Range of Electrons and Positrons

Electrons and positrons behave in essentially the same way with regard to energy loss, slowing down, and penetration through matter. Small differences exist; one was indicated when $dE/dx$ was discussed in Sec. 4.3. Small differences in the values of the range between electrons and positrons should also be expected, and indeed this is the case. Most of the range measurements have been performed with electrons because electrons are used much more frequently than positrons in radiation measurements. For this reason, from this point on, only electrons will be discussed. The reader should be aware that the results are equally applicable for positrons, to a first approximation, but for very accurate results the references listed at the end of this chapter should be consulted.

If the experiment shown in Fig. 4.5 and discussed in Sec. 4.6.1 is repeated with the incident beam consisting of monoenergetic electrons, the result will look as shown in Fig. 4.8. For electrons, the transmission curve does not have a flat part. It decreases gradually to a level which is the background. The range† is equal to the thickness of the material, which is defined by the point where the linear extrapolation of the transmission curve meets the background.

†In many texts, this is called the "extrapolated" range. Since only one type of range is used, there is no need to carry along the world "extrapolated."

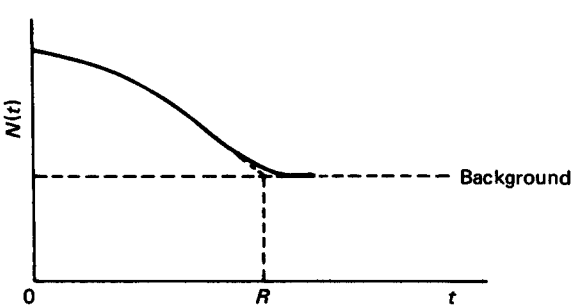


**Figure 4.8** The number of electrons transmitted through thickness $t$. Experiment setup shown in Fig. 4.5.

The semiempirical equation giving the range of electrons for the energy range 0.3 keV to 30 MeV has been developed by Tabata, Ito, and Okabe,[10] based on the experimental results available until 1972. This equation, indicated from now on as the TIO equation, has the following form:

$$R(\text{kg/m}^2) = a_1\left(\frac{\ln[1 + a_2(\gamma - 1)]}{a_2} - \frac{a_3(\gamma - 1)}{1 + a_4(\gamma - 1)^{a_5}}\right) \tag{4.21}$$

where

$$a_1 = \frac{2.335A}{Z^{1.209}} \qquad a_3 = 0.9891 - (3.01 \times 10^{-4}Z)$$

$$a_2 = 1.78 \times 10^{-4}Z \qquad a_4 = 1.468 - (1.180 \times 10^{-2}Z) \tag{4.22}$$

$$a_5 = \frac{1.232}{Z^{0.109}}$$

$A$, $Z$, and $\gamma$ have been defined in Sec. 4.3.

Figures 4.9 and 4.10 show results based on Eq. 4.21, as well as experimental points.

In the case of absorbers that are mixtures or compounds, the atomic number $Z$ and atomic weight $A$ to be used in Eq. 4.22 are given by

$$Z_{\text{ef}} = \sum_i^L w_i Z_i \tag{4.23}$$

$$A_{\text{ef}} = Z_{\text{ef}}\left(\sum_i^L w_i \frac{Z_i}{A_i}\right)^{-1} \tag{4.24}$$

where $w_i$ is the weight fraction of element with atomic number $Z_i$ and atomic weight $A_i$.

**Example 4.11** What is the range of 1-MeV electrons in gold? ($Z = 79$, $A = 197$.)

**Answer** Using Eqs. 4.21 and 4.22,

$$a_1 = \frac{2.335(197)}{79^{1.209}} = 2.336$$

$$a_2 = (1.78 \times 10^{-4})(79) = 0.01406$$

$$a_3 = 0.9891 - (3.01 \times 10^{-4})(79) = 0.965$$

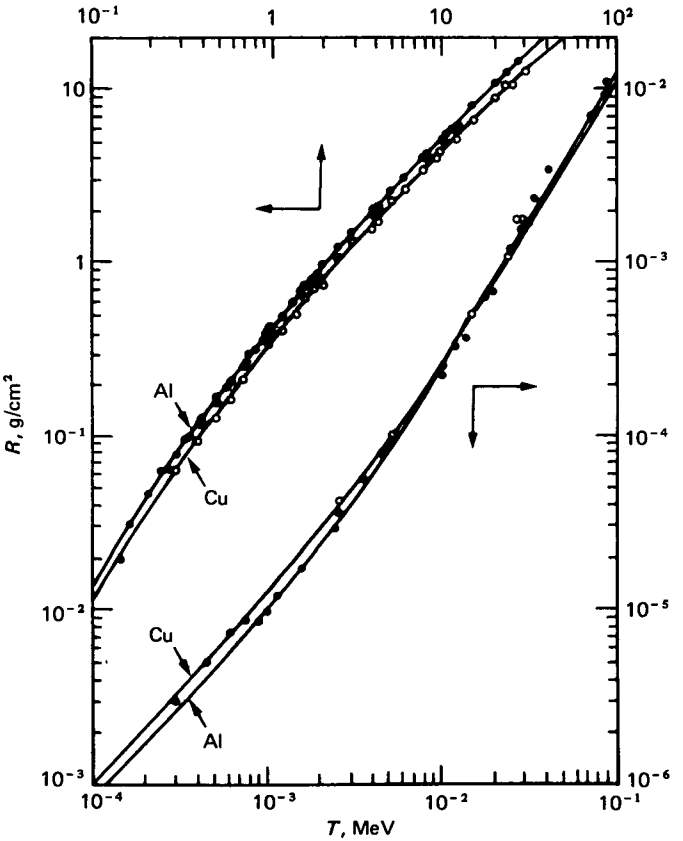


**Figure 4.9** The range of electrons as a function of their kinetic energy as obtained by using Eq. 4.21. The solid circles are experimental data for Al; the open circles are for Cu (from Ref. 10).

$$a_4 = 1.468 - (1.180 \times 10^{-2})(79) = 0.5358$$

$$a_5 = \frac{1.232}{79^{0.109}} = 0.765$$

$$\gamma = \frac{1.511}{0.511} = 2.957$$

$$R = 2.336\left(\frac{\ln(1 + 0.0275)}{0.01406} - \frac{1.8885}{1.895}\right) = 2.18 \text{ kg/m}^2 = 0.218 \text{ g/cm}^2$$

Since the density of gold is $19.3 \times 10^3$ kg/m$^3$, the range in $\mu$m is

$$R = \frac{2.18 \text{ kg/m}^2}{19.3 \times 10^3 \text{ kg/m}^3} = 1.13 \times 10^{-4} \text{ m} = 113\ \mu\text{m}$$

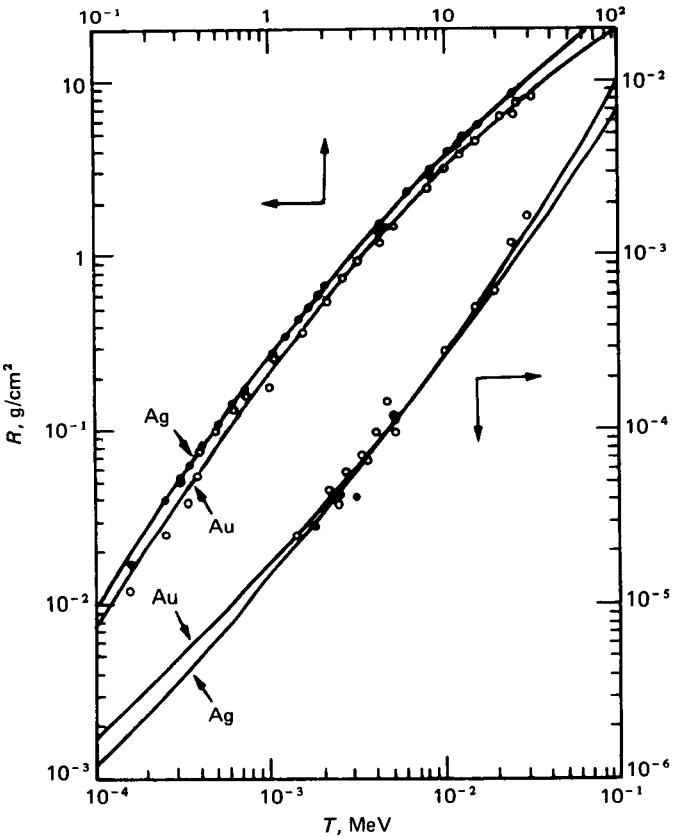


**Figure 4.10** The range of electrons as a function of their kinetic energy as obtained by using Eq. 4.21. The solid circles are experimental data for Ag; the open circles are for Au (from Ref. 10).

**Example 4.12** What is the range of 1-MeV electrons in aluminum? ($Z = 13$, $A = 27$.)

**Answer** Again, using Eq. 4.21 and 4.22,

$$a_1 = \frac{2.335(27)}{13^{1.209}} = 2.837$$

$$a_2 = (1.78 \times 10^{-4})(13) = 2.314 \times 10^{-3}$$

$$a_3 = 0.9891 - (3.01 \times 10^{-4})(13) = 0.985$$

$$a_4 = 1.468 - (1.180 \times 10^{-2})(13) = 1.3146$$

$$a_5 = \frac{1.232}{13^{0.109}} = 0.9315$$

$$R = 2.837\left(\frac{\ln(1.0045)}{0.00231} - \frac{1.928}{3.457}\right) = 3.93\ \text{kg/m}^2 = 0.393\ \text{g/cm}^2$$

Since the density of aluminum is $2.7 \times 10^3$ kg/m$^3$, the range in $\mu$m is

$$R = \frac{3.93\ \text{kg/m}^2}{2.7 \times 10^3\ \text{kg/m}^3} = 1.46 \times 10^{-3}\ \text{m} = 1460\ \mu\text{m}$$

### 4.6.3 Transmission of Beta Particles

Beta particles have a continuous energy spectrum extending from zero energy up to maximum kinetic energy $E_{max}$ (see Sec. 3.7.3). If the transmission experiment shown in Fig. 4.5 is repeated with an incident beam of $\beta$ particles, the result will look as shown in Fig. 4.11. The number of betas $N(t)$ transmitted through a thickness $t$ is very closely represented by

$$N(t) = N(0)e^{-\mu t} \tag{4.25}$$

where $\mu$ is called the mass absorption coefficient.

The value of $\mu$ has been determined experimentally as a function of the maximum beta energy and is given by

$$\mu\ (\text{m}^2/\text{kg}) = 1.7E_{max}^{-1.14} \tag{4.26}$$

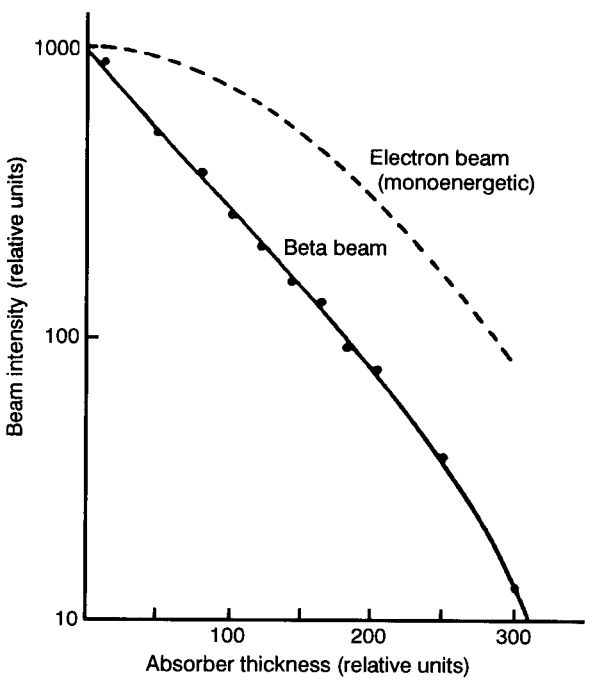


**Figure 4.11** Transmission of betas. A corresponding curve for monoenergetic electrons is also shown with $E_{mono} = E_{max}$.

where $E_{max}$ is in MeV. Notice that $\mu$ is given in units of $m^2/kg$; therefore the thickness $t$ in the exponent of Eq. 4.25 should be in $kg/m^2$. The exponential transmission law represented by Eq. 4.25 is the result of experimental observation. There is no theory predicting it. The range of $\beta$ particles is calculated using Eq. 4.21 for kinetic energy equal to $E_{max}$.

**Example 4.13** What fraction of 2-MeV betas will go through a single Al foil of thickness 0.1 mm?

**Answer** The mass absorption coefficient is, using Eq. 4.26.

$$\mu = 1.7 \times 2^{-1.14} = 0.7714\ m^2/kg$$

The fraction transmitted is, using Eq. 4.25,

$$\frac{N(t)}{N(0)} = e^{-\mu t} = \exp[-0.7714\ m^2/kg(0.1 \times 10^{-3}\ m)(2.7 \times 10^3\ kg/m^3)]$$
$$= \exp(-0.208) = 0.81$$

Therefore, 81 percent of the betas will go through this foil.

### 4.6.4 Energy Loss after Traversing a Material of Thickness $t < R$

One is often required to calculate the energy loss of a charged particle after it traverses a material of thickness $t$. The first step in solving such a problem is to calculate the range of the particle in that medium. If the range is $R < t$, the particle stopped in the medium and the total energy lost is equal to the initial energy of the particle. If $R > t$, the energy loss $\Delta E$ is given by

$$\Delta E = \int_0^t \left(\frac{dE}{dx}\right) dx \tag{4.27}$$

where $dE/dx$ is the total stopping power (ionization-excitation plus radiation loss). If $t \ll R$, one may take $dE/dx$ as constant and obtain

$$\Delta E = \left(\frac{dE}{dx}\right)_0 t \qquad t \ll R \tag{4.28}$$

where $(dE/dx)_0$ is the stopping power calculated for the initial energy of the particle.

If the thickness $t$ is a considerable fraction of the range, $dE/dx$ cannot be considered constant. Then, Eq. 4.27 should be integrated using the appropriate form of $dE/dx$. Since the stopping power is a complicated expression, the integration cannot be carried out by hand. A numerical integration can be performed by a computer. In most cases, however, the following approach gives adequate results.

The thickness $t$ is divided into $N$ segments of length $\Delta x_i$, where

$$\sum_{i=1}^{N} \Delta x_i = t$$

Equation 4.27 takes the form

$$\Delta E = \sum_{i=1}^{N} \left(\frac{dE}{dx}\right)_i \Delta x_i \tag{4.29}$$

where $(dE/dx)_i$ is the stopping power calculated for the kinetic energy of the particle at the beginning of the segment $\Delta x_i$.

There is no general rule as to the best value of the number of segments $N$. Obviously, $N$ should be such that $(dE/dx)_i$ changes by a small but acceptable amount as the particle travels the segment $\Delta x_i$.

**Example 4.14** What is the energy loss of a 10-MeV electron going through 15 mm of aluminum?

**Answer** Using Eq. 4.21 or Fig. 4.9, the range of a 10-MeV electron in aluminum is $R = 20.4$ mm. The particle will emerge, but the thickness of the absorber is a considerable fraction of the range. Therefore, one should use Eq. 4.29.

If one chooses $N = 5$ and equal segments, Eq. 4.29 takes the form

$$\Delta E = \sum_{i=1}^{5} \left(\frac{dE}{dx}\right)_i \Delta x_i \qquad \Delta x_i = 3 \text{ mm}$$

The table below shows how the calculation proceeds.

| $i$ | $T_i$ (MeV) | $dE/dx$ (MeV/mm) | $(\Delta E)_i$ (MeV) | $T_{i+1} = T_i - (\Delta E)_i$ |
|---|---|---|---|---|
| 1 | 10 | 0.605 | 1.815 | 8.185 |
| 2 | 8.185 | 0.568 | 1.704 | 6.481 |
| 3 | 6.481 | 0.530 | 1.590 | 4.891 |
| 4 | 4.891 | 0.492 | 1.476 | 3.415 |
| 5 | 3.415 | 0.457 | 1.373 | 2.042 |

Total energy loss is 7.958 MeV. Using $(dE/dx)_i$, the energy loss would have been equal to 0.605 MeV/mm × 15mm = 9.075 MeV, which is overestimated by about 14%.

## 4.7 STOPPING POWER AND RANGE OF HEAVY IONS ($Z > 2$, $A > 4$)

### 4.7.1 Introduction

The equations presented in Secs. 4.3–4.6 for energy loss and range of charged particles were derived with the assumption that the charge of the particle does not change as the particle traverses the medium. This assumption is certainly

valid for electrons, positrons, protons, and deuterons ($Z = 1$). It holds well for alphas too ($Z = 2$). However, for $Z > 2$, the charge of the particle cannot be assumed constant, and for this reason the energy loss and range calculations require special treatment.

Consider an atom or an ion with speed greater than the orbital velocity of its own electrons. If this particle enters a certain medium, the atomic electrons will be quickly removed from the atom or ion, leaving behind a bare nucleus. The nucleus will keep moving through the medium, continuously losing energy in collisions with the electrons of the medium.† It is probable that the ion will capture an electron in one of these collisions. It is also probable that the electron will be lost in another collision. As the ion slows down and its speed becomes of the same order of magnitude as the orbital speeds of the atomic electrons, the probability for electron capture increases, while the probability for electron loss decreases. When the ion slows down even farther and is slower than the orbiting electrons, the probability of losing an electron becomes essentially zero, while the probability of capturing one becomes significant. As the speed of the ion continues to decrease, a third electron is captured, then a fourth, and so on. At the end, the ion is slower than the least bound electron. By that time, it is a neutral atom. What is left of its kinetic energy is exchanged through nuclear and not electronic collisions. The neutral atom is considered as stopped when it either combines chemically with one of the atoms of the material or is in thermal equilibrium with the medium.

### 4.7.2 The $dE/dx$ Calculation

The qualitative discussion of Sec. 4.7.1 showed how the charge of a heavy ion changes as the ion slows down in the medium. It is this variation of the charge that makes the energy loss calculation very difficult. There is no single equation given $dE/dx$ for all heavy ions and for all stopping materials. Instead, $dE/dx$ is calculated differently, depending on the speed of the ion relative to the speed of the orbital electrons.

The stopping power is written, in general, as the sum of two terms:

$$\frac{dE}{dx} = \left(\frac{dE}{dx}\right)_e + \left(\frac{dE}{dx}\right)_n \tag{4.30}$$

where $(dE/dx)_e$ = electronic energy loss
$(dE/dx)_n$ = nuclear energy loss

An excellent review of the subject is presented by Northcliffe[11] and Lindhard, Scharff, and Schiott.[12] The results are usually presented as universal curves in terms of two dimensionless quantities, the distance $s$ and the energy $\epsilon$, first

†Collisions with nuclei are not important if the particle moves much faster than the atomic electrons.

introduced by Lindhard et al.[10] and defined as follows:

$$s = 4\pi a^2 N \frac{M_1 M_2 x}{(M_1 + M_2)^2} \tag{4.31}$$

$$\epsilon = \frac{a}{r_0}\left(\frac{M_2}{Z_1 Z_2 (M_1 + M_2)}\right)\frac{T}{mc^2} \tag{4.32}$$

where† $a = 0.8853 a_0 (Z_1^{2/3} + Z_2^{2/3})^{-1/2}$
$x$ = actual distance traveled
$a_0 = h^2/me^2$ = Bohr radius = $5.29 \times 10^{-11}$ m
$Z_1, M_1$ = charge and mass of incident particle
$Z_2, M_2$ = charge and mass of stopping material
The parameters $N$, $r_0$, and $mc^2$ have been defined in Sec. 4.3.

At high ion velocities, $v \gg v_0 Z_1^{2/3}$, where $v_0 = e^2/\hbar$ = orbital velocity of the electron in the hydrogen atom, the nuclear energy loss is negligible. The particle has an effective charge equal to $Z_1$, and the energy loss is given by an equation of the form

$$\frac{dE}{dx} \sim \frac{Z_1^2 Z_2}{v^2 A_2} \ln \frac{2mv^2}{I} \tag{4.33}$$

which is similar to Eq. 4.2.

At velocities of the order of $v \approx v_0 Z_1^{2/3}$, the ion starts picking up electrons and its charge keeps decreasing. The energy loss through nuclear collisions is still negligible.

In the velocity region $v \lesssim v_0 Z_1^{2/3}$, the electronic energy loss equation takes the form[10]

$$\left(\frac{d\epsilon}{d\rho}\right)_e = k\epsilon^n \tag{4.34}$$

where

$$k = \xi_e \frac{0.0793 Z_1 Z_2 (A_1 + A_2)^{3/2}}{(Z_1^{2/3} + Z_2^{2/3})^{3/4} A_1^{3/2} A_2^{1/2}}$$

$$\xi_e \approx Z_1^{1/6}$$

and $n$ has a value very close to $\frac{1}{2}$.[12,13] The constant $k$ depends on $Z$ and $A$ only, not on energy, and its value is less than 1. Some typical values are given in Table 4.2.

Table 4.3 shows the kinetic energy per unit atomic mass, as well as the kinetic energy, of several ions for $v = v_0 Z_1^{2/3}$.

The electronic stopping power for different ions and stopping materials is obtained by using the following semiempirical approach.

†The number $0.8853 = (9\pi^2)^{1/3}/2^{7/3}$ is called the Thomas-Fermi constant.

**Table 4.2 Values of $k$ Used in Eq. 4.34**

| $Z_1$ | $A_1$ | $Z_2$ | $A_2$ | $k$ |
|---|---|---|---|---|
| 10 | 50 | 13 | 27 | 0.085 |
| 20 | 60 | 79 | 197 | 0.022 |
| 92 | 238 | 79 | 197 | 0.162 |

The ratio of stopping power for two ions having the same velocity and traveling in the same medium is given by (using Eq. 4.33):

$$\frac{(dE/dx)_{T_1Z_1A_1}}{(dE/dx)_{T_2Z_2A_2}} = \frac{Z_1^2}{Z_2^2} \tag{4.35}$$

The application of Eq. 4.35 to heavy ions should take into account the change of the charge $Z_1$ as the ion slows down. This is accomplished by replacing $Z_1$ with an effective charge,

$$Z_{\text{eff}} = \eta Z_1$$

where $\eta$ is a parameter that depends on energy. The second particle in Eq. 4.35 is taken to be the proton ($Z_2 = A_2 = 1$), thus leading to the form[14-16]

$$\frac{(dE/dx)_{Z_1A_1T_1}}{(dE/dx)_{pT_p}} = \frac{\eta^2 Z_1^2}{\eta_p^2} \tag{4.36}$$

where the effective proton charge $\eta_p$ is given by Eq. 4.37, reported by Booth & Grant[14], and $T_p$ is the proton kinetic energy in MeV:

$$\eta_p^2 = \left[1 - \exp(-150T_p)\right] \exp(-0.835e^{-14.5T_p}) \tag{4.37}$$

**Table 4.3 The Kinetic Energy of Heavy Ions for Several Values of $v = v_0 Z^{2/3}$**

| Ion | $Z_1$ | $v_0 Z_1^{2/3}$ ($\times 10^{-7}$) (m/s) | $\beta$ ($\times 10^2$) | $T/A_1$ | $T$ (MeV) |
|---|---|---|---|---|---|
| C | 6 | 0.72 | 2.4 | 0.27 | 3.3 |
| Al | 13 | 1.2 | 4.04 | 0.76 | 20.7 |
| Ni | 28 | 2.0 | 6.7 | 2.13 | 126 |
| Br | 35 | 2.3 | 7.8 | 2.87 | 230 |
| Ag | 47 | 2.8 | 9.5 | 4.27 | 461 |
| I | 53 | 3.1 | 10.3 | 5.02 | 638 |
| Au | 79 | 4.0 | 13.4 | 8.6 | 1694 |
| U | 92 | 4.5 | 14.9 | 10.57 | 2515 |

Equations giving the value of $\eta$ have been reported by many investigators.[14-17] The most recent equation reported by Forster et al.[17] valid for $8 \leq Z_1 \leq 20$ and for $v/v_0 > 2$ is

$$\eta = 1 - A(Z_1)\exp\left(-0.879\frac{v}{v_0}Z_1^{-0.65}\right) \tag{4.38}$$

with

$$A(Z_1) = 1.035 - 0.4\exp(-0.16Z_1)$$

The proton stopping power is known.[18] Brown[19] has developed an equation of the form

$$\ln\left(\frac{dE}{dx}\right)_p = a + b\ln T_p + C(\ln T_p)^2 \tag{4.39}$$

by least squares fitting the data of Northcliffe and Schilling.[18] The most recent data are those of Janni.[4]

The experimental determination of $dE/dx$ is achieved by passing ions of known initial energy through a thin layer of a stopping material and measuring the energy loss. The thickness $\Delta x$ of the material should be small enough that $dE/dx \approx \Delta E/\Delta x$. Unfortunately, such a value of $\Delta x$ is so small, especially for very heavy ions, that the precision of measuring $\Delta x$ is questionable and the uniformity of the layer has an effect on the measurement. Typical experimental results of stopping power are presented in Fig. 4.12. The data of Fig. 4.12 come from Ref. 13. The solid line is based on the following empirical equation proposed by Bridwell and Bucy[20] and Bridwell and Moak[21]:

$$\frac{dE}{dx}[\text{MeV}/(\text{kg m}^2)] = \frac{2064.5}{A_2}\sqrt{\frac{TA_1Z_2}{Z_1}} \tag{4.40}$$

where $T$ is the kinetic energy of the ion in MeV.

For a compound or mixture, $dE/dx$ can be obtained by using Eq. 4.12 with $(dE/dx)_i$ obtained from Eq. 4.36 or Eq. 4.40.

At velocities $v < v_0 Z_1^{2/3}$, the energy loss through nuclear elastic collisions becomes important. The so-called *nuclear stopping power* is given by the following approximate expression[10]:

$$\left(\frac{d\epsilon}{d\rho}\right)_n = \frac{1}{2\epsilon}\ln(1.294\epsilon) \tag{4.41}$$

While the electronic stopping power $(d\epsilon/d\rho)_e$ continuously decreases as the ion speed $v$ decreases, the nuclear stopping power increases as $v$ decreases, goes through a maximum, and then decreases again (Fig. 4.13).

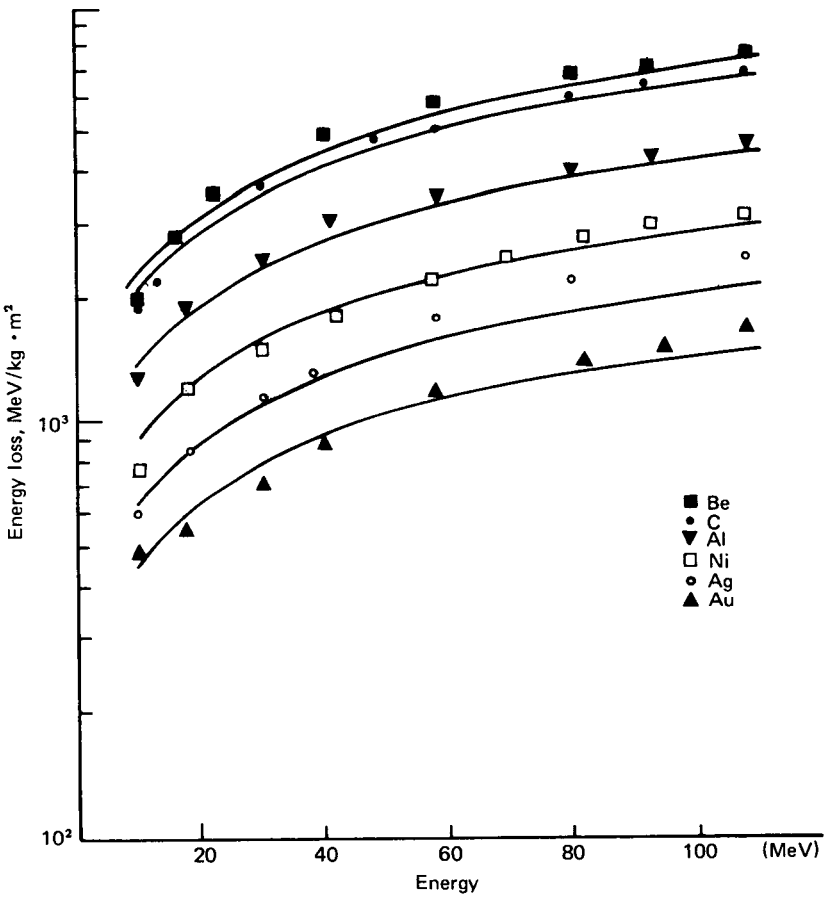


**Figure 4.12** Energy loss of iodine ions in several absorbers (Ref. 13). The curves are based on Eq. 4.40.

### 4.7.3 Range of Heavy Ions

The range of heavy ions has been measured and calculated for many ions and for different absorbers. But there is no single equation—either theoretical or empirical—giving the range in all cases. Heavy ions are hardly deflected along their path, except very close to the end of their track, where nuclear collisions become important. Thus the range $R$, which is defined as the depth of penetration along the direction of incidence, will be almost equal to the pathlength, the actual distance traveled by the ion. With this observation in mind, the range is given by the equation

$$R = \int_0^E \frac{dE}{(dE/dx)_e + (dE/dx)_n} \tag{4.42}$$

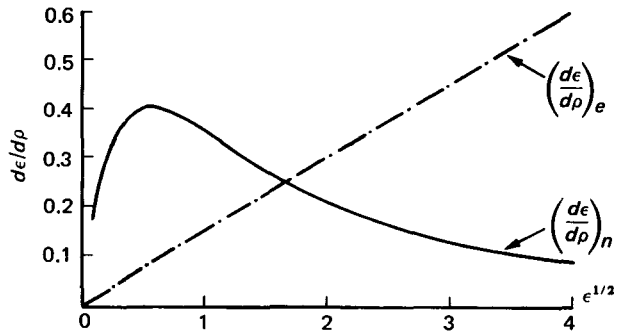


**Figure 4.13** The electronic and nuclear energy loss as a function of the dimensionless energy $\epsilon$ (Ref. 12).

Results of calculations based on Eq. 4.42 are given by many authors. Based on calculations described in Ref. 12, Siffert and Coche[22] present universal graphs for several heavy ions in silicon (Figs. 4.14 and 4.15).

The range of a heavy ion in a compound or mixture is calculated from the range in pure elements by using the equation[23,24]

$$R(\text{kg/m}^2) = \left( \sum_i \frac{w_i}{R_i} \right)^{-1} \tag{4.43}$$

where $R_i$ = range, in kg/m$^2$, in element $i$
$w_i$ = weight fraction of $i$th element

## 4.8 INTERACTIONS OF PHOTONS WITH MATTER

Photons, also called X-rays or $\gamma$-rays, are electromagnetic radiation. Considered as particles, they travel with the speed of light $c$ and they have zero rest mass and charge. The relationship between the energy of a photon, its wavelength $\lambda$, and frequency is

$$E = h\nu = h\frac{c}{\lambda} \tag{4.44}$$

There is no clear distinction between X-rays and $\gamma$-rays. The term X-rays is applied generally to photons with $E < 1$ MeV. Gammas are the photons with $E > 1$ MeV. In what follows, the terms photon, $\gamma$, and X-ray will be used interchangeably.

X-rays are generally produced by atomic transitions such as excitation and ionization. Gamma rays are emitted in nuclear transitions. Photons are also produced as bremsstrahlung, by accelerating or decelerating charged particles. X-rays and $\gamma$-rays emitted by atoms and nuclei are monoenergetic. Bremsstrahlung has a continuous energy spectrum.

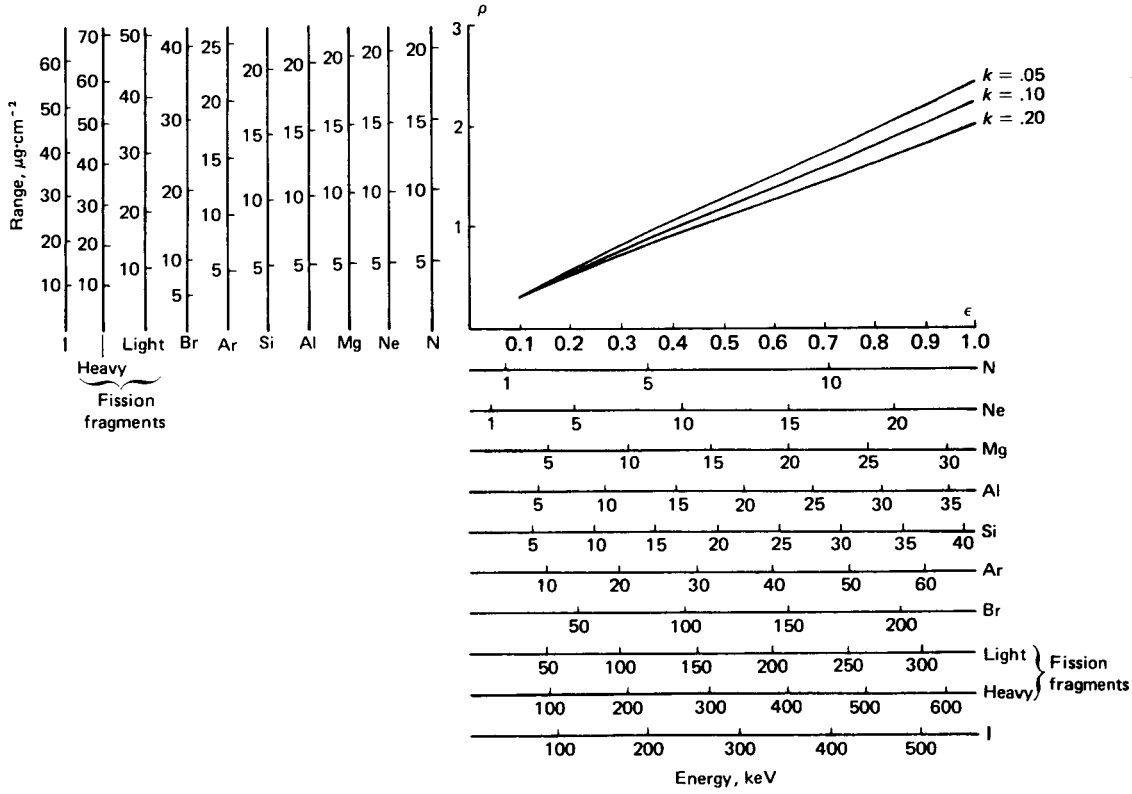


**Figure 4.14** Universal range-energy plot for $\epsilon < 1$. It allows determination of range in silicon for many heavy ions (Ref. 22).

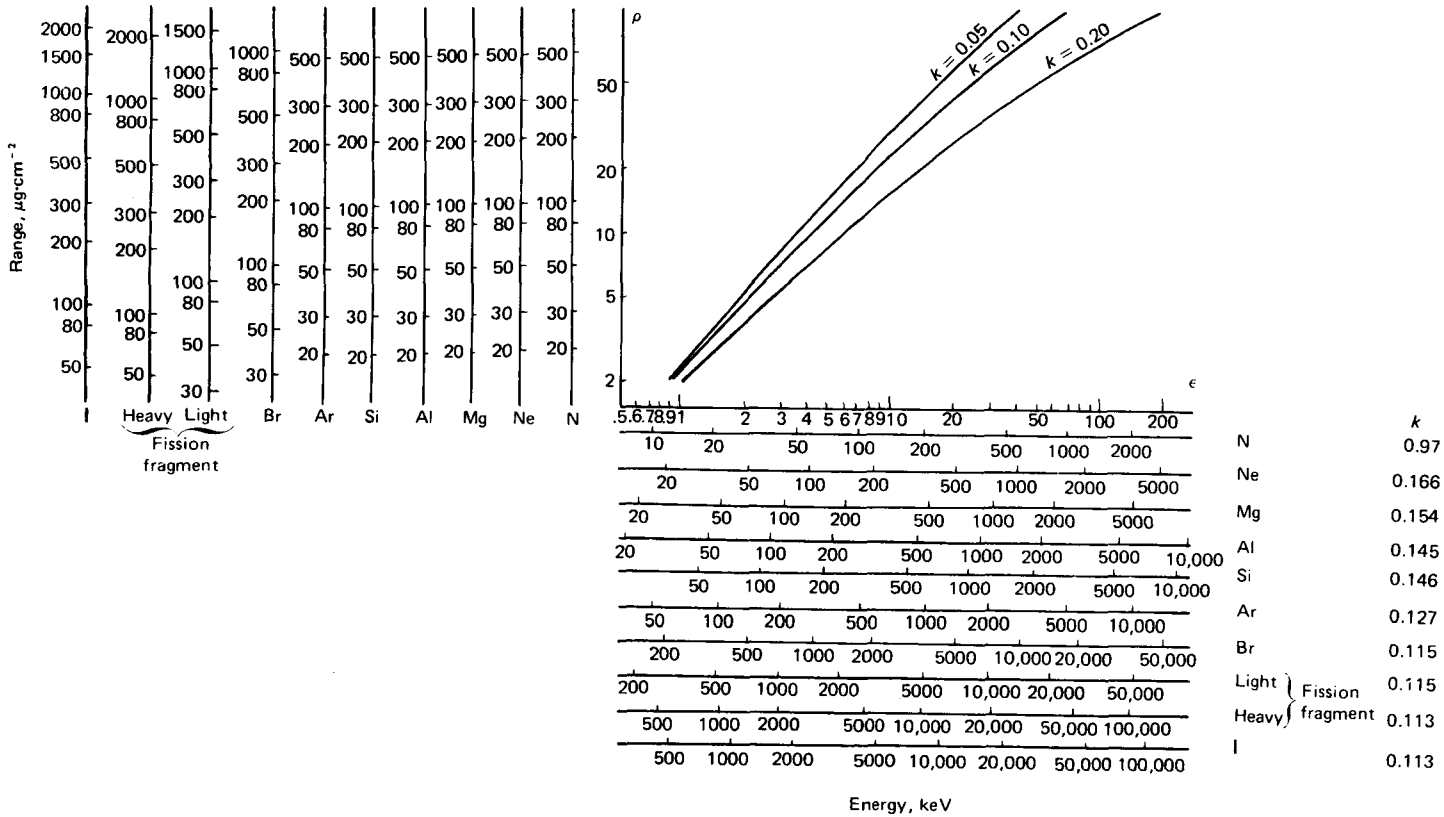


**Figure 4.15** Universal range-energy plot for $\epsilon > 1$. It allows determination of range in silicon for many heavy ions (Ref. 22).

There is a long list of possible interactions of photons, but only the three most important ones will be discussed here: the photoelectric effect, Compton scattering, and pair production.

### 4.8.1 The Photoelectric Effect

The photoelectric effect is an interaction between a photon and a bound atomic electron. As a result of the interaction, the photon disappears and one of the atomic electrons is ejected as a free electron, called the *photoelectron* (Fig. 4.16). The kinetic energy of the electron is

$$T = E_\gamma - B_e \tag{4.45}$$

where $E_\gamma$ = energy of the photon
$B_e$ = binding energy of the electron

The probability of this interaction occurring is called the *photoelectric cross section* or *photoelectric coefficient*. Its calculation is beyond the scope of this book, but it is important to discuss the dependence of this coefficient on parameters such as $E_\gamma$, $Z$, and $A$. The equation giving the photoelectric coefficient may be written as

$$\tau\ (\mathrm{m}^{-1}) = aN\frac{Z^n}{E_\gamma^m}[1 - O(Z)] \tag{4.46}$$

where $\tau$ = probability for photoelectric effect to occur per unit distance traveled by the photon
$a$ = constant, independent of $Z$ and $E_\gamma$
$m, n$ = constants with a value of 3 to 5 (their value depends on $E_\gamma$; see Evans)
$N, Z$ have been defined in Sec. 4.3.

The second term in brackets indicates correction terms of the first order in $Z$. Figure 4.17 shows how the photoelectric coefficient changes as a function of $E_\gamma$ and $Z$. Fig. 4.17 and Eq. 4.46 show that the photoelectric effect is more important for high-$Z$ material, i.e., more probable in lead ($Z = 82$) than in Al ($Z = 13$). It is also more important for $E_\gamma = 10$ keV than $E_\gamma = 500$ keV (for the same material). Using Eq. 4.46, one can obtain an estimate of the photoelectric coefficient of one element in terms of that of another. If one takes the ratio of $\tau$ for two elements, the result for photons of the *same energy* is

$$\tau_2\ (\mathrm{m}^{-1}) = \tau_1\frac{\rho_2}{\rho_1}\left(\frac{A_1}{A_2}\right)\left(\frac{Z_2}{Z_1}\right)^n \tag{4.47}$$

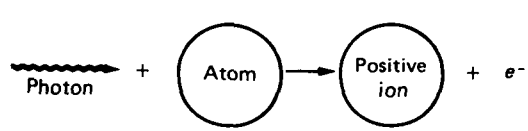


**Figure 4.16** The photoelectric effect.

where $\rho_i$ and $A_i$ are density and atomic weight, respectively, of the two elements, and $\tau_1$ and $\tau_2$ are given in $m^{-1}$. If $\tau_1$ and $\tau_2$ are given in $m^2/kg$, Eq. 4.47 takes the form

$$\tau_2\,(m^2/kg) = \tau_1 \frac{A_1}{A_2}\left(\frac{Z_2}{Z_1}\right)^n \tag{4.47a}$$

### 4.8.2 Compton Scattering or Compton Effect

The *Compton effect* is a collision between a photon and a free electron. Of course, under normal circumstances, all the electrons in a medium are not free but bound. If the energy of the photon, however, is of the order of keV or more, while the binding energy of the electron is of the order of eV, the electron may be considered free.

The photon does not disappear after a Compton scattering. Only its direction of motion and energy change (Fig. 4.18). The photon energy is reduced by a certain amount that is given to the electron. Therefore, conservation of energy gives (assuming the electron is stationary before the collision):

$$T = E_\gamma - E_{\gamma'} \tag{4.48}$$

If Eq. 4.48 is used along with the conservation of momentum equations, the energy of the scattered photon as a function of the scattering angle $\theta$ can be calculated. The result is (see Evans)

$$E_{\gamma'} = \frac{E_\gamma}{1 + (1 - \cos\theta)E_\gamma/mc^2} \tag{4.49}$$

Using Eqs. 4.48 and 4.49, one obtains the kinetic energy of the electron:

$$T = \frac{(1 - \cos\theta)E_\gamma/mc^2}{1 + (1 - \cos\theta)E_\gamma/mc^2}E_\gamma \tag{4.50}$$

A matter of great importance for radiation measurement is the maximum and minimum energy of the photon and the electron after the collision. The minimum energy of the scattered photon is obtained when $\theta = \pi$. This, of course, corresponds to the maximum energy of the electron. From Eq. 4.49,

$$E_{\gamma',\min} = \frac{E_\gamma}{1 + 2E_\gamma/mc^2} \tag{4.51}$$

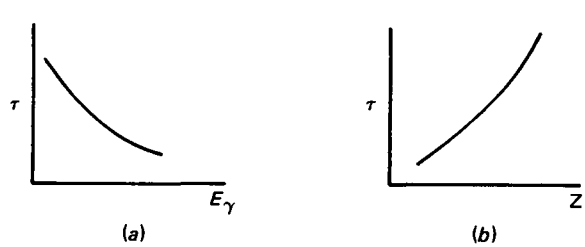


**Figure 4.17** Dependence of the photoelectric cross section on (*a*) photon energy and (*b*) atomic number of the material.

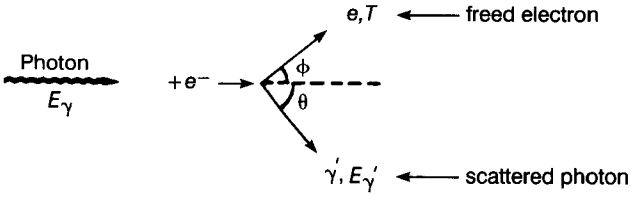


**Figure 4.18** The Compton effect.

and

$$T_{\max} = \frac{2E_\gamma/mc^2}{1 + 2E_\gamma/mc^2} E_\gamma \tag{4.52}$$

The maximum energy of the scattered photon is obtained for $\theta = 0$, which essentially means that the collision did not take place. From Eqs. 4.49 and 4.50,

$$E_{\gamma',\max} = E_\gamma$$
$$T_{\min} = 0$$

The conclusion to be drawn from Eq. 4.51 is that the minimum energy of the scattered photon is greater than zero. Therefore, *in Compton scattering, it is impossible for all the energy of the incident photon to be given to the electron.* The energy given to the electron will be dissipated in the material within a distance equal to the range of the electron. The scattered photon may escape.

**Example 4.15** A 3-MeV photon interacts by Compton scattering. (a) What is the energy of the photon and the electron if the scattering angle of the photon is 90°? (b) What if the angle of scattering is 180°?

**Answer** (a) Using Eq. 4.49,

$$E_{\gamma'} = \frac{3}{1 + (1 - 0)3/0.511} = 0.437 \text{ MeV}$$
$$T = 3 - 0.437 = 2.563 \text{ MeV}$$

(b) Using Eq. 4.51,

$$E_{\gamma',\min} = \frac{3}{1 + (2)3/0.511} = 0.235 \text{ MeV}$$
$$T = 3 - 0.235 = 2.765 \text{ MeV}$$

**Example 4.16** What is the minimum energy of the $\gamma$-ray after Compton scattering if the original photon energy is 0.511 MeV, 5 MeV, 10 MeV, or 100 MeV?

**Answer** The results are shown in the table below (Eq. 4.51 has been used).

| $E_\gamma$ | $(E_\gamma')_{min}$ | $T$ |
|---|---|---|
| 0.511 | 0.170 | 0.341 |
| 5 | 0.243 | 4.757 |
| 10 | 0.25 | 9.75 |
| 100 | 0.25 | 99.75 |

The probability that Compton scattering will occur is called the *Compton coefficient* or the *Compton cross section*. It is a complicated function of the photon energy, but it may be written in the form

$$\sigma(\mathrm{m}^{-1}) = NZf(E_\gamma) \tag{4.53}$$

where $\sigma$ = probability for Compton interaction to occur per unit distance
$f(E_\gamma)$ = a function of $E_\gamma$
If one writes the atom density $N$ explicitly, Eq. 4.53 takes the form

$$\sigma \sim \rho\frac{N_A}{A}Zf(E\gamma) \sim \rho\left(\frac{N_A}{A}\right)\frac{A}{2}f(E_\gamma) \sim \rho\frac{N_A}{2}f(E_\gamma) \tag{4.54}$$

In deriving Eq. 4.54, use has been made of the fact that for most materials, except hydrogen, $A \approx 2Z$ to $A \approx 2.6Z$. According to Eq. 4.54, the probability for Compton scattering to occur is almost independent of the atomic number of the material. Figure 4.19 shows how $\sigma$ changes as a function of $E_\gamma$ and $Z$. If the Compton cross section is known for one element, it can be calculated for any other by using Eq. 4.53 (for photons of the same energy):

$$\sigma_2(\mathrm{m}^{-1}) = \sigma_1\left(\frac{\rho_2}{\rho_1}\right)\left(\frac{A_1}{A_2}\right)\left(\frac{Z_2}{Z_1}\right) \tag{4.55}$$

where $\sigma_1$ and $\sigma_2$ are given in $\mathrm{m}^{-1}$. If $\sigma_1$ and $\sigma_2$ are given in $\mathrm{m}^2/\mathrm{kg}$, Eq. 4.55 takes the form

$$\sigma_2(\mathrm{m}^2/\mathrm{kg}) = \sigma_1\left(\frac{A_1}{A_2}\right)\left(\frac{Z_2}{Z_1}\right) \tag{4.55a}$$

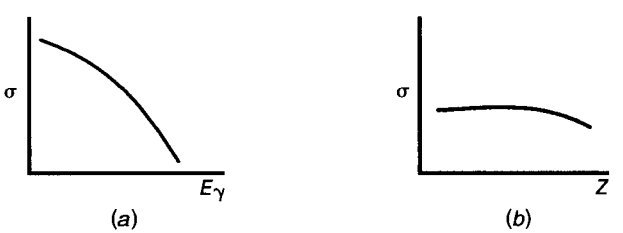


**Figure 4.19** Dependence of the Compton cross section on (*a*) photon energy and (*b*) atomic number of the material.

### 4.8.3 Pair Production

Pair production is an interaction between a photon and a nucleus. As a result of the interaction, the photon disappears and an electron-positron pair appears (Fig. 4.20). Although the nucleus does not undergo any change as a result of this interaction, its presence is necessary for pair production to occur. A $\gamma$-ray will not disappear in empty space by producing an electron-positron pair.†

Conservation of energy gives the following equation for the kinetic energy of the electron and the positron:

$$T_{e^-} + T_{e^+} = E_\gamma - (mc^2)_{e^-} - (mc^2)_{e^+} = E_\gamma - 1.022 \text{ MeV} \tag{4.56}$$

The available kinetic energy is equal to the energy of the photon minus 1.022 MeV, which is necessary for the production of the two rest masses. Electron and positron share, for all practical purposes, the available kinetic energy, i.e.,

$$T_{e^-} = T_{e^+} = \tfrac{1}{2}(E_\gamma - 1.022 \text{ MeV}) \tag{4.57}$$

Pair production eliminates the original photon, but two photons are created when the positron annihilates (see Sec. 3.7.4). These annihilation gammas are important in constructing a shield for a positron source as well as for the detection of gammas (see Chap. 12).

The probability for pair production to occur, called the *pair production coefficient or cross section* is a complicated function of $E_\gamma$ and $Z$ (see Evans and Roy & Reed). It may be written in the form

$$\kappa \ (\text{m}^{-1}) = NZ^2 f(E_\gamma, Z) \tag{4.58}$$

where $\kappa$ is the probability for pair production to occur per unit distance traveled and $f(E_\gamma, Z)$ is a function that changes slightly with $Z$ and increases with $E_\gamma$.

Figure 4.21 shows how $\kappa$ changes with $E_\gamma$ and $Z$. It is important to note that $\kappa$ has a threshold at 1.022 MeV and increases with $E_\gamma$ and $Z$. Of the three coefficients ($\tau$ and $\sigma$ being the other two), $\kappa$ is the only one increasing with the energy of the photon.

†Pair production may take place in the field of an electron. The probability for that to happen is much smaller and the threshold for the gamma energy is $4mc^2 = 2.04$ MeV.

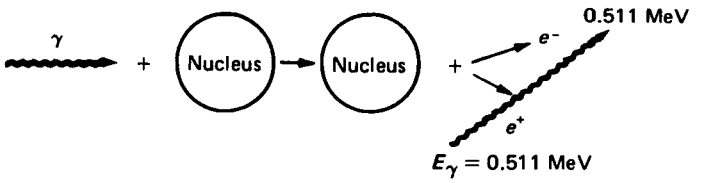


**Figure 4.20** Pair production. The gamma disappears and a positron-electron pair is created. Two 0.511-MeV photons are produced when the positron annihilates.

If the pair production cross section is known for one element, an estimate of its value can be obtained for any other element by using Eq. 4.58 (for photons of the same energy).

$$\kappa_2\,(\mathrm{m}^{-1}) = \kappa_1\left(\frac{\rho_2}{\rho_1}\right)\left(\frac{A_1}{A_2}\right)\left(\frac{Z_2}{Z_1}\right)^2 \tag{4.59}$$

where $\kappa_1$ and $\kappa_2$ are given in $\mathrm{m}^{-1}$. If $\kappa_1$ and $\kappa_2$ are given in $\mathrm{m}^2/\mathrm{kg}$, Eq. 4.59 takes the form

$$\kappa_2\,(\mathrm{m}^2/\mathrm{kg}) = \kappa_1\left(\frac{A_1}{A_2}\right)\left(\frac{Z_2}{Z_1}\right)^2 \tag{4.59a}$$

### 4.8.4 Total Photon Attenuation Coefficient

When a photon travels through matter, it may interact through any of the three major ways discussed earlier. (For pair production, $E_\gamma > 1.022$ MeV.) There are other interactions, but they are not mentioned here because they are not important in the detection of gammas.

Figure 4.22 shows the relative importance of the three interactions as $E_\gamma$ and $Z$ change. Consider a photon with $E = 0.1$ MeV. If this particle travels in carbon ($Z = 6$), the Compton effect is the predominant mechanism by which this photon interacts. If the same photon travels in iodine ($Z = 53$), the photoelectric interaction prevails. For a $\gamma$ of 1 MeV, the Compton effect predominates regardless of $Z$. If a photon of 10 MeV travels in carbon, it will interact mostly through Compton scattering. The same photon moving in iodine will interact mainly through pair production.

The total probability for interaction $\mu$, called the total *linear* attenuation coefficient, is equal to the sum of the three probabilities:

$$\mu\,(\mathrm{m}^{-1}) = \tau + \sigma + \kappa \tag{4.60}$$

Physically, $\mu$ is the probability of interaction per unit distance.

There are tables that give $\mu$ for all the elements, for many photon energies.†

†Tables of mass attenuation coefficients are given in App. D.

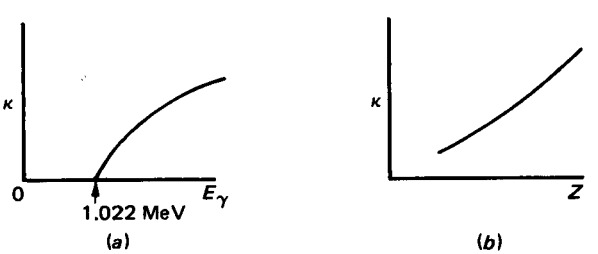


**Figure 4.21** Dependence of the pair production cross section on (*a*) photon energy and (*b*) atomic number of the material.

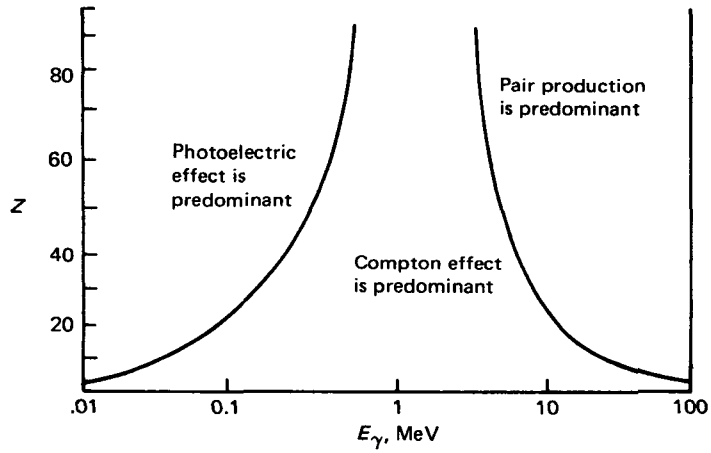


**Figure 4.22** The relative importance of the three major gamma interactions (from *The Atomic Nucleus* by R. D. Evans. Copyright©1972 by McGraw-Hill. Used with the permission of McGraw-Hill Book Company).

Most of the tables provide $\mu$ in units of $m^2/kg$ (or $cm^2/g$), because in these units the density of the material does not have to be specified. If $\mu$ is given in $m^2/kg$ (or $cm^2/g$), it is called the *total mass attenuation coefficient*. The relationship between linear and mass coefficients is

$$\mu\ (m^2/kg) = \frac{\mu\ (m^{-1})}{\rho\ (kg/m^3)} \tag{4.61}$$

Figure 4.23 shows the individual coefficients as well as the total mass attenuation coefficient for lead, as a function of photon energy. The total mass attenuation coefficient shows a minimum because as $E$ increases, $\tau$ decreases, $\kappa$ increases, and $\sigma$ does not change appreciably. However, the minimum of $\mu$ does not fall at the same energy for all elements. For lead, $\mu$ shows a minimum at $E_\gamma \sim 3.5$ MeV; for aluminum, the minimum is at 20 MeV; and for NaI, the minimum is at 5 MeV.

If a parallel beam of monoenergetic photons with intensity $I(0)$ strikes a target of thickness $t$ (Fig. 4.24), the number of photons, $I(t)$, emerging without having interacted in the target is given by

$$I(t) = I(0)e^{-\mu t} \tag{4.62}$$

The probability that a photon will traverse thickness $t$ without an interaction is

$$\frac{\text{number transmitted}}{\text{number incident}} = \frac{I(0)e^{-\mu t}}{I(0)} = e^{-\mu t}$$

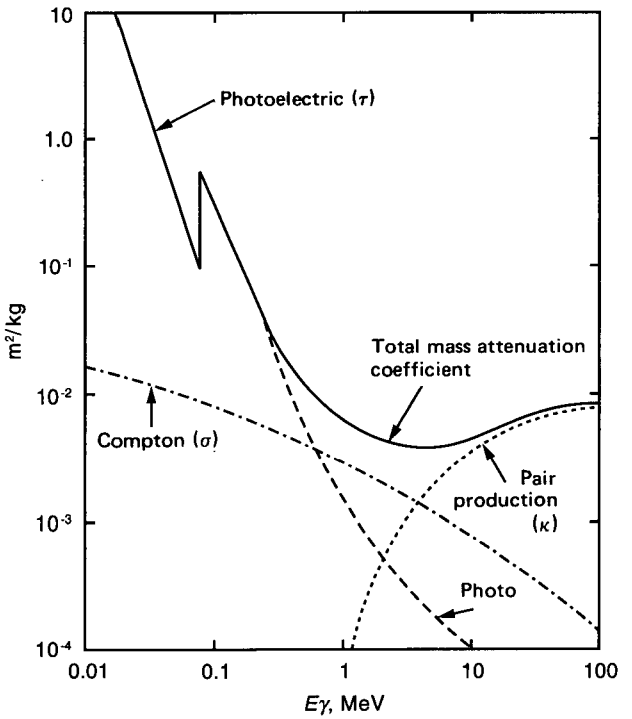


**Figure 4.23** Mass attenuation coefficients for lead ($Z = 82$, $\rho = 11.35 \times 10^3$ kg/m$^3$).

Based on this probability, the average distance between two successive interactions, called the *mean free path* (mfp) ($\lambda$), is given by

$$\lambda\,(\mathrm{m}) = \frac{\int_0^\infty x e^{-\mu x}\,dx}{\int_0^\infty e^{-\mu x}\,dx} = \frac{1}{\mu} \tag{4.63}$$

Thus, the mean free path is simply the inverse of the total linear attenuation coefficient. If $\mu = 10\ \mathrm{m}^{-1}$ for a certain $\gamma$-ray traveling in a certain medium, then the distance between two successive interactions of this gamma in that medium is $\lambda = 1/\mu = 1/10\ \mathrm{m} = 0.10\ \mathrm{m}$.

The total mass attenuation coefficient for a compound or a mixture is calculated by the same method used for $(dE/dx)_c$ in Sec. 4.5. It is easy to show (see Prob. 4.15) that

$$\mu_c\,(\mathrm{m}^2/\mathrm{kg}) = \sum_i w_i\,\mu_i\,(\mathrm{m}^2/\mathrm{kg}) \tag{4.64}$$

where $\mu_c$ = total *mass* attenuation coefficient for a compound or a mixture
$w_i$ = weight fraction of $i$th element in the compound
$\mu_i$ = total *mass* attenuation coefficient of $i$th element

**Example 4.17** What is the total mass attenuation coefficient for 1.25-MeV gammas in NaI?

**Answer** For this compound, the following data apply:

Na: $\mu = 0.00546\ \mathrm{m^2/kg}$ $\quad w = \frac{23}{150} = 0.153$

I: $\mu = 0.00502\ \mathrm{m^2/kg}$ $\quad w = \frac{127}{150} = 0.847$

Using Eq. 4.64,

$$\mu\,(\mathrm{NaI}) = 0.00546(0.153) + 0.00502(0.847) = 0.00509\ \mathrm{m^2/kg} = 0.0509\ \mathrm{cm^2/g}$$

The density of NaI is $3.67 \times 10^3\ \mathrm{kg/m^3}$; hence,

$$\mu\,(\mathrm{m^{-1}}) = 0.00509\ \mathrm{m^3/kg}(3.67 \times 10^3\ \mathrm{kg/m^3}) = 18.567\ \mathrm{m^{-1}} = 0.187\ \mathrm{cm^{-1}}$$

### 4.8.5 Photon Energy Absorption Coefficient

When a photon has an interaction, only part of its energy is absorbed by the medium at the point where the interaction took place. Energy given by the photon to electrons and positrons is considered absorbed at the point of interaction because the range of these charged particles is short. However, X-rays, Compton-scattered photons, or annihilation gammas may escape. The fraction of photon energy that escapes is important when one wants to calculate heat generated due to gamma absorption in shielding materials or gamma radiation dose to humans (see Chap. 16). The gamma energy deposited in any material is calculated with the help of an energy absorption coefficient defined in the following way.

The *gamma energy absorption coefficient* is, in general, that part of the total attenuation coefficient that, when multiplied by the gamma energy, will give the energy deposited at the point of interaction. Equation 4.60 gives the total attenuation coefficient. The *energy absorption coefficient* $\mu_a$ is†

$$\mu_a = \tau + \frac{T_{\mathrm{av}}}{E_\gamma}\sigma + \kappa \tag{4.65}$$

†A more detailed definition of the energy absorption coefficient is given by Chilton et al.

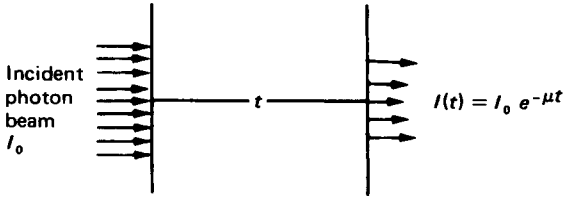


**Figure 4.24** The intensity of the transmitted beam (only particles that did not interact) decreases exponentially with material thickness.

where $T_{av}$ is the average energy of the Compton electron and $\mu_a$ may be a linear or mass energy absorption coefficient, depending on the units (see Sec. 4.8.4).

In writing Eq. 4.65, it is assumed that

1. If photoelectric effect or pair production takes place, all the energy of the gamma is deposited there.
2. If Compton scattering occurs, only the energy of the electron is absorbed. The Compton-scattered gamma escapes.

In the case of photoelectric effect, assumption (1) is valid. For pair production, however, it is questionable because only the energy $E_\gamma - 1.022$ MeV is given to the electron-positron pair. The rest of the energy, equal to 1.022 MeV, is taken by the two annihilation gammas, and it may not be deposited in the medium. There are cases when Eq. 4.65 is modified to account for this effect.[25] Gamma absorption coefficients, as defined by Eq. 4.65, are given in App. D.

**Example 4.18** A 1Ci $^{137}$Cs source is kept in a large water vessel. What is the energy deposited by the gammas in $H_2O$ at a distance 0.05 m from the source?

**Answer** $^{137}$Cs emits a 0.662-MeV gamma. The mass absorption coefficient for this photon in water is (App. D) 0.00327 $m^2/kg$. The total mass attenuation coefficient is 0.00862 $m^2/kg$. The energy deposited at a distance of 0.05 m from the source is ($E_d = \phi\mu_a E_\gamma$)

$$E_d\left(\frac{\text{MeV}}{(\text{kg s})}\right) = \frac{S}{4\pi r^2}e^{-\mu r}\left(\frac{\gamma}{(\text{m}^2\ \text{s})}\right)\left[\mu_a(\text{m}^2/\text{kg})\right]\left[E(\text{MeV}/\gamma)\right]$$

$$= \frac{3.7\times 10^{10}}{4\pi(0.05)^2}(e^{-0.00862(10^3)0.05})0.00327(0.662)$$

$$= 1.66\times 10^9\ \text{MeV}/(\text{kg s}) = 2.65\times 10^{-4}\ \text{J}/(\text{kg s})$$

### 4.8.6 Buildup Factors

Consider a point isotropic monoenergetic gamma source at a distance $r$ from a detector, as shown in Fig. 4.25, with a shield of thickness $t$ between source and detector. The total gamma beam hitting the detector consists of two components.

1. The *unscattered beam* ($\phi_u$) consists of those photons that go through the shield without any interaction. If the source strength is $S(\gamma/\text{s})$, the intensity of the unscattered beam or the unscattered photon flux is given by the simple

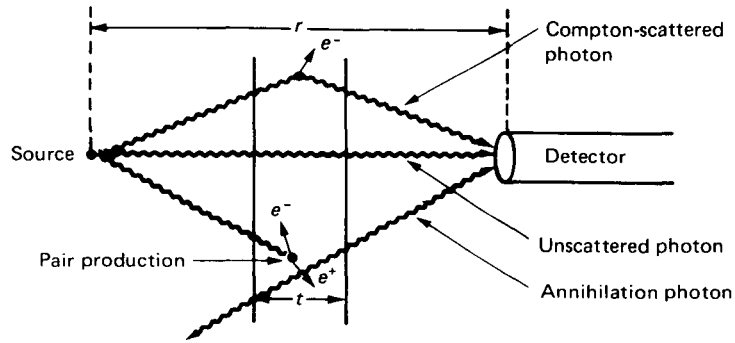


**Figure 4.25** If a point isotropic source is placed behind a shield of thickness $t$, both scattered and unscattered photons will hit the detector.

and exact expression

$$\phi_u(\gamma/\mathrm{m}^2\ \mathrm{s}) = \frac{S}{4\pi r^2} e^{-\mu r} \tag{4.66}$$

2. The *scattered beam* ($\phi_s$) consists of scattered incident photons and others generated through interactions in the shield (e.g., X-rays and annihilation gammas). The calculation of the scattered beam is not trivial, and there is no simple expression like Eq. 4.62 representing it.

The total flux hitting the detector is

$$\phi_{\mathrm{tot}} = \phi_u + \phi_s \tag{4.67}$$

Obviously, for the calculation of the correct energy deposition by gammas, either for the determination of heating rate in a certain material or the dose rate to individuals, the total flux should be used. Experience has shown that rather than calculating the total flux using Eq. 4.67, there are advantages to writing the total flux in the form

$$\phi_{\mathrm{tot}} = B\phi_u \tag{4.68}$$

where $B$ is a buildup factor, defined and computed in such a way that Eq. 4.68 gives the correct total flux. Combining Eqs. 4.67 and 4.68, one obtains

$$B = \frac{\phi_{\mathrm{tot}}}{\phi_u} = 1 + \frac{\phi_s}{\phi_u} \geq 1 \tag{4.69}$$

How will $B$ be determined? Equation 4.69 will be used, of course, but that means one has to determine the scattered flux. Then where is the advantage of using $B$? The advantage comes from the fact that $B$ values for a relatively small number of cases can be computed and tabulated and then, by interpolation, one can obtain the total flux using Eq. 4.68 for several other problems. In other words, the use of the buildup factor proceeds in two steps.

1. Buildup factor values are tabulated for many cases.
2. The appropriate value of $B$ that applies to a case under study is chosen and used in Eq. 4.68 to obtain the total flux.

In general, the buildup factor depends on the energy of the photon, on the mean free paths traveled by the photon in the shield, on the geometry of the source (parallel beam or point isotropic), and on the geometry of the attenuating medium (finite, infinite, slab, etc.).

The formal definition of $B$ upon which its calculation is based is

$$B(E, \mu r) = \frac{\text{quantity of interest due to total flux}}{\text{quantity of interest due to unscattered flux}}$$

Quantities of interest and corresponding buildup factors are shown in Table 4.4

The mathematical formulas for the buildup factors are (assuming a monoenergetic, $E_0$, point isotropic source) as follows:

Number buildup factor:

$$B_N(E_0, \mu r) = \frac{\int_0^{E_0} \phi_{\text{tot}}(r, E)\, dE}{(S/4\pi r^2)e^{-\mu r}} \tag{4.70}$$

Energy deposition buildup factor:

$$B_E(E_0, \mu r) = \frac{\int_0^{E_0} \phi_{\text{tot}}(r, E) E \mu_a^{\text{med}}(E)\, dE}{(S/4\pi r^2)e^{-\mu r}\mu_a^{\text{med}}(E_0)E_0} \tag{4.71}$$

Dose buildup factor:

$$B_D(E_0, \mu r) = \frac{\int_0^{E_0} \phi_{\text{tot}}(r, E) E \mu_a^{\text{tis}}(E)\, dE}{(S/4\pi r^2)e^{-\mu r}\mu_a^{\text{tis}}(E_0)E_0} \tag{4.72}$$

In Eqs. 4.70–4.72, the photon flux $\phi(r, E)$ is a function of space $r$ and energy $E$, even though all photons start from the same point with the same energy $E_0$. Since $B(E, \mu r)$ expresses the effect of scattering as the photons travel the distance $r$, it should not be surprising to expect $B(E, \mu r) \to 1$ as $\mu r \to 0$.

**Table 4.4 Types of Buildup Factors**

| Quantity of interest | Corresponding buildup factor |
|---|---|
| Flux $\phi$ | Number buildup factor |
| Energy deposited in medium | Energy deposition buildup factor |
| Dose (absorbed) | Dose buildup factor |

Note that the only difference between energy and dose buildup factors is the type of gamma absorption coefficient used. For energy deposition, one uses the absorption coefficient for the medium in which energy deposition is calculated; for dose calculations, one uses the absorption coefficient in tissue.

Extensive calculations of buildup factors have been performed,[26-31] and the results have been tabulated for several gamma energies, media, and distances. In addition, attempts have been made to derive empirical analytic equations. Two of the most useful formulas are as follows:

Berger formula:

$$B(E, \mu r) = 1 + a(E)\mu r e^{b(E)\mu r} \tag{4.73}$$

Taylor formula:

$$B(E, \mu r) = A(E)e^{-a_1(E)\mu r} + [1 - A(E)]e^{-a_2(E)\mu r} \tag{4.74}$$

The constants $a(E), b(E), A(E), a_1(E), a_2(E)$ have been determined by fitting the results of calculations to these analytic expressions. Appendix E provides some values for the Berger formula constants. The best equations for the gamma buildup factor representation are based on the so-called "geometric progression" (G-P)[32] form. The G-P function has the form

$$\begin{aligned} B(E, x) &= 1 + (b - 1)(K^x - 1)/(K - 1) \qquad K \neq 1 \\ &= 1 + (b - 1)x \qquad K = 1 \end{aligned} \tag{4.75}$$

$$K(x) = cx^a + d\frac{\tanh[(x/X_k) - 2] - \tanh(-2)}{1 - \tanh(-2)} \tag{4.76}$$

where $x = \mu r$ = distance traveled in mean free paths
$b$ = value of $B$ for $x = 1$
$K$ = multiplication factor per mean free paths
$a, b, c, d, X_k$ = parameters that depend on $E$

Extensive tables of these constants are given in Ref. 31. The use of the buildup factor is shown in Ex. 4.19. More examples are provided in Chap. 16 in connection with dose-rate calculations.

**Example 4.19** A 1-Ci $^{137}$Cs source is kept in a large water tank. What is the energy deposition by the Cs gammas at a distance of 0.5 m from the source?

**Answer** Using the data of Ex. 4.18, the distance traveled by the 0.662-MeV photons in water is $\mu r = (0.00862\ \text{m}^2/\text{kg})(0.5\ \text{m})(10^3\ \text{kg/m}^3) = 4.31$ mean free path. From Ref. 32, the energy deposition buildup factor is $B(0.662, 4.31) = 13.5$. The energy deposition is

$$E_d\left(\frac{\text{MeV}}{\text{kg s}}\right) = \frac{3.7 \times 10^{10}}{4\pi(0.5)^2}e^{-4.31}(0.00327)(0.662)13.5 = 4.62 \times 10^6\ \text{MeV/(kg s)}$$
$$= 7.4 \times 10^{-7}\ \text{J/(kg s)}$$

## 4.9 INTERACTIONS OF NEUTRONS WITH MATTER

Neutrons, with protons, are the constituents of nuclei (see Sec. 3.4). Since a neutron has no charge, it interacts with nuclei only through nuclear forces. When it approaches a nucleus, it does not have to go through a Coulomb barrier, as a charged particle does. As a result, the probability (cross section) for nuclear interactions is higher for neutrons than for charged particles. This section discusses the important characteristics of neutron interactions, with emphasis given to neutron cross sections and calculation of interaction rates.

### 4.9.1 Types of Neutron Interactions

The interactions of neutrons with nuclei are divided into two categories: scattering and absorption.

**Scattering.** In this type of interaction, the neutron interacts with a nucleus, but both particles reappear after the reaction. A scattering collision is indicated as an $(n, n)$ reaction or as

$$n + {}^{A}_{Z}X \rightarrow {}^{A}_{Z}X + n$$

Scattering may be elastic or inelastic. In elastic scattering, the total *kinetic* energy of the two colliding particles is conserved. The kinetic energy is simply redistributed between the two particles. In inelastic scattering, part of the kinetic energy is given to the nucleus as an excitation energy. After the collision, the excited nucleus will return to the ground state by emitting one or more $\gamma$-rays.

Scattering reactions are responsible for neutron's slowing down in reactors. Neutrons emitted in fission have an average energy of about 2 MeV. The probability that neutrons will induce fission is much higher if the neutrons are very slow—"thermal"—with kinetic energies of the order of eV. The fast neutrons lose their kinetic energy as a result of scattering collisions with nuclei of a "moderating" material, which is usually water or graphite.

**Absorption.** If the interaction is an absorption, the neutron disappears, but one or more other particles appear after the reaction takes place. Table 4.5 illustrates some examples of absorptive reactions.

### 4.9.2 Neutron Reaction Cross Sections

Consider a monoenergetic parallel beam of neutrons hitting a thin target† of thickness $t$ (Fig. 4.26). The number of reactions per second, $R$, taking place in

†A thin target is one that does not appreciably attenuate the neutron beam (see Eq. 4.80).

**Table 4.5 Absorptive Reactions**

| Reaction | Name |
|---|---|
| $n + {}^{A}_{Z}\mathrm{X} \rightarrow {}^{A}_{Z-1}\mathrm{Y} + p$ | $(n, p)$ reaction |
| $n + {}^{A}_{Z}\mathrm{X} \rightarrow {}^{A-3}_{Z-2}\mathrm{Y} + {}^{4}_{2}\mathrm{He}$ | $(n, \alpha)$ reaction |
| $n + {}^{A}_{Z}\mathrm{X} \rightarrow {}^{A-1}_{Z}\mathrm{X} + 2n$ | $(n, 2n)$ reaction |
| $n + {}^{A}_{Z}\mathrm{X} \rightarrow {}^{A+1}_{Z}\mathrm{X} + \gamma$ | $(n, \gamma)$ reaction |
| $n + {}^{A}_{Z}\mathrm{X} \rightarrow {}^{A_1}_{Z_2}\mathrm{Y}_1 + {}^{A_2}_{Z_2}\mathrm{Y}_2 + n + n + \cdots$ | fission |

this target may be written as

$$R\ (\text{reactions/s}) = \begin{pmatrix} \text{neutrons per m}^2\ \text{s} \\ \text{hitting the target} \end{pmatrix} \begin{pmatrix} \text{targets exposed} \\ \text{to the beam} \end{pmatrix} \times \begin{pmatrix} \text{probability of interaction} \\ \text{per n/m}^2\ \text{per nucleus} \end{pmatrix}$$

or

$$R = I\ [\text{n}/(\text{m}^2\ \text{s})][N\ (\text{nuclei/m}^3)][a\ (\text{m}^2)][t\ (\text{m})][\sigma\ (\text{m}^2)] \qquad (4.77)$$

where $I$, $a$, and $t$ are shown in Fig. 4.26. The parameter $\sigma$, called the *cross section*, has the following physical meaning:

$\sigma\ (\text{m}^2)$ = probability that an interaction will occur per target nucleus per neutron per $\text{m}^2$ hitting the target

The unit of $\sigma$ is the barn (b).

$$1\ \text{b} = 10^{-24}\ \text{cm}^2 = 10^{-28}\ \text{m}^2$$

Since the nuclear radius is approximately $10^{-15}$ to $10^{-14}$ m, 1 b is approximately equal to the cross-sectional area of a nucleus.

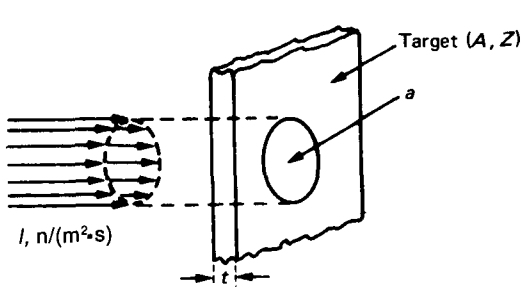


**Figure 4.26** A parallel neutron beam hitting a thin target: $a$ = area of target struck by the beam.

Neutron cross sections are defined separately for each type of reaction and isotope. For the reactions discussed in Sec. 4.9.1, one defines, for example,

$$\sigma_s = \text{elastic scattering cross section}$$
$$\sigma_i = \text{inelastic scattering cross section}$$
$$\sigma_a = \text{absorption cross section}$$
$$\sigma_\gamma = \text{capture cross section}$$
$$\sigma_f = \text{fission cross section}$$

The total cross section—i.e., the total probability that a reaction of any type will take place—is equal to the sum of all the $\sigma$'s:

$$\sigma_{\text{tot}} = \sigma_s + \sigma_i + \sigma_\gamma + \sigma_f + \cdots \tag{4.78}$$

In the notation used here, $\sigma_a = \sigma_\gamma + \sigma_f$.

Neutron cross sections depend strongly on the energy of the neutron as well as on the atomic weight and atomic number of the target nucleus.

Figures 4.27 and 4.28 show the total cross section for two isotopes over the same neutron energy range. Notice the vast difference between the two $\sigma$'s, both in terms of their variation with energy and their value in barns. [All available information about cross sections as a function of energy for all isotopes is contained in the Evaluated Nuclear Data Files (known as ENDF) stored at the Brookhaven National Laboratory, Upton, NY.]

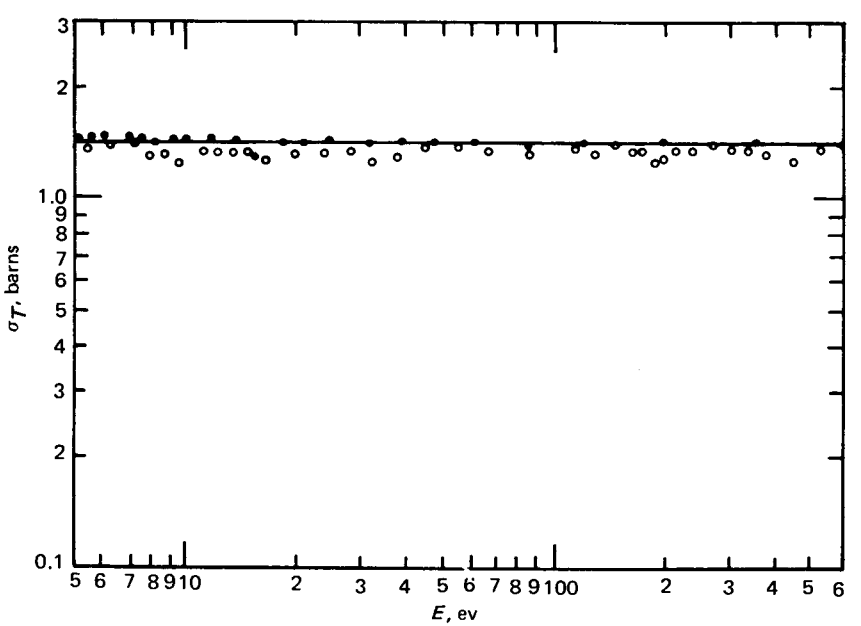


**Figure 4.27** The total neutron cross section of $^{27}$Al from 5 eV to 600 eV (from BNL-325).

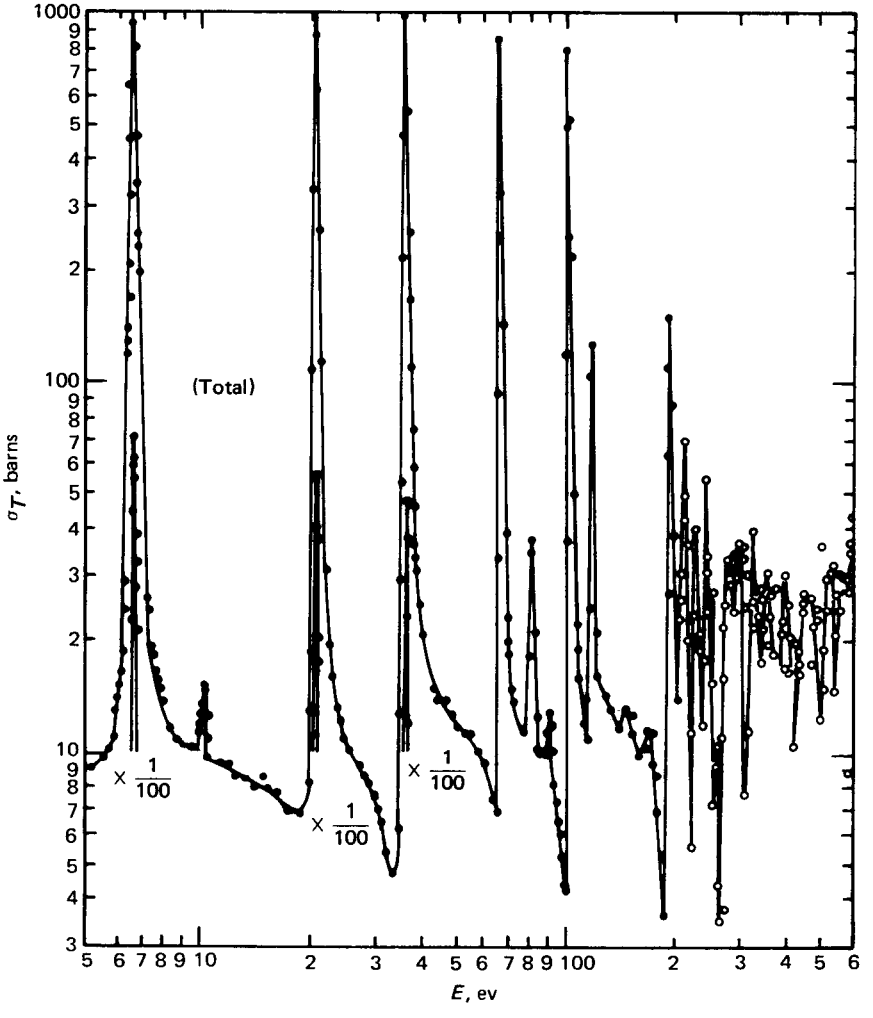


**Figure 4.28** The total cross section of $^{238}U$ from 5 eV to 600 eV (from BNL-325).

The cross section $\sigma$ (b) is called the *microscopic* cross section. Another form of the cross section, also frequently used, is the *macroscopic* cross section $\Sigma$ ($m^{-1}$), defined by the equation

$$\Sigma_i\ (\mathrm{m}^{-1}) = N\ (\mathrm{nuclei/m^3})\left[\sigma_i\ (\mathrm{m}^2)\right] \tag{4.79}$$

and having the following physical meaning:

$\Sigma_i$ = probability that an interaction of type $i$ will take place per unit distance of travel of a neutron moving in a medium that has $N$ nuclei/$m^3$

The macroscopic cross section is analogous to the linear attenuation coefficient of $\gamma$-rays (Sec. 4.8.4). If a parallel beam of monoenergetic neutrons with intensity $I(0)$ impinges upon a material of thickness $t$, the number of neutrons that emerges without having interacted in the material is (see Fig. 4.24)

$$I(t) = I(0)e^{-\Sigma_t t} \tag{4.80}$$

where $\Sigma_t = \Sigma_s + \Sigma_i + \Sigma_a + \cdots$ = total macroscopic neutron cross section.

As with $\gamma$-rays,

$e^{-\Sigma_t t}$ = probability that the neutron will travel distance $t$ without an interaction

The average distance between two successive interactions, the mean free path $\lambda$, is

$$\lambda = \frac{\int_0^\infty xe^{-\Sigma x}\,dx}{\int_0^\infty e^{-\Sigma x}\,dx} = \frac{1}{\Sigma} \tag{4.81}$$

**Example 4.20** What are the macroscopic cross sections $\Sigma_s$, $\Sigma_a$, and $\Sigma_t$ for thermal neutrons in graphite? The scattering cross section is $\sigma_s = 4.8$ b and the absorption cross section is $\sigma_a = 0.0034$ b. What is the mean free path?

**Answer** For graphite, $\rho = 1.6 \times 10^3$ kg/m$^3$ and $A = 12$. Therefore,

$$N = \rho\frac{N_A}{A} = (1.6 \times 10^3)\frac{0.6023 \times 10^{24}}{12 \times 10^{-3}} = 0.0803 \times 10^{30} \text{ atoms/m}^3$$

Using Eq. 4.79,

$$\Sigma_s = (0.0803 \times 10^{30})(4.8 \times 10^{-28}) = 38.5 \text{ m}^{-1} = 0.385 \text{ cm}^{-1}$$

$$\Sigma_a = (0.0803 \times 10^{30})(0.0034 \times 10^{-28}) = 0.027 \text{ m}^{-1} = 0.00027 \text{ cm}^{-1}$$

$$\Sigma_t = \Sigma_s + \Sigma_a = 38.53 \text{ m}^{-1} = 0.3853 \text{ cm}^{-1}$$

The mean free path is

$$\lambda = \frac{1}{\Sigma_t} = 0.0259 \text{ m} = 2.59 \text{ cm}$$

For a mixture of several isotopes, the macroscopic cross section $\Sigma_i$ is calculated by

$$\Sigma_i = \sum_j N_j \sigma_{ij} \tag{4.82}$$

where $\sigma_{ij}$ = microscopic cross section of isotope $j$ for reaction type $i$
$N_j = w_j \rho N_A / A_j$
$w_j$ = weight fraction of $j$th isotope in the mixture
$\rho$ = density of mixture

Equation 4.82 assumes that all the isotopes act independently, i.e., that the chemical-crystal binding forces are negligible. In certain cases, especially for thermal neutrons, these binding forces play an important role and cannot be neglected. In those cases, Eq. 4.82 does not apply.

**Example 4.21** What is the total macroscopic absorption cross section of natural uranium? Natural uranium consists of 0.711 percent $^{235}U$, and the rest is, essentially, $^{238}U$. For thermal neutrons, the absorption cross sections are $\sigma_a$ ($^{235}U$) = 678 b and $\sigma_a$ ($^{238}U$) = 2.73 b.

**Answer** The density of uranium is $19.1 \times 10^3$ kg/m$^3$. Therefore, using Eq. 4.82,

$$\begin{aligned}\Sigma_a(U) &= 0.00711(19.1 \times 10^3)\frac{0.6023 \times 10^{24}}{235 \times 10^{-3}}(678 \times 10^{-28}) \\ &\quad + 0.99289(19.1 \times 10^3)\frac{0.6023 \times 10^{24}}{238 \times 10^{-3}}(2.73 \times 10^{-28}) \\ &= (23.6 + 13.1)\ \mathrm{m}^{-1} = 36.7\ \mathrm{m}^{-1} = 0.367\ \mathrm{cm}^{-1}\end{aligned}$$

### 4.9.3 The Neutron Flux

The neutron flux is a scalar quantity that is used for the calculation of neutron reaction rates. In most practical cases, the neutron source does not consist of a parallel beam of neutrons hitting a target. Instead, neutrons travel in all directions and have an energy (or speed) distribution. A case in point is the neutron environment inside the core of a nuclear reactor. Neutron reaction rates are calculated as follows in such cases.

Consider a medium that contains neutrons of the same speed $v$, but moving in all directions. Assume that at some point in space the neutron density is $n$ (neutrons/m$^3$). If a target is placed at that point, the interaction rate $R$ [reactions/(m$^3$ s)] will be equal to

$$R = \begin{pmatrix}\text{distance traveled by all} \\ \text{neutrons in 1 m}^3\end{pmatrix}\begin{pmatrix}\text{probability of interaction per unit} \\ \text{distance traveled by one neutron}\end{pmatrix}$$

or

$$R = [n\ (\text{neutrons/m}^3)v\ (\text{m/s})][\Sigma\ (\text{m}^{-1})] = nv\Sigma\ [\text{reaction/(m}^3\ \text{s)}]$$

The product $nv$, which has the units of neutrons/(m$^2$ s) and represents the total pathlength traveled per second by all the neutrons in 1 m$^3$, is called the *neutron flux* $\phi$:

$$\phi = nv[n/(\text{m}^2\ \text{s})] \tag{4.83}$$

Although the units of neutron flux are $n/(\text{m}^2\ \text{s})$, the value of the flux $\phi(r)$ at a particular point $r$ does not represent the number of neutrons that would

cross 1 $m^2$ placed at point $r$. The neutron flux is equal to the number of neutrons crossing 1 $m^2$ in 1 s, *only* in the case of a parallel beam of neutrons. Using Eq. 4.83, the expression for the reaction rate becomes

$$R_i = \phi\Sigma_i[(\text{reactions of type } i)/(\text{m}^3\ \text{s})] \tag{4.84}$$

**Example 4.22** What is the fission rate at a certain point inside a nuclear reactor where the neutron flux is known to be $\phi = 2.5 \times 10^{14}$ neutrons/($m^2$ s), if a thin foil of $^{235}U$ is placed there? The fission cross section for $^{235}U$ is $\sigma_f = 577$ b.

**Answer** The macroscopic fission cross section is

$$\Sigma_f = N\sigma_f = (19.1 \times 10^3)\frac{0.6023 \times 10^{24}}{235 \times 10^{-3}}(577 \times 10^{-28})$$
$$= 2824\ \text{m}^{-1} = 28.24\ \text{cm}^{-1}$$

and

$$R_f = \phi\Sigma_f = (2.5 \times 10^{14})2824 = 7.06 \times 10^{17}\ \text{fissions}/(\text{m}^3\ \text{s})$$
$$= 7.06 \times 10^{11}\ \text{fissions}/(\text{cm}^3\ \text{s})$$

Another quantity related to the flux and used in radiation exposure calculations is the *neutron fluence* $F$, defined by

$$F(\text{n/m}^2) = \int_t \phi(t)\, dt \tag{4.85}$$

with the limits of integration taken over the time of exposure to the flux $\phi(t)$.

### 4.9.4 Interaction Rates of Polyenergetic Neutrons

Equation 4.84 gives the reaction rate for the case of monoenergetic neutrons. In practice, and especially for neutrons produced in a reactor, the flux consists of neutrons that have an energy spectrum extending from $E = 0$ up to some maximum energy $E_{max}$. In such a case, the reaction rate is written in terms of an average cross section. Let

$\phi(E)\, dE$ = neutron flux consisting of neutrons with kinetic energy between $E$ and $E + dE$

$\sigma_i(E)$ = cross section for reaction type $i$ for neutrons with kinetic energy $E$

$N$ = number of targets per $m^3$ (stationary targets)

The reaction rate is

$$R\ [(\text{reactions}/(\text{m}^3\ \text{s})] = \int dE\, \phi(E) N\sigma_i(E) \tag{4.86}$$

where the integration extends over the neutron energies of interest. The total

flux is

$$\phi = \int \phi(E)\, dE \tag{4.87}$$

In practice, an average cross section is defined in such a way that, when is multiplied by the total flux, it gives the reaction rate of Eq. 4.86, i.e.,

$$R = \int_E dE\, \phi(E) N \sigma_i(E) = \phi \bar{\Sigma}_i = \phi N \bar{\sigma}_i \tag{4.88}$$

from which the definition of the average cross section is

$$\bar{\sigma}_i = \frac{\int dE\, \phi(E) \sigma_i(E)}{\int \phi(E)\, dE} \tag{4.89}$$

The calculation of average cross sections is beyond the scope of this text. The reader should consult the proper books on reactor physics. The main purpose of this short discussion is to alert the reader to the fact that when polyenergetic neutrons are involved, an appropriate *average* cross section should be used for the calculation of reaction rates.

## PROBLEMS

**4.1** Calculate the stopping power due to ionization and excitation of a 2-MeV electron moving in water. What is the radiation energy loss rate of this particle? What is the total energy radiated?

**4.2** Calculate the stopping power in aluminum for a 6-MeV alpha particle.

**4.3** The window of a Geiger-Muller counter is made of mica and has a thickness of 0.02 kg/m$^2$ ($\rho = 2.6 \times 10^3$ kg/m$^3$). For mica composition, use $NaAl_3Si_3O_{10}(OH)_2$.

(a) What is the minimum electron energy that will just penetrate this window?

(b) What is the energy loss, in MeV/mm, of an electron with the kinetic energy determined in (a) moving in mica?

(c) What is the energy loss, in MeV/mm, of a 6-MeV alpha particle moving in mica?

(d) Will a 6-MeV alpha particle penetrate this mica window?

**4.4** Beta particles emitted by $^{32}P(E_{max} = 1.7$ MeV) are counted by a gas counter. Assuming that the window of the counter causes negligible energy loss, what gas pressure is necessary to stop all the betas inside the counter if the length of the detector is 100 mm? Assume that the gas is argon.

**4.5** What is the kinetic energy of an alpha particle that will just penetrate the human skin? For the skin, assume $t = 1$ mm; $\rho = 10^3$ kg/m$^3$; 65 percent O, 18 percent C, 10 percent H, 7 percent N.

**4.6** Repeat Prob. 4.5 with an electron.

**4.7** Assuming that a charged particle loses energy linearly with distance, derive the function $T = T(x)$, where $T(x)$ = kinetic energy of the particle after going through thickness $x$. The initial kinetic energy is $T_0$, and the range is $R$.

**4.8** A beam of 6-MeV alpha particles strikes a gold foil with thickness equal to one-third of the alpha range. What is the total energy loss of the alpha as it goes through this foil?

**4.9** What is the energy deposited in a piece of paper by a beam of 1.5-MeV electrons? Assume that the paper has the composition $CH_2$, thickness 0.1 mm, and density 800 kg/m$^3$. The incident parallel electron beam consists of $10^8$ electrons/(m$^2$ s). Give your result in MeV/(cm$^2$ s) and J/(m$^2$ s).

**4.10** What is the range of 10-MeV proton in air at 1 atm? What is the range at 10 atm?

**4.11** What is the range of a 4-MeV deuteron in gold?

**4.12** A 1.5-MeV gamma undergoes Compton scattering. What is the maximum energy the Compton electron can have? What is the minimum energy of the scattered photon?

**4.13** The energy of a Compton photon scattered to an angle of 180° is 0.8 MeV. What is the energy of the incident photon?

**4.14** Prove that a gamma scattered by 180°, as a result of a Compton collision, cannot have energy greater than $mc^2/2$, where $mc^2 = 0.511$ MeV is the rest mass energy of the electron.

**4.15** Prove that the attenuation coefficient of gammas for a compound or a mixture can be written as

$$\mu(\mathrm{m}^2/\mathrm{kg}) = \sum_{i=1}^{H} w_i \, \mu_i(\mathrm{m}^2/\mathrm{kg})$$

where $w_i$ = weight fraction of $i$th element
$\mu_i$ = total mass attenuation coefficient of $i$th element

**4.16** A 1.75-MeV $\gamma$-ray hits a 25-mm-thick NaI crystal. What fraction of the interactions of this photon will be photoelectric? What is the average distance traveled before the first interaction occurs? ($\tau = 1.34 \times 10^{-3}\,\mathrm{cm}^2/\mathrm{g}$.)

**4.17** A parallel beam of gammas impinges upon a multiple shield consisting of successive layers of concrete, Fe, and Pb, each layer having thickness 100 mm. Calculate the fraction of gammas traversing this shield. The total attenuation coefficients are $\mu$(concrete) = 0.002 $\mathrm{m}^2/\mathrm{kg}$, $\mu$(Fe) = 0.004 $\mathrm{m}^2/\mathrm{kg}$, and $\mu$(Pb) = 0.006 $\mathrm{m}^2/\mathrm{kg}$; $\rho_{\text{concrete}} = 2.3 \times 10^3\ \mathrm{kg/m^3}$.

**4.18** Assume that a parallel beam of 3-MeV gammas and a parallel beam of 2-MeV neutrons impinge upon a piece of lead 50 mm thick. What fraction of $\gamma$'s and what fraction of neutrons will emerge on the other side of this shield without any interaction? Based on your result, what can you say about the effectiveness of lead as a shield for $\gamma$'s or neutrons? [$\sigma$(2 MeV) = 3.5 b.]

**4.19** What are the capture, fission, and total macroscopic cross section of uranium enriched to 90 percent in $^{235}$U for thermal neutrons? ($\rho = 19.1 \times 10^3\ \mathrm{kg/m^3}$.)

$^{235}$U: $\sigma_\gamma = 101$ b $\quad \sigma_f = 577$ b $\quad \sigma_s = 8.3$ b
$^{238}$U: $\sigma_\gamma = 2.7$ b $\quad \sigma_f = 0 \quad \sigma_s = 8$ b

**4.20** What is the average distance a thermal neutron will travel in 90 percent enriched uranium (see Prob. 4.19) before it has an interaction?

**4.21** The water in a pressurized-water reactor contains dissolved boron. If the boron concentration is 800 parts per million, what is the mean free path of thermal neutrons? The microscopic cross sections are

$H_2O$: $\sigma_s = 103$ b $\quad \sigma_a = 0.65$ b
Boron: $\sigma_s = 4$ b $\quad \sigma_a = 759$ b

## BIBLIOGRAPHY

Brookhaven National Laboratory, "Neutron Cross Sections" (and supplements), BNL-325, Upton, New York, 1958.

Chilton, A. B., Shultis, J. K., and Faw, R. E., *Principles of Radiation Shielding*, Prentice-Hall, Englewood Cliffs, N.J., 1984.

Evans, R. D., *The Atomic Nucleus*, McGraw-Hill, New York, 1972.

Roy, R. R., and Reed, R. D., *Interactions of Photons and Leptons with Matter*, Academic Press, New York, 1968.

Segré, E., *Nuclei and Particles*. W. A. Benjamin, New York, 1968.

Ziegler, J. F. (organizer), *The Stopping and Ranges of Ions in Matter*, 5 vols., Pergamon Press, New York, 1977.

## REFERENCES


1. Berger, M. J., and Seltzer, S. M., NASA SP-3012, 1964.
2. Anderson, H. H., Sorensen, H., and Vadja, P., *Phys. Rev.* **180**:383 (1969).
3. Sorensen, H., and Anderson, H. H., *Phys. Rev.* **8B**:1854 (1973).
4. Janni, J. F., Proton range-energy tables, 1 keV-10 GeV, *Atomic Data Nucl. Data Tables* **27**:147–339 (1982).
5. Berger, M. J., and Seltzer, S. M., NBSIR 82-2550A, 1983.
6. Sternheimer, R. M., *Phys. Rev.* **88**:851 (1952).
7. Sternheimer, R. M., *Phys. Rev.* **103**:511 (1956).
8. Williamson, C. F., Baujot, J. P., and Picard, J., CEA-R-3042 (1966).
9. Bichsel, H., *Phys. Rev.* **112**:1089 (1958).
10. Tabata, T., Ito, R., and Okabe, S., *Nucl. Instrum. Meth.* **103**:85 (1972).
11. Northcliffe, L. C., *Ann. Rev. Nucl. Sci.* **13**:67 (1963).
12. Lindhard, J., Scharff, M., and Schiott, H. E., *Fys Medd.* **33**:14 (1963).
13. Moak, C. D., and Brown, M. D., *Phys. Rev.* **149**:244 (1966).
14. Brown, M. D., and Moak, C. D., *Phys. Rev.* **6B**:90 (1972).
15. Betz, G., Isele, H. J., Rossle, E., and Hortig, G., *Nucl. Instrum. Meth.* **123**:83 (1975).
16. Booth, W., and Grant, I. S., *Nucl. Phys.* **63**:481 (1965).
17. Forster, J. S., Ward, D., Andrews, H. R., Ball, G. G., Costa, G. J., Davies, W. G., and Mitchell, J. V., *Nucl. Instrum. Meth.*, **136**:349 (1976).
18. Northcliffe, L. C., and Schilling, R. F., *Nucl. Data* **A7**:223 (1970).
19. Brown, M. D., "Interaction of Uranium Ions in Solids," Ph.D. thesis, University of Tennessee, 1972 (unpublished).
20. Bridwell, L., and Bucy, S., *Nucl. Sci. Eng.* **37**:224 (1969).
21. Bridwell, L., and Moak, C. D., *Phys. Rev.* **156**:242 (1967).
22. Siffert, P., and Coche, A., "General Characteristics of the Interactions of Nuclear Radiations with Matter and their Consequences," in G. Bertolini and A. Coche (eds.), *Semiconductor Detectors*, Wiley, New York, 1968, pp. 279–300.
23. Hakim, M., and Shafrir, N. H., *Nucl. Sci. Eng.* **48**:72 (1972).
24. Gesini, G., Lucarini, G., and Rustichelli, R., *Nucl. Instrum. Meth.* **127**:579 (1975).
25. Hubbell, J. H., NSRDS-NBS 29, August 1969.
26. Goldstein, H., and Wilkins, J. E., Jr., NYO-3075, Nuclear Development Associates, Inc., 1954.
27. R. G. Jaeger (ed.), *Engineering Compendium on Radiation Shielding* V1, IAEA, New York, 1968.
28. Trubey, D. K., ORNL-RSIC-10, 1966.
29. Eisenhauer, C. M., and Simmons, G. L., *Nucl. Sci. Eng.* **56**:263 (1975).
30. Kuspa, J. P., and Tsoulfanidis, N., *Nucl. Sci. Eng.* **52**:117 (1973).
31. Chilton, A. B., *Nucl. Sci. Eng.* **59**:436 (1979).
32. Trubey, D. K., "New Gamma Buildup Factor Data for Point Kernel Calculations: ANS-6.4.3 Standard Reference Data," ORNL/RSIC-49, 1988.

CHAPTER
# FIVE

# GAS-FILLED DETECTORS

## 5.1 INTRODUCTION

Gas-filled detectors operate by utilizing the ionization produced by radiation as it passes through a gas. Typically, such a counter consists of two electrodes to which a certain electrical potential is applied. The space between the electrodes is filled with a gas (Fig. 5.1). Ionizing radiation, passing through the space between the electrodes, dissipates part or all of its energy by generating electron-ion pairs. Both electrons and ions are charge carriers that move under the influence of the electrical field. Their motion induces a current on the electrodes, which may be measured (Fig. 5.1*a*). Or, through appropriate electronics, the charge produced by the radiation may be transformed into a pulse, in which case particles are counted individually (Fig. 5.1*b*). The first type of counter (Fig. 5.1*a*) is called *current* or *integrating chamber*; the second type (Fig. 5.1*b*) is called *pulse chamber*. To get an idea of what charges and currents one might expect to measure, consider this representative example.

For most gases, the average energy required to produce an electron-ion pair is about 30 eV. This number takes into account all collisions, including those that lead to excitation. If a 3-MeV alpha and beta particle deposits all its energy in the counter, it will produce, on the average,

$$\frac{3 \times 10^6}{30} = 10^5 \text{ electron-ion pairs}$$

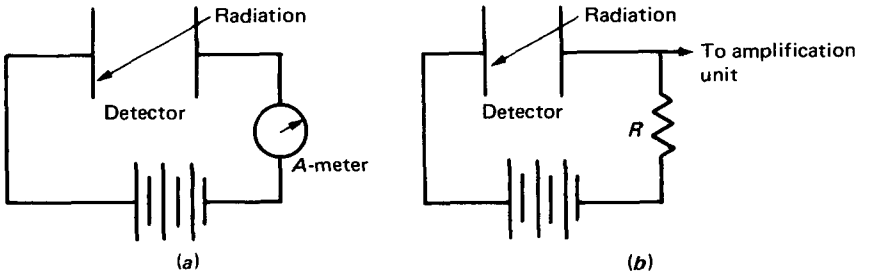


**Figure 5.1** A typical gas-filled detector: (*a*) the direct current produced in the circuit is measured; (*b*) individual pulses are detected.

A typical gas counter† has a capacitance of about 50 pF, and the charge will be collected in a time of the order of 1 $\mu$s. If all the charge created by the 3-MeV particle is collected, the voltage and current expected are of the order of

$$V = \frac{Q}{C} \approx \frac{10^5 \times 1.6 \times 10^{-19}\ \text{C/el}}{50 \times 10^{-12}\ \text{F}} \approx 0.5 \times 10^{-3} V \approx 0.5\ \text{mV}$$

$$i = \frac{Q}{t} \approx \frac{10^5 \times 1.6 \times 10^{-19}}{10^{-6}} A \sim 1.6 \times 10^{-8} A$$

In an ionized gas without an electric field, electrons and positive ions will move at random with an average kinetic energy equal to $\frac{3}{2}kT$, where $k$ = Boltzmann's constant and $T$ = temperature of the gas (Kelvin). When an electric field is present, both electrons and positive ions acquire a net velocity component along the lines of the electric field. Electrons move toward the positive electrode, positive ions toward the negative one. The force on either charge carrier is the same and equal to $F = Ee$, where $E$ = electric field intensity, but the acceleration is quite different. The acceleration $a$ is equal to $F/M$, where $M$ is the mass of the ion or electron. Therefore, the acceleration of an electron will be thousands of times larger than the acceleration of an ion. The time it takes the electrons to reach the positive electrode of a typical counter is about 1 $\mu$s. The corresponding time for the positive ions is about 1 ms, a thousand times longer.

The discussion up to this point has been limited to the effects of the ionization produced directly by the incident particle. This is called *primary* ionization. There are types of gas counters in which the electric field is so strong that the electrons of the primary ionization acquire enough kinetic energy between collisions to produce new electron-ion pairs. These new charges constitute the *secondary* ionization. Primary and secondary ionization are generated within such a short period of time that they contribute to one and the same pulse.

†Although the correct term is gas-filled detector or counter, the short term *gas counter* is frequently used.

## 5.2 RELATIONSHIP BETWEEN HIGH VOLTAGE AND CHARGE COLLECTED

Assume that the following experiment is performed (Fig. 5.2). A radioactive source of constant intensity is placed at a fixed distance from a gas counter. The high voltage (HV) applied to the counter may be varied with the help of a potentiometer. An appropriate meter measures the charge collected per unit time. If the HV applied to the counter is steadily increased, the charge collected per unit time changes as shown in Fig. 5.3. The curve of Fig. 5.3 is divided into five regions, which are explained as follows.

**Region I.** When the voltage is very low, the electric field in the counter is not strong, electrons and ions move with relatively slow speeds, and their recombination rate is considerable. As $V$ increases, the field becomes stronger, the carriers move faster, and their recombination rate decreases up to the point where it becomes zero. Then, all the charge created by the ionizing radiation is being collected ($V = V_1$). Region I is called the *recombination* region.

**Region II.** In region II, the charge collected stays constant despite a change in the voltage because the recombination rate is zero and no new charge is produced. This is called the *ionization* region.

**Region III.** In this region, the collected charge starts increasing because the electrons produce secondary ionization that results in charge multiplication. The electric field is so strong, in a certain fraction of the counter volume, that electrons from the primary ionization acquire enough energy between collisions to produce additional ionization. The gas *multiplication factor*—i.e., the ratio of the total ionization produced divided by the primary ionization—is, for a given voltage, independent of the primary ionization. Thus the output of the counter is proportional to the primary ionization. The pulse height at the output is proportional to the energy dissipated inside the counter; therefore particle

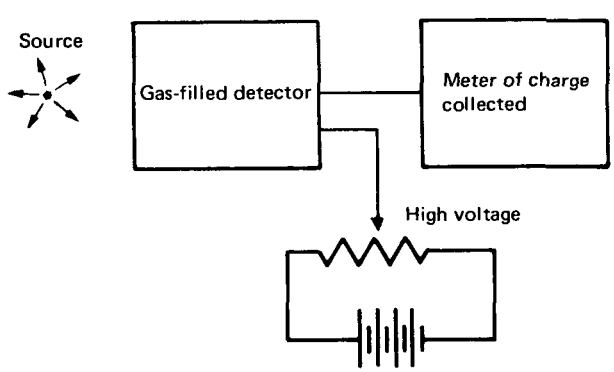


**Figure 5.2** Experimental setup for the study of the relationship between high voltage applied and charge collected.

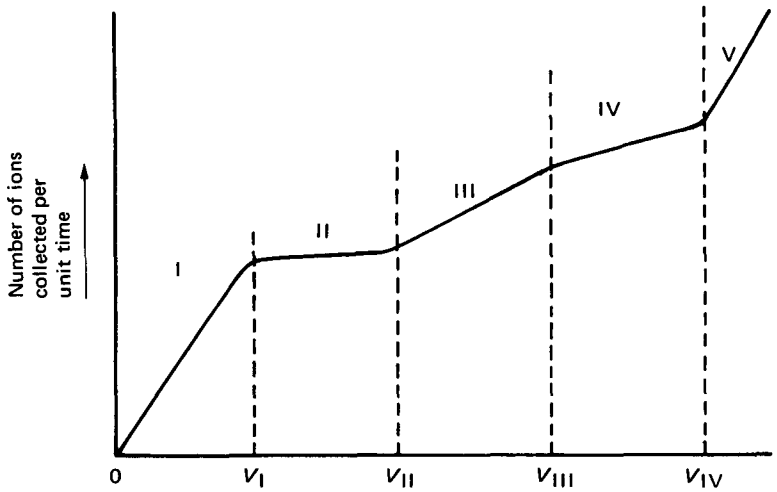


**Figure 5.3** The relationship between voltage applied to the counter and charge collected.

identification and energy measurement are possible. This region is, appropriately enough, called the *proportional* region.

**Region IV.** In this region, the electric field inside the counter is so strong that a single electron-ion pair generated in the chamber is enough to initiate an avalanche of electron-ion pairs. This avalanche will produce a strong signal with shape and height independent of the primary ionization and the type of particle, a signal that depends only on the electronics of the counter. Region IV is called the *Geiger-Müller* (GM) region.

**Region V.** If the applied voltage is raised beyond the value $V_{IV}$, a single ionizing event initiates a continuous discharge in the gas, and the device is not a particle detector anymore. No gas counter should operate with voltage $V > V_{IV}$.

If the graph discussed above is obtained using an $\alpha$, $\beta$, or $\gamma$ source, the results will be as shown in Fig. 5.4.

## 5.3 DIFFERENT TYPES OF GAS-FILLED DETECTORS

Gas counters take their name from the voltage region ion which they operate. No counter operates in region I of Fig. 5.3, because a slight change in voltage will change the signal.

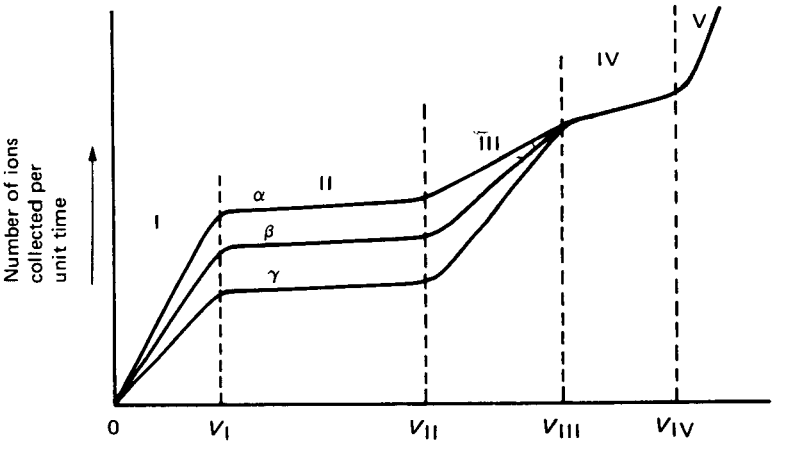


**Figure 5.4** The relationship between charge collected and applied voltage for three different types of particles. In region IV, the curve increases slightly but is the same for all particles.

*Ionization chambers* operate in region II. No charge multiplication takes place. The output signal is proportional to the particle energy dissipated in the detector; therefore measurement of particle energy is possible. Since the signal from an ionization chamber is not large, only strongly ionizing particles such as alphas, protons, fission fragments, and other heavy ions are detected by such counters. The voltage applied is less than 1000 V.

*Proportional counters* operate in region III. Charge multiplication takes place, but the output signal is still proportional to the energy deposited in the counter. Measurement of particle energy is possible. Proportional counters may be used for the detection of any charged particle.

Identification of the type of particle is possible with both ionization and proportional counters. An alpha particle and an electron having the same energy and entering either of the counters, will give a different signal. The alpha particle signal will be bigger than the electron signal. The voltage applied to proportional counters ranges between 800 and 2000 V.

*GM counters* operate in region IV. GM counters are very useful because their operation is simple and they provide a very strong signal, so strong that a preamplifier is not necessary. They can be used with any kind of ionizing radiation (with different levels of efficiency). The disadvantage of GM counters is that their signal is independent of the particle type and its energy. *Therefore, a GM counter provides information only about the number of particles.* Another minor disadvantage is their relatively long dead time (200 to 300 $\mu$s). (For more details about dead time, see Sec. 5.6.2.) The voltage applied to GM counters ranges from 500 to 2000 V.

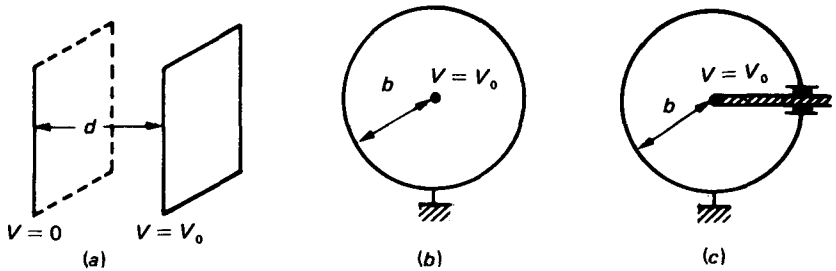


**Figure 5.5** The different geometries of gas-filled detectors: (*a*) parallel plate; (*b*) cylindrical; (*c*) spherical.

Gas counters may be constructed in any of three basic geometries: parallel plate, cylindrical, or spherical (Fig. 5.5). In a parallel-plate chamber, the electric field (neglecting edge effects) is uniform, with strength equal to

$$E = \frac{V_0}{d} \tag{5.1}$$

In the cylindrical chamber, the voltage is applied to a very thin wire, a few mills of an inch in diameter, stretched axially at the center of the cylinder. The cylinder wall is usually grounded. The electric field is, in this case,

$$E(r) = \frac{V_0}{\ln(b/a)} \frac{1}{r} \tag{5.2}$$

where $a$ = radius of the central wire
$b$ = radius of the counter
$r$ = distance from the center of the counter

It is obvious from Eq. 5.2 that very strong electric fields can be maintained inside a cylindrical counter close to the central wire. Charge multiplication is achieved more easily in a cylindrical than in a plate-type gas counter. For this reason, proportional and GM counters are manufactured with cylindrical geometry.

In a spherical counter, the voltage is applied to a small sphere located at the center of the counter. The wall of the counter is usually grounded. The electric field is

$$E(r) = V_0 \frac{ab}{b-a} \frac{1}{r^2} \tag{5.3}$$

where $a$, $b$, and $r$ have the same meaning as in cylindrical geometry. Strong fields may be produced in a spherical counter, but this type of geometry is not popular because of construction difficulties.

A counter filled with a gas at a certain pressure may operate in any of the regions I–IV discussed earlier, depending on a combination of the following

parameters:

1. Size of the counter
2. Size of wire (in cylindrical counters)
3. Gas type
4. Gas pressure
5. Level of high voltage

Normally, gas counters are manufactured to operate in one region only. The user buys an ionization counter, a proportional counter, or a GM counter. The manufacturer has selected the combination of variables 1–4 listed above that results in the desired type of gas counter. The last variable, the high voltage applied, is not a fixed number, but a range of values. The range is specified by the manufacturer, but the user decides on the best possible value of HV.

The rest of this chapter discusses the special characteristics of the three types of gas counters.

## 5.4 IONIZATION CHAMBERS

### 5.4.1 Pulse Formation in an Ionization Chamber

The formation and shape of the signal in an ionization chamber will be analyzed for a parallel-plate counter as shown in Fig. 5.1*b*. The analysis is similar for a cylindrical or a spherical chamber.

Consider the ionization chamber shown in Fig. 5.6. The two parallel plates make a capacitor with capacitance $C$, and with the resistor $R$ an $RC$ circuit is formed. A constant voltage $V_0$ is applied on the plates. The time-dependent

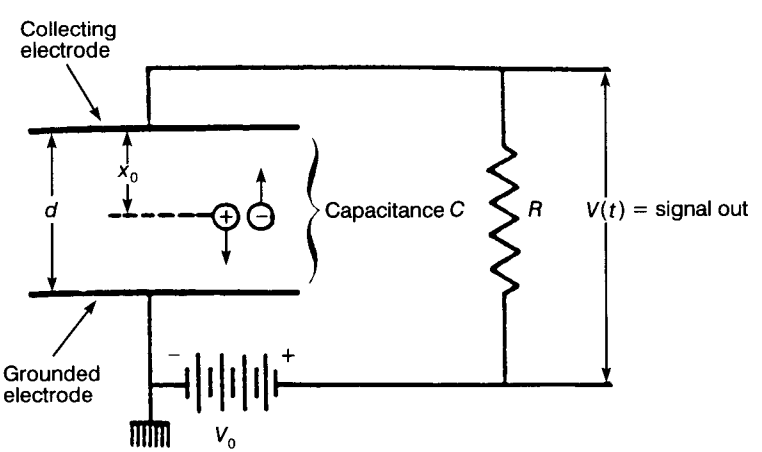


**Figure 5.6** The electronic circuit of a parallel-plate ionization chamber.

voltage $V(t)$ across the resistor $R$ represents the signal. The objective of this section is to obtain the function $V(t)$.

Assume that one electron-ion pair has been formed at a distance $x_0$ from the collecting plate (collector). The electron and the ion start moving in the electric field, and they acquire kinetic energy at the expense of the electrostatic energy stored in the capacitance of the chamber. If the charge moves a distance $dx$, conservation of energy requires that

$$\text{(Work on charges)} = \text{(change in electrostatic energy)}$$

$$eE(dx^+ + dx^-) = d\left(\frac{Q^2}{2C}\right) = \frac{Q}{C}\,dQ \approx V_0(dQ^- + dQ^+) \tag{5.4}$$

where $E$ = electric field intensity
$Q$ = charge on chamber plates
$dQ^+, dQ^-$ = changes in positive, negative charge, respectively

It is assumed that the change in the charge ($dQ$) is so small that the voltage $V_0$ stays essentially constant. The voltage $V(t)$ across the resistor $R$ is the result of this change in the charge and is given by

$$V(t) = \frac{1}{C}\int_0^t dQ(t) = \frac{1}{C}\int_0^t (dQ^+ + dQ^-) \tag{5.5}$$

Substituting in Eq. 5.5 the value of $dQ$ from Eq. 5.4, one obtains

$$V(t) = \frac{1}{C}\int_0^t \frac{e}{V_0}E(dx^+ - dx^-) \tag{5.6}$$

Let

$w^+$ = drift velocity of positive ions
$w^-$ = drift velocity of electrons

In general, the drift velocity is a function of the *reduced field strength* $E/p$, where $p$ is the gas pressure in the chamber.

The derivation up to this point is independent of the chamber geometry. To proceed further requires substitution of the value of the electric field from either Eq. 5.1, 5.2, or 5.3. For a plate-type ionization chamber the field is constant (Eq. 5.1), independent of $x$, and so is the drift velocity. Therefore, Eq. 5.6 becomes

$$V(t) = \frac{e}{Cd}\int_0^t (w^+ + w^-)\,dt = -\frac{e}{Cd}(w^-t + w^+t) \tag{5.7}$$

The drift velocity of the electron is a few thousand times more than the velocity of the ion,† which means the electron will reach the collector plate before the

†Typical values of drift velocities are $w^+ \approx 10$ m/s, $w^- = 10^4 - 10^5$ m/s.

ion has hardly moved. Let

$T^{(+)}$ = time it takes for an ion to reach the cathode

$T^{(-)}$ = time it takes for an electron to reach the collector (anode)

Typical values of these times are

$$T^{(+)} \approx \text{ms} \qquad T^{(-)} \approx \mu\text{s}$$

Equation 5.7 shows that for $t < T^{(-)}$, the voltage $V(t)$ changes linearly with time (Fig. 5.7):

$$V(t) = -\frac{e}{Cd}(w^- + w^+)t \qquad 0 < t \leq T^{(-)} \tag{5.8}$$

For $T > T^{(-)}$, the signal is

$$V(t) = -\frac{e}{Cd}(x_0 + w^+ t) \qquad t > T^{(-)} \tag{5.9}$$

Finally, after $t = T^{(+)}$, the ion reaches the grounded cathode and the signal reaches its maximum (negative) value, which is

$$V(T^+) = -\frac{e}{Cd}x_0 \qquad t > T^{(+)} \tag{5.10}$$

If $N$ electron-ion pairs are produced, the final voltage will be

$$V(T^+) = -\frac{Ne}{Cd}x_0 \qquad t = T^{(+)} \tag{5.11}$$

For $t > T^{(+)}$, the pulse decays with decay constant $RC$ (see Sec. 10.3).

The pulse profile of Fig. 5.7 was derived under the assumption that all ion pairs were produced at $x = x_0$. Actually, the ionization is produced along the track traveled by the incident particle. The final pulse will be the result of the superposition of many pulses with different $T^{(-)}$ values. Because of this effect, the sharp change in slope at $t = T^{(-)}$ will disappear and the pulse will be smoother.

The pulse of Fig. 5.7 is not suitable for counting individual particles because it does not decay quickly enough. A pulse-type counter should produce a signal that decays faster than the average time between the arrival of two successive particles. For example, if the counting rate is 1000 counts/min, a particle arrives at the counter, on the average, every 1/1000 min (60 ms).

In Fig. 5.7, the pulse could be stopped at time $t = T^{(+)}$ by electronic means. Such a technique would produce pulses with height proportional to the total charge generated in the detector, but with a duration of a few hundreds of microseconds, which is unacceptably long. The method used in practice is to "chop off" the pulse at time $t = T^{(-)}$, which amounts to stopping the pulse after only the electrons are collected. The signal is then fed into an $RC$ circuit that, as described in Chap. 10, changes the pulse as shown in Fig. 5.8.

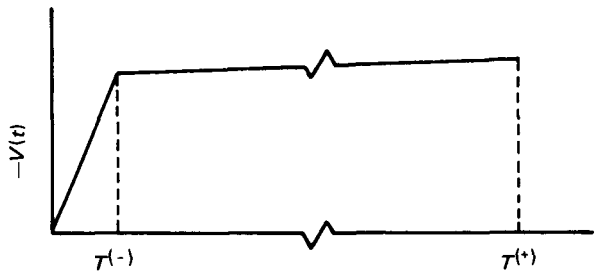


**Figure 5.7** The voltage pulse generated by an ionization chamber.

Let $V_i(t)$ be the signal at the output of the detector that is used as an input to an $RC$ circuit. From Eq. 5.8,

$$V_i(t) = -\frac{e}{Cd}(w^- + w^+)t = kt \tag{5.8a}$$

Using this signal as an input, the output voltage across the resistor $R_0$ is (see Secs. 10.3 and 10.4), for $0 \le t \le T^{(-)}$ (Fig. 5.7),

$$V_0(t) = kC_0R_0(1 - e^{-t/C_0R_0}) \tag{5.12}$$

For $t > T^{(-)}$, $V_i(t)$ is essentially constant, and

$$V_0(t) = kC_0R_0(1 - e^{-T^{(-)}/C_0R_0})e^{-t/R_0C_0} \tag{5.13}$$

The signal $V_0(t)$ is shown in Fig. 5.8*b*. Usually, the $RC$ circuit is the first stage of the preamplifier, which accepts the signal of the ionization chamber.

The disadvantage of the signal in Fig. 5.8*b* is that its maximum value depends on the position where the ionization was produced. Indeed, from Eq. 5.12, one obtains for $t = T^{(-)}$ (noting that $k = -e(w^- + w^+)/Cd \approx -ew^-/Cd$,

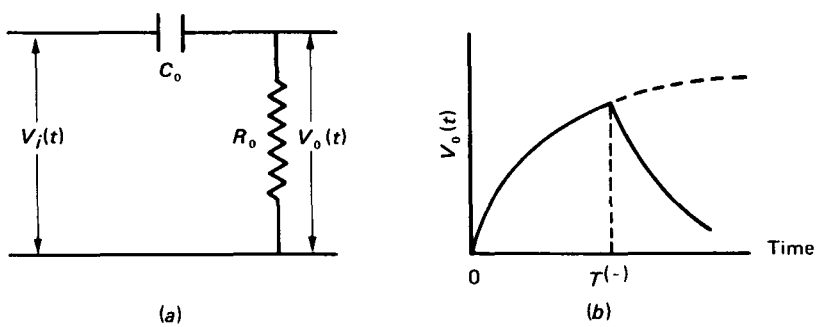


**Figure 5.8** (*a*) The signal $V_i(t)$ is fed into the $RC$ circuit. (*b*) The output of the $RC$ circuit decays quickly with a decay constant $R_0C_0$.

since $w^- \gg w^+$, $T^{(-)} \ll C_0R_0$, and $T^{(-)} = x_0/w^-$)

$$V(T^{(-)}) = -(ew^-/Cd)C_0R_0(1 - e^{-T^{(-)}/C_0R_0}) \approx -(ex_0/Cd) \quad (5.14)$$

Thus the peak value of the pulse in Fig. 5.8*b* depends on $x_0$. This disadvantage can be corrected in several ways. One is by placing a grid between the two plates and keeping it at an intermediate voltage $V_g(0 < V_g < V_0)$. For more details about the "gridded" ionization chamber, the reader should consult the references at the end of this chapter.

The analysis of the pulse formation in a cylindrical or a spherical counter follows the same approach. The results are slightly different because the electric field is not constant (see Eqs. 5.2 and 5.3), but the general shape of the signal is that shown in Fig. 5.7. (See Franzen & Cochran and Kowalski for detailed calculations of the pulse shapes for the three geometries of gas-filled chambers.)

### 5.4.2 Current Ionization Chambers

An ionization chamber of the *current* type measures the average ionization produced by many incoming particles. This is achieved by measuring directly the electrical current generated in the chamber, using either a sensitive galvanometer for currents of $10^{-8}$ A or higher (Fig. 5.9), or an electrometer (sometimes with an amplifier) for currents less than $10^{-8}$ A. In the case of the electrometer, as shown in Fig. 5.10, the current is determined by measuring the voltage drop across the known resistance $R$. The voltage drop may be measured by the electrometer directly or after some amplification.

For current ionization chambers, it is very important to know the relationship between applied voltage and output current (for a constant radiation source). This relationship, which is shown in Fig. 5.11, consists of regions I and II of the graph of Fig. 5.3. The proper operating voltage of the ionization chamber is that for which all the ionization produced by the incident radiation is measured. If this is the case, a slight increase of the applied voltage will result in negligible change of the measured current. The voltage is then called the saturation voltage ($V_s$), and the corresponding current is called saturation current. The value of the saturation current depends on the intensity and type of the radiation source (Fig. 5.11). It also depends, for the same radiation source, on the size and geometry of the chamber as well as on the type and pressure of the gas used. If one considers different gases, other things being equal, the highest current will be produced by the gas with the lowest average energy needed for the production of one electron-ion pair. Typical energies for common gases are given in Table 5.1.

During measurements of the ionization current with an electrometer, one would like to know the response of the measuring instrument if the signal from the ionization chamber changes. Assume that the current of the chamber changes suddenly from a value of $i_1$ to $i_2$. The response of the electrometer is obtained by considering the equivalent electronic circuit of Fig. 5.10, shown in

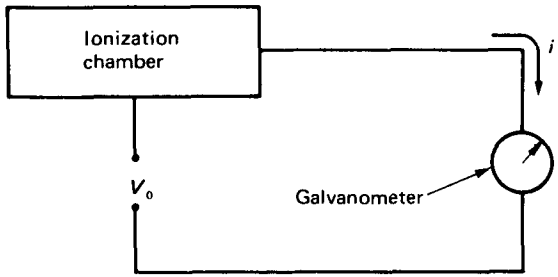


**Figure 5.9** Measurement of the current produced by an ionization chamber by using a galvanometer.

Fig. 5.12. The capacitor $C$ represents the combined capacitance of the chamber and everything else. The resistor $R$ represents a corresponding total resistance for the circuit. The signal to be measured is the voltage $V(t)$, where *for* $t \leq 0$,

$$V_1 = i_R R = i_1 R \tag{5.15}$$

At the $t = 0$, the current changes instantaneously from $i_1$ to $i_2$, and the voltage will eventually become

$$V_2 = i_2 R \tag{5.16}$$

During the transition period, Kirchhoff's first law gives

$$i_2 = i_C + i_R = \frac{dQ(t)}{dt} + \frac{V(t)}{R} = C\frac{dV(t)}{dt} + \frac{V(t)}{R}$$

or

$$\frac{dV(t)}{dt} + \frac{1}{RC}V(t) = i_2/C \tag{5.17}$$

The solution of this differential equation, with the initial condition given by Eq. 5.15, is

$$V(t) = i_2 R + R(i_1 - i_2)e^{-t/RC} \tag{5.18}$$

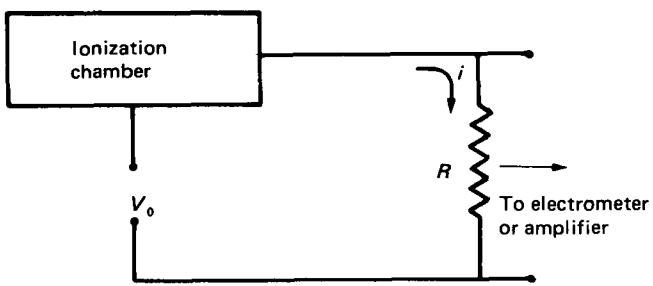


**Figure 5.10** Measurements of the current produced by an ionization chamber by using an electrometer.

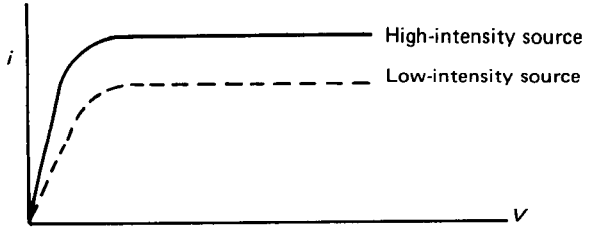


**Figure 5.11** The ionization chamber current as a function of applied voltage.

The function given by Eq. 5.18 is shown in Fig. 5.13. The response of the electrometer is exponential with a rate of change determined by the time constant *RC*. For fast response, the time constant should be as short as practically possible.

## 5.5 PROPORTIONAL COUNTERS

### 5.5.1 Gas Multiplication in Proportional Counters

When the electric field strength inside a gas counter exceeds a certain value, the electrons that move in such a field acquire, between collisions, sufficient energy to produce new ions. Thus, more electrons will be liberated, which in turn will produce more ions. The net effect of this process is multiplication of the primary ionization. The phenomenon is called *gas multiplication.*† To achieve the high field intensity needed for gas multiplication without excessive applied voltage, chambers operating in this mode are usually cylindrical with a very thin wire stretched axially at the center of the counter (Fig. 5.14). The wall of the counter is normally grounded and a positive voltage is applied to the central wire. In

†Also called gas gain or gas amplification.

**Table 5.1 Average Energy Needed for Production of One Electron-Ion Pair**†

| Gas | Energy per pair (eV) |
|---|---|
| H | 36.3 |
| He | 42.3 |
| A | 26.4 |
| Air | 34 |
| $CO_2$ | 32.9 |
| $C_2H_6$ (ethane) | 24.8 |
| $CH_4$ | 27.3 |

†From Franzen and Cochran.

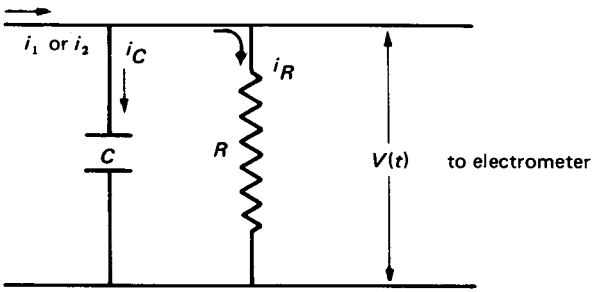


**Figure 5.12** The equivalent electronic circuit of Fig. 5.10.

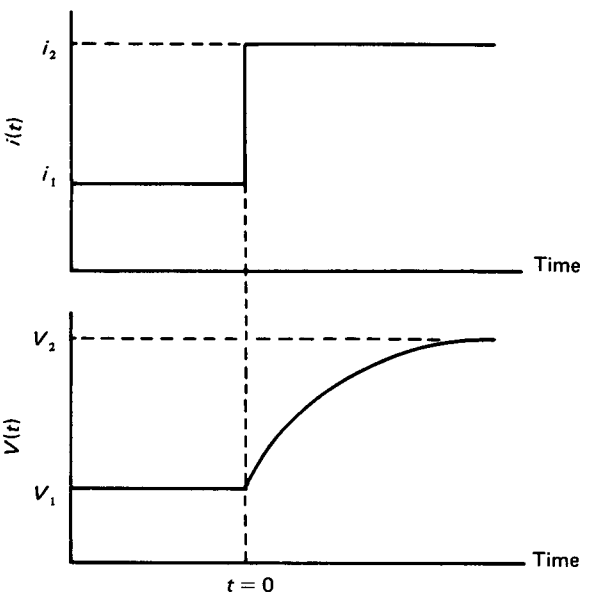


**Figure 5.13** Response of an electrometer to a step change of the ionization current.

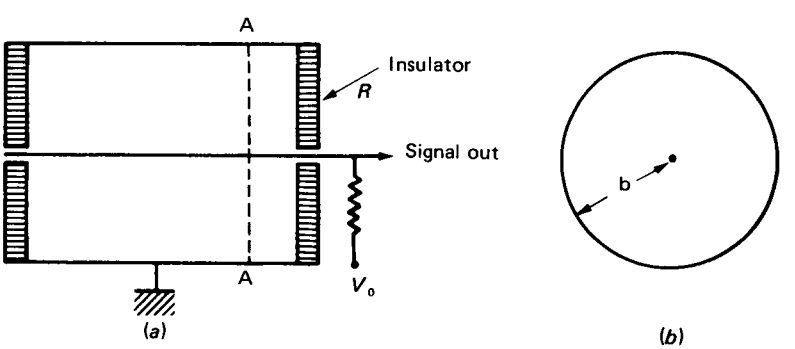


**Figure 5.14** (*a*) A cylindrical gas-filled detector. (*b*) Cross section of the detector at AA.

such a geometry, the electrostatic field inside the chamber is radial and its intensity is

$$E(r) = \frac{V_0}{\ln(b/a)} \frac{1}{r} \tag{5.2}$$

The field intensity increases rapidly as the wire is approached. Since the radius $a$ of the wire is a few mills of an inch and thousands of times smaller than the radius $b$ of the counter, an extremely strong electric field is produced in a fraction of the chamber's volume. This volume is so small that the probability that the incident radiation will produce an electron ion pair in it is negligible.

In addition to the secondary electrons produced by collisions, electrons are also produced by two other processes:

1. Photoelectric interactions
2. Bombardment of the cathode surface by positive ions

The photoelectric interactions are caused by photons that are produced in the counter as a result of the ionization and excitation of the atoms and molecules of the gas. If the chamber is filled with a monatomic gas, these photons produce photoelectrons only when they strike the cathode (wall of cylinder) because they do not have enough energy to ionize the atoms of the gas. If the counter is filled with a gas mixture, however, photons emitted by molecules of one gas may ionize molecules of another.

Electrons are also emitted when the positive ions, which are produced in the chamber, reach the end of their journey and strike the cathode. The significance of this effect depends on the type of material covering the surface of the cathode and, more important, on the type of the gas filling the chamber.

The production of electrons by these processes results in the generation of successive avalanches of ionization because all the electrons, no matter how they are produced, migrate in the direction of the intense electric field and initiate additional ionization. The gas multiplication factor $M$, which is equal to the *total* number of free electrons produced in the counter when *one* pair is produced by the incident radiation, is calculated as follows. Let

$N$ = total number of electrons set free per primary electron-ion pair

$\delta$ = average number of photoelectrons produced per ion pair generated in the counter ($\delta \ll 1$)

The initial avalanche of $N$ electrons will produce $\delta N$ photoelectrons. Each photoelectron produces a new avalanche of $N$ new electrons; therefore the second avalanche consists of $\delta N^2$ electrons. The third avalanche will have $\delta N^3$ electrons, and so on. The total number of electrons per initial ion pair produced is then

$$M = N + \delta N^2 + \delta N^3 + \cdots$$

The magnitude of $\delta N$ depends on the applied voltage. If $\delta N < 1$, the gas multiplication factor is

$$M = \frac{N}{1 - \delta N} \tag{5.19}$$

It should be noted that

1. If $\delta N \ll 1$, the photoelectric effect is negligible and $M = N =$ initial gas multiplication (first avalanche).
2. If $\delta N < 1$, $M$ can become much larger than $N$.
3. If $\delta N \geq 1$, $M \to \infty$, which means that a self-supporting discharge occurs in the counter.

The gas multiplication factor $M$ is a function of the ratio $V_0/\ln(b/a)$ and the product $Pa$, where $P$ is the pressure of the gas in the counter (Rossi & Staub). Experimental results of $M$ values for two gases are shown in Figs. 5.15 and 5.16. Diethorn[1] has obtained the equation

$$\ln M = \frac{V \ln 2}{\overline{\Delta V} \ln(b/a)} \ln \frac{V}{\bar{K} Pa \ln(b/a)} \tag{5.20}$$

where $\overline{\Delta V}$ and $\bar{K}$ are constants of the gas. Equation 5.20 has been tested and found to be valid.[2-4] As Figs. 5.15 and 5.16 show, $M$ increases almost exponentially with applied voltage.

One method by which the strong dependence of $M$ on applied voltage is reduced is by adding a small amount of a polyatomic organic gas in the gas of the counter. One popular mixture is 10 percent $CH_4$ and 90 percent argon. The organic gases, called "quenching" gases, stabilize the operation of the counter by reducing the effect of the secondary processes. They achieve this because

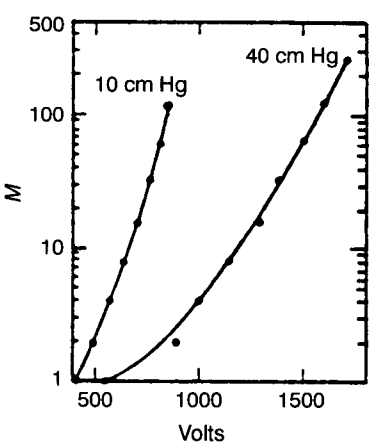


**Figure 5.15** Gas multiplication $M$ versus voltage. Gas is 93.6 percent pure argon ($a = 0.005$ in, $b = 0.435$ in, at two different pressures) (from Rossi and Staub).

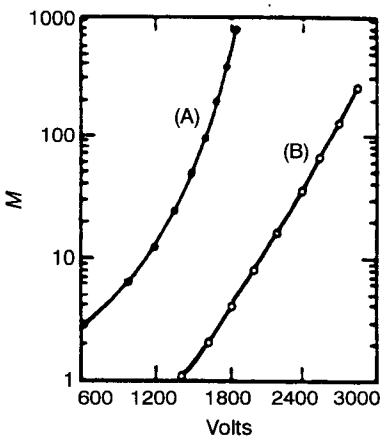


**Figure 5.16** Gas multiplication $M$ versus voltage. Gas is $BF_3$. (A) $a = 0.005$ in, $b = 0.75$ in, $P = 10$ cmHg. (B) $a = 0.005$ in, $b = 0.78$ in, $P = 80.4$ cmHg (from Rossi and Staub).

organic polyatomic molecules

1. dissociate rather than produce electrons when they hit the cathode
2. dissociate when they absorb a photon
3. have lower ionization potential than the molecules of the main gas; as a result, they are ionized in collisions with ions of the main gas and thus prevent the ions from reaching the cathode

The total charge produced in a proportional counter is

$$Q = MNe = M\frac{\Delta E}{W}e \tag{5.21}$$

where $\Delta E$ = energy of the incident particle dissipated in the counter
$w$ = average energy required for production of one electron-ion pair

Equation 5.21 indicates that $Q$ (output) is proportional to the energy deposited in the counter ($\Delta E$). This is the reason why such counters are called proportional. The proportionality holds, however, only if the gas multiplication factor $M$ is constant, independent of the primary ionization. The question then arises, under what conditions is this true?

A proportional counter is strictly proportional as long as the space charge due to the positive ions does not modify too much the electric field around the wire. The magnitude of the space charge is a function of the primary ionization and the gas multiplication. If the primary ionization is very small, the value of $M$ may be $10^5$ to $10^6$ before the space charge affects the proportionality. On the other hand, if the primary ionization is too strong, the critical value of $M$ is smaller. It has been reported[5] that there is a critical maximum value of the charge produced by the multiplication process beyond which proportionality does not hold. That number, obviously, depends on the counter (size, types of gas, etc.).

The events that produce the avalanches of electrons in a proportional counter are statistical in nature. The final multiplication factor $M$ will not be constant but will show statistical fluctuations. The probability that the multiplication will have the value $M$ is, according to Snyder,[6] equal to

$$P(M) = \frac{1}{\overline{M}} \exp\left(-\frac{M}{\overline{M}}\right) \tag{5.22}$$

where $\overline{M}$ = mean multiplication factor. The variance of $M$ is, from Eq. 5.22,

$$\sigma_M^2 = \overline{M}^2 \tag{5.23}$$

### 5.5.2 The Pulse Shape of a Proportional Counter

The shape of the pulse of a proportional counter is understood as one follows the events that lead to the formation of the pulse. A cylindrical counter will be considered, such as that shown in Fig. 5.14.

Assume that the incident particle generated $N$ electron-ion pairs at a certain point inside the counter. The electrons start moving toward the wire (anode). As soon as they reach the region of the strong field close to the wire, they produce secondary ionization. Since all the secondary ionization is produced in the small volume surrounding the wire, the amplitude of the output pulse is independent of the position of the primary ionization. The electrons of the secondary ionization are collected quickly by the wire, before the ions have moved appreciably. The ion contribution to the pulse is negligible because the ions cross only a very small fraction of the potential difference on their way to the anode. The pulse developed in the central wire is almost entirely due to the motion of the ions. As the ions move toward the cathode, the voltage pulse on the wire begins to rise: quickly at first, when the ions are crossing the region of the intense electric field, and slower later, when the ions move into the region of low-intensity field. The voltage pulse as a function of time is given by (Kowalski)

$$V(t) = \frac{Q}{2C \ln(b/a)} \ln\left(1 + \frac{b^2}{a^2}\frac{t}{t_{\text{ion}}}\right) \tag{5.24}$$

where $Q$ is given by Eq. 5.21
$C$ = capacitance of the counter
$t_{\text{ion}}$ = time it takes the ions to reach the cathode
The equation for $t_{\text{ion}}$ is (Kowalski)

$$t_{\text{ion}} = \frac{P \ln(b/a)}{2V_0 \mu_{\text{ion}}}(b^2 - r^2) \tag{5.25}$$

where $P$ = gas pressure
$\mu_{\text{ion}}$ = ion mobility in the field of the counter†
$r$ = point where the ion was produced

†The ion mobility is the proportionality constant between the drift velocity and the reduced field; thus $w^+ = \mu^+ (E/P)$.

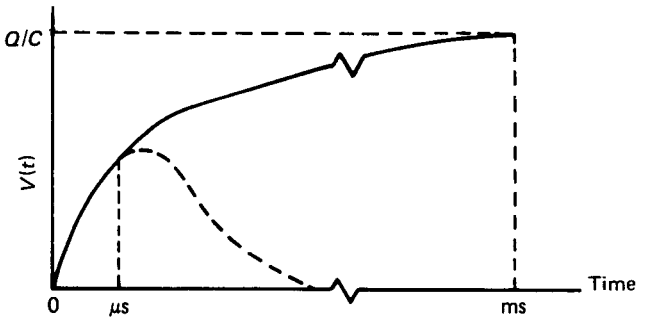


**Figure 5.17** The voltage pulse of a proportional counter.

The pulse $V(t)$ is shown by the solid line of Fig. 5.17. The pulse rises quickly and reaches half of its maximum in time of the order of microseconds. Then it bends and rises at a much slower rate, until about a millisecond later it reaches its final value, $Q/C$.

The pulse of Fig. 5.17 was derived under the assumption that all the ions were produced at the same point. In reality, the ions are produced along the track of the incident particle. This modifies the shape of the pulse during its initial rise but it leaves it virtually unaffected during the later period.

The pulse of Fig. 5.17 is unacceptably long, even for a modest counting rate. As in the case of the ionization chamber, the pulse is "chopped off" at some convenient time with the help of a differentiating circuit (Chap. 10). The result will be a pulse shown by the dashed line in Fig. 5.17.

### 5.5.3 The Change of Counting Rate with High Voltage—The High-Voltage Plateau

When a detector is used for the study of a phenomenon involving counting of particles, the investigator would like to be certain that changes in the counting rate are due to changes in the phenomenon under study and not due to changes of the environment such as atmospheric pressure, temperature, humidity, or voltage. For most radiation measurements, all these factors may be neglected except voltage changes.

Consider a gas-filled counter. For its operation, it is necessary to apply HV, usually positive, which may range from +300 to +3000 V, depending on the counter. For the specific counter used in an experiment, the observer would like to know by what fraction the counting rate will change if the HV changes by a certain amount. It is highly desirable to have a system for which the change in the counting rate is negligible, when the HV changes for a reason beyond the control of the investigator (e.g., change in the 110 V provided by the outlet on the wall, which may, in turn, cause a fluctuation in the output of the HV power supply). For this reason, the response of a counting system to such variations

ought to be known. This information is provided by the HV plateau of the counter. The determination of the HV plateau will be discussed below for a proportional counter. However, the experiment and the results are equally applicable for a GM counter.

The HV plateau is obtained by performing the experiment sketched in Fig. 5.18. A radioactive source, emitting a certain type of particles, is placed at a fixed distance from the counter. The signal from the detector is amplified with the help of a preamplifier and an amplifier. It is then fed through a discriminator, and pulses above the discriminator level are counted by the scaler. The counting rate of the scaler is recorded as a function of the HV, the only variable changed. The result of the experiment is shown in Fig. 5.19 (lower curve). Also shown in Fig. 5.19 (upper curve) is a part of the graph of Fig. 5.3 from regions II (ionization) and III (proportional) with the ordinate now shown as pulse height, which is, of course, proportional to the number of ions collected per unit time. The dashed line represents the discriminator level. The shape of the HV plateau is explained as follows.

For very low voltage ($V < V_A$) the counting rate is zero. The source is there, ionization is produced in the counter, pulses are fed into the amplifier and the discriminator, but the scaler does not receive any signal because all the pulses are below the discriminator level. Hence, the counting rate is zero. As the HV increase beyond $V_A$, more ionization is produced in the counter, some pulse heights generated in it are above the discriminator level and the counting rate starts increasing. The counting rate keeps increasing with HV, since more and more pulses are produced with a height above the discriminator level. This continues up to the point when $V \simeq V_B$. For $V > V_B$, the ionization is still increasing, the pulse height is also increasing, but all the pulses are now above the discriminator level. Since all the pulses are counted, each *pulse being recorded as one regardless of its height*, the counting rate does not change. This continues up to $V \approx V_C$. Beyond that point, the counting rate will start increasing again because the HV is so high that spurious and double pulses may be generated. The counter should not be operated beyond $V = V_C$.

The region of the graph between $V_B$ and $V_C$ is called the *HV plateau*. It represents the operational range of the counter. Although the manufacturer of the detector provides this information to the investigator, it is standard (and safe) practice to determine the plateau of a newly purchased counter before it is used in an actual measurement for the first time.

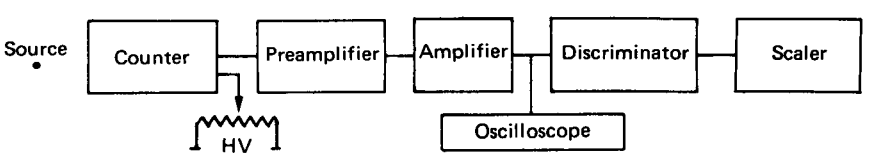


**Figure 5.18** Experimental arrangement for the determination of the HV plateau.

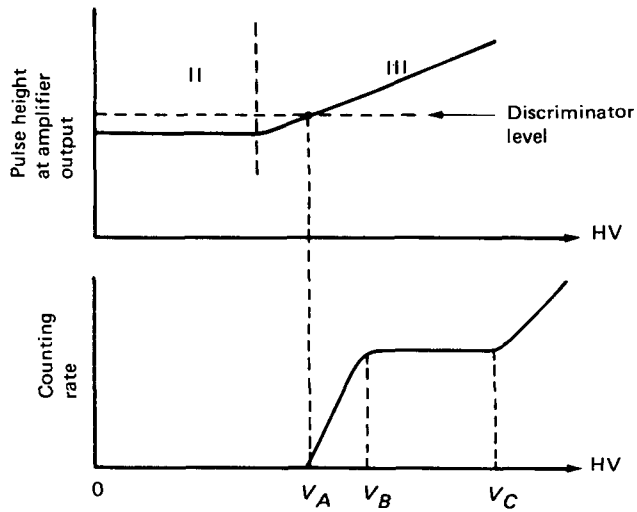


**Figure 5.19** The HV plateau (lower curve).

The plateau of Fig. 5.19 is shown as completely flat. For most counters, the plateau has a positive slope that may be due to spurious counts or to increasing efficiency of the counter, or to both of these effects. Investigation of proportional counters[7] showed that the positive slope is the result of an increase in detector efficiency. For GM counters, on the other hand, the slope of the plateau is due to the production of more spurious counts.

The performance of a counter is expressed in terms of the slope of the plateau given in the form

$$\text{Plateau slope} = \frac{\Delta r/r}{\Delta V} \tag{5.26}$$

where $\Delta r/r$ is the relative change of the counting rate $r$ for the corresponding change in voltage $\Delta V$. Frequently, Eq. 5.26 is expressed in percent change of the counting rate per 100 V change of the high voltage, i.e.,

$$\text{Plateau slope} = \frac{100(\Delta r/r)}{\Delta V}(100) = 10^4\frac{\Delta r/r}{\Delta V} \tag{5.27}$$

**Example 5.1** What is the change of counting rate per 100 V of the plateau for a counter having the plateau shown in Fig. 5.20?

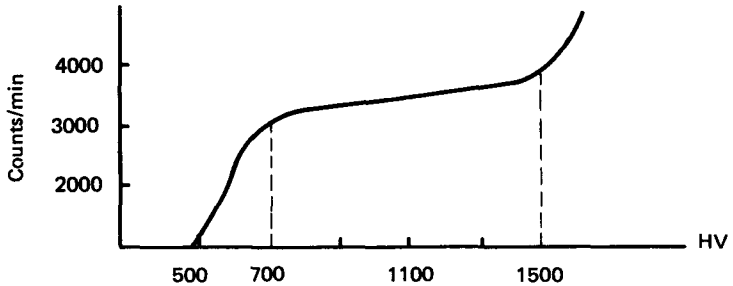


**Figure 5.20** The HV plateau used in Example 5.1.

**Answer** The plateau extends from about 700 to 1500 V. The slope over that region is (using Eq. 5.27),

$$\frac{10^4(r_2 - r_1)/r_1}{V_2 - V_1} = \frac{10^4(3800 - 3000)/3000}{1500 - 700} = 3.3\% \text{ per } 100\ V$$

The location of the plateau of a proportional counter depends on the type of particles being detected. If a source emits two types of particles with significantly different primary ionization, two separate plateaus will be obtained, with the plateau corresponding to the more ionizing particles appearing first. Figure 5.21 shows such a plateau for a proportional counter detecting alpha and beta particles. The existence of two plateaus is a consequence of the fact that in the proportional region, differentiation of the ionization produced by different types of particles is still possible (see region III in Fig. 5.4). In the GM region this distinction is lost, and for this reason GM counters have only one HV plateau regardless of the type of incident radiation (region IV of Fig. 5.4).

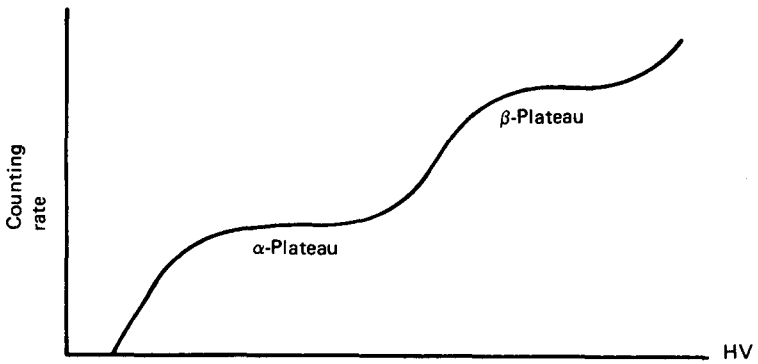


**Figure 5.21** Alpha and beta plateaus of a proportional counter.

## 5.6 GEIGER-MÜLLER COUNTERS

### 5.6.1 Operation of a GM Counter and Quenching of the Discharge

A GM counter is a gas counter that operates in region IV of Fig. 5.3. Its construction and operation are in many ways similar to those of a proportional counter. The GM counter is usually cylindrical in shape, like most of the proportional counters. The electric field close to the central wire is so strong that $N\delta \approx 1$ (see Sec. 5.5.1) and the gas multiplication factor $M$ is extremely high. In a GM counter, a single primary electron-ion pair triggers a great number of successive avalanches. Therefore, the output signal is independent of the primary ionization.

The operation of the GM counter is much more complicated than that of the proportional counter. When the electrons are accelerated in the strong field surrounding the wire, they produce, in addition to a new avalanche of electrons, considerable excitation of the atoms and molecules of the gas. These excited atoms and molecules produce photons when they deexcite. The photons, in turn, produce photoelectrons in other parts of the counter. Thus the avalanche, which was originally located close to the wire, spreads quickly in most of the counter volume. During all this time, the electrons are continuously collected by the anode wire, while the much slower moving positive ions are still in the counter and form a positive sheath around the anode. When the electrons have been collected, this positive sheath, acting as an electrostatic screen, reduces the field to such an extent that the discharge should stop. However, this is not the case because the positive ions eject electrons when they finally strike the cathode, and since by that time the field has been restored to its original high value, a new avalanche starts and the process just described is repeated. Clearly, some means are needed by which the discharge is permanently stopped or "quenched." Without quenching, a GM tube would undergo repetitive discharging. There are two general methods of quenching the discharge.

In *external quenching*, the operating voltage of the counter is decreased, after the start of the discharge until the ions reach the cathode, to a value for which the gas multiplication factor is negligible. The decrease is achieved by a properly chosen $RC$ circuit as shown in Fig. 5.22. The resistance $R$ is so high that the voltage drop across it due to the current generated by the discharge ($i_d$) reduces the voltage of the counter below the threshold needed for the discharge to start (the net voltage is $V_0 - i_d R$). The time constant $RC$, where $C$ represents the capacitance between anode and ground, is much longer than the time needed for the collection of the ions. As a result, the counter is inoperative for an unacceptably long period of time. Or, in other words, its dead time is too long.

The *self-quenching* method is accomplished by adding to the main gas of the counter a small amount of a polyatomic organic gas or a halogen gas.

The organic gas molecules, when ionized, lose their energy by dissociation rather than by photoelectric processes. Thus, the number of photoelectrons,

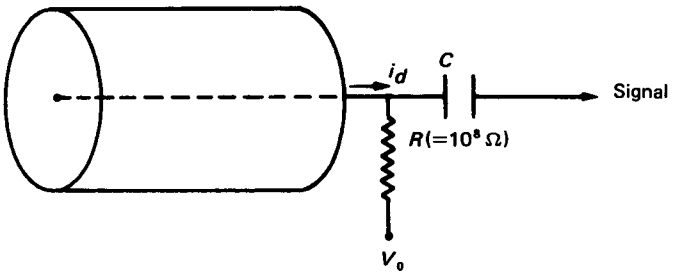


**Figure 5.22** The circuit used for external quenching of a GM counter.

which would spread and continue the avalanche, is greatly reduced. In addition, when the organic ions strike the surface of the cathode, they dissociate instead of causing the ejection of new electrons. Therefore, new avalanches do not start.

GM counters using an organic gas as a quenching agent have a finite lifetime because of the dissociation of the organic molecules. Usually, the GM counters last for $10^8$ to $10^9$ counts. The lifetime of a GM detector increases considerably if a halogen gas is used as the quenching agent. The halogen molecules also dissociate during the quenching process, but there is a certain degree of regeneration of the molecules, which greatly extends the useful lifetime of the counter.

### 5.6.2 The Pulse Shape and the Dead Time of a GM Counter

The signal of a GM counter is formed in essentially the same way as the signal of a proportional counter and is given by the same equation, Eq. 5.24. For GM counters the signal is the result of the sum of the contributions from all the positive ion avalanches produced throughout the volume of the counter. The final pulse is similar in shape to that shown in Fig. 5.17, except that the pulse rises much slower. The shape and height of GM counter pulses are not very important because the pulse is only used to signal the presence of the particle and nothing else. However, how one pulse affects the formation of the next one is important.

As discussed in Sec. 5.6.1, during the formation of a pulse, the electric field in the counter is greatly reduced because of the presence of the positive ions around the anode. If a particle arrives during that period, no pulse will be formed because the counter is insensitive. The insensitivity lasts for a certain time, called the dead time of the counter. Then, the detector slowly recovers, with the pulse height growing exponentially during the *recovery* period. This is illustrated in Fig. 5.23, which shows the change of the voltage and pulse for a typical GM counter. Typical values of dead time are from 100 to 300 $\mu$s. If the dead time is 100 $\mu$s and the counting rate is 500 counts/s, there is going to be a

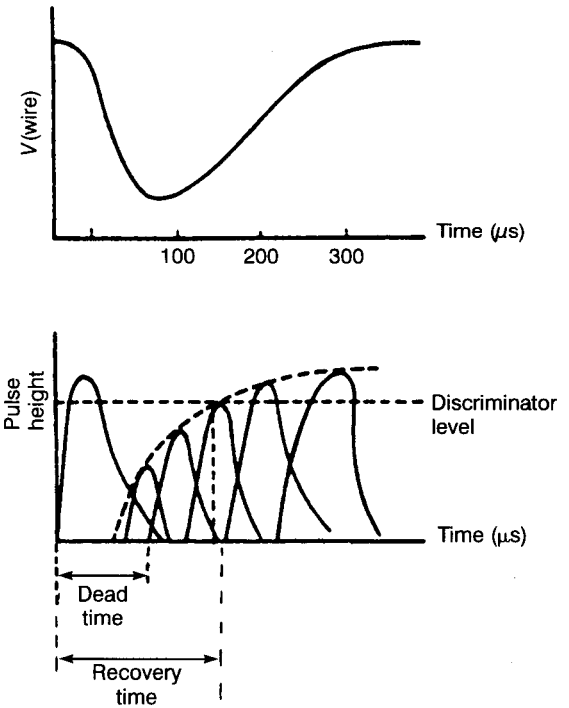


**Figure 5.23** Dead time and recovery time for a GM counter.

5 percent loss of counts due to dead time. Correction for dead time is described in Sec. 2.21.

## 5.7 GAS-FLOW COUNTERS

The gas counters described so far are all sealed. That is, the counter is a closed volume filled with a gas at a certain pressure. The radiation source is placed outside the detector; therefore, the particles have to penetrate the wall of the counter to be counted. In doing so, some particles may be absorbed by the wall and some may be backscattered; in the case of charged particles, they will all lose a certain fraction of their energy. To minimize these effects, most commercial gas counters have a thin window through which the radiation enters the counter. The window may still be too thick for some alpha and low-energy beta particles. For this reason, counters have been developed with the capability of having the source placed inside the chamber.

Gas counters of this type are called *gas-flow counters*. Their name comes from the fact that the gas flows continuously through the counter during operation. This is necessary because the detector cannot be sealed if the source is placed inside the chamber.

Gas-flow counters come in different geometries. Probably the most common one is that of the hemispherical detector as shown in Fig. 5.24. The high voltage is applied to a wire attached to the top of the hemisphere. The gas flows slowly through the counter, the flow rate being controlled by a regulator. At the exit, the gas goes through a liquid (e.g., some oil) and forms bubbles as it comes out. The formation of the bubbles indicates that the gas is flowing, and the rate of bubble formation gives an idea of the gas-flow rate.

Counting with gas-flow counters involves the following steps:

1. The chamber is opened and the sample is placed in its designated location inside the chamber.
2. The chamber is closed.
3. Gas from the gas tank is allowed to flow rapidly through the volume of the counter and purge it (for a few minutes).
4. After the counter is purged, the gas-flow rate is considerably reduced, to a couple of bubbles per second, and counting begins.

There are two advantages in placing the sample inside the detector:

1. The particles do not have to penetrate the window of the counter, where they might be absorbed, scattered out of the detector, or lose energy.
2. Close to 50 percent of the particles emitted by the source have a chance to be recorded in a hemispherical counter, or close to 100 percent in a spherical counter. If the source is placed outside the detector, there are always less than 50 percent of the particles entering the detector.

A hemispherical counter is also called a $2\pi$ counter, while a spherical counter with the source located at its center is called a $4\pi$ counter. Figure 5.24 shows a $2\pi$ counter.

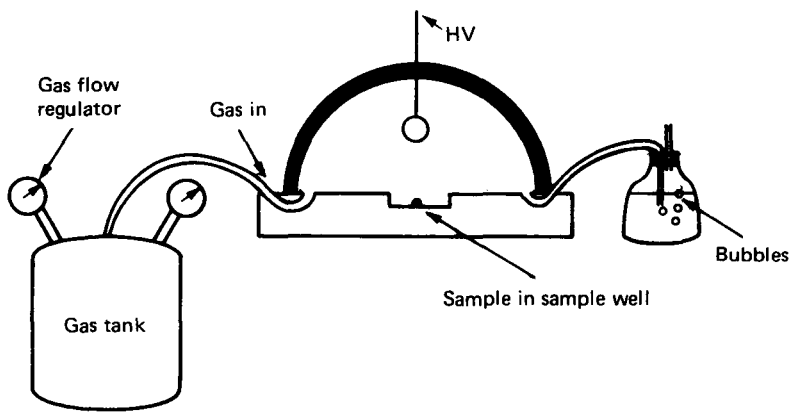


**Figure 5.24** A hemispherical ($2\pi$) gas-flow counter.

Gas-flow counters may operate as proportional or GM counters. In fact, there are commercial models that may operate in one or the other region depending on the voltage applied and the gas used. In a proportional gas-flow counter, the gas is usually methane or a mixture of argon and methane. In the GM region, the gas is a mixture of argon and isobutane.

In some gas-flow counter models, there is provision for placing a very thin window between the sample and the sensitive volume of the counter to reduce the effects of slight contamination of the sample well or of static charges that interfere with the measurement. In the counter of Fig. 5.24, the thin window will be placed on top of the sample well. A different arrangement is shown in Fig. 5.25.

Gas-flow counters are used as low-background alpha-beta detection systems. Requirements for low-background measurements arise in cases where the level of activity from the sample is very low, compared to background. Examples of such cases are samples that monitor contamination of water supplies or of air or ground.

There are commercially available systems that have a background counting rate of less than 1 count/min for betas and a considerably lower rate for alphas. Such a low background is achieved by shielding the counter properly (surrounding it with lead) and using electronic means to reject most of the background radiation. A system offered by one of the manufacturers uses two detectors. The first is the gas-flow counter and the second is a cosmic-ray detector (Fig. 5.26). The two detectors are operated in *anticoincidence* (see Sec. 10.8), which means that events due to particles going through both detectors (e.g., cosmic rays or other radiation from the environment) will not be counted. Only pulses produced by the activity of the sample in the gas-flow counter will be recorded.

Discrimination between alphas and betas can be achieved in many ways. The two methods most frequently used with gas-flow counters are based on range and energy differences. Before these methods are discussed, the reader

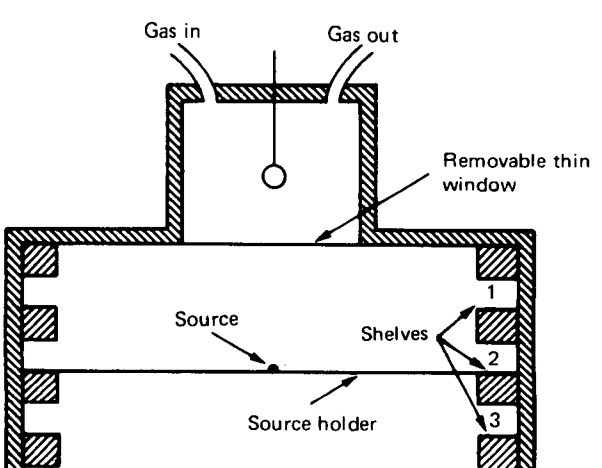


**Figure 5.25** A gas-flow counter with removable thin window and movable source holder.

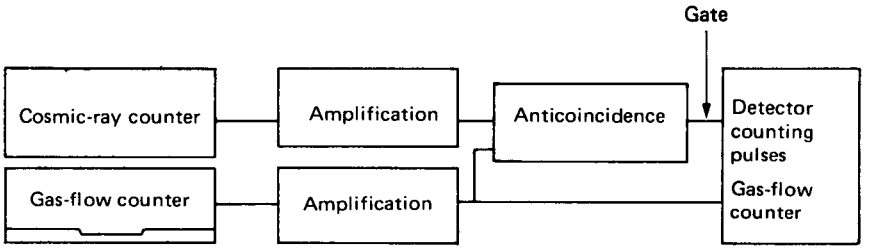


**Figure 5.26** A low-background alpha-beta counting system utilizing two counters and anticoincidence. The anticoincidence output gates the scaler to count only pulses from the gas-flow counter.

should recall that the maximum energy of most beta emitters is less than 2 MeV while the energy of alphas from most alpha emitters is 5–6 MeV.

Because the range of alphas is much shorter than that of betas, a sample can be analyzed for alpha and beta activity by counting it twice: once with a thin foil covering it to stop the alphas, and a second time without the foil to record alphas and betas.

Energy discrimination is based on the difference in pulse height produced by the two types of particles: the alphas, being more energetic, produce higher pulses; thus a simple discriminator at an appropriate level can reject the beta pulses.

### 5.7.1 The Long-Range Alpha Detector (LRAD)

A variation of the gas-flow counter has been developed[8,9] for the detection of alpha contamination. Common alpha particle detectors are limited by the short range of alphas in air. For example, the range of a 6-MeV alpha in air at normal temperature and pressure is about 46 mm. To circumvent this limitation, the LRAD does not measure the alphas directly. Instead, as shown schematically in Fig. 5.27, the ions created by the alphas in air are transported, with the help of airflow, and directed into an ion chamber. There, the current created by the ions is measured by an electrometer. Since the number of ions produced is proportional to the strength of the alpha source, the signal of the electrometer is also proportional to the alpha source strength.

In principle, a similar detector could be developed for any particle that produces ions. However, particles like electrons, gammas, and neutrons generate a much smaller number of ions than alpha particles do, traveling over the same distance. For this reason, an LRAD-type detector would have a smaller sensitivity for these other particles than for alphas. Of course, an LRAD-type detector would operate satisfactorily for the detection of protons, deuterons, and other heavy ions.

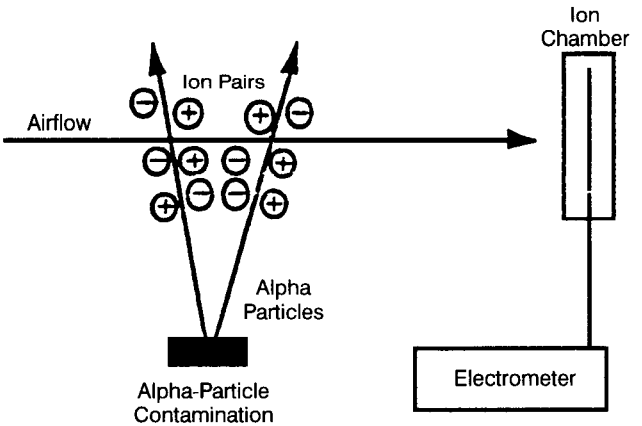


**Figure 5.27** The LRAD detects ions generated by alphas in air with the help of an ion chamber and an electrometer.

### 5.7.2 Internal Gas Counting

An alternative to the gas-flow counter is *internal gas counting*, which is used with low-energy $\beta$-emitters. In internal gas counting, a gaseous form of the radioisotope is introduced into the counter (usually a proportional counter) along with the counting gas. As with gas-flow counters, by having the source inside the counter, losses in the window are avoided and an increase in efficiency is achieved by utilizing a $4\pi$ geometry.

Internal gas counting requires that corrections be made for wall and end effects and for the decrease in electric field intensity at the ends.[10-12] One way to reduce the end effect is to use a spherical proportional counter,[13] in which the anode wire is stretched along a diameter and the cathode is, of course, spherical. The electric field inside the sphere is

$$E = \frac{V}{\ln(b/a)} \frac{1}{r} \tag{5.2}$$

At a certain distance $r$ from the anode, the electric field becomes stronger at the ends of the anode because $b$, the radius of the cathode, gets smaller. However, the supports of the wire tend to reduce the field. By property adjusting the supports, one may make the field uniform. In cylindrical counters, corrections for end effects are applied by a length-compensation method.[10]

Internal gas counting is used for the production of standards. Using this technique, the National Bureau of Standards produced standards of $^{3}H$, $^{14}C$, $^{37}A$, $^{85}K$, $^{131m}Xe$, and $^{133}Xe$.

## 5.8 RATE METERS

A rate meter is a device that measures the average rate of incoming pulses. Rate meters are used for continuous monitoring of an event, where the average counting rate versus time rather than the instantaneous counting rate is needed.

The basic operation of a rate meter is to feed a known charge per pulse into a capacitor that is shunted by a resistor (Fig. 5.28). Let

$$r = \text{counting rate (pulses/s)}$$
$$q = \text{charge per pulse}$$
$$V = \text{voltage across capacitor}$$
$$R = \text{resistance}$$
$$Q = \text{capacitor charge}$$

The net rate of change of $Q$ with respect to time is given by

$$\frac{dQ}{dt} = \text{(charge fed by pulses/s)} - \text{(charge flowing through resistor)}$$

or

$$\frac{dQ}{dt} = rq - \frac{Q}{RC} \tag{5.28}$$

The solution of this differential equation with the initial condition $Q(0) = 0$ is

$$Q(t) = rqRC(1 - e^{-t/RC}) \tag{5.29}$$

or, if one writes the result in terms of the output voltage,

$$V(t) = \frac{Q(t)}{C} = rqR(1 - e^{-t/RC}) \tag{5.30}$$

For time $t \gg RC$, equilibrium is reached and the value of the voltage is

$$V_\infty = rqR \tag{5.31}$$

The signal of a rate meter is the voltage $V_\infty$ given by Eq. 5.31. Notice that $V_\infty$ is independent of the capacitance $C$ and proportional to the counting rate $r$. The voltage $V_\infty$ is measured with an appropriate voltmeter.

If a pulse-type detector is used, the counts accumulated in the scaler have a statistical uncertainty that is calculated as shown in Chap. 2. If a rate meter is used, what is the uncertainty of the measurement? To obtain the uncertainty, one starts with Eq. 5.29, which gives the charge of the capacitor $C$. It is important to note that the charge changes exponentially with time. Thus, the contribution of the charge from a pulse arriving at $t = 0$ is not instantaneous but continues for a period of time.

Consider an observation point $t_0$ (Fig. 5.29). The standard deviation $\sigma_Q$ of the charge collected at $t = t_0$ is the result of contributions from pulses having

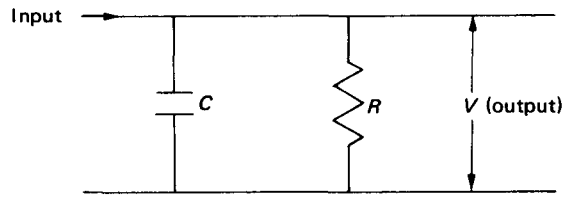


**Figure 5.28** The circuit of a rate meter.

arrived earlier. If the counting rate is $r$, the number of pulses in a time interval $\Delta t$ is, on the average, $r\,\Delta t$. The statistical uncertainty of this number is $\pm\sqrt{r\,\Delta t}$, or the uncertainty of the charge is $\pm q\sqrt{r\,\Delta t}$. One can show that a single pulse arriving at time $t$ contributes to the signal at time $t = t_0$, an amount of charge equal to $q\exp[-(t_0 - t)/RC]$. Therefore, the variance of the charge at time $t = t_0$ is

$$\sigma_Q^2 = \int_0^{t_0} (q\sqrt{r\,dt}\,e^{-(t_0-t)/RC})^2 \tag{5.32}$$

Integration of Eq. 5.32 gives the result

$$\sigma_Q^2 = 0.5q^2 rRC(1 - e^{-2t_0/RC}) \tag{5.33}$$

For $t_0 \gg RC$, Eq. 5.33 takes the form

$$\sigma_Q = q\sqrt{\frac{r(RC)}{2}} \tag{5.34}$$

At equilibrium, $Q = rqRC$ (from Eq. 5.29); therefore,

$$\sigma_r = \frac{\sigma_Q}{qRC} = \sqrt{\frac{r}{2RC}} \tag{5.35}$$

and

$$\frac{\sigma_r}{r} = \sqrt{\frac{1}{2RCr}} \tag{5.36}$$

The quantity $RC$ is the time constant of the circuit shown in Fig. 5.28. Equation 5.36 states that any instantaneous reading on a rate meter has a relative standard error equal to that of a total number of counts obtained by counting for a time equal to $2RC$ (assuming the background is negligible).

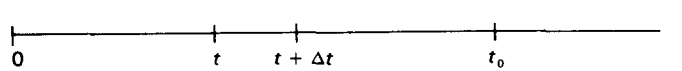


**Figure 5.29** Pulses arriving during $\Delta t$, and at $t$, contribute to $\sigma_Q$ at $t = t_0$.

## 5.9 GENERAL COMMENTS ABOUT CONSTRUCTION OF GAS-FILLED DETECTORS

This section summarizes the important characteristics of gas counters.

**Geometry.** Parallel-plate counters are almost exclusively ionization chambers. The intense fields needed for gas multiplication can be produced only in cylindrical or spherical geometry.

In the cylindrical geometry, which is the most frequently used, the strong electric field exists close to the central wire. The wire is usually made of tungsten or platinum. It has a diameter of 25–100 $\mu$m (few mills of an inch); it must be uniform in radius, without any bends or kinks, and be placed concentrically with the outer cylinder. Of particular importance is the smoothness of the central wire. Any kinks or tiny specks of material attached to its surface amount to pointed tips where very high electric fields are generated. Such a high field is a source of spurious discharges that interfere with counting.

**Gases and pressures used.** For ionization chambers, almost any gas or pressure may be used. Even atmospheric air has been used.

For proportional or GM counters, the noble gases—argon in particular—are normally used. A small percentage of additional gases is also used for quenching purposes. In proportional counters, methane is frequently added to the main gas. The so-called P-10 mixture, consisting of 90 percent argon and 10 percent methane, is extensively used. Another mixture is 4 percent isobutane and 96 percent helium. Several gas pressures have been used. As Figs. 5.15 and 5.16 show, the gas multiplication depends on the pressure. Usually the pressure is less than 1 atm. Of course, gas-flow counters operate at ambient pressure.

As discussed in Sec. 5.6.1, the quenching gas in a GM counter is either an organic polyatomic molecule such as ethyl alcohol, or a halogen such as bromine or chlorine. A typical mixture is 0.1 percent chlorine in neon. The gas pressure in a GM counter is, in most cases, less than 1 atm. The pressure affects the operating voltage.

**Counter window.** When the source is placed outside the counter, it is very important for the radiation to enter the counter after traversing as thin a wall material as possible. Any material in the path of radiation may scatter, absorb, or cause energy loss. This is particularly critical in the measurement of alphas and low-energy betas, which have a very short range. It is not important for neutron and gamma counters.

All counters have walls as thin as possible (or practical), but in addition, many commercial designs have an area on the surface of the counter designated as the "window," consisting of a very thin material. In cylindrical counters, the window is usually the front end of the cylinder (the other end houses electrical connectors). There are some cylindrical counters with windows located on the cylindrical surface.

Materials and thicknesses of windows are

1. Glass, down to 0.30–0.40 kg/m$^2$ (100$\mu$m)
2. Aluminum, 0.25–0.30 kg/m$^2$ (100 $\mu$m)
3. Steel, 0.60–0.80 kg/m$^2$ (80 $\mu$m)
4. Mica, 0.01 kg/m$^2$ (3 $\mu$m)
5. Mylar (plain or aluminized), 0.01 kg/m$^2$
6. Special ultrathin membranes or foils, $\sim 10^{-3}$ kg/m$^2$

## PROBLEMS

**5.1** Sketch the HV plateau of a counter, if all the pulses out of the amplifier have exactly the same height.

**5.2** How would the sketch of Prob. 5.1 change if there are two groups of pulses out of the amplifier (two groups, two different pulse heights)?

**5.3** Sketch counting rate versus discriminator threshold, assuming that the electronic noise consists of pulses in the range $0 < V < 0.1$ V and all the pulses due to the source have height equal to 1.5 V.

**5.4** In a cylindrical gas counter with a central wire radius equal to 25 $\mu$m (0.001 in), outer radius 25 mm ($\sim$ 1 in), and 1000 V applied between anode and cathode, what is the distance from the center of the counter at which an electron gains enough energy in 1 mm of travel to ionize helium gas? (Take 23 eV as the ionization potential of helium.)

**5.5** A GM counter with a mica window is to be used for measurement of $^{14}$C activity. What should the thickness of the window be if it is required that at least 90 percent of the $^{14}$C betas enter the counter?

**5.6** What is the minimum pressure required to stop 6-MeV alphas inside the argon atmosphere of a spherical gas counter with a 25-mm radius? Assume the alpha source is located at the center of the counter.

**5.7** What is the ratio of the saturation ionization currents for a chamber filled with He versus one filled with $CH_4$ (other things being equal)?

**5.8** Show that the variance of $M$ is equal to $\overline{M}^2$ if the probability distribution is given by Eq. 5.22.

**5.9** Calculate the maximum value of the positive ion time given by Eq. 5.25 for a cylindrical counter with a cathode radius equal to 19 mm ($\sim$ 0.75 in) and a central anode wire with a radius of 25 $\mu$m ($\sim$ 0.001 in ). The high voltage applied is 1000 V; the pressure of the gas is 13.3 kPa (10 cmHg), and the mobility of the ions is 13.34 Pa m$^2$/(V s).

**5.10** The observed counting rate of a counter is 22,000 counts/min. What is the error in the true counting rate if the dead time is 300 $\mu$s and no dead-time correction is applied?

## BIBLIOGRAPHY

Eichholz, G. G., and Poston, J. W., *Nuclear Radiation Detection*, Lewis Publishers, Chelsea, Michigan, 1985.

Fenyves, E., and Haiman, O., *The Physical Principles of Nuclear Radiation Measurements*, Academic Press, New York, 1969.

Franzen, W., and Cochran, L. W., "Pulse Ionization Chambers and Proportional Counters," in A. H. Snell (ed.), *Nuclear Instruments and Their Uses*, Wiley, New York, 1962.

Gillespie, A. B., *Signal, Noise and Resolution in Nuclear Counter Amplifiers*, McGraw-Hill, New York, 1953.
Knoll, G. F., *Radiation Detection and Measurement*, 2nd ed., Wiley, New York, 1989.
Kowalski, E., *Nuclear Electronics*, Springer-Verlag, New York-Heidelberg-Berlin, 1970.
Price W. J., *Nuclear Radiation Detection*, McGraw-Hill, New York, 1964.
Rossi, B. B., and Staub, H. H., *Ionization Chambers and Counters*, McGraw-Hill, New York, 1949.
Tait, W. H., *Radiation Detection*, Butterworth, London, 1980.

## REFERENCES

1. Diethorn, W., NYO-0628, 1956.
2. Kiser, R. W., *Appl. Sci. Res.* **8B**:183 (1960).
3. Williams, W., and Sara, R. I., *Int. J. Appl. Rad. Isotopes* **13**:229 (1962).
4. Bennett, E. F., and Yule, T. J., ANL-7763, 1971.
5. Hanna, G. C., Kirkwood, H. W., and Pontecorvo, B., *Phys. Rev.*, **75**:985 (1949).
6. Snyder, H. S., *Phys. Rev.* **72**:181 (1947).
7. Champion, P. J., *Nucl. Instrum. Meth.* **112**:75 (1973).
8. MacArthur, D. W., Allander, K. S., Bounds, J. A., Butterfield, K. B., and McAtee, J. L., *Health Phys.* **63**:324 (1992).
9. MacArthur, D. W., Allander, K. S., Bounds, J. A., and McAtee, J. L., *Nucl. Technol.* **102**:270 (1993).
10. Mann, W. B., Seliger, H. H., Marlow, W. F., and Medlock, R. W., *Rev. Sci. Instrum.* **31**:690 (1960).
11. Garfunkel, S. B., Mann, W. B., Schima, F. J., and Unterweger, M. P., *Nucl. Instrum. Meth.* **112**:59 (1973).
12. Bambynek, W., *Nucl. Instrum. Meth.* **112**:103 (1973).
13. Benjamin, P. W., Kemsholl, C. D., and Redfearn, J., *Nucl. Instrum. Meth.* **59**:77 (1968).

CHAPTER
# SIX

# SCINTILLATION DETECTORS

## 6.1 INTRODUCTION

Scintillators are materials—solids, liquids, gases—that produce sparks or scintillations of light when ionizing radiation passes through them. The first solid material to be used as a particle detector was a scintillator. It was used by Rutherford, in 1910, in his alpha-scattering experiments. In Rutherford's experimental setup, alpha particles hit a zinc sulfide screen and produced scintillations, which were counted with or without the help of a microscope—a very inefficient process, inaccurate and time consuming. The method was abandoned for about 30 years and was remembered again when advanced electronics made possible amplification of the light produced in the scintillator.

The amount of light produced in the scintillator is very small. It must be amplified before it can be recorded as a pulse or in any other way. The amplification or multiplication of the scintillator's light is achieved with a device known as the *photomultiplier tube* (or *phototube*). Its name denotes its function: it accepts a small amount of light, amplifies it many times, and delivers a strong pulse at its output. Amplifications of the order of $10^6$ are common for many commercial photomultiplier tubes. Apart from the phototube, a detection system that uses a scintillator is no different from any other (Fig. 6.1).

The operation of a scintillation counter may be divided into two broad steps:

1. Absorption of incident radiation energy by the scintillator and production of photons in the visible part of the electromagnetic spectrum

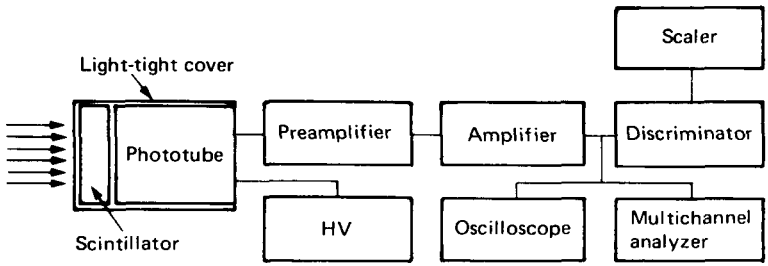


**Figure 6.1** A detection system using a scintillator.

2. Amplification of the light by the photomultiplier tube and production of the output pulse

The sections that follow analyze these two steps in detail. The different types of scintillators are divided, for the present discussion, into three groups:

1. Inorganic scintillators
2. Organic scintillators
3. Gaseous scintillators

## 6.2 INORGANIC (CRYSTAL) SCINTILLATORS

Most of the inorganic scintillators are crystals of the alkali metals, in particular alkali iodides, that contain a small concentration of an impurity. Examples are NaI(Tl), CsI(Tl), CaI(Na), LiI(Eu), and $CaF_2$(Eu). The element in parentheses is the impurity or activator. Although the activator has a relatively small concentration—e.g., thallium in NaI(Tl) is $10^{-3}$ on a per mole basis—it is the agent that is responsible for the luminescence of the crystal.

### 6.2.1 The Mechanism of the Scintillation Process

The luminescence of inorganic scintillators can be understood in terms of the allowed and forbidden energy bands of a crystal. The electronic energy states of an atom are discrete energy levels, which in an energy-level diagram are represented as discrete lines. In a crystal, the allowed energy states widen into bands (Fig. 6.2). In the ground state of the crystal, the uppermost allowed band that contains electrons is completely filled. This is called the *valence band.* The next allowed band is empty (in the ground state) and is called the *conduction band.* An electron may obtain enough energy from incident radiation to move from the valence to the conduction band. Once there, the electron is free to move anywhere in the lattice. The removed electron leaves behind a hole in the valence band, which can also move. Sometimes, the energy given to the electron

is not sufficient to raise it to the conduction band. Instead, the electron remains electrostatically bound to the hole in the valence band. The electron-hole pair thus formed is called an *exciton*. In terms of energy states, the exciton corresponds to elevation of the electron to a state higher than the valence but lower than the conduction band. Thus, the exciton states form a thin band, with the upper level coinciding with the lower level of the conduction band (Fig. 6.2). The width of the exciton band is of the order of 1 eV, whereas the gap between valence and conduction bands is of the order of 8 eV.

In addition to the exciton band, energy states may be created between valence and conduction bands because of crystal imperfections or impurities. Particularly important are the states created by the activator atoms such as thallium. The activator atom may exist in the ground state or in one of its excited states. Elevation to an excited state may be the result of a photon absorption, or of the capture of an exciton, or of the successive capture of an electron and a hole. The transition of the impurity atom from the excited to the ground state, if allowed, results in the emission of a photon in times of the order of $10^{-8}$ s. If this photon has a wavelength in the visible part of the electromagnetic spectrum, it contributes to a scintillation. Thus, production of a scintillation is the result of the occurrence of these events:

1. Ionizing radiation passes through the crystal.
2. Electrons are raised to the conduction band.
3. Holes are created in the valence band.

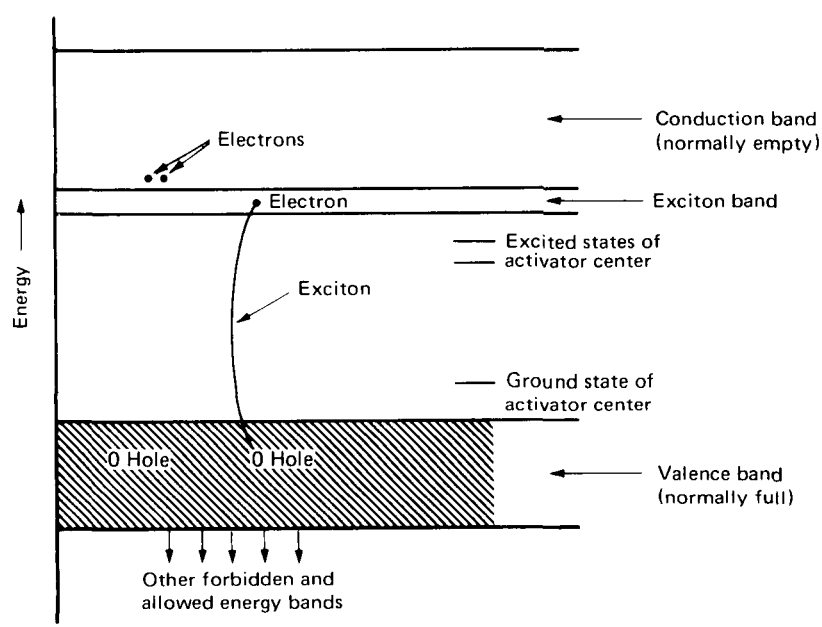


**Figure 6.2** Allowed and forbidden energy bands of a crystal

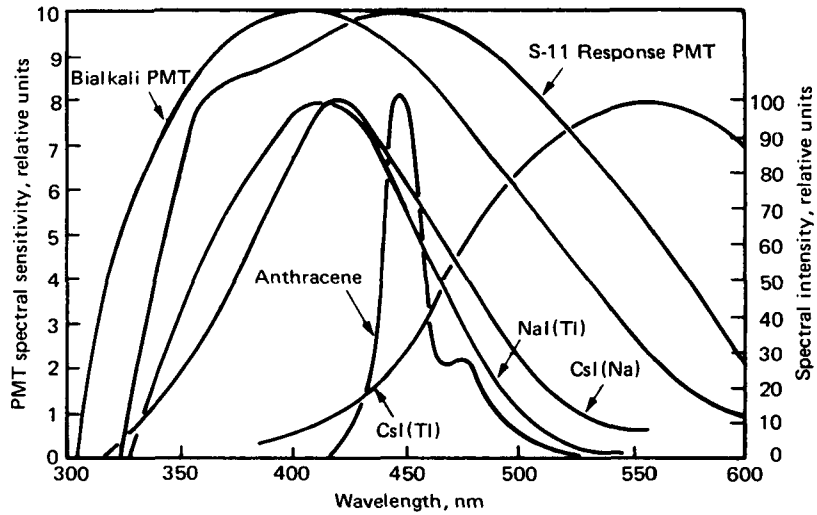


**Figure 6.3** Emission spectra of NaI(Tl), CsI(Tl), CsI(Na), and anthracene, compared to the spectral response of two photocathode materials. PMT, photomultiplier tube (from Harshaw Research Laboratory Report, Harshaw Chemical Company, 1978).

4. Excitons are formed.
5. Activation centers are raised to the excited states by absorbing electrons, holes, and excitons.
6. Deexcitation is followed by the emission of a photon.

The light emitted by a scintillator is primarily the result of transitions of the activator atoms, and not of the crystal. Since most of the incident energy goes to the lattice of the crystal—eventually becoming heat—the appearance of luminescence produced by the activator atoms means that energy is transferred from the host crystal to the impurity. For NaI(Tl) scintillators, about 12 percent of the incident energy appears as thallium luminescence.[1]

The magnitude of light output and the wavelength of the emitted light are two of the most important properties of any scintillator. The light output affects the number of photoelectrons generated at the input of the photomultiplier tube (see Sec. 6.5), which in turn affects the pulse height produced at the output of the counting system. Information about the wavelength is necessary in order to match the scintillator with the proper photomultiplier tube. Emission spectra of NaI(Tl), CsI(Na), and CsI(Tl) are shown in Fig. 6.3. Also shown in Fig. 6.3 are the responses of two phototube cathode materials. Table 6.1 gives the most important properties of some inorganic scintillators.

The light output of the scintillators depends on temperature. Figure 6.4 shows the temperature response of NaI(Tl), Cs(Tl), and CsI(Na).

**Table 6.1 Properties of Certain Inorganic Scintillators**

| Material | Wavelength of maximum emission (nm) | Scintillation efficiency (relative, %) | Decay time ($\mu$s) | Density ($10^3$ kg/m$^3$) |
|---|---|---|---|---|
| NaI(Tl) | 410 | 100 | 0.23 | 3.67 |
| $CaF_2$(Eu) | 435 | 50 | 0.94 | 3.18 |
| CsI(Na) | 420 | 80 | 0.63 | 4.51 |
| CsI(Tl) | 565 | 45 | 1.00 | 4.51 |
| $Bi_4Ge_3O_{12}$ | 480 | 8 | 0.30 | 7.13 |
| $CdWO_4$ | 530 | 20 | 0.90 | 7.90 |
| $^6$LiI(Eu) | 470 | 30 | 0.94 | 3.49 |

### 6.2.2 Time Dependence of Photon Emission

Since the photons are emitted as a result of decays of excited states, the time of their emission depends on the decay constants of the different states involved. Experiments show that the emission of light follows an exponential decay law of the form

$$N(t) = N_0 e^{-t/T} \tag{6.1}$$

where $N(t)$ = number of photons emitted at time $t$
$T$ = decay time of the scintillator (see Table 6.1)

Most of the excited states in a scintillator have essentially the same lifetime $T$. There are, however, some states with longer lifetimes contributing a slow component in the decay of the scintillator known as *afterglow*. It is present to some extent in all inorganic scintillators and may be important in certain measurements where the integrated output of the phototube is used. Two scintillators with negligible afterglow are $CaF_2$(Eu) and $Bi_4Ge_3O_{12}$ (bismuth orthogermanate).

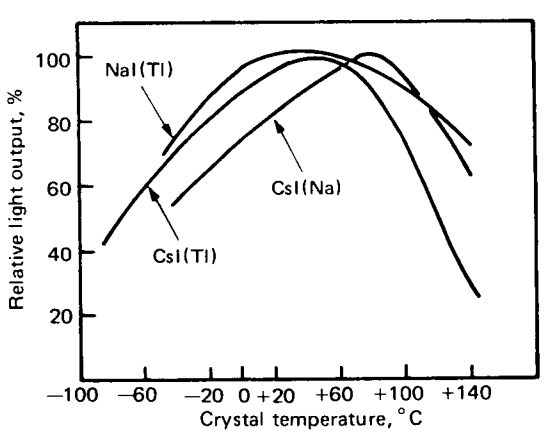


**Figure 6.4** Temperature dependence of light output of NaI(Tl), CsI(Tl), and CsI(Na) (from Harshaw Research Laboratory Report).

In a counting system using a scintillator, the light produced by the crystal is amplified by a photomultiplier tube and is transformed into an electric current having the exponential behavior given by Eq. 6.1. This current is fed into an *RC* circuit as shown in Fig. 6.5, and a voltage pulse is produced of the form

$$V(t) = V_\infty(e^{-t/RC} - e^{-t/T}) \tag{6.2}$$

In practice, the value of *RC* is selected to be of the order of a few hundreds of microseconds. Thus, for short times—i.e., $t \ll RC$, which is the time span of interest—Eq. 6.2 takes the form

$$V(t) = V_\infty(1 - e^{-t/T}) \tag{6.2a}$$

Notice that the rate at which the pulse rises (risetime) is determined by the decay time *T*. In certain measurements, e.g., coincidence-anticoincidence measurements (Chap. 10), the timing characteristics of the pulse are extremely important.

### 6.2.3 Important Properties of Certain Inorganic Scintillators

**NaI(Tl).** NaI(Tl) is the most commonly used scintillator for gamma rays. It has been produced in single crystals of up to 0.75 m (~ 30 in) in diameter and of considerable thickness (0.25 m ≈ 10 in). Its relatively high density ($3.67 \times 10^3$ kg/m$^3$) and high atomic number combined with the large volume make it a

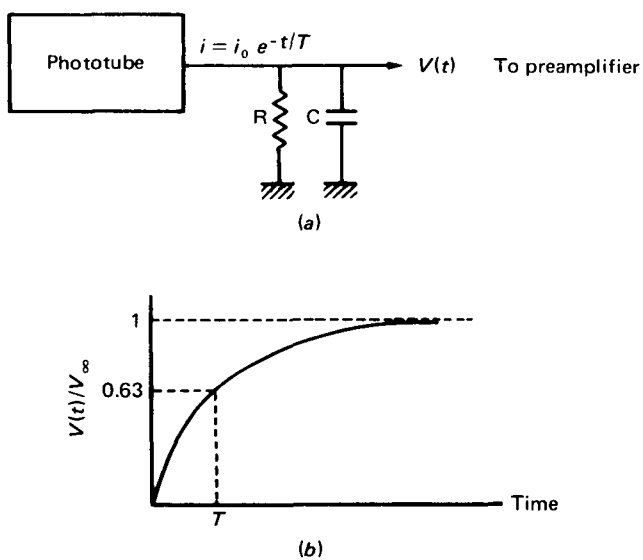


**Figure 6.5** (*a*) A voltage pulse results from the exponential current. (*b*) The shape of the pulse for $RC \gg T$.

$\gamma$-ray detector with very high efficiency. Although semiconductor detectors (Chap. 7 and 12) have better energy resolution, they cannot replace the NaI(Tl) in experiments where large detector volumes are needed.

The emission spectrum of NaI(Tl) peaks at 410 nm, and the light-conversion efficiency is the highest of all the inorganic scintillators (Table 6.1). As a material, NaI(Tl) has many undesirable properties. It is brittle and sensitive to temperature gradients and thermal shocks. It is also so hygroscopic that it should be kept encapsulated at all times. NaI always contains a small amount of potassium, which creates a certain background because of the radioactive $^{40}$K.

**CsI(Tl).** CsI(Tl) has a higher density ($4.51 \times 10^3$ kg/m$^3$) and higher atomic number than NaI; therefore its efficiency for gamma detection is higher. The light-conversion efficiency of CsI(Tl) is about 45 percent of that for NaI(Tl) at room temperature. At liquid nitrogen temperatures (77K), pure CsI has a light output equal to that of NaI(Tl) at room temperature and a decay constant equal to $10^{-8}$ s.[2] The emission spectrum of CsI(Tl) extends from 420 to about 600 nm.

CsI is not hygroscopic. Being softer and more plastic than NaI, it can withstand severe shocks, acceleration, and vibration, as well as large temperature gradients and sudden temperature changes. These properties make it suitable for space experiments. Finally, CsI does not contain potassium.

**CsI(Na).** The density and atomic number of CsI(Na) are the same as those of CsI(Tl). The light-conversion efficiency is about 85 percent of that for NaI(Tl). Its emission spectrum extends from 320 to 540 nm (see Fig. 6.3). CsI(Na) is slightly hygroscopic.

**$CaF_2$(Eu).** $CaF_2$(Eu) consists of low-atomic-number materials, and for this reason makes an efficient detector for $\beta$ particles[3] and X-rays[4] with low gamma sensitivity. It is similar to Pyrex and can be shaped to any geometry by grinding and polishing. Its insolubility and inertness make it suitable for measurements involving liquid radioisotopes. The light-conversion efficiency of $CaF_2$(Eu) is about 50 percent of that for NaI(Tl). The emission spectrum extends from about 405 to 490 nm.

**LiI(Eu).** LiI(Eu) is an efficient thermal-neutron detector through the reaction ${}^6_3\mathrm{Li}(n, \alpha){}^3_1\mathrm{H}$. The alpha particle and the triton, both charged particles, produce the scintillations. LiI has a density of $4.06 \times 10^3$ kg/m$^3$, decay time of about 1.1 $\mu$s, and emission spectrum peaking at 470 nm. Its conversion efficiency is about one-third of that for NaI. It is very hygroscopic and is subject to radiation damage as a result of exposure to neutrons.

**Other inorganic scintillators.** Many other scintillators have been developed for special applications. Examples are $Bi_4Ge_3O_{12}$, $CdWO_4$, and more recently[5] $MF_2$:$UF_4$:$CeF_3$, where M stands for one of the following: Ca, Sr, Ba. This last

scintillator, containing 2 percent $UF_4$ and using Ce as the fluorescing agent, has been used for detection of fission fragments.

## 6.3 ORGANIC SCINTILLATORS

The materials that are efficient *organic scintillators* belong to the class of aromatic compounds. They consist of planar molecules made up of benzenoid rings. Two examples are toluene and anthracene, having the structures shown in Fig. 6.6.

Organic scintillators are formed by combining appropriate compounds. They are classified as unitary, binary, ternary, and so on, depending on the number of compounds in the mixture. The substance with the highest concentration is called the *solvent*. The others are called *solutes*. A binary scintillator consists of a solvent and a solute, while a ternary scintillator is made of a solvent, a primary solute, and a secondary solute. Table 6.2 lists the most common compounds used.

### 6.3.1 The Mechanism of the Scintillation Process

The production of light in organic scintillators is the result of molecular transitions. Consider the energy-level diagram of Fig. 6.7, which shows how the potential energy of a molecule changes with interatomic distance. The ground state of the molecule is at point $A_0$, which coincides with the minimum of the potential energy. Ionizing radiation passing through the scintillator may give energy to the molecule and raise it to an excited state, i.e., the transition $A_0 \rightarrow A_1$ may occur. The position $A_1$ is not the point of minimum energy. The molecule will release energy through lattice vibrations (that energy is eventually dissipated as heat) and move to point $B_1$. The point $B_1$ is still an excited state and, in some cases, the molecule will undergo the transition $B_1 \rightarrow B_0$ accompanied by the emission of the photon with energy equal to $E_{B_1} - E_{B_0}$. This transition, if allowed, takes place at times of the order of $10^{-8}$ s. It should be noted that the energy of the emitted photon $(E_{B_1} - E_{B_0})$ is less than the energy that caused the excitation $(E_{A_1} - E_{A_0})$. This difference is very important because otherwise the emission spectrum of the scintillator would completely coincide with its absorption spectrum and no scintillations would be produced. A more detailed description of the scintillation process is given in the references (see Birks and Ref. 6).

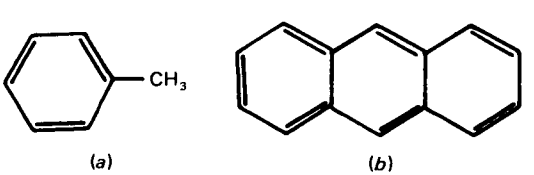


**Figure 6.6** Molecular structure of (*a*) toluene and (*b*) anthracene.

**Table 6.2 Organic Scintillator Compounds†**

| Compound | Formula | Application‡ |
|---|---|---|
| Benzene | $C_6H_6$ | S |
| Toluene | $C_6H_5CH_3$ | S |
| *p*-Xylene | $C_6H_4(CH_3)_2$ | S |
| 1,2,4-Trimethylbenzene (pseudocumene) | $C_6H_3(CH_3)_3$ | S |
| Hexamethylbenzene | $C_6(CH_3)_6$ | S |
| Styrene monomer | $C_6H_5C_2H_3$ | S |
| Vinyltoluene monomer | $C_6H_4CH_3C_2H_3$ | S |
| Naphthalene | $C_{10}H_8$ | S', C |
| Anthracene | $C_{14}H_{10}$ | C |
| Biphenyl | $C_{12}H_{10}$ | S' |
| *p*-Terphenyl | $C_{18}H_{14}$ | C, PS |
| *p*-Quaterphenyl | $C_{24}H_{18}$ | C |
| *trans*-Stilbene | $C_{14}H_{12}$ | C |
| Diphenylacetylene | $C_{14}H_{10}$ | C |
| 1,1',4,4'-Tetraphenylbutadiene | $C_{28}H_{22}$ | SS |
| Diphenylstilbene | $C_{26}H_{20}$ | SS |
| PPO (2,5-diphenyloxazole) | $C_{15}H_{11}NO$ | PS |
| α-NPO [2-(1-Naphthyl)-5-phenyloxazole] | $C_{19}H_{13}NO$ | PS |
| PBD [2-Phenyl,5-(4-biphenylyl)-1,3,4-oxadiazole] | $C_{20}H_{14}N_2O$ | PS |
| BBO [2,5-Di(4-biphenylyl)-oxazole] | $C_{27}H_{19}NO$ | SS |
| POPOP {1,4-Bis[2-(5-phenyloxazolyl)]-benzene} | $C_{24}H_{16}N_2O_2$ | SS |
| TOPOT {1,4-Di-[2-(5-*p*-tolyloxazolyl)]-benzene} | $C_{26}H_{20}N_2O_2$ | SS |
| DiMePOPOP {1,4-Di[2-(4-methyl-5-phenyloxazolyl)]-benzene} | $C_{26}H_{20}N_2O_2$ | SS |

†From [6].

‡S–primary solvent; S'–secondary solvent; PS–primary solute; SS–secondary solute; C–crystal scintillator.

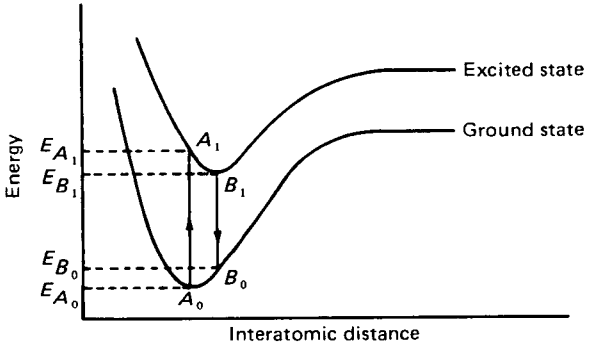


**Figure 6.7** A typical (simplified) energy diagram of a molecule.

One of the important differences between inorganic and organic scintillators is in the response time, which is less than 10 ns for the latter (response time of inorganic scintillators is $\sim 1\ \mu s$; see Table 6.1) and makes them suitable for fast timing measurements (see Chap. 10). Table 6.3 lists important properties of some organic scintillators.

### 6.3.2 Organic Crystal Scintillators

No activator is needed to enhance the luminescence of organic crystals. In fact, any impurities are undesirable because their presence reduces the light output, and for this reason, the material used to make the crystal is purified. Two of the most common organic crystal scintillators are anthracene and *trans*-stilbene.

Anthracene has a density of $1.25 \times 10^3$ kg/m$^3$ and the highest light conversion efficiency of all organic scintillators (see Table 6.3)—which is still only about one-third of the light conversion efficiency of NaI(Tl). Its decay time ($\sim$ 30 ns) is much shorter than that of inorganic crystals. Anthracene can be obtained in different shapes and sizes.

*trans*-Stilbene has a density of $1.15 \times 10^3$ kg/m$^3$ and a short decay time (4–8 ns). Its conversion efficiency is about half of that for anthracene. It can be obtained as a clear, colorless, single crystal with a size up to several millimeters. Stilbene crystals are sensitive to thermal and mechanical shock.

### 6.3.3 Organic Liquid Scintillators

The organic liquid scintillators consist of a mixture of a solvent with one or more solutes. Compounds that have been used successfully as solvents include xylene, toluene, and hexamethylbenzene (see Table 6.2). Satisfactory solutes include *p*-terphenyl, PBD, and POPOP.

In a binary scintillator, the incident radiation deposits almost all of its energy in the solvent but the luminescence is due almost entirely to the solute. Thus, as in the case of inorganic scintillators, an efficient energy transfer is

**Table 6.3 Properties of Certain Organic Scintillators**

| Material | Wavelength of maximum emission (nm) | Relative scintillation efficiency (%) | Decay time (ns) | Density ($10^3$ kg/m$^3$) |
|---|---|---|---|---|
| Anthracene | 445 | 100 | ~30 | 1.25 |
| *trans*-Stilbene | 385 | ~60 | 4–8 | 1.16 |
| NE 102 | 350–450 | ~65 | 2 | 1.06 |
| NE 110 | 350–450 | 60 | 3 | 1.06 |
| NE 213 (liquid) | 350–450 | ~60 | 2 | 0.867 |
| PILOT B | 350–450 | 68 | 2 | 1.06 |
| PILOT Y | 350–450 | 64 | ~3 | 1.06 |

taking place from the bulk of the phosphor to the material with the small concentration (activator in inorganic scintillators, solute in organic ones). If a second solute is added, it acts as a *wavelength shifter*, i.e., it increases the wavelength of the light emitted by the first solute, so that the emitted radiation is better matched with the characteristics of the cathode of the photomultiplier tube.

Liquid scintillators are very useful for measurements where a detector with large volume is needed to increase efficiency. Examples are counting of low-activity $\beta$-emitters ($^3$H and $^{14}$C in particular), detection of cosmic rays, and measurement of the energy spectrum of neutrons in the MeV range (see Chap. 14) using the scintillator NE 213. The liquid scintillators are well suited for such measurements because they can be obtained and used in large quantities (kiloliters) and can form a detector of desirable size and shape by utilizing a proper container.

In certain cases, the radioisotope to be counted is dissolved in the scintillator, thus providing $4\pi$ geometry and, therefore, high detection efficiency. In others, an extra element or compound is added to the scintillator to enhance its detection efficiency without causing significant deterioration of the luminescence. Boron, cadmium, or gadolinium,[7-9] used as additives, cause an increase in neutron detection efficiency. On the other hand, fluorine-loaded scintillators consist of compounds in which fluorine has replaced hydrogen, thus producing a phosphor with a low neutron sensitivity.

### 6.3.4 Plastic Scintillators

The plastic scintillators may be considered as solid solutions of organic scintillators. They have properties similar to those of liquid organic scintillators (Table 6.3), but they have the added advantage, compared to liquids, that they do not need a container. Plastic scintillators can be machined into almost any desirable shape and size, ranging from thin fibers to thin sheets. They are inert to water, air, and many chemicals, and for this reason they can be used in direct contact with the radioactive sample.

Plastic scintillators are also mixtures of a solvent and one or more solutes. The most frequently used solvents are polysterene and polyvinyltoluene. Satisfactory solutes include *p*-terphenyl and POPOP. The exact compositions of some plastic scintillators are given in Ref. 10.

Plastic scintillators have a density of about $10^3$ kg/m$^3$. Their light output is lower than that of anthracene (Table 6.3). Their decay time is short, and the wavelength corresponding to the maximum intensity of their emission spectrum is between 350 and 450 nm. Trade names of commonly used plastic scintillators are Pilot B, Pilot Y, NE 102, and NE 110. The characteristics of these phosphors are discussed in Refs. 11–13. Plastic scintillators loaded with tin and lead have been tried as X-ray detectors in the 5–100 keV range.[14,15] Thin plastic scintillator films (as thin as $20 \times 10^{-5}$ kg/m$^2$ = 20 $\mu$g/cm$^2$) have proven to be useful detectors in time-of-flight measurements[16-18] (see Chap. 13).

## 6.4 GASEOUS SCINTILLATORS

Gaseous scintillators are mixtures of noble gases.[19,20] The scintillations are produced as a result of atomic transitions. Since the light emitted by noble gases belongs to the ultraviolet region, other gases, such as nitrogen, are added to the main gas to act as wavelength shifters. Thin layers of fluorescent materials used for coating the inner walls of the gas container achieve the same effect.

Gaseous scintillators exhibit the following features:

1. Very short decay time
2. Light output per MeV deposited in the gas depending very little on the charge and mass of the particle being detected
3. Very low efficiency for gamma detection

These properties make the gaseous scintillators suitable for the energy measurement of heavy charged particles (alphas, fission fragments, other heavy ions).

## 6.5 THE RELATIONSHIP BETWEEN PULSE HEIGHT AND ENERGY AND TYPE OF INCIDENT PARTICLE

To measure the energy of the incident particle with a scintillator, the relationship between the pulse height and the energy deposited in the scintillator must be known. Because the pulse height is proportional to the output of the photomultiplier, which output is in turn proportional to the light produced by the scintillator, it is necessary to know the light-conversion efficiency of the scintillator as a function of type and energy of incident radiation. The rest of this section presents experimental results for several cases of interest.

### 6.5.1 The Response of Inorganic Scintillators

**Photons.** The response of NaI(Tl) to gammas is linear, except for energies below 400 keV, where a slight nonlinearity is present. Experimental results are shown in Fig. 6.8.[21] More details about the NaI(Tl) response to gammas are given in Chap. 12.

**Charged particles.** For protons and deuterons, the response of the scintillator is proportional to the particle energy, at least for $E > 1$ MeV. For alpha particles, the proportionality begins at about 15 MeV (Fig. 6.9).[22] Theoretical aspects of the response have been studied extensively.[23–26] Today, inorganic scintillators are seldom used for detection of charged particles.

**Neutrons.** Because neutrons are detected indirectly through charged particles produced as a result of nuclear reactions, to find the response to neutrons, one

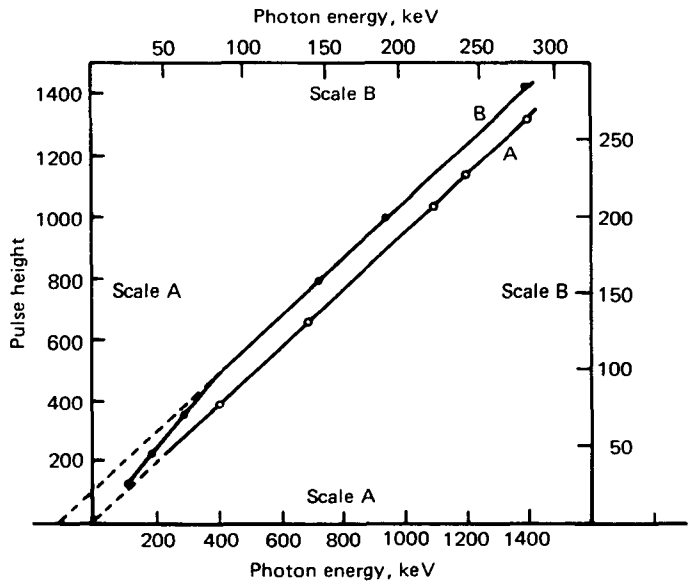


**Figure 6.8** Pulse height versus energy for a NaI(Tl) crystal. The region below 300 keV has been expanded in curve B to show the nonlinearity (from Ref. 21).

looks at the response to alphas and protons. LiI(Eu), which is the crystal used for neutron detection, has essentially the same response as NaI(Tl) (Fig. 6.9).

### 6.5.2 The Response of Organic Scintillators

**Charged particles.** Experiments have shown that organic crystal scintillators (e.g., anthracene) exhibit a direction-dependent response to alphas[27] and protons.[28] An adequate explanation of the direction-dependent characteristics of the response does not exist at present. The user should be aware of the phenomenon to avoid errors.

The response of plastic and liquid scintillators to electrons, protons, and alphas is shown in Figs. 6.10, 6.11, and 6.12.[29-31] Notice that the response is not linear, especially for heavier ions. The response has been studied theoretically by many investigators (Birks and Refs. 32–35).

**Photons and neutrons.** Organic scintillators are not normally used for detection of gammas because of their low efficiency. The liquid scintillators NE 213† is being used for $\gamma$ detection in mixed neutron-gamma fields[36] because of its

†NE 213 consists of xylene, activators, and POPOP as the wavelength shifter. Naphthalene is added to enhance the slow components of light emission. The composition of NE 213 is given as $CH_{1,21}$ and its density as $0.867 \times 10^3$ kg/cm$^3$.

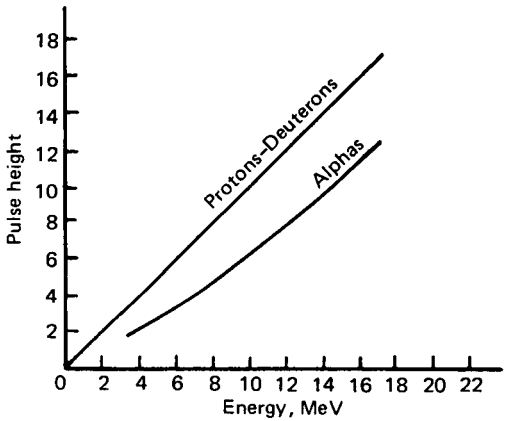


**Figure 6.9** Pulse height versus energy for a NaI(Tl) crystal resulting from charged particles (from Ref. 22).

ability to discriminate against neutrons. Neutrons are detected by NE 213 through the proton-recoil method. More details about the use of the NE 213 scintillator and its response function are given in Chaps. 12 and 14.

## 6.6 THE PHOTOMULTIPLIER TUBE

### 6.6.1 General Description

The photomultiplier tube or phototube is an integral part of a scintillation counter. Without the amplification produced by the photomultiplier, a scintilla-

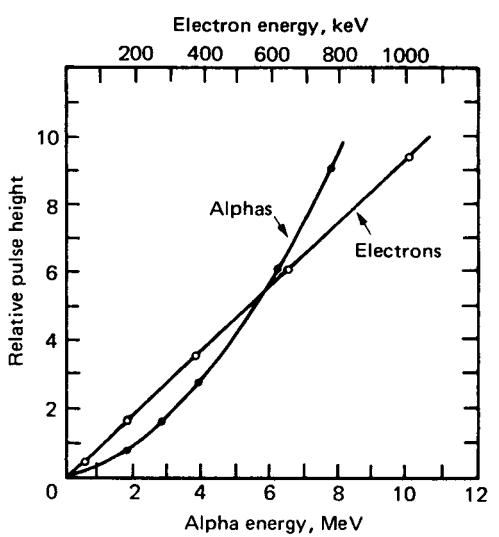


**Figure 6.10** Pulse height versus energy for a liquid scintillator resulting from alphas and electrons (from Ref. 29).

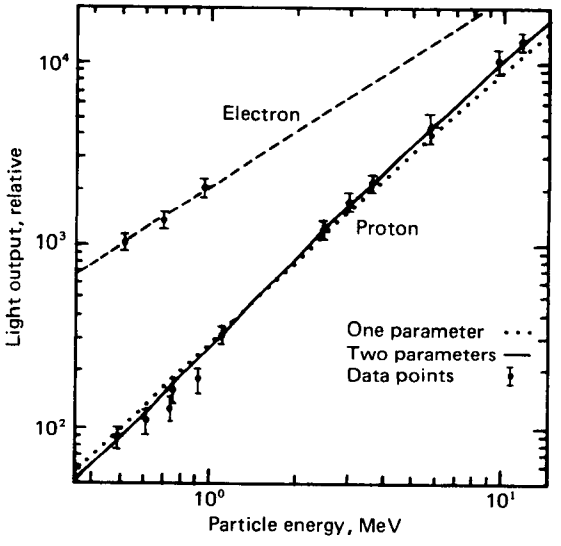


**Figure 6.11** Plastic scintillator (NE 102) response to electrons and protons (from Ref. 30).

tor is useless as a radiation detector. The photomultiplier is essentially a fast amplifier, which in times of $10^{-9}$ s amplifies an incident pulse of visible light by a factor of $10^6$ or more.

A photomultiplier consists of an evacuated glass tube with a photocathode at its entrance and several dynodes in the interior (Fig. 6.13). The anode, located at the end of a series of dynodes serves as the collector of electrons. The photons produced in the scintillator enter the phototube and hit the photocathode, which is made of a material that emits electrons when light strikes it. The electrons emitted by the photocathode are guided, with the help of an electric field, toward the first dynode, which is coated with a substance that emits secondary electrons, if electrons impinge upon it. The secondary electrons from the first dynode move toward the second, from there toward the third, and so on. Typical commercial phototubes may have up to 15 dynodes. The production of secondary electrons by the successive dynodes results in a final amplification of the number of electrons as shown in the next section.

The electric field between dynodes is established by applying a successively increasing positive high voltage to each dynode. The voltage difference between two successive dynodes is of the order of 80–120 V (see Sec. 6.6.2).

The photocathode material used in most commercial phototubes is a compound of cesium and antimony (Cs-Sb). The material used to coat the dynodes is either Cs-Sb or silver-magnesium (Ag-Mg). The secondary emission rate of the dynodes depends not only on the type of surface but also on the voltage applied.

A very important parameter of every photomultiplier tube is the spectral sensitivity of its photocathode. For best results, the spectrum of the scintillator should match the sensitivity of the photocathode. The Cs-Sb surface has a maximum sensitivity at 440 nm, which agrees well with the spectral response of

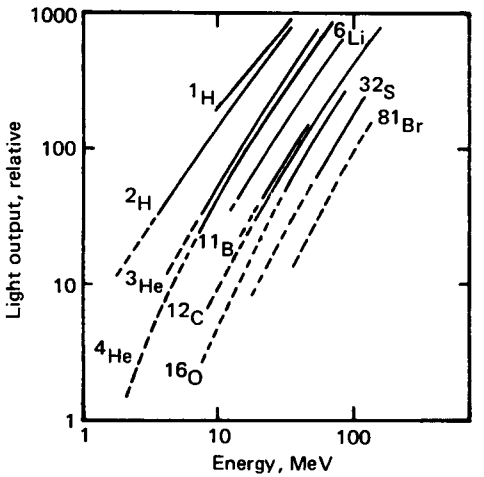


**Figure 6.12** Plastic scintillator (NE 102) response to heavy ions (from Ref. 31).

most scintillators (Tables 6.1 and 6.3). Such a response, called S-11, is shown in Fig. 6.3. Other responses of commercial phototubes are known as S-13, S-20, etc.

Another important parameter of a phototube is the magnitude of its *dark current*. The dark current consists mainly of electrons emitted by the cathode after thermal energy is absorbed. This process is called *thermionic emission*, and a 50-mm-diameter photocathode may release in the dark as many as $10^5$ electrons/s at room temperature. Cooling of the cathode reduces this source of noise by a factor of about 2 per 10–15°C reduction in temperature. Thermionic emission may also take place from the dynodes and the glass wall of the tube, but this contribution is small. Electrons may be released from the photocathode as a result of its bombardment by positive ions coming from ionization of the residual gas in the tube. Finally, light emitted as a result of ion recombination may release electrons upon hitting the cathode or the dynodes. Obviously, the magnitude of the dark current is important in cases where the radiation source

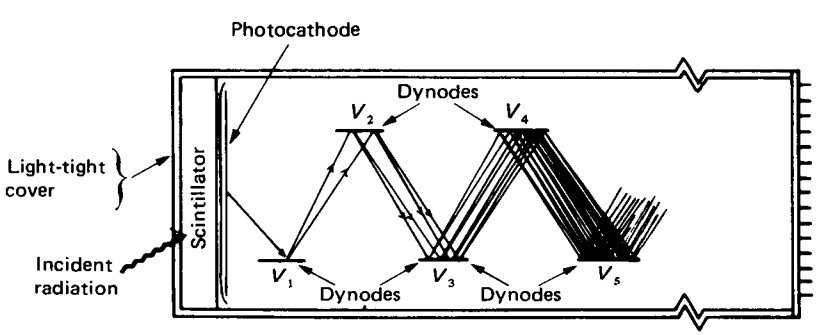


**Figure 6.13** Schematic diagram of the interior of a photomultiplier tube.

is very weak. Both the dark current and the spectral response should be considered when a phototube is to be purchased.

Recall that the electrons are guided from one dynode to the next by an electric field. If a magnetic field is present, it may deflect the electrons in such a way that not all of them hit the next dynode, and the amplification is reduced. Even the earth's weak magnetic field may sometimes cause this undesirable effect. The influence of the magnetic field may be minimized by surrounding the photomultiplier tube with a cylindrical sheet of metal, called *μ-metal*. The μ-metal is commercially available in various shapes and sizes.

Commercial photomultiplier tubes are made with the variety of geometrical arrangements of photocathode and dynodes. In general, the photocathode is deposited as a semitransparent layer on the inner surface of the end window of the phototube (Fig. 6.14). The external surface of the window is, in most phototubes, flat for easier optical coupling with the scintillator (see Sec. 6.7). Two different geometries for the dynodes are shown in Fig. 6.14.

### 6.6.2 Electron Multiplication in a Photomultiplier

The electron multiplication $M$ in a photomultiplier can be written as

$$M = (\theta_1 \epsilon_1)(\theta_2 \epsilon_2) \cdots (\theta_n \epsilon_n) \tag{6.3}$$

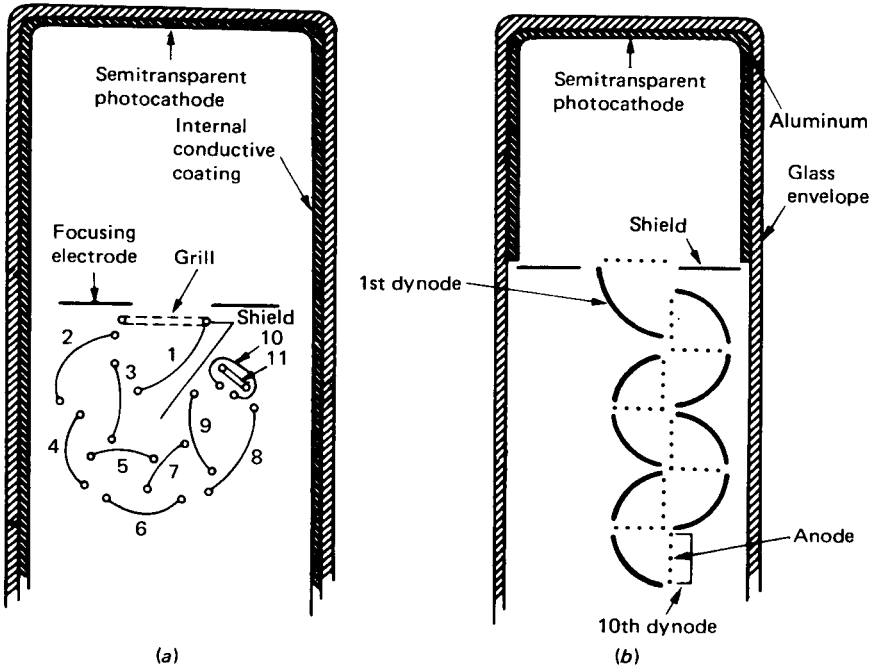


**Figure 6.14** Two dynode arrangements in commercial phototubes: (*a*) Model 6342 RCA, 1–10 are dynodes, 11 is anode; (*b*) Model 6292 DuMont.

where

$$n = \text{number of dynodes}$$

$$\epsilon_i = \frac{\text{number of electrons collected by } i\text{th dynode}}{\text{number of electrons emitted by } (i-1)\text{th dynode}}$$

$$\theta_i = \frac{\text{number of electrons emitted by } i\text{th dynode}}{\text{number of electrons impinging upon } i\text{th dynode}}$$

If $\theta_i$ and $\epsilon_i$ are constant for all dynodes, then

$$M = (\theta\epsilon)^n \tag{6.4}$$

The quantity $\epsilon$ depends on the geometry. The quantity $\theta$ depends on the voltage between two successive dynodes and on the material of which the dynode is made. The dependence of $\theta$ on voltage is of the form

$$\theta = kV^a \tag{6.5}$$

where $V = V_i - V_{i-1}$ = potential difference between two successive dynodes, assumed the same for all dynode pairs

$k, a$ = constants (the value of $a$ is about 0.7)

Using Eq. 6.5, the multiplication $M$ becomes

$$M = \epsilon^n(kV^a)^n = CV^{an} \tag{6.6}$$

where $C = (\epsilon k)^n$ = constant, independent of the voltage.

Equation 6.6 indicates that the value of $M$ increases with the voltage $V$ and the number of stages $n$. The number of dynodes is limited, because as $n$ increases, the charge density between two dynodes distorts the electric field and hinders the emission of electrons from the previous dynode with the lower voltage. In commercial photomultipliers, the number of dynodes is 10 or more. If one takes $n = 10$ and $\epsilon\theta = 4$, typical value, the value of $M$ becomes equal to $10^6$.

To apply the electric field to the dynodes, a power supply provides a voltage adequate for all the dynodes. A voltage divider, usually an integral part of the preamplifier, distributes the voltage to the individual dynodes. When reference is made to *phototube voltage*, one means the total voltage applied. For example, if 1100 V are applied to a phototube with 10 dynodes, the voltage between any two dynodes is 100 V.

## 6.7 ASSEMBLY OF A SCINTILLATION COUNTER AND THE ROLE OF LIGHT PIPES

A scintillation counter consists of the scintillator and the photomultiplier tube. It is extremely important that these two components be coupled in such a way that a maximum amount of light enters the phototube and strikes the photocathode. This section presents a brief discussion of the problems encountered during the assembly of a scintillation counter, with some of the methods used to solve them.

A solid scintillator is coupled to the photomultiplier through the end window of the tube (Fig. 6.15). During the transfer from the scintillator to the photocathode, light may be lost by leaving through the sides and front face of the scintillator, or by being reflected back to the scintillator when it hits the window of the phototube.

To avoid loss of light through the sides and front face, the scintillator is painted with a material that reflects toward the crystal the light that would otherwise escape. Examples of reflecting materials commercially available are alpha alumina and $Al_2O_3$.

To avoid reflection of light from the end window of the phototube, a transparent viscous fluid (such as Dow-Corning 200 Silicone fluid) is placed between the scintillator and the phototube (Fig. 6.15). The optical fluid minimizes reflection because it reduces the change of the index of refraction during the passage of light from the scintillator to the phototube. A sharp change in the index of refraction results in a small critical angle of reflection, which in turn increases total reflection.

In certain experiments, the scintillator has to be a certain distance away from the photocathode. Such is the case if the phototube should be protected from the radiation impinging upon the scintillator or from a magnetic field. Then a *light pipe* is interposed between the scintillator and the phototube. The light pipe is made of a material transparent to the light of the scintillator. Lucite, quartz, plexiglas, and glass have been used in many applications to form light pipes of different lengths and shapes. Light pipes of several feet—sometimes with bends—have been used with success. The optical coupling of the light pipe at both ends is accomplished by the same methods used to couple the scintillator directly to the phototube.

One of the major reasons for using scintillators is their availability in large sizes. In fact, commercially available scintillators are larger than the biggest commercial photomultipliers. In cases where the scintillator is too large, multiple phototubes are coupled to the same crystal. Figure 6.16 shows a NaI(Tl) crystal coupled to six photomultipliers.

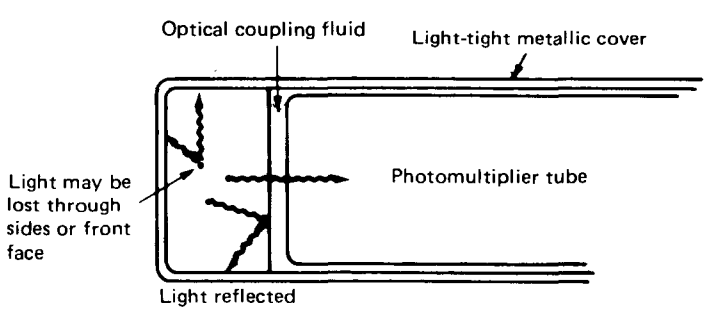


**Figure 6.15** Assembly of a scintillation counter.

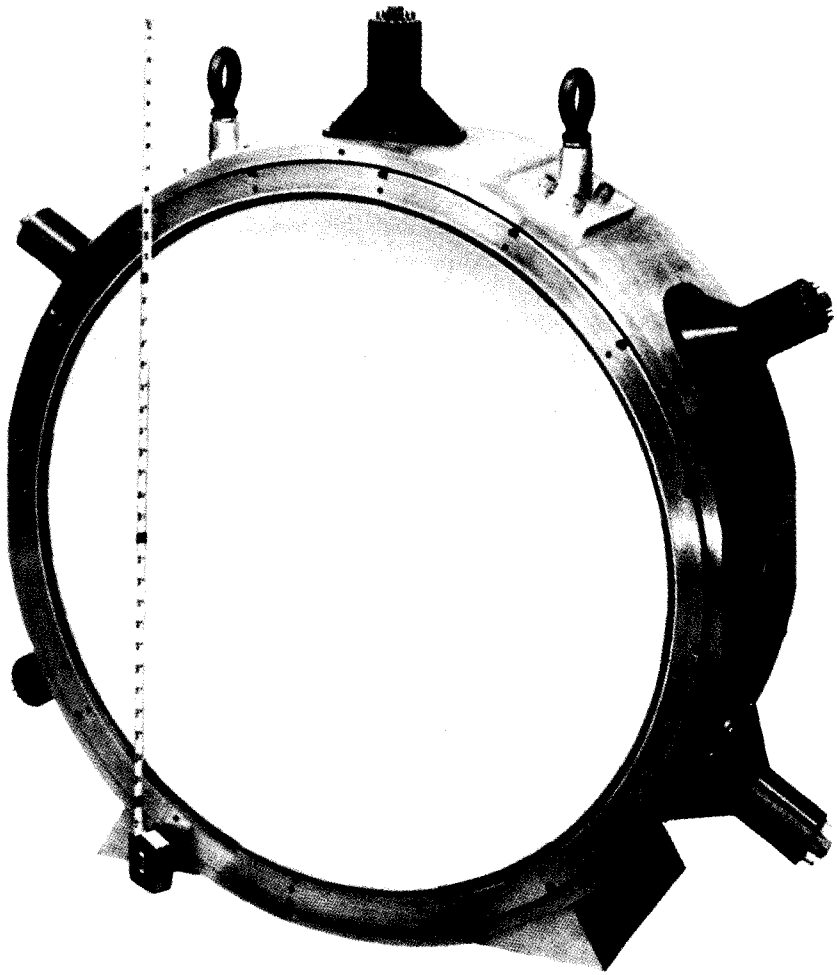

**Figure 6.16** A special 30-in (0.762-m) diameter scintillator crystal coupled to six photomultiplier tubes (from Harshaw Chemical Company).

When a liquid scintillator is used, the phototube is optically coupled to the scintillator through a window of the vessel containing the liquid scintillator. The efficiency of such a counting system increases by using a large volume of liquid and more than one photomultiplier tube (Fig. 6.17).

## 6.8 DEAD TIME OF SCINTILLATION COUNTERS

The *dead time* or *resolving time* is the minimum time that can elapse after the arrival of two successive particles and still result in two separate pulses (see Sec.

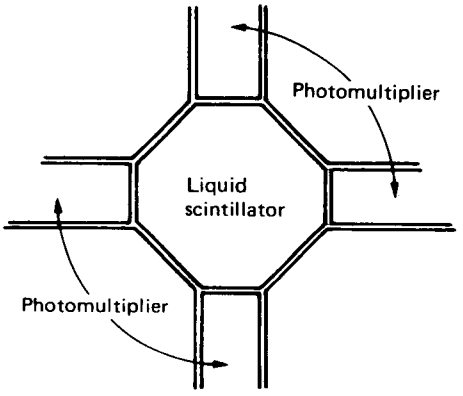


**Figure 6.17** A counting system using a liquid scintillator and four photomultiplier tubes.

2.21). For a scintillation counter this time is equal to the sum of three time intervals:

1. Time it takes to produce the scintillation, essentially equal to the decay time of the scintillator (see Eq. 6.1 and Tables 6.1 and 6.3).
2. Time it takes for electron multiplication in the phototube, of the order of 20–40 ns.
3. Time it takes to amplify the signal and record it by a scaler. The resolving time of commercial scalers is of the order of 1 $\mu$s. The time taken for amplification and discrimination is negligible.

By adding the three above components, the resulting dead time of a scintillation counter is of the order of 1–5 $\mu$s. This is much shorter than the dead time of gas-filled counters, which is of the order of tens to hundreds of microseconds.

Scintillators are detectors with fast response. As seen in Tables 6.1 and 6.3, the risetime of the pulse is very short for all of them. Short risetime is important in measurements that depend on the time of arrival of the particle (see Chap. 10).

## 6.9 SOURCES OF BACKGROUND IN A SCINTILLATION COUNTER

One of the major sources of background in a scintillation counter is the dark current of the phototube (see Sec. 6.6.1). Other background sources are naturally occurring radioisotopes, cosmic rays, and phosphorescing substances.

The holder of a liquid scintillator may contain small amounts of naturally occurring isotopes. In particular, $^{40}$K is always present (isotopic abundance of $^{40}$K is 0.01 percent). Another isotope, $^{14}$C, is a constituent of contemporary organic materials. Solvents, however, may be obtained from petroleum, consisting of hydrocarbons without $^{14}$C.

The term *phosphorescence* refers to delayed emission of light as a result of deexcitation of atoms or molecules. Phosphorescent half-lives may extend to hours. This source of background may originate in phosphorescent substances contained in the glass of the phototube, the walls of the sample holder, or the sample itself.

*Cosmic rays*, which are highly energetic charged particles, produce background in all types of detectors, and scintillators are no exception. The effect of cosmic-ray background, as well as that of the other sources mentioned earlier, will be reduced if two counters are used in coincidence or anticoincidence.

## 6.10 THE PHOSWICH DETECTOR

The phoswich detector is used for the detection of low-level radiation in the presence of considerable background. It consists of two different scintillators coupled together and mounted on a single photomultiplier tube.[1] By utilizing the difference in the decay constants of the two phosphors, differentiation between events taking place in the two detectors is possible. The combination of crystals used depends on the types of particles present in the radiation field under investigation.[37,38]

The basic structure of a phoswich detector is shown in Fig. 6.18. A thin scintillator (scintillator A) is coupled to a larger crystal (scintillator B), which in turn is coupled to the cathode of a single phototube. Two examples of scintillators used are these:

1. NaI(Tl) is the thin scintillator (A) and CsI(Tl) is the thick one (B). Pulses originating in the two crystals are differentiated based on the difference between the 0.25-$\mu$s decay constant of the NaI(Tl) and the 1-$\mu$s decay constant of the CsI(Tl). Slow pulses come from particles losing energy in the CsI(Tl) or in both crystals simultaneously. In a mixed low-energy-high-energy photon field, the relatively fast pulses of the NaI(Tl) will come from the soft

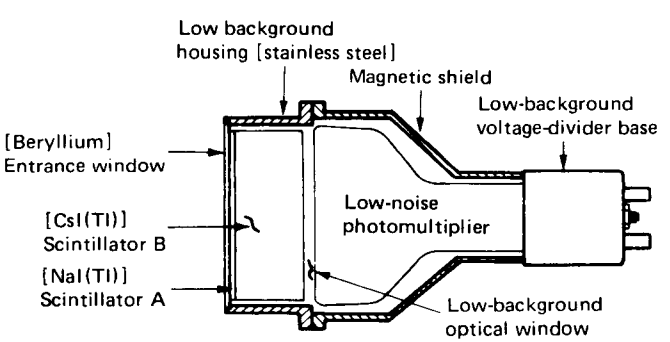


**Figure 6.18** A Phoswich detector (from Harshaw Chemical Company).

component of the radiation. [Soft photons will not reach the CsI(Tl).] Phoswich detectors of this type have been used in X-ray and $\gamma$-ray astronomy, in detection of plutonium in the environment, and in other cases of mixed-radiation fields.

2. $CaF_2$(Eu) is the thin scintillator (A) and NaI(Tl) is the thick one (B). This combination is used for measurements of low-energy beta particles in the presence of a gamma background. The thin (0.1 mm) $CaF_2$(Eu) crystal detects the betas, but is essentially transparent to gammas because of its relatively low atomic number and thickness. A quartz window is usually placed between the two scintillators to stop the betas that did not deposit all their energy in the $CaF_2$(Eu). The fast pulses of the NaI(Tl), which are due to gammas, are time-discriminated against the slower pulses from the $CaF_2$(Eu) ($T = 0.94$ $\mu$s). Thus, the background due to gammas is reduced.

## PROBLEMS

**6.1** If the dead time of a detection system using a scintillator is 1 $\mu$s, what is the gross counting rate that will result in a loss of 2 percent of the counts?

**6.2** A typical dead time for a scintillation detector is 5 $\mu$s. For a gas counter, the corresponding number is 200 $\mu$s. If a sample counted with a gas counter results in 8 percent loss of gross counts due to dead time, what is the corresponding loss in a scintillation counter that records the same gross counting rate?

**6.3** A parallel beam of 1.5-MeV gammas strikes a 25-mm-thick NaI crystal. What fraction of these gammas will have at least one interaction in the crystal ($\mu = 0.0047$ m$^2$/kg)?

**6.4** What is the range of 2-MeV electrons in a plastic scintillator? Assume that the composition of the scintillator is $C_{10}H_{11}$ ($\rho = 1.02 \times 10^3$ kg/m$^3$).

**6.5** Consider two electrons, one with kinetic energy 1 MeV, the other with 10 MeV. Which electron will lose more energy going through a 1-mm-thick plastic scintillator? Consider both ionization and radiation loss. Composition of the scintillator is given in Prob. 6.4. For radiation loss, use

$$Z_{\text{eff}} = \frac{N_H Z_H^2 + N_C Z_C^2}{N_H Z_H + N_C Z_C}$$

**6.6** A phoswich detector consists of a 1-mm-thick NaI(Tl) scintillator coupled to a 25-mm-thick CsI(Tl) scintillator. A 0.1-mm-thick beryllium window protects the NaI(Tl) crystal. If the detector is exposed to a thin parallel beam of 150-keV X-rays and 1.5-MeV $\gamma$ rays, what are the fractions of interactions of each type of photon in each scintillator?

## BIBLIOGRAPHY

Birks, J. B., *The Theory and Practice of Scintillation Counting*, McMillan Co., New York, 1964.

Eichholz, G. G., and Poston, J. W., *Nuclear Radiation Detection*, Lewis Publishers, Chelsea, Michigan 1985.

Fenyves, E., and Haiman, O., *The Physical Principles of Nuclear Radiation Measurements*, Academic Press, New York, 1969.

Knoll, G. F., *Radiation Detection and Measurement*, 2nd ed., Wiley, New York, 1989.

Price, W. J., *Nuclear Radiation Detection*, McGraw-Hill, New York, 1964.
Ross, H., Noakes, J. E., and Spaulding, J. D., *Liquid Scintillation Counting and Organic Scintillators*, Lewis Publishers, Chelsea, Michigan, 1991.
Snell, A. H. (ed.), *Nuclear Instruments and Their Uses*, Wiley, New York, 1962.
Tait, W. H., *Radiation Detection*, Butterworth, London, 1980.

## REFERENCES

1. Heath, R. L., Hofstadter, R., and Hughes, E. B., *Nucl. Instrum. Meth.* **162**:431 (1979). (Review article listing 127 references.)
2. Aliaga-Kelly, D., and Nicoll, D. R., *Nucl. Instrum. Meth.* **43**:110 (1966).
3. Colmenares, C., Shapiro, E. G., Barry, P. E., and Prevo, C. T., *Nucl. Instrum. Meth.* **114**:277 (1974).
4. Campbell, M., Ledingham, K. W. D., Baillie, A. D., and Lynch, J. G., *Nucl. Instrum. Meth.* **137**:235 (1976).
5. Catalano, E., and Czirr, J. B., *Nucl. Instrum. Meth.* **143**:61 (1977).
6. Brooks, F. D., *Nucl. Instrum. Meth.* **162**:477 (1979). (Review article listing 274 references.)
7. Bollinger, L. M., and Thomas, G. E., *Rev. Sci. Instrum.* **28**:489 (1957).
8. Hellstrom, J., and Beshai, S., *Nucl. Instrum. Meth.* **101**:267 (1972).
9. Bergere, R., Beil, H., and Veyssiere, A., *Nucl. Phys.* **A121**:463 (1968).
10. Swank, R. K., *Annu. Rev. Nucl.Sci.* **4**:111 (1954).
11. Walker, J. K., *Nucl. Instrum. Meth.* **68**:131 (1969).
12. Moszynski, M., and Bengtson, B., *Nucl. Instrum. Meth.* **142**:417 (1977).
13. Moszynski, M., and Bengtson, B., *Nucl. Instrum. Meth.* **158**:1 (1979).
14. Eriksson, L. A., Tsai, C. M., Cho, Z. H., and Hurlbut, C. R., *Nucl. Instrum. Meth.* **122**:373 (1974).
15. Becker, J., Eriksson, L., Monberg, L. C., and Cho, Z. H., *Nucl. Instrum. Meth.* **123**:199 (1975).
16. Muga, M. L., Burnsed, D. J., Steeger, W. E., and Taylor, H. E., *Nucl. Instrum. Meth.* **83**:135 (1970).
17. Muga, M. L., *Nucl. Instrum. Meth.* **95**:349 (1971).
18. Batra, R. K., and Shotter, A. C., *Nucl. Instrum. Meth.* **124**:101 (1975).
19. Policarpo, A. J. P. L., Conde, C. A. N., and Alves, M. A. F., *Nucl. Instrum. Meth.* **58**:151 (1968).
20. Morgan, G. L., and Walter, R. L., *Nucl. Instrum. Meth.* **58**:277 (1968).
21. Engelkemeir, B., *Rev. Sci. Instrum.* **27**:989 (1956).
22. Eby, F. S., and Jentschke, W. K., *Phys. Rev.* **96**:911 (1954).
23. Murray, R. B., and Meyer, A., *Phys. Rev.* **122**:815 (1961).
24. Meyer, A., and Murray, R. B., *Phys. Rev.* **128**:98 (1962).
25. Prescott, J. R., and Narayan, G. H., *Nucl. Instrum. Meth.* **75**:51(1969).
26. Hill, R., and Collinson, A. J. L., *Nucl. Instrum. Meth.* **44**:245 (1966).
27. Brand, W., Dobrin, R., Jack, H., Aubert, R. L., and Roth, S., *Con. J. Phys.* **46**:537 (1968).
28. Brooks, F. D., and Jones, D. T. L., *Nucl. Instrum. Meth.*, **121**:69 (1974).
29. Flynn, K. F., Glendenin, C. E., Steinberg, E. P., and Wright, P. M., *Nucl. Instrum. Meth.* **27**:13 (1964).
30. Craun, R. L., and Smith, D. L., *Nucl. Instrum. Meth.* **80**:239 (1970).
31. Becchetti, F. D., Thorn, C. E., and Levine, M. S., *Nucl. Instrum. Meth.* **138**:93 (1976).
32. Chou, C. N., *Phys. Rev.* **87**:376, 904 (1952).
33. Wright, G. T., *Phys. Rev.* **91**:1282 (1953).
34. Voltz, R., Lopes da Silva, J., Laustriat, G., and Coche, A., *J. Chem. Phys.* **45**:3306 (1966).
35. Voltz, R., du Pont, H., and Laustriat, G., *J. Physique* **29**:297 (1968).
36. Ingersoll, D. T., and Wehring, B. W., *Nucl. Instrum. Meth.* **147**:551 (1977).
37. Pastor, C., Benrachi, F., Chambon, B., Cheynis, B., Drain, D., Dauchy, A., Giorni, A., and Morand, C., *Nucl. Instrum. Meth.* **227**:87 (1984).
38. Pouliot, J., Chan, Y., Dacal, A., Harmon, A., Knop, R., Ortiz, M. E., Plagnol, E., and Stokstad, R. G., *Nucl. Instrum. Meth.* **270**:69 (1988).

CHAPTER
# SEVEN

# SEMICONDUCTOR DETECTORS

## 7.1 INTRODUCTION

*Semiconductor detectors* are solid-state devices that operate essentially like ionization chambers. The charge carriers in semiconductors are not electrons and ions, as in the gas counters, but electrons and "holes."[1,2] At present, the most successful semiconductor detectors are made of silicon and germanium. Other materials have been tried, however, with some success, e.g., CdTe and $HgI_2$.

The most important advantage of the semiconductor detectors, compared to other types of radiation counters, is their superior *energy resolution*: the ability to resolve the energy of particles out of a polyenergetic energy spectrum (energy resolution and its importance are discussed in Chaps. 9, 12–14). Other advantages are

1. Linear response (pulse height versus particle energy) over a wide energy range
2. Higher efficiency for a given size, because of the high density of a solid relative to that of a gas
3. Possibility for special geometric configurations
4. Fast pulse risetime (relative to gas counters)
5. Ability to operate in vacuum
6. Insensitivity to magnetic fields

The characteristics of a semiconductor detector depend not only on the type of material used—e.g., Si or Ge—but also on the way the semiconductor is

shaped and treated. The type, size, shape, and treatment of the crystal play a role in the operation and performance of a semiconductor detector.

This chapter first discusses the fundamentals of energy states in crystals, a subject necessary for understanding the creation and movement of electrons and holes in a solid. The properties of semiconductors are discussed next, with special emphasis given to the properties of silicon and germanium. The principle of construction and operation is accompanied by a description of the different types of detectors available in the market. Future prospects in this field are also discussed.

## 7.2 ELECTRICAL CLASSIFICATION OF SOLIDS

Solids are divided according to their electrical conductivity into three groups: conductors, insulators, and semiconductors. If a piece of solid material is placed in an electric field, whether or not current will flow depends on the type of material. If current flows, the material is a *conductor*. If current is zero at low temperatures but larger than zero at higher temperatures, the material is a *semiconductor*. If current is zero at all temperatures, the material is an *insulator*.

*Conductivity* and *electric current* mean motion of electrons, and according to the results of this simple experiment,

1. In conductors, electrons can move freely at any voltage different than zero.
2. In insulators, electrons cannot move under any voltage (except, of course, when the voltage is so high that an electrical discharge occurs).
3. In semiconductors, electrons cannot move at low temperatures (close to absolute zero) under any voltage. As the temperature of a semiconductor increases, however, electrons can move and electric current will flow at moderate voltages.

These properties can be explained by examining the electronic structure of crystals.

### 7.2.1 Electronic States in Solids—The Fermi Distribution Function

In a free atom the electrons are allowed to exist only in certain discrete energy states (Fig. 7.1*a*). In solids, the energy states widen into energy bands. Electrons can exist only in bands 1, 3, and 5, but not in bands 2 and 4 (Fig. 7.1*b*). An electron can move from band 1 to band 3 if

1. The electron acquires the energy $E_g$ necessary to cross the forbidden gap
2. There is an empty state in band 3, which the jumping electron can occupy†

†This constraint is due to the Pauli principle, which forbids two or more electrons to be in the same state.

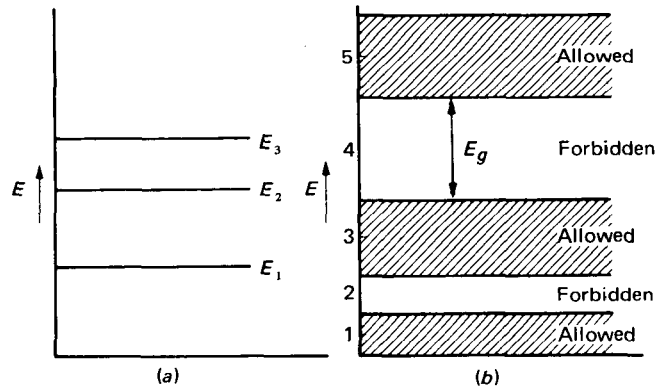


**Figure 7.1** (*a*) The atomic energy levels are discrete lines. (*b*) In a solid, the allowed energy states become energy bands.

The energy distribution of electronic states is described in terms of the following quantities:

$N(E)dE$ = number of electrons per unit volume with energy between $E$ and $E + dE$

$S(E)dE$ = number of allowed electronic energy states, per unit volume, in the energy interval between $E$ and $E + dE$

$P(E)$ = probability that a state of energy $E$ is occupied
= *Fermi distribution function*

Then

$$N(E)\,dE = P(E)[S(E)\,dE] \tag{7.1}$$

The form of $P(E)$ is given by

$$P(E) = \frac{1}{1 + e^{(E-E_f)/kT}} \tag{7.2}$$

where $E_f$ = Fermi energy
$k$ = Boltzmann constant
$T$ = temperature, Kelvin

The *Fermi energy* $E_f$ is a constant that does not depend on temperature but it does depend on the purity of the solid. The function $P(E)$ is a universal function applying to all solids and having these properties (Fig. 7.2):

1. At $T = 0$,

$$P(E) = 1 \qquad E < E_f$$
$$P(E) = 0 \qquad E > E_f$$

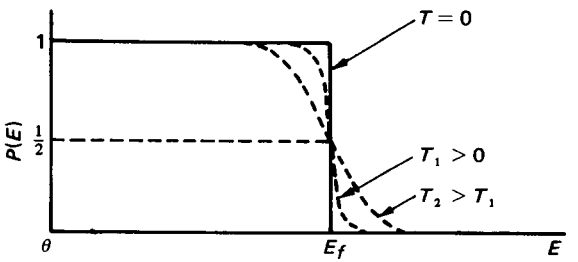


**Figure 7.2** The Fermi distribution function.

2. At any $T$,

$$P(E_f) = \tfrac{1}{2}$$

3. For $T > 0$, the function $P(E)$ extends beyond $E_f$. If $E - E_f \gg kT$, $P(E)$ takes the form

$$P(E) = \frac{1}{1 + e^{(E-E_f)/kT}} \sim \frac{1}{e^{(E-E_f)/kT}} = \exp\left(-\frac{E - E_f}{kT}\right) \qquad (7.3)$$

which resembles the classical Boltzmann distribution.

Notice that at $T = 0$ (Fig. 7.2), all the states are occupied for $E < E_f$ but all the states are empty for $E > E_f$.

### 7.2.2 Insulators

In insulators, the highest allowed band, called the *valence band*, is completely occupied (Fig. 7.3). The next allowed band, called the *conduction band*, is completely empty. As Fig. 7.3 shows, the gap is so wide that the number of occupied states in the conduction band is always zero. No electric field or temperature rise can provide enough energy for electrons to cross the gap and reach the conduction band. Thus, insulators *are* insulators because it is impossible for electrons to be found in the conduction band, where under the influence of an electric field, they would move and generate an electric current.

### 7.2.3 Conductors

In conductors, the conduction band is partially occupied (Fig. 7.4). An electron close to the top of the filled part of this band (point A, Fig. 7.4) will be able to move to the empty part (part B) under the influence of any electric field other than zero. Thus, because of the lack of a forbidden gap, there is no threshold of electric field intensity below which electrons cannot move. Motion of the charge carriers and, consequently, conductivity are always possible for any voltage applied, no matter how small.

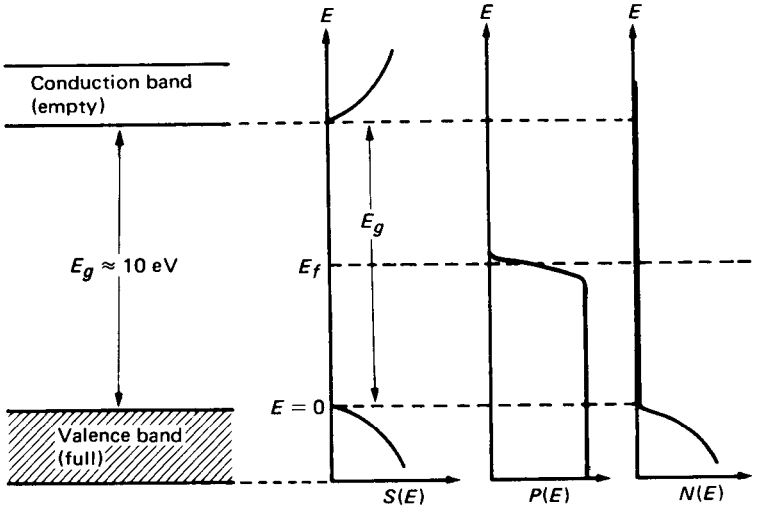


**Figure 7.3** All the energy states in the conduction band of an insulator are empty. Since there are no charge carriers, the conductivity is zero.

## 7.3 SEMICONDUCTORS

In semiconductors, the valence band is full and the conduction band is empty, but the energy gap between these two bands is very small. At very low temperatures, close to $T = 0$, the conductivity of the semiconductors is zero and the energy-band picture looks like that of an insulator (Fig. 7.3). As temperature increases, however, the "tail" of the Fermi distribution brings some electrons into the conduction band and conductivity increases (Fig. 7.5). That is, as temperature increases, some electrons obtain enough energy to cross over to the

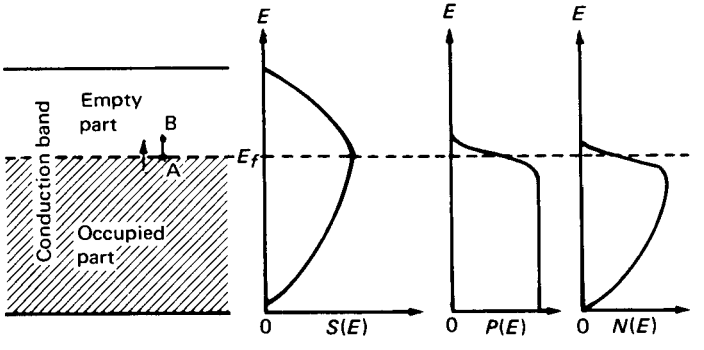


**Figure 7.4** In conductors, the conduction band is partially occupied. If an electric field is applied, the electrons move and conductivity is not zero.

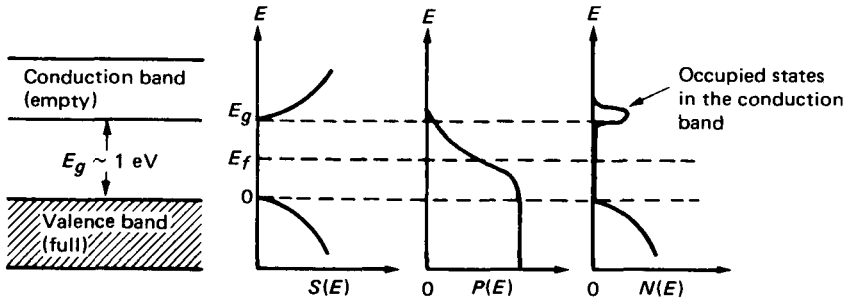


**Figure 7.5** In semiconductors, the energy gap is relatively narrow. As temperature increases, some electrons have enough energy to be able to move to the conduction band and conductivity appears.

conduction band. Once there, they will move under the influence of an electric field for the same reason that electrons of conductors move.

When an electron moves to the conduction band, an empty state is left in the valence band. This is called a *hole*. A hole is the absence of an electron. When the electron moves in one direction, the hole moves in the opposite direction (Fig. 7.6). Holes are treated as particles with positive charges: $-(-e) = +e$. They contribute to the conductivity in the same way electrons do (see Sec. 7.3.2). In a pure and electrically neutral semiconductor, the number of electrons is always equal to the number of holes.

Heat—i.e., temperature increase—is not the only way energy may be given to an electron. Absorption of radiation or collision with an energetic charged particle may produce the same effect. The interaction of ionizing radiation with a semiconductor is a complex process and there is no agreement upon a common model explaining it. One simplified model is the following.

An energetic incident charged particle collides with electrons of the semiconductor and lifts them, not only from the valence to the conduction band but also from deeper lying occupied bands to the conduction band, as shown in Fig. 7.7*a*. Electrons appear in normally empty bands and holes appear in normally fully occupied bands. However, this configuration does not last long. In times of the order of $10^{-12}$ s, the interaction between electrons and holes makes the electrons concentrate at the bottom of the lowest lying unoccupied (conduction) band. The holes, on the other hand, concentrate near the top of the highest full (valence) band. During this deexcitation process, many more electrons and holes are generated. Because of this multistep process, the average energy necessary for the creation of one electron-hole pair is much larger than the energy gap $E_g$. For example, for silicon at room temperature, $E_g = 1.106$ eV, and the average energy for the production of one electron-hole pair is 3.66 eV.

In the absence of an electric field, the final step of the deexcitation process is the recombination of electrons and holes and the return of the crystal to its neutral state.

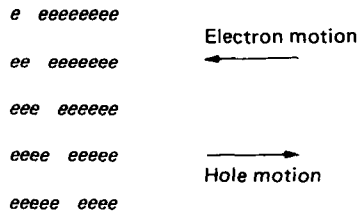


**Figure 7.6** Electrons and holes move in opposite directions. A hole behaves like a positively charged carrier.

### 7.3.1 The Change of the Energy Gap with Temperature

The value of the energy gap $E_g$ (Fig. 7.5) is not constant, but it changes with temperature as shown in Fig. 7.8. For silicon and germanium, $E_g$ initially increases linearly as temperature decreases; but at very low temperatures, $E_g$ reaches a constant value.

The average energy needed to create an electron-hole pair follows a similar change with temperature (Fig. 7.9).

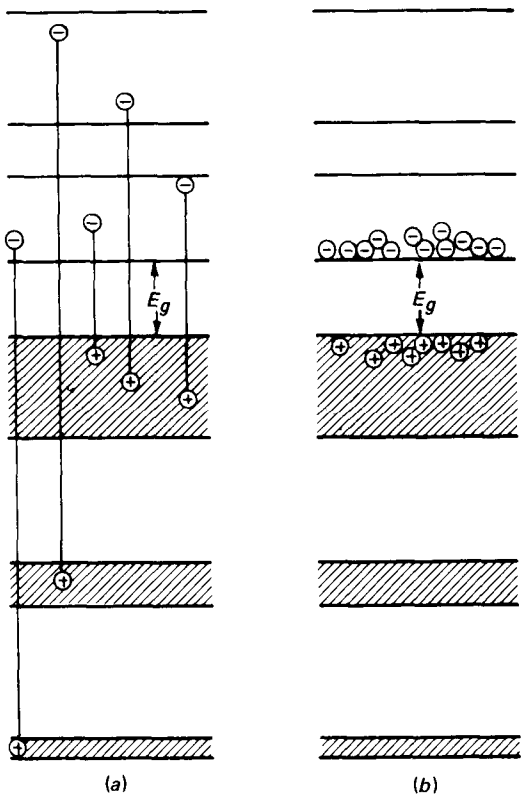


**Figure 7.7** (*a*) Collisions with an energetic charged particle raise electrons to the conduction bands. (*b*) After times of the order of $10^{-12}$ s, electrons and holes tend to deexcite to the upper part of the valence band and lower part of the conduction band, respectively.

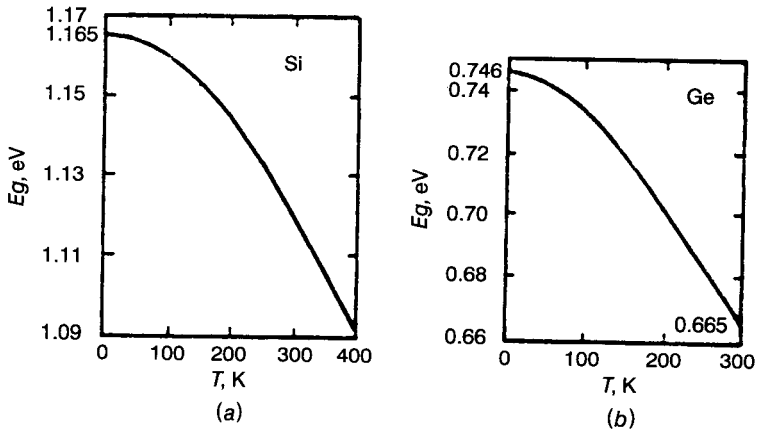


**Figure 7.8** The variation of $E_g$ with temperature: (*a*) for silicon; (*b*) for germanium (from Chap. 1.1.1 of Bertolini & Coche).

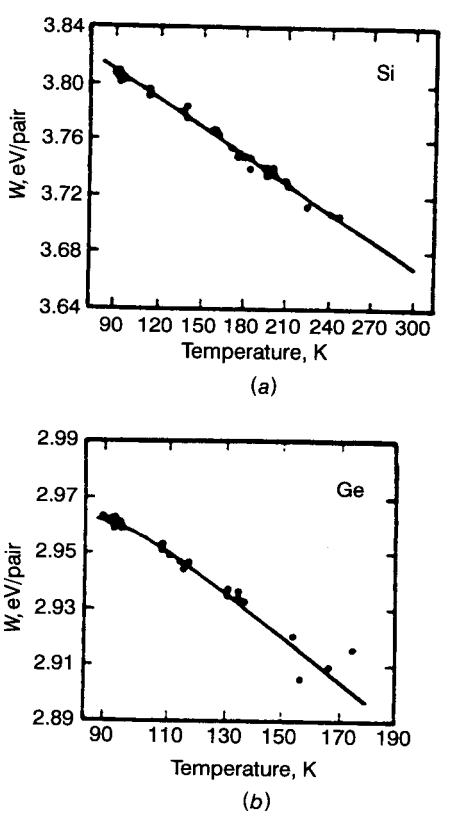


**Figure 7.9** Energy needed to produce an electron-hole pair in (*a*) silicon and (*b*) germanium, as a function of temperature (from Ref. 3).

### 7.3.2 Conductivity of Semiconductors

Conductivity $\sigma$ is the inverse of resistivity and is defined by

$$j = \sigma E \tag{7.4}$$

where $j$ = current density (A/m$^2$)
$\sigma$ = conductivity [A/(V m)]
$E$ = electric field (V/m)

Another expression for the current density is

$$j = eNv \tag{7.5}$$

where $N$ = number of charge carriers/m$^3$
$v$ = speed of carriers

Using Eqs. 7.4 and 7.5, one obtains the following equation:

$$\sigma = eN\frac{v}{E} \tag{7.6}$$

The ratio $v/E$ is given a new name, *mobility of the carrier*:

$$\mu = (v/E) \tag{7.7}$$

All the types of charge carriers present in a medium contribute to the conductivity. In the case of semiconductors, both electrons and holes should be taken into account when conductivity is calculated, and the expression for the conductivity becomes (using Eqs. 7.6 and 7.7).

$$\sigma = e(N_e\mu_e + N_p\mu_p) \tag{7.8}$$

where $N_e$ and $N_p$ are charge carrier concentrations and $\mu_e$ and $\mu_p$ are mobilities of electrons and holes, respectively. According to Eq. 7.8, the conductivity changes if the mobility of the carriers or their concentration or both change.

The mobilities of electrons and holes are independent of the electric field over a wide range of carrier velocities, but they change with temperature. If the temperature decreases, the mobility of both carriers increases. The mobility of electrons and holes in pure germanium as a function of temperature is shown in Fig. 7.10.[4] The mobility changes at $\mu \sim T^{-\alpha}$ with $\alpha \approx 1.5$, for $T < 80$ K. For $T > 80$ K, the value of $\alpha$ is somewhat larger. It is worth noting that for $T < 80$ K, $\mu_n \approx \mu_p$.

In a pure semiconductor, $N_e = N_p$ and each one of these quantities is given by the equation

$$N_e = N_p = AT^{1.5}\exp\left(-\frac{E_g}{2kT}\right) \tag{7.9}$$

where $A$ is a constant independent of $T$.

The motion of the carriers in a semiconductor is also affected by the presence of impurities and defects of the crystal. A small amount of impurities is always present, although impurities are usually introduced deliberately to make

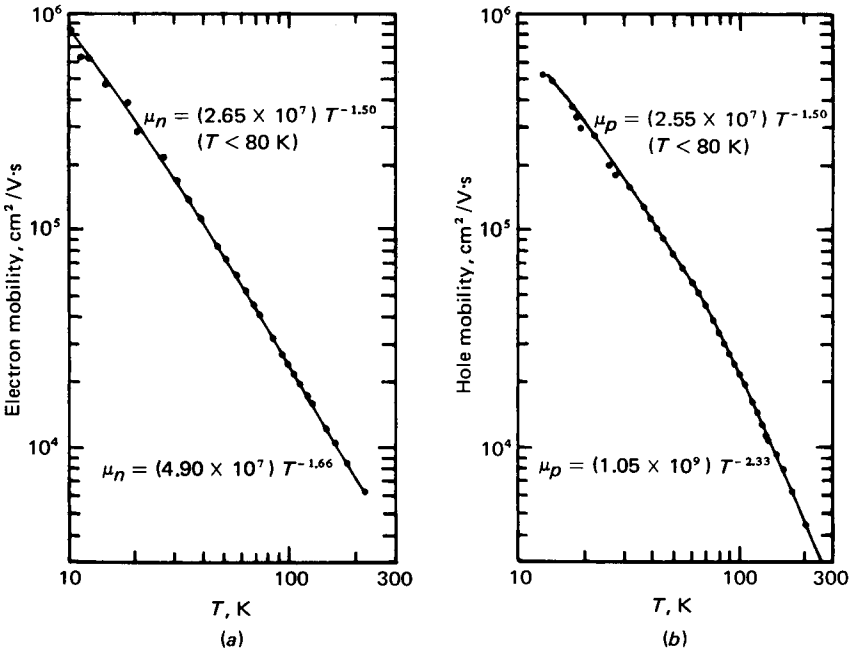


**Figure 7.10** (*a*) Electron mobility versus temperature for *n*-type germanium. (*b*) Hole mobility versus temperature for *p*-type germanium (from Ref. 4).

the properties of the crystal more appropriate for radiation detection (see Sec. 7.3.3). Crystal defects are present too. Even if one starts with a perfect crystal, defects are produced by the incident particles (this is called *radiation damage*). In the language of energy bands, impurities and defects represent new energy states that may trap the carriers. Trapping is, of course, undesirable because it means loss of part of the charge generated by the incident particle.

For semiconductors, the probability that an electron will move from the valence to the conduction level is proportional to the factor (Eq. 7.3)

$$\exp\left(-\frac{E_g}{2kT}\right) \tag{7.10}$$

($E_f$ is located in the middle of the gap; thus $E - E_f = E_g/2$.) Because of the exponential form of Eq. 7.10, there are always some electrons in the conduction band. These electrons produce a leakage current. Obviously, a successful detector should have as low a leakage current as possible to be able to detect the ionization produced by the incident radiation. The leakage current decreases with temperature, and for two different materials it will be smaller for the material with the larger energy gap.

### 7.3.3 Extrinsic and Intrinsic Semiconductors—The Role of Impurities

The properties of a pure semiconductor change if impurities are introduced. With impurities present, new states are created and the semiconductor obtains extra electrons or extra holes, which increase the conductivity of the material.

Actually, pure semiconductors are not available. All materials contain some impurities and for this reason they are called *impure* or *extrinsic*, in contrast to a pure semiconductor, which is called *intrinsic*. In most cases, controlled amounts of impurities are introduced purposely by a process called *doping*, which increases the conductivity of the material by orders of magnitude.

Doping works in the following way. Consider silicon (Si), which has four valence electrons. In a pure Si crystal, every valence electron makes a covalent bond with a neighboring atom (Fig. 7.11*a*). Assume now that one of the atoms is replaced by an atom of arsenic (As), which has five valence electrons (Fig. 7.11*b*). Four of the valence electrons form covalent bonds with four neighboring Si atoms, but the fifth electron does not belong to any chemical bond. It is bound very weakly and only a small amount of energy is necessary to free it, i.e., to move it to the conduction band. In terms of the energy-band model, this fifth electron belongs to an energy state located very close to the conduction band. Such states are called *donor* states (Fig. 7.12), and impurity atoms that create them are called *donor* atoms. The semiconductor with donor atoms has a large number of electrons and a small number of holes. Its conductivity will be due mainly to electrons, and it is called an *n-type* semiconductor (n is for negative).

If a gallium atom is the impurity, three valence electrons are available; thus only three Si bonds will be matched (Fig. 7.13). Electrons from other Si atoms can attach themselves to the gallium atom, leaving behind a hole. The gallium atom will behave like a negative ion after it accepts the extra electron. In terms of the energy-band theory, the presence of the gallium atom creates new states very close to the valence band (Fig. 7.14). These are called *acceptor* states. The impurity is called an *acceptor* atom. For every electron that moves to the acceptor states, a hole is left behind. The acceptor impurity atoms create holes. The charge carriers are essentially positive, and the semiconductor is called *p-type*.

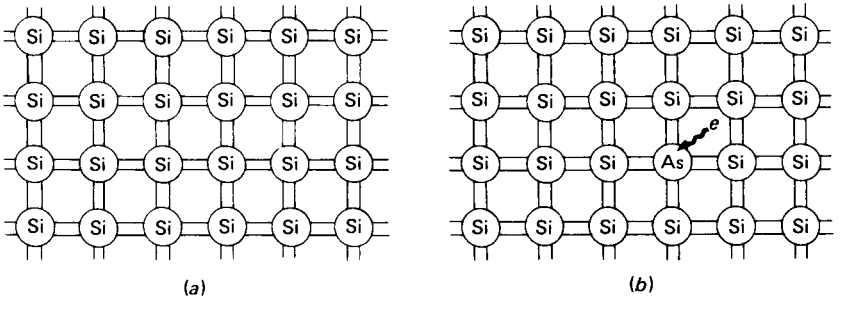


**Figure 7.11** (*a*) Pure (intrinsic) silicon. (*b*) Silicon doped with arsenic. The fifth electron of the arsenic atom is not tightly bound, and little energy is needed to move it to the conduction band.

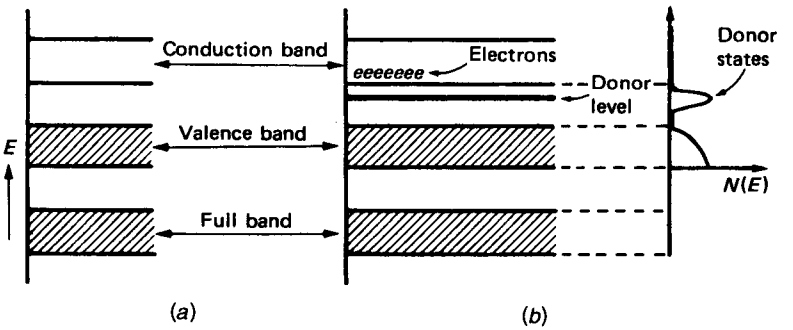


**Figure 7.12** (*a*) Intrinsic and (*b*) n-type semiconductor. New electron states (donor states) are created close to the conduction band.

Interstitial atoms can act as donors or acceptors. Lithium, as an interstitial in either silicon or germanium, creates donor states very close to the conduction band. Copper and nickel introduce donor states midway between the valence and conduction bands. Gold may act as either an acceptor or donor, depending on its position on the lattice.

For every atom of n-type or p-type impurity, an electron or hole is located at the donor or acceptor state, respectively. The material is still neutral, but when conductivity appears,

Electrons are the major carriers for n-type semiconductors.
Holes are the major carriers for p-type semiconductors.

Since the addition of impurities creates new states that facilitate the movement of the carriers, it should be expected that the conductivity of a semiconductor increases with impurity concentration. Figures 7.15 and 7.16 show how the resistivity of germanium and silicon changes with impurity concentration.

The energy gap $E_g$ depends on temperature, as shown in Fig. 7.8, and on the number of impurities and defects of the crystal. With increasing temperatures, if $E_g$ is small as in germanium, the electrical conduction is dominated by electron-hole pairs created by thermal excitation and not by the presence of the impurity atoms. Therefore, at high enough temperatures, any semiconductor can be considered as intrinsic.

Table 7.1 presents the most important physical and electrical properties of silicon and germanium, the two most widely used semiconductors.

## 7.4 THE p-n JUNCTION

### 7.4.1 The Formation of a p-n Junction

As stated in the introduction to this chapter, semiconductor detectors operate like ionization counters. In ionization counters (see Chap. 5), the charges

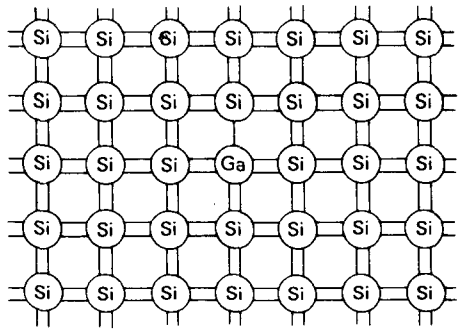


**Figure 7.13** Silicon doped with gallium. One of the covalent bonds is not matched.

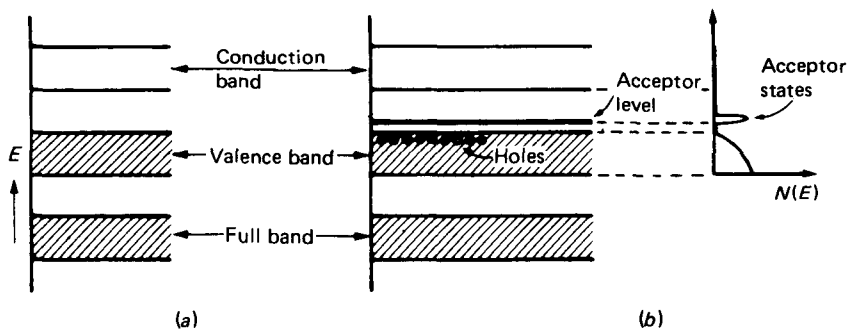


**Figure 7.14** (*a*) Intrinsic and (*b*) p-type semiconductor. New hole states (acceptor states) are created close to the top of the valence band.

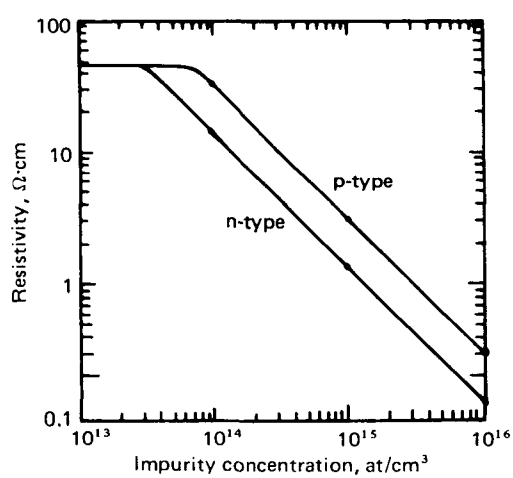


**Figure 7.15** Resistivity as a function of impurity concentration in germanium (from Chap. 1.1.3 of Bertolini & Coche).

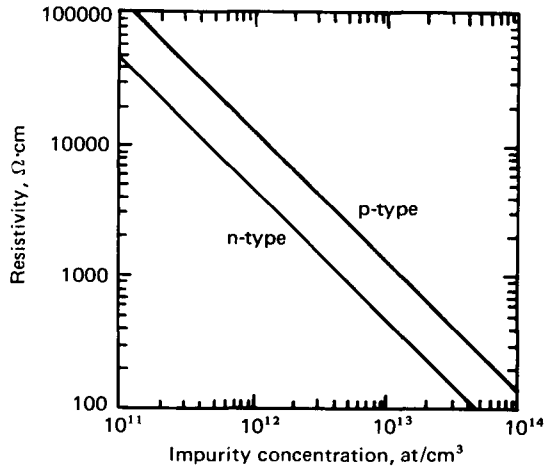


**Figure 7.16** Resistivity as a function of impurity concentration in silicon (from Chap. 1.1.3 of Bertolini & Coche).

produced by the incident radiation are collected with the help of an electric field from an external voltage. In semiconductor detectors, the electric field is established by a process more complicated than in gas counters, a process that depends on the properties of n- and p-type semiconductors. The phenomena involved will be better understood with a brief discussion of the so-called p-n junction.

An n-type semiconductor has an excess of electron carriers. A p-type has excess holes. If a p-type and an n-type semiconductor join together, electrons and holes move for two reasons:

1. Both electrons and holes will move from areas of high concentration to areas of low concentration. This is simply diffusion, the same as neutron diffusion or diffusion of gas molecules.
2. Under the influence of an electric field, both electrons and holes will move, but in opposite directions because their charge is negative and positive, respectively.

Consider two semiconductors, one p-type, the other n-type, in contact, without an external electric field (Fig. 7.17). The n-type semiconductor has a high electron concentration; the p-type has a high hole concentration. Electrons will diffuse from the n- to the p-type; holes will diffuse in the opposite direction. This diffusion will produce an equilibrium of electron and hole concentrations, but it will upset the original charge equilibrium. Originally, both p- and n-type semiconductors were electrically neutral, but as a result of the diffusion, the n-type region will be positively charged, while the p-type region will be negatively charged. After equilibrium is established, a potential difference exists between the two regions. This combination of p- and n-type semiconductor with a potential difference between the two types constitutes a p-n junction.

The potential $V_0$ (Fig. 7.17*a*) depends on electron-hole concentrations and is of the order of 0.5 V. If an external voltage $V_b$ is applied with the positive pole

**Table 7.1 Properties of Si and Ge (from Fenvres and Haiman and Ref. 2)**

| Property | Si | Ge |
|---|---|---|
| Atomic number | 14 | 32 |
| Atomic weight | 28.1 | 72.6 |
| Density (300 K) | $2.33 \times 10^3$ kg/m$^3$ | $5.33 \times 10^3$ kg/m$^3$ |
| Energy gap ($E_g$), 300 K | 1.106 eV | 0.67 eV |
| Energy gap ($E_g$), 0 K | 1.165 eV | 0.75 eV |
| Average energy per electron-hole pair, 77 K | 3.7 eV | 2.96 eV |
| Average energy per electron-hole pair, 300 K | 3.65 eV | – |
| Diffusion voltage ($V_0$) | 0.7 V | 0.4 V |
| Atomic concentration | $5 \times 10^{28}$ m$^{-3}$ | $4.5 \times 10^{28}$ m$^{-3}$ |
| Intrinsic carrier concentration (300 K) | $1.5 \times 10^{16}$ m$^{-3}$ | $2.4 \times 10^{19}$ m$^{-3}$ |
| Intrinsic resistivity (300 K) | $2.3 \times 10^3$ Ω·m | 0.47 Ω·m |
| Intrinsic resistivity (77 K) | ∞ | $5 \times 10^2$ Ω·m |
| Electron mobility (300 K) | 0.1350 m$^2$/V·s | 0.3900 m$^2$/V·s |
| Hole mobility (300 K) | 0.0480 m$^2$/V·s | 0.1900 m$^2$/V·s |
| Electron mobility (77 K) | 4.0–7.0 m$^2$/V·s | 3.5–5.5 m$^2$/V·s |
| Hole mobility (77 K) | 2.0–3.5 m$^2$/V·s | 4.0–7.0 m$^2$/V·s |
| Dielectric constant | 12 | 16 |

connected to the n side, the total potential across the junction becomes $V_0 + V_b$. This is called *reverse bias*. Such external voltage tends to make the motion of both electrons and holes more difficult. In the region of the changing potential, there is an electric field $E = -\partial V/\partial x$. The length $X_0$ of the region where the potential and the electric field exist increases with reverse bias. Calculation

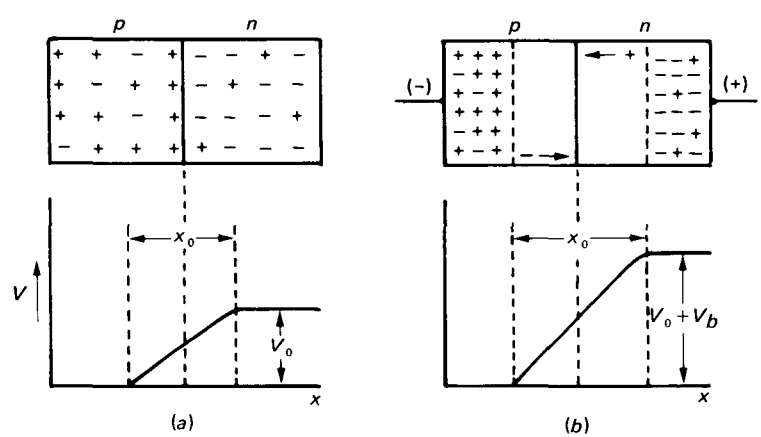


**Figure 7.17** (*a*) A p-n junction without external voltage. (*b*) If a reverse voltage is applied externally, the potential across the junction increases, and so does the depth $x_0$ along which an electric field exists.

shows that

$$X_0 \approx \sqrt{\mu_p \rho (V_0 + V_b)} \qquad \text{for p-type semiconductor} \qquad (7.11a)$$

and

$$X_0 \approx \sqrt{\mu_n \rho (V_0 + V_b)} \qquad \text{for n-type semiconductor} \qquad (7.11b)$$

where $\rho(\Omega \cdot \text{m})$ is the resistivity of the crystal. Application of a negative potential on the n side will have the opposite effect. The total potential difference will be $V_0 - V_b$. This is called *forward bias*. For a successful detector, reverse bias is applied. Since, usually, $V_b \gg V_0$, $X_0 \sim \sqrt{V_b}$.

In practice, a p-n junction is not made by bringing two pieces of semiconductor into contact. Instead, one starts with a semiconductor of one type (say, n-type) and then transforms one end of it into the other type (p-type).

### 7.4.2 The p-n Junction Operating as a Detector

The operation of a semiconductor detector is based, essentially, on the properties of the p-n junction with reverse bias (Fig. 7.18). Radiation incident upon the junction produces electron-hole pairs as it passes through it. For example, if a 5-MeV alpha particle impinges upon the detector and deposits all its energy there, it will create about

$$\frac{5 \times 10^6 \text{ eV}}{3 \text{ eV/pair}} \sim 1.7 \times 10^6 \text{ electron-hole pairs}$$

Electrons and holes are swept away under the influence of the electric field and, with proper electronics, the charge collected produces a pulse that can be recorded.

The performance of a semiconductor detector depends on the region of the p-n junction where the electric field exists (region of width $X_0$, Fig. 7.18). Electrons and holes produced in that region find themselves in an environment similar to what electrons and ions see in a plate ionization chamber (see Sec. 5.4). There are some differences, however, between these two types of detectors.

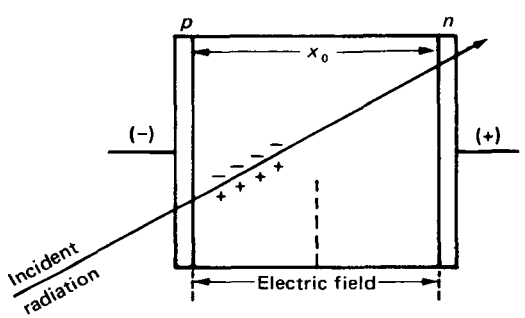


**Figure 7.18** A p-n junction with reverse bias operating as a detector.

In a gas counter, the electron mobility is thousands of times bigger than that of the ions. In semiconductors, the electron mobility is only about two to three times bigger than that of the holes. The time it takes to collect all the charge produced in a gas counter is of the order of milliseconds. In semiconductors, the sensitive region of the counter is only a few millimeters, and the speed of electrons and holes is such that the charge carriers can traverse the sensitive region and be collected in times of the order of $10^{-7}$ s.

It is always the objective in either an ionizatin or a semiconductor detector to collect all the charges produced by the incident particle. This is achieved by establishing an electric field in the detector such that there is zero recombination of electrons and ions (or holes) before they are collected. In a semiconductor detector, even if recombination is zero, some charge carriers may be lost in "trapping" centers of the crystal, such as lattice imperfections, vacancies and dislocations. The incident radiation creates crystal defects that cause deterioration of the detector performance and, thus, reduce its lifetime (see Sec. 7.6).

The capacitance of p-n junction is important because it affects the energy resolution of the detector. For a detector such as that shown in Fig. 7.18, the *capacitance C* is given by

$$C = \epsilon \frac{A}{4\pi X_0} \tag{7.12}$$

where $\epsilon$ = dielectric constant of the material
$A$ = surface area of the detector
$X_0$ = depletion depth (detector thickness)
Combining Eqs. 7.11 and 7.12,

$$C \sim \frac{1}{\sqrt{V_b}}$$

To summarize, a material that will be used for the construction of a detector should have certain properties, the most important of which are the following:

1. *High resistivity*. This is essential, since otherwise current will flow under the influence of the electric field, and the charge produced by the particles will result in a pulse that may be masked by the steadily flowing current.
2. *High carrier mobility*. Electrons and holes should be able to move quickly and be collected before they have a chance to recombine or be trapped. High mobility is in conflict with property (1) because in high-resistivity materials, carrier mobility is low. Semiconductor materials doped with impurities have proven to have the proper resistivity-carrier mobility combination.
3. *Capability of supporting strong electric fields*. This property is related to property (1). Its importance stems from the fact that the stronger the field, the better and faster the charge collection becomes. Also, as the electric field increases, so does the depth of the sensitive region (Eq. 7.11*a*) for certain detectors.

4. *Perfect crystal lattice.* Apart from externally injected impurities, the semiconductor detector material should consist of a perfect crystal lattice without any defects, missing atoms, or interstitial atoms. Any such defect may act as a "trap" for the moving charges.

## 7.5 THE DIFFERENT TYPES OF SEMICONDUCTOR DETECTORS

The several types of semiconductor detectors that exist today differ from one another because of the material used for their construction or the method by which that material is treated. The rest of this section describes briefly the method of construction and the characteristics of the most successful detectors —made of silicon or germanium—and two promising ones made of CdTe and $HgI_2$.

### 7.5.1 Surface-Barrier Detectors

Silicon of high purity, usually n-type, is cut, ground, polished, and etched until a thin wafer with a high-grade surface is obtained. The silicon is then left exposed to air or to another oxidizing agent for several days. As a result of surface oxidization, surface energy states are produced that induce a high density of holes and form, essentially, a p-type layer on the surface (Fig. 7.19). A very thin layer of gold evaporated on the surface serves as the electrical contact that will lead the signal to the preamplifier. In Fig. 7.19, $X_0$ is the depth of the sensitive region, $t$ is the total silicon thickness, and $D$ is the diameter of the detector. The size of the detector is the length (or depth) $X_0$.

### 7.5.2 Diffused-Junction Detectors

Silicon of high purity, normally p-type, is the basic material for this detector type. As with surface-barrier detectors, the silicon piece has the shape of a thin wafer. A thin layer of n-type silicon is formed on the front face of the wafer by applying a phosphorus compound to the surface and then heating the assembly to temperatures as high as 800–1000° C for less than an hour. The phosphorus diffuses into the silicon and "dopes" it with donors (Fig. 7.20). The n-type silicon in front and the p-type behind it form the p-n junction.

Both surface-barrier and diffused-junction detectors are used for the detection of charged particles. To be able to measure the energy of the incident radiation, the size $X_0$ of the detector should be at least equal to the range of the incident particle in silicon. The value of $X_0$ depends on the resistivity of the material (which in turn, depends on impurity concentration) and on the applied voltage, as shown by Eq. 7.11. Blankenship and Borkowski have designed a nomogram relating all these quantities.[5] Figure 7.21 shows a simplified version of the nomogram, and Ex. 7.1 explains its use.

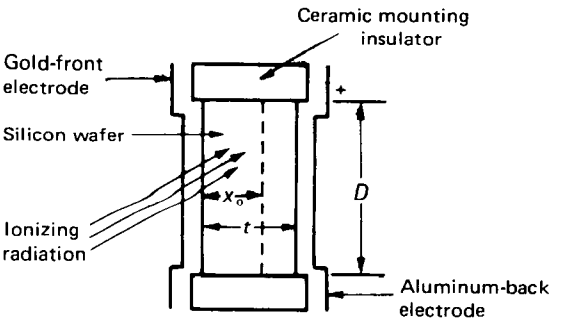


(a)

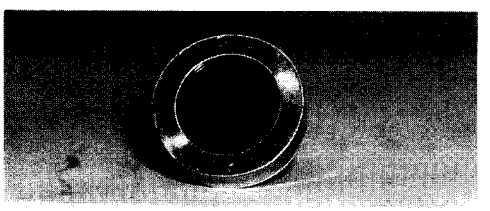

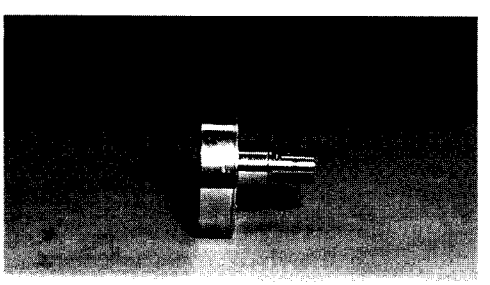

(b)

**Figure 7.19** A typical surface barrier detector: (*a*) a schematic representation; (*b*) photograph of a commercial detector (reproduced from *Instruments for Research and Applied Science* by permission of EG & G ORTEC, Oak Ridge, Tennessee).

**EXAMPLE 7.1** What is the bias needed for a surface-barrier detector made of p-type silicon with resistivity 1.5 k$\Omega$ cm, used for the detection of 10-MeV alpha particles?

**ANSWER** The bias is found by following these steps:

1. Find the range of a 10-MeV alpha particle in silicon. From Sec. 4.6, one obtains $R = 65\ \mu$m (point A in Fig. 7.21).
2. Define point B on the resistivity scale for p-type silicon.
3. Draw the straight line defined by points A and B.
4. The required bias (point C) is the intersection of the line AB with the bias scale ($V_b \simeq 35$ V).

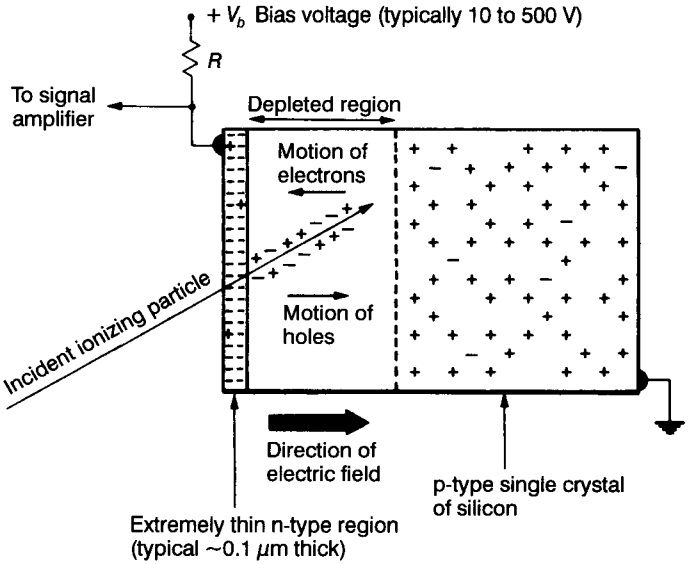


**Figure 7.20** A diffused-junction detector.

The nomogram of Fig. 7.21 also gives the capacitance of the detector. Of course, the capacitance can also be calculated using Eq. 7.11.

### 7.5.3 Silicon Lithium-Drifted [Si(Li)] Detectors

For both surface-barrier and diffused-junction detectors, the sensitive region—i.e., the actual size of the detector—has an upper limit of about 2000 μm. This limitation affects the maximum energy of a charged particle that can be measured. For electrons in Si, the range of 2000 μm corresponds to an energy of about 1.2 MeV; for protons the corresponding number is about 18 MeV; for alphas, it is about 72 MeV. The length of the sensitive region can be increased if lithium ions are left to diffuse from the surface of the detector toward the other side. This process has been used successfully with silicon and germanium and has produced the so-called Si(Li) (pronounced silly) and Ge(Li) (pronounced jelly) semiconductor detectors. Lithium-drifted detectors have been produced with depth up to 5 mm in the case of Si(Li) detectors and up to 12 mm in the case of Ge(Li) detectors.

The lithium drifting process, developed by Pell,[6,7] consists of two major steps: (1) formation of an n-p junction by lithium diffusion, and (2) increase of the depletion depth by ion drifting.

The n-p junction is formed by letting lithium diffuse into a p-type silicon. The diffusion can be accomplished by several methods.[8-11] Probably the simplest method consists of painting a lithium-in-oil suspension onto the surface

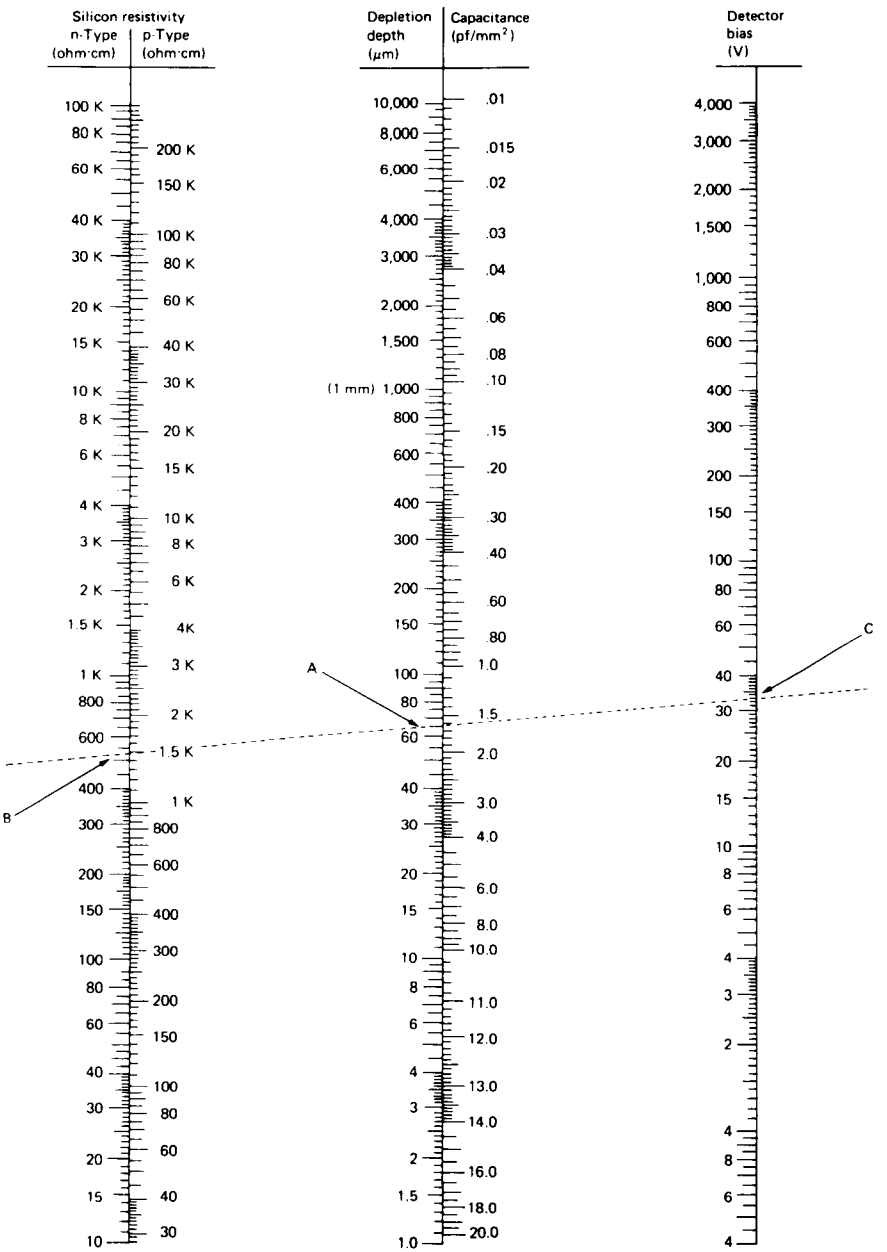


**Figure 7.21** The Blankenship and Borkowski[5] nomogram that relates resistivity, detector thickness, and detector bias. The detector capacitance as a function of detector thickness is also given.

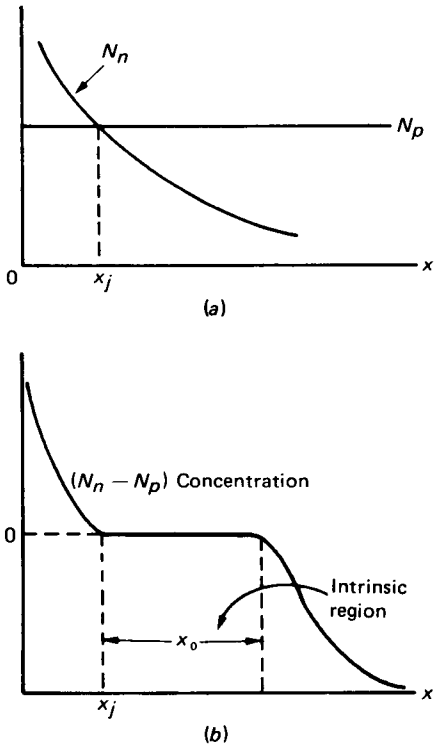


**Figure 7.22** (*a*) During the diffusion of lithium, the donor concentration changes with depth as shown. (*b*) During drifting (at elevated temperature and under reverse bias), and almost intrinsic region is formed with thickness $x_0$.

from which drifting is to begin. Other methods are lithium deposition under vacuum, or electrodeposition. After the lithium is applied on the surface, the silicon wafer is heated at 250–400° C for 3–10 min in an inert atmosphere, such as argon or helium.

Lithium is an n-type impurity (donor atom) with high mobility in silicon (and germanium; see next section). When the diffusion begins, the acceptor concentration ($N_p$) is constant throughout the silicon crystal (Fig. 7.22*a*), while the donor concentration ($N_n$) is high on the surface and zero everywhere else. As the diffusion proceeds, the donor concentration changes with depth, as shown in Fig. 7.22*a*. At the depth $x_j$ where

$$N_n(x_j) = N_p$$

and n-p junction has been formed (Fig. 7.22*b*).

After the diffusion is completed, the crystal is left to cool, the excess lithium is removed, and ohmic contacts are put on the n and p sides of the junction. The contact on the p side is usually formed by evaporating aluminum or gold doped with boron. The contact on the n side can be formed by using pure gold or antimony-doped gold.

Drifting is accomplished by heating the junction to 120–150° C while applying a reverse bias that may range from 25 V up to about 1000 V. In general, the higher the temperature and the voltage are, the faster the drifting proceeds. Depending on the special method used, the semiconductor may be under vacuum or in air or be placed in a liquid bath (e.g., silicon oil or fluorocarbon). The electric field established by the reverse bias tends to move the n-type atoms (lithium) toward the p side of the junction. As a result, the concentration of lithium atoms becomes lower for $x < x_j$ (Fig. 7.22*a*) and higher for $x > x_j$. For $x < x_j$, $N_n$ cannot become less than $N_p$ because then a local electric field would appear pushing the lithium atoms toward the n side. Similarly, for $x > x_j$, $N_n$ cannot increase very much because the local electric field works against such a concentration. Thus, a region is created that looks like an intrinsic semiconductor because $N_n \approx N_p$. For long drifting times, the thickness of the intrinsic region $X_0(t)$ as a function of time is given by

$$X_0(t) = \sqrt{2V\mu_{\mathrm{Li}}t} \tag{7.13}$$

where $V$ = applied voltage

$\mu_{\mathrm{Li}}$ = mobility of Li ions in silicon at the drifting temperature

The mobility of lithium, which increases with temperature,[12] has a value of about $5 \times 10^{-14}$ m$^2$/V s at $T = 150°$ C. Drifting is a long process. Depending on the desired thickness, drifting may take days and sometimes weeks.

**EXAMPLE 7.2** How long will it take to obtain an intrinsic region of 1.5 mm in a silicon wafer drifted at 150° C under a reverse bias of 500 V?

**ANSWER** Using Eq. 7.13 with $\mu_{\mathrm{Li}} = 5 \times 10^{-14}$ m$^2$/V s, one obtains

$$t = \frac{X_0^2(t)}{2V\mu_{\mathrm{Li}}} = \frac{(1.5 \times 10^{-3})^2 \text{ m}^2}{2(500 \text{ V})[5 \times 10^{-14} \text{ m}^2/(\text{V s})]} = 4.5 \times 10^4 \text{ s} = 12.5 \text{ h}$$

After drifting is completed, the Si(Li) detector is mounted on a cryostat, since the best results are obtained if the detector is operated at a very low temperature. Usually, this temperature is 77K, the temperature of liquid nitrogen. Si(Li) detectors may be stored at room temperature for a short period of time without catastrophic results, but for longer periods it is advisable to keep the detector cooled at all times. The low temperature is necessary to keep the lithium drifting at a "frozen" stage. At room temperature, the mobility of lithium is such that its continuous diffusion and precipitation[12] will ruin the detector.

Si(Li) detectors are used for detection of charged particles and especially X-rays. Their characteristics with respect to energy measurements are described in Chaps. 12 and 13.

### 7.5.4 Germanium Lithium-Drifted [Ge(Li)] Detectors

Ge(Li) detectors are not made anymore; they have been replaced by pure germanium crystals. Historically, Ge(Li) detectors dominated the gamma detection field for about 15 years (until about 1985). Since there may still be some Ge(Li)'s operating, a brief discussion is presented in this section.

Ge(Li) detectors are made from horizontally grown or pulled single crystals of germanium. As the crystal is grown, it is doped with acceptor impurities such as indium, gallium, or boron, and becomes a p-type semiconductor. Germanium crystals may be cut to length and shaped by a variety of means, including the use of diamond wheels or band saws. In these mechanical operations, great care must be taken not to fracture the brittle material.

Lithium drifting in germanium follows the same approach as in silicon. The deposition and diffusion of lithium are accomplished by one of the methods discussed in the previous section. The ohmic contacts are made by electrolytic deposition of gold,[13] by using gallium-indium[14] or mercury-indium,[15] or by ion implantation.[16] The drifting process itself takes place at a lower temperature ($< 60°$ C) than for silicon, with the germanium diode in air[17] or immersed in a liquid maintained at its boiling point.[18]

After the drifting process has been completed, the detector is mounted on a cryostat and is always kept at a low temperature (liquid nitrogen temperature $\sim 77$ K). Keeping the Ge(Li) detector at a low temperature is much more critical than for a Si(Li) detector. The mobility of the lithium atoms in germanium is so high at room temperature that the detector will be ruined if brought to room temperature even for a short period of time. If this happens, the detector may be redrifted, but at a considerable cost.

### 7.5.5 Germanium (Ge) Detectors

The production of high-purity germanium (HPGe) with an impurity concentration of $10^{16}$ atoms/cm$^3$ or less has made possible the construction of detectors without lithium drifting.[19–21] These detectors are now designated as Ge, not HPGe, and are simply formed by applying a voltage across a piece of germanium. The sensitive depth of the detector depends on the impurity concentration and the voltage applied, as shown in Fig. 7.23.

The major advantage of Ge versus Ge(Li) detectors is that the former can be stored at room temperature and cooled to liquid nitrogen temperature (77 K) *only* when in use. Cooling the detector, when in use, is necessary because germanium has a relatively narrow energy gap, and at room or higher temperatures a leakage current due to thermally generated charge carriers induces such noise that the energy resolution of the device is destroyed.

Germanium detectors are fabricated in many different geometries, thus offering devices that can be tailored to the specific needs of the measurement. Two examples, the coaxial and the well-type detector, are shown in Fig. 7.24.

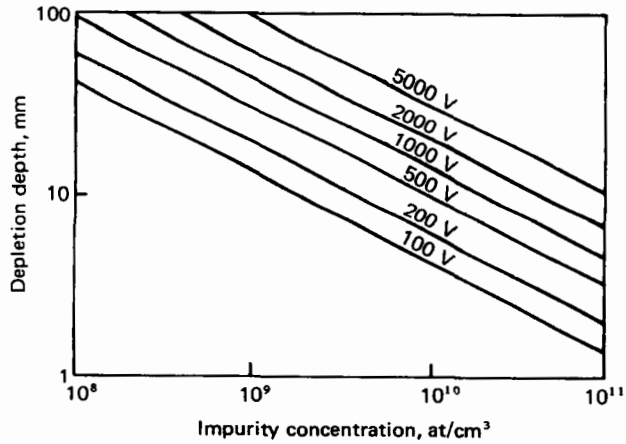


**Figure 7.23** Depletion depth as a function of impurity concentration and applied voltage for planar diodes of high-purity germanium (from Ref. 21).

More details about these detectors are presented in Chap. 12 in connection with $\gamma$-ray spectroscopy.

### 7.5.6 CdTe and $HgI_2$ Detectors

The major disadvantage of lithium-drifted detectors is the requirement for continuous cooling. In the case of Ge detectors, the requirement for cooling

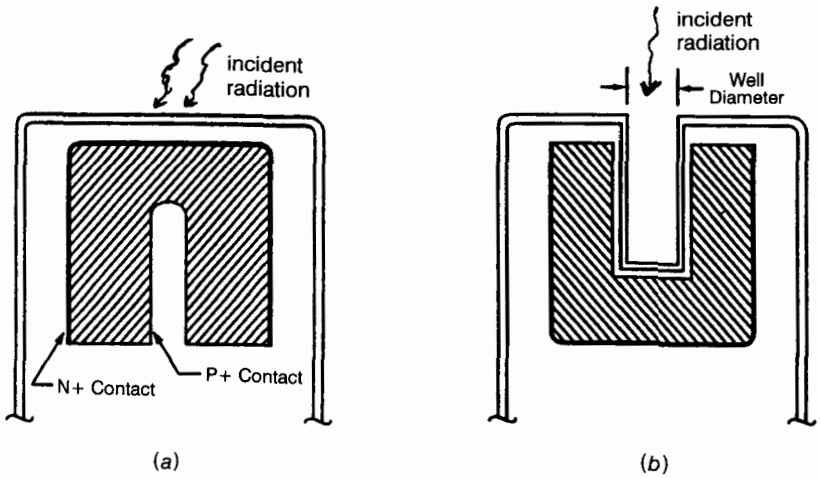


**Figure 7.24** Two examples of geometries used for Ge Detectors; (*a*) coaxial; (*b*) well type (from Canberra Nuclear, *Edition Nine Instruments Catalog*).

during operation is also a disadvantage. Cooling requires a cryostat, which makes the counter bulky and thus impossible to use in cases where only a small space is available; another disadvantage is the cost of continuously buying liquid nitrogen. There is a great incentive, therefore, to develop semiconductor detectors that can be stored and operated at room temperature. Two materials that have been studied and show great promise for the construction of such detectors are CdTe and $HgI_2$.[22-35] A comprehensive review of the state-of-the-art (until 1978) for both materials can be found in Ref. 36.

Successful detectors using CdTe or $HgI_2$ have been constructed with thickness up to 0.7 mm and area 100 $mm^2$ (as of 1978).[31] These detectors are small in size, compared to Si(Li) or Ge(Li) detectors, but the required detector volume depends on the application. For CdTe and $HgI_2$, the favored applications are those that require a small detector volume: monitoring in space,[37] measurement of activity in nuclear power plants,[38] medical portable scanning,[39] or medical imaging devices.[40] Although the detector volume is small, efficiency is considerable because of the high atomic number of the elements involved (Table 7.2). The energy needed for the production of an electron-hole pair is larger for CdTe and $HgI_2$ than it is for Si and Ge; as a result, the energy resolution of the former is inferior to that of the latter (see also Chap. 12). But CdTe and $HgI_2$ detectors are used in measurements where their energy resolution is adequate while, at the same time, their small volume and, in particular, their room-temperature operation offers a distinct advantage over Si(Li) and Ge(Li) detectors.

## 7.6 RADIATION DAMAGE TO SEMICONDUCTOR DETECTORS

The fabrication and operation of a semiconductor detector are based on the premise that one starts with a perfect crystal containing a known amount of impurities. Even if this is true at the beginning, a semiconductor detector will suffer damage after being exposed to radiation. The principal type of radiation damage is caused by the collision of an incident particle with an atom. As a result of the collision, the atom may be displaced into an interstitial position, thus creating an interstitial-vacancy pair known as the *Frenkel defect*. A recoiling

**Table 7.2 Properties of Si, Ge, CdTe, and $HgI_2$**

| Material | Atomic number | Energy gap (eV) | Energy needed to form the pair (eV) |
|---|---|---|---|
| Si | 14 | 1.106 (300 K) | 3.65 (300 K) |
| Ge | 32 | 0.67 (77 K) | 2.96 (77 K) |
| CdTe | 48 and 52 | 1.47 (300 K) | 4.43 (300 K) |
| $HgI_2$ | 80 and 53 | 2.13 (300 K) | 4.22 (300 K) |

**Table 7.3 Particle Fluence That Causes Significant Radiation Damage**

| | Heavy ions (particles/m$^2$) | Alphas ($\alpha$/m$^2$) | Fast neutrons (n/m$^3$) |
|---|---|---|---|
| Junction detectors | $10^{12}$ | $10^{14}$ | |
| Si(Li) | | $10^{12}$ | $10^{14}$ |
| Ge(Li) or Ge | | | $10^{13}$–$10^{14}$ |

atom may have enough energy to displace other atoms; therefore an incident particle may produce many Frenkel defects.

Crystal defects affect the performance of the detector because they may act as trapping centers for electrons and holes or they may create new donor or acceptor states. New trapping centers and new energy states change the charge collection efficiency, the leakage current, the pulse risetime, the energy resolution, and other properties of the detector. The changes are gradual, but the final result is shortening of the detector lifetime.

Electrons and photons cause negligible radiation damage compared to charged particles and neutrons. Heavier and more energetic charged particles cause more damage than lighter and less energetic particles.[2,21] Also, the damage is not the same for all detector types. Table 7.3 gives the fluences that cause considerable radiation damage for different detectors and bombarding particles.

Ge detectors are not affected by gammas, but they are damaged by the neutrons in a mixed n-$\gamma$ field.

## PROBLEMS

**7.1** What is the probability that an electron energy state in Ge will be occupied at temperature $T = 300$ K if the energy state is greater than the Fermi energy by 2 eV?

**7.2** Repeat Prob. 7.1 for $T = 77$ K.

**7.3** The energy gap for diamond is 7 eV. What temperature will provide thermal energy ($kT$) equal to that amount?

**7.4** What should be the maximum thickness of the gold layer covering the front face of a surface barrier detector used for the measurement of 10-MeV alphas, if the energy loss of the alphas traversing the layer should be less than 0.1 percent of the kinetic energy?

**7.5** Repeat Prob. 7.4 for 6-MeV electrons.

**7.6** The thickness of the gold layer covering the front face of a semiconductor detector may be measured by detecting particles entering the detector at two different angles. Calculate that thickness if alphas that enter in a direction perpendicular to the front face register as having energy 4.98 MeV, but those that enter at a 45° angle register as having energy 4.92 MeV.

**7.7** What is the average distance traveled in Si by a 50-KeV gamma before it has an interaction? What is the corresponding distance in Ge?

**7.8** Lithium has been drifted in germanium at 50° C under a reverse bias of 500 V for 2 weeks. What is your estimate of the drifting depth? [$\mu_{Li} = 1.5 \times 10^{-13}$ m$^2$/(V s)]

**7.9** A parallel beam of 0.5-MeV gammas is normally incident upon 2-mm-thick-crystals of Si, Ge, CdTe, and $HgI_2$. What fraction of photons will interact at least once in each crystal?

## BIBLIOGRAPHY

Bertolini, G., and Coche, A., *Semiconductor Detectors*, North-Holland Publishing Co., Amsterdam, 1968.

Brown, W. L., Higinbotham, W. A., Miller, G. L., and Chace, R. L. (eds.), "Semiconductor Nuclear Particle Detectors and Circuits," proceedings of a conference conducted by the Committee of Nuclear Science of the National Academy of Sciences, NAS Publication 1593, Washington, D.C. (1969).

Dearnaley, G., and Northrop, D. C., *Semiconductor Counters for Nuclear Radiations*, E & F.N. Spon. Ltd., London, 1964.

Eichholz, G. G., and Poston, J. W., *Nuclear Radiation Detection*, Lewis Publishers, Chelsea, Michigan, 1985.

Fenyves, E., and Haiman, O., *The Physical Principles of Nuclear Radiation Measurements*, Academic Press, New York, 1969.

Knoll, G. F., *Radiation Detection and Measurement*, 2nd ed., Wiley, New York, 1989.

Price, W. J., *Nuclear Radiation Detection*, McGraw-Hill, New York, 1964.

Tait, W. H., *Radiation Detection*, Butterworth, London, 1980.

## REFERENCES

1. McKenzie, J. M., *Nucl. Instrum. Meth.* **162**:49 (1979).
2. Ewan, G. T., *Nucl. Instrum. Meth.* **162**:75 (1979).
3. Pehl, R. H., Goulding, F. S., Landis, D. A., and Lenzlinger, M., *Nucl. Instrum. Meth.* **59**:45 (1968).
4. Delaet, L. H., Schoenmaekers, W. K., and Guislain, H. J., *Nucl. Instrum. Meth.* **101**:11 (1972).
5. Friedland, S. S., Mayer, J. W., and Wiggins, J. S., *IRE Trans. Nucl. Sci.* **NS-7**(2–3):181 (1960).
6. Pell, E. M., *J. Appl. Phys.* **31**:291 (1960).
7. Mayer, J. W., *J. Appl. Phys.* **33**:2894 (1962).
8. Elliott, J. H., *Nucl. Instrum. Meth.* **12**:60 (1961).
9. Baily, N. A., and Mayer, J. W., *Radiology* **76**:116 (1961).
10. Siffert, P., and Coche, A., *Compt. Rend.* **256**:3277 (1963).
11. Dearnaley, G., and Lewis, J. C., *Nucl. Instrum. Meth.* **25**:237 (1964).
12. Siffert, P., and Coche, A., "Behavior of Lithium in Silicon and Germanium," in G. Bertolini and A. Coche (eds.), *Semiconductor Detectors*, North-Holland Publishing Co., Amsterdam, 1968.
13. Janarek, F. J., Helenberg, H. W., and Mann, H. M., *Rev. Sci. Instrum.* **36**:1501 (1965).
14. Mooney, J. B., *Nucl. Instrum. Meth.* **50**:242 (1967).
15. Hansen, W. L., and Jarrett, B. V., *Nucl. Instrum. Meth.* **31**:301 (1964).
16. Meyer, O., and Haushahn, G., *Nucl. Instrum. Meth.* **56**:177 (1967).
17. Ewan, G. T., and Tavendale, A. J., *Can. J. Phys.* **42**:3386 (1964).
18. Cappellani, E., Fumagulli, W., and Restelli, G., *Nucl. Instrum. Meth.* **37**:352 (1965).
19. Hall, R. N., and Soltys, T. J., *IEEE Trans. Nucl. Sci.* **NS-18**:160 (1971).
20. Hansen, W. L., *Nucl. Instrum. Meth.* **94**:377 (1971).
21. Pehl, R. H., *Physics Today* **30**:11, 50, 53 (1977).
22. Siffert, I., Gonidec, J. P., and Cornet, A., *Nucl. Instrum. Meth.* **115**:13 (1974).
23. Eichinger, P., Halder, N., and Kemmer J., *Nucl. Instrum. Meth.* **117**:305 (1974).
24. Jones, L. T., and Woollam, P. B., *Nucl. Instrum. Meth.* **124**:591 (1975).
25. Iwanczyk, J., and Dabrowski, A. J., *Nucl. Instrum. Meth.* **134**:505 (1976).

26. Siffert, P., *Nucl. Instrum. Meth.* **150**:1 (1978).
27. Dabrowski, A. J., Iwanczyk, J., and Szymczyk, W. M., *Nucl. Instrum. Meth.* **150**:25 (1978).
28. Schieber, M., Beinglass, I., Dishon, G., Holzer, A., and Yaron, G., *Nucl. Instrum. Meth.* **150**:71 (1978).
29. Shalev, S., *Nucl. Instrum. Meth.* **150**:79 (1978).
30. Caine, S., Holzer, A., Beinglass, I., Dishon, G., Lowenthal, E., and Schieber, M., *Nucl. Instrum. Meth.* **150**:83 (1978).
31. Whited, R. C., and Schieber, M. M., *Nucl. Instrum. Meth.* **162**:113 (1979).
32. Ristinen, R. A., Peterson, R. J., Hamill, J. J., and Becchetti, F. D., *Nucl. Instrum. Meth.* **188**:445 (1981).
33. Markakis, J. M., *Nucl. Instrum. Meth.* **263**:499 (1988).
34. Courat, B., Fourrier, J. P., Silga, M., and Omaly, J., *Nucl. Instrum. Meth.* **269**:213 (1988).
35. McKee, B. T. A., Goetz, T., Hazlett, T., and Forkert, L., *Nucl. Instrum. Meth.* **272**:825 (1988).
36. "International Workshop on Mercuric Iodide and Cadmium Telluride Nuclear Detectors," *Nucl. Instrum. Meth.* **150**:1–112 (1978).
37. Lyons, R. B., *Rev. Phys. Appl.* **12**:385 (1977).
38. Jones, L. T., *Rev. Phys. Appl.* **12**:379 (1977).
39. Vogel, J., Ullman, J., and Entine, G., *Rev. Phys. Appl.* **12**:375 (1977).
40. Canali, C., Gutti, E., Kozlov, S. F., Manfredi, P. F., Manfredotti, C., Nava, F., and Quirini, A., *Nucl. Instrum. Meth.* **160**:73 (1979).

CHAPTER
# EIGHT

# RELATIVE AND ABSOLUTE MEASUREMENTS

## 8.1 INTRODUCTION

An *absolute measurement* is one in which the exact number of particles emitted or the exact number of events taking place is determined, for example,

1. Determination of the activity of a radioactive source, i.e., measurement of the number of particles emitted by the source per second
2. Determination of the neutron flux (neutrons per square meter per second) at a certain point in a reactor
3. Measurement of the number of neutrons emitted per fission
4. Measurement of the first cross section for a nuclear interaction

A *relative measurement* is one in which the exact number of particles emitted or the exact number of events taking place is not determined. Instead, a "relative" number of particles or events is measured, a number that has a fixed, but not necessarily known, relationship to the exact number, for example,

1. Determination of the G-M plateau. The relative change of the number of particles counted versus HV is measured. The exact number of particles emitted by the source is not determined; in fact, it is not needed.
2. Determination of half-life by counting the decaying activity of an isotope. The relative change of the number of atoms versus time is measured. The exact number of nuclei decaying per second is not needed.

3. Measurement of the fission cross section for $^{239}Pu$, based on the known fission cross section for $^{235}U$.
4. Determination of the variation of the neutron flux along the axis of a cylindrical reactor. The relative change of the flux from point to point along the axis of the reactor is measured, and not the exact number of neutrons per square meter per second.

Relative measurements are, in most cases, easier than absolute measurements. For this reason, investigators tend to perform the very minimum of absolute measurements and use their results in subsequent relative measurements. One of the most characteristic examples is the determination of the value of nuclear cross sections. Absolute measurements have been performed for very few cross sections. After certain cross sections have been measured, most of the others may be determined relative to the known ones.

This chapter discusses the factors that should be taken into account in performing relative and absolute measurements. Assume that there is a source of particles placed a certain distance away from a detector (Fig. 8.1) and that the detector is connected to a pulse-type counting system. The source may be located outside the detector as shown in Fig. 8.1, or it may be inside the detector (e.g., liquid-scintillation counting and internal-gas counting), and may be isotropic (e.g., particles emitted with equal probability in all directions) or anisotropic (e.g., parallel beam of particles). Both cases will be examined. Let

$S$ = number of particles per second emitted by the source

$r$ = number of particles per second recorded by the scaler

It is assumed that the counting rate $r$ has been corrected for dead time and background, if such corrections are necessary. The measured rate $r$ is related to $S$ by

$$r = f_1 f_2 f_3 \cdots f_n S \tag{8.1}$$

where the $f$ factors represent the effects of the experimental setup on the measurement. These factors may be grouped into three categories, to be discussed in detail in the following sections.

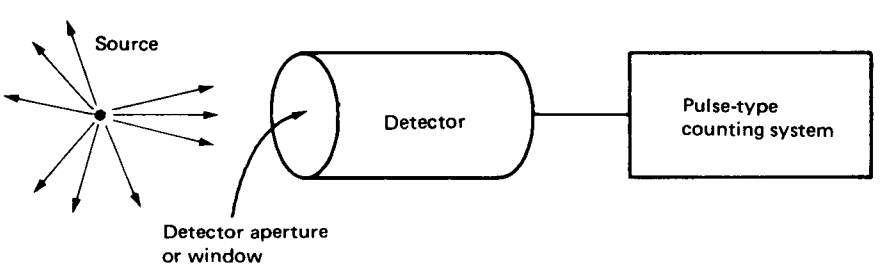


**Figure 8.1** A point isotropic source counted by a pulse-type counting system.

1. *Geometry effects*. The term *geometry* refers to size and shape of source (point, parallel beam, disk, rectangular), size and shape of detector aperture (cylindrical, rectangular, etc.), and distance between source and detector.
2. *Source effects*. The size and, in particular, the way the source is made may have an effect on the measurement. Whether the source is a solid material or a thin deposit evaporated on a metal foil may make a difference. The effect of source thickness is different on charged particles, gammas, and neutrons.
3. *Detector effects*. The detector may affect the measurement in two ways. First, the size and thickness of the detector window (Fig. 8.1) determine how many particles enter the detector and how much energy they lose, as they traverse the window. Second, particles entering the detector will not necessarily be counted. The fraction of particles that is recorded depends on the efficiency of the detector (see Sec. 8.4.2).

## 8.2 GEOMETRY EFFECTS

The geometry may affect the measurement in two ways. First, the medium between the source and the detector may scatter and may also absorb some particles. Second, the size and shape of the source and the detector and the distance between them determine what fraction of particles will enter the detector and have a chance to be counted.

### 8.2.1 The Effect of the Medium between Source and Detector

Consider a source and a detector separated by a distance $d$ (Fig. 8.2). Normally, the medium between the source and detector is air, a medium of low density. For measurements of photons and neutrons, the air has no effect. If the source emits charged particles, however, all the particles suffer some energy loss, and some of them may be scattered in or out of the detector (Fig. 8.2). If this effect

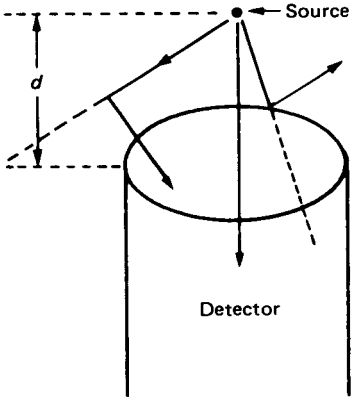


**Figure 8.2** The medium between the source and the detector may scatter and/or absorb particles emitted by the source.

is important for the measurement, it can be eliminated by placing the source and the detector inside an evacuated chamber. If the use of an evacuated chamber is precluded by the conditions of the measurement, then appropriate corrections should be applied to the results.

### 8.2.2 The Solid Angle—General Definition

To illustrate the concept of solid angle, consider a point isotropic source at a certain distance from a detector as shown in Fig. 8.3. Since the particles are emitted by the source with equal probability in every direction, only some of the particles have a chance to enter the detector. That portion is equal to the fractional solid angle subtended by the detector at the location of the source. In the general case of an extended source, the *solid angle* $\Omega$ is defined by

$$\Omega = \frac{\text{number of particles per second emitted inside the space defined by the contours of the source and the detector aperture}}{\text{number of particles per second emitted by the source}} \tag{8.2}$$

The mathematical expression for $\Omega$ is derived as follows (Fig. 8.4). A plane source of area $A_s$ emitting $S_0$ particles/(m$^2$ s), isotropically, is located a distance $d$ away from a detector with an aperture equal to $A_d$. Applying the definition given by Eq. 8.2 for the two differential areas $dA_s$ and $dA_d$ and integrating, one obtains†

$$\Omega = \frac{\int_{A_s}\int_{A_d} (S_0\, dA_s/4\pi r^2)\, dA_d(\hat{\mathbf{n}} \cdot \mathbf{r}/r)}{S_0 A_s} \tag{8.3}$$

†Equation 8.3 applies to isotropic sources: nonisotropic sources, seldom encountered in practice, need special treatment.

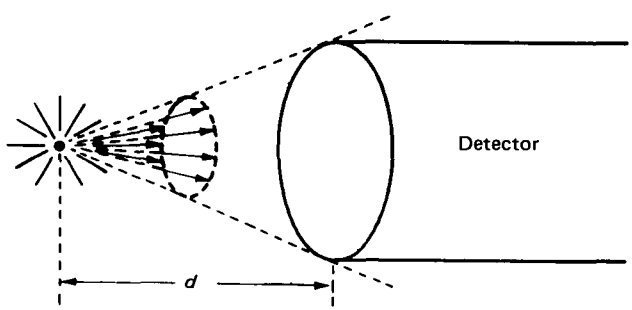


**Figure 8.3** The fraction of particles emitted by a point isotropic source and entering the detector is defined by the solid angle subtended by the detector at the location of the source.

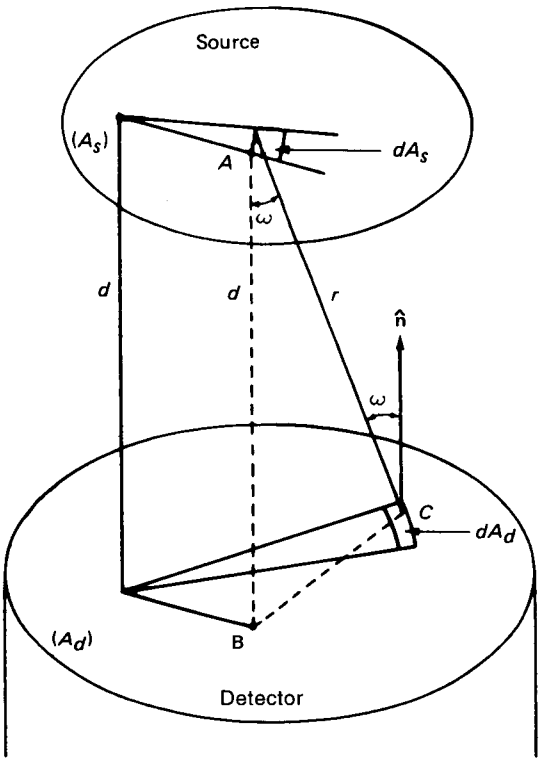


**Figure 8.4** Definition of the solid angle for a plane source and a plane detector parallel to the source.

where $\hat{\mathbf{n}}$ is a unit vector normal to the surface of the detector aperture. Since $\hat{\mathbf{n}} \cdot \mathbf{r}/r = \cos \omega$, Eq. 8.3 takes the form

$$\Omega = \frac{1}{4\pi A_s} \int_{A_s} dA_s \int_{A_d} dA_d \frac{\cos \omega}{r^2} \tag{8.4}$$

Equation 8.4 is valid for any shape of source and detector. In practice, one deals with plane sources and detectors having regular shapes, examples of which are given in the following sections.

As stated earlier, $\Omega$ is equal to the fractional solid angle ($0 \leq \Omega \leq 1$). In radiation measurements, it is called either *solid angle* or *geometry factor*. In this text it will be called the solid angle.

### 8.2.3 The Solid Angle for a Point Isotropic Source and a Detector with a Circular Aperture

The most frequently encountered case of obtaining a solid angle is that of a point isotropic source at a certain distance away from a detector with a circular

aperture (Fig. 8.5). In Eq. 8.4, $\cos \omega = d/r$, and the integration gives

$$\Omega = \frac{1}{2}\left(1 - \frac{d}{\sqrt{d^2 + R^2}}\right) \tag{8.5}$$

From Fig. 8.5,

$$\cos \theta_0 = \frac{d}{\sqrt{d^2 + R^2}} \tag{8.6}$$

Therefore, an equation equivalent to Eq. 8.5 is

$$\Omega = \tfrac{1}{2}(1 - \cos \theta_0) \tag{8.7}$$

It is instructive to rederive Eq. 8.7, not by using Eq. 8.4, but by a method that gives more insight into the relationship between detector size and source-detector distance.

Consider the point isotropic source of strength $S_0$ particles per second located a distance $d$ away from the detector, as shown in Fig. 8.6. If one draws a sphere centered at the source position and having a radius $R_s$ greater than $d$, the number of particles/(m$^2$ s) on the surface of the sphere is $S_0/4\pi R_s^2$. The particles that will hit the detector are those emitted within a cone defined by the location of the source and the detector aperture. If the lines that define this cone are extended up to the surface of the sphere, an area $A_s$ is defined there. $A_s$ is a nonplanar area on the surface of the sphere. The number of particles per second entering the detector is $A_s(S_0/4\pi R_s^2)$ and, using Eq. 8.2, the solid angle

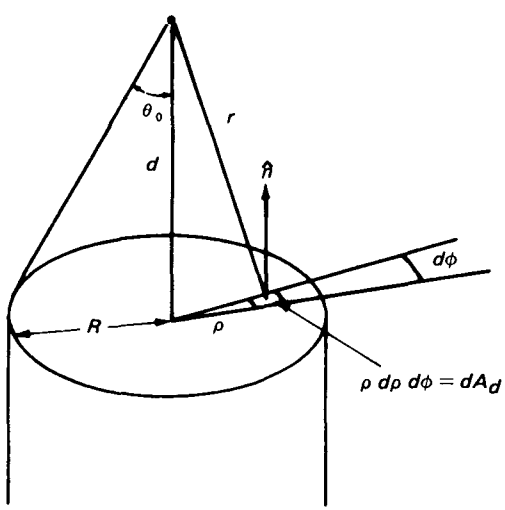


**Figure 8.5** The solid angle between a point isotropic source and a detector with a circular aperture.

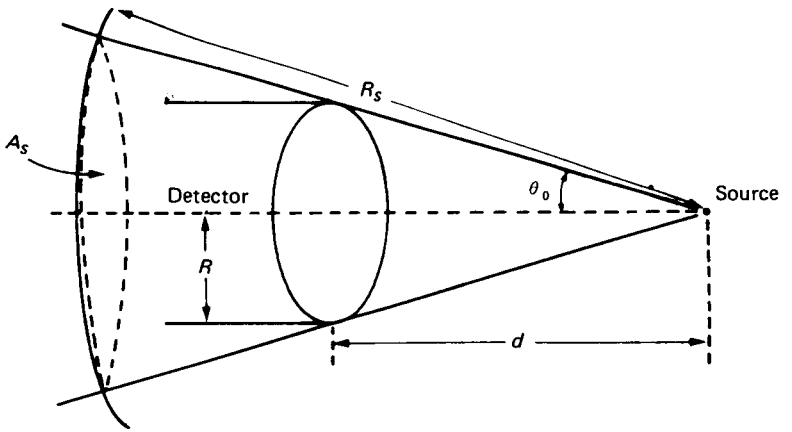


**Figure 8.6** Diagram used for the calculation of the solid angle between a point isotropic source and a detector with a circular aperture.

becomes

$$\Omega = \frac{A_s(S_0/4\pi R_s^2)}{S_0} = \frac{A_s}{4\pi R_s^2}$$

The area $A_s$ is given by (Fig. 8.7):

$$A_s = \int dA_s = \int (R_s\, d\theta)(R_s \sin\theta\, d\phi) = R_s^2 \int_0^{2\pi} d\phi \int_0^{\theta_0} d\theta \sin\theta$$
$$= 2\pi R_s^2(1 - \cos\theta_0)$$

Therefore, the expression for the solid angle becomes

$$\Omega = \frac{A_s}{4\pi R_s^2} = \frac{2\pi R_s^2(1 - \cos\theta_0)}{4\pi R_s^2} = \frac{1}{2}(1 - \cos\theta_0) \tag{8.7a}$$

which is, of course, Eq. 8.7.

If $R \ll d$, Eq. 8.5 takes the form [after expanding the square root (Eq. 8.6) and keeping only the first two terms]

$$\Omega = \frac{R_2}{4d^2} = \frac{\pi R^2}{4\pi d^2} = \frac{\text{detector aperture}}{4\pi d^2} \tag{8.8}$$

Equation 8.8 is valid even for a noncylindrical detector *if the source-detector distance is much larger than any of the linear dimensions of the detector aperture.*

**Example 8.1** A typical Geiger-Muller counter is a cylindrical detector with an aperture 50 mm in diameter. What is the solid angle if a point isotropic source is located 0.10 m away from the detector?

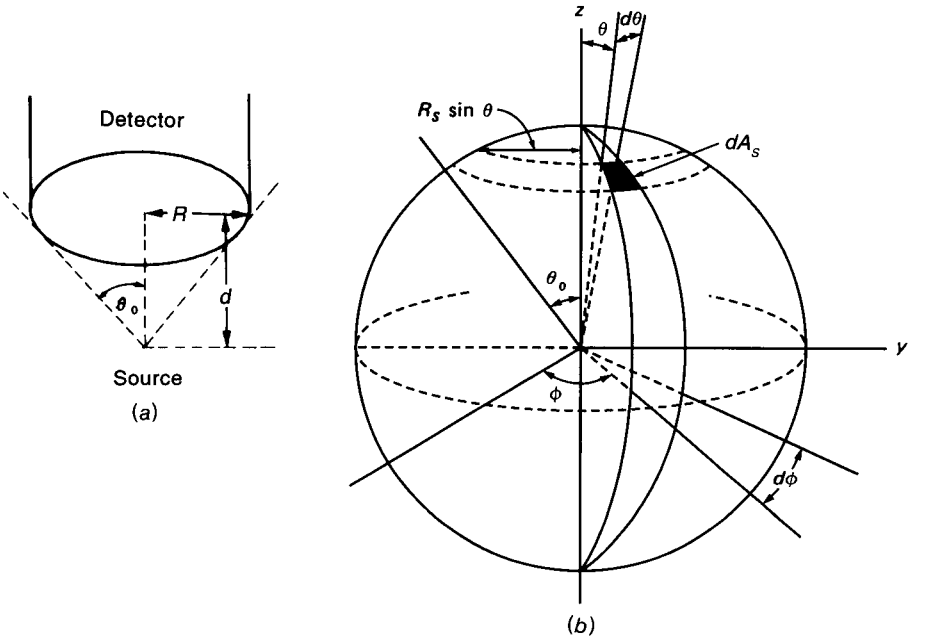


**Figure 8.7** (*a*) The detector is at distance $d$ from the source. (*b*) The source is assumed to be at the center of the sphere. The cone defined by the angle $\theta_0$ determines the area $A_s$ (differential area $dA$) on the surface of the sphere.

**Answer** Using Eq. 8.5 with $d = 0.10$ m and $R = 25$ mm,

$$\Omega = \frac{1}{2}\left[1 - \frac{0.10}{\sqrt{0.10^2 + (25 \times 10^{-3})^2}}\right] = 0.015$$

If $\Omega = 1$, the setup is called a $4\pi$ geometry because the detector sees the full $4\pi$ solid angle around the source. A spherical detector represents such a case (Fig. 8.8*a*). If $\Omega = \frac{1}{2}$, the setup is called a $2\pi$ geometry. Then half of the particles emitted by the source enter the detector (Fig. 8.8*b*).

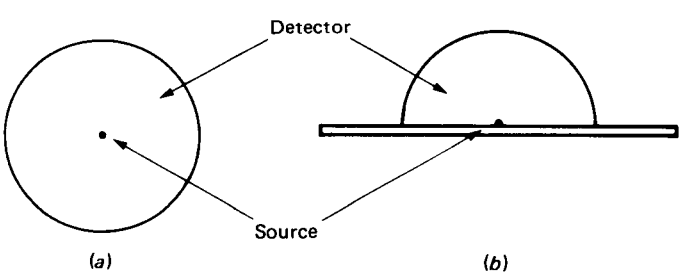


**Figure 8.8** (*a*) $4\pi$ Geometry. (*b*) $2\pi$ Geometry.

### 8.2.4 The Solid Angle for a Disk Source Parallel to a Detector with a Circular Aperture

Consider a disk source parallel to a detector with a circular aperture (Fig. 8.9). Starting with Eq. 8.4, one may obtain an expression involving elliptic integrals[1,2] or the following equation in terms of Bessel functions[3,22]:

$$\Omega = s\int_0^\infty dx\, e^{-xz}\frac{J_1(x)}{x}J_1(xs) \tag{8.9}$$

where $s = R_d/R_s$, $z = d/R_s$, and $J_1(x)$ = Bessell function of the first kind. If $R_d/d$ and $R_s/d$ are less than 1, the following algebraic expression is obtained for the solid angle (see Prob. 8.1):

$$\Omega = \frac{\omega^2}{4}\left\{1 - \frac{3}{4}(\psi^2 + \omega^2) + \frac{15}{8}\left(\frac{\psi^4 + \omega^4}{3} + \psi^2\omega^2\right) - \frac{35}{16}\left[\frac{\psi^6 + \omega^6}{4} + \frac{3}{2}\psi^2\omega^2(\psi^2 + \omega^2)\right]\right\} \tag{8.10}$$

where $\psi = R_s/d$
$\omega = R_d/d$

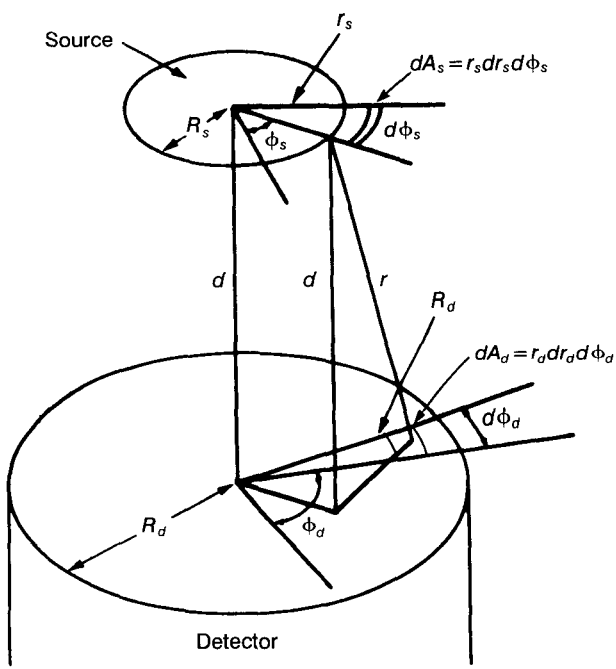


**Figure 8.9** A disk source and a detector with a circular aperture.

The accuracy of Eq. 8.10 increases as $\psi$ and $\omega$ decrease. If $\psi < 0.2$ and $\omega < 0.5$, the error is less than 1 percent.

### 8.2.5 The Solid Angle for a Point Isotropic Source and a Detector with a Rectangular Aperture

Consider the geometry of Fig. 8.10 with a point isotropic source located a distance $d$ away from a detector having a rectangular aperture with area equal to $ab$. The solid angle is given by[4]

$$\Omega = \frac{1}{4\pi} \arctan \frac{ab}{d\sqrt{a^2 + b^2 + d^2}} \tag{8.11}$$

If the source is located at an arbitrary point above the detector, the solid angle is the sum of four terms (Fig. 8.11), each of them similar to Eq. 8.11. As Fig. 8.11 shows, the detector is divided into four rectangles by the lines that determine the coordinates of the point P. The solid angle is then

$$\Omega = \Omega_1 + \Omega_2 + \Omega_3 + \Omega_4$$

where $\Omega_i$ for $i = 1, \ldots, 4$ is given by Eq. 8.11 for the corresponding rectangles.

### 8.2.6 The Solid Angle for a Disk Source and a Detector with a Rectangular Aperture

Consider the geometry shown in Fig. 8.12. A disk source is located at a distance $d$ above a detector having a rectangular aperture with an area equal to $ab$. It is assumed that the center of the source is directly above one corner of the aperture, as shown in Fig. 8.12. The more general case of the arbitrary position of the source is derived from the present example.

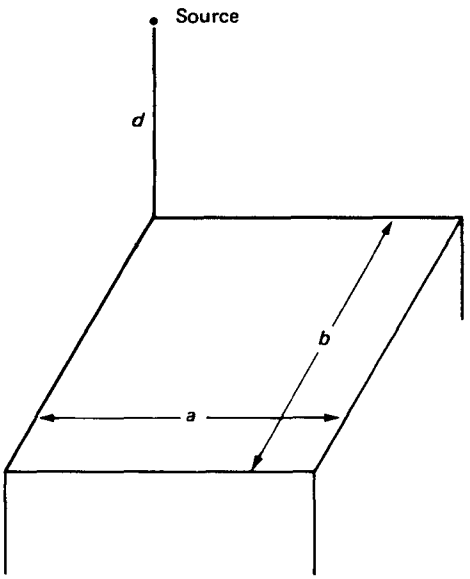


**Figure 8.10** The solid angle between a point isotropic source and a detector with a rectangular aperture. Source is located directly above one corner of the detector.

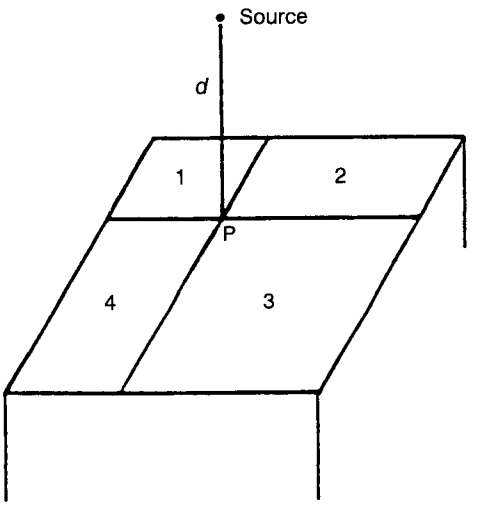


**Figure 8.11** A point isotropic source located at an arbitrary point above a detector with a rectangular aperture. The solid angle is equal to four terms, each given by Eq. 8.11.

The distance $r$ (Fig. 8.12) is equal to

$$r^2 = d^2 + r_S^2 + x^2 + y^2 - 2r_S\sqrt{x^2 + y^2}\cos\left[\phi_s - \cos^{-1}\left(\frac{x}{\sqrt{x^2 + y^2}}\right)\right]$$

Equation 8.4 is then written as

$$\Omega = \frac{1}{4\pi A_S d^2}\int_0^{R_S} dr_S\, r_S \int_0^{2\pi} d\phi_S \int_0^a dx \int_0^b dy \left\{1 + \frac{r_S^2}{d^2} + \frac{x^2}{d^2} + \frac{y^2}{d^2} - 2\frac{r_S}{d}\sqrt{\frac{x^2 + y^2}{d^2}}\cos\left[\phi_s - \cos^{-1}\left(\frac{x}{\sqrt{x^2 + y^2}}\right)\right]\right\} \tag{8.12}$$

As in Sec. 8.2.4, if the ratios $R_s/d$, $a/d$, and $b/d$ are less than 1, the expression in the braces may be expanded in a series. If only the first four terms are kept, the result of the integration is

$$\begin{aligned}\Omega = \frac{\omega_1\omega_2}{4\pi}\Bigg[&1 - \frac{3}{4}\psi^2 - \frac{1}{2}(\omega_1^2 + \omega_2^2) + \frac{1}{8}(5\psi^4 + 3\omega_1^4 + 3\omega_2^4) \\ &+ \frac{5}{4}\psi^2(\omega_1^2 + \omega_2^2) - \frac{35}{64}\psi^6 + \frac{5}{12}\omega_1^2\omega_2^2 - \frac{35}{16}\psi^4(\omega_1^2 + \omega_2^2) \\ &- \frac{7}{32}\psi^2(9\omega_1^4 + 9\omega_2^4 + 10\omega_1^2\omega_2^2) - \frac{7}{16}\omega_1^2\omega_2^2(\omega_1^2 + \omega_2^2) \\ &- \frac{5}{16}(\omega_1^6 + \omega_2^6)\Bigg]\end{aligned} \tag{8.13}$$

where $\omega_1 = a/d$
$\omega_2 = b/d$
$\psi = R_s/d$

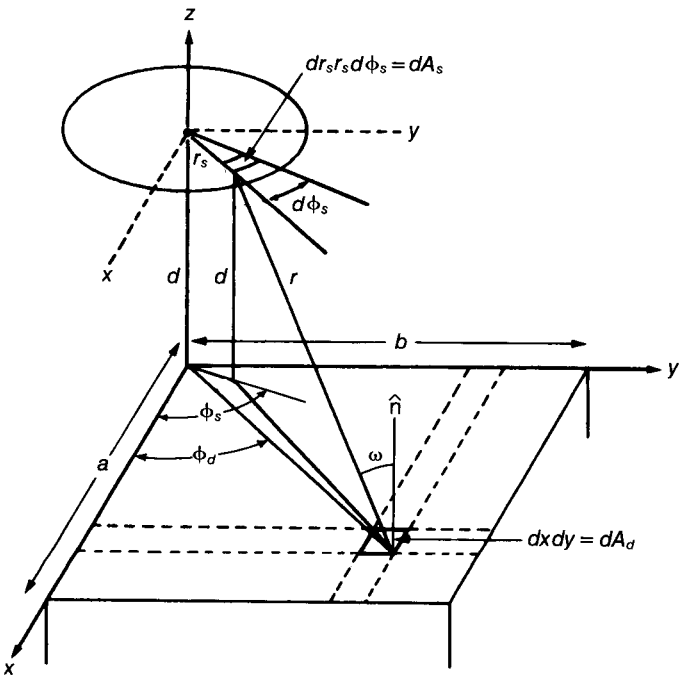


**Figure 8.12** A disk source and a detector with a rectangular aperture.

If the source is located at an arbitrary point above the detector, the solid angle is the sum of four terms as shown in Fig. 8.11.

### 8.2.7 The Use of the Monte Carlo Method for the Calculation of the Solid Angle

The basic equation defining the geometry factor (Eq. 8.4) can be solved analytically in very few cases. Approximate solutions can be obtained either by a series expansion (Eqs. 8.10 and 8.13 are such results) or by a numerical integration or using other approximations,[1,5,6]

A general method that can be used with any geometry is based on a Monte Carlo calculation,[7-10] which simulates, in a computer, the emission and detection of particles. A computer program is written based on a model of the source-detector geometry. Using random numbers, the particle position of birth and the direction of emission are determined. The program then checks whether the randomly selected direction intersects the detector volume. By definition, the ratio of particles hitting the detector to those emitted by the source is equal to the solid angle.

The advantage of a Monte Carlo calculation is the ability to study complicated geometries. The result has an error associated with it that decreases as the number of particles studied increases.

## 8.3 SOURCE EFFECTS

Two source effects are discussed in this section: absorption of particles in the source, and the effect of the backing material that supports the source. Both effects are always important in measurements of charged particles. In some cases, however, they may also be significant in X-ray or thermal-neutron measurements.

### 8.3.1 Source Self-Absorption Factor ($f_a$)

Radioactive substances are deposited on a backing material in thin deposits. But no matter how thin, the deposit has a finite thickness and may cause absorption of some particles emitted by the source. Consider the source of thickness $t$ shown in Fig. 8.13. Particle 1 traverses the source deposit and enters the detector. Particle 2 is absorbed inside the source so that it will not be counted. Therefore, source self-absorption will produce a decrease of the counting rate $r$.

Source self-absorption may be reduced to an insignificant amount but it cannot be eliminated completely. It is always important for charged particles and generally more crucial for heavier particles ($p, \alpha, d$, heavy ions) than for electrons.

Source self-absorption, in addition to altering the number of particles leaving the source, may also change the energy of the particles escaping from it. Particle 1 in Fig. 8.13 successfully leaves the deposit, but it loses some energy as it goes through the deposit. This energy loss is important when the energy of the particle is measured.

An approximate correction for self-absorption can be obtained if the source emits particles following a known attenuation law. As an example, consider a source with thickness $t$ (Fig. 8.14) that has a uniform deposit of a radioisotope emitting $\beta$ particles. Assume that the source gives $S$ betas per second in the direction of the positive $x$ axis. If self-absorption is absent, $S$ betas per second

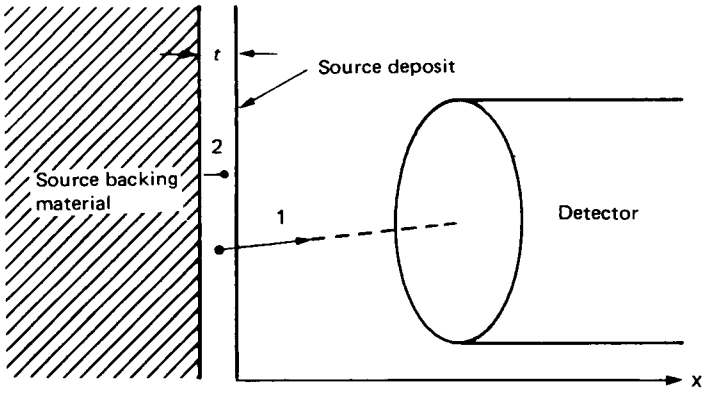


**Figure 8.13** Source self-absorption. Particles may be absorbed in the source deposit.

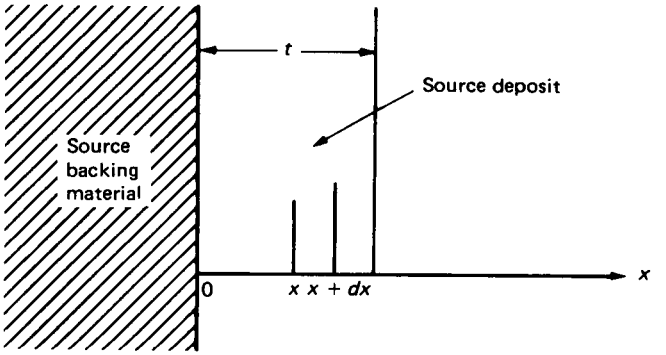


**Figure 8.14** Diagram used for the calculation of the source self-absorption factor for betas.

will leave the source (toward positive $x$). Because of the source thickness, betas produced in $dx$, around $x$, have to successfully penetrate the thickness $(t - x)$ to escape. The probability of escape is $e^{-\mu(t-x)}$, where $\mu$ is the attenuation coefficient for the betas in the material of which the deposit is made. The total number of betas escaping is

$$\int_0^t \frac{dx}{t} S e^{-\mu(t-x)} = \frac{S}{t\mu}(1 - e^{-\mu t})$$

A self-absorption factor $f_a$ is defined by

$$f_a = \frac{\text{number of particles leaving source with self-absorption}}{\text{number of particles leaving source without self-absorption}}$$

Using the result obtained above,

$$f_a = \frac{(S/t\mu)(1 - e^{-\mu t})}{S} = \frac{1}{t\mu}(1 - e^{-\mu t}) \qquad 0 \le f_a \le 1 \qquad (8.14)$$

**Example 8.2** Assume that $^{137}$Cs was deposited on a certain material. The thickness of the deposit is $t = 0.1$ mm. $^{137}$Cs emits betas with $E_{max} = 0.514$ MeV. What is the value of $f_a$ for such a source? The density of cesium is $1.6 \times 10^3$ kg/m$^3$.

**Answer** For betas of $E_{max} = 0.514$ MeV, the attenuation coefficient is (from Chap. 4)

$$\mu = 1.7E_{max}^{-1.14} \qquad \mu = 1.7(0.514)^{-1.14} = 2.14 \text{ m}^2/\text{kg}$$

$$\mu t = (2.14 \text{ m}^2/\text{kg})(0.1 \times 10^{-3} \text{ m})(1.6 \times 10^3 \text{ kg/m}^3) = 0.34$$

Using Eq. 8.14,

$$f_a = \frac{1}{0.34}(1 - e^{-0.34}) = 0.85$$

Therefore, only 85 percent of the betas escape this source. Or, if this effect is not taken into account, the source strength will have an error of 15 percent.†

If the source emits monoenergetic charged particles, essentially all the particles leave the source deposit as long as $t < R$, where $R$ = range of the particles. In practice, the sources for monoenergetic charged particles are such that $t \ll R$, in which case, $f_a \approx 1$. Then the only effect of the source deposit is an energy loss for the particles that traverse it (see also Chap. 13).

### 8.3.2 Source Backscattering Factor ($f_b$)

A source cannot be placed in midair. It is always deposited on a material that is called *source backing* or *source support*. The source backing is usually a very thin material, but no matter how thin, it may backscatter particles emitted in a direction away from the detector (Fig. 8.15). To understand the effect of backscattering, assume that the solid angle in Fig. 8.15 is $\Omega = 10^{-2}$. Also assume that all the particles entering the detector are counted, self-absorption is zero, and there is no other medium that might absorb or scatter the particles except the source backing.

Particle 1 in Fig. 8.15 is emitted toward the detector. Particle 2 is emitted in the opposite direction. Without the source backing, particle 2 would not turn back. With the backing material present, there is a possibility that particle 2 will have scattering interactions there, have its direction of motion changed, and enter the detector. If the counting rate is $r = 100$ counts per minute and there is no backscattering of particles toward the detector, the strength of the source

†A similar calculation of $f_a$ may be repeated for an X-ray or a neutron source. For X-rays the probability of escape $e^{-\mu t}$; for neutrons it is $e^{-\Sigma t}$.

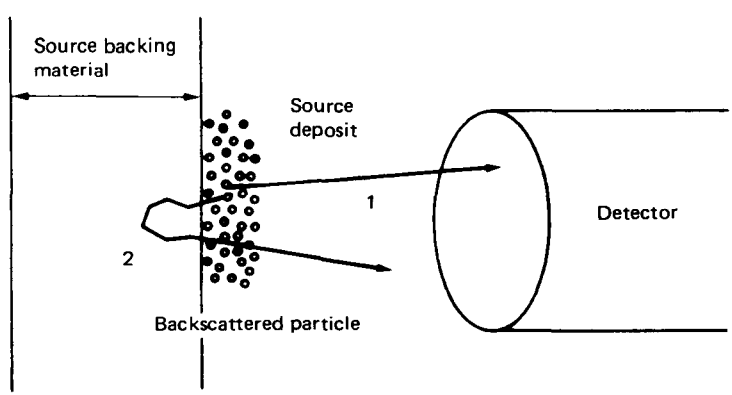


**Figure 8.15** The source backing material backscatters particles and necessitates the use of a backscattering factor $f_b$.

will be correctly determined as

$$S = \frac{r}{\Omega} = \frac{100}{10^{-2}} = 10{,}000 \text{ part./min}$$

If the source backing backscatters 5 percent of the particles, the counting rate will become 105 counts per minute, even though it is still the same source as before. If source backscattering is not taken into account, the source strength will be erroneously determined as

$$S = \frac{r}{\Omega} = \frac{105}{10^{-2}} = 10{,}500 \text{ part./min}$$

To correct properly for this effect, a source backscattering factor ($f_b$) is defined by

$$f_b = \frac{\text{number of particles counted with source backing}}{\text{number of particles counted without source backing}} \tag{8.15}$$

From the definition it is obvious that

$$2 > f_b \geq 1$$

In the example discussed above, $f_b = 1.05$, and the correct strength of the source is

$$S = \frac{r}{\Omega f_b} = \frac{105}{10^{-2} \times 1.05} = 10{,}000 \text{ part./min}$$

The backscattering factor is important, in most cases, only for charged particles. It depends on three variables:

1. Thickness ($b$) of the backing material
2. Particle kinetic energy ($T$)
3. Atomic number of the backing material ($Z$)

The dependence of $f_b$ on thickness $b$ is shown in Fig. 8.16. As $b \to 0$, $f_b \to 1$, which should be expected. For large thicknesses, $f_b$ reaches a saturation

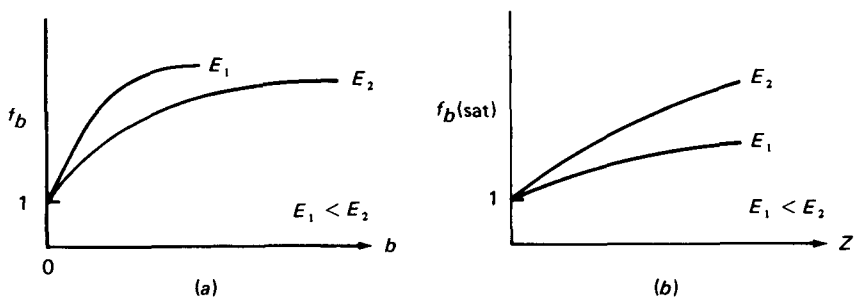


**Figure 8.16** (*a*) The backscattering factor $f_b$ as a function of thickness $b$ of the backing material. (*b*) The saturation backscattering factor as a function of the atomic number $Z$ of the backing material.

value, which should also be expected. Since charged particles have a definite range, there is a maximum distance they can travel in the backing material, be backscattered, and traverse the material again in the opposite direction. Therefore an upper limit for that thickness is $b = R/2$, where $R$ is the range of the particles. Experiments have shown that

$$b_s = b(\text{saturation}) \approx 0.2R$$

The dependence of the saturation backscattering factor of electrons on the kinetic energy and the atomic number of the backing material is given by the following empirical equation,[11,12] based on a least-squares fit of experimental results:

$$f_b(\text{sat}) = 1 + \frac{b_1 \exp(-b_2 Z^{-b_3})}{1 + (b_4 + b_5 Z^{-b_6})\alpha^{(b_7 - b_8/Z)}} \tag{8.16}$$

where the constants $b_i$ for $i = 1, 2, \ldots, 8$ have these values:

$$b_1 = 1.15 \pm 0.06 \qquad b_5 = 15.7 \pm 3.1 \qquad \alpha = \frac{T}{mc^2}$$

$$b_2 = 8.35 \pm 0.25 \qquad b_6 = 1.59 \pm 0.07$$

$$b_3 = 0.525 \pm 0.02 \qquad b_7 = 1.56 \pm 0.02$$

$$b_4 = 0.0185 \pm 0.0019 \qquad b_8 = 4.42 \pm 0.18$$

Figure 8.17 shows the change of $f_b(\text{sat})$ versus kinetic energy $T$ for four elements.

A backscattering correction should be applied to alpha counting in $2\pi$ counters (Fig. 8.8*b*). It has been determined[13-15] that the number of backscat-

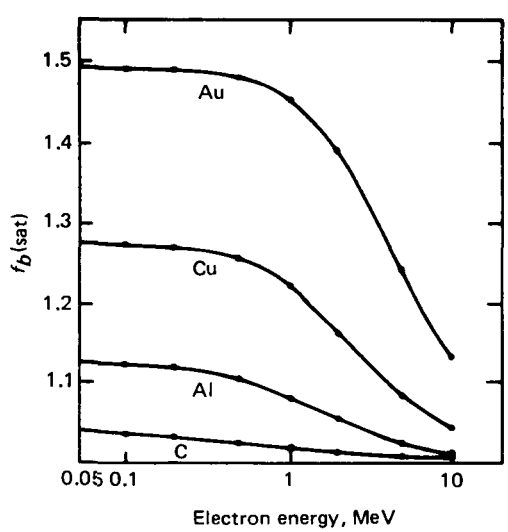


**Figure 8.17** Backscattering factor as a function of energy for C, Al, Cu, and Au. Curves were obtained using Eq. 8.16.

tered alphas is between 0 and 5 percent, depending on the energy of the alphas, the uniformity of the source, and the atomic number of the material forming the base of the counter.

Correction for source backscattering is accomplished in two ways:

1. An extremely thin backing material is used for which $f_b \approx 1$. In general, a low-$Z$ material is used, e.g., plastic, if possible.
2. A thick backing material is used, for which the saturation backscattering factor should be employed for correction of the data.

For accurate results, the backscattering factor should be measured for the actual geometry of the experiment.

## 8.4 DETECTOR EFFECTS

The detector may affect the measurement in two ways. First, if the source is located outside the detector (which is usually the case), the particles may be scattered or absorbed by the detector window. Second, some particles may enter the detector and not produce a signal, or they may produce a signal lower than the discriminator threshold.

### 8.4.1 Scattering and Absorption Due to the Window of the Detector

In most measurements the source is located outside the detector (Fig. 8.18). The radiation must penetrate the detector window to have a chance to be counted. Interactions between the radiation and the material of which the detector wall is made may scatter and/or absorb particles. This is particularly important for low-energy $\beta$ particles.

Figure 8.18 shows a gas-filled counter and a source of radiation placed outside it. Usually the particles enter the detector through a *window* made of a

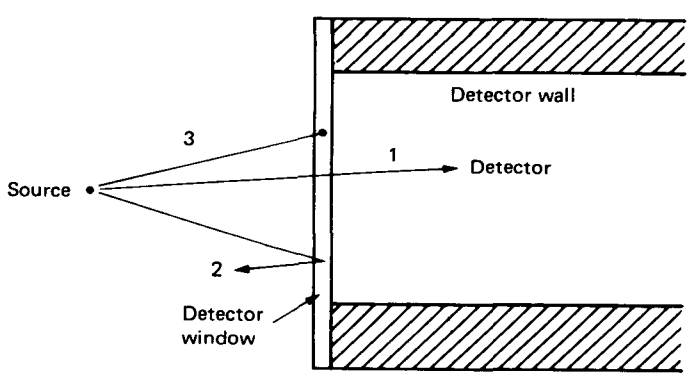


**Figure 8.18** The window of the detector may scatter and/or absorb some of the particles emitted by the source.

very thin material (such as glass, mica, or thin metal). Looking at Fig. 8.18, most of the particles, like particle 1, traverse the window and enter the counter. But, there is a possibility that a particle, like particle 2, may be scattered at the window and never enter the counter. Or, it may be absorbed by the material of the window (particle 3).

In the case of scintillation counters, the window consists of the material that covers the scintillator and makes it light-tight. In some applications the source and the scintillator are placed in a light-tight chamber, thus eliminating the effects of a window.

In semiconductor detectors, the window consists of the metallic layer covering the front face of the detector. That layer is extremely thin, but may still affect measurements of alphas and heavier charged particles because of energy loss there.

There is no direct way to correct for the effect of the window. Commercial detectors are made with very thin windows, but the investigator should examine the importance of the window effect for the particular measurement performed. If there is a need for an energy-loss correction, it is applied separately to the energy spectrum. If, however, there is a need to correct for the number of particles stopped by the window, that correction is incorporated into the detector efficiency.

### 8.4.2 Detector Efficiency ($\epsilon$)

It is not certain that a particle will be counted when it enters a detector. It may, depending on the type and energy of the particle and type and size of detector, go through without having an interaction (particle 1 in Fig. 8.19); it may produce a signal so small it is impossible to record with the available electronic instruments (particle 3); or, it may be prevented from entering the detector by the window (particle 4). In Fig. 8.19, the particle with the best chance of being detected is particle 2.

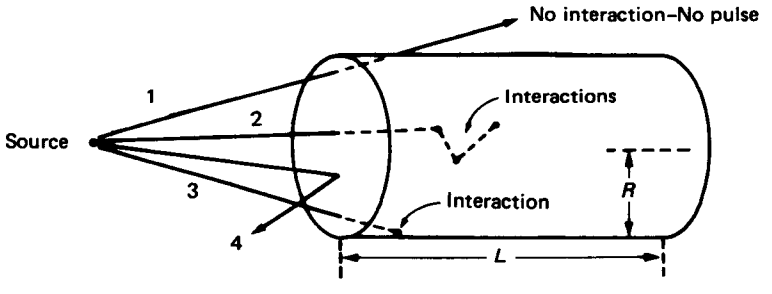


**Figure 8.19** Particles detected are those that interact inside the detector and produce a pulse higher than the discriminator level.

The quantity that gives the fraction of particles being detected is called the *detector efficiency* $\epsilon$, given by

$$\epsilon = \frac{\text{number of particles recorded per unit time}}{\text{number of particles impinging upon the detector per unit time}} \tag{8.17}$$

The detector efficiency depends upon†

1. Density and size of detector material
2. Type and energy of radiation
3. Electronics

**Effect of density and size of detector material.** The efficiency of a detector will increase if the probability of an interaction between the incident radiation and the material of which the detector is made increases. That probability increases with detector size. But larger size is of limited usefulness because the background increases proportionally with the size of the detector, and because in some cases it is practically impossible to make large detectors. (Semiconductor detectors are a prime example.)

The probability of interaction per unit distance traveled is proportional to the density of the material. The density of solids and liquids is about a thousand times greater than the density of gases at normal pressure and temperature. Therefore, other things being equal, detectors made of solid or liquid material are more efficient than those using gas.

**Effect of type and energy of radiation.** Charged particles moving through matter will always have Coulomb interactions with the electrons and nuclei of that medium. Since the probability of interaction is almost a certainty, the efficiency for charged particles will be close to 100 percent. Indeed, detectors for charged particles have an efficiency that is practically 100 percent, regardless of their size or the density of the material of which they are made. For charged particles, the detector efficiency is practically independent of particle energy except for very low energies, when the particles may be stopped by the detector window.

Charged particles have a definite range. Therefore, it is possible to make a detector with a length $L$ such that all the particles will stop and deposit their energy in the counter. Obviously, the length $L$ should be greater than $R$, where $R$ is the range of the particles in the material of which the detector is made.

Photons and neutrons traversing a medium show an exponential attenuation (see Chap. 4), which means that there is always a nonzero probability for a photon or a neutron to traverse any thickness of material without an interaction. As a result of this property, detectors for photons or neutrons have efficiency less than 100 percent regardless of detector size and energy of the particle.

†In gamma spectroscopy, several other efficiencies are being used in addition to this one (see Chap. 12).

**Effect of electronics.** The electronics of a detector affects the counter efficiency indirectly. If a particle interacts in the detector and produces a signal, that particle will be recorded only if the signal is recorded. The signal will be registered if it is higher than the discriminator level, which is, of course, determined by the electronic noise of the counting system. Thus, the counting efficiency may increase if the level of electronic noise is decreased.

As an example, consider a counting system with electronic noise such that the discriminator level is at 1 mV. In this case, only pulses higher than 1 mV will be counted; therefore, particles that produce pulses lower than 1 mV will not be recorded. Assume next that the preamplifier or the amplifier or both are replaced by quieter ones, and the new noise level is such that the discriminator level can be set at 0.8 mV. Now, pulses as low as 0.8 mV will be registered, more particles will be recorded, and hence the efficiency of the counting system increases.

If electronics is included in the discussion, it is the efficiency of the *system* (detector plus electronics) that is considered rather than the efficiency of the counter.

### 8.4.3 Determination of Detector Efficiency

The efficiency of a detector can be determined either by measurement or by calculation. Many methods have been used for the measurement of detection efficiency,[16-18] but the simplest and probably the most accurate is the method of using a calibrated source, i.e., a source of known strength. In Fig. 8.19, assume that the source is a monoenergetic point isotropic source emitting $S$ particles per second. If the true net counting rate is $r$ counts per second, the solid angle is $\Omega$, and the efficiency is $\epsilon$, the equation giving the efficiency is

$$\epsilon(E) = \frac{r}{\Omega F(E) S} \tag{8.18}$$

where $F = f_a f_b \cdots$ is a combination of all the correction factors that may have to be applied to the results. Note that the correction factors and the efficiency depend on the energy of the particle.

Accurate absolute measurements rely on measured rather than calculated efficiencies. Nevertheless, an efficiency calculation is instructive because it brings forward the parameters that are important for this concept. For this reason, two cases of efficiency calculation for a photon detector are presented below.

Consider first a parallel beam of photons of energy $E$ impinging upon a detector of thickness $L$ (Fig. 8.20). The probability that a photon will have at least one interaction in the detector is $1 - e^{-\mu(E)L}$, where $\mu(E)$ is the total linear attenuation coefficient of photons with energy $E$ in the material of which the detector is made. If one interaction is enough to produce a detectable pulse, the efficiency is

$$\epsilon(E) = 1 - e^{-\mu(E)L} \tag{8.19}$$

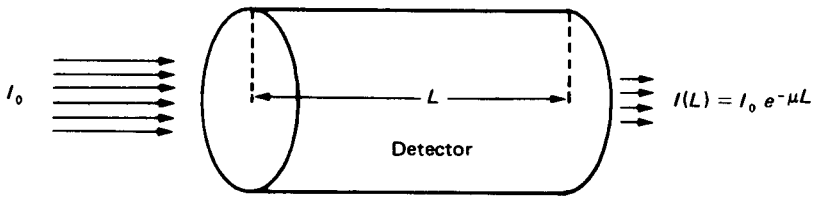


**Figure 8.20** A parallel beam of photons going through a detector of length (thickness) $L$.

Equation 8.19 shows the dependence of $\epsilon(E)$ on

1. The size $L$ of the detector
2. The photon energy (through $\mu$)
3. The density of the material (through $\mu$)

**Example 8.3** What is the efficiency of a 50-mm-long NaI(Tl) crystal for a parallel beam of (a) 2-MeV gammas or (b) 0.5-MeV gammas?

**Answer** (a) From the table in App. D, the total mass attenuation coefficient for 2-MeV gammas in NaI(Tl) is $\mu = 0.00412\ \text{m}^2/\text{kg}$. The density of the scintillator is $3.67 \times 10^3\ \text{kg/m}^3$. Therefore, Eq. 8.19 gives

$$\epsilon = 1 - \exp[-0.00412\ \text{m}^2/\text{kg}(3.67 \times 10^3\ \text{kg/m}^3)0.05\ \text{m}] = 1 - \exp(-0.756)$$
$$= 0.53 = 53\%$$

(b) For 0.50-MeV gammas, $\mu = 0.00921\ \text{m}^2/\text{kg}$. Therefore,

$$\epsilon = 1 - \exp[-0.00921\ \text{m}^2/\text{kg}(3.67 \times 10^3\ \text{kg/m}^3)0.05\ \text{m}] = 1 - \exp(-1.69)$$
$$= 0.81 = 81\%$$

The next case to consider is that of a point isotropic monoenergetic source, at a distance $d$ away from a cylindrical detector of length $L$ and radius $R$ (see Fig. 8.21). For photons emitted at an angle $\theta$, measured from the axis of the detector, the probability of interaction is $1 - \exp[-\mu(E)r(\theta)]$ and the probability of emission between angles $\theta$ and $\theta + d\theta$ is $\frac{1}{2}\sin\theta\, d\theta$. Assuming, as before, that one interaction is enough to produce a detectable pulse, the efficiency is given by

$$\epsilon(E) = \frac{\int_0^{\theta_0} S\{1 - \exp[-\mu(E)r(\theta)]\}\frac{1}{2}\sin\theta\, d\theta}{(S/2)\int_0^{\theta_0}\sin\theta\, d\theta} \tag{8.20}$$

Equation 8.20 shows that the efficiency depends, in this case, not only on $L$, $\mu$, and $E$, but also on the source-detector distance and the radius of the detector. Results obtained by numerically integrating Eq. 8.20 are given in Sec. 12.4.1,

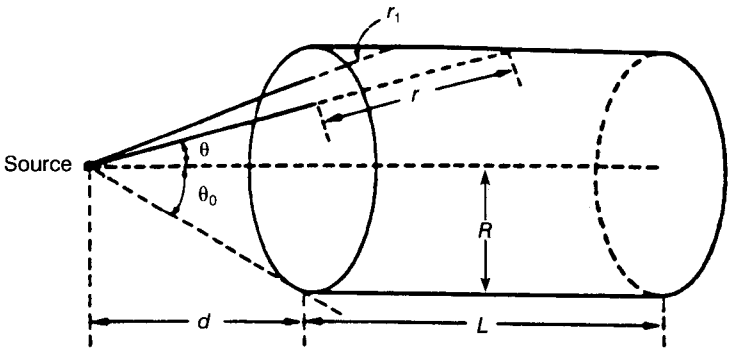


**Figure 8.21** A point isotropic photon source at a distance $d$ away from a cylindrical detector.

where the efficiency of gamma detectors is discussed in greater detail. Many graphs and tables based on Eq. 8.20 can be found in Ref. 20.

Equations 8.19 and 8.20 probably overestimate efficiency, because their derivation was based on the assumption that a single interaction of the incident photon in the detector will produce a detectable pulse. This is not necessarily the case. A better way to calculate efficiency is by determining the energy deposited in the detector as a result of all the interactions of an incident particle. Then one can compute the number of recorded particles based on the minimum energy that has to be deposited in the detector in order that a pulse higher than the discriminator level may be produced. The Monte Carlo method, which is ideal for such calculations, has been used by many investigators[10,21] for that purpose.

Efficiencies of neutron detectors are calculated by methods similar to those used for gammas. Neutrons are detected indirectly through gammas or charged particles produced by reactions of nuclei with neutrons. Thus, the neutron detector efficiency is essentially the product of the probability of a neutron interaction, with the probability to detect the products of that interaction (see Chap. 14).

## 8.5 RELATIONSHIP BETWEEN COUNTING RATE AND SOURCE STRENGTH

Equation 8.18 rewritten in terms of the true net counting rate $r$ gives the relationship between $r$ and the source strength:

$$r = \Omega F \epsilon S \tag{8.21}$$

In terms of gross counts $G$ obtained over time $t_G$ and background count $B$

obtained over time $t_B$, the true net counting rate (Eq. 2.113) is

$$r = \frac{G/t_G}{1 - (G/t_G)\tau} - \frac{B}{t_B} \tag{8.22}$$

where $\tau$ is the counter dead time. Usually the objective of the measurement is to obtain the source strength $S$ using a detection system of known $\Omega$, $F$, and $\epsilon$. Combining Eqs. 8.21 and 8.22, the source strength becomes

$$S = \frac{r}{\Omega F \epsilon} = \frac{1}{\Omega F \epsilon}\left(\frac{G/t_G}{1 - (G/t_G)\tau} - \frac{B}{t_B}\right) \tag{8.23}$$

The error in the value of $S$ is due to errors in the values of $\Omega$, $F$, $\epsilon$, and the statistical error of $r$. In many cases encountered in practice, the predominant error is that of $r$. Then one obtains, from Eq. 8.23,

$$\frac{\sigma_S}{S} = \frac{\sigma_r}{r}$$

That is, the percent error of $S$ is equal to the percent error of the true net counting rate $r$.

**Example 8.4** The geometric setup shown in Fig. 8.22 was used for the measurement of the strength of the radioactive source. The following data were obtained:

$$G = 6000 \qquad B = 400 \qquad \tau = 100\ \mu\text{s} \qquad \epsilon = 0.60 \pm 0.005$$
$$t_G = 10\ \text{min} \qquad t_B = 10\ \text{min} \qquad F = 1 \pm 0.001$$

What is the strength $S$ and its standard error?

**Answer** The true net counting rate $r$ is

$$r = \frac{60000/10}{1 - (6000 \times 100 \times 10^{-6}/10 \times 60)} - \frac{400}{10} = \frac{6000/10}{0.999} - 40$$
$$= 600.6 - 40 \approx 561 \quad \text{counts/min}$$

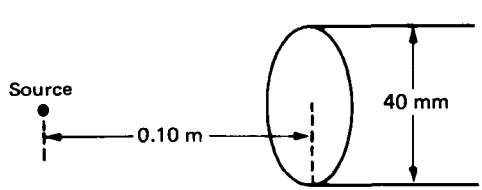


**Figure 8.22** Geometry assumed in Example 8.4.

The standard error of $r$ is (Eq. 2.114)

$$\sigma_r = \sqrt{\left(\frac{1}{1-(G/t_G)\tau}\right)^4 \frac{G}{t_G^2} + \frac{B}{t_B^2}} = \sqrt{\left(\frac{1}{0.999}\right)^4 \frac{6000}{100} + \frac{400}{100}} = 8 \text{ counts/min}$$

Therefore

$$\frac{\sigma_r}{r} = \frac{8}{561} = 1.4\%$$

The solid angle is

$$\Omega = \frac{1}{2}\left(1 - \frac{d}{\sqrt{d^2 + r^2}}\right) = 0.0097$$

Using Eq. 8.23,

$$S = \frac{r}{\Omega F \epsilon} = \frac{561}{(0.0097)(0.60)} = 96{,}392 \text{ part./min}$$

The standard error of $S$ is (Sec. 2.15.1)

$$\frac{\sigma_S}{S} = \sqrt{\left(\frac{\sigma_r}{r}\right)^2 + \left(\frac{\sigma_F}{F}\right)^2 + \left(\frac{\sigma_\epsilon}{\epsilon}\right)^2}$$

$$= \sqrt{(1.4 \times 10^{-2})^2 + \left(\frac{0.001}{1}\right)^2 + \left(\frac{0.005}{0.60}\right)^2} = 1.7 \times 10^{-2} = 1.7\%$$

## PROBLEMS

**8.1** Show that if $R_d/d < 1$ and $R_s/d < 1$, the solid angle between two parallel disks with radii $R_d$ and $R_s$ a distance $d$ apart is given to a good approximation by

$$\Omega = \frac{\omega^2}{4}\left\{1 - \frac{3}{4}(\psi^2 + \omega^2) + \frac{15}{8}\left(\frac{\psi^4 + \omega^4}{3} + \psi^2\omega^2\right) - \frac{35}{16}\left[\frac{\psi^6 + \omega^6}{4} + \frac{3}{2}\psi^2\omega^2(\psi^2 + \omega^2)\right]\right\}$$

where $\psi = R_s/d$ and $\omega = R_d/d$.

**8.2** Show that an approximate expression for the solid angle between two nonparallel disks is

$$\Omega = \frac{\omega^2}{4}\left\{1 - \frac{3}{4}[(\psi^2 + \omega^2(1 + \sin^2\theta)] + \frac{15}{8}\left[\frac{\omega^4 + \psi^4}{3} + \psi^2\omega^2 + \psi^2\left(1 + \frac{1}{4}\omega^2 + \frac{2}{3}\psi^2\right)\sin^2\theta\right]\right\}$$

where $\theta$ is the angle between the planes of the two disks, and $\psi$ and $\omega$ are defined as in Prob. 8.1.

**8.3** Show that the solid angle between a disk source and a detector with a rectangular aperture is given, approximately, by Eq. 8.13 under the conditions given in Sec. 8.2.6.

**8.4** A 1-mCi point isotropic gamma source is located 0.10 m away from a 60° spherical shell of a NaI detector, as shown in the figure below. Assuming that all the pulses at the output of the photomultiplier tube are counted, what is the counting rate of the scaler? The gamma energy is 1.25 MeV.

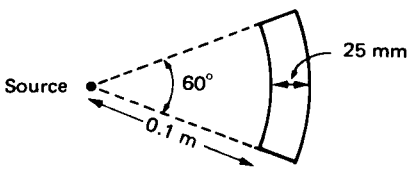


**8.5** Calculate the counting rate for the case shown in the figure below. The source has the shape of a ring and emits $10^6$ part./s isotopically. The background is zero. The detector efficiency is 80 percent, and $F = 1$.

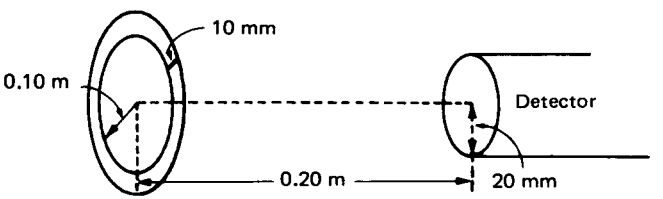


**8.6** Calculate the self-absorption factor for a $^{14}C$ source that has a thickness of 10 $\mu g/cm^2$ ($10^{-4}$ $kg/m^2$); $E_{max} = 156$ keV.

**8.7** An attempt was made to measure the backscattering factor by placing foils of continuously increasing thickness behind the source and observing the change in the counting rate. The foils were of the same material as the source backing. The results of the measurements are given in the table below. Calculate the saturation backscattering factor and the source backscattering factor.

| Thickness behind source (mm) | Counting rate (counts/min) |
|---|---|
| 0.1 (Source backing only) | 3015 |
| 0.15 | 3155 |
| 0.2 | 3365 |
| 0.25 | 3400 |
| 0.3 | 3420 |
| 0.35 | 3430 |
| 0.4 | 3430 |

**8.8** What is the counting rate in a detector with a rectangular aperture measuring 1 mm × 40 mm, if a 1-mCi gamma-ray point isotropic source is 0.10 m away? The efficiency of the detector for these gammas is 65 percent.

**8.9** A radioactive source emits electrons isotropically at the rate of $10^4$ electrons/s. A plastic scintillator having the shape of a cylindrical disk with a 25-mm-radius is located 120 mm away from the source. The efficiency of the detector for these electrons is 95 percent. The backscattering factor is 1.02, and the source self-absorption factor is 0.98. Dead time of the counting system is 5 $\mu$s. How long should one count, under these conditions, to obtain the strength of the source with a standard error of 5 percent? Background is negligible. The only error involved is that due to counting statistics.

**8.10** How would the result of Prob. 8.9 change if the backscattering factor was known with an error of $\pm 1$ percent, the efficiency with an error of $\pm 0.5$ percent, and the source self-absorption factor with an error of $\pm 1$ percent?

**8.11** Calculate the strength of a point isotropic radioactive source if it is given that the gross counting rate is 200 counts/min, the background counting rate is 25 counts/min, the counter efficiency is 0.90, the source detector distance is 0.15 m, and the detector aperture has a radius of 20 mm ($F = 1$). What is the standard error of the results if the error of the gross counting rate is known with an accuracy of $\pm 5$ percent and the background with $\pm 3$ percent? Dead time is 1 $\mu$s.

**8.12** A point isotropic source is located at the center of a hemispherical $2\pi$ counter. The efficiency of this detector for the particles emitted by the source is 85 percent. The saturation backscattering factor is 1.5. The background is $25 \pm 1$ counts/min. What is the strength of the source if 3000 counts are recorded in 1 min? What is the standard error of this measurement?

## REFERENCES


1. Masket, A. V., *Rev. Sci. Instrum.* **28**:191 (1957).
2. Ruffle, M. P., *Nucl. Instrum. Meth.* **52**:354 (1967).
3. Ruby, L., and Rechen, J. B., *Nucl. Instrum. Meth.*, **58**:345 (1968).
4. Gotoh, H., and Yagi, H., *Nucl. Instrum. Meth.* **96**:485 (1971).
5. Gardner, R. P., and Verghese, K., *Nucl. Instrum. Meth.* **93**:163 (1971).
6. Verghese, K., Gardner, R. P. and Felder, R. M., *Nucl. Instrum. Meth.* **101**:391 (1972).
7. Williams, I. R., *Nucl. Instrum. Meth.* **44**:160 (1966).
8. Green, M. V., Aamodt, R. L., and Johnston, G. S., *Nucl. Instrum. Meth.* **117**:409 (1974).
9. Wielopolski, L., *Nucl. Instrum. Meth.* **143**:577 (1977).
10. Beam, G. B., Wielopolski, L., Gardner, R. P., and Verghese, K., *Nucl. Instrum. Meth.* **154**:501 (1978).
11. Tabata, T., Ito, R., and Okabe, S., *Nucl. Instrum. Meth.* **94**:509 (1971).
12. Kuzminikh, V. A., and Vorobiev, S. A., *Nucl. Instrum. Meth.* **129**:561 (1975).
13. Deruytter, A. J., *Nucl. Instrum. Meth.* **15**:164 (1962).
14. Walker, D. H., *Int. J. Appl. Rad. Isot.* **16**:183 (1965).
15. Hutchinson, J. M. R., Nass, C. R., Walker, D. H., and Mann, W. B., *Int. J. Appl. Rad. Isot.* **19**:517 (1968).
16. Waibel, E., *Nucl. Instrum. Meth.* **74**:236 (1969).
17. Waibel, E., *Nucl. Instrum. Meth.* **86**:29 (1970).
18. Waibel, E., *Nucl. Instrum. Meth.* **131**:133 (1975).
19. Bell, P. R., in K. Siegbahn (ed.), *Beta and Gamma-Ray Spectrometry*, Interscience Publishers, New York, 1955, Chap. 5.
20. Heath, R. L., "Scintillation Spectrometry—Gamma-Ray Spectrum Catalogue," IDO-16880-1, 1964.
21. Nakamura, T., *Nucl. Instrum. Meth.* **86**:163 (1970).
22. Ruby, L., *Nucl. Instrum. Meth.* **337**:531 (1994).

CHAPTER
# NINE

# INTRODUCTION TO SPECTROSCOPY

## 9.1 INTRODUCTION

Spectroscopy is the aspect of radiation measurements that deals with measuring the energy distribution of particles emitted by a radioactive source or produced by a nuclear reaction.

This introduction to spectroscopy is complemented by Chap. 11, which discusses methods of analysis of spectroscopic data, and Chaps. 12–14, which present details on spectroscopy of photons, charged particles, and neutrons. This chapter discusses the following broad subjects:

1. Definition of differential and integral spectra
2. Energy resolution of the detector
3. The function of a multichannel analyzer (MCA)

## 9.2 DEFINITION OF ENERGY SPECTRA

A particle energy spectrum is a function giving the distribution of particles in terms of their energy. There are two kinds of energy spectra, differential and integral.

The *differential energy spectrum*, the most commonly studied distribution, is also known as an energy spectrum. It is a function $n(E)$ with the following

meaning:

$$n(E)\,dE = \text{number of particles with energies between } E \text{ and } E + dE$$

or

$$n(E) = \text{number of particles with energy } E \text{ per unit energy interval}$$

The quantity $n(E)\,dE$ is represented by the cross-hatched area of Fig. 9.1.

The *integral energy spectrum* is a function $N(E)$, where $N(E)$ is the number of particles with energy greater than or equal to $E$. The quantity $N(E)$ is represented by the hatched area of Fig. 9.1. The integral energy spectrum $N(E)$ and the differential energy spectrum $n(E)$ are related by

$$N(E) = \int_E^{\infty} n(E)\,dE \tag{9.1}$$

The two examples that follow illustrate the relationship between a differential spectrum and an integral spectrum.

**Example 9.1** Consider a monoenergetic source emitting particles with energy $E_0$. The differential energy spectrum $n(E)$ is shown in Fig. 9.2. Since there are no particles with energy different from $E_0$, the value of $n(E)$ is equal to zero for any energy other than $E = E_0$.

The corresponding integral spectrum $N(E)$ is shown in Fig. 9.3. It indicates that there are no particles with $E > E_0$. Furthermore, the value of $N(E)$ is constant for $E \leq E_0$, since all the particles have energy $E_0$ and only those particles exist. In other words,

$$N(E_0) = \text{number of particles with energy greater than or equal to } E_0 = N(E_1)$$
$$= \text{number of particles with energies greater than or equal to } E_1 \text{ (Fig. 9.3)}$$

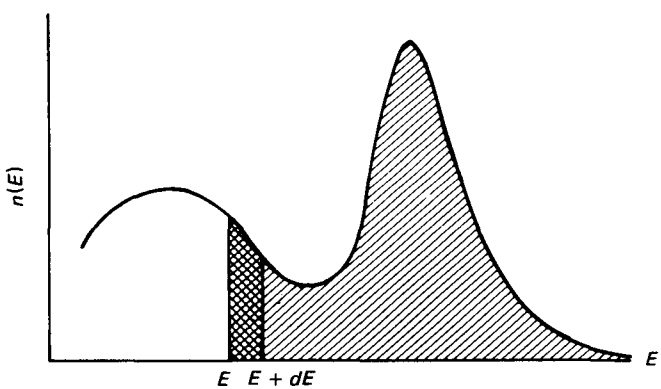


**Figure 9.1** A differential energy spectrum. The quantity $n(E)\,dE$ is equal to the number of particles between $E$ and $E + dE$ (cross-hatched area).

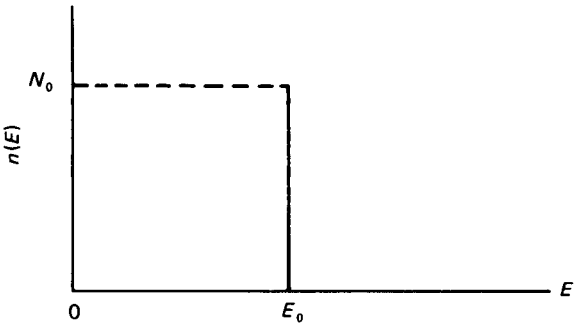


**Figure 9.2** A monoenergetic spectrum. All particles have energy $E_0$.

**Example 9.2** Consider the energy spectrum shown in Fig. 9.4. According to this spectrum, there are 10 particles per MeV at 11, 12, and 13 MeV. The total number of particles is 30. The integral spectrum is shown in Fig. 9.5. Its values at different energies are

| | |
|---|---|
| $N(14) = 0$ | no particles above $E = 14$ MeV |
| $N(13) = 10$ | 10 particles at $E = 13$ MeV and above |
| $N(12) = 20$ | 20 particles at $E = 12$ MeV and above |
| $N(11) = 30$ | 30 particles at $E = 11$ MeV and above |
| $N(10) = 30$ | 30 particles at $E = 10$ MeV and above |
| $N(0) = 30$ | 30 particles above $E = 0$ |

The determination of energy spectra is based on the measurement of pulse-height spectra, as shown in the following sections. Therefore, the definitions of differential and integral spectra given in this section in terms of energy could be expressed equivalently in terms of pulse height. The relationship between particle energy and pulse height is discussed in Sec. 9.5.

## 9.3 MEASUREMENT OF AN INTEGRAL SPECTRUM WITH A SINGLE-CHANNEL ANALYZER

Measurement of an integral spectrum means to count all particles that have energy greater than or equal to a certain energy $E$ or, equivalently, to record all particles that produce pulse height greater than or equal to a certain pulse height $V$. A device is needed that can sort out pulses according to height. Such a device is a *single-channel analyzer* (SCA) operating as a discriminator (integral mode). If the discriminator is set at $V_0$ volts, all pulses with height less than $V_0$ will be rejected, while all pulses with heights above $V_0$ will be recorded. Therefore, a single discriminator can measure an integral energy spectrum. The measurement proceeds as follows.

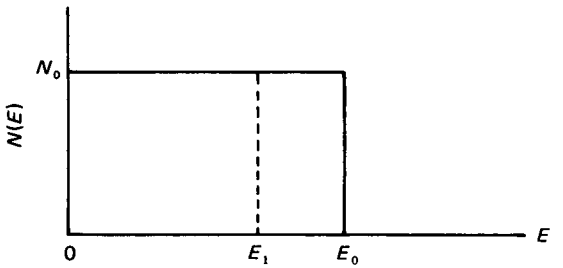


**Figure 9.3** The integral spectrum of a monoenergetic source.

Consider the differential pulse spectrum shown in Fig. 9.6 for which all pulses have exactly the same height $V_0$. To record this spectrum, one starts with the discriminator threshold set very high (higher than $V_0$) and then lowers the threshold by a certain amount $\Delta V$ (or $\Delta E$) in successive steps. Table 9.1 shows the results of this measurement, where $N(V)$ is the number of pulses higher than or equal to $V$. A plot of these results is shown in Fig. 9.7.

## 9.4 MEASUREMENT OF A DIFFERENTIAL SPECTRUM WITH A SINGLE-CHANNEL ANALYZER (SCA)

Measurement of a differential energy spectrum amounts to the determination of the number of particles within a certain energy interval $\Delta E$ for several values of energy; or, equivalently, it amounts to the determination of the number of pulses within a certain interval $\Delta V$, for several pulse heights. A SCA operating in the differential mode is the device that is used for such a measurement.

If the lower threshold of the SCA is set at $V_1$ (or $E_1$) and the window has a width $\Delta V$ (or $\Delta E$), then only pulses with height between $V_1$ and $V_1 + \Delta V$ are recorded. All pulses outside this range are rejected. To measure the pulse spectrum of Fig. 9.6, one starts by setting the lower threshold at $V_1$, where $V_1 > V_0$, with a certain window $\Delta V$ (e.g., $\Delta V = 0.1$ V) and then keeps lowering the lower threshold of the SCA. Table 9.2 shows the results of the measurement, where $n(V)\,\Delta V$ is the number of pulses with height between $V$ and $V + \Delta V$. Figure 9.8 shows these results. It is assumed that the width is $\Delta V = V_i - V_{i+1}$,

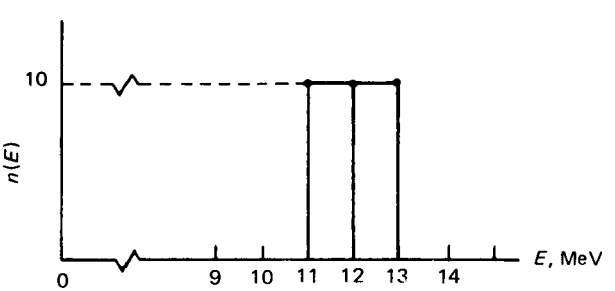


**Figure 9.4** The energy spectrum considered in Ex. 9.2.

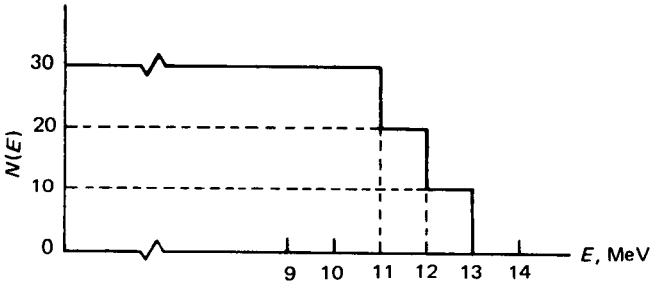


**Figure 9.5** The integral spectrum corresponding to that of Fig. 9.4.

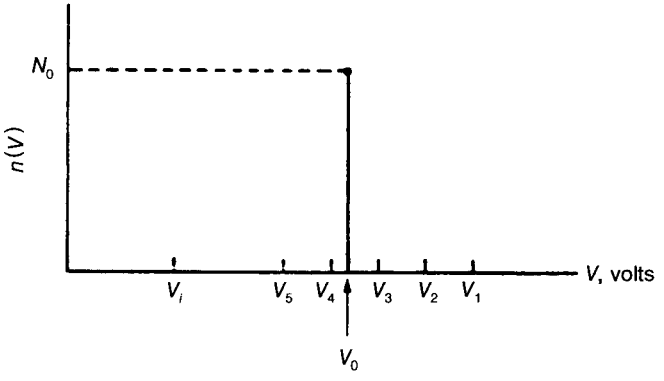


**Figure 9.6** A differential pulse spectrum consisting of pulses with the same height $V_0$.

**Table 9.1 Measurement of Integral Spectrum**

| Discriminator Threshold | $N(V)$ |
|---|---|
| $V_1 > V_0$ | 0 |
| $V_2$ | 0 |
| $V_3$ | 0 |
| $V_4 < V_0$ | $N_0$ |
| $V_5$ | $N_0$ |
| $V_6$ | $N_0$ |
| $V_i < V_0$ | $N_0$ |

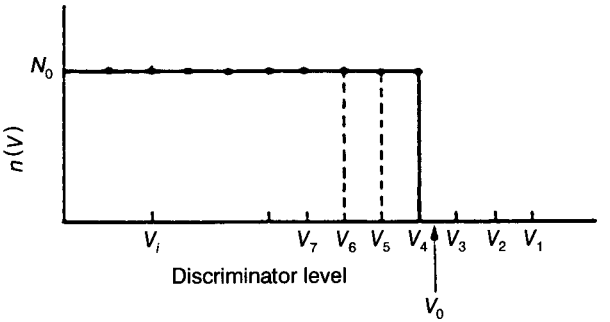


**Figure 9.7** The integral spectrum corresponding to the pulse spectrum of Fig. 9.6.

where $V_i$ are the successive settings of the lower threshold of the SCA. It is important to note that one never measures the value of $n(V)$, but only the product $n(V)\,\Delta V$.

## 9.5 THE RELATIONSHIP BETWEEN PULSE-HEIGHT DISTRIBUTION AND ENERGY SPECTRUM

To determine the energy spectrum of particles emitted by a source, one measures, with the help of a detector and appropriate electronics, the pulse-

**Table 9.2 Measurement of Differential Spectrum**

| SCA threshold | $n(V)\,\Delta V$ |
|---|---|
| $V_1 > V_0$ | 0 |
| $V_2$ | 0 |
| $V_3$ | 0 |
| $V_4 < V_0$ | $N_0$ |
| $V_5$ | 0 |
| $V_i < V_5$ | 0 |

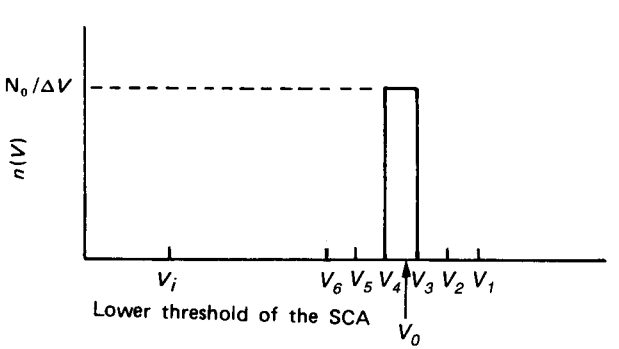


**Figure 9.8** A differential energy spectrum measured with an SCA.

height distribution produced by these particles. Fundamental requirements for the detector and the electronics are as follows:

1. The particle should deposit all its energy or a known constant fraction of it in the detector.
2. The voltage pulse produced by the detector should be proportional to the particles energy dissipated in it, or a known relationship should exist between energy dissipated and pulse height.
3. The electronic amplification should be the same for all pulse heights.

Since the relationship between pulse-height distribution and energy spectrum depends on these three requirements, it is important to discuss them in some detail.

Charged particles deposit all their energy in the detector, as long as their range is shorter than the size of the detector. Gammas do not necessarily deposit all their energy in the detector, regardless of detector size. Neutrons are detected indirectly through other particles produced by nuclear reactions. The energy deposited in the detector depends not only on the energy of the neutron but also on the energy and type of the reaction products.

The events that transform the particle energy into a voltage pulse are statistical in nature. As a result, even if all the particles deposit exactly the same energy in the detector, the output pulses will not be the same but they will have a certain distribution.

The state of commercial electronics is such that the amplification is essentially the same for all pulse heights (see also Sec. 10.11).

As a result of incomplete energy deposition and the statistical nature of the events that take place in the detector, the shape of the pulse-height distribution is different from that of the source energy spectrum. In other words, two spectra are involved in every measurement:

1. The *source spectrum*: This is the energy spectrum of particles emitted by the source.
2. The *measured spectrum*: This is the measured pulse height distribution.

Consider, for example, the measured pulse-height distribution shown in Fig. 9.9*b* produced by a monoenergetic gamma source. This distribution (or spectrum) is obtained using a scintillation counter. The observer records the data shown in Fig. 9.9*b*, which is not identical to that of the source, Fig. 9.9*a*. The objective of the measurement is to obtain the spectrum of Fig. 9.9*a*, but the observer actually measures the distribution shown by Fig. 9.9*b*. The task of the observer is, therefore, to apply appropriate corrections to the measured spectrum to finally obtain the source spectrum.

## 9.6 ENERGY RESOLUTION OF A DETECTION SYSTEM

The quality of the performance of a detection system used for energy measurements is characterized by the width of the pulse-height distribution obtained with particles of the same energy (monoenergetic source). Even in the case where each particle deposits exactly the same energy in the detector, the pulse-height distribution will not be a single line (like that shown in Fig. 9.9*a*); instead, it will have a certain finite width (Fig. 9.10) due to

1. Statistical fluctuations in the number of charge carriers produced in the detector
2. Electronic noise in detector itself, the preamplifier, and the amplifier
3. Incomplete collection of the charge produced in the detector

The *width*, measured at half of the maximum of the bell-shaped curve, is indicated by $\Gamma$ or by full width at half maximum (FWHM). The ability of a detector to identify particles of different energies, called the *energy resolution*, is given either in terms of $\Gamma$ or in terms of the ratio $R(E_0)$, where

$$R(E_0) = \frac{\Gamma}{E_0} \tag{9.2}$$

The width $\Gamma$ is given in energy units, while the ratio $R(E_0)$ is given as a percentage.

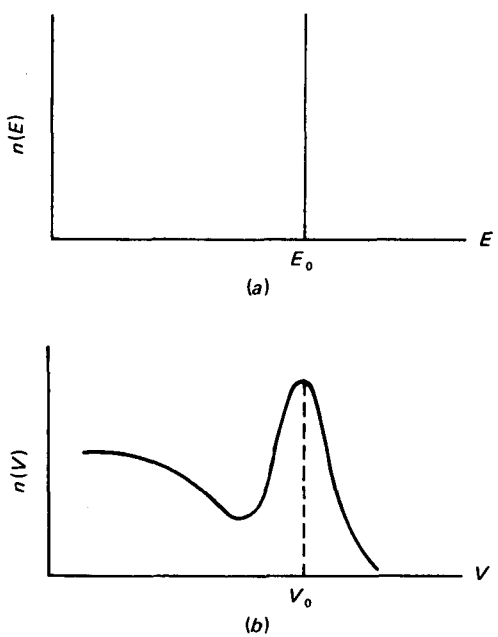


**Figure 9.9** (*a*) The source energy spectrum of a monoenergetic gamma source. (*b*) The pulse-height distribution obtained with a NaI(Tl) scintillation counter.

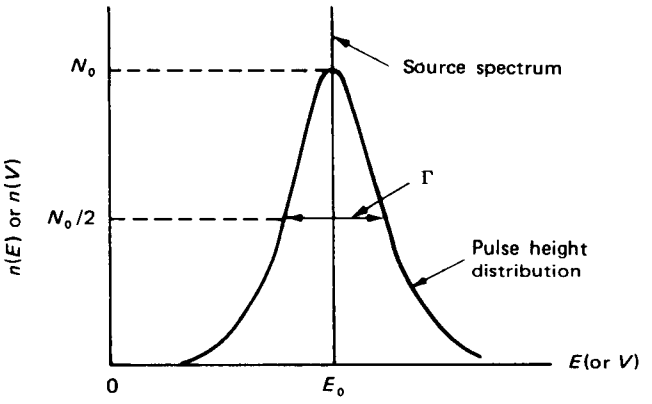


**Figure 9.10** The energy resolution of the detector is given by the width Γ or the ratio $\Gamma/E_0$.

The most important elements affecting the energy resolution of a radiation detection system are the three statistical factors mentioned above in relation to the width Γ. It is worth repeating that in energy measurements it is the energy resolution of the counting system (detector-preamplifier-amplifier) that is the important quantity and not the energy resolution of just the detector.

### 9.6.1 The Effect of Statistical Fluctuations: The Fano Factor

To discuss the effect of the statistical fluctuations on energy resolution, consider a monoenergetic source of charged particles being detected by a silicon semiconductor detector. (The discussion would apply to a gas-filled counter as well.) The average energy $w$ needed to produce one electron-hole pair in silicon is 3.66 eV, although the energy gap ($E_g$) is 1.1 eV. This difference between $w$ and $E_g$ shows that part of the energy of the incident particles is dissipated into processes that do not generate charge carriers. Any process that consumes energy without producing electron-hole pairs is, of course, useless to the generation of the detector signal. If the energy deposited in the detector is $E$, the average number of charge carriers is $E/w$. If the process of the electron-hole generation were purely statistical, Poisson statistics would apply and the standard deviation of the number of pairs would be

$$\sigma = \sqrt{\frac{E}{w}} \tag{9.3}$$

Experience has shown that the fluctuations are smaller than what Eq. 9.3 gives. The observed statistical fluctuations are expressed in terms of the *Fano factor*

$F$,[1] where

$$F = \frac{(\text{standard deviation of the number of pairs produced})^2}{\text{number of pairs produced}}$$

or, using Eq. 9.3,

$$\sigma = \sqrt{\frac{FE}{w}} \tag{9.4}$$

The two extreme values of $F$ are 0 and 1.

$F = 0$ means that there are no statistical fluctuations in the number of pairs produced. That would be the case if all the energy was used for production of charge carriers. $F = 1$ means that the number of pairs produced is governed by Poisson statistics.

Fano factors have been calculated and also measured.[2-7] For semiconductor detectors, $F$ values as low as 0.06 have been reported.[8] For gas-filled counters, reported $F$ values lie between 0.2 and 0.5. Values of $F < 1$ mean that the generation of electron-hole pairs does not exactly follow Poisson statistics. Since Poisson statistics applies to outcomes that are independent, it seems that the ionization events in a counter are interdependent.

The width $\Gamma$ of a Gaussian distribution, such as that shown in Fig. 9.10, is related to the standard deviation $\sigma$ by

$$\Gamma_f = 2\sqrt{2 \ln 2}\, w\sigma \approx 2.355 w\sigma \tag{9.5}$$

Combining Eqs. 9.4 and 9.5,

$$\Gamma_f = 2\sqrt{2(\ln 2) wFE} \tag{9.6}$$

Equation 9.5 shows that the width $\Gamma_f$, which is due to the statistical fluctuations, is roughly proportional to the square root of the energy (the Fano factor is a weak function of energy).

To compare the contribution of the statistical fluctuations to the resolution of different types of detectors at a certain energy, one can use Eqs. 9.2 and 9.6 and write for detectors 1 and 2

$$\frac{R_1}{R_2} = \frac{\Gamma_1/E}{\Gamma_2/E} = \sqrt{\frac{w_1 F_1}{w_2 F_2}} \tag{9.7}$$

It can be seen from Eq. 9.7 that the resolution is better for the detector with the smaller average energy needed for the creation of a charge carrier pair (and smaller Fano factor). Thus, the energy resolution of a semiconductor detector ($w \sim 3$ eV, $F < 0.1$) should be expected to be much better than the resolution of a gas-filled counter ($w \approx 30$ eV, $F \approx 0.2$), and indeed it is (see Chaps. 12 and 13).

### 9.6.2 The Effect of Electronic Noise on Energy Resolution

The electronic noise consists of a small voltage variation around the zero line (Fig. 9.11), with average voltage $\bar{v}_n \neq 0$. To see the effect of the noise on the energy resolution, consider pulses of constant height $V$. In the absence of noise, the FWHM of the distribution of these pulses is zero. If noise is present, the pulses will be superimposed on the noise with the results that the pulses are not of equal height any more (Fig. 9.12), and that the pulses form a Gaussian distribution centered at $V$ and having a width equal to $\Gamma_n = 2\sqrt{2 \ln 2}\, \sigma_n$. The width $\Gamma_n$ is due to the noise only and has nothing to do with statistical effects in the detector.

The *signal-to-noise ratio* is frequently the quantity used to indicate the magnitude of the noise. It is defined by

$$\text{Signal-to-noise ratio} = \frac{\text{mean pulse height}}{\text{noise standard deviation}} = \frac{V}{\sigma_n}$$

Or, one can write

$$\frac{V}{\sigma_n} = 2\sqrt{2 \ln 2}\, \frac{V}{\Gamma_n} = \frac{2\sqrt{2 \ln 2}}{R} \tag{9.8}$$

where $R$ is given by Eq. 9.2. This last equation may be rewritten as

$$R = \frac{2\sqrt{2 \ln 2}}{V/\sigma_n} \tag{9.8a}$$

to show that the higher the signal-to-noise ratio is, the better the resolution becomes (other things being equal, of course).

### 9.6.3 The Effect of Incomplete Charge Collection

The effect of incomplete charge collection in gas counters is small compared to the effect of the statistical fluctuations. In semiconductor detectors, incomplete charge collection is due to trapping of carriers. The amount of charge trapped is approximately proportional to the energy deposited in the detector, which in turn, is proportional to the energy of the incident particles.[9] For this reason, the resolution is affected by trapping effects more at high energy than at low energy. As discussed in Chap. 7, trapping effects depend on the material of which the detector is made and on radiation damage suffered by the semiconductor.

**Figure 9.11** The electronic noise.

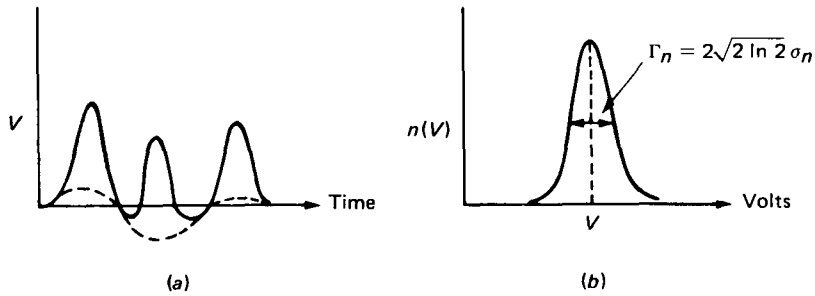


**Figure 9.12** (*a*) The pulses are superimposed on the noise, as a result of which (*b*) they show a distribution with a width that depends on the standard deviation of the noise.

Usually, the effect of incomplete charge collection is included in the statistical fluctuations.

### 9.6.4 The Total Width Γ

The total width Γ (or the total energy resolution) is obtained by adding in quadrature the contributions from the statistical effects ($\Gamma_f$) and from the noise and incomplete charge collection ($\Gamma_n$). Thus,

$$\Gamma = \sqrt{\Gamma_f^2 + \Gamma_n^2} \tag{9.9}$$

For gas and scintillator counters, the main contribution comes from the statistical fluctuations. For semiconductor detectors at low energies, measurements have shown that $\Gamma_n \gtrsim \Gamma_f$. At higher energies this is reversed, since $\Gamma_n$ is essentially independent of energy while $\Gamma_f$ increases with it (see Eq. 9.6).

## 9.7 DETERMINATION OF THE ENERGY RESOLUTION—THE RESPONSE FUNCTION

Depending on the type and energy of the incident particle and the type of the detector, a monoenergetic source produces a pulse-height distribution that may be a Gaussian (Fig. 9.10) or a more complicated function (Fig. 9.9). In either case, one concludes that although all the particles start at the source with the same energy, there is a probability that they may be recorded within a range of energies. That probability is given by the *response function* or *energy resolution function* $R(E, E')$ of the detection system, defined as

$R(E, E')\,dE$ = probability that a particle emitted by the source with energy $E'$ will be recorded with energy between $E$ and $E + dE$

One measures, of course, a pulse-height distribution, but the energy calibration of the system provides a one-to-one correspondence between energy and pulse height. If one defines

$$S(E)\,dE = \text{source spectrum} = \text{number of particles emitted by the source with energy between } E \text{ and } E + dE$$

and

$$M(E)\,dE = \text{measured spectrum} = \text{number of particles recorded as having energy between } E \text{ and } E + dE$$

then the three functions $R(E, E')$, $S(E)$, and $M(E)$ are related by

$$M(E) = \int_0^\infty R(E, E')S(E')\,dE' \tag{9.10}$$

Equation 9.10 is an integral equation with the source spectrum $S(E)$ being the unknown. The procedure by which $S(E)$ is obtained, after $R(E, E')$ and $M(E)$ have been determined, is called *unfolding* of the measured spectrum. Methods of unfolding are discussed in Chaps. 11–14.

To determine the response function of a detection system at energy $E$, the energy spectrum of a monoenergetic source emitting particles with that energy is recorded. Since the resolution changes with energy, the measurement is repeated using several sources spanning the energy range of interest. The response function can also be calculated, as shown in Chaps. 12–14. Figure 9.13 shows response functions for several commonly encountered cases.

## 9.8 THE IMPORTANCE OF GOOD ENERGY RESOLUTION

The importance of good energy resolution becomes obvious if the energy spectrum to be measured consists of several energies. Consider as an example the source spectrum of Fig. 9.14, consisting of two energies $E_1$ and $E_2$. Assume that this spectrum is measured with a system having energy resolution equal to $\Gamma$,† and examine the following cases.

**Case I: $E_2 - E_1 > 2\Gamma$.** The measured spectrum is shown in Fig. 9.15 for this case. The system can *resolve* the two peaks—i.e., the two peaks can be identified as two separate energies.

**Case II: $E_2 - E_1 = 2\Gamma$.** This case is shown in Fig. 9.16. The peaks can still be resolved.

† $\Gamma$ may be different at $E_1$ and $E_2$. However, the difference is very small since $E_1$ and $E_2$ are close. For the present discussion, the same $\Gamma$ will be used at $E_1$ and $E_2$.

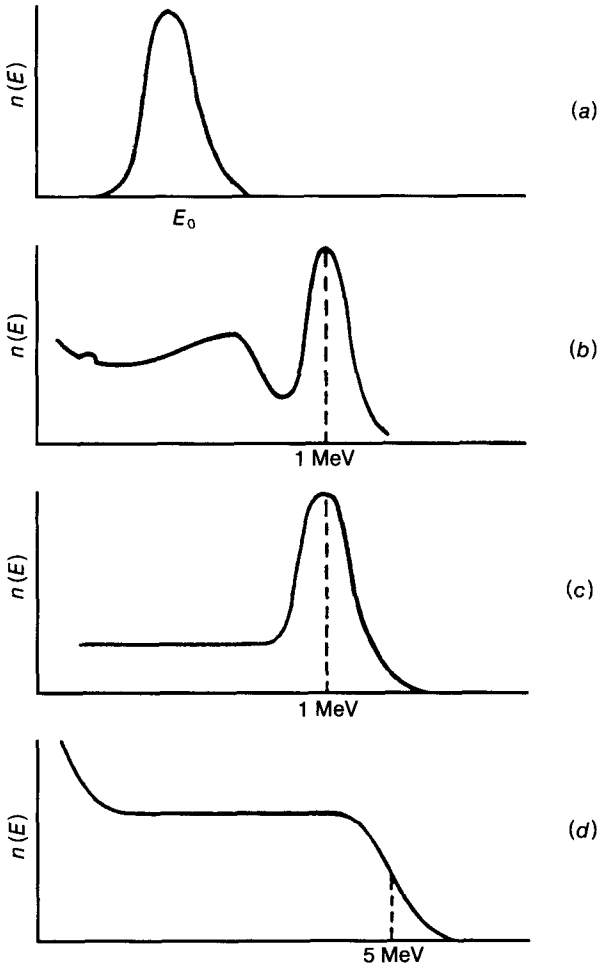


**Figure 9.13** Four examples of response functions (*a*) 5-MeV Alpha particles detected by a silicon surface barrier detector (Chap. 13), or 20-keV X-rays detected by a Si(Li) reactor (Chap. 12). (*b*) 1-MeV Gamma ray detected by a NaI(Tl) crystal (Chap. 12). (*c*) 1-MeV Electrons detected by a plastic scintillator (Chap. 13). (*d*) 5-MeV Neutrons detected by an NE 213 organic scintillator (Chap. 14).

**Case III:** $E_2 - E_1 = \Gamma$. This case is shown in Fig. 9.17. The solid line shows how the measured spectrum will look as the sum of the two peaks (dashed lines).

It is obvious that it is difficult to identify two distinct peaks if $E_2 - E_1 = \Gamma$, and the situation will be worse if $E_2 - E_1 < \Gamma$.

The three cases examined above intend to show how important good energy resolution is for the measurement of spectra with many energy peaks. If the response function of the detector is not known and the measured spectrum shows no well-identified peaks, the following criterion is used for the energy resolution required to identify the peaks of about equal magnitude:

To be able to resolve two energy peaks at $E_1$ and $E_2$, the resolution of the system should be such that $\Gamma \leq |E_1 - E_2|$.

**Figure 9.14** Source spectrum consisting of two distinct energies.

## 9.9 BRIEF DESCRIPTION OF A MULTICHANNEL ANALYZER (MCA)

To measure an energy spectrum of a radioactive source means to record the pulse-height distribution produced by the particles emitted from the source, which is achieved with the use of an instrument called the multichannel analyzer (MCA). Multichannel analyzers are used in either of two different modes: the *pulse-height analysis* (PHA) mode or the *multichannel scaling* (MCS) mode.

The MCS mode is used to count events as a function of time. The individual channels of the memory count all incoming pulses for a preset time width $\Delta t$. After time $\Delta t$, the counting operation is switched automatically to the next channel in the memory, thus producing in the end a time sequence of the radiation being detected. For example, if the radiation source is a short-lived isotope, the MCS mode will provide the exponential decay curve that can be used for the measurement of the half-life of this isotope. The MCS mode is also useful for Mossbauer experiments.

The PHA mode is the traditional function of an MCA and is used to sort out incoming pulses according to their height and store the number of pulses of a particular height in a corresponding address of the MCA memory called the *channel number*.

In the PHA mode, an MCA performs the function of a series of SCAs placed adjacent to one another. When only one SCA with width $\Delta E$ is used, the experimenter has to sweep the spectrum by moving the lower threshold of the SCA manually (see Sec. 9.4). On the other hand, if one had many SCAs, all counting simultaneously, the whole spectrum would be recorded simultaneously.

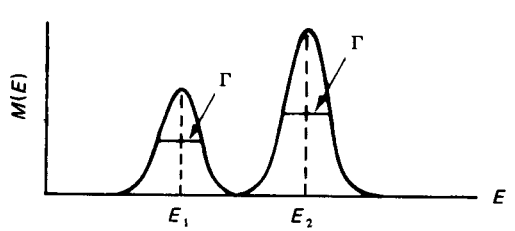


**Figure 9.15** Measured spectrum for Case I: $2\Gamma < E_2 - E_1$.

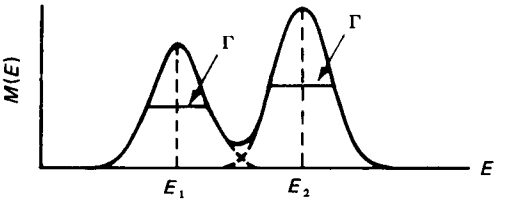


**Figure 9.16** Measured spectrum for Case II: $2\Gamma = E_2 - E_1$.

This is exactly what the MCA does, although its principle of operation is not based on a series of SCAs.

Figure 9.18 shows a simplified block diagram of an MCA. In the PHA mode, the incoming pulse enters into a unit called the *analog-to-digital converter* (ADC). The ADC *digitizes* the pulse amplitude: it produces a number proportional to the height of the pulse, a number that determines the channel where the pulse will be stored. The size of the ADC, given in terms of channels, defines the absolute resolution of the system. Actually, the ADC determines the number of discrete parts into which the pulse height can be subdivided. Commercial ADCs have at the present time a size up to 16384 channels, with the full scale adjustable in steps of 256, 512, 1024, etc., channels.

The number of discrete parts (channels) into which the input pulse range (0 to +10 V) is divided is called the *conversion gain*. The conversion gain is set by a stepwise control knob located on the front of the instrument. As an example, if the conversion gain is set at 2048 channels, it means that the maximum pulse height (10 V) is divided into that many parts. Therefore, the resolution of the MCA at this setting is

$$10\ \text{V}/2048 = 4.88\ \text{mV/channel}$$

More details about the operation and characteristics of ADCs are given in Sec. 10.12.

The memory of the MCA is a data-storage unit arranged in a series of channels. Every channel is capable of storing up to $2^{20} - 1$ data (pulses), in most cases. Commercial MCAs have memories with up to 16384 channels. Normally, the MCA provides for selection and use of the full memory, only half of it, or one-fourth of it. Transfer of data from one fraction of the memory to another is also possible.

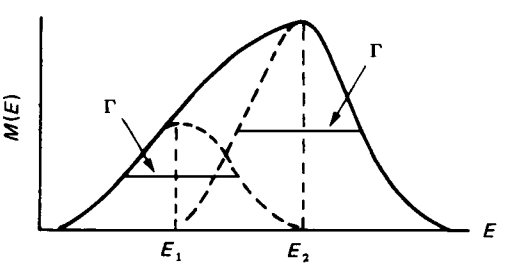


**Figure 9.17** Measured spectrum for Case III: $\Gamma = E_2 - E_1$.

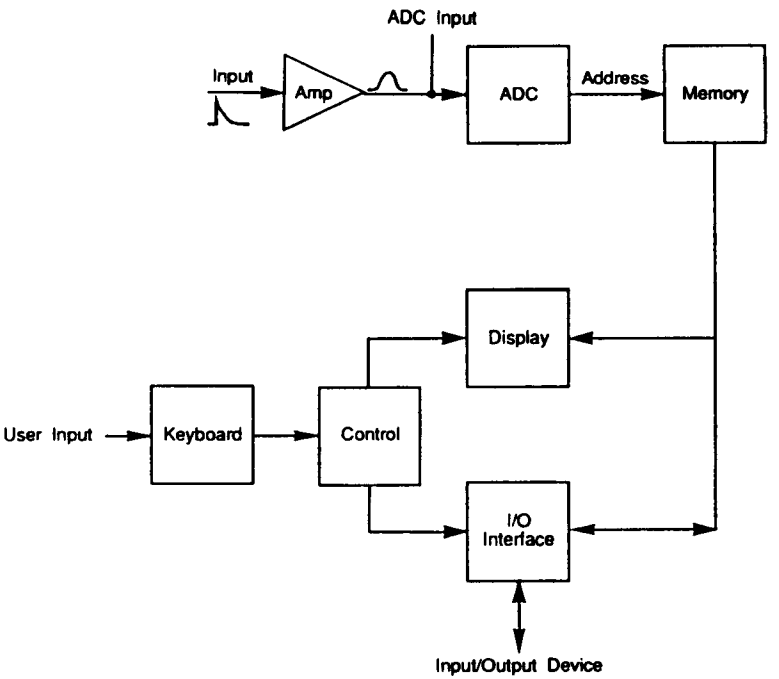


**Figure 9.18** Block diagram showing the components of an MCA counting system (modified from Ref. 10).

In the PHA mode, the first channel of the region used is called *channel zero* and records, in almost all late model MCAs, the live time of the analysis, in seconds. If the full memory or the first half or first quarter of the memory is used, channel zero is the address 0000. If the second half of 4096 memory is used, channel zero is address 2048; if the second quarter is used, channel zero is address 1024; and so on.

How does one determine the size of the MCA memory needed for a specific experiment? The decision is made based on the requirements for the PHA mode. One equation frequently used is

$$\text{Number of channels} = h\frac{\text{energy range of interest (keV)}}{\Gamma(\text{keV})} \tag{9.11}$$

where $\Gamma$ is the FWHM of the detector used. The factor $h$ is equal to the number of channels at or above the FWHM of the peak. Its value is between 3 and 5.

As an example, assume that the energy range of interest is 0 to 2.0 MeV and consider a NaI(Tl) and a Ge detector. The resolution of the NaI(Tl) detector is

about 50 keV. Therefore, the minimum number of channels is ($h = 5$)

$$5\left(\frac{2000}{50}\right) \approx 200 \text{ channels}$$

The resolution of a Ge detector is about 2 keV. Now, the number of channels is

$$5\left(\frac{2000}{2}\right) \approx 5000 \text{ channels}$$

The user should remember that the ADC, not the memory, determines the absolute resolution of an MCA. An MCA with an ADC of 1000 channels and a memory of 2000 channels has an actual resolution of only 1000 channels.

In using an MCA to record a spectrum, there is "dead time" involved, which is, essentially, the time it takes to store the pulse in the appropriate channel. That time depends on and increases with the channel number. More details about the MCA dead time are given in Sec. 10.12 in connection with the discussion of ADCs.

Commercial MCAs have a meter that shows, during counting, the percentage of dead time. They also have timers that determine the counting period in *live time* or *clock time*. In clock time mode, the counting continues for as long as the clock is set up. In live time mode, an automatic correction for dead time is performed. In this case, the percent dead time indication can be used to determine the approximate amount of actual time the counting will take. For example if the clock is set to count for 5 min (in live mode) and the dead time indicator shows 25 percent, the approximate actual time of this measurement is going to be

$$\text{Actual time} = \frac{\text{live time}}{1 - (\text{dead time fraction})} = \frac{300 \text{ s}}{1 - 0.25} = 400 \text{ s}$$

Modern MCAs can do much more than just store pulses in memory. They are computers that may, depending on the hardware and software available, be able to

1. Perform the energy calibration of the system
2. Determine the energy of a peak
3. Integrate the area over a desired range of channels
4. Identify an isotope, based on the energy peaks recorded, etc.

## 9.10 CALIBRATION OF A MULTICHANNEL ANALYZER

The calibration of an MCA follows these steps:

1. *Determination of range of energies involved.* Assume this is $0 \leq E \leq E_m$ (MeV).

2. *Determination of preamplifier-amplifier setting.* Using a source that emits particles of known energy, one observes the signal generated on the screen of the oscilloscope. It should be kept in mind that the maximum possible signal at the output of the amplifier is 10 V. In energy spectrum measurements, one should try to stay in the range 0–9 V.

Assume that the particle energy $E_1$ results in pulse height $V_1$. Is this amplification proper for obtaining a pulse height $V_m \leq 10$ V for energy $E_m$? To find this out, the observer should use the fact that pulse height and particle energy are proportional. Therefore,

$$\frac{V_m}{E_m} = \frac{V_1}{E_1} \rightarrow V_m = \frac{E_m}{E_1} V_1$$

If $V_m < 10$ V, then the amplification setting is proper. If $V_m \geq 10$ V, the amplification should be reduced. (If $V_m < 2$ V, amplification should be increased. It is good practice, but not necessary, to use the full range of allowed voltage pulses.) The maximum pulse $V_m$ can be changed by changing the amplifier setting.

3. *Determination of MCA settings.* One first decides the part of the MCA memory to be used. Assume that the MCA has a 1024-channel memory and it has been decided to use 256 channels, one-fourth of the memory. Also assume that a spectrum of a known source with energy $E_1$ is recorded and that the peak is registered in channel $C_1$. Will the energy $E_m$ be registered in $C_m < 256$, or will it be out of scale?

The channel number and energy are almost proportional,† i.e., $E_i \sim C_i$. Therefore

$$\frac{C_m}{E_m} \approx \frac{C_1}{E_1} \rightarrow C_m \approx \frac{E_m}{E_1} C_1$$

If $C_m \leq 256$, the setting is proper and may be used. If $C_m > 256$, a new setting should be employed. This can be done in one of two ways or a combination of the two:

1. The fraction of the memory selected may be changed. One may use 526 channels of 1024, instead of 256.
2. The conversion gain may be changed. In the example discussed here, if a peak is recorded in channel 300 with conversion gain of 1024, that same peak will be recorded in channel 150 if the conversion gain is switched to 512.

There are analyzer models that do not allow change of conversion gain. For such an MCA, if $C_m$ is greater than the total memory of the instrument, one should return to step 2 and decrease $V_m$ by reducing the gain of the amplifier.

†The correct equation is $E = a + bC$, but $a$ is small and for this argument it may be neglected; proper evaluation of $a$ and $b$ is given in step 4 of the calibration procedure.

4. *Determination of the energy-channel relationship.* Calibration of the MCA means finding the expression that relates particle energy to the channel where a particular energy is stored. That equation is written in the form

$$E = a_1 + a_2C + a_3C^2 + \cdots \tag{9.12}$$

where $C$ = channel number and $a_1, a_2, a_3, \ldots$ are constants.

The constants $a_1, a_2, a_3, \ldots$ are determined by recording spectra of sources with known energy. In principle, one needs as many energies as there are constants. In practice, a large number of sources is recorded with energies covering the whole range of interest, and the constants are then determined by a least-squares fitting process (see Chap. 11).

Most detection systems are essentially linear, which means that Eq. 9.12 takes the form

$$E = a_1 + a_2C \tag{9.13}$$

**Example 9.3** Obtain the calibration constants for an MCA based on the spectrum shown in Fig. 9.19. The peaks correspond to the following three energies:

$$E_1 = 0.662 \text{ MeV} \qquad C_1 = 160$$
$$E_2 = 1.173 \text{ MeV} \qquad C_2 = 282.5$$
$$E_3 = 1.332 \text{ MeV} \qquad C_3 = 320$$

**Answer** Plotting energy versus channel on linear graph paper, one obtains the line shown in Fig. 9.20, which indicates that the linear equation, Eq. 9.13, applies, and one can determine the constants $a_1$ and $a_2$ from the slope and the zero intercept of the straight line. From Fig. 9.20, the value of $a_2$ is

$$a_2 = \frac{950 - 400}{230 - 97.5} = 4.15 \text{ keV/channel}$$

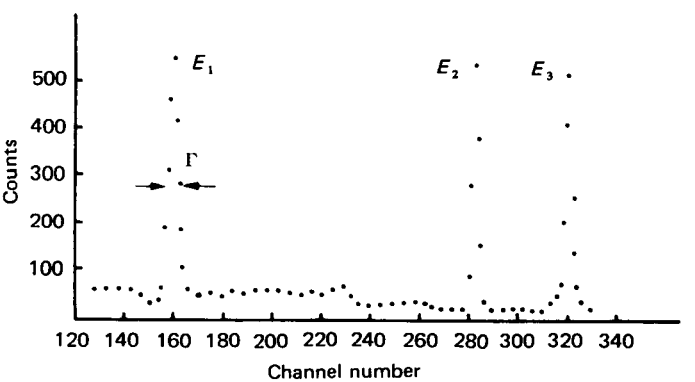


**Figure 9.19** A gamma spectrum used for calibration of an MCA.

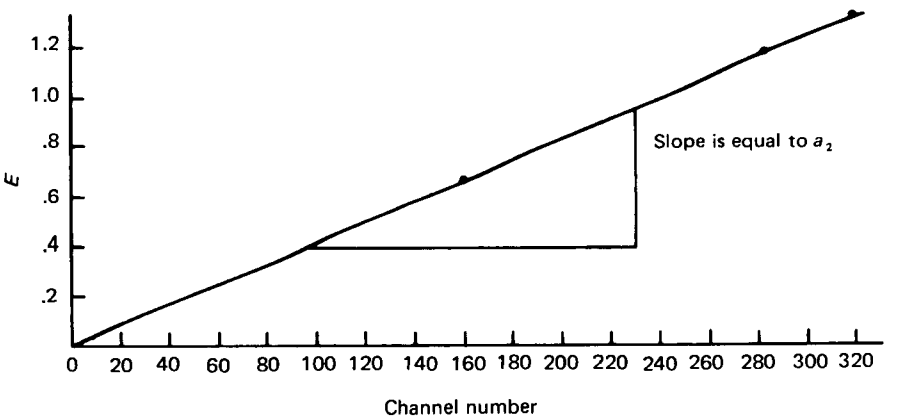


**Figure 9.20** Plot of energy versus channel number. In this case, the relationship is linear.

The constant $a_1$ is equal to the zero-intercept of the line.† In the present case, it is almost zero. Based on these results, the calibration equation of this MCA is $E = 4.15C$.

5. *Calculation of the energy resolution.* By definition, the energy resolution is $R = \Gamma/E$, where $\Gamma$ is the FWHM of the peak of energy $E$. Therefore, using Eq. 9.13,

$$R = \frac{\Gamma}{E} = \frac{(a_1 + a_2C_R) - (a_1 - a_2C_L)}{E} = \frac{a_2(C_R - C_L)}{E} \tag{9.14}$$

where $C_R$ and $C_L$ are the channel numbers on either side of the peak at half of its maximum. If $a_1$ is zero, the resolution is given by

$$R = \frac{a_2(C_R - C_L)}{a_2C_{\text{peak}}} = \frac{C_R - C_L}{C_{\text{peak}}} \tag{9.15}$$

For peak $E_1$ (Fig. 9.19),

$$C_L = 158 \qquad C_{\text{peak}} = 160 \qquad C_R = 162$$

Therefore

$$R = \frac{162 - 158}{160} = 2.5\%$$

or $\Gamma = a_2(C_R - C_L) = 4.15(4) = 16.6$ keV.

†Most commercial MCAs have a hand-screw adjustment that makes $a_1$ equal to zero.

## PROBLEMS

**9.1** Sketch the integral spectrum for the differential spectrum shown in the figure below.

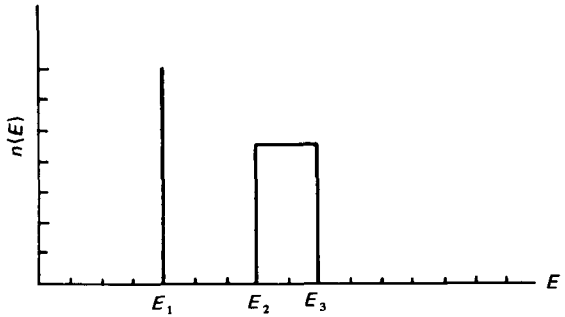


**9.2** Sketch the differential energy spectrum for the integral spectrum shown in the figure below.

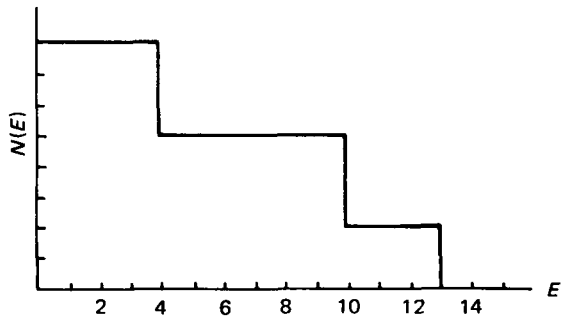


**9.3** Sketch the integral spectrum for the differential spectrum shown in the figure below.

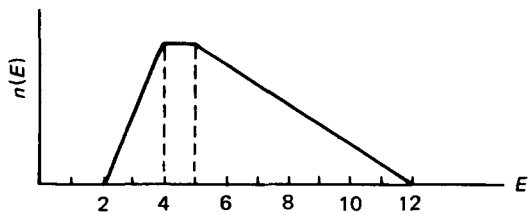


**9.4** If the energy resolution of a NaI(Tl) scintillator system is 11 percent at 600 keV, what is the width $\Gamma$ of a peak at that energy?

**9.5** What is the maximum energy resolution necessary to resolve two peaks at 720 keV and 755 keV?

**9.6** Prove that if a detection system is known to be linear, the calibration constants are given by

$$a_1 = \frac{E_2C_1 - E_1C_2}{C_1 - C_2} \qquad a_2 = \frac{E_1 - E_2}{C_1 - C_2}$$

where $E_1$ and $E_2$ are two energies recorded in channels $C_1$ and $C_2$, respectively.

**9.7** Shown in the following figure is the spectrum of $^{22}$Na, with its decay scheme. Determine the calibration constants of the MCA that recorded this spectrum, based on the two peaks of the $^{22}$Na spectrum.

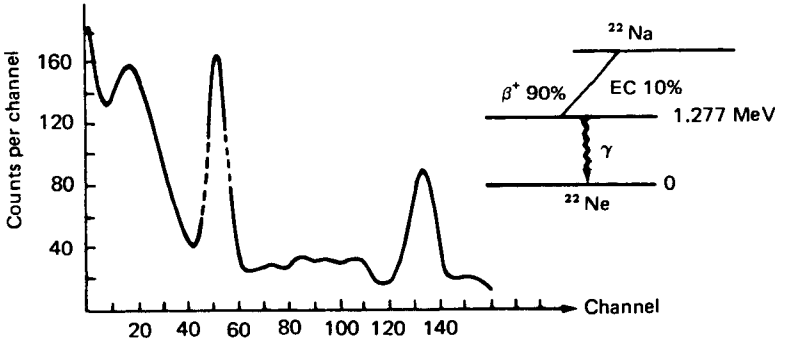


**9.8** In Prob. 9.7, the channel number cannot be read exactly. What is the uncertainty of the calibration constants $a_1$ and $a_2$ if the uncertainty in reading the channel is one channel for either peak?

**9.9** Assume that the energy resolution of a scintillation counter is 9 percent and that of a semiconductor detector is 1 percent at energies around 900 keV. If a source emits gammas at 0.870 MeV and 0.980 MeV, can these peaks be resolved with a scintillator or a semiconductor detector?

**9.10** Consider the two peaks shown in the accompanying figure. How does the peak at $E_2$ affect the width of the peak at $E_1$ and vice versa? What is the width $\Gamma$ for either peak?

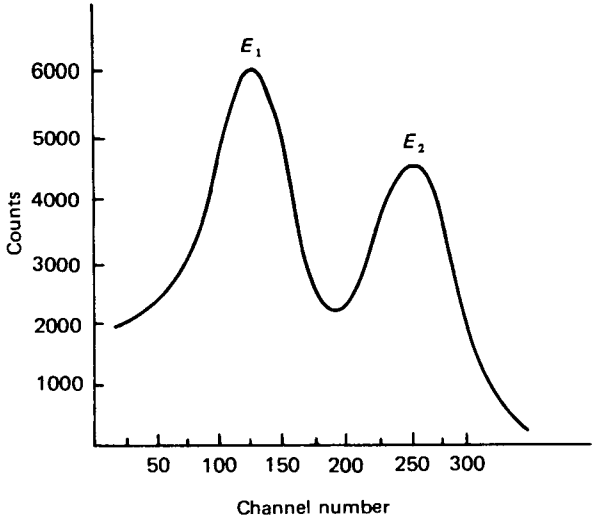


## REFERENCES

1. Fano, U., *Phys. Rev.* **72**:26 (1947).
2. van Roosbroeck, W., *Phys. Rev.* **139A**:1702 (1965).
3. Goulding, F. S., *Nucl. Instrum. Meth.* **43**:1 (1966).

4. Mann, H. M., Bilger, H. R., and Sherman, I. S., *IEEE* **NS-13**(3):352 (1966).
5. Deshpande, R. Y., *Nucl. Instrum. Meth.* **57**:125 (1967).
6. Hashiba, A., Masuda, K., and Doke, T., *Nucl. Instrum. Meth.* **227**:305 (1984).
7. Kase, M., Akioka, T., Mamyoda, H., Kikuchi, J., and Doke, T., *Nucl. Instrum. Meth.* **227**:311 (1984).
8. Pehl, R. H., and Goulding, F. S., *Nucl. Instrum. Meth.* **81**:329 (1970).
9. Ewan, G. T., *Nucl. Instrum. Meth.* **162**:75 (1979).
10. Canberra Industries, Inc. *Edition Nine Instruments Catalog*, Meriden, CT.

CHAPTER
# TEN

# ELECTRONICS

## 10.1 INTRODUCTION

This chapter presents a brief and general description of electronic units used in radiation measurements. The subject is approached from the viewpoint of "input-output"—i.e., the input and output signals of every component unit or instrument are presented with a minimum of discussion on circuitry. The objective is to make the reader aware of the capabilities and limitations of the different types of units and, at the same time, create the capacity to choose the right component for a specific counting system.

Details about construction and operation of electronic components and systems are given in books specializing on that subject. A few such texts are listed in the bibliography at the end of the chapter. Also, the vendors of nuclear instruments provide manuals for their products with useful information about their operation.

## 10.2 RESISTANCE, CAPACITANCE, INDUCTANCE, AND IMPEDANCE

To understand what factors affect the formation, transmission, amplification, and detection of a detector signal, it is important to comprehend the function of resistance, capacitance, inductance, and impedance, which are the basic constituents of any electronic circuit. For this reason, a brief review of these concepts is offered.

The *resistance R* is a measure of how difficult (or easy) it is for an electric current to flow through a conductor. The resistance is defined by Ohm's law as the ratio of a voltage to current flowing through a conductor (Fig. 10.1*a*). The resistance is measured in ohms (Ω). If a potential difference of 1 V generates a current of 1 A, the resistance is 1 Ω; that is,

$$R = \frac{V}{i} \tag{10.1}$$

*Capacitance C* is the ability to store electrical charge. A capacitor usually consists of two conductors separated by an insulator or a dielectric (Fig. 10.1*b*). Every conductor, e.g., simple metal wire, has a certain capacitance. The capacitance is measured in farads (F). If a charge of 1 coulomb produces a potential difference of 1 V between the two conductors forming the capacitor, then its capacitance is 1 F; that is,

$$C = \frac{q}{V} \tag{10.2}$$

If the voltage across the capacitor is constant, no current flows through it; i.e., a capacitor acts as an open circuit to dc voltage. If, however, the voltage changes, a current flows through the capacitor equal to

$$i = \frac{dq}{dt} = C\frac{dV}{dt} \tag{10.3}$$

*Inductance* refers to the property of conductors to try to resist a change in a magnetic field. If the current flowing through a conductor changes with time (in which case the magnetic field produced by the current also changes), a potential difference is induced that opposes the change. The induced potential difference $V_L$ is given by (Fig. 10.1*c*)

$$V_L = L\frac{di}{dt} \tag{10.4}$$

where $L$ is called the inductance of the conductor and is measured in henrys (H). If a current change of 1 A/s induces a potential difference of 1 V, the inductance is 1 H. An inductor is usually indicated as a coil (Fig. 10.1*c*), but any

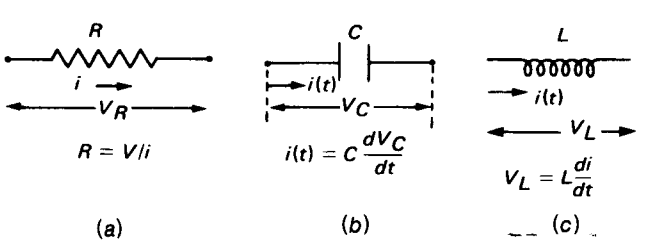


**Figure 10.1** (*a*) A resistor. (*b*) A capacitor. (*c*) An inductor (coil).

conductor, e.g., a metal wire, has a certain inductance. No pure inductor exists because there is always some ohmic resistance and some capacitance in the wires making the coils.

Capacitance and inductance are important for time-varying signals. To be able to introduce and discuss the pertinent concepts, consider a sinusoidal voltage signal with maximum voltage $V_m$ and frequency $\omega$ applied to an $RC$ circuit, as shown in Fig. 10.2:

$$V(t) = V_m \sin \omega t \tag{10.5}$$

Kirchhoff's second law applied to this circuit gives

$$V_m \sin \omega t - \frac{q}{C} = Ri \tag{10.6}$$

Differentiating Eq. 10.6 with respect to time,

$$V_m \omega \cos \omega t - \frac{i}{C} = R\frac{di}{dt} \tag{10.7}$$

The current flowing through the circuit is sinusoidal with frequency $\omega$ but with a phase difference relative to the input voltage. Let us call this phase difference $\varphi$. Then, we can write for the current

$$i(t) = i_m \sin(\omega t + \varphi) \tag{10.8}$$

To evaluate the phase difference $\varphi$, substitute Eq. 10.8 into Eq. 10.7 and compute the resulting expression at some convenient value of the time $t$ (in this case, $t = \pi/2\omega$; see Prob. 10.1). The result is

$$\tan \varphi = \frac{1}{RC\omega} \tag{10.9}$$

Note that as $R \to 0$, $\tan \varphi \to \infty$ and $\varphi \to \pi/2$. The voltage across the capacitor is given by

$$V_c(t) = \frac{q}{C} = \frac{1}{C}\int i_m \sin(\omega t + \varphi)\, dt = -\frac{i_m}{C\omega}\cos(\omega t + \varphi)$$
$$= \frac{i_m}{C\omega}\sin\left(\omega t + \varphi - \frac{\pi}{2}\right)$$

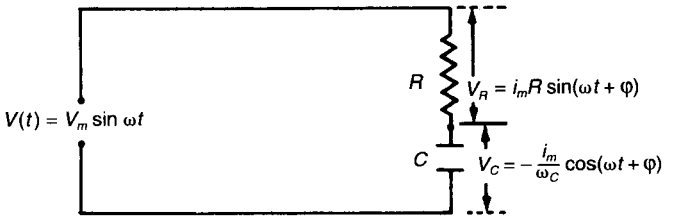


**Figure 10.2** The interaction of an $RC$ circuit with a sinusoidal input.

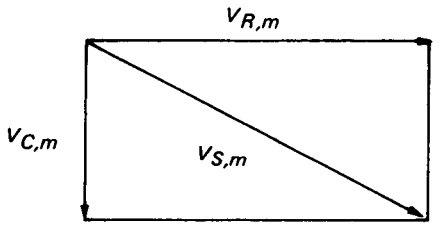


**Figure 10.3** The addition of the peak potentials in an *RC* circuit.

At every time $t$, the instantaneous potentials $V(t)$, $V_R(t)$, and $V_C(t)$ satisfy the equation

$$V(t) = V_R(t) + V_C(t) \tag{10.10}$$

The peak potentials, however, are not additive linearly because their maxima do not occur at the same time. To find the correct relationship, apply Eq. 10.7 at time $t = -(\varphi/\omega)$ with $i(t)$ from Eq. 10.8. The result is

$$i_m = \frac{V_m}{R}\cos\varphi = \frac{V_m}{R}\frac{1}{\sqrt{1+\tan^2\varphi}} = \frac{V_m}{\sqrt{R^2 + (1/\omega^2C^2)}} \tag{10.11}$$

Equation 10.11 is the analog of Ohm's law for the *RC* circuit. The "resistance" of the circuit is called the impedance $Z$ and is given by

$$Z = \sqrt{R^2 + (1/\omega^2C^2)} \tag{10.12}$$

Pictorially, the relationships expressed by Eqs. 10.11 and 10.12 are shown in Fig. 10.3. The quantity $R_c = 1/\omega C$ is called the capacitive resistance. The impedance $Z$, as well as $R$ and $R_c$, are measured in ohms.

Consider now an *LR* circuit as shown in Fig. 10.4. If the voltage given by Eq. 10.5 is applied at the input, Kirchhoff's second law gives, in this case,

$$V_m \sin\omega t - L\frac{di}{dt} = iR \tag{10.13}$$

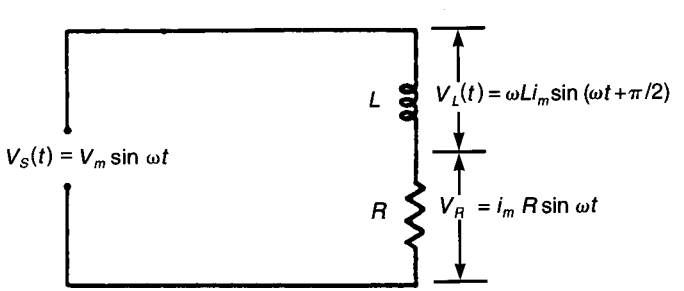


**Figure 10.4** The interaction of an *LR* circuit with a sinusoidal input.

As in the $RC$ circuit, the current will have the frequency $\omega$ and a phase difference $\varphi$, relative to the voltage. The current may be written as

$$i(t) = i_m \sin(\omega t - \varphi) \tag{10.14}$$

Substituting the value of the current from Eq. 10.14 into Eq. 10.13 and evaluating the resulting expression at $t = 0$ (see Prob. 10.2), one obtains

$$\tan \varphi = \frac{L\omega}{R} \tag{10.15}$$

which is the phase difference in the $LR$ circuit (equivalent to Eq. 10.9). To find the relationship between the peak values, Eq. 10.13 is evaluated at time $t = \varphi/\omega$. The result is

$$i_m = \frac{V_m}{L\omega} \sin \varphi = \frac{V_m}{L\omega} \frac{\tan \varphi}{\sqrt{1 + \tan^2 \varphi}} = \frac{V_m}{\sqrt{R^2 + L^2\omega^2}} \tag{10.16}$$

Thus, the impedance of an $LC$ circuit is

$$Z = \sqrt{R^2 + L^2\omega^2} \tag{10.17}$$

The quantity $R_L = L\omega$ is called the inductive reactance. If a circuit contains all three elements, $R$, $L$, $C$, it can be shown (see Prob. 10.3) that the phase difference and impedance are given by

$$\tan \varphi = \frac{\omega L - (1/\omega C)}{R} \tag{10.18}$$

$$Z = \sqrt{R^2 + [\omega L - (1/\omega C)]^2} \tag{10.19}$$

Every electronic component has a characteristic impedance. When a signal is transmitted from a unit with a high-impedance output to a low-impedance input, there is going to be a loss in the signal unless an impedance-matching device is used to couple the two units. Manufacturers of preamplifiers and amplifiers quote the impedance of the input and output for their products. Coaxial cables have an impedance between 90 and 100 Ω.

## 10.3 A DIFFERENTIATING CIRCUIT

A *differentiating circuit* consists of a capacitor and a resistor (Fig. 10.2). If a time-dependent voltage $V_i(t)$ is applied at the input, Eq. 10.10 relating the instantaneous values of the three voltages involved (Fig. 10.5) becomes

$$\frac{q(t)}{C} + Ri = \frac{q(t)}{C} + R\frac{dq(t)}{dt} = V_i(t) \tag{10.20}$$

where $q(t)$ is the charge of the capacitor at time $t$. If the input signal is a step

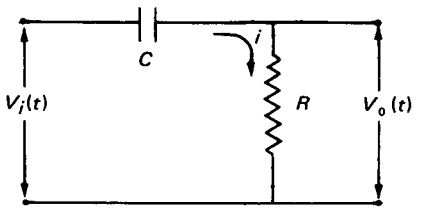


**Figure 10.5** A *CR* shaping circuit (differentiator).

function (Fig. 10.6), the output voltage is given (after solving Eq. 10.20) by

$$V_0(t) = R\frac{dq(t)}{dt} = V_{i,m}e^{-t/RC} \tag{10.21}$$

Figure 10.7 shows the output voltage if the input signal is a rectangular pulse of height $V_{i,m}$ and duration $T$. Notice that if $RC \ll T$, the output signal represents the derivative of the input. Indeed, from Eq. 10.20, if $RC \ll T$, then

$$\frac{V_i(t)}{R} = \frac{q}{RC} + \frac{dq}{dt} \approx \frac{q}{RC}$$

or

$$\frac{1}{R}\frac{dV_i}{dt} = \frac{1}{RC}\frac{dq}{dt} = \frac{1}{RC}i$$

Thus,

$$V_0(t) = iR = R\frac{dq}{dt} = RC\frac{dV_i}{dt} \tag{10.22}$$

and for this reason, this circuit is called a *differentiator*. If $V_i(t)$ is the pulse from a detector, the effect of differentiation is to force the pulse to decay faster.

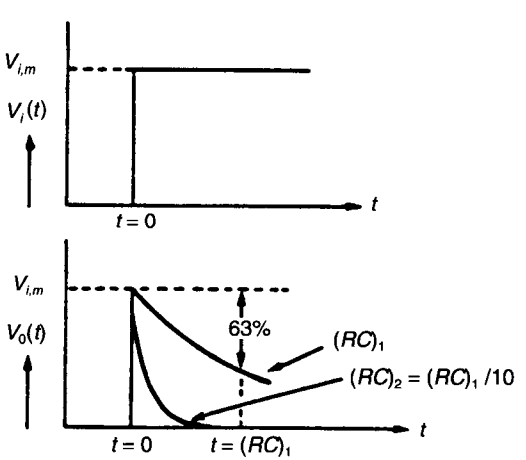


**Figure 10.6** The output signal of a *CR* shaping circuit for a step input.

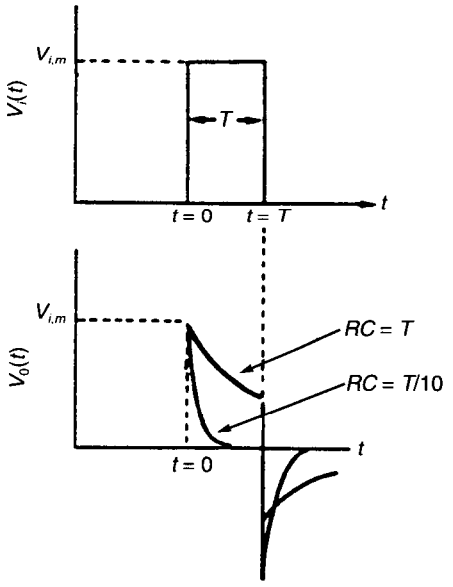


**Figure 10.7** The response of a *CR* circuit to a rectangular pulse.

As shown in Sec. 10.2, for a sinusoidal signal the peak value of the potential across the resistor of an *RC* circuit is related to the peak of the input signal by

$$\frac{V_{0,m}}{V_{i,m}} = \frac{R}{\sqrt{R^2 + R_C^2}} = \frac{R}{\sqrt{R^2 + 1/\omega^2 C^2}} \tag{10.23}$$

where $\omega = 2\pi f$ and $f$ is the frequency of input signal. According to Eq. 10.23, as the frequency decreases, the fraction of the signal appearing at the output of the differentiator also decreases, approaching zero for very low frequencies. For this reason, this circuit is called a *high-pass filter*. The output of the filter as a function of frequency is shown in Fig. 10.8. If the signal is not purely sinusoidal, it may be decomposed into a series of sine components with frequencies that are multiples of a fundamental one (this is called Fourier analysis). Going through

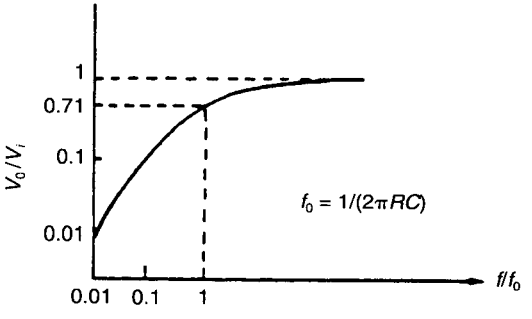


**Figure 10.8** The output of a differentiator (high-pass) filter as a function of input frequency.

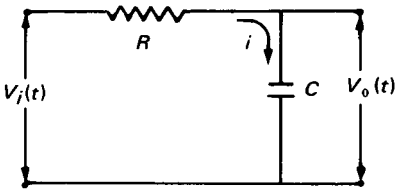


**Figure 10.9** An *RC* shaping circuit (integrator).

the high-pass filter, the lower frequencies will be attenuated more than the higher ones.

## 10.4 AN INTEGRATING CIRCUIT

An *integrating circuit* also consists of a resistor and a capacitor, but now the output signal is taken across the capacitor (Fig. 10.9). Equation 10.20 applies in such a case too, and the output signal as a result of a step input is given by

$$V_0(t) = \frac{q(t)}{C} = V_{i,m}(1 - e^{-t/RC}) \tag{10.24}$$

Input and output signals are shown in Fig. 10.10. Figure 10.11 shows the output voltage if the input signal is a rectangular pulse of height $V_{i,m}$ and duration $T$. If $RC \gg T$, the output signal looks like the integral of the input. Indeed, from Eq. 10.20,

$$\frac{V_i(t)}{R} = \frac{q(t)}{CR} + \frac{dq(t)}{dt}$$

which gives, if $RC \gg T$,

$$\frac{V_i(t)}{R} \approx \frac{dq}{dt}$$

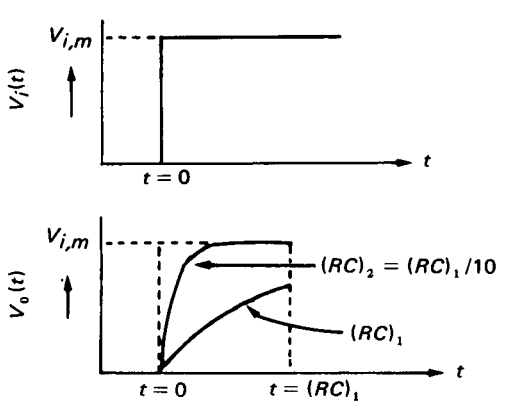


**Figure 10.10** The output signal of an *RC* shaping circuit for a step input (top).

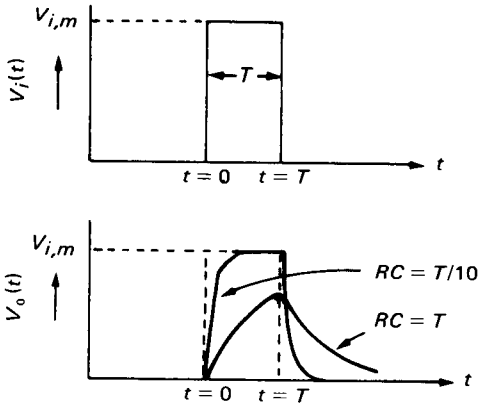


**Figure 10.11** The response of an $RC$ circuit to a rectangular pulse.

Then, from Eq. 10.24,

$$V_0(t) = \frac{q(t)}{C} = \frac{1}{RC}\int V_i(t)\,dt \tag{10.25}$$

and for this reason, this circuit is called an *integrator*.

For a sinusoidal input signal, the peak value of the voltage across the capacitor is related to the peak value of the input signal by

$$\frac{V_{0,m}}{V_{i,m}} = \frac{R_C}{\sqrt{R^2 + R_C^2}} = \frac{1/\omega C}{\sqrt{R^2 + 1/\omega^2 C^2}} \tag{10.26}$$

As the frequency increases, the ratio given by Eq. 10.26 decreases, and for this reason this circuit is called a *low-pass filter*. Going through the filter, lower frequencies fare better than the higher ones. The output of the filter as a function of frequency is shown in Fig. 10.12.

## 10.5 DELAY LINES

Any signal transmitted through a coaxial cable is delayed by a time $T = \sqrt{LC}$ seconds per unit length, where $L$ is the inductance per unit length and $C$ is the

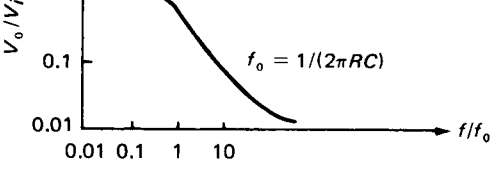


**Figure 10.12** The output of an integrator (low-pass) filter as a function of input frequency.

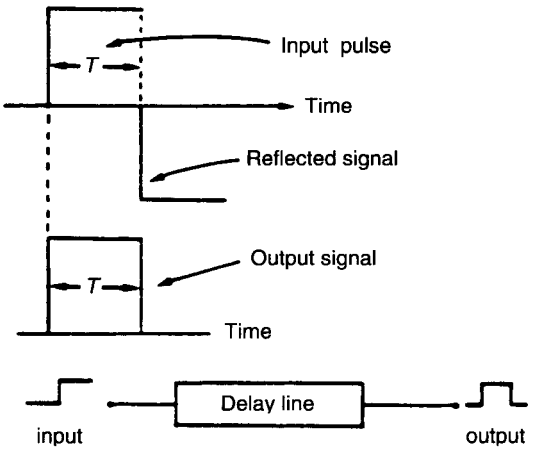


**Figure 10.13** The use of a delay line to form a rectangular pulse.

capacitance per unit length. For ordinary coaxial cables, the delay is about 5 ns/m. For larger delays, the central conductor of the cable is spiraled to increase the inductance per unit length.

Commercial delay lines are a little more complicated than a simple cable. They are used not only to delay a signal, but also to produce a rectangular pulse for subsequent pulse shaping or for triggering another electronic unit (e.g., a scaler). The formation of the rectangular pulse is achieved by reflecting the delayed signal at the end of the delay line, bringing it back to the input and adding it to the original signal (Fig. 10.13). A double delay line produces the double rectangular pulse shown in Fig. 10.14.

## 10.6 PULSE SHAPING

The pulse produced at the output of a radiation detector has to be modified or *shaped* for better performance of the counting system. There are three reasons that necessitate pulse shaping:

1. *To prevent overlap.* Each pulse should last for as short a period of time as possible, and then its effect should be abolished so that the system may be

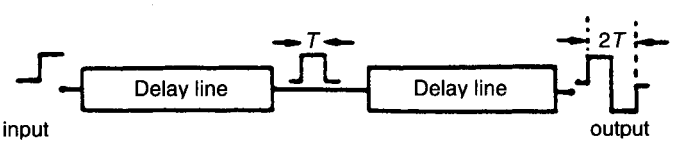


**Figure 10.14** The effect of a double delay line.

ready for the next pulse. Without pulse shaping, the detector signal lasts so long that pulses overlap. If only the number of particles is counted, pulse overlap leads to loss of counts (dead time loss). In spectroscopy measurements, pulse overlap worsens the resolution.

2. *To improve the signal-to-noise ratio.* Noise created in the detector and the early amplification stages accompanies the detector signal. Appropriate pulse shaping can enhance the signal while at the same time reduce the noise. Thus, the signal-to-noise ratio will improve, which in turn, leads to better energy resolution.
3. *For special pulse manipulation.* The detector pulse may, in certain applications, need special pulse shaping to satisfy the needs of certain units of the counting system. As an example, the signal at the output of the amplifier needs to be stretched before it is recorded in the memory of a multichannel analyzer (see Sec. 10.12).

The pulse-shaping methods used today are based on combinations of *RC* circuits and delay lines. For example, the use of a *CR–RC* circuit combination produces the pulse shown in Fig. 10.15. The exact shape and size of the output pulse depends on the relative magnitudes of the time constants $C_1R_1$ and $C_2R_2$. The use of the *CR–RC* circuit combination provides, in addition to pulse shaping, a better signal-to-noise ratio by acting as high-pass and low-pass filter for undesired frequencies.

If one adds more *RC* integrating circuits, the pulse will approach a Gaussian shape (Fig. 10.16).

If one applies a *CR–RC–CR* combination, the result is a doubly differentiated pulse as shown in Fig. 10.17. Commercial amplifiers usually provide either singly or doubly differentiated pulses. In all cases, the final pulse is the result of repeated application of *CR–CR* circuits. Figure 10.18 shows such pulses produced by the application of many *RC* and *CR* circuits, called unipolar and bipolar pulses, respectively. Pulse shaping using a delay line and an *RC* circuit is shown in Fig. 10.19.

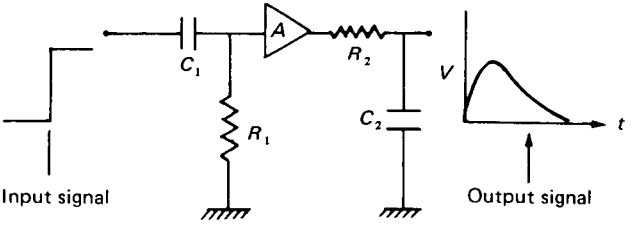


**Figure 10.15** An example of *CR–RC* shaping. The triangle indicates the amplification unit (A) that isolates the two shaping circuits.

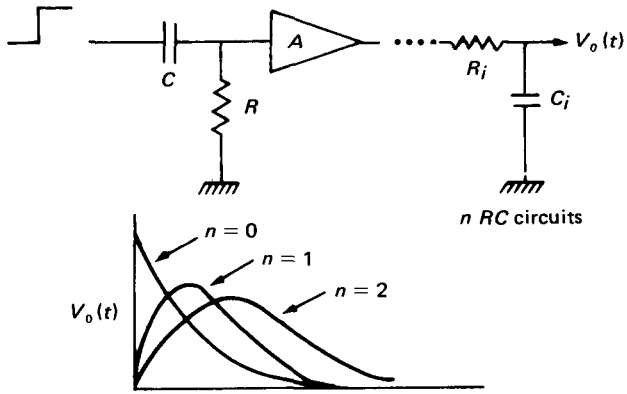


**Figure 10.16** The output pulse after using many shaping circuits. The triangle indicates the amplification unit that isolates any two consecutive shaping circuits.

## 10.7 TIMING

The term *timing* refers to the determination of the time of arrival of a pulse. Timing experiments are used in measurement of the time development of an event (e.g., measurement of the decay of a radioactive species), measurement of true coincident events out of a large group of events, and discrimination of different types of particles based on the different time characteristics of their pulse (pulse-shape discrimination).

Timing methods are characterized as "slow" or "fast" depending on the way the signal is derived. Slow timing signals are generated by an integral discriminator or a timing single-channel analyzer. In either case, timing is obtained by using a shaped signal at the output of an amplifier. Fast timing signals are based on the unshaped pulse at the output of the detector or on a signal shaped specifically for timing.

Many timing methods have been developed over the years. All the methods pick the time based on a certain point in the "time development" of the pulse,

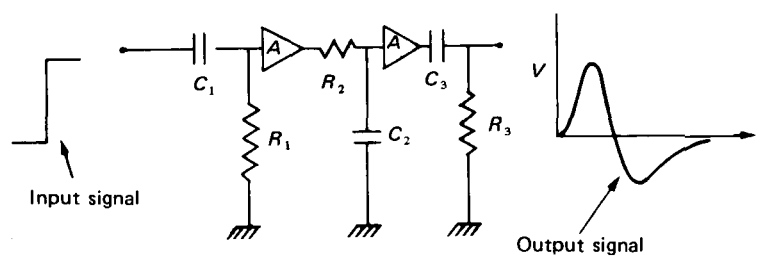


**Figure 10.17** A doubly differentiated pulse.

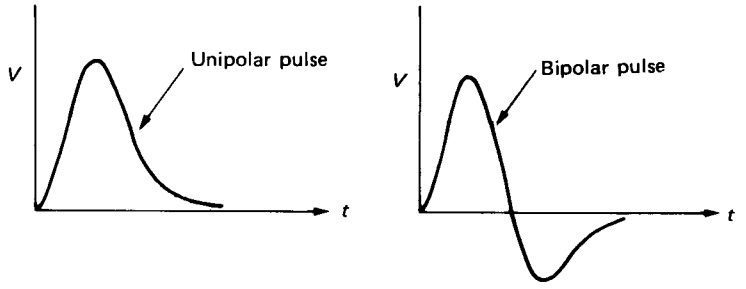


**Figure 10.18** A unipolar and bipolar pulse as a result of the application of many CR and RC circuits.

but they differ in the way that point is selected. Three methods are discussed here.[1-5]

### 10.7.1 The Leading-Edge Timing Method

The leading-edge timing method determines the time of arrival of a pulse with the help of a discriminator, as shown in Fig. 10.20. A discriminator threshold is set and the time of arrival of the pulse is determined from the point where the pulse crosses the discriminator threshold.[†]

The leading-edge timing method is simple, but it introduces uncertainties because of "jitter" and "walk" (Fig. 10.21). *Jitter* is another name for electronic noise. The timing uncertainty due to jitter depends on the amplitude of the noise and the slope of the signal close to the discriminator threshold. *Walk* originates when differences in the rate of pulse-risetime cause pulses starting at the same point in time to cross the discriminator level at different positions. Walk can be reduced by setting the discriminator level as low as possible or by restricting the amplitude range of the acceptable pulses. Both of these corrective measures, however, introduce new difficulties. Setting the discriminator

[†]Rectangular pulses such as the ones shown in Fig. 10.20 are called logical pulses.

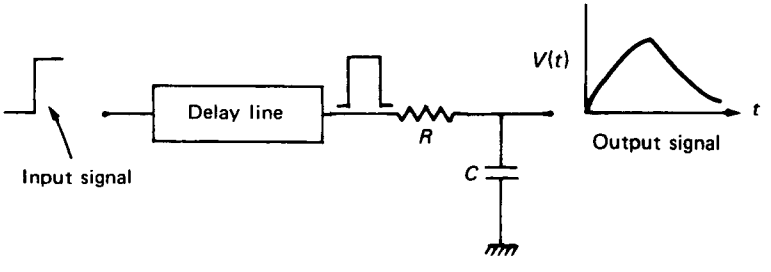


**Figure 10.19** Pulse shaping using a single delay line and an *RC* circuit.

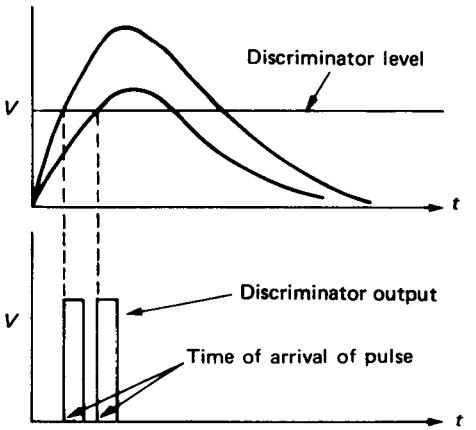


**Figure 10.20** The time of arrival of the pulse is determined from the instant at which the pulse crosses the discriminator threshold.

level too close to the noise level may allow part of the random noise to be counted. Limiting the range of acceptable pulses reduces the counting rate.

### 10.7.2 The Zero-Crossing Timing Method

The zero-crossing method reduces the errors due to jitter and walk by picking the time from the zero crossing of a bipolar pulse (Fig. 10.22). Ideally, all the pulses cross the zero at the same point, and the system is walk free. In practice, there is some walk because the position of zero crossing depends on pulse risetime.† The dependence on pulse risetime is particularly important for Ge detectors because the pulses produced by Ge detectors exhibit considerable variations in their time characteristics. To reduce the uncertainties still present with the zero-crossing method, the constant-fraction method has been developed specifically for Ge detectors.

†Pulse risetime is taken as the time it takes the pulse to increase from 10 percent to 90 percent of its value.

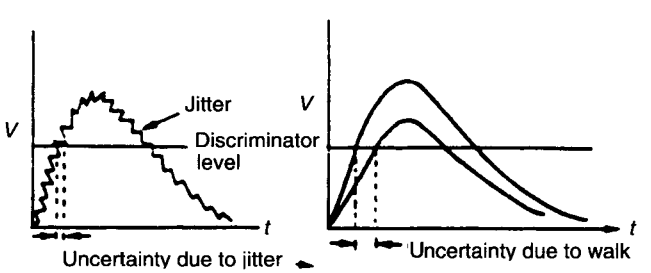


**Figure 10.21** Timing uncertainty due to jitter and walk.

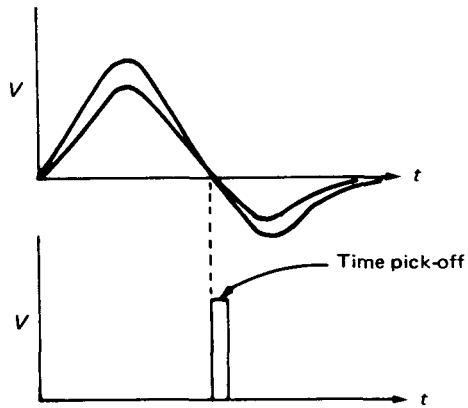


**Figure 10.22** Timing by the zero-crossing method.

### 10.7.3 The Constant-Fraction Timing Method

The principle of constant-fraction timing is shown in Fig. 10.23. First, the original pulse (Fig. 10.23*a*) is attenuated by a factor $f$ equal to the fraction of the pulse height on which the timing will be based (Fig. 10.23*b*). The original pulse is inverted and delayed (Fig. 10.23*c*) for a time longer than its risetime. Finally, the signals in Figs. 10.23*c* and 10.23*b* are added to give the signal in Fig. 10.23*d*. The time pick-off, taken as the zero-crossing point, is thus defined by the preselected fraction of the pulse height and is independent of the pulse amplitude. It can be shown that pulses with the same risetime always give the same zero-crossing time.

## 10.8 COINCIDENCE-ANTICOINCIDENCE MEASUREMENTS

There are times in radiation measurements when it is desirable or necessary to discard the pulses due to certain types of radiation and accept only the pulses from a single type of particle or from a particle or particles coming from a specific direction. Here are two examples of such measurements.

1. *Detection of pair-production events.* When pair production occurs, two 0.511-MeV gammas are emitted back-to-back. To insure that only annihilation photon are counted, two detectors are placed 180° apart, and only events that register simultaneously (coincident events) in both detectors are recorded.

2. *Detection of internal conversion electrons.* Radioisotopes emitting internal conversion (IC) electrons also emit gammas and X-rays. The use of a single detector to count electrons will record not only IC electrons but also Compton electrons produced in the detector by the gammas. To eliminate the Compton electrons, one can utilize the X-rays that are emitted simultaneously with the IC electrons. Thus, a second detector is added for X-rays and the counting system

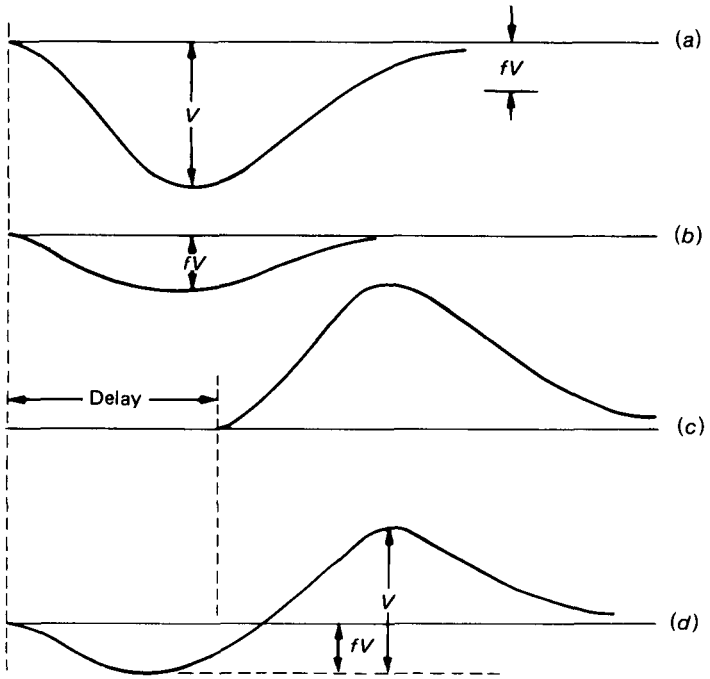


**Figure 10.23** Timing by the constant-fraction technique.

is required to record only events that are coincident in these two detectors. This technique excludes the detection of Compton electrons.

Elimination of undesirable events is achieved by using a coincidence (or anti-coincidence) unit. Consider the counting system shown in Fig. 10.24. The source emits particles detected by detectors 1 and 2. After amplification, the detector signals are fed into a timing circuit, which in turn generates a pulse signifying the time of occurrence in the detector of the corresponding event (1) or (2). The timing signals are fed into a coincidence unit, so constructed that it produces an output signal only when the two timing pulses are coincident. If the objective is to count only the number of coincident events, the output of the coincidence unit is fed into a scaler. If, on the other hand, the objective is to measure the energy spectrum of particles counted by detector 1 in coincidence with particles counted by detector 2, the output signal of the coincidence unit is used to "gate" a multichannel analyzer (MCA) that accepts the energy pulses from detector 1. The gating signal permits the MCA to store only those pulses from detector 1 that are coincident with events in detector 2.

In theory, a true coincidence is the result of the arrival of two pulses at exactly the same time. In practice, this "exact coincidence" seldom occurs, and for this reason a coincidence unit is designed to register as a coincident event those pulses arriving within a finite but short time interval $\tau$. The interval $\tau$,

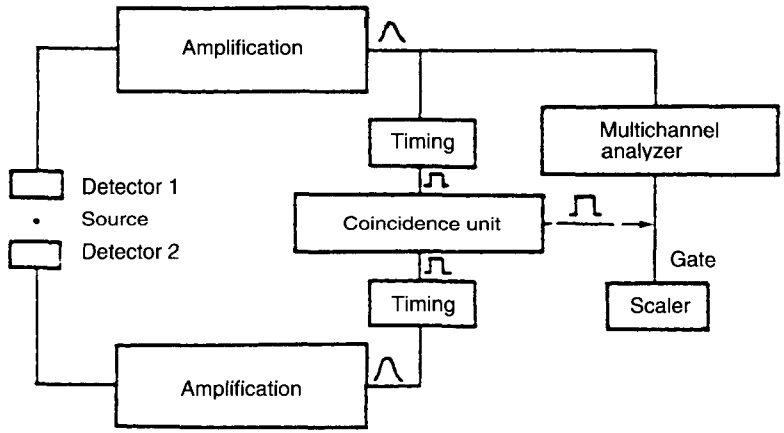


**Figure 10.24** A simple coincidence measurement setup.

called the *resolving time* or the *width* of the coincidence, is set by the observer. Typical values of $\tau$ are 1–5 $\mu$s for "slow" coincidence and 1–10 ns for "fast" coincidence measurements. By introducing the width $\tau$, the practical definition of coincidence is

Two or more events are coincident if they occur within the time period $\tau$.

According to this definition, events (1) and (2) or (2) and (3) in Fig. 10.25 are coincident, but events (1) and (3) are not.

As stated earlier, the coincidence unit is an electronic device that accepts pulses (events) in two or more input channels and provides an output signal *only* if the input pulses arrive within the time period $\tau$. The logic of a coincidence unit is shown in Fig. 10.26.

An anticoincidence unit is an electronic device that accepts pulses (events) in two input channels and provides an output signals *only* if the two events *do not* arrive within the time period $\tau$. The logic of an anticoincidence unit is shown in Fig. 10.27

Figures 10.26 and 10.27 both show a "coincidence" unit as the instrument used because, commercially, a single component is available that, with the flip of a switch, is used in the coincidence or anticoincidence mode.

For a successful coincidence or anticoincidence measurement, the detector signals should not be delayed by any factors other than the time of arrival of the particles at the detector. If it is known that it takes longer to generate the signal

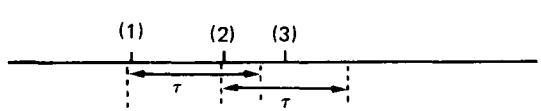


**Figure 10.25** Events (1) and (2) or events (2) and (3) are coincident. Events (1) and (3) are not.

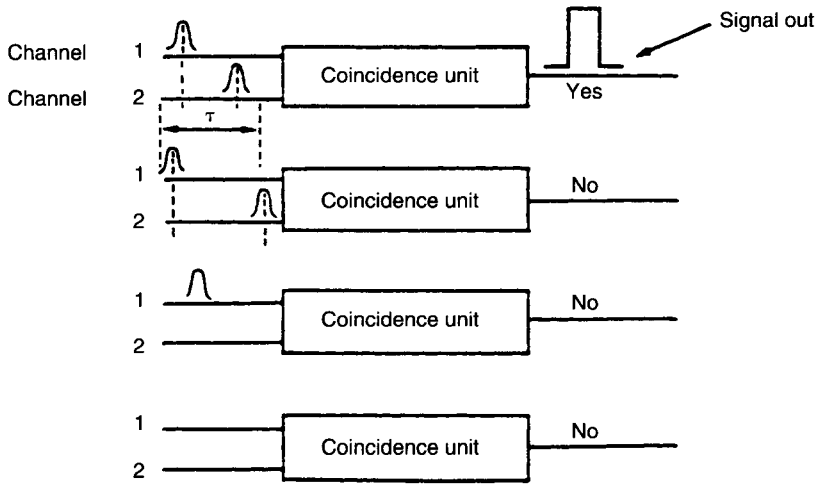


**Figure 10.26** The logic of a coincidence unit with two input channels.

in one detector than in another, the signal from the fast detector should be delayed accordingly to compensate for this difference. This compensation is accomplished by passing the signal through a delay line before it enters the coincidence unit. A delay line is always needed if the detectors used in the coincident measurement are not identical. The value of the relative delay needed is determined as follows.

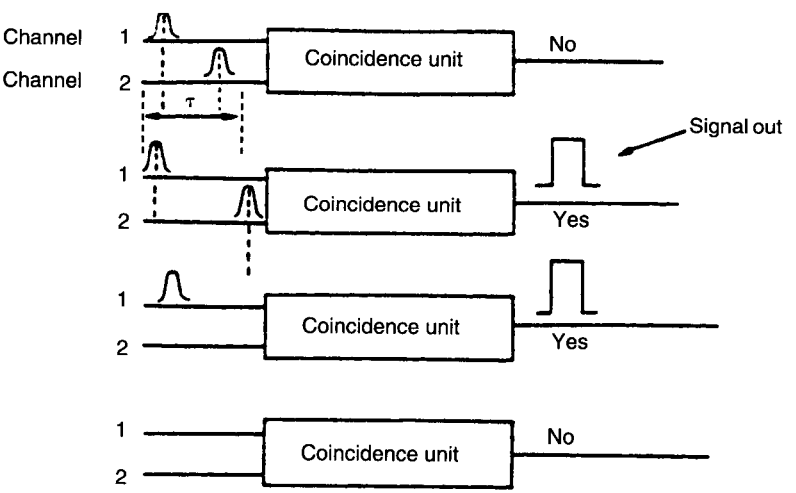


**Figure 10.27** The logic of an anticoincidence unit.

Consider what is probably the simplest type of coincidence circuit, the additive type shown in Fig. 10.28. The coincidence unit is summing the input pulses. When two pulses overlap, their sum exceeds a discriminator threshold and the unit produces an output pulse. If the width of the input pulse is $T$, the resolving time is essentially $\tau = 2T$. Assume now that a system has been set up as shown in Fig. 10.24, with the addition of a delay line in channel 2 between the timing and the coincidence units. If one measures the number of coincidences as a function of the delay between the two signals, the result will be the delay or resolving-time curve shown in Fig. 10.29. The proper relative delay is the value corresponding to the center of the flat region. The ideal (rectangular) curve will be obtained if the time jitter is zero.

Since the pulses from the two detectors arrive randomly, a certain number of accidental (or chance) coincidences will always be recorded. Let

$$r_1 = \text{counting rate of detector 1}$$
$$r_2 = \text{counting rate of detector 2}$$
$$r_a = \text{accidental coincidence rate}$$

Consider a single pulse in channel 1. If a pulse occurs in channel 2 within the time period $\tau$, then a coincidence will be registered. Since the number of pulses in channel 2 during time $\tau$ is $r_2\tau$, the rate of accidental coincidences is

$$r_a = r_1 r_2 \tau \tag{10.27}$$

Equation 10.27 gives accidental coincidences of first order. Corrections for multiple coincidences of higher order have also been calculated.[6, 7]

If $S$ is the strength of the source, $\epsilon_1$ and $\epsilon_2$ the efficiencies, $\Omega_1$ and $\Omega_2$ the solid angle factors, and $F_1$ and $F_2$ any other factors that affect the measurement of particles counted by detectors 1 and 2 (see Chap. 8), then the true coinci-

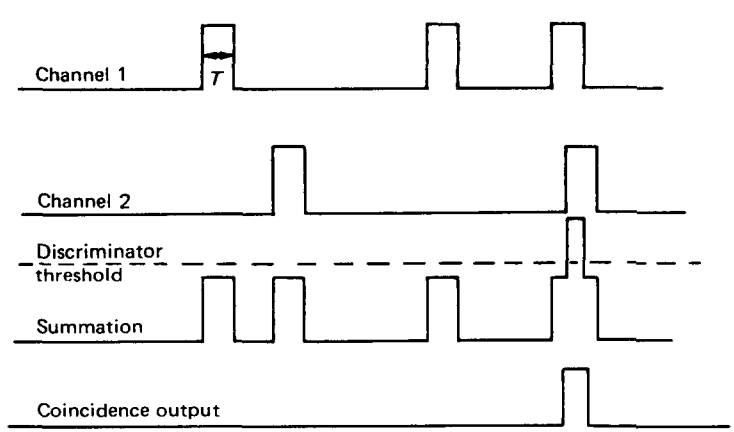


**Figure 10.28** The coincidence circuit of the additive type.

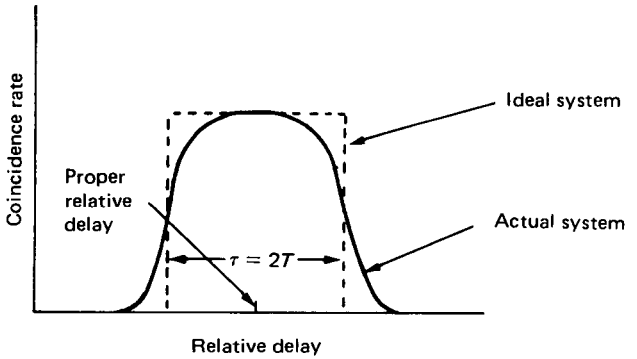


**Figure 10.29** The delay or resolving-time curve.

dence rate $r_t$ is given by

$$r_t = S\epsilon_1\epsilon_2\Omega_1\Omega_2F_1F_2 \tag{10.28}$$

and from Eq. 10.27 the accidental coincidence rate is

$$r_a = S^2\epsilon_1\epsilon_2\Omega_1\Omega_2F_1F_2\tau \tag{10.29}$$

The *figure of merit* in a coincidence experiment is the ratio

$$Q = \frac{r_t}{r_a} = \frac{1}{S\tau} \tag{10.30}$$

which should be as high as possible. Equation 10.30 shows that this ratio improves when $S$ and $\tau$ decrease. Unfortunately, the values for both of these quantities have constraints. The value of $\tau$ is limited by the performance of the detector and by the electronics. The source strength $S$ has to be of a certain value for meaningful counting statistics to be obtained in a reasonable time. It is interesting to note that when the source strength increases, both true and accidental coincidence rates increase but the ratio $Q$ (Eq. 10.30) decreases, because $r_t \propto S$ but $r_a \propto S^2$.

Another coincidence technique involves the use of a *time-to-amplitude converter* (TAC). A TAC is an electronic unit that converts the time difference between two pulses into a voltage pulse between 0 and 10 V. The height of the pulse is proportional to the time difference between the two events. The time spectrum of the two detectors is stored directly in the MCA. A "time" window is set around the coincidence peak (Fig. 10.30). A second window of equal width is set outside the peak to record accidental coincidences only.

The advantages of using a TAC are

1. No resolving curve need be taken.
2. No resolving time is involved.

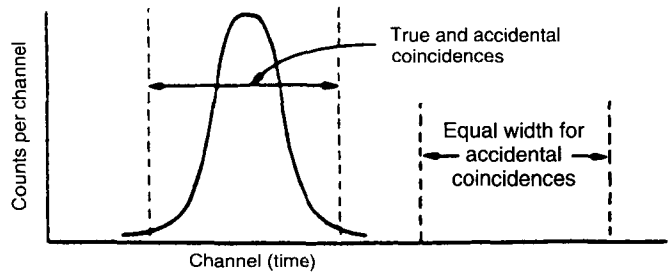


**Figure 10.30** An MCA spectrum taken with a TAC

3. The number of channels and the range of time intervals analyzed may be changed over a wide range by simply changing the conversion gain of the MCA.

Most TACs cannot distinguish the sequence of events—i.e., they cannot tell if a pulse from channel 1 precedes a pulse from channel 2 and vice versa. To avoid this ambiguity and also to create a measurable difference between the pulses, the signal from one detector is usually shifted by a fixed delay.

Figure 10.31 shows what is now a common counting system for $\gamma$-$\gamma$ coincidence measurements using a NaI(Tl) detector and a Ge(Li) detector. The initials ADC stand for analog-to-digital converter (see Sec. 10.12).

## 10.9 PULSE-SHAPE DISCRIMINATION

Pulse-shape discrimination (PSD) is the name given to a process that differentiates pulses produced by different types of particles in the same detector. Although PSD has found many applications, its most common use is to discriminate between pulses generated by neutrons and gammas in organic scintillators (see also Chap. 14), and it is this type of PSD that will be discussed.

Measurement of the amount of light produced in organic scintillators by neutrons and gammas shows that both the differential and integral light intensities are different as functions of time. Figure 10.32, presenting the results of Kuchnir & Lynch,[8] illustrates this point. It is obvious that the pulses from neutrons and gammas have different time characteristics, and it is this property that is used as the basis for PSD.

Many different methods have been proposed and used for successful PSD.[9-14] One method doubly differentiates the detector pulse, either using *CR* circuits or a delay line, and bases the PSD on the time interval between the beginning of the pulse and the zero crossing point. This time interval, which is

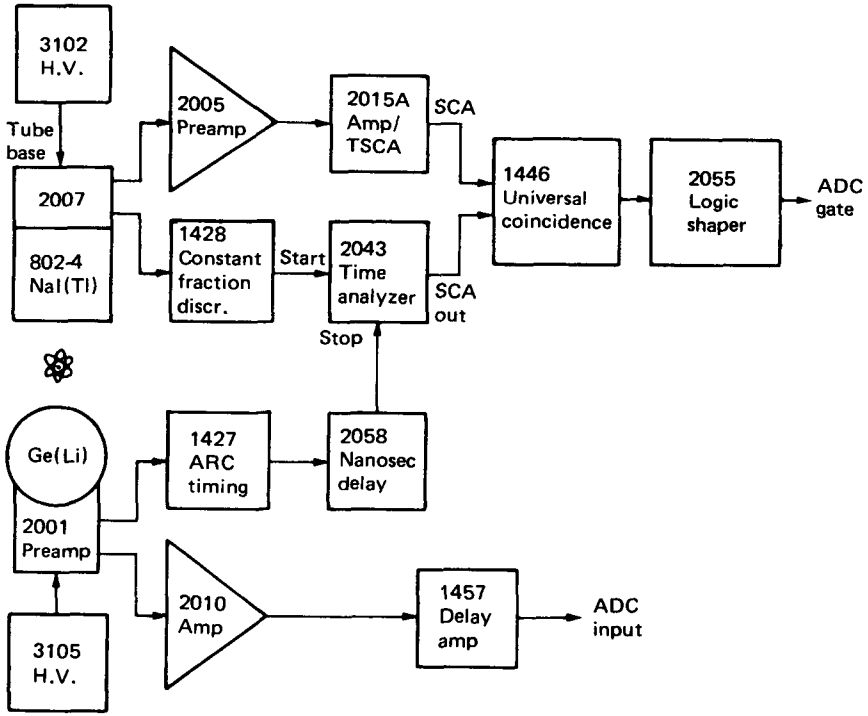


**Figure 10.31** A NaI–Ge(Li) $\gamma$-$\gamma$ coincidence system (from Ref. 25; numbers indicate Canberra models).

essentially independent of the pulse amplitude but depends on the pulse shape, is usually converted into a pulse by means of a TAC. The pulse from the TAC may be used to gate the counting system. Figure 10.33 shows a block diagram for such a counting system. The result of $n$-$\gamma$ discrimination is usually a spectrum that resembles Fig. 10.34. Actually, the $\gamma$ peak is due to electrons produced by the gammas, and the neutron peak is due to protons recoiling after collisions with the incident neutrons. More details of this method of neutron detection are given in Chap. 14.

A second method, introduced by Brooks,[12] integrates the charge from the early part of the pulse and compares it to the total charge. A third method, introduced by Kinbara and Kumahara,[13] differentiates $n$-$\gamma$ pulses by a measurement of the risetime of the pulse. A final example of a PSD technique is that used by Burrus and Verbinski,[14,15] based on a design by Forté.[16] Details of the circuitry are given in Refs. 14 and 15. This PSD method produces a large positive pulse output for neutrons and a small positive or a large negative pulse for gammas.

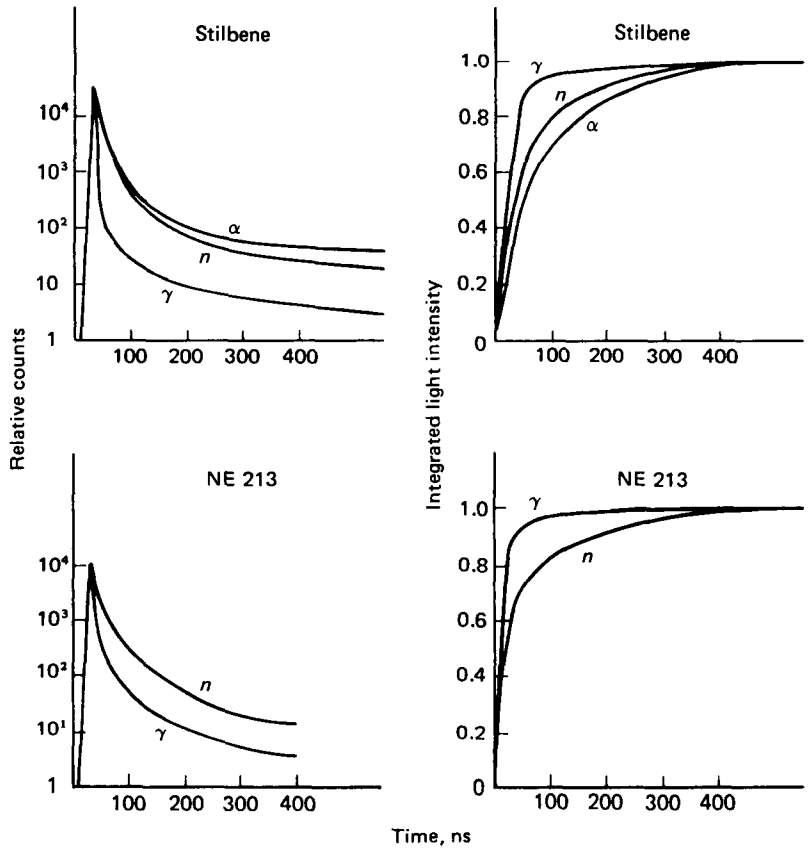


**Figure 10.32** The light produced by neutrons and gammas in stilbene and NE 213. Light intensity is shown at left: integrated light intensity is shown at right (based on data of Ref. 8).

## 10.10 PREAMPLIFIERS

In Sec. 1.5.5, a few general comments were made about preamplifiers. It was stated that the primary purpose of the preamplifier is to provide an optimum coupling between the detector and the rest of the counting system. A secondary purpose of the preamplifier is to minimize any sources of noise, which will be transmitted along with the pulse and thus may degrade the energy resolution of the system. This second objective, low noise, is particularly important with semiconductor detectors, which are the counters offering the best energy resolution.

There are three basic types of preamplifiers: charge-sensitive, current-sensitive, and voltage-sensitive. The voltage-sensitive preamplifier is not used in spectroscopy because its gain depends on the detector capacitance, which in turn depends on the detector bias. The charge-sensitive preamplifier is the most

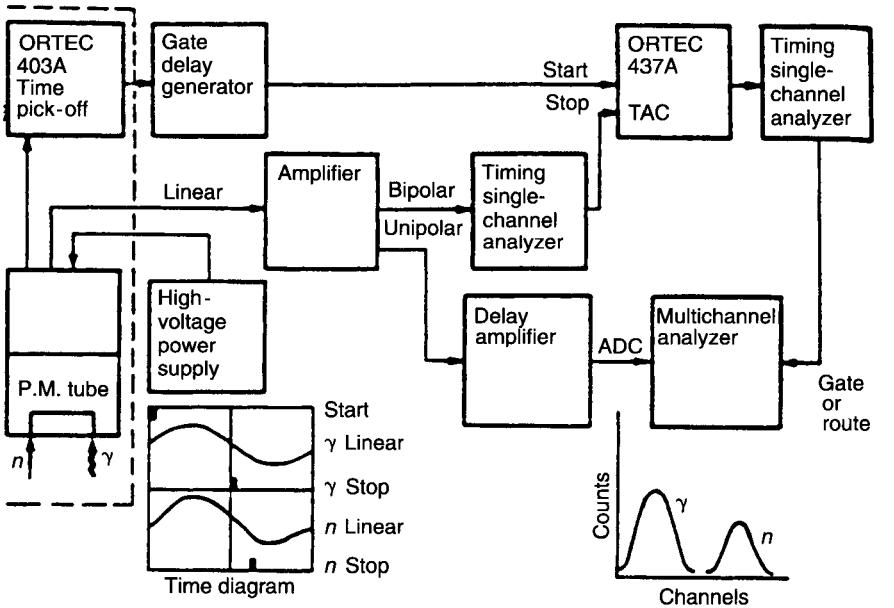


**Figure 10.33** A block diagram for a PSD system (reproduced from *Instruments for Research and Applied Sciences* by permission of EG &G ORTEC, Oak Ridge, Tennessee).

commonly used in spectroscopic measurements and the only type used with semiconductor detectors.

To understand the basic features of a charge-sensitive preamplifier, consider the basic circuit associated with a semiconductor detector, shown in Fig. 10.35. The high-voltage (HV) bias applied to the detector is usually connected through the detector to the first stage of the charge-sensitive preamplifier. In Fig. 10.35, $C_f$ is the feedback capacitor ($\sim$ 1 pF) and $R_f$ is the feedback resistor ($\sim$ 1000 M$\Omega$).[17] The triangle with the letter A indicates the first stage of the preamplifier, which today is usually a field-effect transistor (FET). The FET is a p-n junction with reverse bias, exhibiting extremely low noise. The type of coupling shown in Fig. 10.35 is called dc coupling. There is an ac coupling, too,

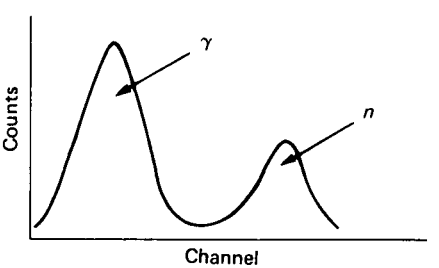


**Figure 10.34** The result of $\gamma$-$n$ discrimination using PSD.

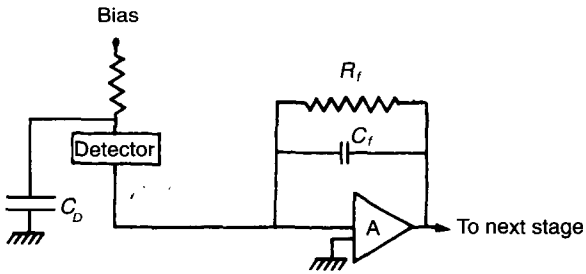


**Figure 10.35** The first stage of a charge-sensitive preamplifier dc-coupled to the bias circuit.

in which the detector is coupled to the FET through a coupling capacitor (see Nicholson, p. 110).

The detector sees the FET stage as a large capacitor of magnitude $AC_f$. As long as $AC_f \gg C_i$, where $C_i$ is the total input capacitance consisting of the detector capacitance $C_D$, the cable capacitance, etc., the voltage at the output of the preamplifier is equal to

$$V_0 = \frac{Q}{C_f} \tag{10.31}$$

where $Q$, the charge produced in the detector, is given by

$$Q = \frac{Ee}{w} \tag{10.32}$$

where $E$ = energy of the particle
$e$ = electronic charge = $1.6 \times 10^{-19}$ coulombs
$w$ = average energy required to produce one electron-hole pair

The major components of $C_i$ are the detector capacitance $C_D$ and that of the cables between the detector and the preamplifier. Both of these components are controlled by the user to a certain extent.

The noise of the charge-sensitive preamplifier depends on three parameters: the noise of the input FET, the input capacitance $C_i$, and the resistance connected to the input. The noise can be determined by injecting a charge $Q$, equivalent to $E$, into the preamplifier and measuring the amplitude of the generated pulse. Commercial preamplifiers are provided with a test input for that purpose. In general, the noise expressed as the width (keV) of a Gaussian distribution increases as input capacitance increases (Fig. 10.36).

The output pulse of the preamplifier has a fast risetime (of the order of nanoseconds) followed by a slow exponential decay, ~ 100 $\mu$s (Fig. 10.37). The useful information in the pulse is its amplitude and its risetime. The risetime is particularly important when the signal is going to be used for timing. The observer should be aware that the risetime increases with external capacitance. The preamplifier pulse is shaped in the amplifier by the methods described in Sec. 10.6.

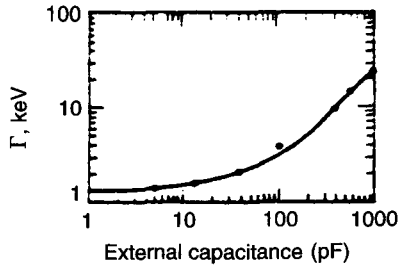


**Figure 10.36** The dependence of noise on external capacitance for a typical charge-sensitive preamplifier (from *Instruments for Research and Applied Sciences* by permission of EG & G ORTEC, Oak Ridge, Tennessee).

The *sensitivity* (or *gain*) of a charge-sensitive preamplifier is expressed by the ratio $V/E$, where $V$ is given by Eq. 10.31. For a 1-MeV particle in a germanium detector, the sensitivity is (using $C_f \approx 5$ pF)

$$\frac{V}{E} = \frac{Q}{EC_f} = \frac{Ee}{EC_f w} = \frac{e}{C_f w} = \frac{1.6 \times 10^{-19}}{(5 \times 10^{-12})(3 \times 10^{-6})} \sim 10 \text{ mV/MeV}$$

A current-sensitive preamplifier is used to transform fast current pulses produced by a photomultiplier into a voltage pulse. The current-sensitive preamplifier is an amplifying instrument. The sensitivity (or gain) of such a unit is expressed as $V_{out}/I_{in}$, i.e., in mV/mA with typical values of the order of 500 mV/mA. The risetime of the pulse is $\sim 1$ ns.

## 10.11 AMPLIFIERS

As explained in Sec. 1.5.6, the amplifier plays the two roles of amplifying and shaping the signal. The need for amplification is obvious. The output signal of the preamplifier, being in the range of a few millivolts, cannot travel very far or be manipulated in any substantial way without losing the information it carries or being itself lost in the noise. Commercial amplifiers consisting of many amplification stages increase the amplitude of the input signal by as many as 2000 times, in certain models.

The need for shaping the signal was explained in Sec. 10.6. The type of shaping that is applied depends on the requirements of the measurement. For spectroscopy measurements where good energy resolution is the important

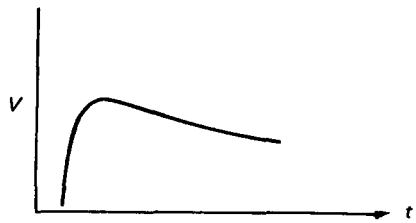


**Figure 10.37** Typical pulse from a charge-sensitive preamplifier.

parameter, pulse shaping should not decrease the signal-to-noise ratio. For timing measurements, depending on the method of time pick-off, the signal may be singly or doubly differentiated or be shaped by a single or double delay line.

For a good measurement, the amplifier should satisfy many requirements.[18-23] Not all types of measurements, however, require the same level of performance. For example, if one measures only the number of particles and not their energy, the precision and stability of the amplification process can be relatively poor. It is in spectroscopy measurements, particularly measurements using semiconductor detectors, that the requirements for precision and stability are extremely stringent. Since the energy resolution of Ge detectors is of the order of 0.1 percent, the dispersion of the pulses due to the amplification process should be much less, about 0.01 percent.

An ideal spectroscopy amplifier should have a constant amplification for pulses of all amplitudes without distorting any of them. Unfortunately, some pulse distortion is always present because of electronic noise, gain drift due to temperature, pulse pile-up, and limitations on the linearity of the amplifier.

The effect of electronic noise on energy resolution was discussed in Sec. 9.6.2. Random electronic noise added to equal pulses makes them unequal (see Fig. 9.12). Gain drift of an amplifier is caused by small changes in the characteristics of resistors, capacitors, transistors, etc., as a result of temperature changes. The value of the gain drift, always quoted by the manufacturer of the instrument, is for commercial amplifiers of the order of 0.005 percent per °C or less.

Since the time of arrival of pulses is random, it is inevitable that a pulse may arrive at a time when the previous one did not fully decay. Then the incoming pulse "piles up" on the tail of the earlier one and appears to have a height different from its true one. Pulse pile-up depends on the counting rate.

The linearity of an amplifier is expressed as differential and integral.

*Differential nonlinearity* is a measure of the change in amplifier gain as a function of amplifier input signal. Referring to Fig. 10.38, the differential

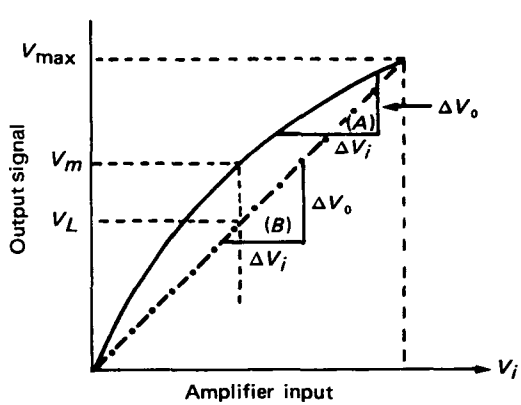


**Figure 10.38** Diagram used for the definition of differential and integral linearity of an amplifier. The output signal of a perfect amplifier plotted versus input signal should give the straight line shown (-·-·-·).

nonlinearity in percent is given by

$$\frac{(\Delta V_0/\Delta V_i)_A}{(\Delta V_0/\Delta V_i)_B}(100) \tag{10.33}$$

In Eq. 10.33, the numerator is the slope of the amplifier gain curve at the point where the nonlinearity is measured, and the denominator is the slope of the straight line as shown in Fig. 10.38.

*Integral nonlinearity* is defined as the maximum vertical deviation between the straight line shown in Fig. 10.38 and the actual amplifier gain curve, divided by the maximum rated output of the amplifier. Referring to Fig. 10.38, the integral nonlinearity in percent is given by

$$\frac{V_m - V_L}{V_{\max}}(100) \tag{10.34}$$

The integral nonlinearity is one of the specifications of commercial amplifiers and has a value of about 0.05 percent or less over the range 0–10 V.

There are many types of commercial amplifiers designed to fit the specific needs of spectroscopic or timing measurements. Companies like Canberra, EG & G ORTEC, etc., offer a wide selection of such instruments.

## 10.12 ANALOG-TO-DIGITAL CONVERTERS (ADC)

As discussed in Sec. 9.9, the backbone of an MCA is the analog-to-digital converter (ADC), the unit that digitizes the input pulse height and assigns it to a specific channel. Many types of ADCs have been developed, but the most frequently used is the Wilkinson type.[24]

The Wilkinson-type ADC operates as shown in Fig. 10.39. When a pulse enters the MCA, two events are initiated:

1. A capacitor starts charging.
2. An input gate prevents the acceptance of another pulse until the previous one is fully processed and registered.

The capacitor keeps charging until the peak of the pulse is reached. At that point in time, two new events are initiated:

1. The voltage on the charged capacitor is discharged by a constant current.
2. An oscillator clock starts. The clock stops its oscillations when the capacitor is fully discharged.

The number of oscillations during this time—called *rundown* or *conversion time*—is proportional to the pulse height and constitutes the information that determines the channel number in which that pulse will be stored.

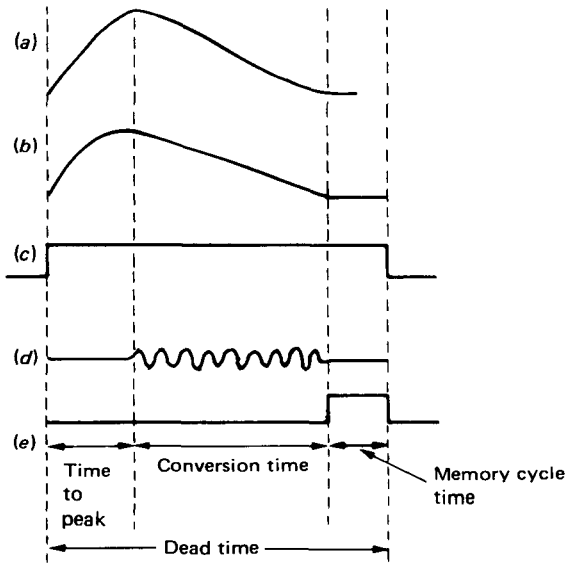


**Figure 10.39** The processing of the pulse in a Wilkinson ADC. (*a*) Input pulse. (*b*) Charge capacitor voltage. (*c*) Gate stops other pulses. (*d*) Oscillator clock. (*e*) Pulse storage.

A variation of this method is shown in Fig. 10.40. The steps followed in this case are

1. The input pulse is stretched in such a way that its flat portion is proportional to its height.
2. At the moment the pulse reaches its maximum (time $t_1$), a linear ramp generator is triggered, producing a voltage $C$.

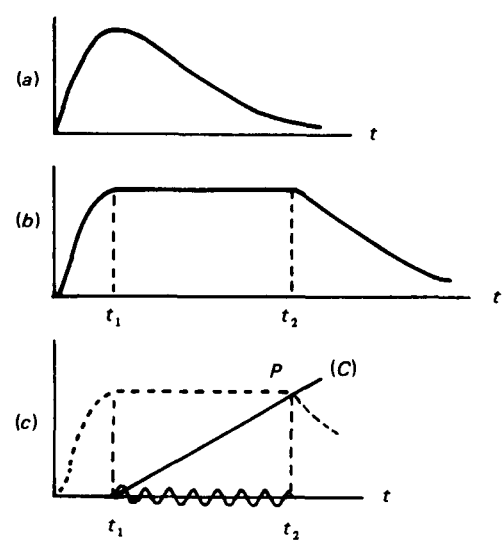


**Figure 10.40** The processing of the pulse by the ADC. (*a*) Input pulse. (*b*) Input pulse stretched; flat part proportional to pulse height. (*c*) Ramp voltage and oscillator clock start at $t_1$.

3. At the same moment ($t_1$), a gate signal is produced and an oscillator clock is turned on.

When the voltage ramp signal reaches the flat part of the stretched pulse ($P$), the gate signal turns the clock off. Thus, the time interval ($t_2 - t_1$) and, therefore, the number of oscillations during ($t_2 - t_1$) are again proportional to the height of the pulse. This second method of ADC operation (Fig. 10.40) is not favored because it is difficult to keep the pulse height constant for the time interval ($t_2 - t_1$).

Figure 10.39 shows, in addition to the principle of operation of the Wilkinson ADC, the reason for the dependence of the MCA dead time on the channel number. The dead time consists of three components:

1. Pulse risetime
2. Conversion time
3. Memory cycle time (time it takes to store the digitized signal)

Of the three components, the second is the most important because it depends on the channel number. One can reduce the size of the conversion time by using a clock with higher frequency. Today's ADCs use quartz-stabilized clocks with a frequency of up to 450 MHz. Obviously, for a Wilkinson ADC, the higher the clock frequency is, the shorter the dead time will be. The equation for dead time is written as

$$\tau(C) = a_1 + 0.01(C + X)\ \mu\text{s} \tag{10.35}$$

where a typical value of $a_1$ is 1.5 $\mu$s, $C$ = address (channel) count, and $X$ = effective digital offset.[25] The digital offset is a capability offered by modern ADCs of subtracting a certain number of channels from the converted channel number before the data are introduced into the memory. One application of digital offset is to enhance resolution in a measurement performed with a small MCA. For example, with a 1000-channel MCA and an 8000 channel ADC, a 7000 digital offset allows data to be recorded for the top eighth of the spectrum only. A fixed dead time (FDT) ADC has also been developed for certain applications.[25]

The resolution of an ADC is expressed in terms of channels. It represents the maximum number of discrete voltage increments into which the maximum input pulse can be subdivided. ADC resolutions range from 4096 to 16,384 channels. Since commercial amplifiers can provide a maximum 10-V pulse, an ADC with a resolution of 4096 channels may subdivide 10 V into 4096 increments. Another quantity used is the conversion gain of the ADC. The conversion gain may be considered as a subset of the resolution. An ADC with a resolution of 16,384 channels may be used, depending on the application, with a conversion gain of 4096, or 8192, or 16,384 channels.

The accuracy of the ADC is expressed in terms of its differential and integral nonlinearity. The *differential nonlinearity* describes the uniformity of address widths over the entire range of the ADC. To make this point better

understood, assume that a 1000-channel ADC is used to process pulses with maximum height of 10 V. Then the average address width is $10/1000 = 10\text{mV/channel}$. The ideal ADC should provide a conversion of 10 mV/channel at any channel. Any deviation between this width and the actual one is expressed by the differential nonlinearity. Mathematically, if

$$\overline{\Delta V} = \text{average width}$$

$$\Delta V_{max} = \text{maximum width}$$

$$\Delta V_{min} = \text{minimum width}$$

then the differential nonlinearity is given by the equation

$$\%\ \text{Differential nonlinearity} = \frac{\Delta V_{max} - \Delta V_{min}}{\overline{\Delta V}}(100) \qquad (10.36)$$

Commercial ADCs have differential nonlinearity of the order of $\pm 0.5$ percent to $\pm 1$ percent.

The *integral nonlinearity* is defined as the maximum deviation of any address (ADC channel) from its nominal position, determined by a linear plot of address (ADC channel) versus input pulse amplitude (Fig. 10.41). The maximum pulse height $V_{max}$ corresponds to the maximum address $N_{max}$. If $N$ is the address number with the maximum deviation between the actual and nominal pulse heights, the integral nonlinearity is given by the equation

$$\%\ \text{Integral nonlinearity} = \frac{V_{nom} - V_{act}}{V_{max}}(100) \qquad (10.37)$$

Modern commercial ADCs have integral nonlinearity of the order of $\pm 0.05$ percent over 98–99 percent of the full range.

The integral nonlinearity affects the centroid position of energy peaks, which in turn affects the calibration of the system as well as the identification of unknown energy peaks.

## 10.13 MULTIPARAMETER ANALYZERS

The MCA is an instrument that stores events by a single parameter, namely, pulse height. When the need arises, however, there are many experiments for

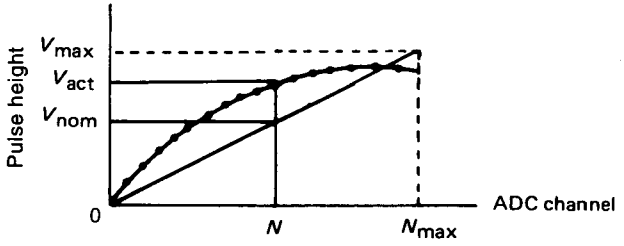


**Figure 10.41** The definition of integral nonlinearity is based on a linear plot of ADC channel versus pulse amplitude.

the study of events in terms of more than one parameter. Such requirements occur in

1. Coincidence measurements where the energy spectrum from both detectors need be analyzed
2. Simultaneous measurement of energy and mass distribution of fission fragments
3. Study of energy and angular dependence of nuclear reactions involving many particles, etc.

The "direct" method of multiparameter analysis would be to use an arrangement such that all parameters but one are limited to a narrow range (by using a single-channel analyzer) and the remaining parameter is recorded by an MCA. After an adequate number of events have been recorded, the value of one of the fixed parameters is changed, and the measurement is repeated. This process continues until all values of all parameters are covered. Obviously, such an approach is cumbersome and time consuming.

A more efficient way of performing the measurement is by storing the information simultaneously for more than one parameter. For example, consider a coincidence measurement involving two detectors (Fig. 10.42). The detector signals are fed into a coincidence unit, which then is used to gate the corresponding ADCs. The amplified detector pulses that are coincident are thus digitized by the ADCs, and the information is stored in the memory of the system. Any event that reaches the memory is defined like a point in a two-dimensional space. For example, if a pulse from $ADC_1$ has the value 65 (i.e., ADC channel 65) and one from $ADC_2$ has the value 18, the event is registered as 6518 (assuming 100 channels are available for each parameter). The measured data may be stored in the computer, for subsequent analysis, and may also be displayed on the screen of the monitor for an immediate preliminary assessment of the results. The results of a dual-parameter system such as that shown in Fig. 10.42 constitute a three-dimensional histogram as shown by Fig. 10.43.

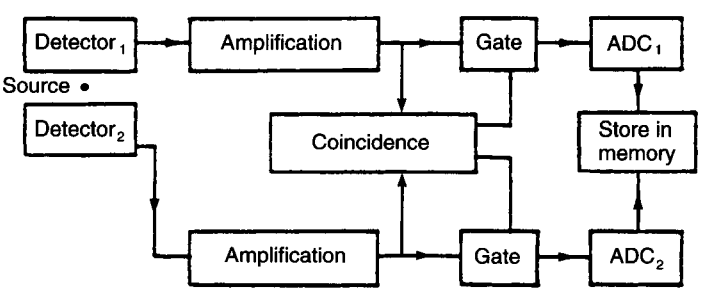


**Figure 10.42** A two-parameter measurement.

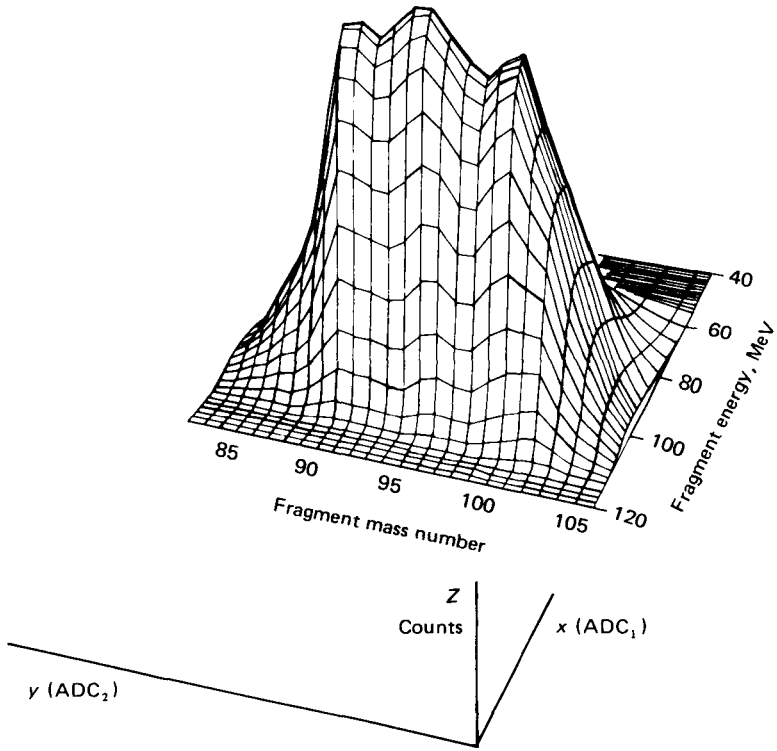


**Figure 10.43** A sample of the output from a two-parameter system (from Ref. 26).

One of the difficulties with multiparameter measurements is to secure sufficient memory capacity to register all possible events. The necessary storage increases exponentially with the number of parameters. For a $k$ parameter measurement with $N$ channels per parameter, the capacity of the memory should be $N^k$. Thus a two-parameter system with 100 channels per parameter needs $10^4$ memory locations. If both parameters are registered in 1000 channels, the requirements are $10^6$ locations.

## PROBLEMS

**10.1** Prove that the phase difference between voltage and current maximum values in an $RC$ circuit is given by $\varphi = \tan^{-1}(1/RC\omega)$.

**10.2** Prove that the phase difference between voltage and current maximum values in a $LR$ circuit is given by $\varphi = \tan^{-1}(L\omega/R)$.

**10.3** Prove that (a) the phase difference between voltage and current maximum values in an $RCL$ circuit is given by

$$\varphi = \tan^{-1}\left[\frac{\omega L - (1/\omega C)}{R}\right]$$

and (b) the impedance is given by $Z = \sqrt{R^2 + [\omega L - (1/\omega C)]^2}$.

**10.4** Prove that the output signal of a differentiating circuit is, for a step input, equal to

$$V_0(t) = V_i e^{-t/RC}$$

**10.5** Show that the output signal of a differentiating circuit is given by

$$V_0(t) = \frac{V_i}{\tau} RC(1 - e^{-t/RC})$$

when the input signal is given by $V_i(t) = V_i t/\tau$.

**10.6** Show that the output signal of an integrating circuit is, for a step input, equal to

$$V_0(t) = V_i(1 - e^{-t/RC})$$

**10.7** Show that the output signal of a differentiating circuit is given by

$$V_0(t) = V_i \frac{1}{1 - \tau/RC}(e^{-t/RC} - e^{-t/\tau})$$

when the input signal is $V_i(1 - e^{-t/\tau})$.

**10.8** A coincidence measurement has to be performed within a time $T$. Show that the standard deviation of the true coincidence rate is given by

$$\sigma_t = \frac{1}{\sqrt{T}}\left(\sqrt{r_a + r_t} + \sqrt{r_a}\right)$$

where $r_a$ = accidental coincidence rate
$r_t$ = true coincidence rate

## BIBLIOGRAPHY

Kowalski, E., *Nuclear Electronics*, Springer-Verlag, New York, 1970.
Malmstadt, H. V., Enke, C. G., and Toren, E. C., *Electronics for Scientists*, W. A. Benjamin, New York, 1963.
Nicholson, P. W., *Nuclear Electronics*, Wiley, London, 1974.

## REFERENCES

1. Chase, R. L., *Rev. Sci. Instrum.* **39**:1318 (1968).
2. Gedcke, D. A., and McDonald, W. J., *Nucl. Instrum. Meth.* **55**:377 (1967).
3. Maier, M. R., and Sperr, P., *Nucl. Instrum. Meth.* **87**:13 (1970).
4. Strauss, M. G., Larsen, R. N., and Sifter, L. L., *Nucl. Instrum. Meth.* **46**:45 (1967).
5. Graham, R. L., Mackenzie, I. K., and Ewan, G. T., *IEEE Trans. NS 13* **1**:72 (1966).
6. Viencent, C. H., *Nucl. Instrum. Meth.* **127**:421 (1975).
7. Smith, D., *Nucl. Instrum. Meth.* **152**:505 (1978).
8. Kuchnir, F. T., and Lynch, F. J., *IEEE Trans. NS 15* **3**:107 (1968).
9. Alexander, T. K., and Goulding, F. S., *Nucl. Instrum. Meth.* **13**:244 (1961).
10. Heistek, L. J., and Van der Zwan, L., *Nucl. Instrum. Meth.* **80**:213 (1970).
11. McBeth, G. W., Lutkin, J. E., and Winyard, R. A., *Nucl. Instrum. Meth.* **93**:99 (1971).
12. Brooks, F. D., *Nucl. Instrum. Meth.* **4**:151 (1959).
13. Kinbara, S., and Kumahara, T., *Nucl. Instrum. Meth.* **70**:173 (1969).
14. Burrus, W. R., and Verbinski, V. V., *Nucl. Instrum. Meth.* **67**:181 (1969).

15. Verbinski, V. V., Burrus, W. R., Love, T. A., Zobel, W., and Hill, N. W., *Nucl. Instrum. Meth.* **65**:8 (1968).
16. Forté, M., Konsta, A., and Moranzana, C., *Electronic Methods for Discrimination of Scintillation Shapes* (IAEA Conf. Nucl. Electr. Belgrade, 1961) NE-59.
17. Brenner, R., *Rev. Sci. Instrum.* **40**:1011 (1969).
18. Nowlin, C. H., and Blankenship, J. L., *Rev. Sci. Instrum.* **36**:1830 (1965).
19. Fairstein, E., and Hahn, J., *Nucleonics 23*, no. 7:56 (1965).
20. Fairstein, E., and Hahn, J., *Nucleonics 23*, 9:81 (1965).
21. Fairstein, E., and Hahn, J., *Nucleonics 23*, no. 11:50 (1965).
22. Fairstein, E., and Hahn, J., *Nucleonics 24*, no. 1:54 (1966).
23. Fairstein, E., and Hahn, J., *Nucleonics 24*, no. 3:68 (1966).
24. Wilkinson, D. H., *Philos. Soc.* **46**:508 (1950).
25. Canberra Industries, Inc., *Edition Nine, Instruments Catalog*, Meriden, CT, 1993.
26. Diorio, G., and Wehring, B. W., *Nucl. Instrum. Meth.* **147**:487 (1977).

CHAPTER
# ELEVEN

# DATA ANALYSIS METHODS

## 11.1 INTRODUCTION

Raw† experimental data seldom give the answer to the problem that is the objective of the measurement. In most cases, additional calculations or analysis of the raw data is necessary. The analysis of the raw data may consist of a simple division of the counts recorded in a scaler by the counting time to obtain counting rates, may require fitting an analytical function to the data, or may necessitate unfolding of a measured spectrum.

Whatever the analysis of the data may entail, there are some general methods helpful to the analyst. The objective of this chapter is to present a brief introduction to these general methods and principles of data analysis.

## 11.2 CURVE FITTING

The results of most experiments consist of a finite number of values (and their errors) of a dependent variable $y$ measured as a function of the independent variable $x$ (Fig. 11.1). The objective of the measurement of $y = y(x)$ may be one

†Raw data consist of the numbers obtained by the measuring device, e.g., a scaler, a clock, or a voltmeter.

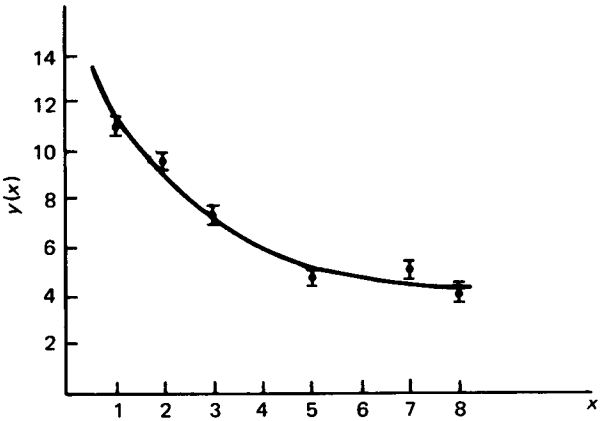


**Figure 11.1** Experimental results consist of the values of the dependent variable $y(x)$ and their errors. The curve was drawn to help the eye.

of the following:

1. To find how $y$ changes with $x$
2. To prove that $y = y(x)$ follows a theoretically derived function
3. To use the finite number of measurements of $y(x)$ for the evaluation of the same function at intermediate points or at values of $x$ beyond those measured

These objectives could be immediately achieved if the function $y(x)$ were known. Since it is not, the observer tries to determine it with the help of the experimental data. The task of obtaining an analytic function that represents $y(x)$ is called *curve fitting*.

The first step in curve fitting is to plot the data ($y$ versus $x$) on linear graph paper (Fig. 11.1). A smooth curve is then drawn, following as closely as possible the general trend of the data and trying to have an equal number of points on either side of the curve. The experimental points always have an error associated with them, so the smooth curve is not expected to pass through all the measured $(x, y)$ points. Obviously, there is no guarantee that the smooth curve so drawn is the "true" one. Criteria that may help the observer draw a curve with a certain degree of confidence are then needed. Such criteria exist and are described in Sec. 11.4.

After the data are plotted and a smooth curve is drawn, the observer has to answer two questions:

1. What type of function would represent the data best (e.g., exponential, straight line, parabola, logarithmic)?
2. After the type of function is decided upon, how can one determine the best values of the constants that define the function uniquely?

Since there exist an infinite number of functions, the observer would like to have certain criteria or rules that limit the number of possible functions. While no such formal set of criteria exists, the following suggestions have proved useful.

First, the observer should utilize any a priori knowledge about $y(x)$ and $x$. Examples are restrictions of $x$ and $y$ within a certain range (e.g., in counting experiments both $x$ and $y$ are positive) or information from theory that suggests a particular function (e.g., counting data follow Poisson statistics).

Second, the observer should try the three simple expressions listed next, before any complicated function is considered.

1. The linear relation (straight line)

$$y(x) = ax + b \tag{11.1}$$

   where $a$ and $b$ are constants to be determined based on the data. A linear relationship will be recognized immediately in a linear plot of $y(x)$ versus $x$.
2. The exponential relationship

$$y(x) = ae^{-bx} \tag{11.2}$$

   If the data can be represented by such a function, a plot on semilog paper—i.e., a plot of $\ln y$ versus $x$—will give a straight line.
3. The power relationship

$$y(x) = ax^b \tag{11.3}$$

   If the data can be represented by this expression, a plot on log-log paper—i.e., a plot of $\ln y$ versus $\ln x$—will give a straight line.

Third, the observer should know that a polynomial of degree $N$ can always be fitted exactly to $N + 1$ pieces of data (see also Sec. 11.3–11.5).

If no satisfactory fit can be obtained by using any of these suggestions, the analyst should try more complicated functions. Plotting the data on special kinds of graph paper, such as reciprocal or probability paper may be helpful. After the type of function is found, the constants associated with it are determined by a least-squares fit (see Sec. 11.4).

There is software now available that accepts a table of data points as input and tests possible fits of this data set to a large number of analytic functions. At the end of the operation, both the function representing the best fit and a degree of "confidence" are provided.

## 11.3 INTERPOLATION SCHEMES

It was mentioned in Sec. 11.2 that one of the reasons for curve fitting is to be able to evaluate the function $y(x)$ at values of $x$ for which measurements do not exist. An alternative to curve fitting that can be used for the calculation of

intermediate $y(x)$ values is the method of interpolation. This section presents one of the basic interpolation techniques—the *Lagrange formula*. Many other formulas exist that the reader can find in the bibliography of this chapter (e.g., see Hildebrand, and Abramowitz and Stegan's *Handbook or Mathematical Functions*).

Assume that $N$ values of the dependent variable $y(x)$ are known at the $N$ points $x_i$, $x_a \le x_i \le x_b$ for $i = 1, \ldots, N$. The pairs of data $(y_i, x_i)$ for $i = 1, \ldots, N$, where $y(x_i) = y_i$, may be the results of an experiment or tabulated values. Interpolation means to obtain a value $y(x)$ for $x_a < x < x_b$ based on the data $(y_i, x_i)$, when the point $x$ is not one of the $N$ values for which $y(x)$ is known.

The Lagrange interpolation formula expresses the value $y(x)$ in terms of polynomials (up to degree $N - 1$ for $N$ pairs of data). The general equation is

$$y(x) = \sum_{i=0}^{M} P_i(x) y(x_i) \qquad M \le N - 1 \tag{11.4}$$

where

$$P_i(x) = \frac{\prod_{j=0, j \ne i}^{M} (x - x_j)}{\prod_{j=0, j \ne i}^{M} (x_i - x_j)} \qquad M \le N - 1 \tag{11.5}$$

The error associated with Eq. 11.4 is given by

$$\text{Error}[y(x)] = \prod_{j=0}^{M} (x - x_j) \frac{y^{M+1}(\xi)}{(M+1)!} \qquad M \le N - 1 \tag{11.6}$$

where $y^{M+1}(\xi)$ is the $(M + 1)$ derivative of $y(x)$ evaluated at the point $\xi$, $x_a < \xi < x_b$. Since $y(x)$ is not known analytically, the derivative in Eq. 11.6 has to be calculated numerically.

Equation 11.4 is the most general. It uses all the available points to calculate any new value of $y(x)$ for $x_a < x < x_b$. In practice, people use only a few points at a time, as the following two examples show.

**Example 11.1** Derive the Lagrange formula for $M = 1$.

**Answer** If $M = 1$, Eq. 11.4 takes the form (also using Eq. 11.5)

$$y(x) = \sum_{i=0}^{1} P_i(x) y(x_i) = \frac{x - x_1}{x_0 - x_1} y_0 + \frac{x - x_0}{x_1 - x_0} y_1 \tag{11.7}$$

where $y_i = y(x_i)$. The points $x_0$ and $x_1$ could be anywhere between $x_a$ and $x_b$, but the point $x$ should be $x_0 \le x \le x_1$.

To calculate $y(x)$ at any $x$, Eq. 11.7 uses two points, one on either side of $x$, and for this reason it is called the *Lagrange two-point interpolation formula*. Equation 11.7 may be written in the form

$$y(x) = y_0 + \frac{x - x_0}{x_1 - x_0}(y_1 - y_0) \tag{11.8}$$

which shows that the two-point formula amounts to a linear interpolation.

The error associated with the two-point formula is obtained from Eq. 11.6:

$$\text{Error}[y(x)] = (x - x_0)(x - x_1)\frac{y^{(2)}(\xi)}{2}$$

where $y^{(2)}(\xi)$ is the second derivation evaluated at $\xi, x_0 \le \xi < x_1$.

**Example 11.2** Derive the Lagrange formula for $M = 2$.

**Answer** If $M = 2$, Eq. 11.4 takes the form

$$y(x) = \sum_{i=0}^{2} P_i(x)y(x_i) = \frac{(x - x_i)(x - x_2)}{(x_0 - x_1)(x_0 - x_2)}y_0 + \frac{(x - x_0)(x - x_2)}{(x_1 - x_0)(x_1 - x_2)}y_1 + \frac{(x - x_0)(x - x_1)}{(x_2 - x_0)(x_2 - x_1)}y_2 \tag{11.9}$$

To calculate $y(x)$ at any point $x$, Eq. 11.9 uses three points $x_0, x_1, x_2$ with $x_0 \le x \le x_2$, and is called the *Lagrange three-point interpolation formula*. The three-point formula amounts to a parabolic representation of the function $y(x)$ between any three points.

The error associated with the three-point formula is (applying again Eq. 11.6):

$$\text{Error}[y(x)] = (x - x_0)(x - x_1)(x - x_2)\frac{y^{(3)}(\xi)}{3!}$$

where $y^{(3)}(\xi)$ is the third derivative evaluated at $\xi, x_0 \le \xi < x_2$.

**Example 11.3** Calculate the value of the function $f(x)$ at $x = 11.8$ from the table below using the Lagrange two- and three-point interpolation formulas. The data are plotted in Fig. 11.2.

| $x$ | $f(x)$ |
|---|---|
| 10 | 30.5 |
| 11 | 33.0 |
| 12 | 35.8 |
| 13 | 36.7 |
| 14 | 37.2 |

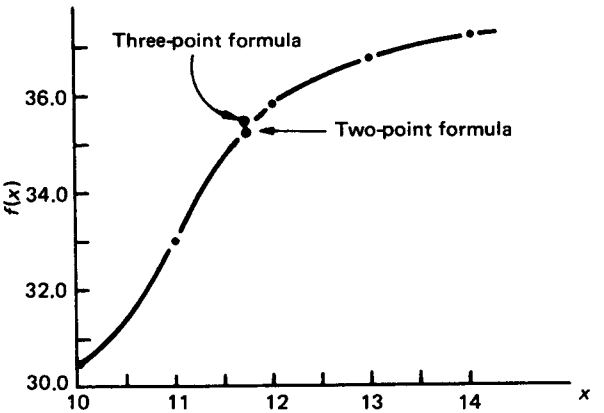


**Figure 11.2** A plot of the data used in Ex. 11.3.

**Answer** (a) Using the two-point formula (Eq. 11.7), one has $x_0 = 11$, $x_1 = 12$, $y_0 = 33.0$, $y_1 = 35.8$.

$$y(x) = y(11.8) = \frac{11.8 - 12}{11 - 12}(33.0) + \frac{11.8 - 11}{12 - 11}(35.8) = 35.2$$

(b) Using the three-point formula (Eq. 11.9), one has $x_0 = 11$, $x_1 = 12$, $x_2 = 13$, $y_0 = 33$, $y_1 = 35.8$, $y_2 = 36.7$.

$$y(11.8) = \frac{(11.8 - 12)(11.8 - 13)}{(11 - 12)(11 - 13)}(33) + \frac{(11.8 - 11)(11.8 - 13)}{(12 - 11)(12 - 13)}(35.8)$$
$$+ \frac{(11.8 - 11)(11.8 - 12)}{(13 - 11)(13 - 12)}(36.7) = 3.96 + 34.37 - 2.94 = 35.4$$

The error of $y(x)$ associated with the interpolation is, for the first case only,

$$\text{Error}[y(x)] = (x - x_0)(x - x_1)\frac{y^{(2)}(\xi)}{2}$$

The second derivative evaluated at $\xi = \frac{1}{2}(x_0 + x_1)$ is

$$y^{(2)}(\xi) = \frac{4(y_1 - 2y + y_0)}{(x_1 - x_0)^2}$$

Thus the error is

$$\text{Error}[y(x)] = (11.8 - 11)(11.8 - 12)\frac{4(35.8 - 2(35.2) + 33)}{2(1^2)} = 0.512$$

or $0.512/35.2 = 0.014 = 1.4\%$.

## 11.4 LEAST-SQUARES FITTING

Assume that an observer obtained the experimental data $y_i = y(x_i)|_{i=1;N}$. It is often desirable to find a function that can represent the data, i.e., to find a function that can be fitted to the data. Let such a function be written as

$$f(x, a_1, a_2, \ldots, a_M) \qquad M < N$$

where $a_m|_{m=1,M}$ are parameters to be determined. According to the method of least squares, the best values of the parameters $a_M$ are those that minimize the quantity

$$Q = \sum_{i=1}^{N} w_i[y_i - f(x_i)]^2 \tag{11.10}$$

where $w_i|_{i=1,N}$ are weighting functions. Minimization of $Q$ is achieved by requiring

$$\frac{\partial Q}{\partial a_m} = 0 \qquad m = 1, \ldots, M \tag{11.11}$$

Before Eq. 11.11 is solved, it should be pointed out that the observer decides about the form of the function $f(x)$ and the weighting functions $w_i$. The form of $f(x)$ is obtained by the curve-fitting methods discussed in Sec. 11.2. The weighting functions are selected based on the type of data and the purpose of the fit. For example, if the data are the result of a counting experiment, $w_i = 1/\sigma_i^2$, where $\sigma_i$ is the standard deviation of $y_i$.

There are two types of least-squares fit, linear and nonlinear. *Linear least-squares fit* is based on a function $f(x)$ of the form

$$f(x, a_1, a_2, \ldots, a_M) = \sum_{m=1}^{M} a_m \phi_m(x) \tag{11.12}$$

where the $\phi_m(x)$ are known functions of $x$.

*Nonlinear least-squares fit* is based on a function $f(x)$ nonlinear in $a_m$, such as

$$f(x, a_1, a_2, \ldots, a_M) = a_1 \cos(a_2 x)$$

The interested reader should consult the bibliography of this chapter (see Bevington) for further information on nonlinear least-squares fit.

For a linear least-squares fit, the parameters $a_m|_{m=1,M}$ are determined from Eq. 11.11, with Eq. 11.12 giving the form of $f(x)$. The result is

$$\frac{\partial Q}{\partial a_k} = \frac{\partial}{\partial a_k}\left\{\sum_{i=1}^{N} w_i\left[y_i - \sum_{m=1}^{M} a_m \phi_m(x_i)\right]^2\right\} \qquad k = 1, \ldots, M \tag{11.13}$$

If one defines

$$A_{km} = \sum_{i=1}^{N} w_i \phi_k(x_i)\phi_m(x_i) \qquad k, m = 1, \ldots, M \tag{11.14}$$

and

$$B_k = \sum_{i=1}^{N} w_i y_i \phi_k(x_i) \qquad k = 1, \ldots, M \tag{11.15}$$

then Eq. 11.13 takes the form

$$\sum_{m=1}^{M} A_{km} a_m = B_k \qquad k = 1, \ldots, M \tag{11.16}$$

Equation 11.16 forms a system of $M$ linear nonhomogeneous equations for the $M$ unknowns $a_m|_{m=1,M}$ and can be solved by using any of the standard methods (e.g., Kramer's rule). In matrix notation, the solution is

$$a_m = \mathbf{A}^{-1}\mathbf{B} \tag{11.17}$$

where **A** and **B** are matrices with elements given by Eqs. 11.14 and 11.15.

If the function $f(x)$ is a polynomial, then

$$f(x, a_1, a_2, \ldots, a_m) = \sum_{m=1}^{M} a_m x^{m-1} \tag{11.18}$$

Equations 11.14 and 11.15 take the form [since $\phi_k(x) = x^{k-1}$]

$$A_{km} = \sum_i w_i x_i^{k-1} x_i^{m-1} \tag{11.19}$$

$$B_k = \sum_i w_i y_i x_i^{k-1} \tag{11.20}$$

The notation used in Eqs. 11.19 and 11.20 and in the next section is $\sum_{i=1}^{N} \to \sum_i$.

### 11.4.1 Least-Squares Fit of a Straight Line

If the function represented by Eq. 11.18 is a straight line, then

$$f(x_i, a_1, a_2) = a_1 + a_2 x_i \tag{11.21}$$

Thus, Eqs. 11.19 and 11.20 become

$$A_{11} = \sum_i w_i \qquad A_{12} = \sum_i w_i x_i = A_{21} \qquad A_{22} = \sum_i w_i x_i^2$$

$$B_1 = \sum_i w_i y_i \qquad B_2 = \sum_i w_i y_i x_i$$

Then, Eq. 11.16 takes the forms

$$A_{11} a_i + A_{12} a_2 = B_1$$
$$A_{21} a_1 + A_{22} a_2 = B_2$$

which are solved to give

$$a_1 = \frac{1}{D}\left[\left(\sum_i w_i y_i\right)\left(\sum_i w_i x_i^2\right) - \left(\sum_i w_i y_i x_i\right)\left(\sum_i w_i x_i\right)\right] \tag{11.22}$$

$$a_2 = \frac{1}{D}\left[\left(\sum_i w_i\right)\left(\sum_i w_i y_i x_i\right) - \left(\sum_i w_i x_i\right)\left(\sum_i w_i y_i\right)\right] \tag{11.23}$$

and

$$D = \left(\sum_i w_i\right)\left(\sum_i w_i x_i^2\right) - \left(\sum_i w_i x_i\right)^2 \tag{11.24}$$

The variance of $a_1$ and $a_2$ is obtained by using the principle of propagation of error presented in Chap. 2.

$$\sigma_{a_m}^2 = \sum_i \left(\frac{\partial a_m}{\partial y_i}\right)^2 \sigma_{y_i}^2 \qquad m = 1, 2 \tag{11.25}$$

where $\sigma_{y_i}$ = standard error of $y_i = \sigma_i$.

In many cases, the standard deviation of $y_i$ defines the weighting functions, and specifically, analysts use

$$w_i = \frac{1}{\sigma_i^2}$$

Then, Eq. 11.25 gives

$$\sigma_{a_1}^2 = \frac{1}{D}\sum_i \frac{x_i^2}{\sigma_i^2} \tag{11.26}$$

$$\sigma_{a_2}^2 = \frac{1}{D}\sum_i \frac{1}{\sigma_i^2} \tag{11.27}$$

where $D$ is given by Eq. 11.24 with $w_i = 1/\sigma_i^2$. Equations 11.22–11.27 are further simplified if all the $\sigma_i$ have the same value.

### 11.4.2 Least-Squares Fit of General Functions

A straight-line least-squares fit is not limited to linear functions of $x$. It may be used with functions such as the exponential ($y = ae^{bx}$) or the power relationship ($y = ax^b$) after an appropriate transformation of variables. For example, the exponential function can be written as

$$\ln y = \ln a + bx \tag{11.28}$$

which is of the form given by Eq. 11.21 after setting

$$y' = \ln y \qquad a_1' = \ln a \qquad a_2' = b$$

When the variable is transformed, it is necessary to obtain the standard deviation of the new variable. In general, if one sets

$$y' = g(y)$$

then the standard deviation of $y'(x)$ is

$$\sigma_i' = \frac{\partial g(y_i)}{\partial y_i}\sigma_i \tag{11.29}$$

In the example given above, $y' = \ln y$ and

$$\sigma_i' = \frac{\partial(\ln y_i)}{\partial y_i}\sigma_i = \frac{\sigma_i}{y_i} \tag{11.30}$$

Therefore, if a transformation is applied to the function, all the $\sigma_i$ in Eqs. 11.26 and 11.27 should be replaced by the values given by Eq. 11.30.

If the parameters $a_m$ are transformed, the standard deviation of the new constant is again determined by Eq. 11.29. In the example given above, $a' = \ln a$ and

$$\sigma_{a'} = \frac{\sigma_a}{a} \tag{11.31}$$

Table 11.1 presents a number of functions that can be cast into a linear (or polynomial) form by a transformation of variables. It should be emphasized that although the functions shown in Table 11.1 are not linear in $x$, the least-squares fit is still linear. An example of a function $f(x, a_1, \ldots)$ that represents a nonlinear least-squares fit is

$$f(x, a_1, a_2, \ldots) = a_1 \cos(a_2 x)$$

**Example 11.4** The following table gives neutron-absorption cross-section values and their errors as a function of neutron kinetic energy. Determine the analytic function that fits this data set.

| $T_n$ (eV) | $\sigma_a(b)$ | Error ($b$) |
|---|---|---|
| 1 | 1000 | 50 |
| 4 | 540 | 23 |
| 10 | 290 | 19 |
| 20 | 225 | 15 |
| 50 | 160 | 11 |
| 80 | 108 | 10 |
| 100 | 105 | 9 |

**Table 11.1 Functions That Can Be Changed into a Form Suitable for a Linear Least-Squares Fit**

| Function $y(x)$ | Transformation | | | Function used in the least-squares fit |
|---|---|---|---|---|
| $y = ae^{bx}$ | $y' = \ln y$ | $a' = \ln a$ | | $y' = a' + bx$ |
| $y = ax^b$ | $y' = \ln y$ | $a' = \ln a$ | $x' = \ln x$ | $y' = a' + bx'$ |
| $y = a \exp\left[-\frac{(x-a)^2}{2\sigma^2}\right]$ | $y' = \ln y$ | | | $y' = a_1 + a_2 x + a_3 x^2$ |
| $y = a_1 + a_2 x^b + a_3 x^{2b}$ | $x' = x^b$ | | | $y' = a_1 + a_2 x' + a_3 x'^2$ |
| $y = a_1 x^{b_1} + a_2 x^{b_2}$ | $y' = yx^{-b_1}$ | $x' = x^{b_2 - b_1}$ | | $y' = a_1 + a_2 x'$ |

**Answer** If one plots the data on log-log paper, the result is very close to a straight line (see Fig. 11.3). Therefore, the function to use is

$$\ln \sigma_a = a_1 + a_2 \ln T_n$$

If one takes $w_i = 1/\sigma_i^2$ and applies Eqs. 11.22–11.27, the result is

$$a_1 = 6.925 \qquad a_2 = -0.495 \qquad \frac{\sigma_{a_1}}{a_1} = 0.6\%$$

$$\sigma_{a_1} = 0.039 \qquad \sigma_{a_2} = 0.015 \qquad \frac{\sigma_{a_2}}{a_2} = 3\%$$

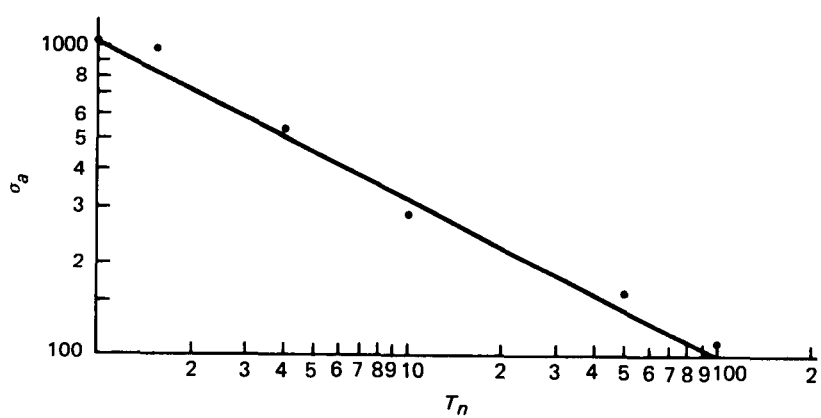


**Figure 11.3** The least-squares fit to the data of Ex. 11.4.

## 11.5 FOLDING AND UNFOLDING

To define the problems of folding and unfolding, consider the functions

$$\begin{aligned} S(x) &\qquad 0 < x < \infty \\ M(x) &\qquad 0 < x < \infty \\ R(x, x') &\qquad 0 < x, x' < \infty \end{aligned}$$

where the function $R(x, x')$ is normalized to 1:

$$\int_0^\infty R(x, x')\, dx = 1 \tag{11.32}$$

*Folding* the function $S(x)$ with the function $R(x, x')$ to obtain the function $M(x)$ means to perform the integration

$$M(x) = \int_0^\infty R(x, x') S(x')\, dx' \tag{11.33}$$

*Unfolding* means to obtain the function $S(x)$, knowing $M(x)$ and $R(x, x')$. Thus, folding is an integration, as shown by Eq. 11.33. Unfolding, on the other hand, entails solving the integral equation, Eq. 11.33—known as the *Fredholm equation*—for the unknown function $S(x)$.

In the field of radiation measurements, folding and (especially) unfolding are very important operations that have to be applied to the experimental data. In most radiation measurements, the variable $x$ is the energy of the particle, and for this reason the discussion in this section will be based on that variable. The reader should be aware, however, that $x$ may represent other quantities, such as time, velocity, or space variables. If $x$ is the energy of the particle, the functions $S(x)$, $M(x)$, and $R(x, x')$ have the following meanings (also given in Sec. 9.7):

$S(E)\, dE$ = source spectrum = number of particles emitted by the source with energy between $E$ and $E + dE$

$M(E)\, dE$ = measured spectrum = number of particles recorded as having energy between $E$ and $E + dE$

$R(E, E')\, dE$ = response of the detector = probability that a particle emitted by the source with energy $E'$ will be recorded with energy between $E$ and $E + dE$

As explained in Chap. 9, the response function is measured using monoenergetic sources. A monoenergetic source is represented mathematically by the *delta function* ($\delta$ function), which has these properties (Fig. 11.4):

$$\delta(E - E_0) = 0 \qquad E \neq E_0$$

$$\int_{E_1}^{E_2} \delta(E - E_0)\, dE = \begin{cases} 1 & \text{if } E_1 < E_0 < E_2 \\ 0 & \text{otherwise} \end{cases} \tag{11.34}$$

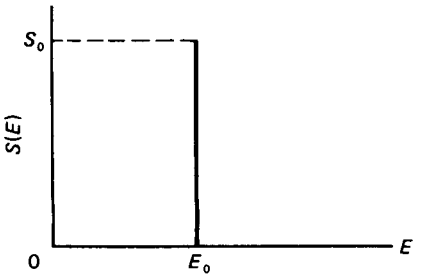


**Figure 11.4** A monoenergetic source spectrum.

Thus, the $\delta$ function is equal to zero everywhere except at $E = E_0$, which is, of course, what the energy spectrum of a monoenergetic source represents. Because of the property expressed by Eq. 11.34, integrals involving the $\delta$ function are immediately evaluated. For any function $f(E)$, one obtains

$$\int_{E_1}^{E_2} f(E)\delta(E - E_0)\, dE = f(E_0) \qquad E_1 < E_0 < E_2 \tag{11.35}$$

because there is no contribution to the integral except at $E = E_0$. For the same reason, if $E_0$ is outside the limits of integration, then

$$\int_{E_1}^{E_2} f(E)\delta(E - E_0)\, dE = 0 \qquad \begin{cases} E_0 < E_1 \\ E_0 > E_2 \end{cases} \tag{11.36}$$

Assume that a monoenergetic source emitting $S_0$ particles per second (Fig. 11.4) is used to measure the response function. If one substitutes the expression for this source,

$$S(E) = E_0\delta(E - E_0) \tag{11.37}$$

into Eq. 11.33, the result is

$$M(E) = \int_0^\infty R(E, E')S_0\delta(E' - E_0)\, dE' = S_0 R(E, E_0) \tag{11.38}$$

Equation 11.38 shows that the measured spectrum is indeed equal to the response function in the case of a monoenergetic source.

### 11.5.1 Examples of Folding

In radiation measurements, *folding* means to obtain the shape of the measured spectrum when the source and the detector response are known. Several examples of folding using a Gaussian distribution as the response function are presented next.

**Example 11.5** The source spectrum is a step function:

$$S(E) = \begin{cases} S_0 & E \geq E_0 \\ 0 & E < E_0 \end{cases}$$

What is the measured spectrum?

**Answer**

$$M(E) = \int_0^\infty \frac{dE'}{\sqrt{2\pi}\,\sigma} \exp\left[-\frac{(E-E')^2}{2\sigma^2}\right] S(E')$$

$$= S_0 \int_{E_0}^\infty \frac{dE'}{\sqrt{2\pi}\,\sigma} \exp\left[-\frac{(E-E')^2}{2\sigma^2}\right]$$

$$M(E) = \frac{S_0}{2}\left[1 + \operatorname{erf}\left(\frac{E-E_0}{\sqrt{2}\,\sigma}\right)\right]$$

where

$$\operatorname{erf}\left(\frac{E-E_0}{\sqrt{2}\,\sigma}\right) = \text{error function} = \frac{1}{\sqrt{2\pi}} \int_0^{(E-E_0)/\sigma} e^{-t^2/2}\,dt$$

Figure 11.5 shows the three functions involved.

**Example 11.6** The source spectrum is a square spectrum:

$$S(E) = \begin{cases} S_0 & E_1 \leq E \leq E_2 \\ 0 & \text{otherwise} \end{cases}$$

What is the measured spectrum?

**Answer**

$$M(E) = \int_0^\infty \frac{dE'}{\sqrt{2\pi}\,\sigma} \exp\left[-\frac{(E-E')^2}{2\sigma^2}\right] S(E')$$

$$= S_0 \int_{E_1}^{E_2} \frac{dE'}{\sqrt{2\pi}\,\sigma} \exp\left[-\frac{(E-E')^2}{2\sigma^2}\right]$$

$$= \frac{S_0}{2}\left[\operatorname{erf}\left(\frac{E_2-E}{\sqrt{2}\,\sigma}\right) - \operatorname{erf}\left(\frac{E_1-E}{\sqrt{2}\,\sigma}\right)\right]$$

Figure 11.6 shows the functions involved.

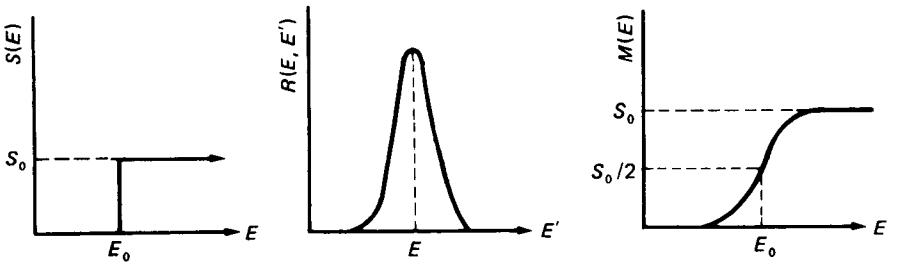


**Figure 11.5** A step function folded with a Gaussian.

**Example 11.7** The source spectrum is a Gaussian centered at $E = E_0$:

$$S(E) = \frac{S_0}{\sqrt{2\pi}\,\sigma_S} \exp\left[-\frac{(E - E_0)^2}{2\sigma_S^2}\right]$$

What is the measured spectrum?

**Answer**

$$M(E)^{\dagger} = \int_{-\infty}^{\infty} \frac{dE'}{\sqrt{2\pi}\,\sigma} \exp\left[-\frac{(E - E')^2}{2\sigma^2}\right] \frac{S_0}{\sqrt{2\pi}\,\sigma_S} \exp\left[-\frac{(E - E_0)^2}{2\sigma_S^2}\right]$$

$$= \frac{S_0}{\sqrt{2\pi}(\sigma_S^2 + \sigma^2)^{1/2}} \exp\left[-\frac{(E - E_0)^2}{2(\sigma^2 + \sigma_S^2)}\right]$$

Figure 11.7 shows the three functions involved. It is worth noting that if a Gaussian is folded with another Gaussian, their standard deviations add in quadrature.

†The integral of Eq. 11.33 may be extended to $-\infty$ because the Gaussian drops off quickly to a negligible value for $E < 0$.

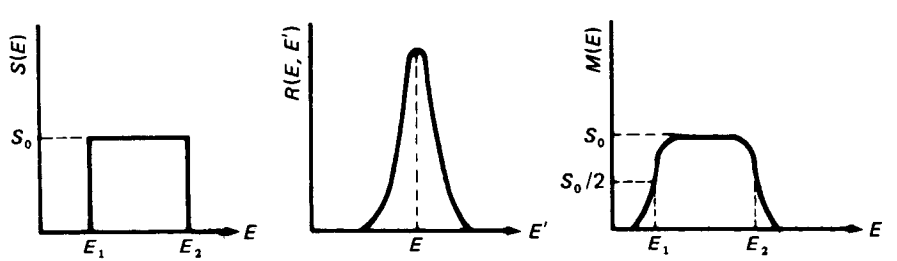


**Figure 11.6** A "square" function folded with a Gaussian.

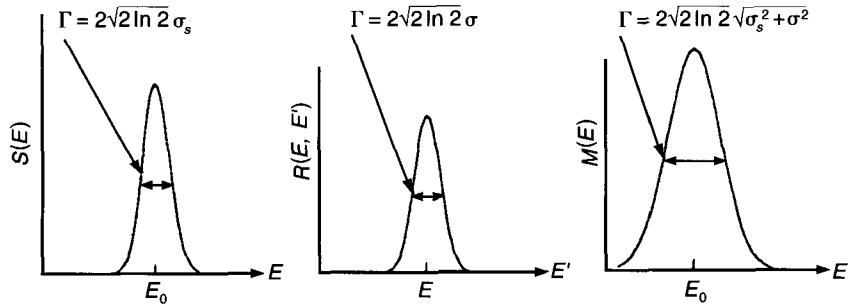


**Figure 11.7** A Gaussian folded with a Gaussian gives a third Gaussian, which has a larger width.

**Example 11.8** The source spectrum is a Lorentzian centered at $E_0$:

$$S(E) = \frac{\Gamma_S/2\pi}{(E - E_0)^2 + \Gamma_S^2/4}$$

and the response function is also a Lorentzian with width $\Gamma$. What is the measured spectrum?

**Answer**

$$M(E) = \int_{-\infty}^{\infty} \frac{\Gamma/2\pi}{(E - E')^2 + \Gamma^2/4} \frac{\Gamma_S/2\pi}{(E' - E_0)^2 + \Gamma_S^2/4} dE'$$

$$= \frac{(\Gamma + \Gamma_S)/2\pi}{(E - E_0)^2 + (\Gamma + \Gamma_S)^2/4}$$

Figure 11.8 shows the three functions involved. Notice that by folding a Lorentzian with a Lorentzian, the result is a third Lorentzian with width equal to the sum of the two widths.

### 11.5.2 The General Method of Unfolding

This section discusses methods of unfolding, assuming that an energy spectrum is measured with a multichannel analyzer or any other device that divides the measured spectrum into energy bins. As stated at the beginning of Sec. 11.5, unfolding means to solve the Fredholm-type integral equation

$$M(E) = \int_0^{\infty} R(E, E')S(E')\, dE' \tag{11.39}$$

for the unknown function $S(E)$. Before possible methods of solution of Eq. 11.39 are discussed, it is important to note that no spectrometer measures

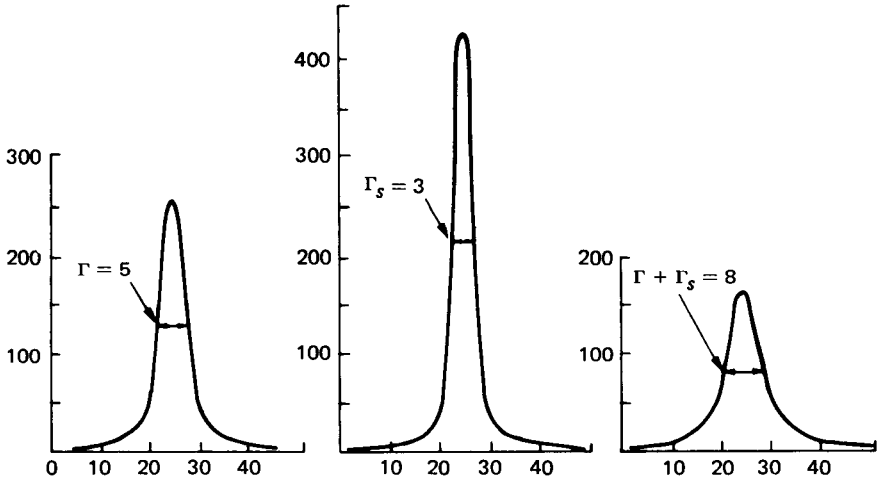


**Figure 11.8** A Lorentzian folded with a Lorentzian gives a third Lorentzian with a width equal to the sum of the widths of the first two distributions.

$M(E)$. What is measured is the quantity

$$M_i = \int_{E_i}^{E_{i+1}} M(E)\, dE \tag{11.40}$$

where $E_{i+1} - E_i = \Delta E_i$ = energy "bin" of the spectrometer. For a multichannel analyzer, $\Delta E_i$ represents the width of one of the channels. Therefore, one never measures a continuous function $M(E)$ but obtains instead a histogram consisting of the quantities $M_i$ (see Fig. 11.9). As a first approximation, $M(E_i) \approx M_i/\Delta E_i$.

An analytic solution of Eq. 11.39 is immediately obtained if the detector

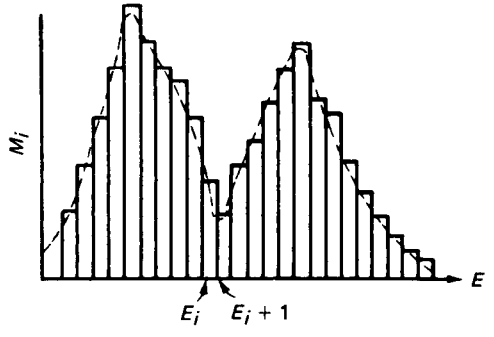


**Figure 11.9** The spectrometer produces a histogram, i.e., the quantities $M_i$, and not the continuous function $M(E)$ shown by the dashed line.

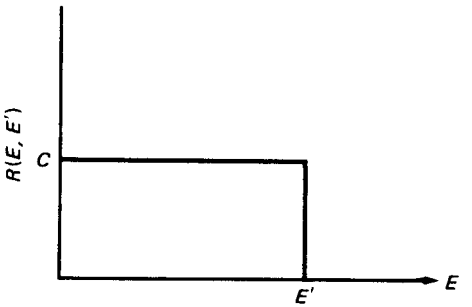


**Figure 11.10** A step-function response.

response is a $\delta$ function. Indeed, if $R(E, E') = \delta(E - E')$, then

$$M(E) = \int_0^\infty \delta(E - E')S(E')\,dE' = S(E)$$

This case is not encountered in practice because there is no detector with such a response function; it indicates only that with perfect energy resolution there is no need for unfolding. In general, the more the detector response resembles a $\delta$-function, the more the measured spectrum looks like the source spectrum.

A second type of response that gives an analytic solution, in principle, is a step function† (Fig 11.10). Let

$$R(E, E') = \begin{cases} \dfrac{C}{E'} & 0 < E \le E' \\ 0 & \text{otherwise} \end{cases} \tag{11.41}$$

where $C$ is a normalization constant. Then Eq. 11.39 takes the form

$$M(E) = \int_E^\infty \frac{C}{E'} S(E')\,dE' \tag{11.42}$$

The lower limit of the integral has been set equal to $E$ because if the response function is that given by Eq. 11.41, no source particles with energy $E' < E$ can contribute to $M(E)$. Upon differentiation,[1-4] Eq. 11.42 gives

$$S(E) = \frac{E}{C}\left|\frac{dM(E)}{dE}\right| \tag{11.43}$$

which is the desired solution. This method of unfolding is known as the *differentiation method.*

Since only the quantities $M_i$ (Eq. 11.40) are obtained, and not the function $M(E)$, the differentiation indicated by Eq. 11.43 must be performed numerically. There are several computer codes that perform such differentiation.

†The response of proton-recoil counters resembles a step function (see Chap. 14).

The most general method of unfolding is based on a transformation of Eq. 11.39 into a matrix equation. Equation 11.39 may be rewritten as

$$M(E) = \sum_{j}^{NR} \int_{E_j}^{E_{j+1}} R(E, E')S(E')\, dE' \tag{11.44}$$

where the integral over $E'$ has been written as a sum of integrals over $NR$ energy intervals $\Delta E_j = E_{j+1} - E_j$. Next, Eq. 11.44 is integrated over $E$ to give (see Eq. 11.40)

$$M_i = \int_{E_i}^{E_{i+1}} dE\, M(E) = \sum_{j}^{NR} \int_{E_i}^{E_{i+1}} dE \int_{E_j}^{E_{j+1}} R(E, E')S(E')\, dE' \tag{11.45}$$

Equation 11.45 is still exact. To proceed further, one needs an approximation for the source spectrum $S(E)$. Two approximations and corresponding methods of solving the resulting matrix equation are presented in the next two sections.

### 11.5.3 An Iteration Method of Unfolding

There are several iteration methods. The method presented here is useful for slowly varying spectra and has been used successfully to unfold beta spectra.[5]

The source spectrum $S(E)$ is approximated over any interval $\Delta E_j$ by the expression

$$S(E') = \frac{S_j}{\Delta E_j} \tag{11.46}$$

Using Eq. 11.46 and defining

$$R_{ij} = \frac{1}{\Delta E_j} \int_{E_i} dE \int_{E_j} dE'\, R(E, E') \tag{11.47}$$

then Eq. 11.45 takes the form

$$M_i = \sum_{i} R_{ij} S_j \qquad i, j = 1, NR \tag{11.48}$$

or, in matrix notation,

$$\mathbf{M} = \mathbf{R} \cdot \mathbf{S} \tag{11.49}$$

A formal solution of Eq. 11.49 is

$$\mathbf{S} = \mathbf{R}^{-1}\mathbf{M} \tag{11.50}$$

where $\mathbf{R}^{-1}$ is the inverse of the matrix with elements given by Eq. 11.47. Although in principle, Eq. 11.50 represents a solution to the unfolding problem, in practice the matrix inversion is not always achieved or leads to a solution with a large error.

The iteration method to be discussed here starts with Eq. 11.48 and uses the measured spectrum as the first guess of the iteration procedure.[5]

$$S_j^{(1)} = M_j \qquad j = 1, NR$$

This source spectrum when substituted into Eq. 11.48 gives

$$M_j^{(1)} = \sum_i R_{ij} S_j^{(1)} \qquad j = 1, NR$$

The error of $S_j^{(1)}$ is taken to be

$$S_j - S_j^{(1)} = M_j - M_j^{(1)} \qquad j = 1, NR$$

and the new guess for the second iteration is

$$S_j^{(2)} = S_j^{(1)} + \left[M_j - M_j^{(1)}\right] \qquad j = 1, NR$$

Substitution into Eq. 11.48 gives

$$M_j^{(2)} = \sum R_{ij} S_i^{(2)} \qquad i = 1, NR$$

and so on. The $n$th iteration uses

$$S_j^{(n)} = S_j^{(n-1)} + \left[M_j - M_j^{(n-1)}\right] \qquad j = 1, NR$$

and is the solution to the problem if the difference $|M_j - M_j^{(n)}|$ for $j = 1, \ldots, NR$ is acceptably small. This iteration method converges in less than five iterations and gives good results.

### 11.5.4 Least-Squares Unfolding

A different approximation for the source spectrum, used with neutrons, assumes that $S(E)$ can be represented as a sum of $NS$ discrete components.[6-8] Therefore, one can write

$$S(E') = \sum_{j=1}^{NS} X_j \delta(E' - E_j) \tag{11.51}$$

Using Eq. 11.51 and defining

$$\mathbf{A}_{ij} = \frac{1}{E_i - E_{i-1}} \int_{E_{i-1}}^{E_i} R(E, E_j)\, dE \tag{11.52}$$

then Eq. 11.45 takes the form

$$M_i = \sum_{j=1}^{NS} A_{ij} X_j \begin{cases} i = 1, \ldots, NR \\ j = 1, \ldots, NS \end{cases} \tag{11.53}$$

or in matrix notation,

$$\mathbf{M} = \mathbf{AX} \tag{11.54}$$

If $NR = NS$, the formal solution of Eq. 11.54 is, as with Eq. 11.49,

$$\mathbf{X} = \mathbf{A}^{-1}\mathbf{M} \tag{11.55}$$

Because of the difficulties of matrix inversion, a least-squares solution has been attempted with $NR > NS$. If $NR < NS$, no unique solution exists, but an acceptable one has been obtained.

The least-squares unfolding starts with Eq. 11.53 and minimizes the quantity

$$Q = \sum_{i=1}^{NR} w_i \left( M_i - \sum_{j=1}^{NS} A_{ij} X_i \right)^2 \tag{11.56}$$

The weighting factors $w_i$ are usually taken to be the inverse of the variance of $M_i$. The minimization is achieved by setting

$$\frac{\partial Q}{\partial X_k} = 0 \qquad k = 1, \ldots, NS$$

which gives

$$\sum_{i=1}^{NR} w_i A_{ik} \left( M_i - \sum_{j=1}^{NS} A_{ij} X_j \right) = 0 \qquad k = 1, \ldots, NS \tag{11.57}$$

and can be solved for $X_j$ for $j = 1, NS$. Equation 11.57 may be written in matrix form[6]

$$\mathbf{X} = (\mathbf{A}^T \mathbf{W} \mathbf{A})^{-1} \mathbf{A}^T \mathbf{W} \mathbf{M} \tag{11.58}$$

where $\mathbf{A}^T$ = transpose of $\mathbf{A}$.

Computer round-off errors in completing the matrix inversion shown by Eq. 11.58 lead to large oscillations in the solution $\mathbf{X}$. The oscillations can be reduced if the least-squares solution is "constrained." Details of least-squares unfolding with constraints are given in Refs. 6 and 7.

## 11.6 DATA SMOOTHING

The smoothing of raw experimental data is a controversial subject because it represents manipulation of the data without clear theoretical justification. However, smoothing is generally accepted as common practice, since experience has shown that it is beneficial in certain cases to the subsequent analysis of the data, for example, in identification of energy peaks in complex gamma energy spectra (Chap. 12) and unfolding of neutron energy spectra (Chap. 14). Data smoothing should be viewed as an attempt to filter out the statistical fluctuations without altering the significant features of the data.

To illustrate how data smoothing is performed, consider again $N$ measurements $y_i|_{i=1,N}$, where $y_i = y(x_i)$. Smoothing, which is applied to the values of $y_i$, is an averaging process. In the simplest case, one adds a fixed odd number of $y_i$

values, takes the arithmetic average of the sum, and sets the smoothed value of $y_i$ at the center of the group equal to this average. Next, the first point of the group is dropped, the next point is added at the other end of the group, and the process is repeated for all $y_i$ points. In general, the "smoothing" equation takes the form

$$y_i = \frac{1}{M} \sum_{j=-n}^{j=n} C_j y_{i+j} \tag{11.59}$$

where $C_j$ = coefficients that depend on the method of smoothing (see below)
$M$ = normalization constant
$n$ = index showing the number of points used in the smoothing process (the index $n$ means that $2n + 1$ points were used for smoothing)
$y_i$ = smoothed value, replacing the old $y_i$ in the middle of $2n + 1$ points

The coefficients $C_j$ are determined by least-squares fitting a polynomial of order $m$ to $2n + 1$ data points[9-11] and taking the smoothed value equal to the value of the polynomial in the middle point (Fig. 11.11). To illustrate the method, a few examples are given below. The least-squares fit will be based on Eqs. 11.18–11.20.

**Three-point zeroth-order smoothing.** From Eq. 11.18,

$$f(x) = a_1$$

From Eq. 11.19,

$$A_{11} = \sum_{i=1}^{3} w_i = \sum_i 1 = 3$$

From Eq. 11.20,

$$B_1 = \sum_i^{3} w_i y_i = \sum_{i=1}^{3} y_i$$

From Eq. 11.16,

$$a_1 = \frac{B_1}{A_{11}} = \frac{1}{3} \sum_{i=1}^{3} y_i$$

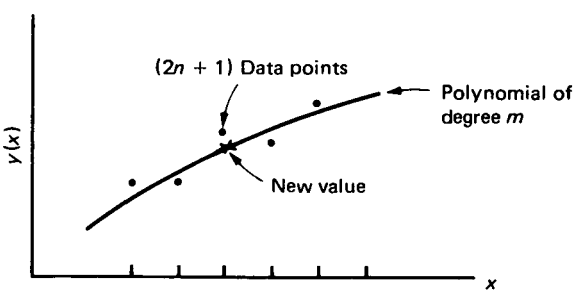


**Figure 11.11** Data smoothing. A polynomial of degree $m$ is fitted to $(2n + 1)$ data points, and the smoothed value is equal to the value of the polynomial in the middle point.

Therefore, if three-point zeroth-order smoothing is applied (Fig. 11.12), the constants of Eq. 11.59 are

$$M = 3 \qquad C_1 = C_2 = C_3 = 1$$

and

$$y_i = \tfrac{1}{3}(y_{i-1} + y_i + y_{i+1}) \tag{11.60}$$

**Five-point zeroth-order smoothing.** Following the same steps as above, one obtains

$$M = 5 \qquad C_i = 1 \qquad i = 1,5$$

and

$$y_i = \tfrac{1}{5}(y_{i-2} + y_{i-1} + y_i + y_{i+1} + y_{i+2}) \tag{11.61}$$

**Three-point first-order smoothing.** From Eq. 11.18, $f(x) = a_1 + a_2 x$. Using Eqs. 11.19, 11.20, and 11.16, one can solve for the values of $M$ and $C_i$. If the $x_i$ points are equally spaced, the result is identical with three-point zeroth-order smoothing (Eq. 11.60). This is true, in general, for equally spaced $x_i$; that is, the result of smoothing with an even-order polynomial is the same as that with a polynomial of the next higher order. Table 11.2 gives the values of $M$ and $C_j$ for second-order smoothing.

As an example of using the various equations, Fig. 11.13 shows results of three-point zeroth-order smoothing and five-point second-order smoothing, i.e., using Eqs. 11.60 and 11.62:

$$y_i = \tfrac{1}{35}(-3y_{i-2} + 12y_{i-1} + 17y_i + 12y_{i+1} - 3y_{i+2}) \tag{11.62}$$

If the total number of points is $N$, the number of smoothed points is $N - 2n$ for $(2n + 1)$-point smoothing because the first smoothed point is $i = n + 1$ and the last one is $N - n$. The smoothing process can be repeated if necessary—i.e., one may smooth data that were previously smoothed.[9]

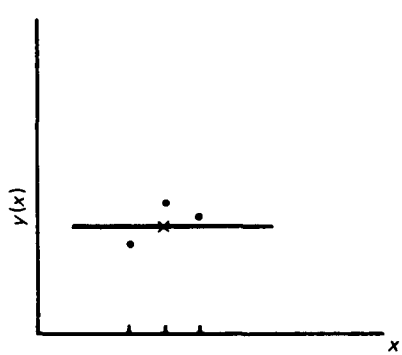


**Figure 11.12** Three-point, zeroth-order smoothing.

**Table 11.2 Coefficients for Second-Order Smoothing†**

| $n$ | 5 | 7 | 9 | 11 |
|---|---|---|---|---|
| $M$ | 35 | 21 | 231 | 429 |
| $C_{-5}$ | | | | 36 |
| $C_{-4}$ | | | −21 | 9 |
| $C_{-3}$ | | −2 | 14 | 44 |
| $C_{-2}$ | −3 | 3 | 39 | 69 |
| $C_{-1}$ | 12 | 6 | 54 | 84 |
| $C_0$ | 17 | 7 | 59 | 89 |
| $C_1$ | 12 | 6 | 54 | 84 |
| $C_2$ | −3 | 3 | 39 | 69 |
| $C_3$ | | −2 | 14 | 44 |
| $C_4$ | | | −21 | 9 |
| $C_5$ | | | | −36 |

†From reference 9.

One of the difficulties in data smoothing is the choice of the correct value for $n$. Unfortunately, there are no strict criteria for the selection of $n$. The analyst should be guided mainly by experience and by the general effects of smoothing on the results. In particular, if the data represent energy spectra with many peaks, the smoothed spectrum may tend to flatten the peaks and fill the valleys.

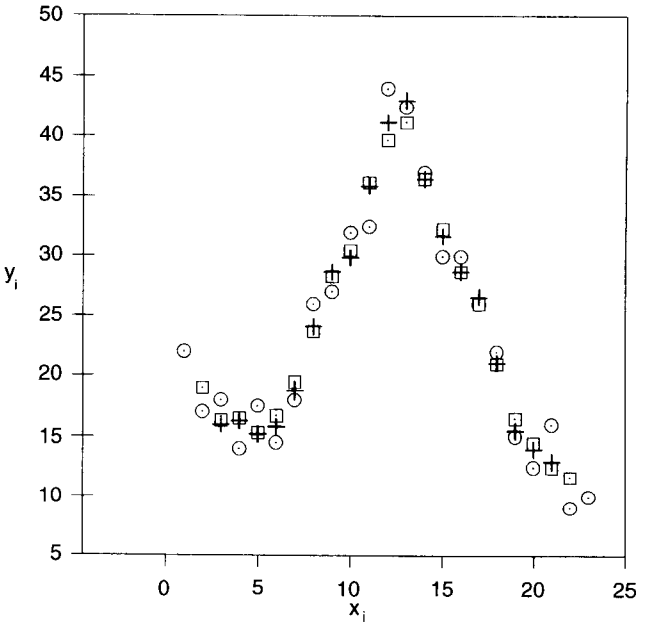


**Figure 11.13** The same data smoothed with two different equations. Circles are original data, squares are data smoothed with Eq. 11.60, and crosses are data smoothed with Eq. 11.62.

The general smoothing equation may be written as

$$Z_i = \sum_j R_{i-j} Y_j \tag{11.63}$$

which has the same form as the folding-unfolding matrix equations (Eq. 11.48). Thus, smoothing may be considered as folding the data ($y_i$) with the weights ($R_{i-j}$) as the response function. Taking it one step further, one may perform smoothing by using a continuous function, i.e., a Gaussian. Then

$$Z(x) = \int G(x, x') y(x')\, dx' \tag{11.64}$$

The operation indicated by Eq. 11.64 has been applied to neutron spectroscopic data.[12]

## PROBLEMS

**11.1** The table below shows radioactive decay data from a certain isotope. Using least-squares fit, determine the half-life of the isotope. What is the error of the half-life as determined by this set of data?

| $t$(min) | Counts | $t$(min) | Counts |
|---|---|---|---|
| 0 | 500 | 6 | 164 |
| 1 | 430 | 7 | 130 |
| 2 | 310 | 8 | 92 |
| 3 | 265 | 9 | 89 |
| 4 | 240 | 10 | 75 |
| 5 | 186 | | |

**11.2** The numbers below represent values of cosine for the corresponding angles.

| Angle: | 5° | 10° | 15° | 20° | 25° | 30° |
|---|---|---|---|---|---|---|
| Cosine: | 0.99619 | 0.98481 | 0.96593 | 0.93969 | 0.90631 | 0.86603 |

Obtain cosine values, by interpolation, for 22° using Lagrange's three-point interpolation formula. Evaluate the error of your result. Compare the error with its correct value.

**11.3** Prove Eqs. 11.22 to 11.24.

**11.4** Obtain the least-squares fit equations for a quadratic fit.

**11.5** Prove that the result of folding a step function with a Gaussian is

$$M(E) = \frac{S_0}{2}\left[1 + \operatorname{erf}\left(\frac{E - E_0}{\sqrt{2}\,\sigma}\right)\right]$$

where the source spectrum is

$$S(E) = \begin{cases} S_0 & E \geq E_0 \\ 0 & \text{otherwise} \end{cases}$$

**11.6** Prove that the result of folding a Gaussian with a Gaussian is

$$M(E) = \frac{1}{\sqrt{2}\,\pi\sqrt{(\sigma^2 + \sigma_S^2)}} \exp\left[-\frac{(E - E_0)^2}{2(\sigma^2 + \sigma_S^2)}\right]$$

where the source spectrum is centered at $E_0$ and has a standard deviation $\sigma_S$.

**11.7** Prove that the result of folding an exponential function $e^{-aE}$ with a Gaussian is

$$M(E) = e^{a^2\sigma^2/2}e^{-aE}$$

**11.8** What is the measured spectrum $M(E)$ if the detector response is a step function of the form $R(E, E') = C(E')/E'$ and the source emits two types of particles at energy $E_1$ and $E_2$?

**11.9** What is the measured spectrum $M(E)$ if the detector response is a step function, as in Prob. 11.8, and the source spectrum is

$$S(E) = \frac{S_0}{E_2 - E_1} \qquad E_1 \le E \le E_2$$

and is zero otherwise.

**11.10** The following data represent results of counting an energy peak. How does the full width at half maximum of the peak change if one applies (a) three-point zeroth-order smoothing and (b) five-point second-order smoothing?

| Channel | Counts | Channel | Counts |
|---|---|---|---|
| 10 | 12 | 17 | 34 |
| 11 | 10 | 18 | 26 |
| 12 | 14 | 19 | 18 |
| 13 | 14 | 20 | 10 |
| 14 | 24 | 21 | 12 |
| 15 | 30 | 22 | 9 |
| 16 | 40 | | |

## BIBLIOGRAPHY

Abramowitz, M., and Stegan, I. A. (eds.), *Handbook of Mathematical Functions*, National Bureau of Standards, Applied Mathematics Series, 55, June 1964.

Bevington, R. P., *Data Reduction and Error Analysis for the Physical Sciences*, McGraw-Hill, New York, 1969.

Hildebrand, F. B., *Introduction to Numerical Analysis*, McGraw-Hill, New York, 1956.

Householder, A. S., *Principles of Numerical Analysis*, McGraw-Hill, New York, 1953.

## REFERENCES

1. Bennet, F. F., and Yule, T. J., ANL-7763, 1971.
2. Ciallela, C. M., and Devanney, J. A., *Nucl. Instrum. Meth.* **60**:269 (1968).
3. Toms, M. E., *Nucl. Instrum. Meth.* **92**:61 (1971).

4. Johnson, R. H., and Wehring, B. W., ORNL/RSIC-40, p. 33, 1976.
5. Tsoulfanidis, N., Wehring, B. W., and Wyman, M. E., *Nucl. Instrum. Meth.* **73**:98 (1969).
6. Burrus, W. R., and Verbinski, V. V., *Nucl. Instrum. Meth.* **67**:181 (1969).
7. Kendrick, H., and Sperling, S. M., GA-9882, 1970.
8. Johnson, R. H., Ingersoll, D. T., Wehring, B. W., and Dorning, J. J., *Nucl. Instrum. Meth.* **145**:337 (1977).
9. Savitzky, A., and Golay, M. J. E., *Anal. Chem.* **36**:1627 (1964).
10. Yule, H. P., *Nucl. Instrum. Meth.* **54**:61 (1967).
11. Yule, H. P., *Anal. Chem.* **38**:103 (1966).
12. Johnson, R. H., Wehring, B. W., and Dorning, J. J., *Nucl. Sci. Eng.* **73**:93 (1980).

CHAPTER
# TWELVE

# PHOTON (GAMMA-RAY AND X-RAY) SPECTROSCOPY

## 12.1 INTRODUCTION

Photons, i.e., gamma-rays and X-rays, may be treated either as electromagnetic waves or as particles. An *electromagnetic wave* is characterized by its wavelength $\lambda$ or frequency $\nu$. A *photon* is a particle having zero charge and zero rest mass, traveling with the speed of light, and having an energy $E = h\nu$, where $h =$ Planck's constant. The wave properties of a photon are used for low-energy measurements only. In all other cases, detection of photons is based on their interactions as particles.

This chapter first examines the mechanisms of detection in photon counters and then discusses the spectroscopic characteristics of the different types of X-ray and $\gamma$-ray detectors.

## 12.2 MODES OF ENERGY DEPOSITION IN THE DETECTOR

Photons are detected by means of the electrons they produce when they interact in the material of which the detector is made. The main interactions are photoelectric effect, Compton scattering, and pair production. The electrons (or positrons) produced by these interactions deposit their energy in the counter and thus generate a voltage pulse that signifies the passage of the photon. The height of the voltage pulse is proportional to the energy deposited in the

detector. Since the objective is to measure the energy of the incident photon, the question arises: Is this voltage pulse proportional to the energy of the incident particle? To provide an answer, one must examine how the photon interacts and what happens to its energy.

### 12.2.1 Energy Deposition by Photons with $E < 1.022$ MeV

A photon with $E < 1.022$ MeV can interact only through the photoelectric or the Compton effect. If a photoelectric interaction takes place, the photon disappears and an electron appears with energy equal to $E - B_e$, where $B_e$ is the binding energy of that electron. The range of electrons in a solid, either a scintillator crystal or a semiconductor, is so short that it can be safely assumed that all the electron energy will be deposited in the detector (Fig. 12.1*a*). If the interaction occurs very close to the wall, the electron may deposit only part of its energy in the counter (Fig. 12.1*b*), but the probability of this happening is small. In practice, one assumes that all the photoelectrons deposit all their energy in the detector. This energy is less than the energy of the incident photon by the amount $B_e$, the binding energy of the electron. What happens to the energy $B_e$?

After a photoelectric effect takes place, an electron from one of the outer atomic shells drops into the empty inner state in about $10^{-8}$ s. This electronic transition is followed by an X-ray or by an Auger electron (see Chap. 4). The Auger electron will also deposit its energy in the detector. The X-ray with energy in the low keV range ($\sim$ 100 keV or less) interacts again photoelectrically and generates another electron.† The net result of these successive interactions is that the part $B_e$ of the incident photon energy is also deposited in the counter. All these events take place within a time of the order of $10^{-8}$ s. Since the formation of the voltage pulse takes about $10^{-6}$ s, both parts of the energy—namely, $E - B_e$ = energy of photoelectron and $B_e$ = energy of the X-ray—contribute to the same pulse, the height of which is proportional to

†For thin detectors, or detectors made of high-$Z$ material—e.g., CdTe or $HgI_2$—some X-rays may escape, thus forming the so called "escape peaks" (see Sec. 12.8).

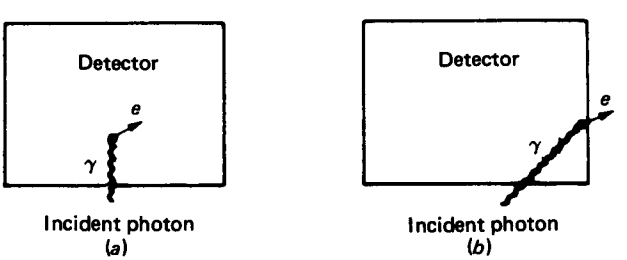


**Figure 12.1** As a result of a photoelectric interaction, the photon disappears. (*a*) All the energy of the electron is deposited in the detector. (*b*) Part of the energy is deposited in the wall.

$(E - B_e) + B_e = E =$ incident photon energy. The conclusion is, therefore, that if the photon interacts via photoelectric effect, the resulting pulse has a height proportional to the incident particle energy.

If Compton scattering takes place, only a fraction of the photon energy is given to an electron. A scattered photon still exists carrying the rest of the energy. The energy of the electron is deposited in the detector. But what happens to the energy of the scattered photon?

The scattered photon may or may not interact again inside the detector. The probability of a second interaction depends on the size of the counter (Fig. 12.2), on the position of the first interaction, on the energy of the scattered photon, and on the material of which the detector is made. Unless the detector is infinite in size, there is always a chance that the scattered photon may escape, in which case a pulse will be formed with height proportional to an energy that is *less* than the energy of the incident photon.

From the study of the Compton effect (Chap. 4), it is known that Compton electrons have an energy range from zero up to a maximum energy $T_{max}$, which is

$$T_{max} = E - \frac{E}{1 + 2E/mc^2} \tag{12.1}$$

where $mc^2 = 0.511$ MeV, the rest mass energy of the electron. Therefore, if the interaction is Compton scattering, pulses are produced from Compton electrons with heights distributed from $V = 0$ volts, corresponding to $T_{min} = 0$, up to a maximum height $V_{max}$ volts corresponding to the maximum energy $T_{max}$. Figures 12.3 to 12.5 illustrate how a monoenergetic photon spectrum is recorded as a result of photoelectric and Compton interactions.

Figure 12.3 shows the source spectrum. In the case of perfect energy resolution, this monoenergetic source produces in an MCA the measured spectrum shown by Fig. 12.4. Some photons produce pulses that register in channel $C_0$, corresponding to the source energy $E_0$, and thus contribute to the main peak of the spectrum, which is called the full-energy peak. The Compton

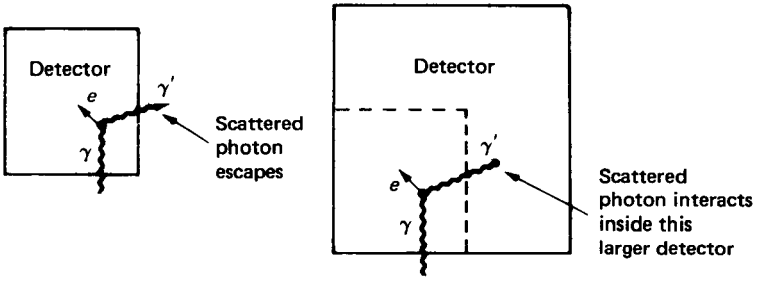


**Figure 12.2** As a result of Compton scattering, part of the photon energy may escape.

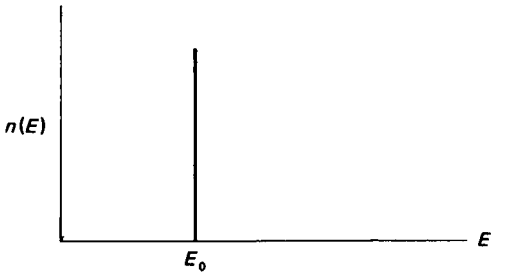


**Figure 12.3** A monoenergetic gamma spectrum (source spectrum).

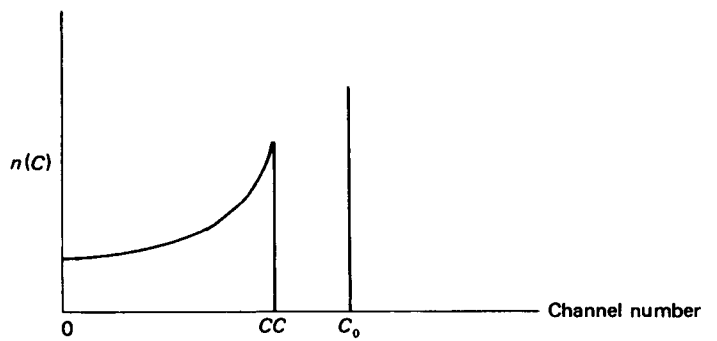


**Figure 12.4** The pulse height spectrum obtained from the source spectrum of Fig. 12.3, in the absence of statistical effects in the detector (perfect energy resolution).

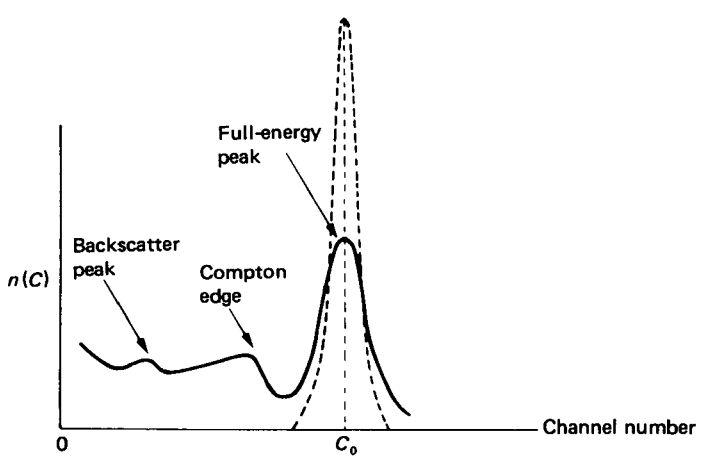


**Figure 12.5** The measured pulse height spectrum for the source spectrum of Fig. 12.3. The statistical effects in the detector broaden both the peak and the Compton continuum part of the spectrum. The dashed line shows the spectrum that would have been recorded in the absence of the Compton continuum.

electrons are responsible for the continuous part of the spectrum, extending from zero channel up to channel *CC* and called the *Compton continuum*. The end of the Compton continuum, called the *Compton edge*, corresponds to the energy given by Eq. 12.1. Since no detector exists with perfect energy resolution, the measured spectrum looks like that of Fig. 12.5.

Sometimes the Compton interaction occurs very close to the surface of the detector or in the material of the protective cover surrounding the detector (Fig. 12.6).† Then there is a high probability that the electron escapes and only the energy of the scattered photon is deposited in the detector. The minimum energy $E_{\min}$ of the scattered photon is given by

$$E_{\min} = \frac{E}{1 + 2E/mc^2} \tag{12.2}$$

Occasionally, a rather broad peak, corresponding to the energy given by Eq. 12.2, is observed in $\gamma$-ray spectra. This peak is called the *backscatter peak* (Fig. 12.5).

The fraction of counts recorded outside the full-energy peak depends on the energy of the gamma and on the size of the detector. The energy of the photon determines the ratio $\sigma/\mu$ of the Compton scattering coefficient to the total attenuation coefficient. The lower the gamma energy is, the smaller this ratio becomes. Then a greater fraction of photons interacts photoelectrically and is recorded in the full-energy peak, thus reducing the Compton continuum part of the spectrum. As an example, consider gammas with energy 100 keV and 1 MeV, and a Ge(Li) detector. For 100-keV gammas in germanium, the ratio $\sigma/\mu$ is $0.9/3.6 \approx 0.25$ (Fig. 12.31), which indicates that 25 percent of the interactions are Compton and 75 percent photoelectric. The number of pulses in the Compton continuum should be equal to or less than one-third the number recorded under the full energy peak. At 1 MeV, the ratio $\sigma/\mu$ is about $0.4/0.42 \approx 0.95$, which means that about 95 percent of the interactions are Compton and only 5 percent photoelectric. Thus, the Compton continuum due to 1-MeV photons is the largest part of the spectrum.

The magnitude of the Compton continuum is also affected by the size of the detector (Fig. 12.2). The larger the detector is, the greater the probability of a second Compton interaction. If the detector size could become infinite, the Compton continuum would disappear.

### 12.2.2 Energy Deposition by Photons with $E > 1.022$ MeV

If $E > 1.022$ MeV, pair production is possible, in addition to photoelectric effect and Compton scattering. As a result of pair production, the photon

†Backscattering may also take place in the source itself, or in the shield surrounding the detector.

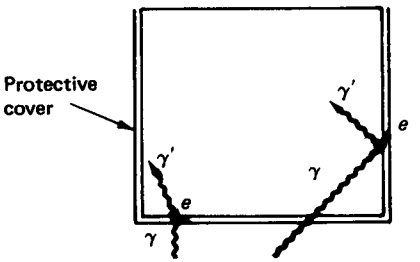


**Figure 12.6** If Compton scattering occurs close to the surface of the detector, the only energy deposited may be that of the scattered photon.

disappears and an electron-positron pair appears, at the expense of 1.022 MeV transformed into the pair's rest masses. The total kinetic energy of the electron-positron pair is

$$T_{e^-} + T_{e^+} = T = (E - 1.022)\ \text{MeV}$$

The kinetic energy of the pair is deposited in the counter (the arguments are the same as for photoelectrons or Compton electrons). Therefore, pulses proportional to the energy $T = E - 1.022$ MeV are certainly produced, but what happens to the energy of 1.022 MeV?

The positron slows down and reaches the end of its range in a very short time, shorter than the time needed for pulse formation. Sometimes while in flight, but most of the time at the end of its track, it combines with an atomic electron, the two annihilate, and two gammas are emitted, each with energy 0511 MeV.† There are several possibilities for the fate of these annihilation gammas.

1. The energy of both annihilation gammas is deposited in the detector. Then, a pulse height proportional to energy

$$(E - 1.022)\ \text{MeV} + 1.022\ \text{MeV} = E$$

   is produced.
2. Both annihilation photons escape. A pulse height proportional to energy $(E - 1.022)$ MeV is formed.
3. One annihilation photon escapes. A pulse height proportional to energy

$$(E - 1.022)\ \text{MeV} + 0.511\ \text{MeV} = (E - 0.511)\ \text{MeV}$$

   is formed.

If the pair production event takes place on or close to the surface of the detector, it is possible that only one of the annihilation photons enters the counter. In such a case, a pulse height proportional to energy 0.511 MeV is formed.

†There is a small probability that three gamma may be emitted. This event has a negligible effect on spectroscopy measurements.

Peaks corresponding to these energies could be identified, but this does not mean that they are observed in every $\gamma$-ray spectrum. The number, energy, and intensity of peaks depend on the size of the detector, the geometry of the source (is it collimated or not?), and the energies of the gammas in the spectrum. If a source emits only one gamma, the measured spectrum will certainly show

1. The full energy peak, corresponding to $E$ (this is the highest energy peak)
2. The Compton edge, corresponding to energy

$$E - \frac{E}{1 + 2E/mc^2}$$

Other peaks that may be observed are

3. Backscatter peak, with energy

$$\frac{E}{1 + 2E/mc^2}$$

4. The *single-escape peak* with energy $(E - 0.511)$ MeV
5. The *double-escape peak* with energy $(E - 1.022)$ MeV

Figure 12.7 presents the spectrum of $^{24}$Na. The single- and double-escape peaks due to the 2.754-MeV gamma are clearly shown. The single- and double-

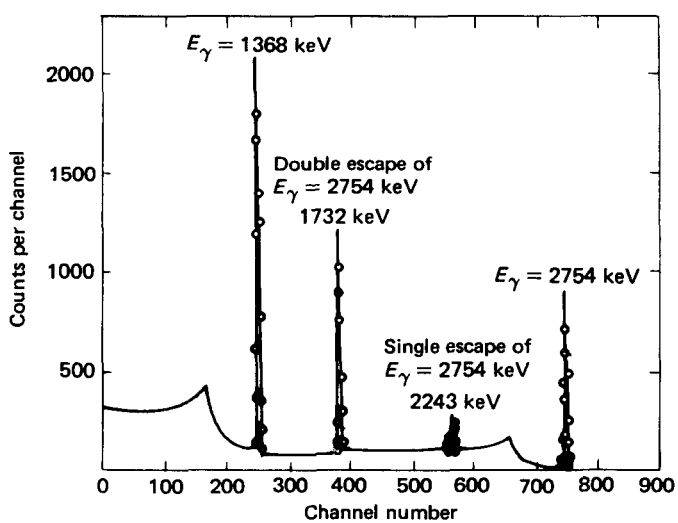


**Figure 12.7** A gamma spectrum showing single- and double-escape peaks (from Chap. 4.4.2 of Bertolini and Coche).

escape peaks are very important when complex gamma spectra are recorded. The observer should be extremely careful to avoid identifying them falsely as peaks produced by gammas emitted from the source.

If the source is a positron emitter, a peak at 0.511 MeV is always present. The positron-emitting isotope $^{22}$Na is such an example. It emits only one gamma with energy 1.274 MeV, yet its spectrum shows two peaks. The second peak is produced by 0.511-MeV annihilation photons emitted after a positron annihilates (Fig. 12.8).

The Compton continuum, present in gamma energy spectra recorded either by a NaI(Tl) scintillator or by a Ge detector, is a nuisance that impedes the analysis of complex spectra. It is therefore desirable to eliminate or at least reduce that part of the spectrum relative to the gamma energy peak. One way to achieve this is to use two detectors and operate them in anticoincidence. Such an arrangement, known as the *Compton-suppression spectrometer*, is shown in Fig. 12.9. A large NaI(Tl) scintillator surrounds a Ge detector, and the two detectors are operated in anticoincidence. The energy spectrum of the central

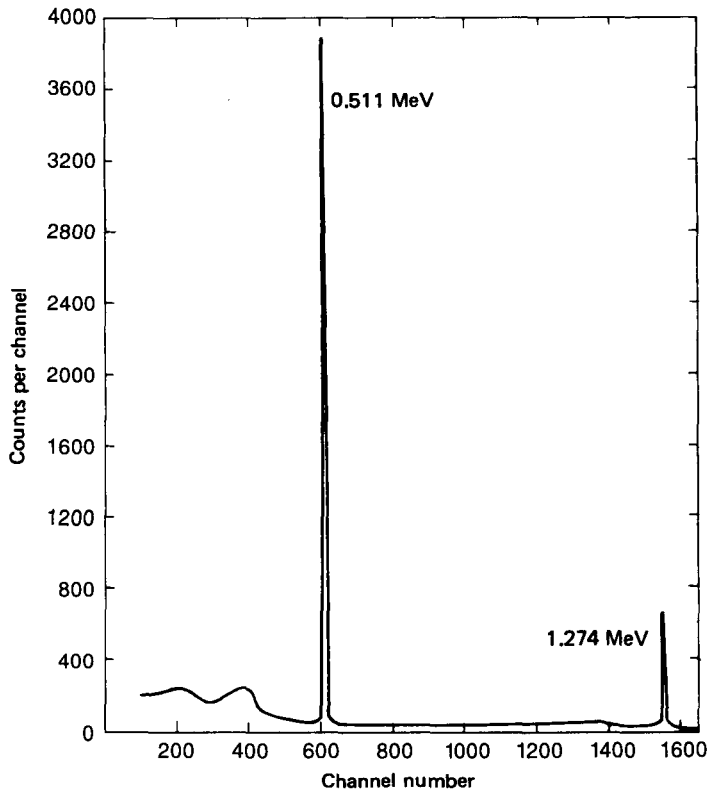


**Figure 12.8** The $^{22}$Na spectrum showing the 1.274-MeV peak and the 0.511-MeV peak that is due to annihilation gammas.

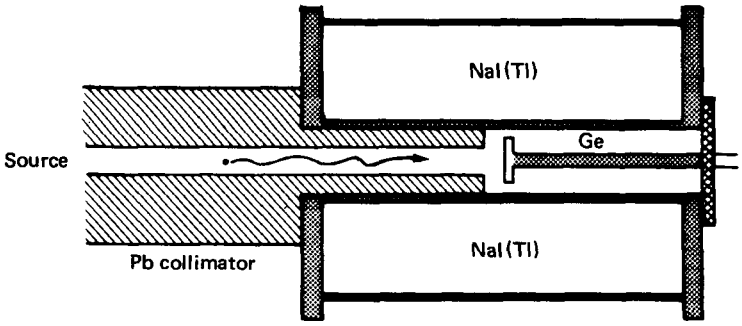


**Figure 12.9** Diagram of a Compton suppression spectrometer using a NaI(Tl) and a Ge detector. The two detectors are operated in anticoincidence, with the Ge recording the energy spectrum.

detector [the Ge in this case] will consist of pulses that result from total energy absorption in that detector. Figure 12.10 shows the $^{60}$Co spectrum obtained with and without Compton suppression.

## 12.3 EFFICIENCY OF X-RAY AND GAMMA-RAY DETECTORS: DEFINITIONS

There are four types of efficiency reported in the literature:

1. Total detector efficiency
2. Full-energy peak efficiency

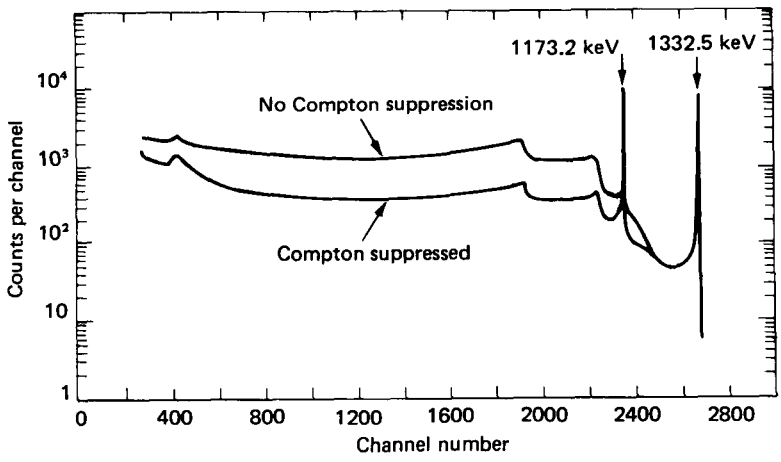


**Figure 12.10** The $^{60}$Co spectrum recorded with and without Compton suppression. Notice that the ordinate is in logarithmic scale.

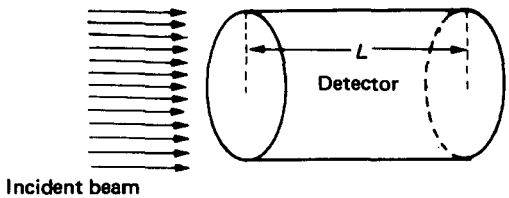


**Figure 12.11** The geometry assumed in the definition of intrinsic efficiency.

3. Double-escape peak efficiency
4. Single escape peak efficiency

The first two are much more frequently used than the last two. All four efficiencies may be intrinsic, absolute, or relative. The individual definitions are as follows.

*Intrinsic total detector efficiency* is the probability that a gamma of a given energy which strikes the detector will be recorded. The geometry assumed for the calculation or measurement of this efficiency is shown in Fig. 12.11.

*Absolute total detector efficiency* is the probability that a gamma emitted from a specific source will be recorded in the detector. The geometry assumed for the absolute efficiency is shown in Fig. 12.12. The intrinsic efficiency (Fig. 12.11) depends on the energy of the gamma $E$ and the size of the detector $L$. The absolute total efficiency (Fig. 12.12) depends on, in addition to $E$ and $L$, the radius of the detector $R$ and the source-detector distance $d$. Therefore the absolute total efficiency, as defined here, is the product of intrinsic efficiency times the solid angle fraction (see also Chap. 8).

*Full-energy peak efficiency is defined as follows*:

$$\begin{pmatrix}\text{Full-energy peak}\\ \text{efficiency}\end{pmatrix} = \begin{pmatrix}\text{total detector}\\ \text{efficiency}\end{pmatrix} \times \frac{\begin{pmatrix}\text{counts in full-}\\ \text{energy peak}\end{pmatrix}}{\begin{pmatrix}\text{total counts in}\\ \text{spectrum}\end{pmatrix}} \tag{12.3}$$

The ratio by which the total detector efficiency is multiplied in Eq. 12.3 is called the *peak-to-total ratio* ($P$). Figure 12.13 shows how $P$ is measured.

The *double-escape peak efficiency* is important if the energy of the gamma $E$ is greater than about 1.5 MeV, in which case pair production becomes important. The energy of the double-escape peak, equal to $E - 1.022$ MeV, is used

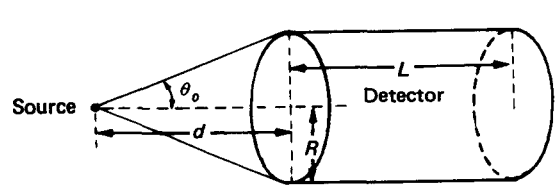


**Figure 12.12** The geometry assumed in the definition of absolute efficiency.

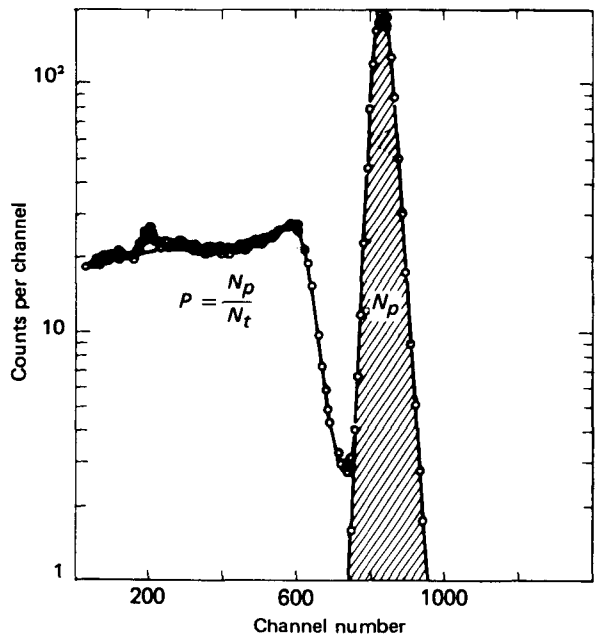


**Figure 12.13** The peak-to-total ratio is equal to the number of counts under the peak ($N_p$) divided by the total number of counts ($N_t$).

for identification of certain isotopes. This kind of efficiency is defined by

$$\begin{pmatrix}\text{Double-escape}\\ \text{peak efficiency}\end{pmatrix} = \begin{pmatrix}\text{total detector}\\ \text{efficiency}\end{pmatrix} \times \frac{\begin{pmatrix}\text{counts in double-}\\ \text{escape peak}\end{pmatrix}}{\begin{pmatrix}\text{total counts in}\\ \text{spectrum}\end{pmatrix}} \tag{12.4}$$

The *single-escape peak efficiency* is important also for $E > 1.5$ MeV, and its definition is analogous to that of the double-escape peak:

$$\begin{pmatrix}\text{Single-escape}\\ \text{peak efficiency}\end{pmatrix} = \begin{pmatrix}\text{total detector}\\ \text{efficiency}\end{pmatrix} \times \frac{\begin{pmatrix}\text{counts in single-}\\ \text{escape peak}\end{pmatrix}}{\begin{pmatrix}\text{total counts in}\\ \text{spectrum}\end{pmatrix}} \tag{12.5}$$

The double- and single-escape peak efficiencies are used with semiconductor detectors only. In the above definitions, if the total detector efficiency is replaced by intrinsic, the corresponding full-energy, single-, and double-escape peak efficiencies are also considered intrinsic.

*Relative* efficiency may be obtained for all the cases discussed above. In general,

$$(\text{Relative efficiency})_i = \frac{(\text{absolute efficiency})_i}{\text{efficiency of a standard}} \tag{12.6}$$

where the subscript $i$ refers to any one of the efficiencies defined earlier.

Depending on the type of detector and measurement, the user selects the efficiency to be used. For quantitative measurements, the absolute total efficiency of the detector has to be used at some stage of the analysis of the experimental data.

## 12.4 DETECTION OF PHOTONS WITH NaI(Tl) SCINTILLATION COUNTERS

Of all the scintillators existing in the market, the NaI crystal activated with thallium, NaI(Tl), is the most widely used for the detection of $\gamma$-rays. NaI(Tl) scintillation counters are used when the energy resolution is not the most important factor of the measurement. They have the following advantages over Ge(Li) and Si(Li) detectors:

1. They can be obtained in almost any shape and size. NaI(Tl) crystals with size 0.20 m (8 in) diameter by 0.20 m (8 in) thickness are commercially available.
2. They have rather high efficiency (see Sec. 12.4.1).
3. They cost less than semiconductor detectors.

A disadvantage of all scintillation counters, in addition to their inferior energy resolution relative to Si(Li) and Ge(Li) detectors, is the necessary coupling to a photomultiplier tube.

NaI(Tl) detectors are offered in the market today either as crystals that may be ordered to size or as integral assemblies mounted to an appropriate photomultiplier tube.[1-3] The integral assemblies are hermetically sealed by an aluminum housing. Often, the housing is chrome-plated for easier cleaning. The phototube itself is covered by an antimagnetic $\mu$-metal that reduces gain perturbations caused by electric and magnetic fields surrounding the unit.

The front face of the assembly is usually the "window" through which the photons pass before they enter into the crystal. The window should be as thin as possible to minimize the number of interactions of the incident photons in the materials of the window. Commercially available NaI(Tl) counters used for $\gamma$-ray detection have an aluminum window, which may be as thin as 0.5 mm (0.02 in). X-ray scintillation counters usually have a beryllium window, which may be as thin as 0.13 mm (0.005 in). Beryllium is an excellent material because it allows less absorption thanks to its low atomic number ($Z = 4$).

### 12.4.1 Efficiency of NaI(Tl) Detectors

The intrinsic efficiency of NaI(Tl) detectors (see Fig. 12.11) is essentially equal to $1 - \exp[-\mu(E)L]$, where

$\mu(E)$ = total attenuation coefficient in NaI for photons with energy $E$

$L$ = length of the crystal

A plot of $\mu(E)$ for NaI as a function of photon energy is shown in Fig. 12.14.

The efficiency increases with crystal size. The user should be aware, however, that when the detector volume increases, the background counting rate increases too. In fact, the background is roughly proportional to the crystal volume, while the efficiency increases with size at a slower than linear rate. Thus, there may be a practical upper limit to a useful detector size for a given experiment.

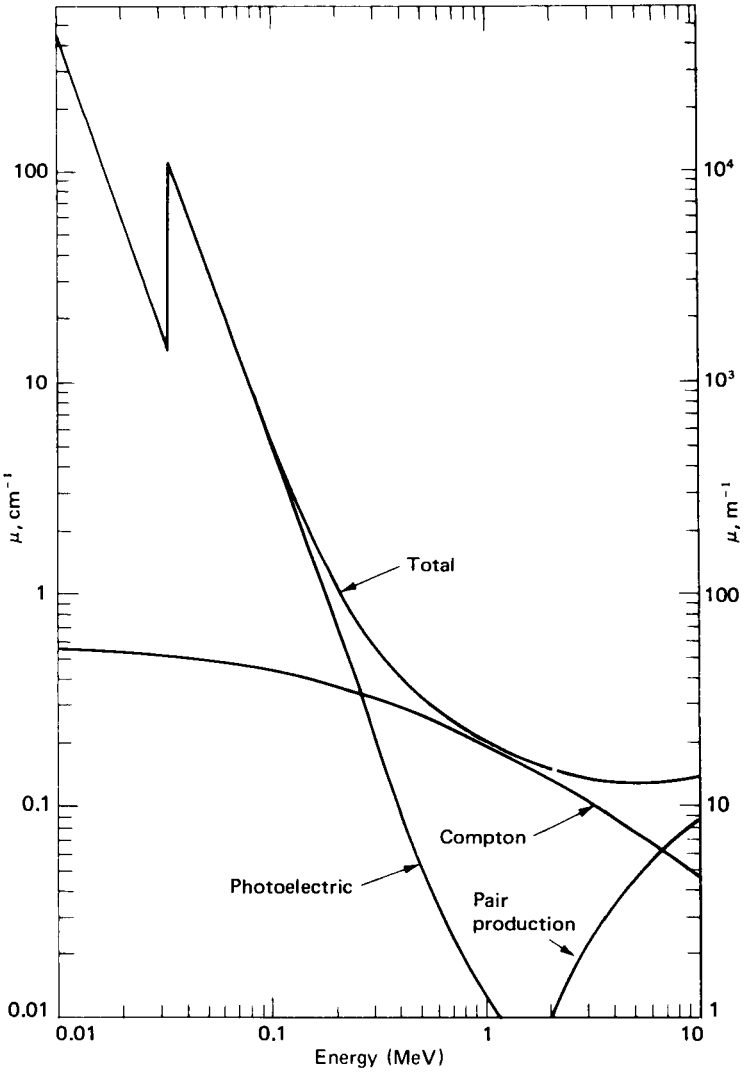


**Figure 12.14** The photon linear attenuation coefficients for NaI(Tl) (from Ref. 3).

Calculated absolute total efficiencies of a NaI crystal are given in Fig. 12.15 for several source-detector distances. They have been obtained by integrating Eq. 8.20, which is repeated here (refer to Figs. 8.21 and 12.12 for notation):

$$\epsilon(E) = \frac{\int_0^{\theta_0} S\{1 - \exp[-\mu(E)r(\theta)]\}\frac{1}{2}\sin\theta\, d\theta}{(S/2)\int_0^{\theta_0}\sin\theta\, d\theta} \tag{8.20}$$

or

$$\epsilon(E) = \frac{\int_0^{\theta_1}\{1 - \exp[-\mu(E)L/\cos\theta]\}\sin\theta\, d\theta}{1 - \cos\theta_0} + \frac{\int_{\theta_1}^{\theta_0}(1 - \exp\{-\mu(E)[(R/\sin\theta) - (d/\cos\theta)]\})\sin\theta\, d\theta}{1 - \cos\theta_0}$$

where $\theta_1 = \tan^{-1}[R/(d + L)]$
$\theta_0 = \tan^{-1}(R/d)$

The inherent approximation of Eq. 8.20 is that it considers detected every photon that interacted at least once inside the detector.

In Fig. 12.15, note that the efficiency decreases with energy up to about 5 MeV. Beyond that point, it starts increasing because of the increase in the pair

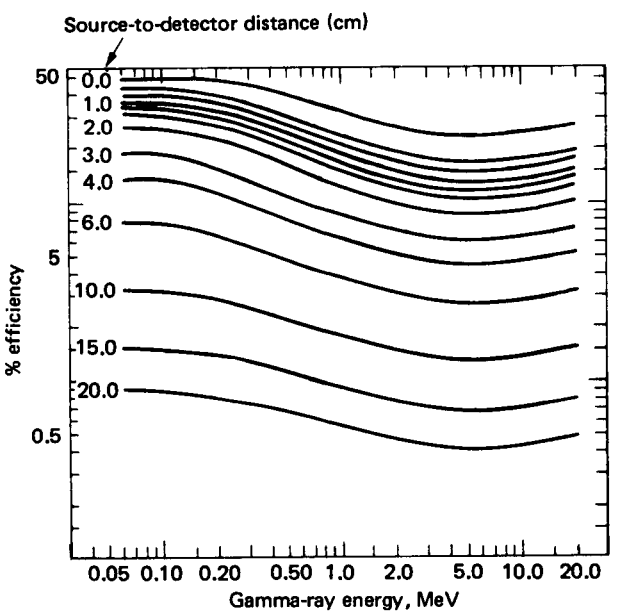


**Figure 12.15** Calculated absolute total efficiencies of a 3 in ×3 in (76.2 mm × 76.2 mm) NaI(Tl) scintillator as a function of energy for different source-detector distances (from Ref. 3).

production probability. Figure 12.16 shows how the peak-to-total ratio (see Fig. 12.13) changes with energy for a source located 0.10 m from detectors of different sizes.

### 12.4.2 Analysis of Scintillation Detector Energy Spectra

NaI(Tl) scintillators are seldom used as gamma-ray spectrometers because their energy resolution is inferior to that of semiconductor detectors. Despite this fact, a brief discussion of the methods of analysis of NaI(Tl) spectra is instructive because it helps point out differences and similarities between the responses of NaI(Tl) and Ge(Li) detectors.

If a NaI(Tl) scintillator is used to detect a photon spectrum consisting of many gamma energies, the measured spectrum will be the summation of spectra

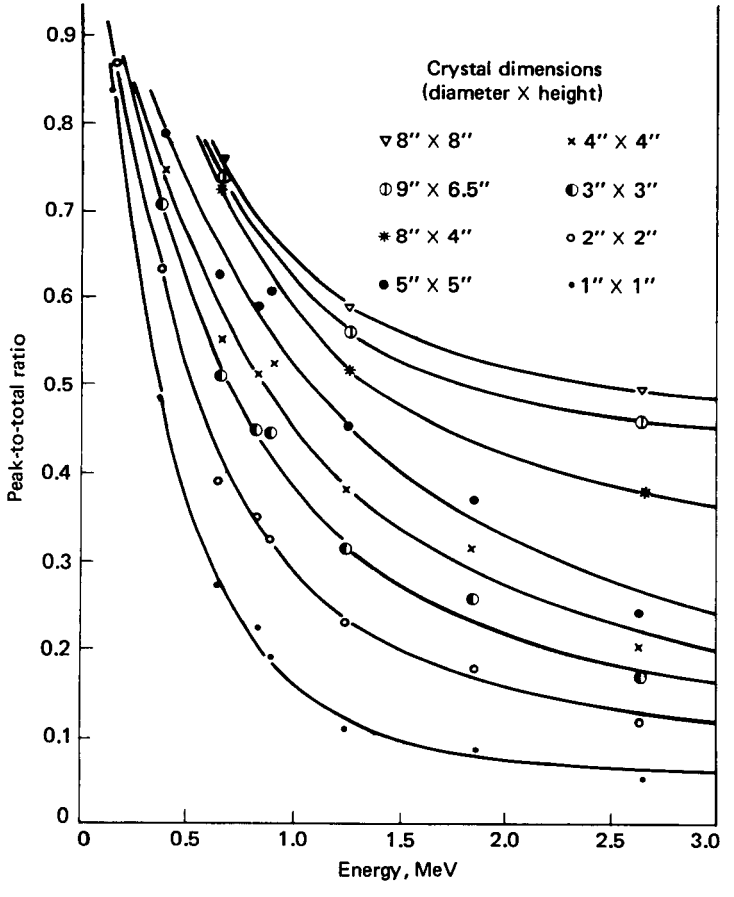


**Figure 12.16** Peak-to-total ratio as a function of energy for NaI(Tl) scintillators of different sizes. The source-to-detector distance is 0.10 m (from Ref. 3).

similar to those shown in Fig. 12.5. To identify individual energies from a complex spectrum, one unfolds the measured spectrum (see Chap. 11). Unfolding, in turn, requires the knowledge of the detector response function.

Response functions of NaI(Tl) detectors, obtained by Heath et al.,[4,5] are shown in Fig. 12.17. These authors measured the response for several gamma energies and then used an interpolation scheme to derive the three dimensional plot of Fig. 12.17. A modified Gaussian of the form

$$y(x) = y_0\left\{1 + \alpha_1(x - x_0)^4 + \alpha_2(x - x_0)^{12}\exp\left[-\frac{(x - x_0)^2}{b_0}\right]\right\} \quad (12.7)$$

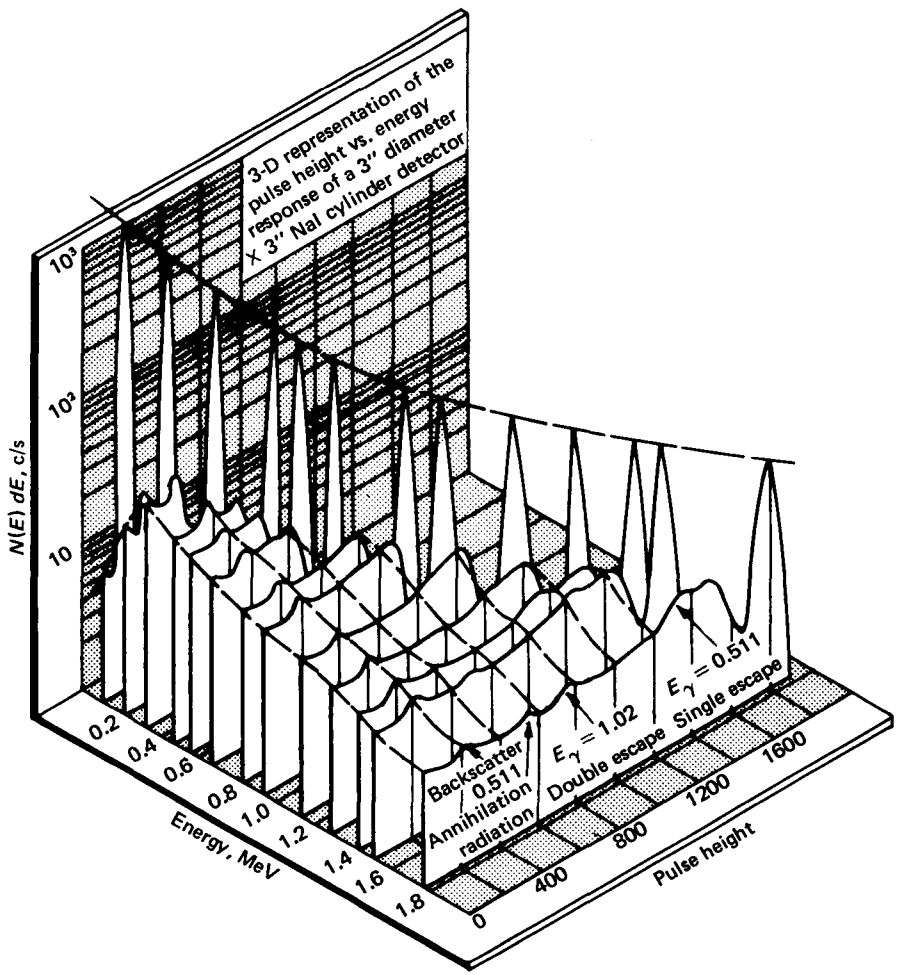


**Figure 12.17** A three-dimensional representation of NaI(Tl) response functions (from Ref. 4).

gave a successful fit to individual gamma peaks. The five parameters $y_0$, $x_0$, $b_0$, $\alpha_1$, and $\alpha_2$ were determined by least-squares fit. The parameter $x_0$ shows the location of the peak, and $b_0$ is related to the full width at half maximum (FWHM) by $\Gamma = 2\sqrt{2(\ln 2)b_0}$. Figure 12.18 shows the measured and calculated response functions for $^{137}$Cs. Unfolding of the spectrum was achieved by using these response functions in a computer program that determines energy and intensity of individual gammas based on a least-squares fit and iteration technique.[5]

The energy resolution of NaI(Tl) detectors is quoted in terms of the percent resolution for the 0.662-MeV gamma of $^{137}$Cs. Using the best electronics available, this resolution is about 7 percent and the FWHM is about 46 keV. As mentioned in Chap. 9, the FWHM is roughly proportional to the square root of the energy. For this reason, the resolution in percent deteriorates as the energy decreases. For 10-keV X-rays, the best resolution achieved is about 40 percent, which makes the FWHM about 4 keV.

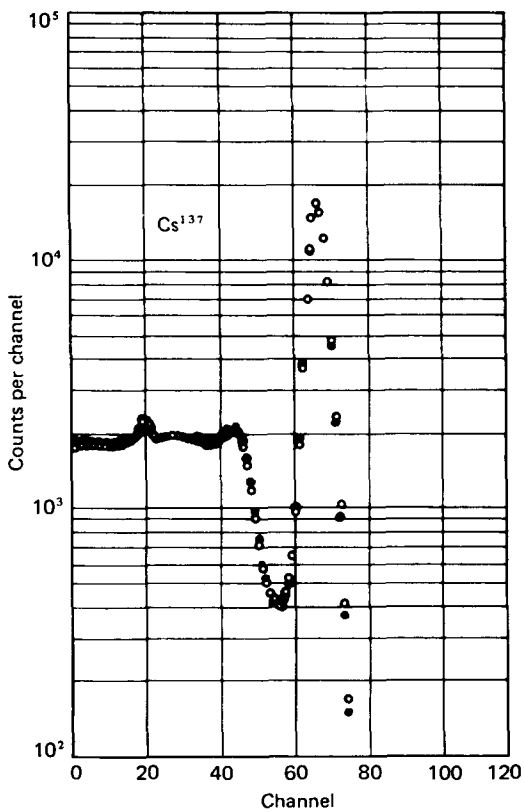


**Figure 12.18** Comparison of the measured (solid circles) and calculated (open circles) response functions for $^{137}$Cs (from Ref. 4).

## 12.5 DETECTION OF GAMMAS WITH AN NE 213 ORGANIC SCINTILLATOR

The NE 213 organic scintillator has emerged as one of the leading fast neutron spectrometers (see Chap. 14). As a gamma spectrometer, the NE 213 scintillator has an efficiency lower than that of NaI(Tl) and an energy resolution that is poor compared to that of semiconductor detectors. There are certain applications, however, where high-energy resolution is not the most important factor. One such application is detection of gammas in a mixed neutron-gamma field. There, the ability of the NE 213 scintillator to discriminate against neutrons makes it an attractive gamma detector.

Because gammas are detected by the NE 213 scintillator mainly through Compton interactions, the response function of the detector consists of the Compton continuum. The response function has been calculated[6] and measured[7] for several gamma energies. Figure 12.19 shows a comparison of calculated and measured response functions.

To obtain the gamma spectrum from the source, the measured NE 213 spectrum must be unfolded. Results of matrix-inversion unfolding applied to the measured spectrum of $^{24}$Na are shown in Figs. 12.20 and 12.21. The spectrum shown in Fig. 12.21 was obtained by unfolding the spectrum of Fig. 12.20 with the code FORIST,[8] which is a variation of the code FERDOR.[9] Both codes use

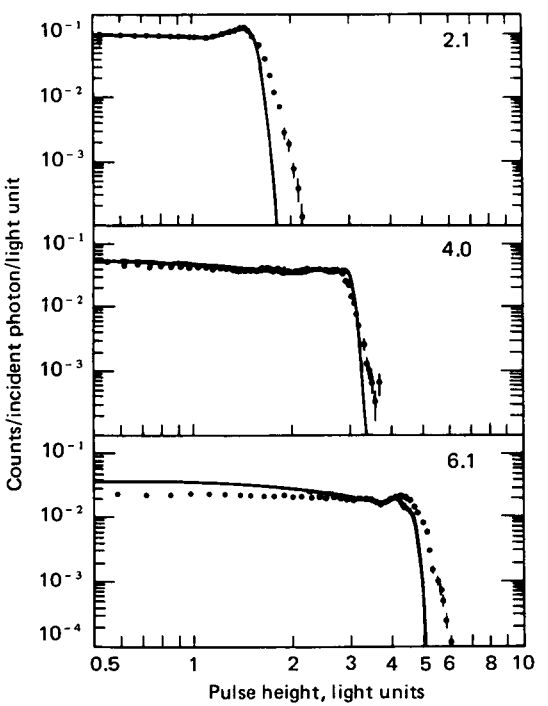


**Figure 12.19** Comparison of measured (point) and calculated (line) NE 213 response functions for 2.1-, 4.0-, and 6.1-Me gamma rays (from Ref. 7).

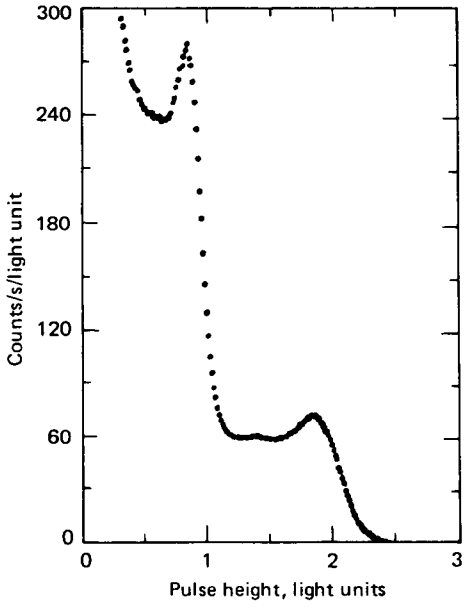


**Figure 12.20** Gamma-ray pulse height spectrum produced by NE 213 for a $^{24}$Na source. The two Compton edges are due to the 1.37- and 0.75-MeV gammas (from Ref. 7).

the least-squares unfolding method described in Sec. 11.5.4. Another program used for gamma spectra analysis is called SAMPO, adapted for use with microcomputers.[10]

## 12.6 DETECTION OF X-RAYS WITH A PROPORTIONAL COUNTER

Gas-filled chambers operating in the proportional counter range are used in certain special applications for the detection of X-rays with energy less than 100

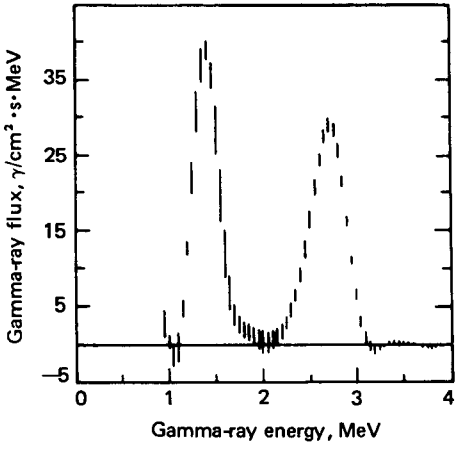


**Figure 12.21** The spectrum of Fig. 12.20, unfolded with the code FORIST. The vertical error bars show $\pm 1$ standard error due to counting statistics (from Ref. 7).

keV. At this energy range, the photons interact only through the photoelectric effect. Since the photoelectric cross section increases as $Z^m$, with $m \approx 3$–5, it is important to have a window made of very low-$Z$ material and a gas with as high a $Z$ value as possible.

X-ray proportional counters are usually cylindrical with a very thin beryllium window located either on the side or at the front end. They use a gas that is a mixture of a noble gas—He, Ne, Ar, Kr, Xe—with methane, at a pressure of about 1 atm.

The energy resolution of these counters is such that the FWHM is 1–2 keV at 20 keV. Thus, proportional counters are superior to scintillation counters in this energy range.

## 12.7 DETECTION OF GAMMAS WITH Ge DETECTORS

As mentioned in Sec. 7.5.5, the Ge(Li) detectors have been replaced by Ge detectors, which are devices that use hyper pure germanium (impurity concentration $10^{16}$ atoms/m$^3$ or less). The main advantage of Ge over Ge(Li) detectors is that the former should be kept at low temperatures only when in use; the latter must be kept cool at all times.

The cooling of Ge detectors is achieved by permanently mounting the detector on a cryostat. The cryostat consists of a reservoir or Dewar containing the cooling medium and a vacuum chamber housing the detector. The Dewar is made of two concentric metal containers (Fig. 12.22) with the space between the two containers evacuated for thermal insulation. In one design, called the "dipstick" (Fig 12.22*a*), the detector is housed in a separate vacuum chamber and the cooling rod is made of copper. The cooling medium is usually liquid

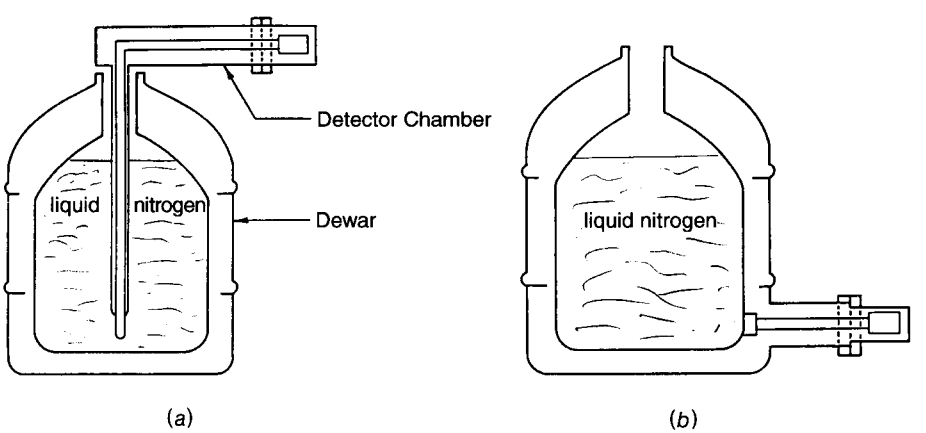


**Figure 12.22** (*a*) A dipstick cryostat (cross section). (*b*) An integral cryostat (cross section) (courtesy of Canberra Nuclear).

nitrogen (boiling temperature −196°C, or 77 K). In another design, called the integral cryostat (Fig. 12.22*b*), there is a common vacuum chamber for both the Dewar and the detector. One version of the integral cryostat is provided with a rotary vacuum seal, which allows the detector chamber to be rotated 180°. With respect to cooling, one manufacturer (Canberra) has designed and is offering a cryoelectric cryostat that uses a commercial refrigerator with helium gas as the refrigerant.

The vacuum chamber that contains the detector is made of stainless steel. The chamber protects the detector from dirt and, by being evacuated, prevents condensation of vapor on the detector surface or electrical discharge when high voltage is applied to the detector. A metal envelope, with a very thin window at its end for the passage of the incident photons, surrounds the detector. The window is made of beryllium, aluminum, or a carbon composite fiber. Transmission characteristics of several window thicknesses are shown in Fig. 12.23. Most commercial cryostats include the preamplifier as a standard component.

Reduction of background in any measurement is very important. It becomes absolutely necessary in cases when the sample to be counted is a very weak radiation source and its activity barely exceeds the background. Complete elimination of the background radiation is impossible, but reduction of it is feasible by using special shields. Common shields are made of lead or steel and are 0.10–0.15 m thick. Figure 12.24 shows a typical arrangement of the cryostat, the detector, and the shield. Photographs of two commercial detectors, cryostats, and multichannel analyzers are shown in Fig. 12.25.

### 12.7.1 Efficiency of Ge Detectors

The efficiency of Ge detectors quoted in the list of specifications by the manufacturer may be a relative full-energy peak efficiency or an absolute

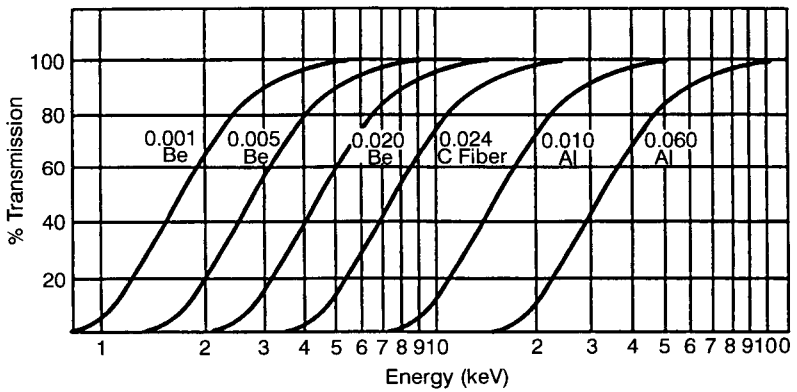


**Figure 12.23** Transmission characteristics of various detector windows. The thicknesses shown are in mils of inches (courtesy of Canberra Nuclear).

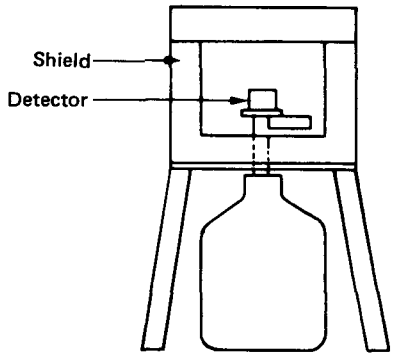


**Figure 12.24** A typical arrangement of the detector, the shield, and the cryostat.

efficiency. Relative efficiencies are referenced in terms of the absolute full-energy peak efficiency of a 76 mm × 76 mm (3 in × 3 in) NaI(Tl) crystal. The measurement (or calculation) is based on the 1.33-MeV peak of $^{60}$Co. It is assumed that a $^{60}$Co source of known strength is positioned 0.25 m away from the face of the detector. A count is taken for a period of time, and the absolute full-energy peak efficiency of the Ge(Li) detector is determined by dividing the total number of counts under the 1.33-MeV peak (shaded area, Fig. 12.26) by the number of photons emitted from the source during the same time period. This absolute efficiency is divided by $1.2 \times 10^{-3}$, which is the absolute efficiency of a 3 in × 3 in NaI(Tl) crystal 0.25 m from the source, to give the relative efficiency quoted in the specifications.

Absolute efficiencies as a function of energy for four types of Ge detectors are shown in Figs. 12.27–12.30. In Fig. 12.27, a Ge wafer is used to make what the manufacturer calls a low-energy Ge (LEGe) detector. In this detector, a p + contact is fabricated on the front face and the cylindrical surface with implanted boron; on the rear face, an n + contact is formed with lithium diffused along a spot that is smaller than the full rear area of the device. The efficiency of this detector is dropping for energies below 5 keV because of absorption in the Be window; at the other end of the graph, the efficiency drops for $E > 100$ keV because of a corresponding decrease in the value of the total linear attenuation coefficient of gamma rays in Ge (Fig. 12.31). A coaxial Ge detector and its efficiency are shown in Fig. 12.28. The contacts of this detector are formed by diffused lithium (n contact) and by implanted boron (p contact). The diffused-lithium n contact is given by the manufacturer as 0.5 mm thick. A variation of the coaxial detector, called the reverse-electrode (REGe) detector and its efficiency are shown in Fig. 12.29. In the REGe detector the electrodes are opposite to those of the "normal" coaxial: the p-type electrode (formed by ion-implanted boron) is on the outside, and the n-type contact (formed by diffused lithium) is on the inside. This electrode arrangement leads to decreased window thickness (the p contact may be as thin as 0.3 $\mu$m; the Be window is ~ 0.5 mm), which, in turn, results in higher efficiency at lower energy (compare efficiency curves of Figs. 12.28 and 12.29). Finally, in Fig. 12.30 a Ge well-type

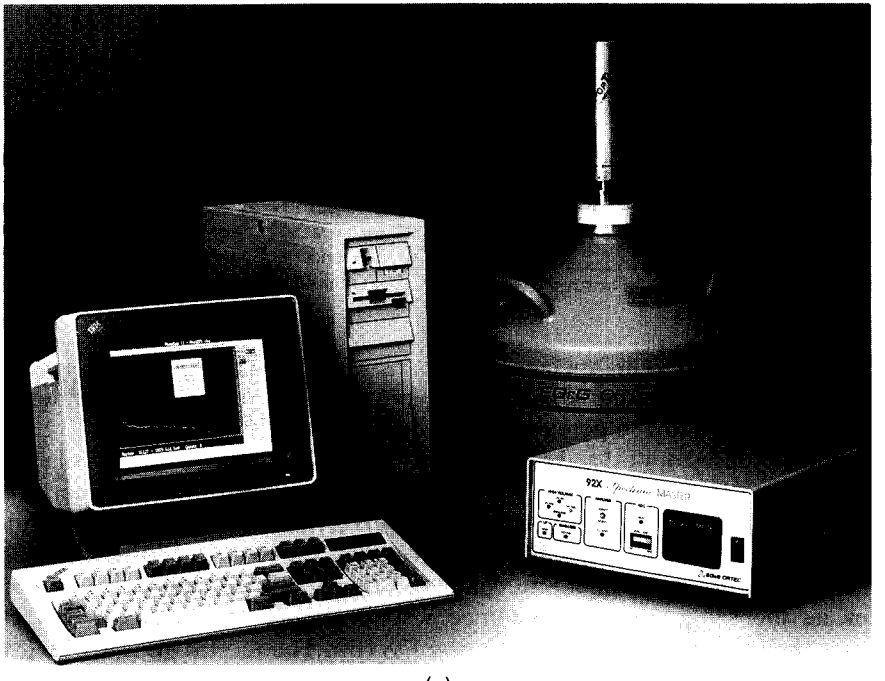

(a)

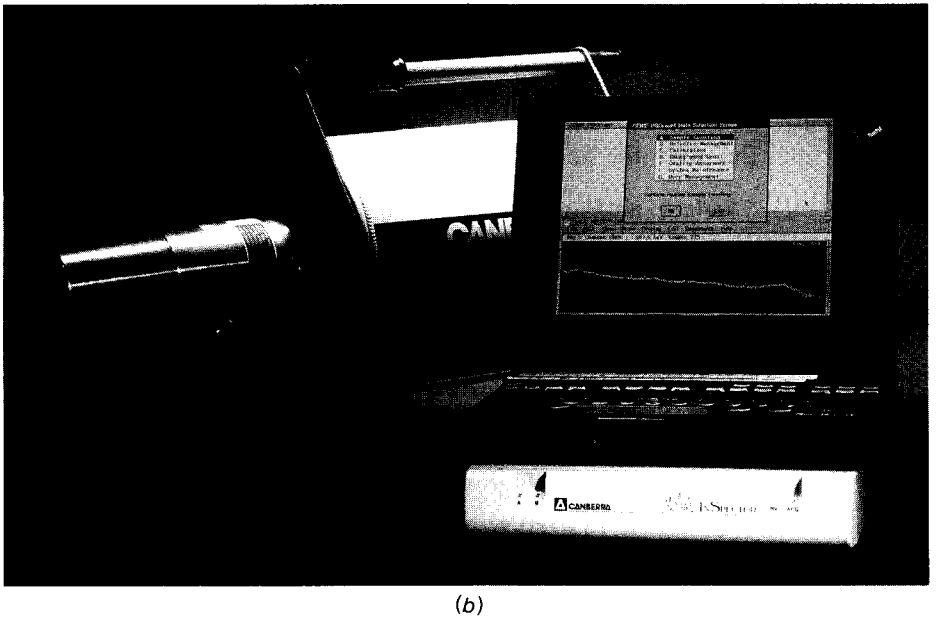


(b)

**Figure 12.25** (*a*) Ge detector with its cryostat and multichannel analyzer (reproduced from Instruments for Research and Applied Sciences by permission of EG & G ORTEC, Oak Ridge, Tennessee). (*b*) Portable Ge detector system with its cryostat and multichannel analyzer (courtesy of Canberra Nuclear).

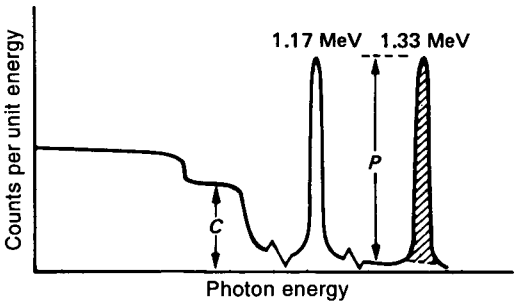


**Figure 12.26** A sketch of the $^{60}$Co spectrum, indicating how it is used for efficiency and peak-to-Compton ratio determination.

detector is shown. The special characteristic of this device is its increased efficiency due to its particular geometry. The solid angle approaches $4\pi$, resulting in close to 100 percent efficiency in a certain energy range.

For Ge detectors other than the well-type, the efficiency is low, relative to Na(Tl) scintillation counters. This statement holds true for Si(Li) detectors as well (see Sec. 12.9). Lower efficiency, however, is more than compensated for by the better energy resolution of the semiconductor detector. Figure 12.32 illustrates the outstanding resolution characteristics of a semiconductor detector by showing the same spectrum obtained with a NaI(Tl) and a Ge(Li) detector. Notice the tremendous difference in the FWHM. The Ge(Li) gives a FWHM = 1.9 keV, while the NaI(Tl) gives FWHM $\approx$ 70 keV.

Consider a case of 10,000 counts being recorded by a 3 in $\times$ 3 in Na(Tl) detector under the 1.33-MeV peak of $^{60}$Co. A Ge detector with 10 percent relative efficiency will record only 1000 counts. The FWHM of the Na(Tl) peak is 70 keV; the corresponding width of the Ge peak is about 2 keV. Since the total number of counts under the peak is proportional to the product of the FWHM times the peak, the heights of the two peaks are related by

$$\frac{\text{Height of Ge peak}}{\text{Height of NaI(Tl) peak}} \approx \frac{(1000/2)}{(10{,}000/70)} = \frac{70}{20} = 3.5$$

Thus, even though the Ge detector is only 10 percent efficient, relative to the NaI(Tl) crystal, it produces a peak that is 3.5 times higher.

Another parameter specified by the manufacturer of Ge detectors is the *peak-to-Compton ratio* (PCR). Looking at Fig. 12.26, the PCR is defined by the equation

$$\text{PCR} = \frac{\text{height of 1.33-MeV peak}}{\left(\begin{array}{c}\text{average height of Compton}\\ \text{plateau of 1.33-MeV peak}\end{array}\right)}$$

The average of the plateau is taken between 1040 and 1096 keV, in accordance with IEEE Standard No. 325-1971.[11] The PCR is important because it indicates the capability of the detector to identify low-energy peaks in the presence of

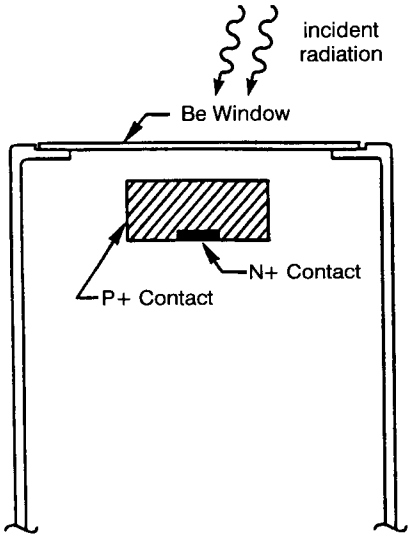


(a)

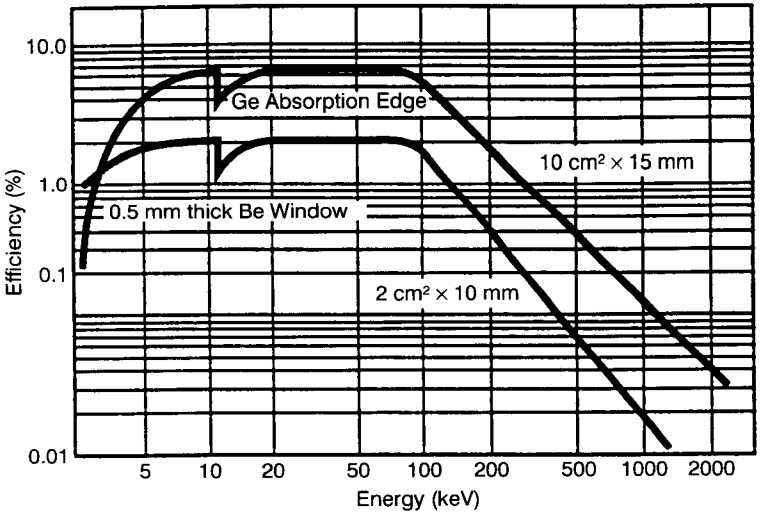


(b)

**Figure 12.27** (*a*) LEGe detector. (*b*) Absolute efficiency as a function of energy for a detector size shown on the graph and 2.5-cm distance assumed between source and detector (from Canberra, Ref. 2).

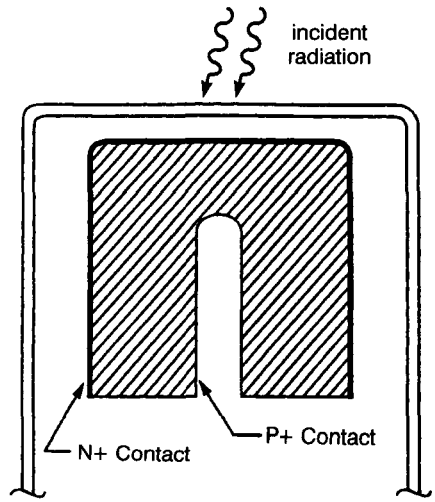


(a)

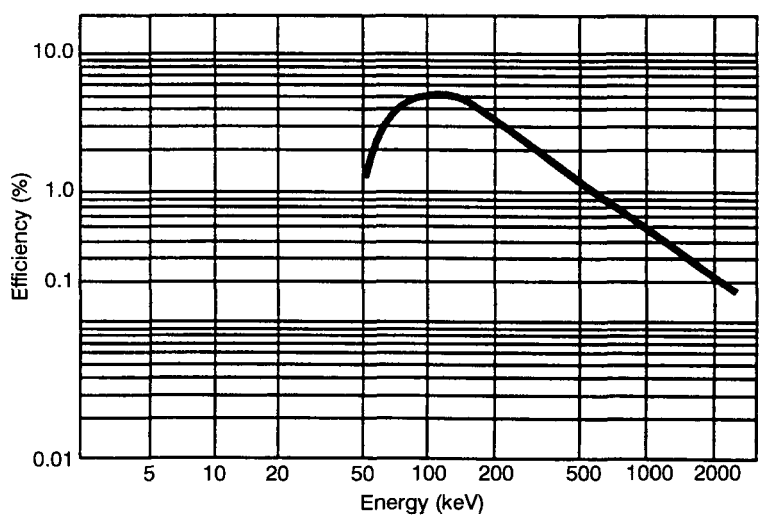


(b)

**Figure 12.28** (*a*) Coaxial Ge detector. (*b*) Absolute efficiency as a function of energy for a distance of 2.5 cm between source and detector (from Canberra, Ref. 2).

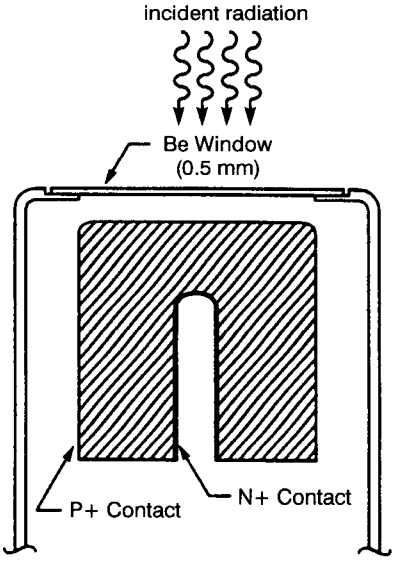


(a)

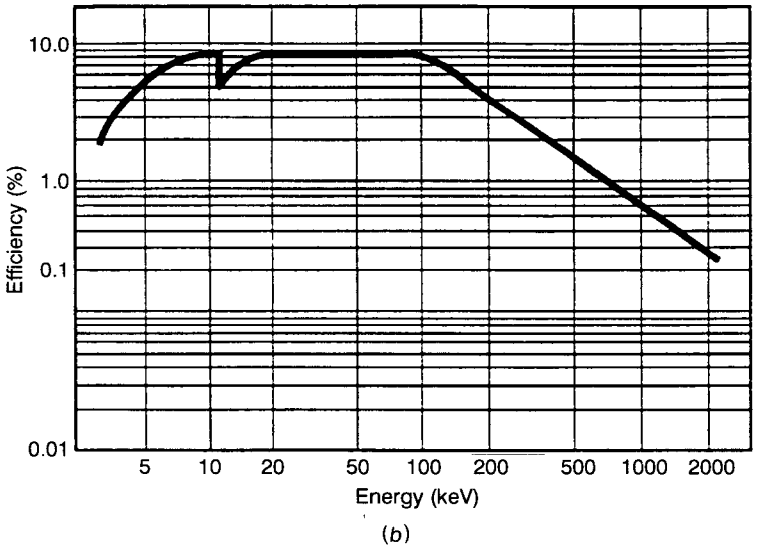


(b)

**Figure 12.29** (*a*) REGe coaxial detector. (*b*) Absolute efficiency as a function of energy for a distance of 2.5 cm between source and detector (from Canberra, Ref. 2).

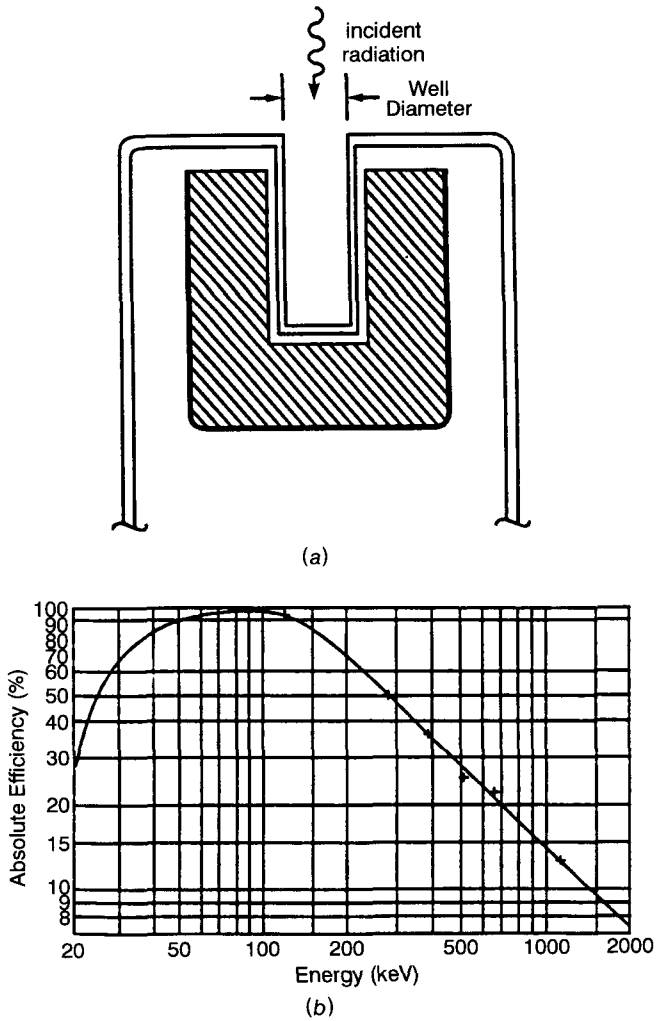


**Figure 12.30** (*a*) A Ge well-type detector. (*b*) Absolute detector efficiency for a detector with 40-mm depth and 10-mm-diameter well. Source assumed placed at the bottom of the well.

stronger peaks of higher energy. PCR values of 30:1 are common, but higher values have also been reported.

For the analysis of complex gamma spectra, it is helpful to have an analytic function that represents the efficiency of the detector as a function of energy. Many semiempirical equations have been developed to fit the efficiency of Ge(Li) detectors.[11-20] Three examples are given here.

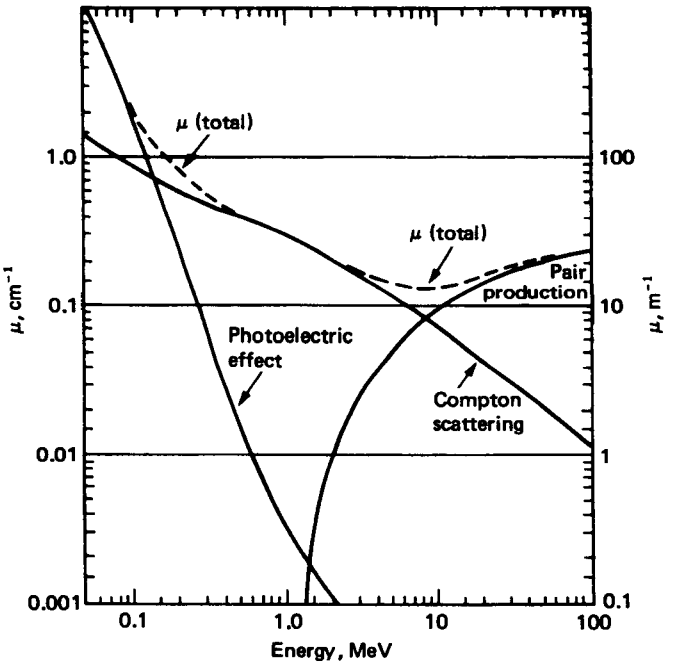


**Figure 12.31** Photon attenuation coefficients for germanium. The dashed line is the approximate total linear attenuation coefficient.

**The Freeman-Jenkin Equation[11].**

$$\epsilon = 1 - \exp(-\tau x) + \sigma A \exp(-BE) \tag{12.8}$$

where $\tau$ = photoelectric coefficient
$x$ = thickness of the detector
$\sigma$ = Compton coefficient
$A, B$ = constants to be determined from measurement

Equation 12.8 was used to determine the *relative* efficiency of a cylindrical and a trapezoidal detector over the range 500–1500 keV, with an accuracy of about 1 percent.

**The Mowatt Equation[17].**

$$\epsilon = a_1 F' \exp(-\mu_{Ge} a_2) \left[ \frac{\tau + \sigma a_3 \exp(-a_4 E)}{\tau + \sigma} \right] [1 - \exp(-\mu_{Ge} a_5)] \tag{12.9}$$

where $F' = \Pi_i \exp(-\mu_i x_i)$ = product of attenuation factors outside the intrinsic region
$a_1$ = normalization factor

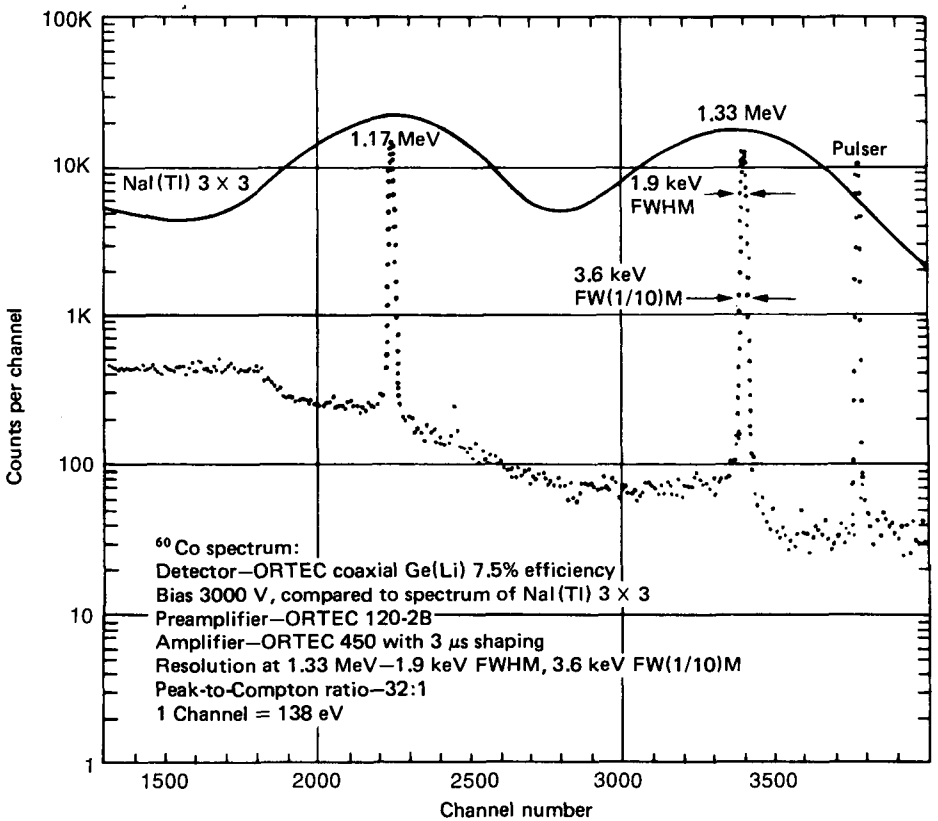


**Figure 12.32** The $^{60}$Co spectrum obtained with a NaI(Tl) scintillator and a Ge(Li) detector (reproduced from *Instruments for Research and Applied Sciences* by permission of EG & G ORTEC, Oak Ridge, Tennessee).

$a_2$ = the thickness of the germanium front dead layer
$a_3, a_4$ = constants to be determined from measurement
$a_5$ = effective detector depth

Equation 12.9 is an improvement over Eq. 12.8 because it takes into account absorption in the window (through the factor $F'$) and in the dead layer of the detector [through the factor $\exp(-\mu_{Ge} a_2)$]. Mowatt's equation, developed for planar detectors, gives the efficiency with an accuracy of 1.5 percent over the range 100–1400 keV.

**McNelles–Campbell Equation[14].**

$$\epsilon = \left(\frac{a_1}{E}\right)^{a_2} + a_3 \exp(-a_4 E) + a_5 \exp(-a_6 E) + a_7 \exp(-a_8 E) \quad (12.10)$$

where $a_1$ through $a_8$ are constants to be determined from measured gamma

spectra. Equation 12.10, developed for coaxial detectors, predicts the efficiency with an accuracy of 0.2 percent over the energy range 160–1333 keV. Further testing of 12.10 showed[20] that the last term involving the constants $a_7$ and $a_8$ has a negligible effect on the result.

Equations 12.8–12.10 are given just as examples that indicate the general energy dependence of the efficiency curve. What is done in practice is to measure the efficiency as a function of energy using calibrated sources emitting gammas of known energies and intensities.[11–15,21] A table of gamma energies used for calibration is given in App. C.

### 12.7.2 Energy Resolution of Ge Detectors

The energy resolution of a Ge detector is given in terms of the FWHM ($\Gamma$). The width $\Gamma$ consists of the following two components:

$$\Gamma_d = \text{width due to detector effects}$$

$$\Gamma_e = \text{width due to effects of electronics}$$

Since these two components are uncorrelated, they are added in quadrature to give the total width, $\Gamma$,

$$\Gamma = \sqrt{\Gamma_d^2 + \Gamma_e^2} \tag{12.11}$$

As shown in Chap. 9, the width $\Gamma_d$ is energy dependent and is given by

$$\Gamma_d = 2\sqrt{(2 \ln 2) FEw} \tag{12.12}$$

where $F$ is the Fano factor and $w$ is the average energy needed to produce an electron-hole pair. For germanium, at the operational temperature of 77 K, $w = 2.97$ eV. Thus,

$$\Gamma_d \text{ (keV)} = 0.1283\sqrt{FE \text{ (keV)}} \tag{12.13}$$

The width $\Gamma_e$ increases when the detector capacitance increases. The detector capacitance, in turn, generally increases with detector size and may change with detector bias. Good Ge detectors have a flat capacitance-bias relationship over most of the range of bias voltage applied.

The capacitance of the detector has an effect on the energy resolution because it influences the performance of the charge-sensitive preamplifier that accepts the detector signal. The contribution of the preamplifier to the value of $\Gamma_e$ increases with the input capacitance. One of the manufacturers, Canberra, reports a 0.570-eV $\Gamma_e$ with zero input capacitance and a slow increase with higher values as shown in Fig. 12.32. Clearly, the resolution improves if the capacitance is kept low. The other component of the input capacitance comes from items like connectors and cables. Reduction of the length of input cable and of connectors' capacitance is helpful. For the best resolution with a given system, the preamplifier should be located as close to the detector as possible.

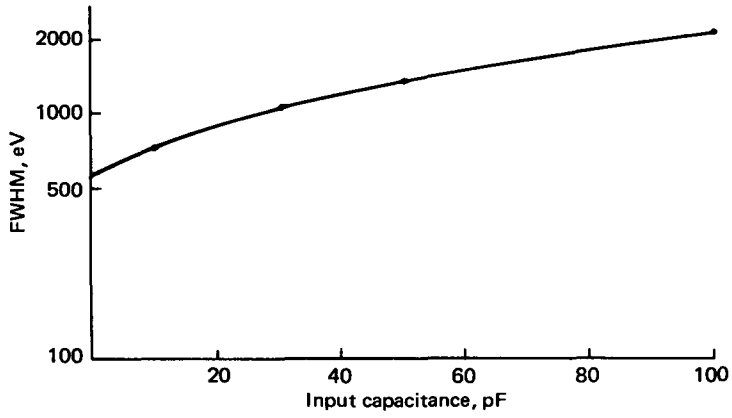


**Figure 12.33** The dependence of $\Gamma_e$ on input capacitance for a charge-sensitive preamplifier (from Ref. 2).

Large Ge detectors commercially available today have capacitance as high as 30 pF, which results in a value of $\Gamma_e = 1.06$ keV (Fig. 12.33). Combining the two contributions $\Gamma_d$ and $\Gamma_e$ in accordance with Eq. 12.11, one gets

$$\Gamma\ (\text{keV}) = \sqrt{(0.1283)^2 FE\ (\text{keV}) + 1.06^2} \tag{12.14}$$

A typical value of the Fano factor for $0.1 < E < 10$ MeV is 0.16. Substitution in Eq. 12.14 gives

$$\Gamma\ (\text{keV}) = \sqrt{(2.63 \times 10^{-3})E\ (\text{keV}) + 1.06^2} \tag{12.15}$$

Equation 12.15 shows that for low energies, the resolution is determined by electronic noise. For higher energies, the energy contribution predominates. Consider two cases:

Case 1: $E = 100$ keV

$$\Gamma = \sqrt{(2.63 \times 10^{-3})100 + 1.06^2} = \sqrt{0.263 + 1.12} = 1.2\ \text{keV}$$

Case 2: $E = 1000$ keV

$$\Gamma = \sqrt{(2.63 \times 10^{-3})1000 + 1.062} = \sqrt{2.63 + 1.12} = 1.9\ \text{keV}$$

The energy resolution versus gamma energy is shown in Fig. 12.34 for the four detectors depicted in Figs. 12.27–12.30. Usually, the resolution is given in terms of the FWHM at 5.9, 122, and 1332 keV.

### 12.7.3 Analysis of Ge Detector Energy Spectra

Despite the superb energy resolution of Ge detectors compared to that of NaI(Tl) scintillators (see Fig. 12.32), analysis of complex gamma spectra is

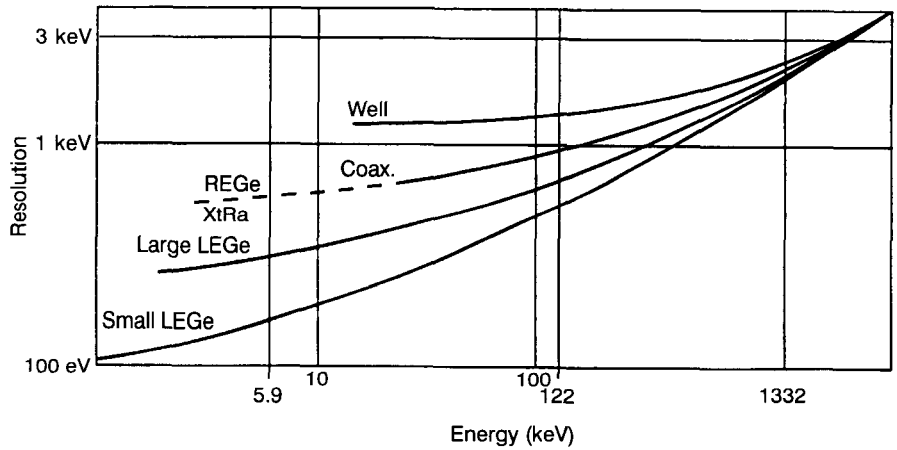


**Figure 12.34** Typical energy resolution versus gamma energy for Ge detectors (from Canberra, Ref. 2).

necessary. Figure 12.35 shows a typical Ge energy spectrum. Analysis of the spectrum entails, first, assignment of energy to the peaks of the spectrum and, second, the determination of the number of counts (i.e., the area) for each peak.

The energy assignment to the peaks of the spectrum is accomplished by calibrating the detector with a source that emits gammas of known energy and intensity. As explained in Sec. 9.10, calibration means to determine the con-

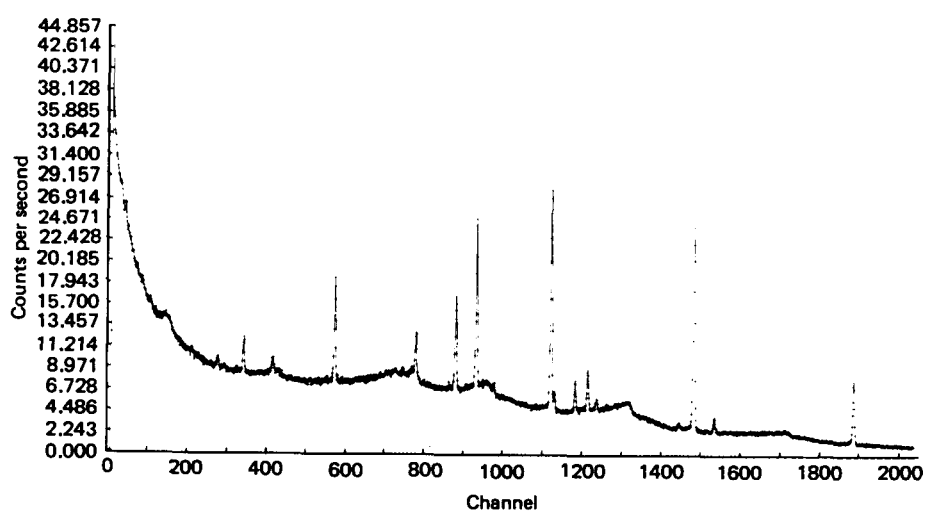


**Figure 12.35** A gamma-ray energy spectrum recorded with a Ge detector. (This is the spectrum from a human hair sample irradiated in a reactor.)

stants of the equation

$$E = a_1 + a_2C + a_3C^2 \tag{12.16}$$

where $C$ is the channel number (for most systems, $a_3$ is very small, or zero). When the energy assignment is performed, the observer should be aware of the following general features of a gamma spectrum recorded by a Ge detector:

1. For $E_\gamma < 2$ MeV, the full-energy peak is intense and almost Gaussian in shape.
2. At higher energies ($E_\gamma > 2$ MeV) the double-escape peak ($E_{DE} = E_\gamma - 1.022$ MeV) becomes prominent. The single-escape peak is present too (see Fig. 12.7).
3. In spectra taken with thin Ge(Li) detectors, one may see the germanium "escape" peaks. The escape peaks (EP) have energy equal to

$$E_{EP} = E_\gamma - E_k$$

   where $E_k$ is the K X-ray energy of germanium. The escape peaks are due to the loss of the energy carried away by the escaping K X-ray of germanium. This energy is equal to 9.9 keV for the $K_\alpha$ and 11.0 keV for the $K_\beta$ X-ray of germanium. Figure 12.36 shows the $^{139}$Ce X-ray spectrum with the escape peaks marked.
4. When the front surface of the detector is covered by a metal, characteristic X-rays of that metal are emitted if the incident radiation consists of photons

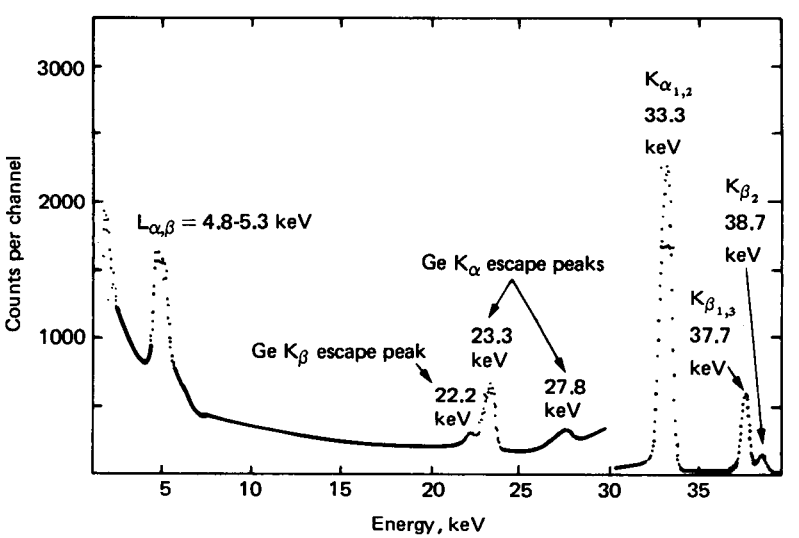


**Figure 12.36** The X-ray spectrum resulting from the decay of $^{139}$Ce. The Ge escape peaks are clearly seen (from Ref. 54).

with energy greater than the K X-ray energy of that metal. Gold, which is sometimes used, emits a $K_\alpha$ X-ray with energy 68 keV and five L X-rays between 9 and 13 keV.

The determination of the area under a peak—i.e., the absolute intensity of a particular gamma energy—is not as straightforward as the assignment of energy, because the area under a peak includes contributions from other gammas. The methods that have been developed for the determination of the area can be classified into two groups: methods that treat the data (i.e., counts per channel) directly, and methods that fit a known function to the data.

Methods that treat the data directly give the area under the peak by adding the counts from all the channels in the region of the peak and subtracting a "base background." The methods differ in the way they define the "base" and the number of channels that define the peak (a review of the methods is given in Refs. 22 and 23). Figures 12.37 and 12.38 show graphically three of the methods.

**Method 1.** A straight line is used to separate the peak from the base,[22,24] and the net area under the peak (NPA) is calculated using the equation (Fig. 12.37*a*)

$$\text{NPA} = \sum_{i=L}^{R} a_i - (a_L + a_R)\frac{R - L + 1}{2} \tag{12.17}$$

where $a_i$ = number of counts in channel $i$
$L$ = channel number at left limit of photopeak
$R$ = channel number at right limit of photopeak

**Method 2.** Here, the background (Fig. 12.37*b*) is defined as the average count in a region equal to $3\Gamma$ (3 FWHM), extending $1.5\Gamma$ on both sides of the peak. The gross count under the peak is taken as the sum of all the counts in the channels corresponding to $3\Gamma$. The net peak area is then given by

$$\text{NPA} = G - B_L - B_R \tag{12.18}$$

**Method 3.** This method, due to Quittner,[25] fits a polynomial, using the least-squares technique, to the data from $2k_L + 1$ and $2k_R + 1$ channels (Fig. 12.38) on either side of the peak. The base line is constructed in such a way that at $X_L$ and $X_R$ (shown in Fig. 12.38) it has the same magnitude $(p_L, p_R)$ and slope $(q_L, q_R)$ as the fitted polynomial. The net area under the peak is now given by the equation

$$\text{NPA} = \sum_{i=-W_L}^{W_R} \left(a_{x_p+i} - b_{x_p+i}\right) \tag{12.19}$$

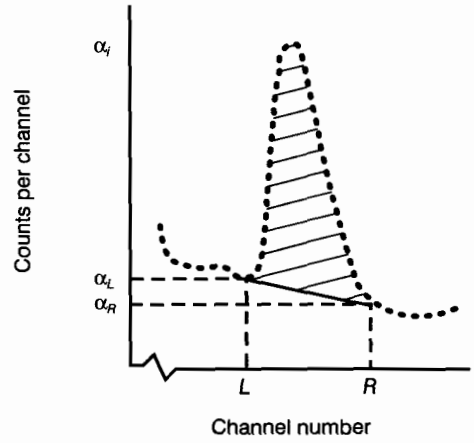


(a)

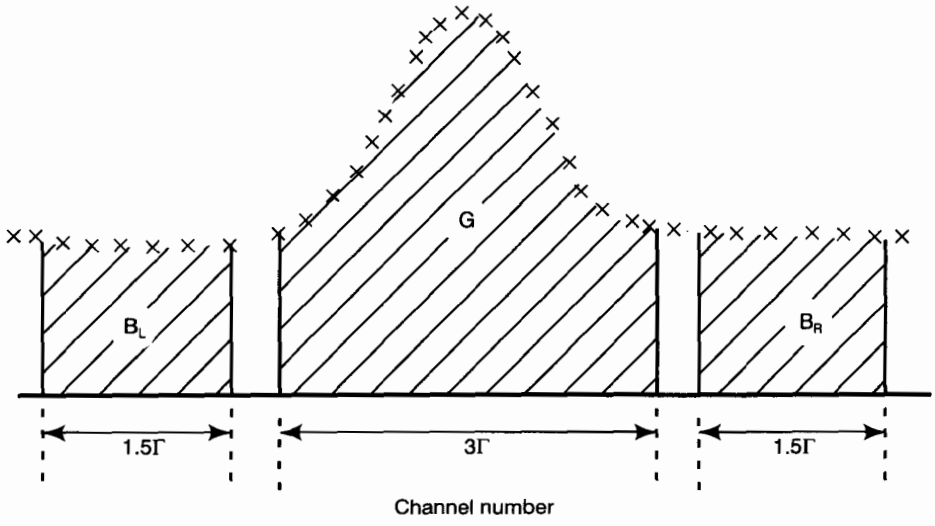


(b)

**Figure 12.37** Determination of the net area under the peak. (*a*) A straight line is used to define the base. (*b*) An average background is subtracted from the gross count.

where the value of $b$ is, in terms of a third-degree polynomial, equal to

$$b(x) = p_L + q_L(x - x_L) + \left[\frac{-q_R - 2q_L}{l_L + l_R} + \frac{3(p_R - p_L)}{(l_L + l_R)^2}\right](x - x_L)^2 + \left[\frac{q_L + q_R}{(l_L + l_R)^2} + \frac{2(p_L - p_R)}{(l_L + l_R)^3}\right](x - x_L)^3 \tag{12.20}$$

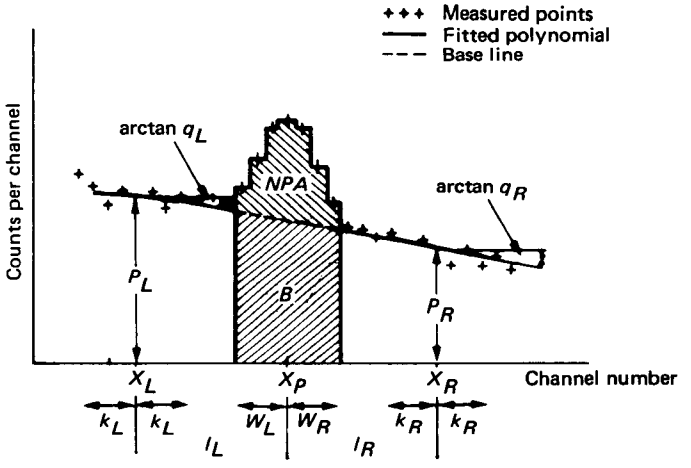


**Figure 12.38** Determination of the area under the peak using the method of Quittner (from Ref. 25).

Quittner's method is quite accurate if the peaks are separated by about 20 channels.

Today, the most widely used methods are those that fit an analytic function to each peak. After the fit is accomplished, the analytic function is used for the calculation of quantities of interest such as the area and the centroid (position) of the peak.

The principle of obtaining the fit is simple and essentially the same for all the methods.[4,5,26–34] Let $y_i|_{i=1,N}$ be the experimental point—i.e., the counts in channels $x_i|_{i=1,N}$—and $f(x, a_1, a_2, \ldots)$ be a function that will represent a single peak. The parameters $a_1, a_2, \ldots$ are determined by minimizing the quantity

$$\sum_i W_i[y_i - f(x_i, a_1, a_2, \ldots)]^2$$

i.e., by a least-squares technique, where the weighting factors $W_i$ usually are the inverse of the variance of $y_i$. The fitting function consists of a Gaussian plus modifying functions. Three examples are

1. $f = G(x) + B + Cx = y_0 \exp\left[-\dfrac{(x - x_0)^2}{2\sigma^2}\right] + B + Cx$

   Here, a Gaussian describes the peak, and the linear function $B + Cx$ describes the background.[26]

2. $f = G(x)\left[1 + a_1(x - x_0)^{m_1} + a_2(x - x_0)^{m_2}\right]$ (from Ref. 27)

3. $f = G(x) + B + S + D$ (from Ref. 34)

where $B$ = linear background
$S$ = step function = $A\{1 - \text{erf}[(x_0 - x)/\sigma\sqrt{2}]\}$
$D$ = tail function having an exponential form on the left of the peak and a Gaussian on the right

In addition to the methods discussed so far, there are others that use mixed techniques.[35,36] No matter what the method is, the analysis has to be done by computer, and numerous computer codes have been developed for that purpose. Examples are the codes SAMPO,[28] SISYPHUS-II and SHIFTY-II,[5] HYPERMET,[36] and GAUSS.[37]

The determination of the absolute intensity of a gamma requires that the efficiency of the detector be known for the entire energy range of interest. The efficiency is determined from information provided by the energy spectrum of the calibration source. Using the known energy and intensity of the gammas emitted by the source, a table is constructed giving efficiency of the detector for the known energy peaks. The efficiency at intermediate points is obtained either by interpolation or, better yet, by fitting an analytic form to the data of the table (see Sec. 12.7.1).

As in the case of minimum detectable activity (Sec. 2.20), two types of errors are encountered when one tries to identify peaks in a complex energy spectrum.[38] Type I arises when background fluctuations are falsely identified as true peaks. Type II arises when fluctuations in the background obscure true peaks. Criteria are set in the form of confidence limits (see Sec. 2.20 and Ref. 38) that can be used to avoid both types of errors.

### 12.7.4 Timing Characteristics of the Pulse

For certain measurements, like coincidence-anticoincidence counting or experiments involving accelerators, the time resolution of the signal is also important, in addition to energy resolution. For timing purposes, it is essential to have pulses with constant risetime.

No detector produces pulses with exactly the same risetime. This variation is due to the fact that electrons are produced at different points inside the detector volume, and thus traverse different distances before they reach the point of their collection. As a result, the time elapsing between production of the charge and its collection is not the same for all the carriers

Consider a true coaxial detector, shown in Fig. 12.39*a* (see also Fig. 7.26). Since the electric field is radial, electrons and holes will follow a trajectory perpendicular to the axis of the detector. The maximum time required for collection of the charge corresponds to electron-holes being produced either at $A$ or $C$. That time $t$ is equal to $t \approx (AC)/v$, where $AC$ is the detector thickness and $v$ is the speed of electrons or holes. For a detector bias of about 2000 V and the size shown in Fig. 12.39*a*, $v \approx 0.1$ mm/ns = $10^5$ m/s, which gives a maximum collection time of 120 ns. The best risetime corresponds to electron-holes generated at point $B$ (Fig. 12.39*a*) and is equal to about 60 ns.

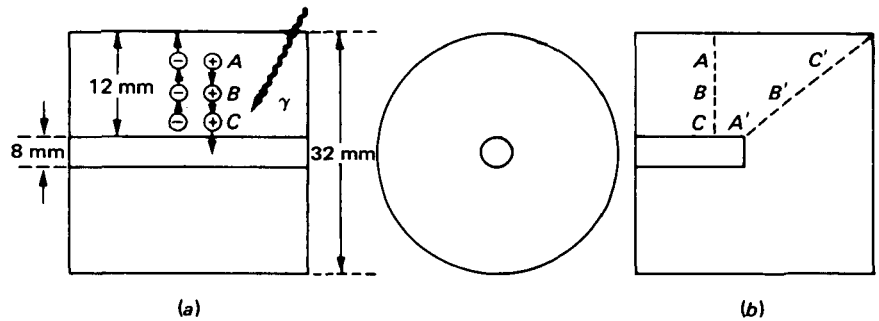


**Figure 12.39** (*a*) In a true coaxial detector, electrons and holes travel along the direction *ABC*. (*b*) In wrap-around coaxial detectors, the carriers may travel along *ABC* but also along the longer path *A'B'C'*.

The pulse risetime is essentially equal to the collection time. For the detector shown in Fig. 12.39*a*, the risetime will vary between 60 and 120 ns. For other detector geometries the variation in risetime is greater because the electrons and holes, following the electric field lines, may travel distances larger than the thickness of the detector core (Fig. 12.39*b*). The variation in risetime for the detector of Fig. 12.39*b* will be between 60 and 200 ns. The distribution of pulse risetimes for commercial detectors is a bell-type curve, not exactly Gaussian, with a FWHM of less than 5 ns.

## 12.8 CdTe AND $HgI_2$ DETECTORS AS GAMMA SPECTROMETERS

A great advantage for CdTe and $HgI_2$ detectors,[39-48] compared to Ge and Si(Li) detectors, is that they can operate at room temperature (see also Sec. 7.5.6). At this time, they can be obtained in relatively small volumes, but they still have an intrinsic efficiency of about 75 percent at 100 keV because of the high atomic number of the elements involved. The energy resolution of CdTe detectors is 18 percent at 6 keV and 1.3 percent at 662 keV. The corresponding numbers for $HgI_2$ are 8 percent and 0.7 percent.[45]

The $HgI_2$ detectors are very useful for the measurement for X-rays with energy less than 10 keV. In that energy range, resolutions of 245 eV at 1.25 keV[49] and 295 eV at 5.9 keV[50] have been reported.

As with small Ge detectors, X-ray escape peaks are present in spectra taken with these CdTe and $HgI_2$ detectors. Figure 12.40 shows the spectrum of the 59.5-keV X-rays and $\gamma$-rays from $^{241}$Am taken with a CdTe detector. The escape peaks due to the $K_\alpha$ X-rays of cadmium (23 keV) and tellurium (27 keV) are clearly seen.

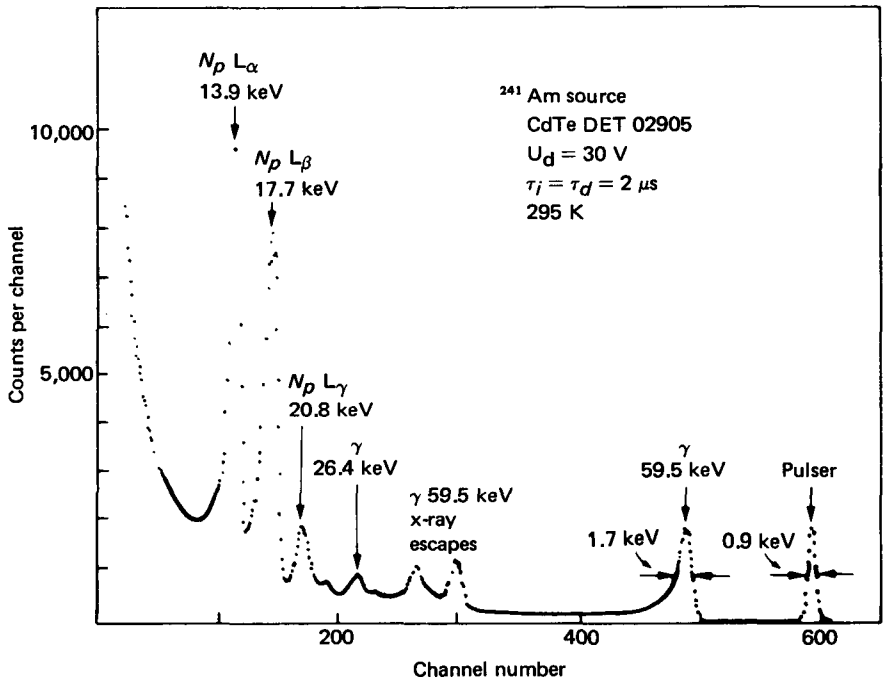


**Figure 12.40** The 59.5-keV X-ray of $^{241}$Am detected with a CdTe detector (from Ref. 42).

## 12.9 DETECTION OF X-RAYS WITH A Si(Li) DETECTOR

Si(Li) detectors are generally used as X-ray spectrometers for $E < 50$ keV. They need cooling and therefore require a cryostat. Their energy resolution and efficiency are better than those of a Ge(Li) detector for $E < 50$ keV. Figure 12.41 shows how the resolution changes with energy. The FWHM is again given by Eq. 12.11. Using a value of $w = 3.7$ eV per electron-hole pair for silicon at 77 K and Fano factor equal to 0.1, the width $\Gamma$ becomes

$$\Gamma\ (\text{eV}) = \sqrt{2.05E\ (\text{eV}) + \Gamma_e^2} \tag{12.21}$$

The width $\Gamma_e$ is indicated as "electronic noise" in Fig. 12.41. Of the three types of X-ray detectors mentioned—scintillation, proportional, and semiconductor counters—the Si(Li) detector has the best energy resolution for X-rays. This fact is demonstrated in Fig. 12.42, which shows the same energy peak obtained with the three different detectors. Notice that only the Si(Li) detector can resolve $K_\alpha$ and $K_\beta$ lines, an ability absolutely necessary for the study of fluorescent X-rays for most elements above oxygen. The manganese fluorescence spectrum obtained with a Si(Li) detector is shown in Fig. 12.43

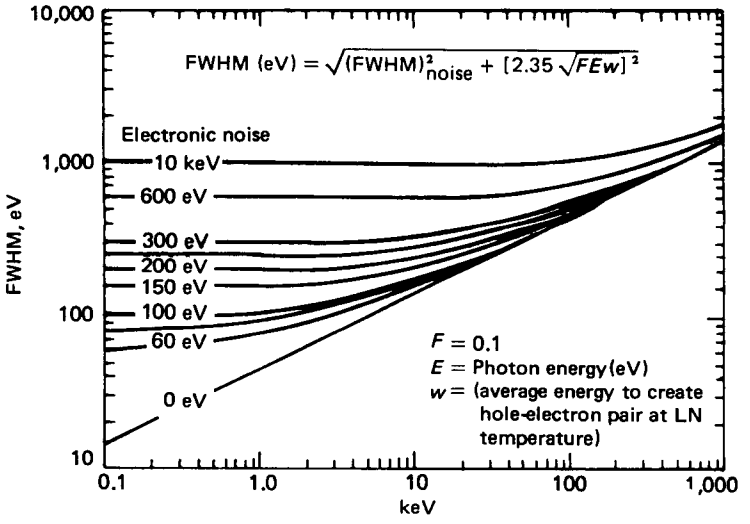


**Figure 12.41** Si(Li) detector energy resolution as a function of X-ray energy (from Ref. 2). What is indicated as electronic noise is the width $\Gamma_e$.

The dependence of Si(Li) detector efficiency on the X-ray energy is shown in Fig. 12.44. For $E < 3$ keV, the efficiency drops because of absorption of the incident X-rays by the beryllium detector window. For $E > 15$ keV, the efficiency falls off because of the decrease of the total linear attenuation coefficient of X-rays in silicon (Fig. 12.45).

## 12.10 DETECTION OF X-RAYS WITH A CRYSTAL SPECTROMETER

The measurement of X-ray energy by wavelength-dispersive crystal spectrometers is based on the phenomenon of diffraction of electromagnetic waves from a crystal (see Compton and Allison, and Cullity). Consider an X-ray of wavelength $\lambda$ incident at an angle $\theta$ on a crystal with interplanar spacing $d$ (Fig. 12.46). The incident X-rays will be scattered by the atoms of the crystal in all directions, but as a result of the periodicity of the atom positions, there are certain directions along which constructive interference of the scattered photons takes place. The direction of constructive interference of the diffracted beam is given by the Bragg condition

$$n\lambda = 2d \sin \theta \tag{12.22}$$

where $n$ is the order of reflection ($= 1, 2, 3, \ldots$). Equation 12.22 states that for constructive interference, the path difference between any two rays (photons) must be an integral number of wavelengths. In Fig. 12.46, the path difference for rays 1 and 2 is $BC + CD = 2d \sin \theta = n\lambda$.

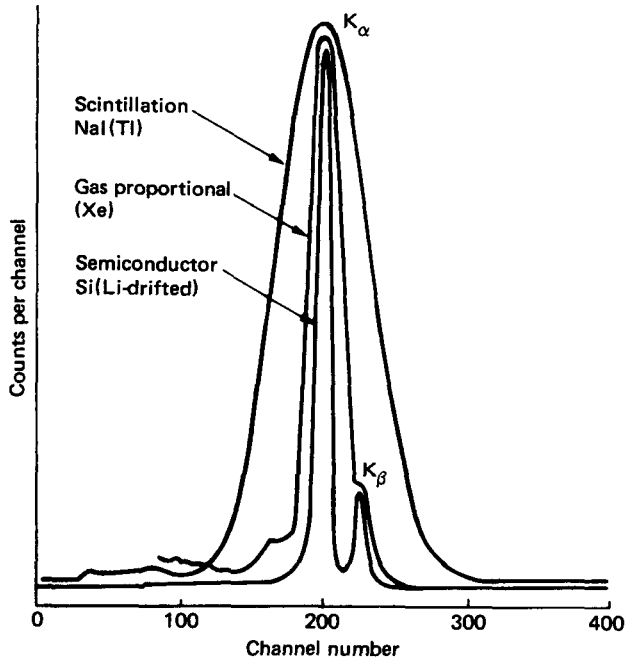


**Figure 12.42** Demonstration of the superior energy resolution of Si(Li) detectors by showing the same peak recorded with a NaI(Tl) scintillator and a gas-filled proportional counter (from Ref. 55).

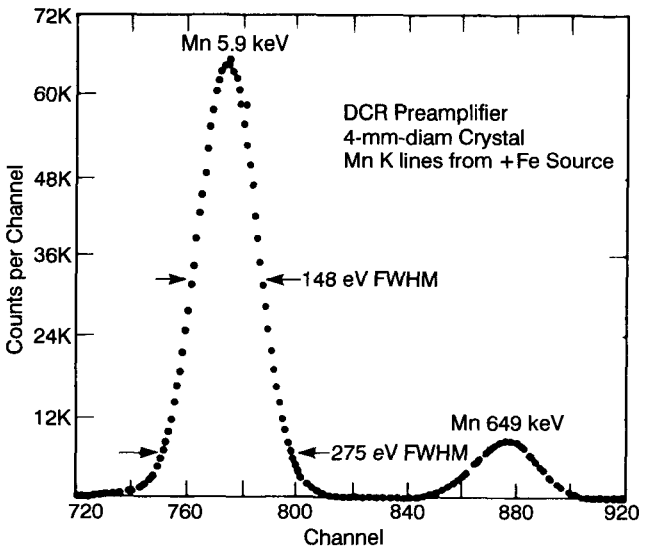


**Figure 12.43** The manganese fluorescence spectrum obtained with a Si(Li) detector (from Ref. 1).

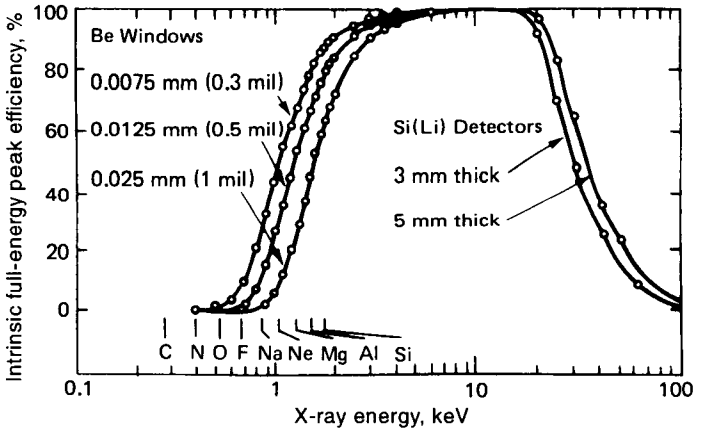


**Figure 12.44** Si(Li) detector efficiency as a function of X-ray energy for different beryllium window thicknesses (from Ref. 2).

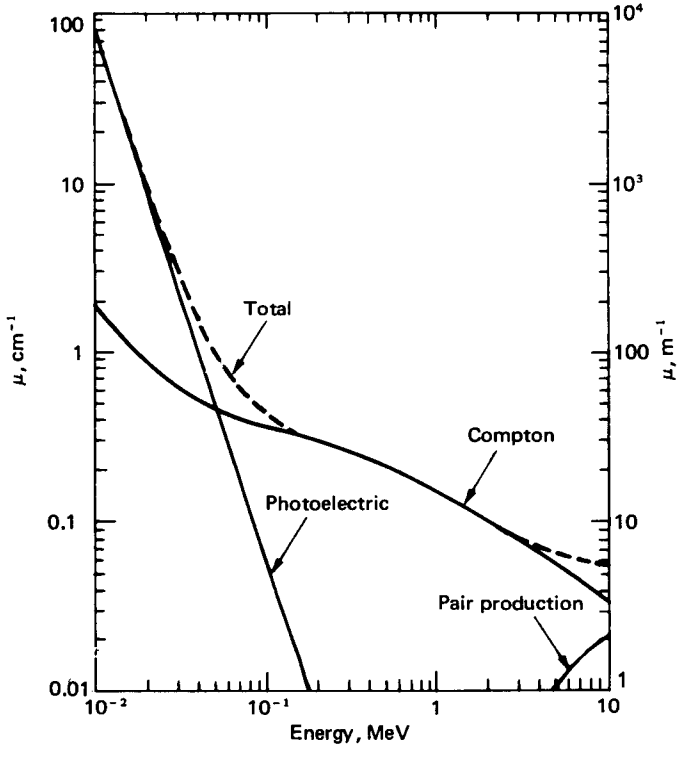


**Figure 12.45** Linear photon attenuation coefficients for silicon.

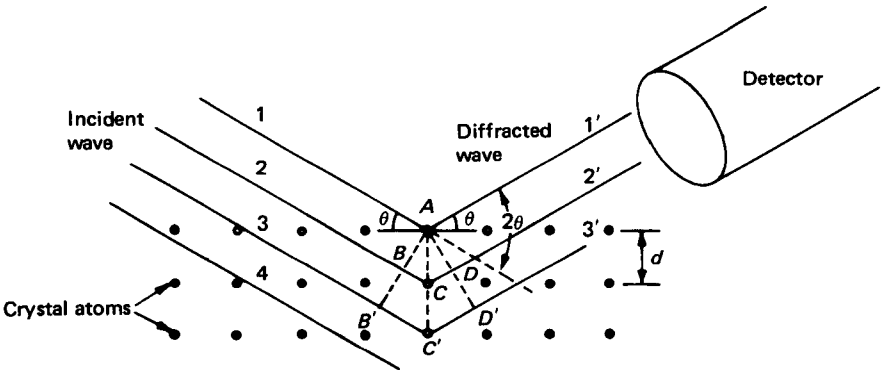


**Figure 12.46** Diffraction of electromagnetic waves by a crystal. The detector counts photons being diffracted at an angle $\theta$, i.e., photons having wavelength $\lambda$ satisfying Eq. 12.18.

The order of reflection $n$ may take any value (for a given $\theta$ and $d$) provided $\sin\theta < 1$, and is physically equal to the number of wavelengths by which the paths of X-rays scattered by two adjacent planes are different. Figure 12.46 shows first-order reflection if the path difference between rays 1 and 2 is 1 wavelength ($BC + CD = \lambda$); between 1 and 3 is 2 wavelengths ($B'C' + C'D' = 2\lambda$); between 1 and 4 is 3 wavelengths, and so on. Second-order reflection would mean that $BC + CD = 2\lambda$; therefore, first-, second-, third-, ..., $n$th-order reflections satisfy the equations

$$\begin{aligned} \lambda &= 2d\sin\theta_1 \\ 2\lambda &= 2d\sin\theta_2 \\ 3\lambda &= 3d\sin\theta_3 \\ &\vdots \\ n\lambda &= 2d\sin\theta n \end{aligned}$$

Reflections of order higher than 1 act as "contamination" in X-ray measurements. Fortunately, the first-order reflection is always much more intense than higher-order ones (second-order reflection is about 20 percent the intensity of the first).

The diffracted photons are detected by a counter set to accept the radiation emerging at an angle $\theta$ (Fig. 12.46), i.e., set to accept photons of wavelength $\lambda$, or energy

$$E = \frac{1.2399}{\lambda\,(\text{nm})}\ \text{keV} \tag{12.23}$$

According to Eq. 12.22, if one uses an X-ray detector set at an angle $\theta$ (Fig. 12.47) to detect diffracted photons of wavelength $\lambda$, the counting rate is zero at any angle different from $\theta$. In practice, this does not happen. As the angle $\theta$

changes from rotating the crystal around an axis perpendicular to the plane formed by the incident and diffracted beams, the counting rate of the detector will have a maximum at $\theta = \theta_0$, where $\lambda = 2d \sin \theta_0$, but it will gradually go to zero as shown in Fig. 12.48. The curve of Fig. 12.48, known as the *rocking curve* of the crystal, is the result of incomplete destructive interference of the diffracted X-rays. The rocking curve is the equivalent of the Gaussian response function of a detector to a monoenergetic photon source. However, its origin is not statistical, as the following discussion shows.

As stated earlier, the Bragg condition (Eq. 12.22) indicates that the waves (photons) scattered by the different crystal planes have a path difference equal to an integral number of wavelengths along the direction $\theta$ satisfying Eq. 12.22. But what if the angle $\theta$ is such that the path difference is only a fraction of a wavelength? The destructive interference of the scattered waves is not complete and the result is radiation of lower amplitude. This partial constructive interference may happen because of three reasons:

1. *Finite thickness of the crystal.* A crystal with finite thickness consists of a finite number of planes. For any angle $\theta_0$, there are planes with no matching partner to create the correct phase difference in scattered radiation for complete destructive interference. The width $\Gamma_t$ of the rocking curve, due to the finite thickness of the crystal, is given by (see Cullity)

$$\Gamma_t = \frac{0.9\lambda}{t \cos \theta_0} \tag{12.24}$$

   where $t$ is the crystal thickness. Notice that $\Gamma_t$ depends on the wavelength, the thickness, and the diffraction angle. If $t \gtrsim 1$ mm, the width $\Gamma_t$ is negligible for the cases encountered in practice.
2. *Nonparallel incident rays.* It is impossible to produce a beam consisting of exactly parallel rays. Thus, at any angle $\theta_0$ there are X-rays hitting the crystal

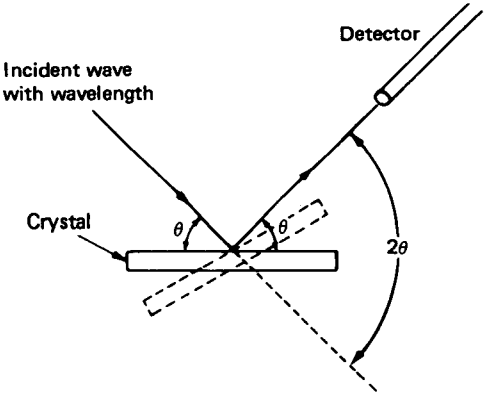


**Figure 12.47** The rocking curve of the crystal is obtained by rotating the crystal and keeping source and detector fixed.

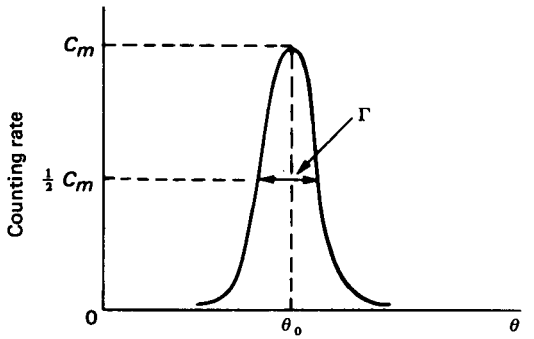


**Figure 12.48** The rocking curve of a crystal.

at an angle slightly different from $\theta_0$. The magnitude of this effect depends on the collimation of the beam.

3. *Mosaic structure of the crystal.* Real crystals do not consist of a single uninterrupted lattice. Instead, they are made up of small regions, each region being a perfect lattice but having a slightly different orientation with respect to the next one (Fig. 12.49).

One of the most difficult and important tasks in the use of a crystal spectrometer is correct alignment of the instrument and accurate measurement of the diffraction angle. At any position, the diffraction angle $\theta$ is taken as the angle corresponding to the maximum of the rocking curve. In most cases, what is measured is $2\theta$ (Fig. 12.47) instead of $\theta$. Of course, for an accurate measurement, the experimenter must know the crystal parameters and the crystal planes giving the reflection, in addition to the angle $\theta$.

### 12.10.1 Types of Crystal Spectrometers

Crystal spectrometers can be used in two ways (Fig. 12.50). The first is to use the spectrometer as a means to obtain monochromatic radiation, which then strikes a sample (Fig. 12.50*a*). The second is to use it for the measurement of the energy of the radiation emerging from the sample (Fig. 12.50*b*). In most cases the sample emits fluorescent radiation, and for this reason the instrument is

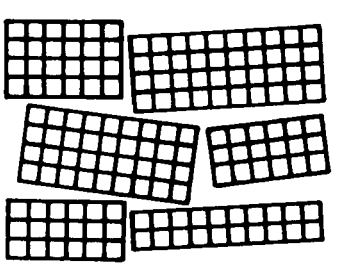

**Figure 12.49** The mosaic structure of real crystals. Each block represents a perfect crystal.

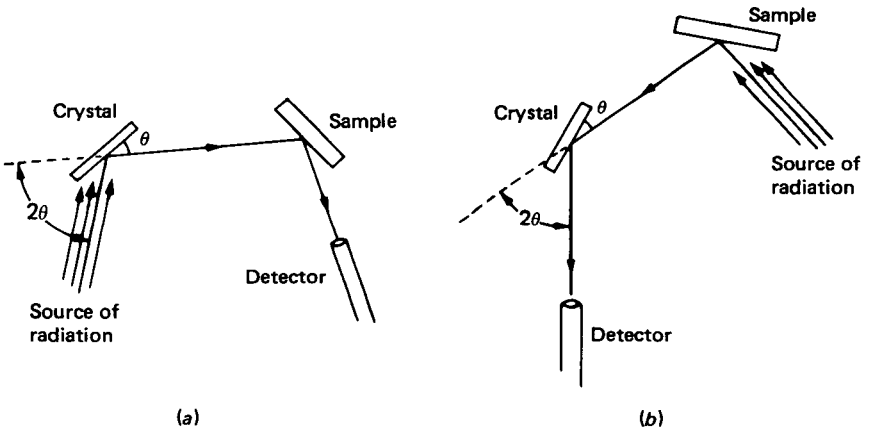


**Figure 12.50** Two examples of using a fluorescent spectrometer.

called a *fluorescent spectrometer*. The diffracted radiation reaching the counter is strongly attenuated, first at the crystal and a second time at the sample. A very small fraction of the incident radiation reaches the counter. It is therefore important to design a spectrometer that provides maximum intensity. Considerable improvement in intensity is achieved if the crystal, the X-ray source, and the detector are located on the same circle, and the crystal is bent to twice the radius of that circle (Fig. 12.51).[51-53] In addition to the reflection spectrometer shown in Fig. 12.51, called the *Johansson type*, others based on transmission through the crystal have also been constructed.

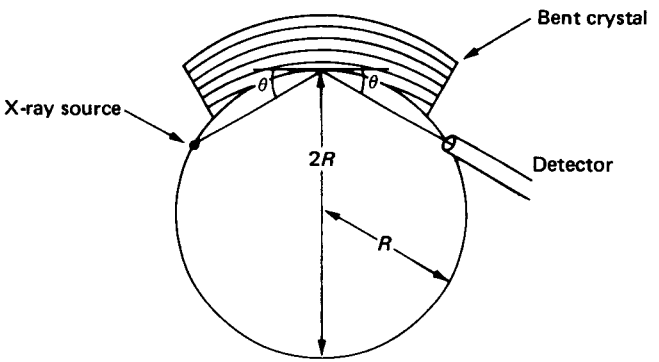


**Figure 12.51** The geometry of a bent-crystal spectrometer.

### 12.10.2 Energy Resolution of Crystal Spectrometers

The resolution of crystal spectrometers is traditionally expressed as the *resolving power*, which is the inverse of the energy resolution:

$$\text{Resolving power} = \frac{E}{\Delta E} = \frac{\lambda}{\Delta\lambda} = \frac{\tan\theta}{\Delta\theta} = \frac{nk}{2d(\Delta\theta)E}\left(1 - \frac{n^2k^2}{4d^2E^2}\right)^{-1/2} \tag{12.25}$$

where $k = 1.2399$ keV · nm, the constant of Eq. 12.23. The uncertainty of the angle $\Delta\theta$ depends on crystal properties (rocking curve), the size of the source, and the size of the detector. The experimentally obtained rocking curve (Fig. 12.48) includes all the contributions to $\Delta\theta$; thus its width $\Gamma$ is

$$\Gamma = \sqrt{\Gamma_t^2 + \Gamma_g^2} \tag{12.26}$$

where $\Gamma_g$ = width due to the geometry (collimator, source, detector)
$\Gamma_t$ = width due to crystal imperfections and size, given by Eq. 12.24

For practical cases of interest, $\Gamma_t \ll \Gamma_g$ and $\Gamma \approx 0.5°$. The resolving power and the resolution of a crystal spectrometer as a function of energy are shown in Fig. 12.52. It should be pointed out that the X-ray detector used with the crystal spectrometer need not have an extremely good energy resolution, because it is the resolution of the analyzing crystal that determines the spectroscopic capabilities of the system, not that of the detector. The X-ray counter may be a proportional counter or a Si(Li) detector.

**Example 12.1** What is the energy resolution of an X-ray crystal spectrometer for 6-keV X-rays using a crystal with $d = 0.15$ nm and $\Delta\theta = 0.3°$?

**Answer** Using Eq. 12.25, the resolution is ($n = 1$)

$$\frac{\Delta E}{E} = \frac{2d(\Delta\theta)E}{k}\sqrt{1 - \frac{k^2}{4d^2E^2}} = \frac{2(0.15)(0.0052)(6)}{1.2399}\sqrt{1 - \frac{1.2399^2}{4(0.15)^2(6)^2}}$$
$$= 0.0055 = 0.55\%$$

One can improve the resolution by decreasing $\Delta\theta$ or using a crystal with a smaller interplanar distance.

The energy range over which crystal spectrometers can be used is determined, in principle, from the Bragg condition (Eq. 12.22) and the requirement that $0 < \sin\theta < 1$. Using Eq. 12.22 and assuming $\theta_{\min} \approx 0.5°$, $d = 0.2$ nm,† and

†Crystals frequently used are mica, $(33\bar{1})$ planes, $d = 0.15$ nm; LiF, (200) planes, 0.201 nm; NaCl, (200) planes, 0.082 nm.

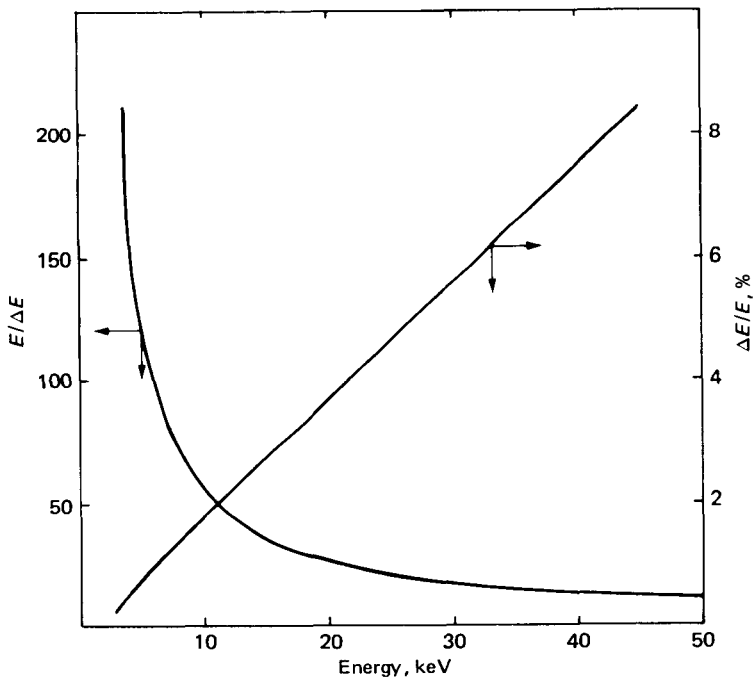


**Figure 12.52** Resolving power and energy resolution of a crystal spectrometer as a function of X-ray energy (data used: $n = 1$, $d = 0.2$ nm, $\Delta\theta = \frac{1}{3}°$).

$n = 1$, the limits are

$$3 \text{ keV} < E < 350 \text{ keV}$$

In practice, the upper limit is about 50 keV because Si(Li) detectors have better resolution beyond that energy. Advantages and disadvantages of crystal spectrometers versus Si(Li) detectors are summarized in Table 12.1.

**Table 12.1 Advantages and Disadvantages of a Crystal Spectrometer and a Si(Li) Detector**

| | Crystal spectrometer | Si(Li) detector |
|---|---|---|
| Energy resolution (6.4 keV) | ~10 eV | ~150 eV |
| Data collection | One energy at a time | All energies at once |
| Efficiency | Low | High |
| Position, relative to sample | Certain distance away from sample | Very close to sample |

## PROBLEMS

**12.1** The Compton edge of a $\gamma$-ray peak falls at 0.95 MeV. What is the energy of the photon? What is the energy of the backscatter peak?

**12.2** Sketch the energy spectrum you would expect to get from isotopes having the decay schemes shown in the figure below. Explain energy and origin of all peaks. You may assume either a NaI(Tl) or a Ge(Li) detector.

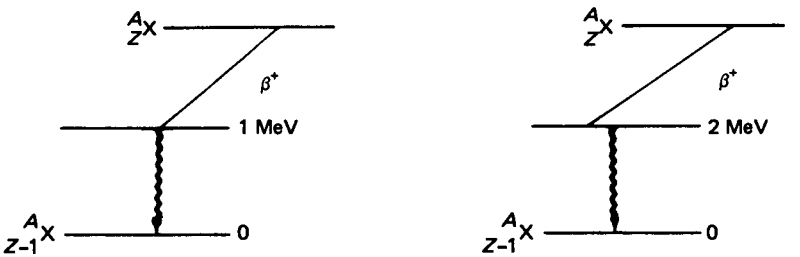


**12.3** A liquid sample is contaminated with equal amounts (mass, not activity) of $^{131}I$ and $^{137}Cs$. Sketch the energy spectra you expect to see if you use (a) a NaI(Tl) crystal with 7 percent energy resolution for the cesium peak, and (b) a Ge(Li) detector with energy resolution given by Eq. 12.15. Assume the same number of channels is used with both detectors. Relevant data for the two isotopes are given in the table below. Assume that the sample is placed at a distance of 0.20 m from the detectors. The NaI(Tl) is a 3 in × 3 in crystal. The efficiency of the Ge(Li) detector is given by Fig. 12.28.

| $^{131}I$ | | $^{137}Cs$ | |
|---|---|---|---|
| $E$ (MeV) | Intensity (%) | $E$ (MeV) | Intensity (%) |
| 0.284 | 5 | 0.662 | 85 |
| 0.364 | 82 | | |
| 0.637 | 6.8 | | |
| 0.723 | 1.6 | | |
| Half-life = 8.05 d | | Half-life = 30 y | |

**12.4** An isotope emits two gammas with energies 0.8 and 1.2 MeV and intensities 30 and 100 percent, respectively. Assume that a Ge(Li) detector 5 mm thick is used for the measurement of this spectrum. Also assume that all the photons are normally incident upon the detector. Calculate the ratio of counts under the 0.8-MeV spectrum to counts under the 1.2-MeV spectrum.

**12.5** What is the width above which the two peaks of Mn shown in Fig. 12.43 cannot be resolved?

**12.6** Will the peaks of Fig. 12.40 be resolved with a gas-filled proportional counter, assuming the best possible resolution for that type of counter?

**12.7** What is the efficiency of a 50-mm-long proportional counter filled with a mixture of xenon (20 percent) and methane at a pressure of 1 atm for a parallel beam of 10-keV X-rays (geometry of Fig. 12.11)?

**12.8** Verify the efficiency values for 1-keV X-rays, shown in Fig. 12.44 for a Si(Li) detector.

**12.9** Other things being equal, what is the ratio of intrinsic efficiencies of Si(Li) and Ge(Li) detectors 3 mm thick for 50-keV X-rays?

**12.10** Prove that the energy of a photon is related to its wavelength by

$$E = \frac{1.2399}{\lambda\,(\text{nm})}\ (\text{keV})$$

**12.11** A crystal spectrometer will be used for analysis of fluorescent X-rays. If the required resolution is 0.1 percent and the angular aperture cannot be less than 0.5°, what is the lattice interplanar distance needed? Assume first-order reflection. The energy of the X-rays is between 4 and 6 keV.

## BIBLIOGRAPHY

Compton, A. H., and Allison, S. K., *X Rays in Theory and Experiment*, Van Nostrand, New York, 1943.
Cullity, B. D., *Elements of X-Ray Diffraction*, Addison-Wesley, Reading, Mass., 1956.
Evans, R. D., *The Atomic Nucleus*, McGraw-Hill, New York, 1972.
Knoll, G. F., *Radiation Detection and Measurement*, 2nd ed., Wiley, New York, 1989.
Price, W. J., *Nuclear Radiation Detection*, McGraw-Hill, New York, 1964.
*A Handbook of Radioactivity Measurements Procedures*, NCRP Report No. 58, 1978.

## REFERENCES

1. Ortec catalogue and brochures (1976 and 1979).
2. Canberra catalogue and brochures (1979, 1980, and 1993, 9th ed.).
3. Harshaw Chemical Company Brochure (1978).
4. Heath, R. L., Helmer, R. G., Schmittroth, L. A., and Cazier, G. A., *Nucl. Instrum. Meth.* **47**:281 (1967).
5. Helmer, R. G., Heath, R. L, Schmittroth, L. A., Jayne, G. A., and Wagner, L. M., *Nucl. Instrum. Meth.* **47**:305 (1967).
6. Lurie, N. A., Harris, L., Jr., and Young, T. C., *Nucl. Instrum. Meth.* **129**:543 (1975).
7. Ingersoll, D. T., and Wehring, B. W., *Nucl. Instrum. Meth.* **147**:551 (1977).
8. "FORIST Spectra Unfolding Code," RSIC Computer Code Collection PSR-92, ORNL (1975).
9. "COOLC and FERDOR Spectra Unfolding Codes," RSIC Computer Code Collection, RSR-17, ORNL.
10. Aarnio, P. A., Routt, J. T., Sandberg, J. V., and Windberg, M. J., *Nucl. Instrum. Meth.* **219**:173 (1984).
11. Calibration and Usage of Germanium Detectors for Measurement of Gamma-Ray Emission of Radionuclides," ANSI N 42.14-1978 (1978).
12. Freeman, J. M., and Jenkin, J. G., *Nucl. Instrum. Meth.* **43**:269 (1966).
13. Campbell, J. L., and McNelles, L. A., *Nucl. Instrum. Meth.* **101**:153 (1972).
14. McNelles, L. A., and Campbell, J. L., *Nucl. Instrum Meth.* **109**:241 (1973).
15. Abreu, M. C., Maio, A. A., and D'Oliveira, M. J. T., *Nucl. Instrum. Meth.* **123**:295 (1975).
16. Tokcan, G., and Cothern, C. R., *Nucl. Instrum. Meth.* **64**:219 (1968).
17. Mowatt, R. S., *Nucl. Instrum. Meth.* **70**:237 (1969).
18. Papadellis, T., and Hontzeas, S., *Nucl. Instrum. Meth.* **73**:210 (1969).
19. Hajnal, F., and Klusek, C., *Nucl. Instrum. Meth.* **122**:559 (1974).
20. Singh, R., *Nucl. Instrum. Meth.* **136**:543 (1976).
21. Cecil, F. E., Wilkinson, F. J., III, Ristinen, R. A., and Rieppo, R., *Nucl. Instrum. Meth.* **234**:479 (1985).
22. Baedecker, P. A., *Anal. Chem.* **43**:405 (1971).

23. Kokta, L., *Nucl. Instrum. Meth.* **112**:245 (1973).
24. Covell, D. F., *Anal. Chem.* **31**:1785 (1959).
25. Quittner, P., *Nucl. Instrum. Meth.* **76**:115 (1969).
26. Mariscotti, M. A., *Nucl. Instrum. Meth.* **50**:309 (1967).
27. Helmer, R. G., Heath, R. L., Putnam, M., and Gipson, D. H., *Nucl. Instrum. Meth.* **57**:46 (1967).
28. Routti, J. T., and Prussin, S. G., *Nucl. Instrum. Meth.* **72**:125 (1969).
29. Robinson, D. C., *Nucl. Instrum. Meth.* **78**:120 (1970).
30. Kern, J., *Nucl. Instrum. Meth.* **79**:233 (1970).
31. McNelles, L. A., and Campbell, J. L., *Nucl. Instrum. Meth.* **127**:73 (1975).
32. Jorch, H. H., and Campbell, J. L., *Nucl. Instrum. Meth.* **143**:551 (1977).
33. DeLotto, I., and Ghirardi, A., *Nucl. Instrum. Meth.* **143**:617 (1977).
34. Campbell, J. L., and Jorch, H. H., *Nucl. Instrum. Meth.* **159**:163 (1979).
35. Connelly, A. L., and Black, W. W., *Nucl. Instrum. Meth.* **82**:141 (1970).
36. Phillips, G. W., and Marlow, K. W., *Nucl. Instrum. Meth.* **137**:525 (1976).
37. Cline, J. E., Putnam, M. H., and Helmer, R. G., "GAUSS-VI, A Computer Program for the Automatic Analysis of Gamma-Ray Spectra from Ge(Li) Spectrometers," ANCR-1113 (1973).
38. Head, J. H., *Nucl. Instrum. Meth.* **98**:419 (1972).
39. Siffert, P., Gonidec, J. P., and Cornet, A., *Nucl. Instrum. Meth.* **115**:13 (1974).
40. Jones, L. T., and Woollam, P. B., *Nucl. Instrum. Meth.* **124**:591 (1975).
41. Siffert, P., *Nucl. Instrum. Meth.* **150**:1 (1978).
42. Dabrowski, A. J., Iwanczyk, J., Szymczyk, W. M., Kokoschinegg, P., and Stelzhammer, J., *Nucl. Instrum. Meth.* **150**:25 (1978).
43. Schieber, M., Beinglass, I., Dishon, G., Holzer, A., and Yaron, G., *Nucl. Instrum. Meth.* **150**:71 (1978).
44. Shaler, J., *Nucl. Instrum. Meth.* **150**:79 (1978).
45. Whited, R. C., and Schieber, M. M., *Nucl. Instrum. Meth.* **162**:113 (1979).
46. Markakis, J. M., *Nucl. Instrum. Meth.* **263**:499 (1988).
47. Courat, B., Fourrier, J. P., Silga, M., and Omaly, J., *Nucl. Instrum. Meth.* **269**:213 (1988).
48. McKee, B. T. A., Goetz, T., Hazlett, T., and Forkert, L., *Nucl. Instrum. Meth.* **272**:825 (1988).
49. Dabrowski, A. J., Iwanczyk, J. S., Barton, J. B., Huth, G. C., Whited, R., Ortale, C., Economou, T. E., and Turkevich, A. L., *IEEE Trans. Nucl. Sci.* **NS-28**(1):536 (1981).
50. Iwanczyk, J. S., Dabrowski, A. J., Huth, G. C., Del Duca, A., and Schnepple, W., *IEEE Trans. Nucl. Sci.* **NS-28**(1):579 (1981).
51. Johansson, T., *Z. Physik* **82**:507 (1933).
52. Cauchois, Y., *Ann. Phys.* **1**:215 (1934).
53. DuMond, J. W. M., *Rev. Sci. Instr.* **18**:626 (1947).
54. Palms, J. M., Venugopala Pao, P., and Wood, R. D., *Nucl. Instrum. Meth.* **64**:310 (1968).
55. Muggleton, A. H. F., *Nucl. Instrum. Meth.* **101**:113 (1972).

CHAPTER
# THIRTEEN

# CHARGED-PARTICLE SPECTROSCOPY

## 13.1 INTRODUCTION

A charged particle going through any material will have interactions affecting its detection in two ways. First, the energy spectrum is distorted because of the energy loss caused by the interactions in any mass interposed between source and detector. Second, a particle entering the active detector volume will interact there at least once and will be detected, i.e., the efficiency is practically 100 percent.

Because any energy loss outside the detector is undesirable, the task of the experimenter is to design a spectrometer with zero mass between the source and the detector. Such an ideal system cannot be built, and the only practical alternative is a spectrometer that results in such a small energy loss outside the detector that reliable corrections can be applied to the measured spectrum.

In certain measurements, the particles do not stop in the detector, but they go through it and emerge with only a fraction of their energy deposited in the detector. Then a correction to the spectrum of the exiting particles will have to be applied because of *energy straggling*, a term used to describe the statistical fluctuations of energy loss. Energy straggling should not be confused with the statistical effects that result in the finite energy resolution of the detector.

For heavy ions, a phenomenon called the *pulse height defect* (PHD) seems to have an important effect on energy calibration. As a result of the PHD, the relationship between pulse height and ion energy is mass dependent. In semiconductor detectors, experiments have shown that the PHD depends on the

orientation of the incident ion beam relative to the crystal planes of the detector. This phenomenon is called channeling.

To avoid unnecessary energy loss, the source of the charged particles should be prepared with special care. The heavier the ion, the more important the source thickness becomes and the more difficult the source preparation is.

This chapter discusses the subjects of energy loss and straggling, pulse height defect, energy calibration methods, and source preparation, from the point of view of their effect on spectroscopy. All the effects are not equally important for all types of particles. Based on similarity in energy loss behavior, the charged particles are divided into three groups, as in Chap. 4:

1. Electrons and positrons
2. Alphas, protons, deuterons, tritons
3. Heavy ions ($Z > 2$, $A > 4$)

Energy straggling, which is a phenomenon common to all particles, is discussed first. Then the other effects are analyzed separately for each particle group.

## 13.2 ENERGY STRAGGLING

If a monoenergetic beam of charged particles traverses a material of thickness $\Delta x$, where $\Delta x$ is less than the range of the particles in that medium, the beam will emerge from the material with a distribution of energies. The broadening of the beam is due to the statistical fluctuations of the energy loss processes. Simply stated, the incident particle participates in a great number of collisions as it travels the distance $\Delta x$, and loses a certain fraction of its energy in every collision. However, neither the number of collisions nor the energy lost per collision is constant, resulting in a distribution of energies called *energy straggling*.

Energy straggling plays no role in the measurement of the total energy of the charged particle. It does play a significant role, however, in transmission-type experiments where the particle emerges from a detector after depositing only a fraction of its energy in it.

Consider a monoenergetic beam of particles with kinetic energy $T_0$ (Fig. 13.1) going through a thickness $\Delta x$ that is a fraction of the particle range. The average energy $\overline{T}$ of the emerging particles is

$$\overline{T} = T_0 - \int_0^{\Delta x} \left( \frac{dE}{dx} \right) dx \tag{13.1}$$

where $dE/dx$ is the stopping power of the medium for the incident particle (see Chap. 4). In most cases, $\overline{T} < T_p$, where $T_p$ is the most probable energy of the particles after going through the thickness $\Delta x$.

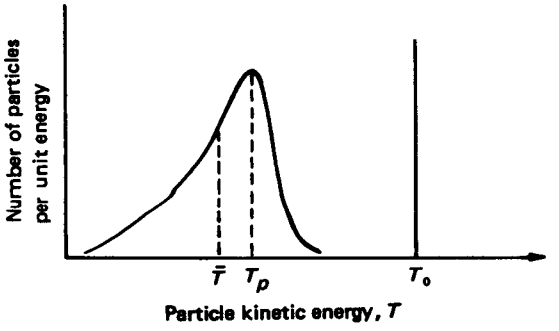


**Figure 13.1** A monoenergetic beam will exhibit an energy distribution after going through a material of thickness $\Delta x < R$.

The shape of the energy distribution shown in Fig. 13.1 is determined by the parameter $k$,

$$k = \frac{\xi}{\Delta E_{\max}} \tag{13.2}$$

where $\xi$ is roughly equal to the mean energy loss of the particle traversing the thickness $\Delta x$, and $\Delta E_{\max}$ is the maximum energy transfer to an atomic electron in one collision. The expressions for $\xi$ and $\Delta E_{\max}$ are

$$\xi = 2\pi r_0^2 mc^2 \frac{Z_1^2 N Z_2}{\beta^2} \Delta x \tag{13.3}$$

$$\Delta E_{\max} = 2mc^2 \frac{\beta^2}{1-\beta^2}\left[1 + \left(\frac{m}{M_1}\right)^2 + 2\frac{m}{M_1}\frac{1}{\sqrt{1-\beta^2}}\right]^{-1} \tag{13.4a}$$

All the symbols in Eqs. 13.3 and 13.4$a$ have been defined in Sec. 4.3, except $Z_1$, the charge of the incident particle, and $Z_2$, the atomic number of the stopping material. For nonrelativistic particles ($\beta \ll 1$), which are much heavier than electrons, Eq. 13.4$a$ takes the form

$$\Delta E_{\max} = \frac{4mM_1}{(m+M_1)^2} T \tag{13.4b}$$

If $M \gg m$, then Eq. 13.4$b$ takes the form $\Delta E_{\max} = 4(m/M_1)T$.

For small values of $k (k \leq 0.01)$, a small number of collisions takes place in the stopping medium and the resulting distribution is asymmetric with a low-energy tail. Landau[1] first investigated this region and obtained a universal asymmetric curve. The case of intermediate $k$ values ($0.1 < k < 10$) was first investigated by Symon[2] and later by Vavilov.[3] The Vavilov distribution was checked and was found to agree with experiment.[4] For small $k$, the Vavilov distribution takes the shape of the Landau result, while for large $k$, when the number of collisions is large, it becomes a Gaussian. Figure 13.2 shows how the distribution changes as a function of $k$. Many other authors have studied special cases of the energy straggling problem.[5-11]

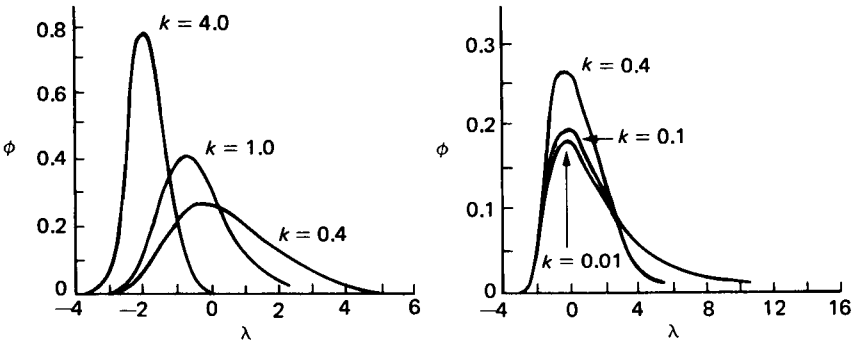


**Figure 13.2** The Vavilov distribution shown for various values of the parameter $k$. The quantity $\phi$ is a measure of the probability that a particle will lose energy between $T$ and $T + dT$ in traversing thickness $\Delta x$. The parameter $\lambda = (T - \bar{T})/\xi - 0.423 - \beta^2 - \ln k$ (from Ref. 11).

The variance of the energy straggling distribution was first calculated† by Bohr[12] using a classical model. Bohr's result is

$$\sigma_E^2 = \overline{(\Delta T)^2} - \left(\overline{\Delta T}\right)^2 = 4\pi r_0^2 (mc^2)^2 Z_1^2 Z_2 N \Delta x \tag{13.5}$$

where $\Delta T$ = energy loss in a specific case

$\overline{\Delta T}$ = average energy loss given by (Eq. 13.1) $T_0 - \bar{T}$

The width $\Gamma$ of the distribution is equal to $(2\sqrt{2\ln 2})(\sigma_E)$.

Livingston and Bethe[13] obtained a different expression by incorporating quantum-mechanical concepts into the calculation. Their result is

$$\sigma_E^2 = 4\pi r_0^2 (mc^2)^2 Z_1^2 N \left( Z_2' + \sum_i \frac{8}{3} \frac{I_i Z_i}{\Delta E_{\max}} \ln \frac{\Delta E_{\max}}{I_i} \right) \Delta x \tag{13.6}$$

where $Z_2'$ = effective atomic number of the stopping material

$I_i, Z_i$ = ionization potential and number of electrons, respectively, in the $i$th atomic shell of the stopping material

$\Delta E_{\max}$ is given by Eq. 13.4*a*. A third expression for $\sigma_E^2$ was obtained by Titeica.[14] It is worth noting that Bohr's result (Eq. 13.5) is independent of the particle energy, while the Beth-Livingston (Eq. 13.6) and the Titeica result have a small energy dependence.

The expressions for $\sigma_E^2$ mentioned above were all obtained by taking into account electronic collisions only. Nuclear collisions (see Chap. 4) are rare, but they cause large energy losses. As a result, they do not contribute significantly to the average energy loss but they do influence the energy distribution by giving it a low-energy tail. (The energy *loss* distribution will have a high-energy tail.)

†The calculation is presented by Evans and by Segré (see bibliography of this chapter).

The width of the energy distribution after the beam traverses a thickness $\Delta x$ consists of a partial width $\Gamma_s$ due to straggling and a second one $\Gamma_d$ due to the resolution and noise of the detection system. The total width $\Gamma$ is obtained by adding the two partial widths in quadrature:

$$\Gamma = \sqrt{\Gamma_s^2 + \Gamma_d^2} \tag{13.7}$$

The energy straggling is measured with an experimental setup shown schematically in Fig. 13.3. A source, a detector, and a movable absorber are housed in an evacuated chamber, to avoid any energy loss as the particles travel from the source to the detector. The width $\Gamma_d$ is measured first by recording the particle energy spectrum with the absorber removed. Then the absorber is put into place and the measured spectrum gives the width $\Gamma$. The straggling width is, using Eq. 13.7,

$$\Gamma_s = \sqrt{\Gamma^2 - T_d^2} \tag{13.8}$$

By using absorbers of different thicknesses, the width $\Gamma_s$ may be studied as a function of $\Delta x$. Measurements of this type have been performed by many people, especially with alpha particles.[15,16] For small thicknesses, the experimental results agree with theory, but for large thicknesses the theory underestimates the width. Figure 13.4 shows results for thin and thick silver foils. It should be noted that according to the theory (Eqs. 13.5 and 13.6), the width $\Gamma_s$ is proportional to $\sqrt{\Delta x}$, assuming that $Z_1$ does not change as the particle traverses the thickness $\Delta x$.

Energy straggling is more pronounced for electrons than for heavier particles for three reasons. First, electrons are deflected to large angles and may lose up to half of their energy in one collision. Second, large-angle scattering increases their path-length. Third, electrons radiate part of their energy as bremsstrahlung. All three effects tend to increase the fluctuations of the energy loss. Results of electron transmission and straggling measurements have been reported by many observers. A typical spectrum of straggled electrons is shown in Fig. 13.5, which compares the experimental result[17] with a Monte Carlo calculation.[18]

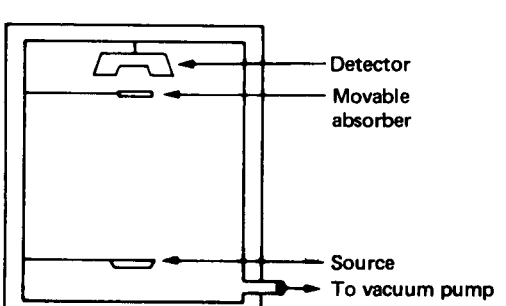


**Figure 13.3** The experimental setup used in the study of energy straggling.

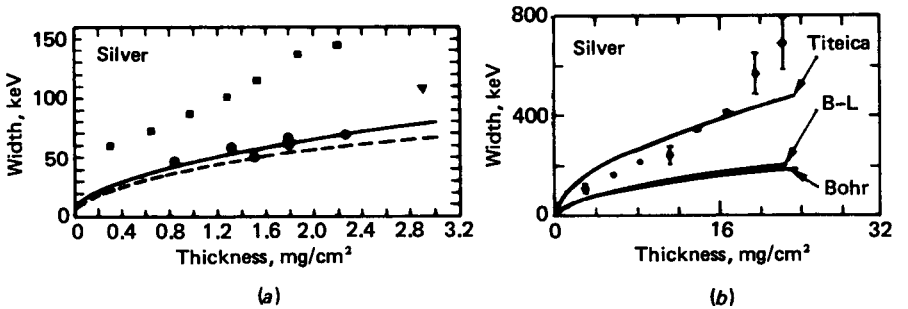


**Figure 13.4** Alpha-particle energy straggling for (*a*) thin, and (*b*) thick foils of silver. [(*a*) Data (●) from Ref. 16; (■) measurements of Sykes & Harris (Ref. 59); (---) calculation from Ref. 12; (——) calculation from Ref. 13; (▼) measurements from Ref. 15; (*b*) Experimental points from Ref. 15; the lines are results of calculations.]

*Range straggling* is a phenomenon related to energy straggling by the equation

$$\sigma_R^2 = \left(\frac{dE}{dx}\right)^{-2} \sigma_E^2 \tag{13.9}$$

where $\sigma_R^2$ is the range variance. Range straggling refers to the pathlength distribution of monoenergetic particles traversing the same absorber thickness (for more details see Sec. 22.5 of Evans). For spectroscopy measurements, only energy straggling is important.

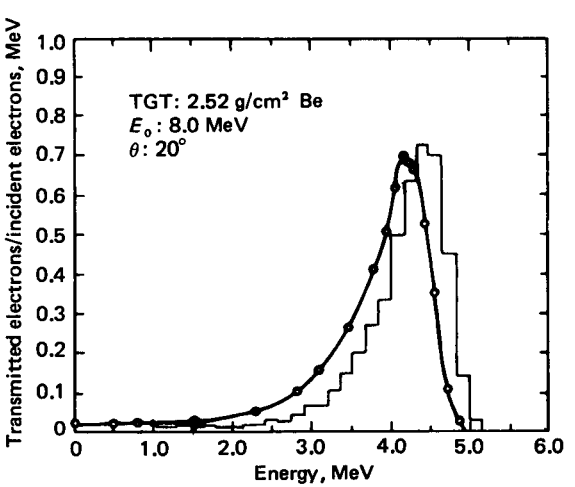


**Figure 13.5** Energy spectrum of 8-MeV electrons transmitted through 2.52 g/cm$^2$ of Be and observed at 20° from the direction of the incident beam. The histogram is the result of a Monte Carlo calculation (Ref. 18), The experimental points are from Ref. 17.

## 13.3 ELECTRON SPECTROSCOPY

Under the common title of electron spectroscopy, this section discusses the most important problems of electron, positron, and beta-ray energy measurements: back-scattering, energy resolution and detector response functions, energy calibration, and source preparation.

### 13.3.1 Electron Backscattering

Electrons moving through a detector behave differently from heavier charged particles in two respects. First, as a result of successive collisions with atomic electrons, the incident electrons may be deflected by more than 90°, i.e., they may be backscattered. Second, electrons slowing down lose part of their energy as bremsstrahlung.† In general, the effect of bremsstrahlung production on spectrum distortion is small. Backscattering in the detector, on the other hand, is important, and therefore corrections to the measured spectrum have to be applied. The effect of backscattering on electron energy spectra is discussed in this section.

Consider a monoenergetic electron beam of energy $T_0$ impinging normally up a detector of thickness $x$, where $x > R(T_0)$ (Fig. 13.6) and $R(T_0)$ is the range of electrons of energy $T_0$ in the material of which the detector is made. Most of the incident electrons will deposit all their energy in the detector (electron A, Fig. 13.6) and thus generate a pulse proportional to $T_0$. But some electrons (like B or C or D, Fig. 13.6) are scattered out of the detector before they deposit all their energy in it. Such particles will give rise to a pulse smaller than that corresponding to energy $T_0$. As a result of electron backscattering, the energy spectrum of a monoenergetic source will have a full-energy peak and a low-energy tail, as shown in Fig. 13.7.[19–23] The fraction of electrons recorded in the tail

1. Increases with the atomic number of the detector material

†Every charged particle slowing down radiates part of its energy. For particles other than electrons, however, and for the energies considered here, the bremsstrahlung can be ignored (see Chap. 4).

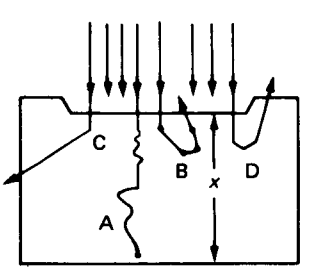


**Figure 13.6** Some of the electrons incident upon the detector are backscattered and deposit only part of their energy in it.

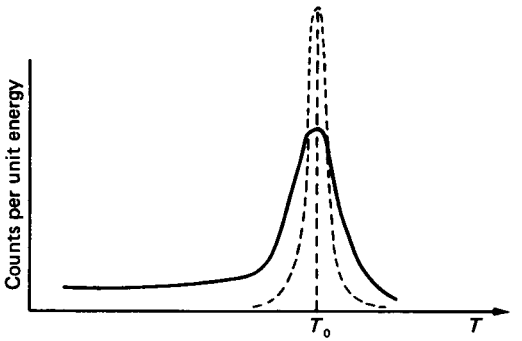


**Figure 13.7** The dashed line shows the measured spectrum without backscattering in the detector. The solid line shows the same spectrum with backscattering.

2. Changes slowly with the energy $T_0$
3. Increases as the incident angle of the beam deviates from the normal

An electron energy spectrum measured with a plastic scintillator is shown in Fig. 13.8. It is represented extremely well by the following analytic function, which was developed by Tsoulfanidis et al.[20] and is shown in Fig. 13.9.

$$R(E, E') = \frac{1}{2}\frac{b}{E'}\operatorname{erfc}\left(\frac{E - E'}{\sigma\sqrt{2}}\right) + \frac{1 - b}{\sigma\sqrt{2\pi}}\exp\left[-\frac{1}{2}\frac{(E - E')^2}{\sigma^2}\right] \tag{13.10}$$

where

$$\operatorname{erfc}(x) = 1 - \frac{2}{\sqrt{\pi}}\int_0^x \exp(-t^2)\,dt$$

and

$\sigma$ = standard deviation of the Gaussian
$b$ = fraction of electrons in the tail

The backscattering fraction $b$ is given by

$$b = \left[1 + \sqrt{2\pi}\left(\frac{g}{\tau} - \frac{1}{2}\right)\frac{\sigma}{E'}\right]^{-1} \tag{13.11}$$

where (Fig. 13.9) $g$ is the height of the peak and $\tau$ is height of the backscattering tail.

Similar results have been obtained with a Si(Li) detector.[20,23] More references on the subject are given by Bertolini and Coche (see their Sec. 4.3.3). Semiempirical formulas giving the value of $b$ as a function of $Z$ and $T$ have been developed by many authors,[24,25] but such equations are of limited general value because the response function and the backscattering depend on the geometry of the system; for this reason, response function and backscattering should be measured for the actual experimental setup of the individual observer.

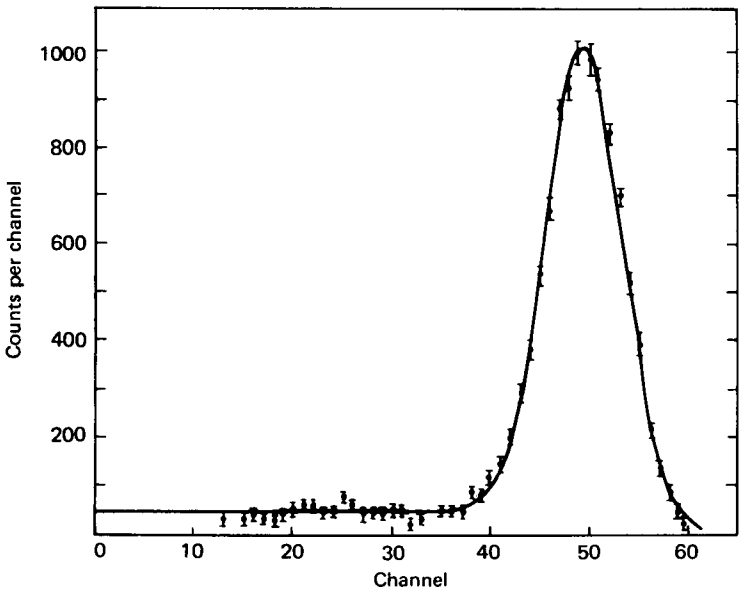


**Figure 13.8** The $^{113}$Sn internal conversion electron spectrum obtained with a plastic scintillator. The solid line was obtained using Eq. 13.10 (from Ref. 20).

### 13.3.2 Energy Resolution and Response Function of Electron Detectors

The best energy resolution for electrons is obtained using silicon semiconductor detectors, with the possible exception of magnetic spectrometers. Silicon detectors may be surface-barrier or Si(Li) detectors. The surface-barrier detectors operate at room temperature, while the Si(Li) detectors give best results when cooled to liquid nitrogen temperatures. The energy resolution of semiconductor detectors is determined by the electronic noise alone. It deteriorates as the area and the sensitive depth of the detector increase. For commercial detectors the full width at half maximum (FWHM) ranges from about 7 to 30 keV.

The energy resolution of scintillators, plastic scintillators in particular, is much worse. It is of the order of 8–10 percent at 1 MeV, which gives a FWHM of 80–100 keV. For scintillators the FWHM is roughly proportional to $\sqrt{E}$. Plastic scintillators have two advantages over semiconductor detectors: the backscattering fraction is less for scintillators because of their lower atomic number, and the timing characteristics are extremely useful for certain types of measurements. The pulse risetime is about 0.1 ns for a plastic scintillator, while for a silicon detector it is between 1 and 10 ns.

The response function of electron detectors is of the form shown in Fig. 13.9. Because of the low-energy tail, if one measures a continuous spectrum (e.g., one beta spectrum or a mixture of beta spectra), the measured spectrum will be higher than the source spectrum at the low-energy end and lower at the

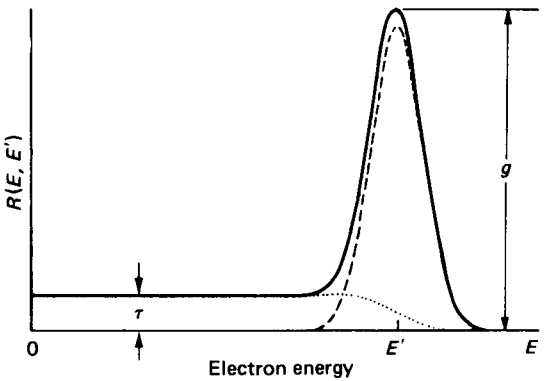


**Figure 13.9** Analytical response function for monoenergetic electrons measured by a thin plastic scintillator. Shown are the backscattering tail ( ··· ) an the Gaussian (---).

high-energy end, as shown in Fig. 13.10. Therefore, spectrum unfolding is necessary to shift back to their proper energy all the betas that were incorrectly recorded at lower energies because of backscattering. The iteration method of unfolding, described in Sec. 11.5.3, is suitable for beta spectra. The spectrum shown in Fig. 13.10 was unfolded using that method.

### 13.3.3 Energy Calibration of Electron Spectrometers

The energy calibration of any spectrometer requires the use of sources of known energy and preferably of monoenergetic sources. Monoenergetic electron sources are provided by accelerators and by radioisotopes emitting internal-conversion (IC) electrons (see Chap. 3).

The advantage of the accelerators is their ability to provide a monoenergetic beam with any desired energy from zero up to the upper limit of the machine. The disadvantages are their expensive operation and the fact that the spectrometer has to be moved to the accelerator beam.

IC emitters are relatively inexpensive to obtain and very easy to handle. They have the disadvantage that they emit not only IC electrons but also gammas. Thus, when a spectrum is recorded, the result includes both IC electrons and Compton electrons created by gammas that interact in the detector. One may eliminate the Compton electrons by utilizing the X-rays that are also given off by the IC source. The X-rays are emitted in coincidence with the IC electrons, while the gammas, and therefore the Compton electrons too, are not. Thus, if the IC electrons are counted in coincidence with the X-rays, the Compton electrons will not be recorded.

IC sources emit K, L, ..., electrons. The energy resolution of silicon semiconductor detectors is so good that separation of the K, L, ..., electrons is possible. Figure 13.11 shows the IC electron energy spectrum of $^{207}$Bi, one of the most widely used calibration sources. The excellent energy resolution of the detector distinguishes K, L, and M electrons. The $K_\alpha$ and $K_\beta$ X-rays, which accompany the IC process, are also known.

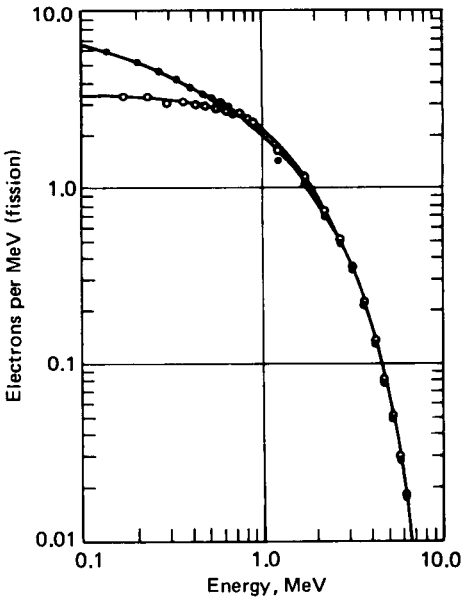


**Figure 13.10** Measured (●) and unfolded (○) beta spectra from $^{235}U$ fission fragments. Unfolding removes the effect of backscattering in the detector; thus, it reduces the spectrum at the low-energy end (from Ref. 26).

Pure beta-emitting isotopes exist and may be used for calibration, but only after the energy spectrum is cast into a form called the *Kurie plot*. The beta spectrum is continuous and extends from zero energy up to a maximum end point kinetic energy (see Fig. 13.12). Because of the shape of the spectrum, it is impossible to accurately determine the end point energy. However, from the

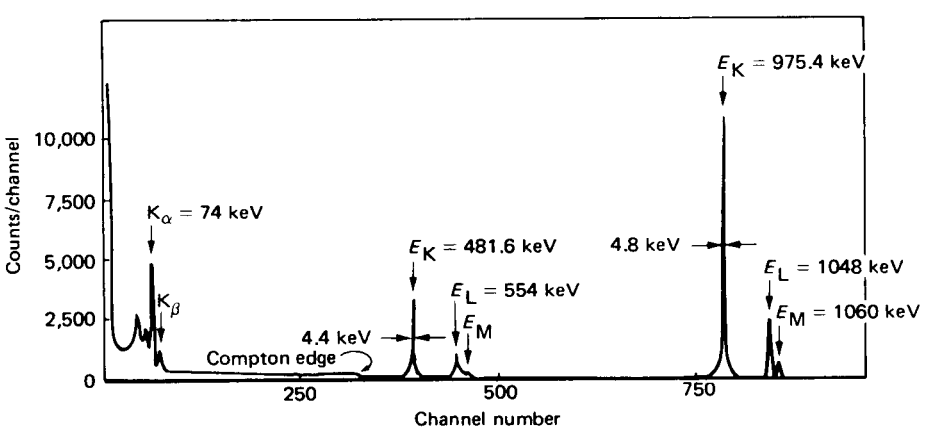


**Figure 13.11** The $^{207}Bi$ internal conversion electron spectrum obtained with a silicon semiconductor detector (from Ref. 27).

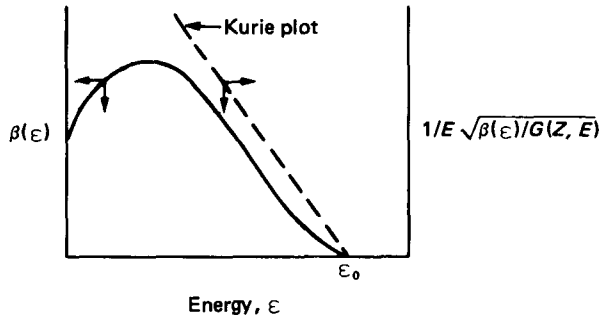


**Figure 13.12** A typical beta energy spectrum (solid line) and its Kurie plot (dashed line).

theory of beta decay, it is known that the beta spectrum may be written as[28]

$$\frac{1}{E}\sqrt{\frac{\beta(\epsilon)}{G(Z,E)}} = k(\epsilon_0 - \epsilon) \tag{13.12}$$

where $\epsilon$ = beta kinetic energy in units of $mc^2$
$E = \mathrm{T} + mc^2 = (\epsilon + 1)mc^2$ = total energy
$G(Z, E)$ = modified Fermi function of $\beta$ decay
$k$ = constant independent of energy (for allowed transitions)
If the left-hand side of Eq. 13.12 is plotted against $\epsilon$, the result is a straight line that crosses the energy axis at $\epsilon = \epsilon_0$. The Kurie plot is a straight line for allowed beta transitions. A "forbidden" beta decay will show an upward curvature at the end.[28]

### 13.3.4 Electron Source Preparation

Preparation of electron or beta sources is accomplished by observing these two rules:

1. The source backing material should be as thin as possible, to avoid backscattering from the source.
2. The source cover should be as thin as possible, to avoid any unnecessary energy loss there.

One way to make a source is by following these steps:

1. A liquid solution of the radioisotope is obtained.
2. A thin piece of Mylar or metallic foil (a few microns thick) is mounted on a metal ring (see Fig. 13.13). This is the source support.
3. Using a pipette, a small amount of the radioisotope is placed on the source support.
4. The source support is then placed under a heat lamp until the liquid evaporates. The heat lamp should be located inside a properly monitored fume hood.

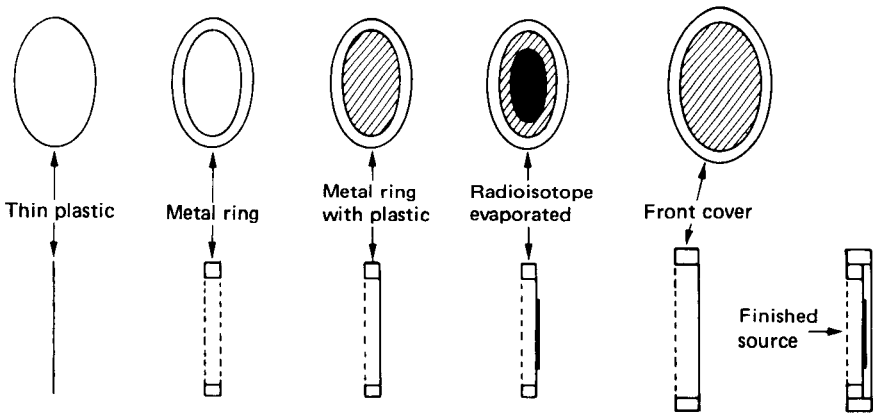


**Figure 13.13** Preparation of an electron source.

5. Steps 3 and 4 are repeated as many times as necessary to achieve the required source strength.
6. The source is sealed by placing a ring with an extremely thin cover (again a few microns thick) on its front face, as shown in Fig. 13.13.

There are many commercial outfits that sell $\beta$ sources with specified characteristics of intensity, source backing, and source cover. Detailed description of the source preparation, for all types of charged particles, is given in a review article by van de Eijk et al.[29] and also in Refs. 30-32.

## 13.4 ALPHA, PROTON, DEUTERON, AND TRITON SPECTROSCOPY

Protons, deuterons, tritons, and alpha particles behave similarly as far as energy loss and straggling are concerned. As they travel in a medium, they are deflected very little from their direction of incidence, as a result of which backscattering is insignificant and their range is almost equal to their pathlength.

To avoid significant energy loss, the particles must go through as small a mass as possible when they move from the source to the detector. This is accomplished by making the source cover and the detector window as thin as possible. The entrance window of such detectors consists of a metallic layer, usually gold, with a thickness of $4 \times 10^{-4}$ kg/m$^2$ (40 $\mu$g/cm$^2$) or less. The measurements are performed in an evacuated chamber to avoid energy loss in air.

The discussion in the rest of this section uses examples from alphas, but the points made are valid for the other particles of this group. Alphas have been studied and used much more extensively than the others, providing a basis for discussion.

### 13.4.1 Energy Resolution and Response Function of Alpha Detectors

The best energy resolution is obtained with silicon surface-barrier detectors. Most detector manufacturers quote the resolution obtained for the 5.486-MeV alphas of $^{241}$Am. A typical spectrum obtained with a detector having 25 mm$^2$ active area and 100 $\mu$m sensitive depth is shown in Fig. 13.14. The resolution deteriorates somewhat as the detector size increases. Since the response function of alpha detectors is a narrow Gaussian, there is no need to unfold a measured monoenergetic alpha spectrum.

### 13.4.2 Energy Calibration

All isotopes with $Z > 82$ emit alphas in the energy range 4 MeV $< T <$ 8 MeV, each isotope giving off more than one group of alphas. A particular isotope is selected to be used for calibration based on the energy of the alphas, the presence of other interfering radiations, and its half-life. For example, the isotope $^{241}_{95}$Am is very popular because it has a 432-year half-life and its only other radiation emitted is $^{237}$Np X-rays. Other isotopes frequently used are $^{210}$Po, $^{226}$Ra, and $^{252}$Cf. Alpha sources with $T_\alpha > 8$ MeV, as well as sources of protons, deuterons, and tritons of any energy, can be provided by accelerators only.

### 13.4.3 Source Preparation

The main precaution taken in the preparation of an alpha source using an alpha-emitting radioisotope is to cover its front face with the thinnest possible layer of material. Commercial sources are made by sandwiching the radioisotope between two thin foils. Figure 13.15 shows a $^{241}$Am source made by the Amersham Corporation.

Alpha-emitting isotopes are considered extremely hazardous when ingested, and in particular when they enter the lungs. To avoid accidental exposure, the user should always be certain that the source cover has not been damaged. The user should also be aware that all alpha sources emit a small number of

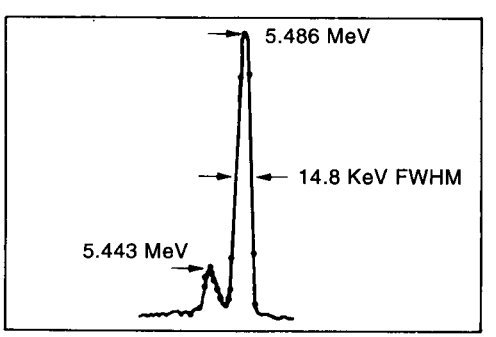


**Figure 13.14** The $^{241}$Am alpha spectrum obtained with a silicon surface-barrier detector (from Canberra).

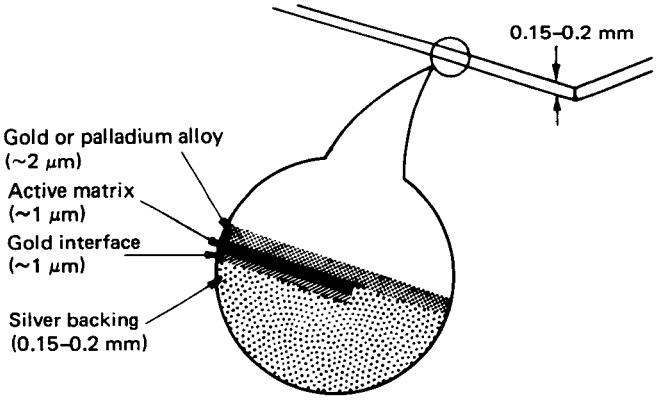


**Figure 13.15** A $^{241}$Am source (from Amersham Corp.).

neutrons, produced either through $(\alpha, n)$ reactions with the source-supporting material or from spontaneous fission of the radioisotope itself.

## 13.5 HEAVY-ION ($Z > 2$) SPECTROSCOPY

Heavy-ion spectroscopy is different from that of lighter charged particles because of the pulse-height defect (PHD), which makes the energy calibration equation mass dependent.

### 13.5.1 The Pulse-Height Defect

The measurement of particle energy with any type of detector is based on the assumption that the charge collected at the output of the detector is proportional to the energy of the incident particle. The assumption is valid if all the particle energy is lost in ionizing collisions and all the charge produced is collected, i.e., no recombination takes place.

It has been known for many years that heavy ions moving in gases lose part of their energy in nonionizing collisions with nuclei. The same phenomenon, PHD, has been observed in semiconductor detectors. The PHD, which is negligible for alphas and lighter particles, is defined as the difference between the energy of a heavy ion and that of a light ion (usually an alpha particle) that generates the same pulse height in the detector. Experimental results showing this phenomenon are presented in Fig. 13.16.[33] Notice that for alphas and carbon ions, the relationship between energy and pulse height is linear. Nickel and silver ions show a small PHD. Heavier ions (Au, U) show a significant PHD.

The PHD is the result of three contributing defects:[33–38]

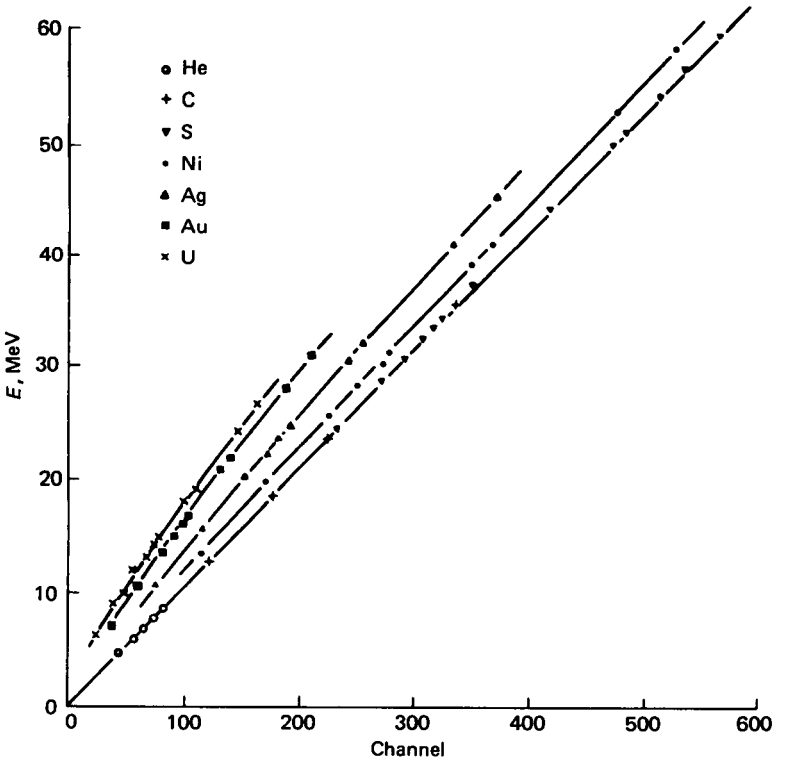


**Figure 13.16** The relationship between energy and pulse height (channel) for ions with different masses (from Ref. 33).

1. The *nuclear defect* is due to nuclear collisions. As a result of such collisions, the moving ion imparts energy upon other nuclei. The recoiling nuclei lose their energy partly in electronic ionizing collisions and partly in nuclear nonionizing ones. The nuclear defect has been calculated[36] based on the work of Bohr[1] and of Lindhard et al.[39] (see also Chap. 4).
2. The *recombination defect* arises from incomplete collection of the charge produced in the detector. A heavy ion is a strongly ionizing particle. It creates a dense plasma of electron-hole pairs along its path, a plasma that reduces the electric field established by the external bias applied to the detector. The reduction of the electric field intensity hinders the drifting of the electrons and holes and thus increases the probability of recombination. The calculation of this defect is not so easy as that of the nuclear one, but an approximate calculation was performed by Wilkins et al.[33]
3. The *window defect* is due to energy loss in the dead layer (window) of the front surface of the detector. It can be obtained from the thickness of the window and the stopping power of the ion. The thickness of the window can

be measured by determining the change in pulse height as a function of the incident angle (see Problem 7.6).

The PHD for iodine and for argon ions has been measured by Moak et al.,[40] using the *channeling effect* in silicon. Pulse-height distributions were measured by first aligning the direction of incident ions with the [110] crystal axis of the silicon surface-barrier detector and then by letting the ions impinge at an angle with respect to the same axis. In the first case, the ions moved along the channel between two planes (*channeled* ions); in the second, they did not (*unchanneled* ions). The channeled ions showed an energy resolution about three times better than that of unchanneled ones, and essentially no PHD (Fig. 13.17). This result can be explained by assuming that the channeled ions traveling between atomic planes lose all their energy in ionizing collisions, all the way to the end of their track. Similar results have been obtained with $^{235}$U fission fragments[34] and $^{252}$Cf fission fragments.[41]

The lack of nuclear collisions for channeled ions is not the only phenomenon that affects the pulse height. It is known that the electron density is much reduced along the channel. As a result, the electronic stopping power is lower and, consequently, so is the charge density produced by the heavy ion. Thus, not only the nuclear but also the recombination defect is reduced for the channeled ions.

The PHD increases slowly with ion energy, as shown in Fig. 13.18.

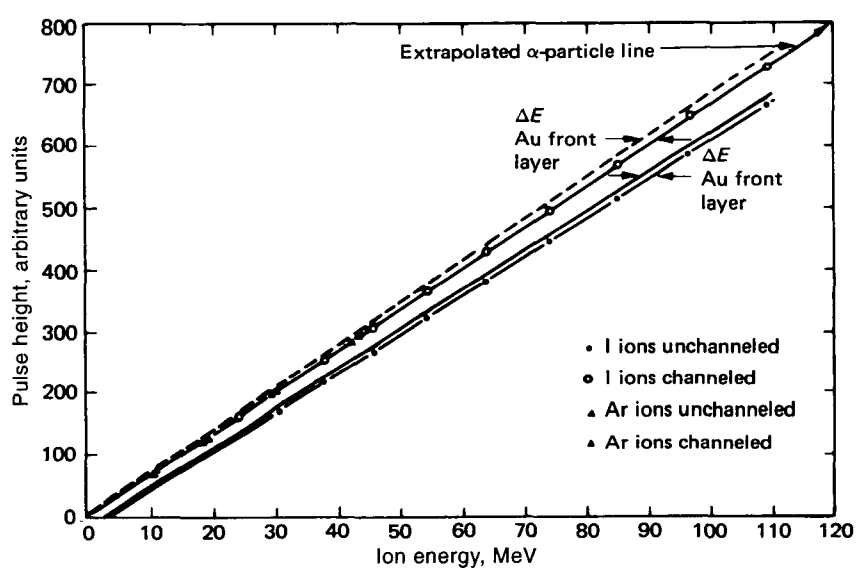


**Figure 13.17** Pulse-height response of a Si surface-barrier detector for "channeled" and "unchanneled" ions (from Ref. 40).

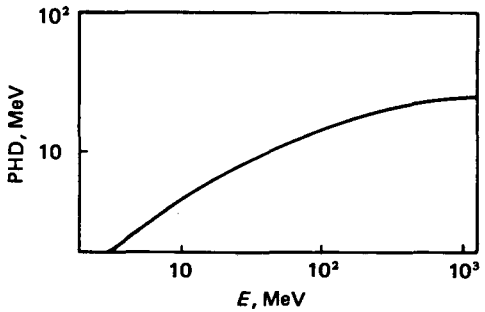


**Figure 13.18** The dependence of the pulse height defect on ion energy (from Ref. 33). The numbers correspond, approximately, to uranium ions.

### 13.5.2 Energy Calibration: The Schmitt Method

The relationship between the pulse height $h$ and the kinetic energy $T$ of a heavy ion was determined by Schmitt et al.[42,43] to be of the form

$$T = (a + bM)h + c + dM \tag{13.13}$$

where $M$ is the mass of the ion and $a$, $b$, $c$, and $d$ are constants. The calibration of the detector, i.e., the determination of the constants $a$, $b$, $c$, and $d$, can be achieved in two ways. The first is an absolute calibration, and the second is a relative one.

Absolute energy calibration is performed with the help of an accelerator. One measures the pulse heights of four monoenergetic beams of ions with known mass. Substitution of the known energy, mass, and pulse height into Eq. 13.13 provides four equations with four unknowns that can be solved for the constants $a$, $b$, $c$, and $d$.

For fission-fragment measurements, a relative calibration is used. The calibration constants of Eq. 13.13 are determined in terms of two pulse heights $H$ and $L$ of a fission-fragment spectrum (Fig. 13.19), where $H$ and $L$ represent pulse height corresponding to the mid-point at three-quarters maximum of the heavy or light fragment peak, respectively. The equations for the constants are

$$a = \frac{a_1}{L - H} \tag{13.14}$$

$$b = \frac{a_2}{L - H} \tag{13.15}$$

$$c = a_3 - aL \tag{13.16}$$

$$d = a_4 - bL \tag{13.17}$$

and the constants $a_1, a_2, a_3, a_4$ for $^{252}$Cf and $^{235}$U fission fragments are given in Table 13.1.

The constants $a_1$, $a_2$, $a_3$, and $a_4$ do not depend on the detector. The quality of the detector with respect to energy resolution is determined from a set of criteria developed by Schmitt and Pleasonton[43] and shown in Table 13.2. Figure 13.19 explains the symbols used (see also Ref. 45).

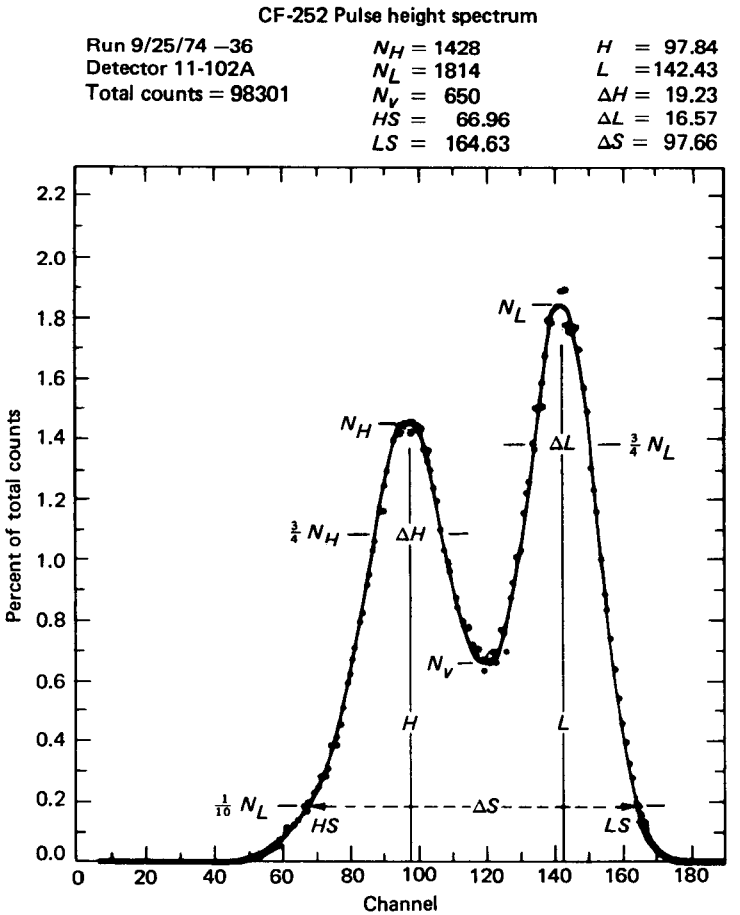


**Figure 13.19** The $^{252}$Cf fission-fragment spectrum used for the determination of the detector calibration constants (from Ref. 44).

**Table 13.1 Schmitt Calibration Constants for $^{252}$Cf and $^{235}$U Fission Fragments[42,46]**

| Constant | $^{252}$Cf | $^{235}$U |
|---|---|---|
| $a_1$ | 24.0203 | 30.9734 |
| $a_2$ | 0.03574 | 0.04596 |
| $a_3$ | 89.6083 | 87.8626 |
| $a_4$ | 0.1370 | 0.1345 |

**Table 13.2 Acceptable Parameters for a $^{252}$Cf Fission-Fragment Spectrum**

| Spectrum parameters | Expected values | Spectrum of Fig. 13.19 |
|---|---|---|
| $N_L/N_V$ | 2.9 | 2.79 |
| $N_H/N_V$ | 2.2 | 2.20 |
| $N_L/N_H$ | 1.3 | 1.27 |
| $\Delta L/(L-H)$ | 0.36 | 0.37 |
| $\Delta H/(L-H)$ | 0.44 | 0.43 |
| $(H-HS)/(L-H)$ | 0.69 | 0.69 |
| $(LS-L)/(L-H)$ | 0.48 | 0.50 |
| $\Delta S/(L-H)$ | 2.17 | 2.19 |

### 13.5.3 Calibration Sources

Monoenergetic heavy ions necessary for energy calibration can be provided only by accelerators. Fission fragments, which are heavy ions, cover a wide spectrum of energies (Fig. 13.19). The isotope $^{252}$Cf is a very convenient source of fission fragments produced by the spontaneous fission of that isotope. Uranium, plutonium, or thorium fission fragments can only be produced after fission is induced by neutrons; therefore, a reactor or some other intense neutron source is needed.

### 13.5.4 Fission Foil Preparation

Fission foils are prepared by applying a coat of fissile material of the desired thickness on a thin metal backing. Details of several methods of foil preparation are given in Refs. 29–32. A technique used for the preparation of uranium foils is described here.

Enriched uranium in the form of uranium nitrate hexahydrate crystals is dissolved in ethanol until it forms a saturated solution. A small amount of collodion is added to the solution to improve its spreading characteristics. A thin metal foil—e.g., nickel—that serves as the backing material is dipped into the solution and then heated in an oven in a controlled temperature environment. The heating of the foil is necessary to remove organic contaminants and to convert the uranium nitrate into uranium oxides (mostly $U_3O_8$). The temperature is critical because if it is too high, part of the uranium diffuses into the backing material, causing fragment energy degradation. Dipping produces a two-sided foil. If the material is applied with a paint brush, a one-sided foil is formed.

The dipping (or brush-painting) and heating is repeated as many times as necessary to achieve the desired foil thickness. The thickness of the foil is determined by weighing it before and after the uranium deposition or, better yet, by counting the alphas emitted by the uranium isotopes. Most of the alphas come from $^{234}$U; therefore the fraction of this isotope in the uranium must be known.

## 13.6 THE TIME-OF-FLIGHT SPECTROMETER

The time-of-flight (TOF) method, which is also used for the measurement of neutron energy (see Sec. 14.8), has been applied successfully for the determination of the mass of fission fragments and other heavy ions.

The principle of TOF is simple. A beam of ions is directed along a flight path of length $L$ (Fig. 13.20). The time $t$ it takes the ions to travel the distance $L$ determines their speed $V = L/t$. This information, combined with the measurement of the energy of the particle, gives the mass (nonrelativistically):

$$M = \frac{2Et^2}{L^2} \tag{13.18}$$

The errors in determining the mass come from uncertainty in energy, $\Delta E$, in time, $\Delta t$, and in length of the flight path, $\Delta L$. The mass resolution is then given by

$$\frac{\Delta M}{M} = \sqrt{\left(\frac{\Delta E}{E}\right)^2 + \left(\frac{2\,\Delta t}{t}\right)^2 + \left(\frac{2\,\Delta L}{L}\right)^2} \tag{13.19}$$

Usually, the system is designed in such a way that $\Delta L/L$ is negligible compared to the other two terms of Eq. 13.19. Assuming that this is the case, consider the sources of uncertainty in energy and time.

The uncertainty $\Delta E/E$ is the resolution of the detector measuring the energy of the ion. The best energy resolution that can be achieved with silicon surface-barrier detectors is about 1.5–2 percent. The resolution can be improved with magnetic or electrostatic analyzers (DiIorio and Wehring[47] achieved 0.3 percent energy resolution using an electrostatic analyzer).

The time $t$ it takes the particle to travel the distance $L$ is the difference between a START and a STOP signal (Fig. 13.20). The STOP signal is generated by the detector, which measures the energy of the ion. This detector is usually a surface-barrier detector. The START signal is generated by a transmission counter, also called the $\delta E$ detector. The ion loses a tiny fraction of its energy going through the START detector.

Several types of $\delta E$ detectors have been used.[48] Examples are totally depleted surface-barrier detectors,[49,50] thin ($\sim 10^{-3}$ kg/m$^2$ = 100 $\mu$g/cm$^2$) plastic scintillators,[51] ionization chambers,[52] and secondary-electron emission

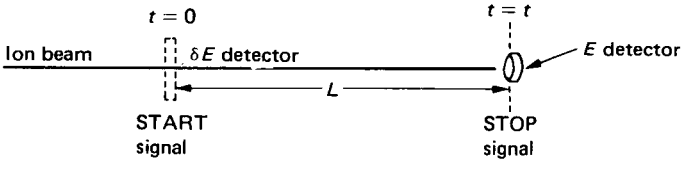


**Figure 13.20** The principle of time-of-flight for the determination of the mass of heavy ions.

detectors.[47,53–56] Secondary-electron emission detectors fall into two categories. In the first, the ions traverse a thin foil (e.g., carbon foil $10^{-4}$ kg/m$^2$ = 10 $\mu$g/cm$^2$ thick) and generate secondary electrons that are accelerated and focused to strike a scintillator coupled to a photomultiplier tube. In the second category belong the *channel electron multipliers* (CEM) and the *microchannel plates* (MCP).

A CEM is essentially a thin glass tube ($\sim$ 1 mm diameter) shaped into a spiral, with its inside surface coated with a semiconducting material that is also a good secondary electron emitter. An accelerating field is created in the tube by applying a high voltage along its length. Electrons multiply as they proceed down the tube. Figure 13.21 shows one possible arrangement for the use of a CEM.

An MCP is a glass disk perforated with a large number of small-diameter (10–100 $\mu$m) holes or channels. Each channel is a glass tube coated with a resistive secondary electron-emitting material. If a voltage is applied, each channel acts as an electron multiplier.

The state of the art of $\delta E$ detector systems is such that $\Delta t < 100$ ps has been achieved and the flight path $L$ can become long enough that the time $T \approx 100$–$300$ ns. Thus, the time resolution of TOF measurements is

$$\frac{\Delta t}{t} \approx \frac{100 \times 10^{-3}\ \text{ns}}{200\ \text{ns}} \approx 5 \times 10^{-4} \approx 0.05\%$$

and the mass resolution (Eq. 13.19) is essentially limited by the energy resolution. The mass measurement is actually the measurement of the mass number $A$ ($\Delta M/M = \Delta A/A$). Since $A$ is an integer, the lowest limit for mass resolution is $\Delta A < 1$. Assuming $\Delta A = 0.7$, Fig. 13.22 gives the ion energy necessary for such resolution as a function of $A$ and $L/\Delta t$.[57] For heavy ions, mass resolution as low as $\Delta A = 0.2$ has been reported.[50]

If the mass of the ion is known, the TOF technique can be used to determine the energy of the ion with a resolution much better than with any detector in use today. Indeed, if $\Delta M = 0$, Eq. 13.19 gives

$$\frac{\Delta E}{E} = 2\frac{\Delta t}{t} \approx \frac{200 \times 10^{-3}\ \text{ns}}{200\ \text{ns}} \approx 0.1\%$$

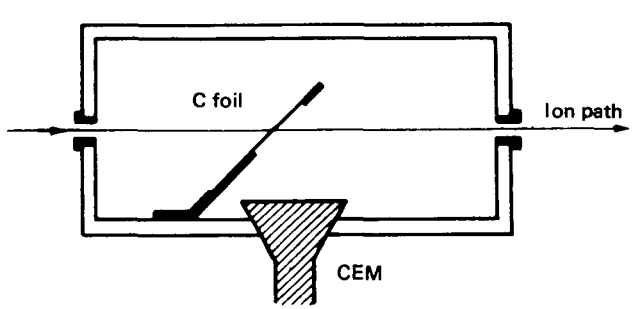


**Figure 13.21** The use of a CEM as a $\delta E$ detector.

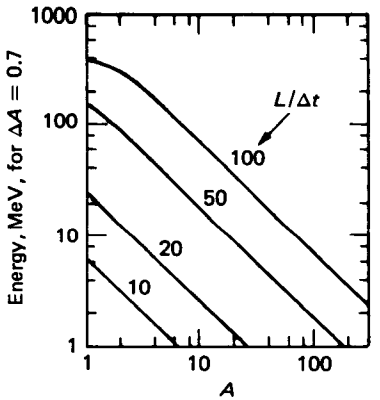


**Figure 13.22** Energy of ion at which adjacent isotopes can be resolved, as a function of $A$, for different values of $L/\Delta t$ (from Ref. 57).

## 13.7 DETECTOR TELESCOPES ($E\,dE/dx$ DETECTORS)

The TOF method discussed in the previous section measures the energy and the mass of the ion. This section presents a method that identifies the atomic number $Z$ and the mass number $A$ of the particle.[58]

Identification of $A$ and $Z$ is possible by making use of a *detector telescope* consisting of a very thin detector measuring $dE/dx$ and a thick detector that stops the particle. The geometric arrangement is similar to that shown in Fig. 13.20. The particle traverses the thin detector after depositing there an energy equal to $(dE/dx)t$ (where $t$ is the detector thickness), and stops in the "$E$ detector." The total energy of the particle is obtained from the sum of the two detector signals. The product $E\,dE/dx$ can be written, using Eq. 4.2 or 4.33, as

$$E\frac{dE}{dx} = k_1 M Z_{\text{ef}}^2 \ln\left(k_2 \frac{E}{M}\right) \tag{13.20}$$

where $Z_{\text{ef}}$ is the effective charge of the ion. Since the logarithmic term changes very slowly with energy, Eq. 13.20 gives a value for $MZ_{\text{ef}}^2$.

Another method, giving better results, is based on the fact that the range of heavy ions is given, over a limited energy range, by an equation of the form

$$R = C\frac{E^b}{MZ_{\text{ef}}^2} \tag{13.21}$$

where $b$ is a constant. If a particle deposits energy $\delta E = (dE/dx)t$ in a detector of thickness $t$ and then deposits energy $E$ in the second detector, one can say that the range of the particle with energy $E + \delta E$ is $t$ units longer than the range of the same particle with energy $E$. Using Eq. 13.21, one can write

$$MZ_{\text{ef}}^2 \approx \frac{[(E + \delta E)^b - E^b]}{t} \tag{13.22}$$

Thus, Eq. 13.22 provides the value of $MZ_{\text{ef}}^2$ since $t$, $E$, and $\delta E$ are known. The constant $b$ is also assumed to be known for the ion of interest.

Equations 13.20 to 13.22 were written in terms of the mass $M$ of the particle. For nonrelativistic particles, $M$ has a nonintegral value very close to the value of $A$, which in turn, is given by an integer. This is fortunate because $Z$ also assumes integral values only, and the product $MZ^2$ assumes unique values for many particles. For example, for protons, deuterons, tritons, and alphas, the value of $MZ^2$ is 1, 2, 3, and 16, respectively.

## 13.8 MAGNETIC SPECTROMETERS

Magnetic spectrometers (or analyzers) are instruments that exhibit high-energy resolution. They are used mainly in experiments involving high-energy particles, but they can be used with low-energy particles as well. Energy resolutions achieved with this type of spectrometer are of the order of $\Delta E/E \approx 10^{-4}$ for high-energy electrons[60] and $\Delta E/E \approx 10^{-3}$ for heavy ions.[61]

Many types of magnetic spectrometers have been developed, differing mainly in the shape of the magnetic field used.[60–65] The basic principle common to all of them is the action of the force from a magnetic field on a moving charged particle. If a particle with charge $Ze$ moves with velocity $\mathbf{v}$ in a magnetic field of strength $\mathbf{B}$, the force $\mathbf{F}$ on the particle is given by

$$\mathbf{F} = Ze\mathbf{v} \times \mathbf{B} \tag{13.23}$$

Since the magnetic force is always perpendicular to the direction of motion of the particle, it does not change the energy but only the direction of motion of the particle. If the velocity is perpendicular to the magnetic field, the particle trajectory will form a circle of radius $\rho$ given by the equation

$$\frac{M^* v^2}{\rho} = ZevB \tag{13.24}$$

which after rearrangement becomes

$$M^* v = ZeB\rho \tag{13.25}$$

where $M^* = M/\sqrt{1-\beta^2}$, the total mass of the particle.

Equation 13.25 is the basis of magnetic spectroscopy. It expresses the fact that the momentum of the particle is proportional to the quantity $B\rho$, called the *magnetic rigidity* of the particle. The relationship between kinetic energy and rigidity is obtained from the equation linking energy and momentum (see Chap. 3). The relativistic equation for the kinetic energy $T$ is

$$T = \sqrt{(Mc^2)^2 + Z^2e^2(B\rho)^2} - Mc^2 \tag{13.26}$$

The nonrelativistic equation is

$$T = \frac{Z^2e^2(B\rho)^2}{2M} \tag{13.27}$$

To understand how a magnetic spectrometer works, consider two particles with momenta $M_1v_1$ and $M_2v_2$ coming into a space with a constant magnetic field $B$ (Fig. 13.23). Assuming that the magnetic field is perpendicular to the velocity and also perpendicular to the plane of the figure, the two particles will move along circular paths of radii $\rho_1$ and $\rho_2$ given by Eq. 13.25. If the particles are allowed to complete half a circle, they will hit the "focal" plane at points A and B. Thus, if one determines $\rho_1$ and $\rho_2$ and the charge of the particles is known, the momentum can be determined from Eq. 13.25. If the mass of the particle is also known, the energy can be determined from Eq. 13.26 or 13.27. Obviously, for a given rigidity $B\rho$, the energy $T$ depends on the factor $Z^2/M$. If one determines the energy by other means—e.g., by using a semiconductor detector—the magnetic spectrometer may give the $Z^2/M$ value.

In practice, the value of $B$ is accurately known; therefore, the real task is the accurate determination of the radius $\rho$. The radius $\rho$ (or the distance $2\rho$) is measured with the help of position-sensitive detectors placed at the focal plane. Any uncertainty in the value of $\rho$, or in general in the value of $B\rho$, introduces an uncertainty in the value of energy. If all the particles move in parallel paths when they enter the spectrometer, the energy resolution obtained from Eq. 13.26 or Eq. 13.27 is given by

*Relativistic*

$$\frac{\Delta T}{T} = \left(1 + \frac{Mc^2}{Mc^2 + T}\right)\frac{\Delta(B\rho)}{B\rho} \tag{13.28}$$

*Nonrelativistic*

$$\frac{\Delta T}{T} = 2\frac{\Delta(Be)}{B\rho} \tag{13.29}$$

The position can be determined with an accuracy of less than a millimeter. Since a typical value of $\rho$ is 0.80 m, the expected resolution is

$$\frac{\Delta T}{T} \approx \frac{\Delta\rho}{\rho} \approx \frac{1}{800} \approx 10^{-3}$$

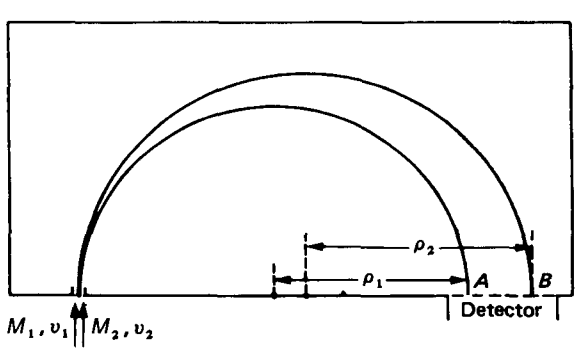


**Figure 13.23** Two particles with velocities $v_1$ and $v_2$ follow trajectories with radius $\rho_1$ and $\rho_2$ respectively, and are separated spatially (points $A$ and $B$).

As shown in Fig. 13.23, the particles enter the spectrometer through a slit, whose size defines the solid angle accepting particles from the source. This solid angle should be as large as possible, because the more particles that enter the spectrometer, the less the necessary counting time is. Since magnetic spectrometers are commonly used with accelerators, reduction of the counting time means less operational time for the accelerator. When the solid angle increases, however, the probability also increases that particles with nonparallel paths will enter the spectrometer. Such particles will not focus at the same point even if they have the same momentum. This "defocusing" is a difficult problem, corrected by using magnetic fields that focus at a spot or a line of the detector all the particles entering through a certain solid angle and having the same momentum.

The first magnetic spectrometers used photographic plates for the detection of the deflected particles. Today, position-sensitive semiconductor detectors or multiwire proportional chambers are used (see Sec. 13.10). These detectors are better than photographic plates because they have the capability of on-line data collection, provide time information for coincidence experiments, and measure the energy of the particle.

## 13.9 ELECTROSTATIC SPECTROMETERS

Electrostatic spectrometers (or analyzers) do not have such extensive use as magnetic spectrometers. They are only used for certain types of experiments where an electrostatic field is more convenient than a magnetic one.

An electrostatic spectrometer uses a radial electric field formed between two cylindrical electrodes, as shown in Fig. 13.24. If there is a potential difference $V$ between the electrodes $EF$ and $E'F'$, the electric field in the space

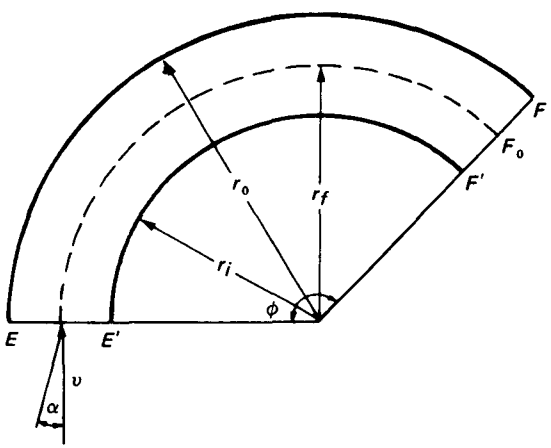


**Figure 13.24** An electrostatic spectrometer using a radial field.

between the two electrodes is equal to

$$\left[\frac{V}{\ln(r_0/r_i)}\right]\frac{1}{r}$$

where $r$ is the distance from the center of the electrodes. A particle entering the spectrometer at $EE'$ with velocity **v** perpendicular to $EE'$ will follow under the influence of the radial force

$$F = (Ze)\left[\frac{V}{\ln(r_0/r_i)}\right]\frac{1}{r} \tag{13.30}$$

a circular path of radius $r_f$. It can be shown[66] that particles entering at $EE'$ with the same speed but traveling along a direction slightly different from the normal to $EE'$ will focus at the point $F_0$, provided the angle $\phi = \pi/\sqrt{2} = 127°17'$ (Fig. 13.24). All the particles that arrive at $F_0$ have a kinetic energy that can be calculated in terms of the radius $r_f$ and the strength of the electric field.[67] More details about the focusing properties and energy resolution of electrostatic spectrometers can be found in Refs. 68–70. Electrostatic analyzers with parallel plates have also been constructed.

## 13.10 POSITION-SENSITIVE DETECTORS

Detectors that in addition to the measurement of the energy also indicate the position of the particle have been developed for application with magnetic or electrostatic spectrometers and for imaging devices used in biological and medical research. As discussed in Secs. 13.8 and 13.9, magnetic or electrostatic spectrometers are mostly used with high-energy particles. Biological and medical imaging devices, on the other hand, involve mostly X-rays and, in general, low-energy radiation. It is because of the latter use that position-sensitive detectors are briefly discussed here.

### 13.10.1 Position-Sensitive Semiconductor Detectors

Most of the position-sensitive semiconductor detectors determine the position of the incident particle by employing the method of *resistive-charge division*.[71] To illustrate the method, consider the detector in Fig. 13.25. The detector is a reverse-biased p-n junction with electrodes on both front and back. The front electrode with considerable resistivity has two electrical contacts a distance $L$ apart. The back electrode has low resistivity and provides a good electrical contact to the base material. When a particle enters the detector, electrons and holes are created that move under the influence of the electric field. If the resistivity of the front electrode is homogeneous, and charge-sensitive low-impedance amplifiers are used, the charge collected at one of the two contacts of the front electrode is proportional to the distance between the point of impact

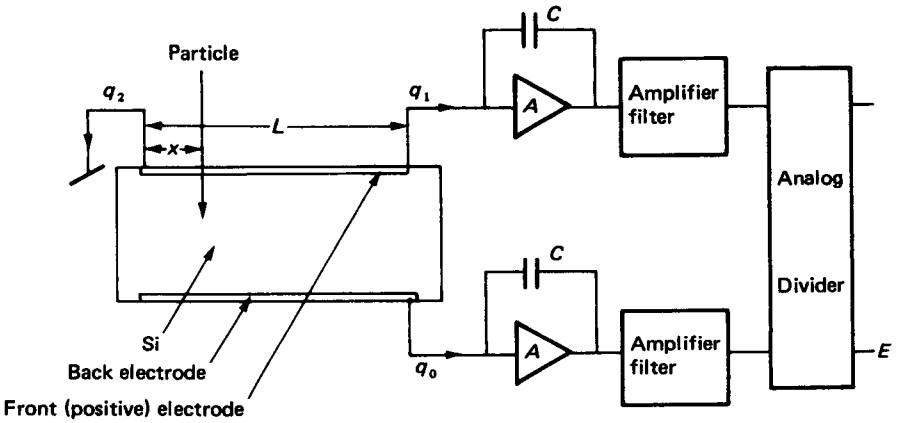


**Figure 13.25** A position-sensitive semiconductor detector using resistive-charge division (from Ref. 71).

and the other contact. The total charge $q_0$ collected through the single contact of the back side is, of course, proportional to the energy deposited in the sensitive region of the junction. This technique of determining the position by comparing the signals from $q_1$ and $q_0$ is called the *amplitude method.*

The signal $q_1$ changes with time, as shown in Fig. 13.26. The timescale is in units of the time constant $\tau_D = R_D C_D$, where $R_D$ and $C_D$ are the resistance and capacitance of the detector, respectively. Figure 13.26 shows that the risetime of the signal depends on the position. This property is the basis of a second technique for determination of position, called the *time method.* The position is

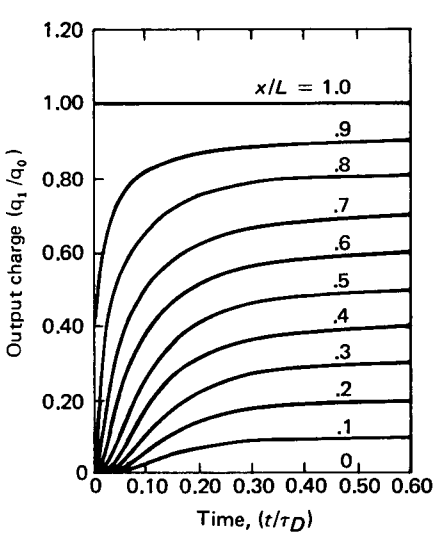


**Figure 13.26** Time dependence of the position signal for different positions of incidence (from Ref. 71).

now determined from the difference in arrival times of the signals from the charges $q_1$ and $q_2$ (Fig. 13.25).

The detector described above is of the "continuous" type. Position-sensitive detectors of the "discrete" type have also been developed.[72] They consist of individual semiconductor elements all placed on the same base material, with each element connected to its own preamplifier-amplifier system. Two-dimensional detectors of the continuous type[73] as well as of the discrete type[74] have also been tried.

### 13.10.2 Multiwire Proportional Chambers

Mulitwire proportional chambers (MWPC)† have been developed for use as position-sensitive focal detectors for magnetic spectrometers.[76–86] They can provide excellent position resolution, operate with counting rates as high as $10^6$ counts/s, and provide a large solid angle at the focal plane of the spectrometer.

The basic design of an MWPC is shown in Fig. 13.27. A series of thin, equally spaced anode wires is positioned between two parallel plates serving as cathodes. A noble gas mixed with an organic component fills the space between the cathodes. A positive voltage is applied to the anode wires. When a particle goes through the counter, electrons and ions are created by the processes explained in Chap. 5. The electric field close to the wires is so intense that the primary electrons acquire enough energy to produce secondary ionization. Thus, an avalanche of electrons is produced that is collected within a time of 1 ns, but that leaves behind a cloud of positive ions.

It is significant that the pulse produced by the counter is not due to the motion of the electrons, but to that of the ions.[76] As the positive ions move away from the anode wires, they generate a fast-rising ($\sim$ 10 ns) negative pulse that gradually slows down and lasts a few microseconds. The pulse induced in the neighboring wires is positive. Thus, the active wire (the wire close to the trajectory of the particle) is distinguished from the others. The signals from the wires are processed and read by either digital or analog systems.[77]

The position resolution depends on the spacing between the wires, but it is better than the actual size of the spacing. The smallest wire spacing is about 1

†Single-wire position-sensitive proportional counters operating by charge division (as described in Sec., 13.10.1) have also been used.[75]

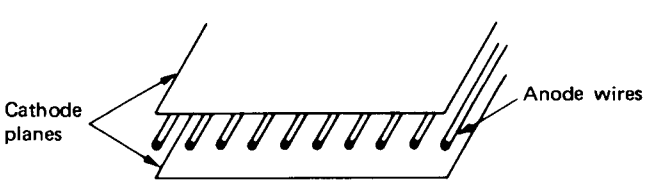


**Figure 13.27** The basic design of an MWPC.

mm, while position resolutions better than 100 $\mu$m have been reported.[87,88] Such space resolution has been achieved because the position is determined from the well-defined centroid of the charge distribution generated by the passage of the particle.

A variation of the detector described above is the so-called "drift chamber." The drift chamber determines the position from the time it takes the electrons produced by the incoming particle to drift to the nearest anode wire.[89] A two-dimensional MWPC has also been constructed for detection of neutrons scattered from biological samples.[90] It is a $^3$He gas-filled counter that detects neutrons through the $(n, p)$ reaction.

## PROBLEMS

**13.1** Prove that the maximum energy transfer to an electron as a result of a collision with a particle of mass $M$ and speed $v = \beta c$ is equal to

$$\Delta E_{\max} = 2mc^2 \frac{\beta^2}{1-\beta^2}\left[1 + \left(\frac{m}{M}\right)^2 + 2\frac{m}{M}\frac{1}{\sqrt{1-\beta^2}}\right]^{-1}$$

**13.2** Show that $\Delta E_{\max}$ of Prob. 13.1 takes the form

$$\Delta E_{\max} = \frac{4mM}{(m+M)^2}T$$

if $T = \frac{1}{2}Mv^2$ (nonrelativistic particle) and $m \ll M$.

**13.3** Calculate the energy loss of a 6-MeV alpha particle going through an aluminum foil with thickness equal to one-fourth of the range of the alpha (remember $dE/dx$ is not constant as the particle slows down).

**13.4** A monoenergetic beam of 10-MeV alpha particles goes through a nickel foil with a thickness equal to 1/30 of the range of the alphas. What is the width of the emerging beam (in keV)? If the emerging particles are counted by a silicon detector with a resolution of 15 keV, what is the total width of the measured alpha beam (measurement performed in vacuum)?

**13.5** What is the thickness of a nickel foil that will cause energy loss equal to 1/50 of the energy of a 10-MeV proton traversing it?

**13.6** Show that the backscattering fraction of electrons is given by

$$b = \left[1 + \sqrt{2\pi}\left(\frac{g}{\tau} - 0.5\right)\frac{\sigma}{E'}\right]^{-1}$$

where $g$, $\tau$, and $E'$ are defined in Fig. 13.9; $\sigma$ is the standard deviation of the Gaussian.

**13.7** If the stopping power for a heavy ion can be represented by the equation

$$\frac{dE}{dx} = k\sqrt{E} + b$$

where $k$ and $b$ are constants, what is the expression for the range as a function of energy for such ions? What is the energy of the ion as a function of distance traveled?

**13.8** If the expression for $dE/dx$ given for Prob. 13.7 is valid, what fraction of the initial kinetic energy of the ion is lost in the first half of its range?

**13.9** A thin fission foil was prepared using natural uranium. Calculate the ratio of alpha activities due to the isotopes $^{234}$U, $^{235}$U, and $^{238}$U. The abundance $a$ and half-lives of the three isotopes are

$$^{234}U: \quad a = 0.0057\% \qquad T_{1/2} = 2.47 \times 10^5 \text{ y}$$

$$^{235}U: \quad a = 0.711\% \qquad T_{1/2} = 7.10 \times 10^8 \text{ y}$$

$$^{238}U: \quad a = 99.283\% \qquad T_{1/2} = 4.51 \times 10^9 \text{ y}$$

Assume that every decay gives off an alpha; i.e., neglect decay by spontaneous fission.

**13.10** Verify the curves of Fig. 13.22.

**13.11** Prove that the energy resolution of a magnetic spectrometer is given (relativistically) by the equation

$$\frac{\Delta T}{T} = \left(1 + \frac{Mc^2}{Mc^2 + T}\right)\frac{\Delta(B\rho)}{B\rho}$$

(Definition of the symbols used is given in Sec. 13.8.)

## BIBLIOGRAPHY

Bertolini, G., and Coche, A. (eds.), *Semiconductor Detectors*, Wiley Interscience, New York, 1968.
Evans, R. D., *The Atomic Nucleus*, McGraw-Hill, New York, 1972.
Segré, E., *Nuclei and Particles*, W. A. Benjamin, New York, 1965.
Siegbahn, K. (ed.), *Alpha, Beta and Gamma-Ray Spectroscopy*, North Holland Publishing Co., Amsterdam, 1965, vols. 1 and 2.

## REFERENCES

1. Landau, W., *J. Phys. USSR* **8**:201 (1944).
2. Symon, K., thesis, Harvard 1958, "Experts in High Energy Particles," Prentice-Hall, Englewood Cliffs, N.J., 1952.
3. Vavilov, P. V., *JETP* **5**:749 (1957).
4. Maccabee, H. D., Raju, M. R., and Tobias, L. A., *IEEE Nucl. Sci.* **13**(3):176 (1966).
5. Blunk, O., and Leisegang, S., *Z. Physik* **128**:500 (1950).
6. Tschalar, C., *Nucl. Instrum. Meth.* **61**:141 (1968).
7. Tschalar, C., *Nucl. Instrum. Meth.* **64**:237 (1968).
8. Clarke, N. M., *Nucl. Instrum. Meth.* **96**:497 (1971).
9. Ispirian, K. A., Murgarian, A. T., and Zuerev, A. M., *Nucl. Instrum. Meth.* **117**:125 (1974).
10. Ermilova, V. C., Kotenko, L. P., and Merzon, G. I. *Nucl. Instrum. Meth.* **145**:444 (1977).
11. Skyrme, D. J., *Nucl. Instrum. Meth.* **57**:61 (1967).
12. Bohr, N., *Philos. Mag.* **30**:581 (1915).
13. Livingston, M. S., and Bethe, H., *Rev. Mod. Phys.* **9**:245 (1937).
14. Titeica, S., *Bull. Soc. Roumaine Phys.* **38**:81 (1939).
15. Comfort, J. R., Decker, J. F., Lynk, E. T., Scully, M. D., and Quinton, A. R., *Phys. Rev.* **150**:249 (1966).
16. Strittmatter, R. B., and Wehring, B. W., *Nucl. Instrum. Meth.* **135**:173 (1976).
17. Lonergan, J. A., Jupiter, C. P., and Merkel, G., *J. Appl. Phys.* **41**:678 (1970).
18. Berger, M. J., and Seltzer, S. M., "ETRAN Monte Carlo Code System for Electron and Photon Transport Through Extended Media," NBS-9836 and NBS-9837 (1968).
19. Rogers, P. C., and Gordon, G. E., *Nucl. Instrum. Meth.* **37**:259 (1965).

20. Tsoulfanidis, N., Wehring, B. W., and Wyman, M. E., *Nucl. Instrum. Meth.* **73**:98 (1969).
21. Wohn, F. K., Clifford, J. R., Carlson, G. H., and Talbert, W., Jr., *Nucl. Instrum. Meth.* **101**:343 (1972).
22. Schupferling, H. M., *Nucl. Instrum. Meth.* **123**:67 (1975).
23. Dakuba, T., and Gilboy, W. B., *Nucl. Instrum. Meth.* **150**:479 (1978).
24. Tabata, T., Ito, R., and Okabe, S., *Nucl. Instrum. Meth.* **94**:509 (1971).
25. Kuzminikh, V. A., and Vorobiev, S. A., *Nucl. Instrum. Meth.* **129**:561 (1975).
26. Tsoulfanidis, N., Wehring, B. W., and Wyman, M. E., *Nucl. Sci. Eng.* **43**:42 (1971).
27. Meyer, O., and Langmann, H. J., *Nucl. Instrum. Meth.* **39**:119 (1966).
28. Segré, E., *Nuclei and Particles*, Benjamin, New York, 1965, p. 348.
29. Van de Eijk, W., Oldenhof, W., and Zehner, W., *Nucl. Instrum. Meth.* **112**:343 (1973).
30. Lowenthal, G. C., and Wyllie, H. A., *Nucl. Instrum. Meth.* **112**:353 (1973).
31. Dobrilovic, L., and Simovic, M., *Nucl. Instrum. Meth.* **112**:359 (1973).
32. Adair, H. L., and Kuehn, P. R., *Nucl. Instrum. Meth.* **114**:327 (1974).
33. Wilkins, B. D., Fluss, M. J., Kaufman, S. B., Cross, C. E., and Steinberg, E. P., *Nucl. Instrum. Meth.* **92**:381 (1971).
34. Sullivan, W. J., and Wehring, B. W., *Nucl. Instrum. Meth.* **116**:29 (1974).
35. Caywood, J. M., Mead, C. A., and Mayer, J. W., *Nucl. Instrum. Meth.* **79**:329 (1970).
36. Haines, E. L., and Whitehead, A. B., *Rev. Sci. Instrum.* **37**:190 (1966).
37. Finch, E. C., and Rodgers, A. L., *Nucl. Instrum. Meth.* **113**:29 (1973).
38. Finch, E. C., *Nucl. Instrum. Meth.* **113**:41 (1973).
39. Lindhard, J., Scharff, M., and Schiott, H. E., *Fys. Medd.* **33**:1 (1963).
40. Moak, C. D., Dabbs, J. W. T., and Walker, W. W., *Rev. Sci. Instrum.* **1131**:37 (1966).
41. Britt, H. C., and Wegner, H. E., *Rev. Sci. Instrum.* **34**:274 (1963).
42. Schmitt, H. W., Kiker, W. E., and Williams, C. W., *Phys. Rev.* **137**:B837 (1965).
43. Schmitt, H. W., and Pleasonton, F., *Nucl. Instrum. Meth.* **40**:204 (1966).
44. Bucher, R. G., Ph.D. thesis, University of Illinois, 1975.
45. Long, A. B., Wehring, B. W., and Wyman, M. E., *Rev. Sci. Instrum.* **1566**:39 (1968).
46. Schmitt, H. W., Gibson, W. M., Neiler, J. H., Walter, F. J., and Thomas, T. D., *Proceedings of IAEA Conf. on the Physics and Chemistry of Fission*, **1**:531 (1965).
47. DiIorio, G. J., and Wehring, B. W., *Nucl. Instrum. Meth.* **147**:487 (1977).
48. Betts, R. R., *Nucl. Instrum. Meth.* **162**:531 (1979).
49. Pleyer, H., Kohlmeyer, B., Schneider, W. F. W., and Bock, R., *Nucl. Instrum. Meth.* **96**:363 (1971).
50. Zediman, B., Henning, W., and Kovar, D. G., *Nucl. Instrum. Meth.* **118**:361 (1974).
51. Gelbke, C. K., Hildenbrabd, K. D., and Bock, R., *Nucl. Instrum. Meth.* **95**:397 (1971).
52. Barrette, J., Braun-Munzinger, P., and Gelbke, C. K., *Nucl. Instrum. Meth.* **126**:181 (1975).
53. Dietz, E., Bass, R., Reiter, A., Friedland, V., and Hubert, B., *Nucl. Instrum. Meth.* **97**:581 (1971).
54. Schneider, W. F. W., Kohlmeyer, B., and Bock, R., *Nucl. Instrum. Meth.* **123**:93 (1975).
55. Pfeffer, W., Kohlmeyer, B., and Schneider, W. F. W., *Nucl. Instrum. Meth.* **107**:121 (1973).
56. Wiza, J. L., *Nucl. Instrum. Meth.* **162**:587 (1979).
57. Butler, G. W., Poskanzer, A. M., and Landis, D. A., *Nucl. Instrum. Meth.* **89**:189 (1970).
58. Goulding, F. S., and Harvey, B. G., *Annu. Rev. Nucl. Sci.* **25**:167 (1975).
59. Sykes, D. A., and Harris, S. J., *Nucl. Instrum. Meth.* **101**:423 (1972).
60. Bertoxzi, W., Hynes, M. V., Sargent, C. P., Turchinetz, W., and Williamson, C., *Nucl. Instrum. Meth.* **162**:211 (1979).
61. Fulbright, H. W., *Nucl. Instrum. Meth.* **162**:355 (1979).
62. Enge, H. A., *Nucl. Instrum. Meth.* **162**:161 (1979).
63. Laurent, H., and Schapira, J. P., *Nucl. Instrum. Meth.* **162**:181 (1979).
64. Mladjenovic, M. S., *Nucl. Instrum. Meth.* **162**:193 (1979).
65. Bartholomew, G. A., and Lee-Whiting, G. E., *Nucl. Instrum. Meth.* **162**:239 (1979).
66. Hughes, A. L., and Rojansky, V., *Phys. Rev.* **34**:284 (1929).
67. Rogers, F. T., Jr., *Rev. Sci. Instrum.* **8**:22 (1937).
68. Rogers, F. T., Jr., *Rev. Sci. Instrum.* **11**:19 (1939).

69. Rogers, F. T., Jr., *Rev. Sci. Instrum.* **14**:216 (1943).
70. Rogers, F. T., Jr., *Rev. Sci. Instrum.* **22**:723 (1951).
71. Laegsgaard, E., *Nucl. Instrum. Meth.* **162**:93 (1979).
72. Haase, E. L., Fawzi, M. A., Saylor, D. P., and Vellen, E., *Nucl. Instrum. Meth.* **97**:465 (1971).
73. Kalbitzer, S., Barer, R., Melzer, W., and Stumpfi, W., *Nucl. Instrum. Meth.* **54**:323 (1967).
74. Hofker, W. K., Oosthock, D. P., Hoeberechts, A. M. E., Van Dantzig, X., Mulder, K., Obserski, J. E. J., Koerts, L. A., Dieperink, J. H., Kok, E., and Rumphorst, R. F., *IEEE Trans.* **NS-13**(3):208 (1966).
75. Ford, J. L. C., Jr., *Nucl. Instrum. Meth.* **162**:277 (1979).
76. Charpak, G., *Nature* **270**:479 (1977).
77. Ball, G. C., *Nucl. Instrum. Meth.* **162**:263 (1979).
78. Allemond, R., Bourdel, J., Roudant, E., Convert, P., Ibel, K., Jacobe, J., Cotton, J. P., and Farnoux, B., *Nucl. Instrum. Meth.* **126**:29 (1975).
79. Beardsworth, E., Fischer, J., Iwata, S., Lavine, M. J., Rudeka, V., and Thorn, C. E., *Nucl. Instrum. Meth.* **127**:29 (1975).
80. Glussel, P., *Nucl. Instrum. Meth.* **140**:61 (1977).
81. Kitahara, T., and Isozumi, Y., *Nucl. Instrum. Meth.* **140**:263 (1977).
82. Fischer, J., Okuno, H., and Walenta, A. H., *Nucl. Instrum. Meth.* **151**:451 (1978).
83. Gustaldi, V., et al., *Nucl. Instrum. Meth.* **156**:297 (1978).
84. Lindgren, L. J., and Sandell, A., *Nucl. Instrum. Meth.* **219**:149 (1984).
85. Fuzesy, R. Z., Hadley, N. J., and Robrish, P. R., *Nucl. Instrum. Meth.* **223**:40 (1984).
86. Doll, P., Brady, F. P., Ford, T. D., Garrett, R., Krupp, H., and Klages, H. O., *Nucl. Instrum. Meth.* **270**:437 (1988).
87. Lacy, J. L., and Lindsey, R. S., *Nucl. Instrum. Meth.* **119**:483 (1974).
88. Bertozzi, W., Hynes, M. V., Sargent, C. P., Creswell, C., Dunn, P. C., Hirsch, A., Leitch, M., Norum, B., Rad, F. N., and Susanuma, T., *Nucl. Instrum. Meth.* **141**:457 (1977).
89. Breskin, A., Charpak, G., Gabioud, B., Sauli, F., Trantner, N., Duinker, W., and Schultz, G., *Nucl. Instrum. Meth.* **119**:9 (1974).
90. Alberi, J., Fischer, J., Radeka, V., Rogers, L. C., and Schoenborn, B., *Nucl. Instrum. Meth.* **127**:507 (1975).

CHAPTER
# FOURTEEN

# NEUTRON DETECTION AND SPECTROSCOPY

## 14.1 INTRODUCTION

Since neutrons do not directly ionize atoms, they are detected "indirectly" upon producing a charged particle or a photon, which is then recorded with the help of an appropriate detector. The charged particle or the photon is the result of a neutron interaction with a nucleus. If the mechanism of the interaction is known, information about the neutron can be extracted by studying the products of the reaction. Many types of interactions are used, divided into absorptive and scattering reactions.

Absorptive reactions are $(n, \alpha)$, $(n, p)$, $(n, \gamma)$, or $(n, \text{fission})$. In the case of an $(n, \gamma)$ reaction, the neutron may be detected through the interactions of the gamma emitted at the time of the capture, or it may be detected through the radiation emitted by the radioisotope produced after the neutron is captured. The radioisotope may emit $\beta^-$ or $\beta^+$ or $\gamma$ or a combination of them. By counting the activity of the isotope, information is obtained about the neutron flux that produced it. This is called the activation method. If the reaction is fission, two fission fragments are emitted; being heavy charged particles, these are detected easily.

The main scattering reaction used is neutron-proton collision, called the *proton-recoil method.* The knocked-out proton is the particle recorded.

With the exception of the proton-recoil method, which functions for fast neutrons only ($E_n > 1.0$ keV), all the other interactions can be used with neutrons of any energy. However, at every neutron energy, one method may be better than another. The best method will be selected based on the neutron

energy, the purpose of the experiment (is it number or energy of neutrons measured, or both?), and the physical constraints of the measurement (e.g., inside a reactor core or outside).

This chapter discusses in detail all the neutron detection methods mentioned above, as well as the Bragg crystal spectrometer, the time-of-flight method, compensated ion chambers, and self-powered neutron detectors (SPND). Other specialized neutron detectors, such as fission track recorders and thermoluminescent dosimeters, are described in Chap. 16.

## 14.2 NEUTRON DETECTION BY ($n$, CHARGED PARTICLE) REACTION

There are many nuclear reactions of the type ($n$, charged particle) used for neutron detection. In general, endothermic reactions are used for fast neutrons, and exothermic ones for thermal neutrons. The endothermic reactions will be discussed in Sec. 14.6.

The most useful exothermic reactions are listed in Table 14.1, along with their $Q$ values and the value of the cross section for thermal neutrons.

The charged particles from any one of the reactions of Table 14.1 share an amount of kinetic energy equal to $Q + E_n$, where $E_n$ is the neutron kinetic energy. The large $Q$ values make detection of the products very easy, regardless of the value of $E_n$, but at the same time make measurement of the energy of slow neutrons practically impossible. The neutron energy would be measured from the pulse height, which is proportional to $Q + E_n$. However, if the pulse corresponds to energy of the order of MeV (because of the $Q$ value), a small change in $E_n$ will produce a variation in the pulse that is undetectable. For example, the fractional change of a 1-MeV pulse due to 1-keV change in neutron kinetic energy is $(1.001 - 1.000)/1.000 = 0.1$ percent, which is less than the best energy resolution of alpha-particle detectors. Therefore, the measurement of neutron energy is possible only when $E_n$ amounts to a considerable fraction of the $Q$ value.

**Table 14.1 Exothermic Reactions Used for Neutron Detection**

| Reaction | Charged particles produced | $Q$ Value (MeV) | $\sigma$ (b) for $E_n = 0.025$ eV |
|---|---|---|---|
| ${}^{10}_{5}B(n, \alpha){}^{7}_{3}Li$ | $\alpha$, ${}^{7}Li$ | 2.78 | 3840 |
| ${}^{6}_{3}Li(n, \alpha){}^{3}_{1}H$ | $\alpha$, ${}^{3}H$ | 4.78 | 937 |
| ${}^{3}_{2}He(n, p){}^{3}_{1}H$ | $p$, ${}^{3}H$ | 0.765 | 5400 |

### 14.2.1 The $BF_3$ Counter

The $(n, \alpha)$ reaction with ${}^{10}_{5}B$ is probably the most useful reaction for the detection of thermal neutrons because

1. The reaction cross section is large.
2. The energy dependence of the cross section is of the $1/v$ type.
3. ${}^{10}_{5}B$ is a constituent of the compound $BF_3$, which may be used as the gas of a proportional gas counter.

The $BF_3$ counter is a proportional counter filled with $BF_3$ gas, usually enriched to more than 90 percent in ${}^{10}B$ (about 20 percent of natural boron is ${}^{10}B$; the rest is ${}^{11}B$). The $BF_3$ counter detects the alpha and the lithium particles produced by the reaction

$$ {}^{10}_{5}B + {}^{1}_{0}n \rightarrow {}^{4}_{2}\text{He} + {}^{7}_{3}\text{Li} + 2.78 \text{ MeV} $$

With thermal neutrons, the ${}^{7}Li$ nucleus is left in an excited state about 96 percent of the time. In that case, the $Q$ value of the reaction is 2.30 MeV and the ${}^{7}Li$ nucleus goes to the ground state by emitting a gamma with energy equal to $2.78 - 2.30 = 0.480$ MeV. This photon may also be used for the detection of the neutron.

The relationship between counting rate and neutron flux is derived as follows. Let

$n(E)\,dE$ = number of neutrons/m$^3$ with kinetic energy between $E$ and $E + dE$

$\phi(E)\,dE = v(E)n(E)\,dE$ = neutron flux consisting of neutrons with kinetic† energy between $E$ and $E + dE$

$v(E)$ = neutron speed for energy $E$ (m/s)

$E_m$ = upper limit of neutron energy considered

$N$ = number of ${}^{10}B$ atoms per unit volume

$V$ = volume of the counter

$\sigma(E) = \sigma(v)$ = cross section of the $(n, \alpha)$ reaction for neutron energy $E$

Assuming that the neutron flux is uniform over the detector volume, the reaction rate $R$ is given by

$$ R \text{ (reactions/s)} = VN\int_0^{E_m} \sigma(E)\phi(E)\,dE \tag{14.1} $$

The ${}^{10}B$ cross section has a $1/v$ dependence‡ over a wide range of neutron

†In Chap. 3, the symbol $T$ was used to denote kinetic energy. That was necessary because the discussion involved kinetic and total energy. In this chapter, $E$ is used for the kinetic energy of the neutron.

‡The ${}^{11}B$ cross section is quite different. Equation 14.2 represents only the ${}^{10}B$ cross section.

energies; i.e., it can be written as

$$\sigma(E) = \sigma_0 \frac{v_0}{v(E)} = \sigma_0 \sqrt{\frac{E_0}{E}} \tag{14.2}$$

where $\sigma_0$ is the cross section at some known speed $v_0 = \sqrt{2E_0/M}$, and $M$ is the neutron mass. If Eq. 14.2 is substituted into Eq. 14.1, the reaction rate takes the form

$$R = NV\sigma_0 v_0 n \text{ (reactions/s)} \tag{14.3}$$

where $n$ is the total number of neutrons per unit volume, or

$$n = \int_0^{E_m} n(E)\, dE \tag{14.4}$$

Equation 14.3 shows that the reaction is proportional to the total neutron density. $BF_3$ counters are most frequently used for the detection of thermal neutrons, for which one can calculate an average neutron speed $\bar{v}$ given by

$$\bar{v} = \frac{\int_0^{E_m} v(E)n(E)\, dE}{\int_0^{E_m} n(E)\, dE} \tag{14.5}$$

and a total flux $\phi$, given by

$$\phi = \int_0^{E_m} \phi(E)\, dE = \int_0^{E_m} v(E)n(E)\, dE \tag{14.6}$$

Under these conditions, Eq. 14.3 takes the form

$$R = NV\sigma_0 \frac{v_0}{\bar{v}} \phi \tag{14.7}$$

Thus, if $\bar{v}$ is known, the reaction rate is proportional to the total neutron flux $\phi$. For example, for the commonly encountered Maxwell-Boltzmann distribution of thermal neutrons, $\bar{v} = 2v_p/\sqrt{\pi}$, where $v_p$ is the most probable neutron speed.

The derivation of Eqs. 14.3 and 14.7 was based on the assumption that the neutron flux is uniform over the volume of the counter. A measure of the flux uniformity is the value of the factor $\exp(-\Sigma_t l)$, where

$\Sigma_t$ = total macroscopic cross section for the gas of the counter, averaged over all the neutron energies present

$l$ = a characteristic dimension of the counter (usually the diameter or the length of a cylindrical counter)

If $\exp(-\Sigma_t l) \approx 1$, the flux may be taken as uniform over the detector volume.

**Example 14.1** Consider a $BF_3$ counter with a diameter of 0.05 m ($\simeq$ 2 in) and length 0.30 m ($\simeq$ 12 in) filled with $BF_3$ gas, 96 percent enriched to $^{10}B$, at a

pressure of 1 atm and used for the detection of 0.0253 eV neutrons. Should the user take into account flux depression in the counter?

**Answer** The factor $\exp(-\Sigma_t l)$ should be calculated. For the worst case, consider $l$ = length of the counter. The total macroscopic cross section is

$$\Sigma_t = N(BF_3)[0.96\sigma(^{10}B) + 0.04\sigma(^{11}B) + 3\sigma(F)]$$
$$\approx \frac{0.6022}{22{,}400}(0.96)(3840) = 0.0991 \text{ cm}^{-1} = 9.91 \text{ m}^{-1}$$

For the calculation of $\Sigma_t$, the cross sections of $^{11}B$ and F were neglected because they are much smaller than that of $^{10}B$. The "depression factor" is

$$\exp(-\Sigma_t l) = \exp[(-9.91)(0.30)] = \exp(-2.97) = 0.05$$

If $l$ is the diameter of the counter, then

$$\exp(-\Sigma_t l) = \exp[(-9.91)(0.05)] = \exp(-0.496) = 0.61$$

One concludes that flux depression is considerable in this case, and the flux cannot be taken as uniform over the counter volume.

If the $BF_3$ counter is used for the detection of a polyenergetic neutron spectrum, instead of a monoenergetic neutron source, average cross sections should be used for the calculation (Section 4.9.4 explains how average cross sections are obtained).

As a first approximation, the efficiency of a $BF_3$ counter is equal to

$$\epsilon = \frac{\Sigma_a}{\Sigma_t}[1 - \exp(-\Sigma_t l)][\exp(-\Sigma_t^w t_w)] \tag{14.8}$$

where $\Sigma_t$ and $\Sigma_a$ are total and absorptive neutron macroscopic cross sections, respectively, for $BF_3$, and $l$ is the dimension of the counter parallel to the direction of the neutron beam. $\Sigma_t^w$ and $t_w$ are the total macroscopic cross section and thickness, respectively, for the material of which the wall or the front window of the counter is made. Equation 14.8 was derived under the assumptions that

1. All neutrons travel the same distance inside the counter (parallel beam).
2. Every neutron interaction in the wall or the front window of the counter removes the neutron from the beam.

**Example 14.2** What is the efficiency of a $BF_3$ counter enriched to 96 percent in $^{10}B$, 0.04 m (1.57 in) in diameter, 0.30 m ($\sim$ 12 in) long, for a parallel beam of 1-eV neutrons? The $BF_3$ pressure in the counter is 53,329 Pa (40 cmHg). Consider two cases:

(a) The beam is directed parallel to the axis of the counter.
(b) The beam is perpendicular to the axis of the counter.

Assume that the wall and the window of the counter are made of aluminum and are 2 mm thick. Take the total neutron cross section for Al at 1 eV to be 1.5 b.

**Answer** Equation 14.8 will be used. At 1 eV for $BF_3$ enriched to 96 percent to $^{10}B$, $\Sigma_a \approx \Sigma_t \approx \Sigma_a\ (^{10}B)$. To find the microscopic cross section at 1 eV, use Eq. 14.2 and the value of $\sigma_a = 3840$ b at $E_n = 0.025$ eV.

$$\sigma_a(1\text{ eV}) = 3840\frac{v_0(0.025\text{ eV})}{v(1\text{ eV})} = 3840\sqrt{\frac{0.025}{1}} = 607\text{ b}$$

$$\Sigma_a = 0.96\left(\frac{53{,}329}{101{,}325}\right)\left(\frac{0.6022}{22{,}400}\right)(607) = 0.0082\text{ cm}^{-1} = 0.82\text{ m}^{-1}$$

For aluminum,

$$\Sigma_t^w t_w = 1.5(2.7)\left(\frac{0.6022}{27}\right)(0.2) = 0.018$$

(a) If the beam is parallel to the counter axis, $l = 0.30$ m and

$$\epsilon = [1 - \exp(\Sigma_a l)][\exp(-\Sigma_t^w t_w)] = (0.18)(0.982) = 0.214 = 21.4\%$$

(b) If the beam is perpendicular to the axis, all the neutrons do not travel the same distance inside the cylindrical counter. Assuming that the incident neutrons form a narrow beam that hits the counter at the center, $l =$ diameter $= 0.04$ m. Then,

$$\epsilon = \{1 - \exp[(-0.82)(0.04)]\}(0.982) = (0.032)(0.982) = 0.032 = 3.2\%$$

The specifications of commercial $BF_3$ counters consist of sensitivity, dimensions, composition of the filling gas, operating voltage, and maximum operating temperature.

The sensitivity $S$ is defined as the ratio

$$S = \frac{\text{true net counting rate}}{\text{neutron flux}} = \frac{r}{\phi} \tag{14.9}$$

and is given in terms of counts/s per neutron/(m$^2$ s). The parameters affecting the sensitivity can be seen by noting that

$$r = \epsilon_p R = g - b \tag{14.10}$$

where $\epsilon_p$ = efficiency of the counter for detection of the charged particles produced
$b$ = background counting rate
$g$ = gross counting rate
$R$ = reaction rate given by Eq. 14.7

Since the charged particles are generated inside the volume of the detector, the efficiency $\epsilon_p$ is practically equal to 1. Also, the background rate may be made negligible because the pulses produced by the charged particles are well above

the electronic noise. Thus, a proper discriminator level may be set to eliminate almost all the background. Under these conditions, $R = g$ and the equation for the sensitivity becomes

$$S = \frac{R}{\phi} = NV\sigma_0 \frac{v_0}{\bar{v}} \tag{14.11}$$

Equation 14.11 indicates that for a certain neutron spectrum, the sensitivity is proportional to boron density (i.e., pressure of the $BF_3$ gas) and volume of the counter.

The number of boron atoms decreases with exposure, and so does the sensitivity. The decrease is expressed by a factor having the form

$$\exp(-\sigma_a \phi t)$$

where $\phi t$ in neutrons/m$^2$ is the fluence to which the counter was exposed. Since the average value of $\sigma_a$ for thermal neutrons reacting with $^{10}B$ is of the order of $10^{-25}$ m$^2$ (1000 b), the fluence necessary to cause an appreciable change in sensitivity is of the order of $10^{25}$ neutrons/m$^2$.

Typical specifications of commercial counters are the following.

*Sensitivity:* 5 counts per second per n/(cm$^2$ s)
*Dimensions:* Almost any dimensions
*Pressure of* $BF_3$: From a little less than 1 to about 2 atm (202 kPa). An increase in pressure requires an increase in the operating voltage.
*Operating voltage:* $BF_3$ counters show an almost flat plateau (see Chap. 5) extending over 1000 V or more. Typical operating voltages range from 1000 to 3000 V.
*Temperature:* Maximum operating temperature is about 100°C.

### 14.2.2 Boron-Lined Counters

Boron-lined counters are gas-filled proportional counters that employ the same reaction as the $BF_3$ counter, except that the $^{10}B$ is coated on the walls of the counter. Since the $(n, \alpha)$ reactions take place in a thin layer close to the wall (Fig. 14.1), only one of the two particles has a chance of entering the sensitive volume of the counter and producing a pulse; the other stops in the wall. The sensitivity increases with the thickness of the $^{10}B$ coating. That thickness,

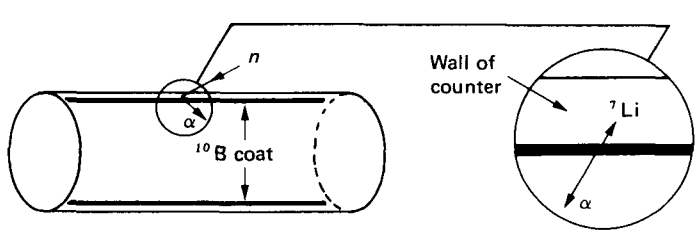


**Figure 14.1** A $^{10}B$-lined counter.

however, cannot exceed the range of the alphas produced. The advantage of boron-lined over the $BF_3$ counters is the flexibility of using a gas more appropriate than $BF_3$. Then the operating voltage is less and the counter is less sensitive to gamma rays. For this reason, boron-lined counters may be used to detect neutrons in intense gamma fields.

Both $BF_3$ and boron-lined counters are mainly used for the measurement of the number (not energy) of thermal neutrons.

### 14.2.3 $^6$Li Counters

Neutron detection by $^6$Li is based on the reaction

$$^6_3\text{Li} + ^1_0n \rightarrow ^4_2\text{He} + ^3_1\text{H} + 4.78\ \text{MeV}$$

The cross section for this reaction is of the $1/v$ type up to 10 keV, with a value of 937 b at 0.025 eV. Lithium is used either as LiF or as the component of a scintillator.

A neutron spectrometer based on LiF[1] consists of a thin slice of $^6$LiF ($\sim 30 \times 10^{-5}$ kg/m$^2$ = 30 $\mu$g/cm$^2$) sandwiched between two surface-barrier silicon detectors. When neutrons strike the LiF, charged-particle pairs ($^4$He–$^3$H) are produced and are detected simultaneously by the two detectors. The pulses from the detectors are amplified and then summed to produce a single pulse, which is proportional to the energy of the neutron plus the $Q$ value of the reaction.

There are many inorganic scintillators based on lithium. $^6$LiI(Eu) has been used for neutron energy measurements from 1 to 14 MeV with 10 percent energy resolution.[2] It has good efficiency for low-energy neutrons, but activation of iodine creates some problems. The most widely used lithium scintillator was developed by Ginther and Schulman[3] and Voitovetskii et al.[4] It is a cerium-activated scintillating glass containing $Li_2O$. The proportion of the cerium activator affects the efficiency of luminescence. A series of measurements of many properties of commercially available glasses has been reported recently by Spowart.[5,6] Today one can buy these glasses in a large variety of thicknesses (0.5–25 mm), sizes (up to 125 mm in diameter), Li contents (up to 11 percent), and $^6$Li enrichments (up to 95 percent). The efficiency of $^6$Li glass as a function of neutron energy is shown in Fig. 14.2.

To increase the efficiency, $^6$Li glass scintillators with thickness about 13 mm and diameter 110 mm have been optically coupled to one or more photomultiplier tubes through light pipes.[8,9] To avoid moderation of the incident neutrons, the light pipe should not contain hydrogenous material. One problem with such thick scintillators is considerable scattering of the incident neutrons. The scattered neutrons add an exponential tail to the primary neutron signal, a tail that should be included in the time resolution function of the instrument in time-of-flight measurements.

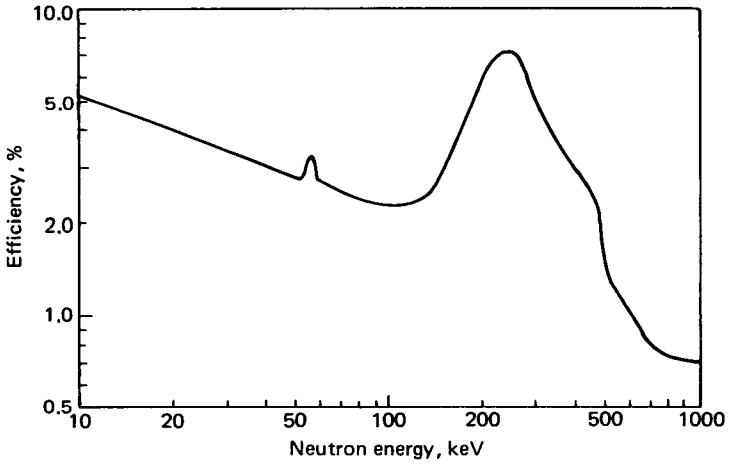


**Figure 14.2** The efficiency of $^6$Li glass as a function of neutron energy, with glass thickness 12.7 mm (from Ref. 7).

A different type of arrangement, using a $^6$LiI(Eu) scintillator to detect the neutrons after they are moderated, is the *Bonner* ball (or sphere).[10,11] Using the Bonner ball, neutrons are detected by a $^6$LiI(Eu) scintillator, a $BF_3$ tube, or an $^3$He counter placed at the center of polyethylene spheres with sizes ranging from 51 to 305 mm (2–12 in) in diameter. Using the Bonner sphere, the neutron energy is determined on the basis of the difference in moderating efficiency for the spheres of different sizes. Because the Bonner sphere is primarily used as a neutron dosimeter, it is discussed in more detail in Chap. 16.

### 14.2.4 $^3$He Counters

Neutron detection by $^3$He is based on the reaction

$$^3_2\text{He} + ^1_0n \rightarrow ^1_1\text{H} + ^3_1\text{H} + 765 \text{ keV}$$

The cross section for this reaction is quite high for thermal neutrons (5400 b at 0.025 eV) and varies as $1/v$ from 0.001 eV to 0.04 eV.

One type of helium neutron spectrometer consists of two surface-barrier silicon detectors facing each other, with the space between them filled with helium at a pressure of a few atmospheres (this is similar to the $^6$LiF spectrometer described in Sec. 14.2.3).

Proportional counters filled with $^3$He are widely used, especially in time-of-flight measurements (see Sec. 14.8). The efficiency of the counter can be increased by increasing the pressure. Figure 14.3 shows the efficiency of a $^3$He counter as a function of neutron energy for three different pressures. One of the problems of $^3$He counters is the *wall effect*. If the reaction takes place close to

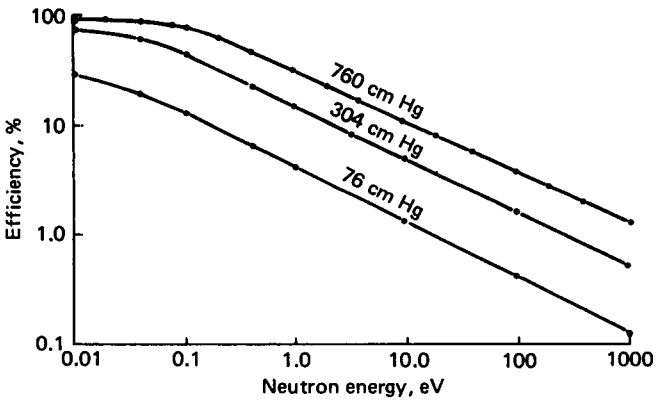


**Figure 14.3** Efficiency of $^3$He-filled proportional counter as a function of neutron energy.

the wall of the counter, there is a high probability that only a fraction of the charged-particle energy will be deposited in the counter. As a result, smaller size pulses are produced which do not come under the main peak. There are two ways to overcome this effect. One is to use a large-diameter counter, in which case the fraction of reactions occurring near the wall is smaller. The other is to increase the stopping power of the gas. Increase in stopping power is achieved either by increasing the pressure of the gas or by adding a small fraction of another gas, such as krypton, with a higher stopping power. Increase in stopping power is accompanied, however, by an increase in gamma sensitivity and a decrease in pulse risetime. Fast risetime is important for time-of-flight measurements.

The pressure of the gas and the operating voltage are higher in $^3$He than in $BF_3$ counters. The pressure of the $^3$He is usually between 404 and 1010 kPa (4–10 atm), and the operating voltage is 3000–5000 V.

## 14.3 FISSION CHAMBERS

Fission chambers are gas counters that detect the fragments produced by fission. The fission fragments, being massive charged particles with $Z \approx +20e$ and kinetic energy 60–100 MeV, have a short range even in a gas. They produce such an intense ionization that gas multiplication is not necessary. Thus, fission chambers operate in the ionization region.

In the most common type of fission counter, the interior surface of the detector is coated with a fissile isotope (Fig. 14.4). When fission takes place, one of the fission fragments (denoted as $FF_1$ in Fig. 14.4) is emitted toward the center of the counter and is detected. The other ($FF_2$) stops in the fissile deposit or the wall of the counter. The counting rate of a fission counter is proportional

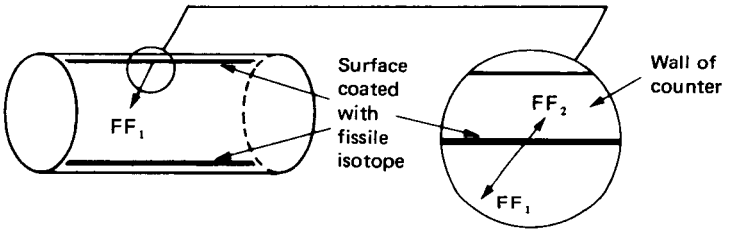


**Figure 14.4** A fission counter.

to the fission rate, which in turn, is proportional to the neutron flux. The relationship among these three quantities is similar to the equations given for the $BF_3$ counter.

For relative measurements, the thickness of the fissile material coating is not very critical except that it should be less than the range of the fission fragments. For absolute measurement, however—i.e., measurements for which every fission should be detected—at least one fission fragment from each fission should produce a recorded pulse. To achieve this, the thickness of the coating must be limited so that fission fragments being produced anywhere in the layer of the fissile material generate a pulse larger than that of alphas, betas, or gammas, which are always present.† Pulses from gammas present a problem only when the counter is used in an extremely intense gamma field. Pulses from alphas, however, are always present and should be discriminated from those of fission fragments. Fortunately, the difference between the ionization produced by alphas and that produced by fission fragments is so large that such discrimination is easy. Figure 14.5 shows a typical integral pulse-height spectrum. Notice that the alpha pulses start at such a low level that a discriminator level can be set to cut them off.

Fission counters may be used for detection of either fast or thermal neutrons. If the counter wall is coated with $^{235}U$, essentially only thermal neutrons are detected because the $^{235}U$ fission cross section for thermal neutrons is about 500 times higher than that of fast neutrons. If the counter is coated with $^{238}U$ or $^{232}Th$, only fast neutrons with kinetic energy greater than 1 MeV are detected because the fission cross section of these isotopes has a threshold at about that energy.

Fission counters are used for detection of the number and not the energy of neutrons. They can be used, however, for differentiation of thermal and fast-neutron flux by using a combination of $^{235}U$- and $^{238}U$-coated counters (see also Sec. 14.6).

The sensitivity of a fission counter decreases with exposure because of the depletion of the fissile isotope (the same phenomenon as depletion of boron

†All fissile isotopes emit alpha particles. Betas and gammas may be emitted either by the fissile isotope or by fission fragments.

atoms—see Sec. 14.2.1). The decrease in sensitivity may be halted, to a certain extent, if the counter wall is coated with a mixture of fertile and fissile materials. One such combination is 90 percent $^{234}U$ and 10 percent $^{235}U$. The $^{235}U$ is partially replenished with new atoms produced by neutron capture in $^{234}U$. A $^{235}U$–$^{238}U$ combination will have a similar effect, thanks to $^{239}Pu$ produced as a result of neutron capture in $^{238}U$.

Fission counters are used extensively for both out-of-core and in-core measurements of neutron flux in nuclear flux in nuclear reactors. In out-of-core situations, they monitor the neutron population during the early stages of power ascension when the neutron flux level is very low. For in-core measurements, fission counters are used for flux mapping (and consequently, determination of the core power distribution). They are manufactured as long thin cylindrical probes that can be driven in and out of the core with the reactor in power. Typical commercial fission counters for in-core use have diameters of about 1.5 mm (0.06 in), use uranium enriched to at least 90 percent in $^{235}U$ as the sensitive material, and can be used to measure neutron fluxes up to $10^{18}$ neutrons/(m$^2$ · s) [$10^{14}$ neutrons/(cm$^2$ s)].

Another method of measuring fission rates is by using fission track detectors, as discussed in Sec. 16.9.3.

## 14.4 NEUTRON DETECTION BY FOIL ACTIVATION

### 14.4.1 Basic Equations

Neutron detection by foil activation is based on the creation of a radioisotope by neutron capture, and subsequent counting of the radiation emitted by that radioisotope. Foil activation is important not only for neutron flux measurements but also for neutron activation analysis, which is the subject of Chap. 15. This section presents the basic equations involved.

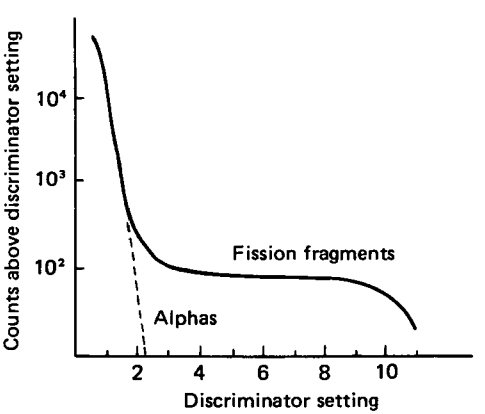


**Figure 14.5** An integral pulse-height spectrum taken with a fission counter.

Consider a target being irradiated in a neutron flux $\phi(E)$, where

$\sigma_i(E)$ = neutron absorption cross section of isotope $A_i$ at neutron energy $E$

$\lambda_{i+1}$ = decay constant of isotope with atomic mass number $A_i + 1(A_{i+1})$

$\sigma_{i+1}(E)$ = neutron absorption cross section of isotope $A_{i+1}$ at neutron energy $E$

$N_i(t)$ = number of atoms of nuclide with atomic mass number $A_i$, present at time $t$

$m$ = mass of target (normally this is the mass of the element whose isotope $A_i$ captures the neutron)

$a_i$ = weight fraction in the sample of isotope $A_i$

As a result of neutron absorption, the following processes take place:

1. Target atoms of atomic mass number $A_i$ are destroyed.
2. Atoms with atomic mass number $A_{i+1}$ are produced.
3. Atoms of type $A_{i+1}$ decay.
4. Atoms of type $A_{i+1}$ may be destroyed by absorbing a neutron.

For the target isotope (${}^{A_i}_{Z_i}\mathrm{X}$), the reaction involved is

$$ {}^{A_i}_{Z_i}\mathrm{X} + n \rightarrow {}^{A_{i+1}}_{Z_i}\mathrm{X} $$

The destruction of these atoms proceeds according to the equation

$$ -\frac{dN_i(t)}{dt} = N_i(t)\int_0^\infty dE\, \sigma_i(E)\phi(E) \tag{14.12} $$

In Eq. 14.12 and all others in this section, it is assumed that the presence of the target does not disturb the flux; i.e., the foil does not cause depression of the flux. Corrections that take into account foil self-absorption can be found in Chap. 11 in Beckurts and Wirtz and in Ref. 12. The integral over energy in Eq. 14.12 is usually expressed as

$$ \int_0^\infty dE\, \sigma_i(E)\phi(E) = \bar{\sigma}_i\int_0^\infty \phi(E)\, dE = \bar{\sigma}_i\phi = \sigma_i\phi \tag{14.13} $$

That is, an average cross section is used, even though the overbar that indicates averaging is normally dropped. From now on, Eq. 14.13 will be used without the overbar, but the reader should keep in mind that $\sigma$ is an average over the neutron energy spectrum.

The solution of Eq. 14.12 is, using Eq. 14.13,

$$ N_i(t) = N_i(0)e^{-\sigma_i\phi t} \tag{14.14} $$

where

$$ N_i(0) = \frac{a_i m N_A}{A_i} = \text{number of atoms of isotope } A_i \text{ at } t = 0 $$

The net production of the $A_{i+1}$ isotope is expressed by

$$\frac{dN_{i+1}(t)}{dt} = \text{production-destruction-decay}$$

or

$$\frac{dN_{i+1}(t)}{dt} = N_i(t)\sigma_i\phi - N_{i+1}(t)\sigma_{i+1}\phi - \lambda_{i+1}N_{i+1}(t) \tag{14.15}$$

With initial condition $N_{i+1}(t) = 0$, the solution of Eq. 14.15 is

$$N_{i+1}(t) = \frac{\sigma_i N_i(0)\phi}{\lambda_{i+1} + \sigma_{i+1}\phi - \sigma_i\phi}\{\exp(-\sigma_i\phi t) - \exp[-(\lambda_{i+1} + \sigma_{i+1}\phi)t]\} \tag{14.16}$$

The activity of this target, $A_{i+1}(t)$, is, after irradiation for time $t$,

$$A_{i+1}(t) = N_{i+1}(t)\lambda_{i+1} = \frac{\sigma_i N_i(0)\phi}{1 + (\sigma_{i+1} - \sigma_i)\phi/\lambda_{i+1}}\{\exp(-\sigma_i\phi t) - \exp[-(\lambda_{i+1} + \sigma_{i+1}\phi)t]\} \tag{14.17}$$

Equation 14.17 refers to the most general case. In practice, targets are selected in such a way that

1. The fraction of target nuclei destroyed is negligible, i.e., $\sigma_i\phi t \ll 1$.
2. The radioisotope produced has a neutron absorption cross section such that $\lambda_{i+1} \gg \sigma_{i+1}\phi$.

If conditions (1) and (2) are met, Eq. 14.17 takes the form

$$A_{i+1}(t) = \sigma_i N_i(0)\phi[1 - \exp(-\lambda_{i+1}t)] \tag{14.18}$$

which is the more familiar form of the activity or activation equation.

If one plots activity as a function of irradiation time, the result is Fig. 14.6. Two regions are observed.

1. For irradiation times that are short compared to the half-life of the radioisotope produced, the activity increases linearly with time. Indeed, if $\lambda_{i+1}t \ll 1$, then $e^{-\lambda_{i+1}t} \approx 1 - \lambda_{i+1}t$ and

$$A_{i+1}(t) \approx \sigma_i N_i(0)\phi\lambda_{i+1}t = \sigma_i N_i(0)\phi\frac{\ln 2}{T_{i+1}}t$$

   where $T_{i+1}$ is the half-life of the isotope produced.
2. For irradiation times many times longer than the half-life of the radioisotope, the activity reaches a saturation value ($A_s$). Theoretically, the saturation activity

$$A_s = \sigma_i N_i(0)\phi \tag{14.19}$$

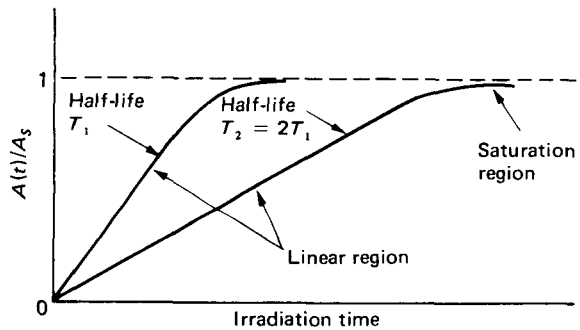


**Figure 14.6** Activity versus irradiation time (shown as a fraction of saturation activity).

is reached for $t = \infty$. In practice, the activity produced is taken as equal to $A_s$ for $t \approx 6$–$7$ half-lives.

Table 14.2 gives the fraction of saturation activity produced for several irradiation times.

**Example 14.3** The isotope $^{197}$Au is irradiated in a thermal neutron flux of $10^{18}$ neutrons/(m$^2 \cdot$ s). The cross section for neutron capture is 99 b, and the half-life of the radioactive $^{198}$Au produced is 2.7 days. (a) How long does the sample have to be irradiated for 0.1 percent of the target atoms to be destroyed? (b) What is the irradiation time necessary to produce 95 percent of saturation activity? (c) If the mass of the sample is $4 \times 10^{-6}$ kg, what is the irradiation time necessary to produce $7.4 \times 10^4$ Bq (2 $\mu$Ci) of activity?

**Answer**

(a) Using Eq. 14.14,

$$\frac{N(t)}{N(0)} = 0.999 = e^{-\sigma\phi t} \quad \text{or} \quad t = \frac{1}{\sigma\phi} \ln \frac{1}{0.999}$$

$$t = \frac{1}{(99 \times 10^{-28})10^{18}} \ln \frac{1}{0.999} = 1.01 \times 10^5 \text{ s} = 28 \text{ h}$$

**Table 14.2 Fraction of Saturation Activity Produced as a Function of Irradiation Time**

| Irradiation time (in half-lives) | $A_{i+1}(t)/A_s$ |
|---|---|
| 4 | 0.937 |
| 5 | 0.969 |
| 6 | 0.984 |
| 7 | 0.992 |
| 8 | 0.996 |

(b) Using Eq. 14.18, the irradiation time $t$ should be such that $1 - \exp(-\lambda t) = 0.95$ or

$$t = \frac{T}{\ln 2} \ln\left(\frac{1}{1 - 0.95}\right) = 11.67 \text{ days}$$

(c) Using Eq. 14.18,

$$A(t) = \sigma N(0)\phi(1 - e^{-\lambda t}) = \sigma m \frac{N_A}{A} \phi(1 - e^{\lambda t})$$

It is useful to evaluate $A_s$ first, because if $A_s$ is less than the activity desired, it is impossible to obtain such activity under the conditions given.

The saturation activity is

$$A_s = \sigma m \frac{N_A}{A} \phi = (99 \times 10^{-28})(4 \times 10^{-6}) \frac{0.6022 \times 10^{24}}{197 \times 10^{-3}} \times 10^{18}$$
$$= 1.21 \times 10^{11} \text{ Bq}$$

In this example, $A_s$ is greater than $A(t)$ and the required irradiation time $t$ is

$$t = -\frac{T}{\ln 2} \ln\left[1 - \frac{A(t)}{A_s}\right] = -\frac{2.7 \text{ days}}{\ln 2} \ln\left(1 - \frac{7.4 \times 10^4}{1.21 \times 10^{11}}\right) = 0.21 \text{ s}$$

### 14.4.2 Determination of the Neutron Flux by Counting the Foil Activity

As shown in Eq. 14.18, the activity of the irradiated foil is proportional to the neutron flux. Determination of the flux requires measurement of the activity, a task accomplished as follows.

Let the irradiation time be $t_0$. In practice, counting of the foil starts some time after irradiation stops, and it is customary to consider the end of irradiation as time $t = 0$ (Fig. 14.7). At time $t$ after irradiation stops, the activity is, using Eq. 14.18,

$$A_{i+1}(t) = N_i(0)\sigma_i\phi[1 - \exp(-\lambda_{i+1}t_0)]e^{-\lambda_{i+1}t} \tag{14.20}$$

If the sample is counted between $t_1$ and $t_2$, the number of disintegrations in that

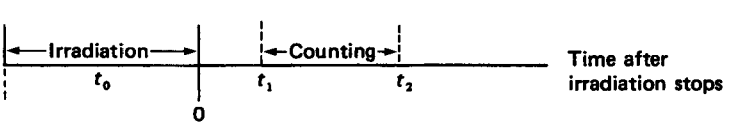


**Figure 14.7** Timescale for counting an irradiated sample. Time $t = 0$ coincides with the end of the irradiation period.

period is

$$D(t_1, t_2) = \int_{t_1}^{t_2} A_{i+1}(t)\, dt = \frac{N_i(0)\sigma_i\phi}{\lambda_{i+1}}[1 - \exp(-\lambda_{i+1}t_0)](e^{-\lambda_{i+1}t_1} - e^{-\lambda_{i+1}t_2}) \tag{14.21}$$

Assuming that one counts particles with energy $E_k$ for which $e_k$ is the probability of emission per decay, and the counting system is such that

$\epsilon_k$ = the efficiency of the detection of particles with energy $E_k$
$\Omega$ = solid angle
$B$ = background counts recorded in time $T = t_2 - t_1$

then the gross counts recorded, $G_k$, will be

$$G_k = \epsilon_k e_k F\Omega \frac{N_i(0)\sigma_i\phi}{\lambda_{i+1}}[1 - \exp(-\lambda_{i+1}t_0)](e^{-\lambda_{i+1}t_1} - e^{-\lambda_{i+1}t_2}) + B \tag{14.22}$$

The factor $F$ in Eq. 14.22 takes into account any other corrections (i.e., backscattering, foil self-absorption) that may be necessary (see Sec. 8.3). If dead-time correction is necessary, it should be applied to $G_k$.

The flux $\phi$ is determined from Eq. 14.22 if all the other factors are known. There are two types of factors in Eq. 14.22:

1. Factors that depend on the sample $[N_i(0), \sigma_i, \lambda_{i+1}, e_k]$, which are assumed to be known with negligible error
2. Factors that depend on the counting system $(\epsilon, F, \Omega, B)$, which are the main sources of error

To determine the flux distribution only, not the absolute value of the flux, foils are placed at known positions $x_j$ and are irradiated for a time $t_0$. The foils are then counted using the same detector. At any point $x_j$, the flux may be written as

$$\phi(x_j) = \frac{L[G_k(x_j) - B_j]}{m_j C_j} \tag{14.23}$$

where the subscript $j$ indicates position of the foil and

$$m_j = \text{mass of foil at position } j$$

$$C_j = [\exp(-\lambda_{i+1}t_1) - \exp(-\lambda_{i+1}t_2)]_j$$

$$L = \lambda_{i+1}\left(\epsilon_k e_k F\Omega \frac{N_A}{A_i}[1 - \exp(-\lambda_{i+1}t_0)]\right)^{-1}$$

($L$ includes all the factors that are common to all the foils.)

The title of this section includes the word *foil* because the sample to be irradiated is used in the form of a thin foil of the order of 1 mm thick or less. The mass of the foil is only a few milligrams. Small thin foils are used because

1. A thick sample will absorb so many neutrons that the radiation field will be perturbed and the measurement will not give the correct flux.
2. A thick sample will cause a depression of the flux in its interior. In such a case, correction factors will have to be applied to all the equations of this section that contain the flux $\phi$.
3. If the radioisotope emits $\beta$ particles, increased thickness will not necessarily increase the counting rate, because only particles emitted close to the surface within a thickness less than the range will leave the target and have a chance to be recorded.
4. There is no purpose in producing more activity than is necessary.

Foil activation may be used for detection of the number of either fast or thermal neutrons. The use of foils for fast-neutron energy measurements is discussed in Sec. 14.6. Foil activation is not used generally for measurement of the energy of thermal neutrons.

## 14.5 MEASUREMENT OF A NEUTRON ENERGY SPECTRUM BY PROTON RECOIL

Detection of neutrons by proton recoil is based on collisions of neutrons with protons and subsequent detection of the moving proton. Since neutrons and protons have approximately the same mass, a neutron may, in one collision, transfer all its kinetic energy to the proton. However, there is a possibility that the struck proton may have any energy between zero and the maximum possible, as a result of which the relationship between a neutron energy spectrum and a pulse-height distribution of the struck protons is not simple. It is the objective of this section to derive a general expression for this relationship. The sections that follow show its application for specific detectors.

Consider the case of a neutron with kinetic energy $E_n$ colliding with a proton at rest (Fig. 14.8). To calculate the proton kinetic energy after the collision, one must apply the equations of conservation of energy and linear momentum (Eqs. 3.81–3.83) using $Q = 0$ and $M_n = M_p$. The result for $E_p$, the proton kinetic energy as a function of the recoil angle $\theta$, is

$$E_p = E_n \cos^2 \theta \tag{14.24}$$

In a neutron-proton collision, the maximum value of angle $\theta$ is 90°, and the minimum 0°; therefore, the limits of the proton energy are $0 \leq E_p \leq E_n$. For neutron energies up to about 14 MeV, the $(n - p)$ collision is isotropic in the center-of-mass system; as a consequence, there is an equal probability for the

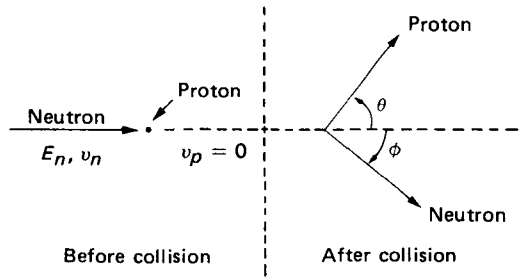


**Figure 14.8** Neutron-proton collision kinematics.

proton to have any energy between zero and $E_n$ in the laboratory system. That is, if $p(E)\,dE$ is the probability that the proton energy is between $E$ and $E + dE$, after the collision, then

$$p(E)\,dE = \frac{dE}{E_n} \tag{14.25}$$

The function $p(E)$ is shown in Fig. 14.9. What is important for the observer is not $p(E)$ but the proton pulse-height distribution produced by the detector. The relationship between the pulse-height distribution and the neutron spectrum is derived as follows. Let

$\phi(E_n)\,dE_n$ = neutron energy spectrum = flux of neutrons with energy between $E_n$ and $E_n + dE_n$

$N(E_p)\,dE_p$ = proton recoil energy spectrum = number of protons produced (by collisions with neutrons) with energy between $E_p$ and $E_p + dE_p$

$R(E, E_p)\,dE$ = response function of the detector = probability that a proton of energy $E_p$ will be recorded as having energy between $E$ and $E + dE$ (defined before in Sec. 11.5)

$M(E)\,dE$ = measured spectrum = number of protons measured with energy between $E$ and $E + dE$

The measured spectrum $M(E)$ is the pulse-height distribution in energy scale. The response function $R(E, E_p)$ takes into account the finite energy

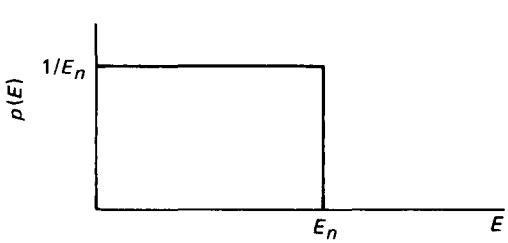


**Figure 14.9** The proton energy distribution after a $(n, p)$ collision that is isotropic in the center of mass system of the two particles.

resolution of the detector and the relationship between energy deposition and pulse height.

Assuming isotropic scattering in the center of mass system, the proton energy spectrum is

$$N(E_p)\,dE_p = N_H T \int_0^{E_{\max}} \sigma(E_n)\phi(E_n)\,dE_n \frac{dE_p}{E_n} H(E_n - E_p) \tag{14.26}$$

where $N_H$ = number of hydrogen atoms exposed to the neutron beam
$T$ = time of measurement of the recoil protons
$H(E_n - E_p)$ = step function; $H(E_n - E_p) = 1 | E_n \geq E_p$, zero otherwise
$\sigma(E_n)$ = elastic scattering cross section for $(n, p)$ collisions

The measured energy spectrum is then given by

$$M(E)\,dE = \int_0^{E_{\max}} dE\, R(E, E_p) N(E_p)\,dE_p \tag{14.27}$$

In Eqs. 14.26 and 14.27, the energy $E_{\max}$ is the upper limit of the neutron energy spectrum. Equation 14.27 may be rewritten in the form

$$M(E) = \int_0^{E_{\max}} dE_n\, k(E, E_n)\phi(E_n) \tag{14.28}$$

where

$$k(E, E_n) = \int_0^{E_{\max}} dE_p R(E, E_p) N_H T \frac{\sigma(E_n)}{E_n} H(E_n - E_p) \tag{14.29}$$

Equation 14.28 has the form of the folding integral (see also Sec. 11.5), while Eq. 14.29 gives the "composite" response function for the proton recoil spectrometer.

**Example 14.4** As a first application of Eq. 14.28, consider the case of a monoenergetic neutron spectrum and a detector with a Gaussian response function. What is the measured spectrum?

**Answer** Substituting the Gaussian response function

$$R(E, E_p) = \frac{1}{\sqrt{2\pi}\,\sigma} \exp\left[-\frac{(E - E_p)^2}{2\sigma^2}\right]$$

into Eq. 14.29 and performing the integration, assuming $E/\sigma \gg 1$, one obtains†

$$k(E, E_n) = \frac{N_H T \sigma(E_n)}{2E_n}\left[1 + \operatorname{erf}\left(\frac{E_n - E}{\sqrt{2}\,\sigma}\right)\right]$$

†There are two $\sigma$'s involved here: $\sigma(E)$ is the cross section at energy $E$; $\sigma$ without an argument is the standard deviation of the Gaussian.

where

$$\operatorname{erf}\left(\frac{x}{\sqrt{2}}\right) = \sqrt{\frac{2}{\pi}} \int_0^x e^{-t^2/2}\, dt$$

Substituting the value of $k(E, E_n)$ and the monoenergetic flux $\phi(E_n) = S\delta(E_n - E_0)$ into Eq. 14.28 and performing the integration, one obtains

$$M(E) = S\frac{N_H T\sigma(E_0)}{2E_0}\left[1 + \operatorname{erf}\left(\frac{E_0 - E}{\sqrt{2}\,\sigma}\right)\right] \tag{14.30}$$

The function $M(E)$ given by Eq. 14.30 is shown in Fig. 14.10. It is essentially the same function as that shown in Fig. 14.9, except for the rounding off at the upper energy limit caused by the Gaussian detector response.

The task of neutron spectroscopy is to obtain the neutron energy spectrum $\phi(E)$, which means to unfold Eq. 14.28. Two general methods used to unfold this equation are discussed next.

### 14.5.1 Differentiation Unfolding of Proton Recoil Spectra

If $R(E, E_p) = \delta(E - E_p)$, then the response function of the proton recoil spectrometer is (using Eq. 14.29)

$$k(E, E_n) = N_H T\frac{\sigma(E_n)}{E_n}$$

and Eq. 14.28 takes the form

$$M(E) = N_H T\int_E^{E_{\max}} dE_n\, \frac{\sigma(E_n)}{E_n}\phi(E_n) \tag{14.31}$$

The lower limit of the integral is set equal to $E$ because at any energy $E$, only neutrons with energy $E_n > E$ can contribute to $M(E)$. Equation 14.31 may be solved by differentiation to give

$$\phi(E) = \frac{E}{N_H T\sigma(E)}\left|\frac{dM(E)}{dE}\right| \tag{14.32}$$

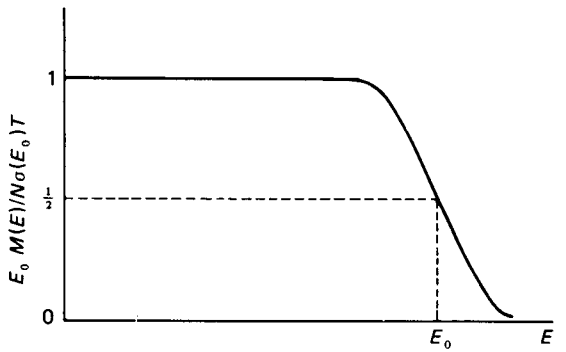


**Figure 14.10** The measured monoenergetic neutron spectrum obtained with a detector having a Gaussian response ($S = 1$).

The evaluation of the derivative in Eq. 14.32 is performed by numerical techniques, since it is not the spectrum $M(E)$ that is measured but its "binned" equivalent,

$$\int_{E_i}^{E_{i+1}} M(E)\, dE = M_i \tag{14.33}$$

where $M_i$ is the number of counts in channel $i$ of the spectrometer. Several investigators[13-17] applied least-squares fit techniques to numerically perform the differentiation of Eq. 14.32. Usually, each $M_i$ is assigned the energy corresponding to the midpoint of the channel and an $M$th-order polynomial is least-squares fit to that point and the preceding and following $N$ points [this is an $M$th-order, $(2N + 1)$-point fit]. The derivative of the polynomial at the mid-point is used as the derivative $[dM(E)/dE]_i$. This method has the disadvantage that it slightly hardens the unfolded spectrum.

An improved differentiation technique[18] consists of first smoothing the true spectrum $\phi(E)$ to obtain a "smoothed" true spectrum $\phi_s(E)$, given by

$$\phi_s(E) = \int_0^\infty G(E, E')\phi(E')\, dE' \tag{14.34}$$

where $G(E, E')$ is a smoothing function normalized to 1. Substituting Eq. 14.32 into Eq. 14.34, one obtains[18]

$$\phi_s(E) \simeq \sum_{i=1}^{NC} \frac{1}{NT}\left[\frac{E_{i+1}}{\sigma(E_{i+1})}G(E, E_{i+1}) - \frac{E_i}{\sigma(E_i)}G(E, E_i)\right]M_i \tag{14.35}$$

where $NC$ is the number of channels, $M_i$ is given by Eq. 14.33, and the assumption is made that the quantity $[E'/\sigma(E')]G(E, E')$ approaches zero at both limits of integration of Eq. 14.34. Results obtained with Eq. 14.35 and a Gaussian smoothing function show no spectrum hardening.

### 14.5.2 The FERDOR Unfolding Method

The unfolding code FERDOR based on the work of Burrus[19] is described in several articles.[20,21] The measured spectrum given by Eq. 14.28 is written in the form

$$M_i = \int_0^{E_{\max}} dE_n\, k_i(E_n)\phi(E_n) \qquad i = 1, NC \tag{14.36}$$

where

$$k_i(E') = \int_{E_i}^{E_{i+1}} dE\, k(E, E') \tag{14.37}$$

$E_{i+1} - E_i = \Delta E_i$ = width of the spectrometer channel at energy $E_i$

$NC$ = number of spectrometer channels

The functions $k_i(E)$, which represent the detector response, can be measured at selected energies or can be computed.[22]

The code FERDOR, instead of obtaining $\phi(E)$, calculates the quantities $S_k$ given by

$$S_k = \int_0^{E_{\max}} W_k(E)\phi(E)\,dE \qquad k = 1, NW \tag{14.38}$$

where $W_k(E)$ = *window function*, chosen by the observer
$NW$ = number of window functions

There are many interpretations of Eq. 14.38, all equally valid:

1. If $W_k(E)$ is taken as the response of an "ideal" detector, then the $S_k$'s are the elements of an "ideal" measured spectrum.
2. The functions $W_k(E)$ are smoothing functions for the true spectrum $\phi(E)$.
3. The $S_k$'s are linear functions of the true spectrum $\phi(E)$ that have to be calculated. For example, if $W_k(E)$ is a cross section, the corresponding $S_k$ is a reaction rate; if $W_k(E)$ is a flux-to-dose conversion factor, then $S_k$ is the dose rate; or if $W_k(E) = 1$, then $S_k$ is the integral spectrum.

The functions $W_k(E)$ used by FERDOR are Gaussians with a standard deviation given by

$$\sigma_k = \frac{w_k E_k}{2\sqrt{2\ln 2}} \tag{14.39}$$

where $w_k = \Gamma_k/E_k$, and its value is set by the user. The code calculates the $S_k$'s and their uncertainties based on the values of $k_i(E)$, $M_i$, and the statistical errors of $M_i$, using a constrained least-squares method.

Experience has shown that the proper values of $w_k$ depend on both the shape of the neutron spectrum and the statistical errors of $M_i$, and that small changes in the $w_k$ cause large changes in the errors of the result.[23] This effect has been mitigated in the code FORIST,[24] which is a modification of FERDOR.[†] In FORIST, the value of $w_k$ is obtained by an iterative process in terms of the desired statistical error of the result $S_k$. Choosing the widths $w_k$ by this method improves the resolution of the unfolded spectrum, for a fixed desired statistical error.

### 14.5.3 Proportional Counters Used as Fast-Neutron Spectrometers

Proportional counters filled with hydrogen or methane are used for the measurement of neutron spectra in the energy range 1 keV $< E_n <$ 2 MeV. Neither hydrogen nor methane are equally useful over the full energy range. Hydrogen-filled counters are used for $E_n <$ 100 keV. For higher neutron energy, greater stopping power is needed, and for this reason, methane is used instead of hydrogen. Methane-filled counters do not give good results for $E_n <$ 100 keV because of spectrum distortion from carbon recoils.

[†]The codes FERDOR and FORIST are available through the Radiation Shielding Information Center of Oak Ridge National Laboratory.[25,26]

The efficiency of a proportional counter, like that of any other gas counter, depends on its size, the composition and pressure of the gas, and the energy of the incident neutrons. Knowledge of the neutron cross section for interactions with hydrogen and carbon over the energy range of interest is necessary for efficiency calculations. The hydrogen cross section is known to better than 1 percent for neutron energies between 0.2 and 22 MeV. The carbon cross section is less accurately known for $E_n > 2$ MeV. In addition to elastic scattering, other carbon reactions, such as $(n, n')$, $(n, \alpha)$, and $(n, p)$, are important for $E_n > 4.8$ MeV and should be included in the response function of the counter. Table 14.3 gives hydrogen and carbon cross sections for $0.2 < E_n < 20$ MeV.

The relationship between the neutron spectrum and the measured pulse-height distribution is given by Eq. 14.28. The response function $k(E, E_n)$ (Eq. 14.29) may be measured or calculated. In either case, the following effects have to be taken into account in obtaining $k(E, E_n)$:[14-17,27,28]

**Wall-and-end effects.** Tracks of protons generated close to the wall or close to the ends of the counter have a high probability for incomplete energy deposition and collection of ionization. Proton-recoil tracks close to the wall are truncated by collisions with the wall material before the struck proton deposits all its energy in the counter. Protons being produced close to the end of the counter

**Table 14.3 Total Hydrogen and Carbon Cross Sections for $0.2 < E_n < 20$ MeV[22]**

| Neutron energy (MeV) | $\sigma_t(^1\mathrm{H})$ (b) | $\sigma_t(^{12}\mathrm{C})$ (b) |
|---|---|---|
| 0.2015 | 9.523 | 4.260 |
| 0.3220 | 7.719 | 3.857 |
| 0.4265 | 6.712 | 3.583 |
| 0.6170 | 5.532 | 3.174 |
| 0.9035 | 4.515 | 2.720 |
| 1.205 | 3.902 | 2.345 |
| 1.613 | 3.287 | 1.965 |
| 2.234 | 2.737 | 1.606 |
| 3.329 | 2.183 | 1.760 |
| 4.236 | 1.827 | 1.943 |
| 4.919 | 1.616 | 1.198 |
| 6.017 | 1.422 | 1.094 |
| 7.038 | 1.246 | 1.023 |
| 8.029 | 1.137 | 1.466 |
| 10.00 | 0.940 | 1.140 |
| 11.98 | 0.801 | 1.259 |
| 14.01 | 0.693 | 1.360 |
| 16.06 | 0.605 | 1.431 |
| 17.81 | 0.541 | 1.448 |
| 19.91 | 0.483 | 1.450 |
| 21.81 | 0.442 | 1.445 |

and moving toward either end enter into a region of lower electric field where there is little or no gas multiplication and where there is, consequently, incomplete collection of the charge produced.

As a result of wall-and-end effects, lower energy pulses are generated that tend to increase the response function toward the lower energies (Fig. 14.11). Corrections for this effect have been calculated,[17,29] but unfortunately each calculation applies only to a specific geometry.

The magnitude of wall-and-end effects increases as the size of the counter decreases. It also increases as the neutron energy increases. In fact, for neutrons in the MeV range, the distortion of the spectrum due to these effects becomes so significant that it sets the upper energy limit ($\sim$ 2 MeV) for the use of a proportional counter as a spectrometer.

**Electric field distortion.** The gas multiplication in a proportional counter depends on the intensity of the electric field. Close to the ends of a cylindrical counter, the strength of the electric field becomes gradually less intense than in most of the counter volume. This effect produces lower pulses from proton recoils at the ends of the counter. Detectors with large length-to-diameter ratio are less affected by this problem. Theoretical corrections of this effect have been developed and successfully applied.[17]

**Effect of carbon recoils.** Neutrons detected by methane-filled counters collide not only with hydrogen nuclei but also with carbon atoms. The ionization produced by carbon recoils is indistinguishable from that produced by protons. However, carbon recoils produce pulses that are smaller than those from protons because of differences in both kinematics and ionization ability. The maximum fraction of neutron energy that can be imparted to a carbon nucleus in one collision is 0.28 (versus 1 for a hydrogen nucleus), and the relative ionization efficiency of a carbon to a proton recoil is about 0.5.[28] Thus, the effect of carbon recoils is to add pulses at the low-energy region of the response

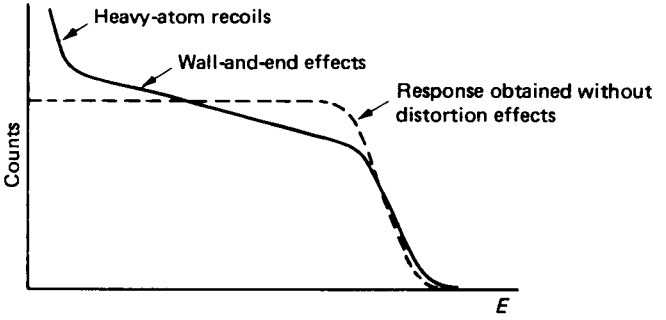


**Figure 14.11** Distortion of the response function because of wall-and-end effects and heavy-atom recoils.

function (Fig. 14.11). Carbon-recoil effects are so significant for $E_n < 100$ keV that methane-filled counters are not usable below this energy.

**Variation of energy needed to produce one ion pair.** The measured spectrum may differ from the proton-recoil spectrum because of nonlinearity in the relationship between proton energy and ionization produced. That relationship is expressed by the quantity $w(E)$, defined as the energy needed by a proton of energy $E$ to produce one electron-ion pair. To be able to use a counter as a spectrometer, the value of $w(E)$ should be accurately known for the gas of the counter for all energies below the maximum neutron energy measured. Experiments have shown that the value of $w(E)$ is essentially constant for hydrogen for neutron energies about $\sim 20$ keV. Below that energy, $w(E)$ changes slightly with energy.[17,28] For methane, $w(E)$ seems to be essentially constant between 100 keV and 1 MeV.[28]

**Gamma-ray discrimination.** Proportional counters used in a mixed neutron-gamma field detect both types of radiation. Discrimination of $\gamma$-ray pulses has been accomplished by utilizing the fact that the Compton electrons produced by the gammas have longer range than proton recoils. The *time-of-rise method*, which is now almost universally used, takes advantage of the faster risetime of the proton pulse relative to that of the electrons. Proton range is so much shorter than electron range that all the ions produced by the proton arrive at the anode at about the same time and generate a pulse with a fast risetime. On the other hand, ions produced by electrons along their path arrive at the anode over a period of time and generate a pulse with a slower risetime. Thus, using appropriate electronics, the pulses from gammas can be rejected.

**Finite resolution of proton detector.** The resolution of a proportional counter for monoenergetic protons is derived from two factors. One is a statistical broadening that depends on the number of ion pairs produced. The other is a "mechanical" broadening due to imperfections in the design of the counter and impurities in the filling gas. At an energy of 615 keV, the energy resolution is of the order of 4 percent, but it deteriorates to about 60 percent at 1 keV.

Response functions of proportional counters have been measured and calculated by several people. Verbinski and Giovannini[28] gave a critical study of response functions of gas-filled counters as well as a comparative study of the different codes used to unfold their spectra. Figures 14.12 and 14.13 show measured and calculated response functions for methane- and hydrogen-filled proportional counters.

Coarse calibration of proportional counters is achieved by using $^3$He and $N_2$ as additives in the gas of the counter and employing the reactions

$$^{14}\mathrm{N}(n,p)^{14}\mathrm{C} \qquad Q = 626 \text{ keV}$$

$$^{3}\mathrm{He}(n,p)^{3}\mathrm{H} \qquad Q = 765 \text{ keV}$$

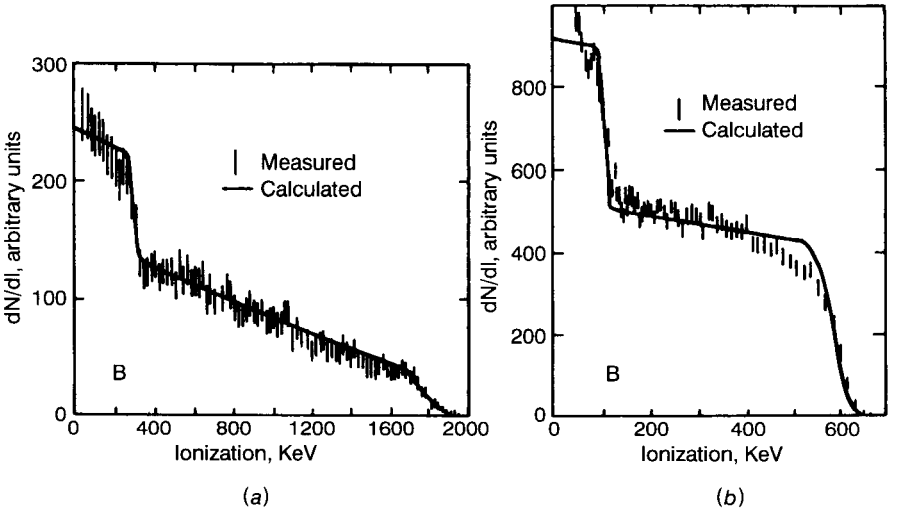


**Figure 14.12** Measured and calculated response functions for a methane-filled proportional counter (1.5 in diameter, 3.5 atm pressure). (*a*) At 75°C, 1772 keV. (*b*) At 75°C, 592 keV. (From Ref. 28; $dN/dI$ is the proton ionization spectrum.)

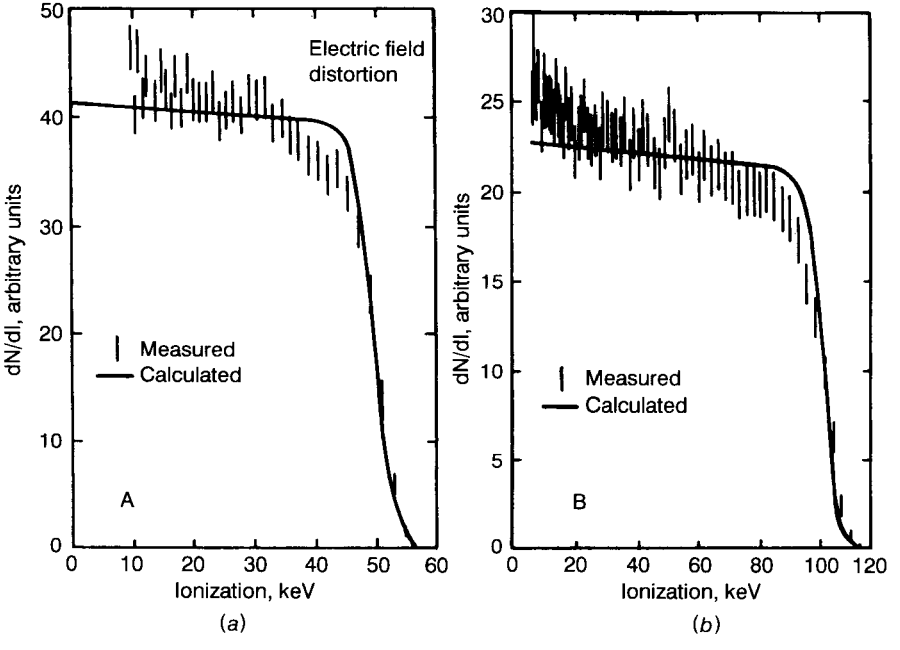


**Figure 14.13** Measured and calculated response functions for a cylindrical hydrogen-filled proportional counter (1.5 in diameter, 2.6 atm pressure, $H_2$ + 5 percent $N_2$). (*a*) Electric field distortion, 45°C, 50 keV; (*b*) 45°C, 100 keV. (From Ref. 28; $dN/dI$ is the proton ionization spectrum.)

Fine calibration is obtained by placing the detector inside neutron filters made of aluminum, NaCl, and Teflon.[30] The filters generate dips in the unfolded spectrum, which coincide with the energies of cross-section resonances of the corresponding isotope. Fine calibration is achieved when the energies of the dips of the unfolded spectrum coincide with the energies of the resonances.

### 14.5.4 Organic Scintillators Used as Fast-Neutron Spectrometers

Organic scintillators have proven to be excellent fast-neutron detectors because they have high and known efficiency, good energy resolution, and low sensitivity to gammas. The high efficiency is due to their hydrogen content (1.1 hydrogen atoms per carbon atom, density about $10^3$ kg/m$^3$ = 1 g/cm$^3$), the relatively high hydrogen cross section (2.5 b for 2.5-MeV neutrons), and the ability to make and use them in large sizes. Organic scintillators are the main detectors used for neutron spectroscopy from $\sim$ 10 keV to 200 MeV. An excellent review of organic scintillator properties is given in Ref. 31.

Stilbene scintillators were used as early as 1957. Stilbene as a crystal is very sensitive to mechanical and thermal shock and shows an anisotropic response to neutrons—i.e., neutrons incident from different directions, with respect to the crystal lattice, produce different light output. Liquid organic scintillators have none of these problems; in addition, they have higher H/C ratio, and light production from carbon recoils relatively lower than in stilbene. For all these reasons, liquid organic scintillators are almost exclusively used for detecting fast neutrons.

The NE series† of organic scintillators has been studied in detail and used extensively,[22,28,31,32] in particular NE 213. The NE 213 scintillator, which is most commonly used, consists of xylene, activators, the organic compound POPOP (as a wavelength shifter), and naphthalene, which is added to improve light emission. The density of NE 213 is about 870 kg/m$^3$ (0.87 g/cm$^3$), and its composition is taken to be $CH_{1.21}$.

As the size of an organic scintillator increases, the efficiency increases, the energy resolution deteriorates, and the background increases. The optimum size for MeV neutrons seems to be a scintillator with a volume $10^{-4}$ m$^3$ (100 cm$^3$), i.e., a cylinder 50 mm in diameter and 50 mm tall. The efficiency of the NE 213 scintillator has been determined by Verbinski et al.[22] using a combination of measurements and Monte Carlo calculations for 20 neutron energies between 0.2 and 22 MeV.

The response of an organic scintillator to monoenergetic neutrons depends on effects similar to those discussed in the previous section for proportional counters, with the exception of electric field distortions. The most important cause of a response different from the ideal rectangular distribution shown in Fig. 14.9 is the nonlinear relation between the energy of the proton and the amount of light produced by the scintillation process. For organic scintillators,

†Manufactured by Nuclear Enterprises, Winnipeg, Ontario, Canada.

the light production by protons and heavier ions is essentially proportional to the $\frac{3}{2}$ power of the energy deposited[22] in the energy range 0.3 MeV $< E <$ 4 MeV, and linear for lower energies.[33] The light production by electrons varies almost linearly with energy[33] (Fig. 14.14).

Response functions for the NE 213 organic scintillator were first obtained by Verbinski et al.[22] These authors measured the NE 213 response for 20 energies between 0.2 and 22 MeV and then normalized the spectra to Monte Carlo calculations. One additional response was constructed at 10 MeV from Monte Carlo calculations and from interpolation of the measured responses at 8 and 12 MeV. These 21 neutron response functions are included in the FERDOR/COOLC package,[25] but they constitute an insufficient response matrix. Ingersoll and Wehring,[34,36] using an interpolation scheme, expanded these data into an 81-column matrix, and used it successfully to unfold neutron spectra up to 20 MeV. This expanded matrix, along with a measured gamma-ray response function,[34] is included in the FORIST code package.[26] Figure 14.15 shows typical response functions for monoenergetic neutrons up to 8.12 MeV. Figure 14.16 shows a pulse-height distribution and an unfolded spectrum. Two other unfolding methods can be found in Refs. 37 and 38.

Neutron-gamma discrimination is essential for satisfactory performance of an organic scintillator as a neutron spectrometer. Fortunately, rejection of gamma pulses can be achieved by electronic means. The method is called pulse-shape discrimination (PSD) and is based on the difference in scintillator response to gamma- and neutron-associated events. The electrons, which are produced by gammas, cause scintillations at a rate faster than that due to protons produced by neutrons. Thus, the electron pulses, which are associated with photon interactions, have a faster risetime than the proton pulses associated with neutrons. There are many PSD circuits. All of them generate a pulse with amplitude dependent upon the fast and slow components of the scintillation. The PSD circuit used by Burrus and Verbinski[20] produces a large positive pulse for neutrons and a small positive or large negative pulse for gammas.

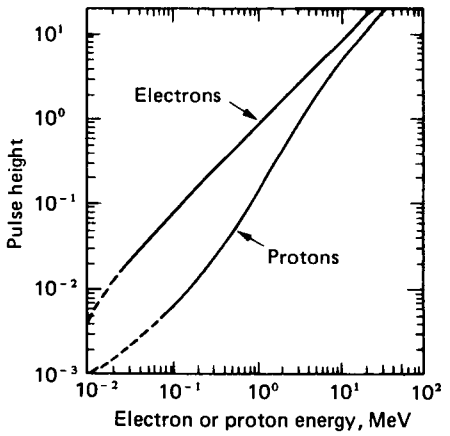


**Figure 14.14** Light response of NE 110 (plastic) and NE 213 scintillator as a function of electron and proton energy (from Ref. 35).

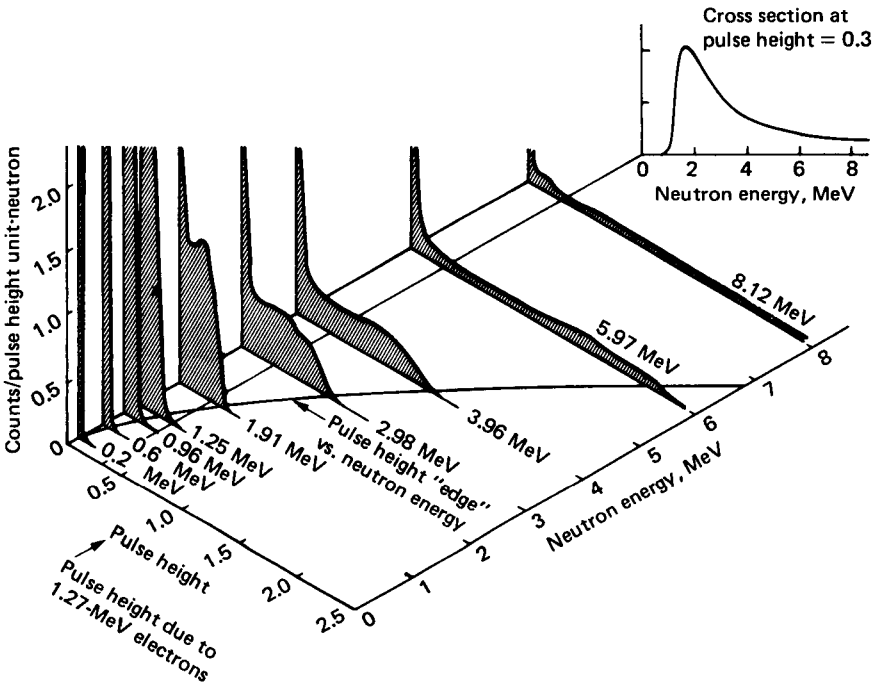


**Figure 14.15** Response functions of NE 213 spectrometer. The curves represent the quantity $k_i(E)$, Eq. 14.37 (from Ref. 20).

Johnson et al.[36] used a time-to-amplitude converter to generate a signal proportional to the risetime of the pulses produced in the scintillator (Fig. 14.17).

Organic scintillators can be used in time-of-flight measurements because they have shown timing resolution less than 1 ns[31] (see Sec. 14.8).

## 14.6 DETECTION OF FAST NEUTRONS USING THRESHOLD ACTIVATION REACTIONS

Detection of fast neutrons by threshold activation reactions (or threshold detectors) is based on the existence of an energy threshold for certain reactions of neutrons with nuclei. Thus, if one activates a foil made of such nuclei, the activity of the foil will give a measure of the neutron flux above the threshold. Consider, for example, the $(n, \alpha)$ and $(n, 2n)$ cross sections of $^{27}$Al an $^{46}$Ti shown in Fig. 14.18. If Al and Ti foils are irradiated, the activity produced (activity of $^{24}$Na and $^{45}$Ti) will be a measure of the neutron flux above $\sim$ 5 MeV and $\sim$ 13 MeV, respectively.

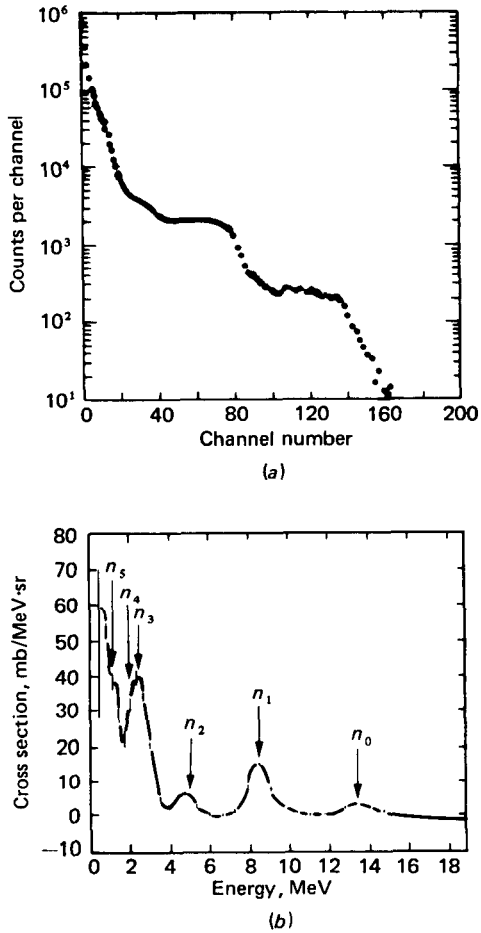


**Figure 14.16** Pulse-height distribution and unfolded neutron spectrum obtained with a 46-mm × 46.5-mm diameter NE 213 organic scintillator (from Ref. 20).

The main advantages of this technique, over the use of other spectrometers, are as follows:

1. The foils have a small volume and a low cross section; therefore, they do not disturb the neutron field.
2. The foils are almost insensitive to gammas.
3. Their small size makes the location of foils possible in places where no other spectrometer would fit.
4. The counting equipment does not have to be carried to the radiation area.

As shown in Sec. 14.4, the saturation activity $A_s$ of a foil is given by

$$A_s = N\int_{E_{th}}^{\infty} \sigma(E)\phi(E)\,dE \tag{14.40}$$

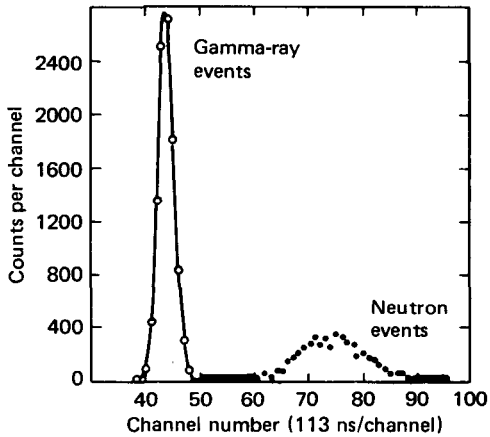


**Figure 14.17** Risetime spectrum of gamma-ray and neutron events recorded by a NE 213 organic scintillator (from Ref. 36).

where $N$, $\sigma(E)$, and $\phi(E)$ have been defined in Sec. 14.4 and $E_{th}$ is the energy threshold for the cross section $\sigma(E)$. Table 14.4 gives a partial list of the many reactions one can use to cover a given neutron energy range. In general, reactions are selected according to the energy range of the neutron spectrum and the counting equipment available. There are, however, criteria that make certain reactions and certain foils more desirable than others:

1. The cross section for the reaction should be well known as a function of energy.
2. The type, energy, and relative intensity of the radiations of the product of the reaction should be well known.
3. The half-life of the radionuclide produced should be well known and should be at least several minutes long.
4. The foil material should be available in high purity, to avoid interference reactions caused by impurities.

To determine the neutron flux as a function of energy by the threshold reaction technique, one irradiates $n$ foils and obtains $n$ equations for the saturation activity per target nucleus,†

$$A_i = N\int_{E_{th,i}}^{\infty} \sigma_i(E)\phi(E)\,dE \,|i = 1, n \tag{14.41}$$

Note that the activity $A_i$ is not the total activity of the foil but only the activity due to the reaction associated with the cross section $\sigma_i(E)$. For example, if one

†If saturation activity cannot be obtained because of long half-life, an appropriate time-correction factor is used.

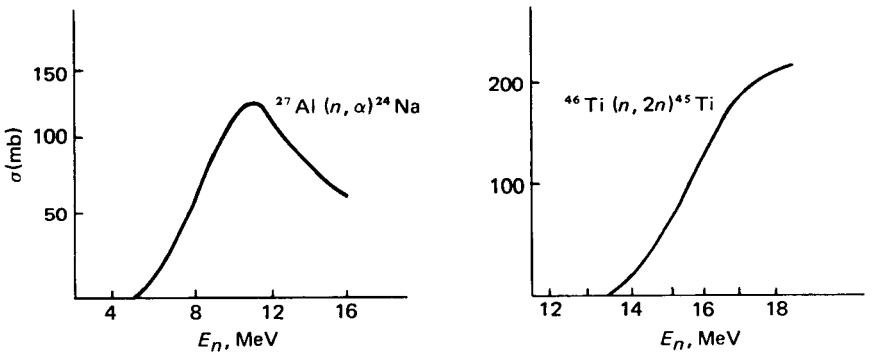


**Figure 14.18** The $(n, \alpha)$ and $(n, 2n)$ cross sections for $^{27}$Al and $^{46}$Ti.

**Table 14.4 A List of Threshold Reactions**

| Material | Reaction | Threshold (MeV) | Half-life of product |
|---|---|---|---|
| Teflon | $^{19}$F$(n, 2n)^{18}$F | 11.6 | 109.7 min |
| Li | $^{7}$Li$(n, \alpha n')^{3}$H | 3.8 | – |
| Mg | $^{24}$Mg$(n, p)^{24}$Na | 6 | 15 h |
| Al | $^{27}$Al$(n, \alpha)^{24}$Na | 4.9 | 15 h |
| Al | $^{27}$Al$(n, p)^{27}$Mg | 3.8 | 9.45 min |
| Ti | $^{46}$Ti$(n, p)^{46}$Sc | 5.5 | 83.3 d |
| Ti | $^{47}$Ti$(n, p)^{47}$Sc | 2.1 | 3.41 d |
| Ti | $^{48}$Ti$(n, p)^{48}$Sc | 6.8 | 43.7 h |
| Fe | $^{56}$Fe$(n, p)^{56}$Mn | 4.9 | 2.58 h |
| Fe | $^{54}$Fe$(n, p)^{54}$Mn | 2.2 | 312.5 d |
| Co | $^{59}$Co$(n, \alpha)^{56}$Mn | 5.2 | 2.58 h |
| Ni | $^{58}$Ni$(n, 2n)^{57}$Ni | 13 | 36 h |
| Ni | $^{58}$Ni$(n, p)^{58}$Co | 2.9 | 71.3 d |
| Cu | $^{63}$Cu$(n, 2n)^{62}$Cu | 11.9 | 9.8 min |
| Cu | $^{63}$Cu$(n, \alpha)^{60}$Co | 6.1 | 5.27 y |
| Zn | $^{64}$Zn$(n, p)^{64}$Cu | 2 | 12.7 h |
| I | $^{127}$I$(n, 2n)^{126}$I | 9.3 | 13 d |
| Au | $^{197}$Au$(n, 2n)^{196}$Au | 8.6 | 6.17 d |
| Np | $^{237}$Np$(n, \text{fission})^{140}$Ba† | 0.5 | 12.8 d |
| U | $^{238}$U$(n, \text{fission})^{140}$Ba† | 1.45 | 12.8 d |

†Various fission products are available for counting, e.g., $^{95}$Zn, $^{103}$Ru, $^{140}$La. $^{140}$Ba is shown as typical.

irradiates an aluminum foil, the total activity will be the result of the $(n, \alpha)$ and $(n, p)$ reactions listed in Table 14.4 and the $(n, \gamma)$ reaction that will also occur. If the user intends to examine the $(n, p)$ reaction, the activity that should be used in Eq. 14.41 is that of $^{27}$Mg. Activity due to $^{24}$Na [from the $(n, \alpha)$ reaction] and $^{28}$Al [from the $(n, \gamma)$ reaction] should be disregarded.

It is advantageous, but not necessary, to choose reactions that result in the same type of radiation being emitted by all the foils used. Then the same counting equipment can be used with all the foils. The most common choice is gammas, and the detector is a Ge spectrometer.

**Example 14.5** Consider two foils made of materials with neutron absorption cross sections as shown below:

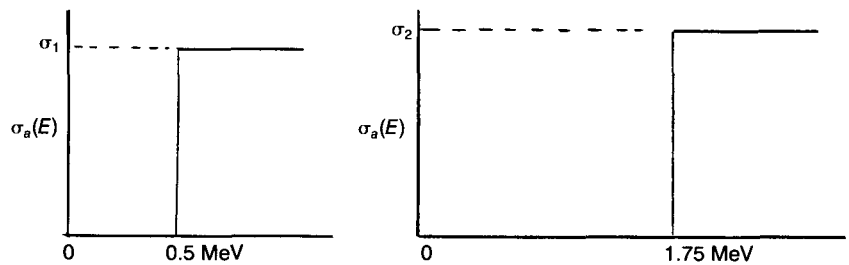


The foils were exposed to a fast-neutron flux for 2 hours. The half-life of the radioisotope produced by the first foil is 10 min, and of the second is 5 hours.

(a) Write the activation equations and sketch activity produced versus irradiation time for both foils.
(b) What information about the neutron spectrum can one obtain from this measurement?

**Answer** The activation equation is

$$A_i(t) = N_i \sigma_i \phi (1 - e^{-\lambda_i t}) = A_{\text{sat},i}(1 - e^{\lambda_i t})$$

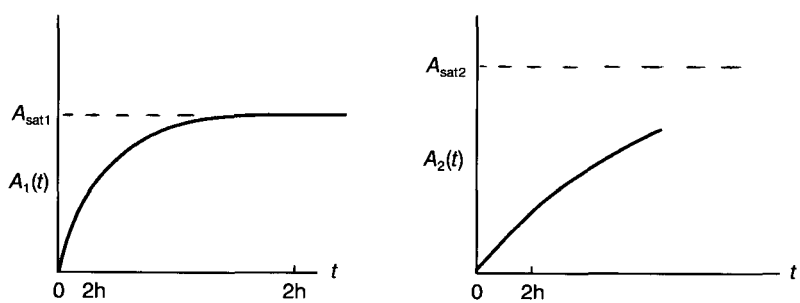

The saturation activity is an integral over the neutron spectrum (Eq. 14.40):

$$A_{\text{sat1}} = N_1 \int_{0.5}^{\infty} \sigma_1(E)\phi(E)\,dE \qquad A_{\text{sat2}} = N_2 \int_{1.75}^{\infty} \sigma_2(E)\phi(E)\,dE$$

Since the cross sections are constants,

$$A_{\text{sat1}} = N_1 \sigma_1 \int_{0.5}^{\infty} \phi(E)\,dE, \qquad A_{\text{sat2}} = N_2 \sigma_2 \int_{1.75}^{\infty} \phi(E)\,dE$$

These expressions show that (a) from foil 1, one can get the number of neutrons above 0.5 MeV, and (b) from foil 2, one can get the number of neutrons above 1.75 MeV. Subtracting the two activities gives information about the number of neutrons between 0.5 and 1.75 MeV.

The calculation of $\phi(E)$ based on Eq. 14.41 is another case of unfolding. Usually the flux is expressed in terms of a number of energy groups $G$. If $G < n$, unfolding of Eq. 14.41 is a simple case of least-squares fit. Unfortunately, in most cases of practical interest, $G > n$, and the only way to obtain $\phi(E)$ is to assume a certain a priori form for it and then try to improve upon this initial guess. The result depends on the choice of the input spectrum, the set of threshold reactions chosen, the errors of the measured activities, and the uncertainties of the cross sections involved. The several unfolding codes that are used differ mainly in the choice of the input spectrum. A brief description of four such codes, SAND-II,[39] SPECTRA,[40] relative deviation minimization method (RDMM),[41] and LSL-M2[42] is given next.

### 14.6.1 The Code SAND-II

The code SAND-II assumes an estimate of the flux $\phi_j^{(0)}|_{j=1,G}$, and for subsequent iterations applies a nonlinear adjustment to the flux. For the $k$th iteration,

$$\phi_j^{(k+1)} = \phi_j^{(k)} \exp C_j^{(k)} \qquad j = 1, \ldots, G \tag{14.42}$$

where $C_j^{(k)}$ is the $k$th iteration correction term for the $j$th flux group. The value of $C_j^{(k)}$ depends on weighting factors, which in turn, are calculated from the measured activities. The activity of every foil is written in terms of the flux as shown by Eq. 14.43:

$$A_{ij}^{(k)} = \sigma_{ij}\phi_j^{(k)}(E_{j+1} - E_j) \tag{14.43}$$

where $\sigma_{ij}$ = $i$th foil cross section averaged over flux of group $j$
$A_{ij}^{(k)}$ = *the portion of* $A_i$ contributed by neutrons in the $j$th group, during the $k$th iteration

To avoid spurious variations introduced to the result by the iteration, SAND-II applies smoothing[43,44] to the weighting factors used for the calculation of the flux correction factor $C_j^{(k)}$. Experience has shown that SAND-II is better than either SPECTRA or RDMM.

### 14.6.2 The Code SPECTRA

The code SPECTRA assumes that the flux is a piecewise-linear function of energy; i.e., for any energy group $j$, one can write

$$\phi(E) = \frac{E - E_j}{E_{j+1} - E_j}\phi_{j+1} + \frac{E_{j+1} - E}{E_{j+1} - E_j}\phi_j \tag{14.44}$$

The flux $\phi(E)$ from Eq. 14.44 is introduced into Eq. 14.41, and the integration is performed to give a matrix equation $\mathbf{A} = \mathbf{S\Phi}$, where $\mathbf{A}$ is an $n \times 1$ vector whose components are the measured activities, $\mathbf{S}$ is an $n \times G$ matrix whose elements are integrals of the cross section of the form

$$S_{ij} = \int_{E_{j-1}}^{E_j} \frac{E - E_{j-1}}{E_j - E_{j-1}}\sigma_i(E)\,dE + \int_{E_j}^{E_{j+1}} \frac{E_{j+1} - E}{E_{j+1} - E_j}\sigma_i(E)\,dE \tag{14.45}$$

and $\Phi$ is a $G \times 1$ vector whose components are the desired fluxes. The best flux $\Phi$ is that flux that minimizes the quantity

$$\sum_{i=1}^{n}\left(\frac{A_i - A_{ci}}{A_i}\right)^2$$

where $A_i$ and $A_{ci}$ are measured and calculated activities, respectively.

### 14.6.3 The Relative Deviation Minimization Method (RDMM)

The RDMM[41] assumes that the flux can be represented as a series of linearly independent functions,

$$\phi_m(E) = W(E)\sum_{k=1}^{m} a_k\psi_k(E) \tag{14.46}$$

where $W(E)$ = weighting function (e.g., $e^{-E}$)
$a_k$ = coefficients of the expansion
$\psi_k(E)$ = polynomial, simple or orthogonal (e.g., Laguerre or Chebyshev polynomials may be used)

Equation 14.46 represents an iterative procedure for the evaluation of the flux, because a new term is added to the expansion, after each iteration, up to a maximum of $n$. The best approximation for the flux is that which minimizes the quantity

$$Q(m, a_1, a_2, \ldots, a_m) = \sum_{i=1}^{n}\left[\frac{A_i - \int_0^\infty \sigma_i(E)\phi_m(E)\,dE}{A_i}\right]^2 \tag{14.47}$$

By taking the derivatives

$$\frac{\partial Q}{\partial a_k} = 0 \qquad k = 1, m \tag{14.48}$$

one obtains $m$ equations that can be solved for the constants $a_k|_{k=1,m}$.

### 14.6.4 The LSL-M2 Unfolding Code

The LSL-M2 program package determines the neutron energy spectrum based on information obtained from a combination of neutron flux calculations and threshold foil activation measurements. The results of LSL-M2 are used primarily for the determination of radiation damage to reactor components and specimens irradiated by neutrons. The package consists of three programs. The program ACT converts measured activities to reaction rates, taking into account the reactor power history. The program CALACT calculates the reaction rates using appropriate cross sections and computed neutron fluxes. The third program, FLXPRO, converts data from one energy group structure to another, applying appropriate interpolation and extrapolation procedures.

The LSL-M2 performs a nonlinear least-squares adjustment procedure based on the logarithm of the ratio $A_C/A_M$, where

$$A_C = \sum_{g=1}^{G} \phi_g \sigma_g$$

are the calculated reaction rates based on $G$ energy groups and $A_M$ are the corresponding measured reaction rates. Based on the discrepancies between the $\ln(A_C/A_M)$ values, the initially computed fluxes $\phi_g$ are adjusted so that, after a few iterations, there is acceptable agreement between measured and calculated reaction rates. The least-squares adjustment takes into account the random errors for both calculated and measured quantities. The final product of the computation is the adjusted neutron spectrum $\phi_g|_g = 1, G$ that generates the acceptable values of $A_C$. The mathematical details are given in Refs. 42 and 45.

## 14.7 NEUTRON ENERGY MEASUREMENT WITH A CRYSTAL SPECTROMETER

The measurement of neutron energy with a crystal spectrometer is based on the same principle of Bragg diffraction as is the measurement of X-ray energy (see Sec. 12.10).

A neutron with kinetic energy $E$ has a de Broglie wavelength equal to

$$\lambda = \left(\frac{h}{p}\right) = \frac{0.028602}{\sqrt{E\ (\text{eV})}}\ \text{nm} = \frac{0.28602}{\sqrt{E\ (\text{eV})}}\ \text{Å} \tag{14.49}$$

where $h$ = Planck's constant

$p = Mv = \sqrt{2ME}$ = linear momentum of the neutron

Neutrons with wavelength $\lambda$ incident upon a crystal with interplanar distance $d$ are scattered by the atoms of the crystal. As a result of constructive interference, a diffracted neutron beam appears at an angle $\theta$ satisfying the Bragg condition (Fig. 14.19),

$$n\lambda = 2d \sin\theta \tag{14.50}$$

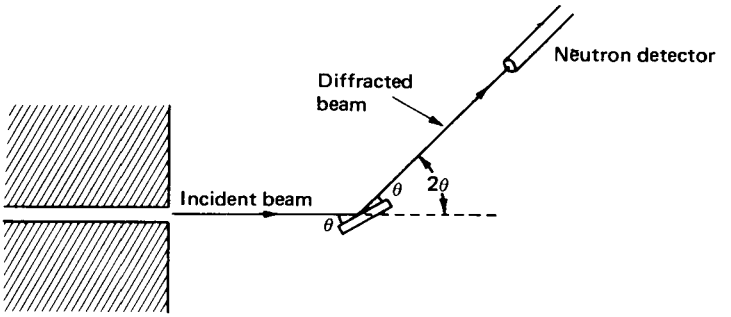


**Figure 14.19** The arrangement of a neutron diffraction spectrometer.

where $n$ is the order of reflection (see Sec. 12.10). If the incident beam is polyenergetic, the neutron detector set at an angle $\theta$ will detect neutrons of wavelength $\lambda$ satisfying Eq. 14.50, i.e., neutrons having kinetic energy $E$ related to $\lambda$ by

$$E\ (\text{eV}) = \frac{8.191 \times 10^{-4}}{\lambda^2\ (\text{nm})^2} \tag{14.51}$$

Neutron crystal spectrometers are used either to analyze a polyenergetic neutron source or, more frequently, to provide a source of monoenergetic neutrons. Considering again Fig. 14.19, even though the incident beam may consist of neutrons of many energies, the neutrons diffracted at an angle $\theta$ constitute a monoenergetic neutron beam of energy given by Eq. 14.51.

Monoenergetic neutron sources at the energy range provided by crystal spectrometers are necessary for the study of low-energy neutron cross sections with resonances. Consider, as an example, the total neutron cross section of iridium shown in Fig. 14.20. To be able to measure the resonances of this cross section, one needs neutron energy resolution less than 0.1 eV, resolution that can be achieved only with crystal spectrometers[46,47] or time-of-flight measurements (see Sec. 14.8).

Most of the discussion presented in Sec. 12.10 for X-ray crystal spectrometers is also valid for neutron spectrometers (i.e., rocking curve, alignment, higher order reflections, types of spectrometers). There are some differences, however, which are discussed next.

The resolving power of a neutron crystal spectrometer is given (based on Eqs. 14.49 and 14.50) by

$$\frac{E}{\Delta E} = \frac{\lambda}{2\,\Delta\lambda} = \frac{\tan\theta}{2\,\Delta\theta} = \frac{nk}{4(\Delta\theta)d\sqrt{E}}\left(1 - \frac{n^2k^2}{4d^2E}\right)^{-1/2} \tag{14.52}$$

where $k = 0.028602\ \text{nm}\cdot(\text{eV})^{1/2}$, the constant of Eq. 14.49. This function, as

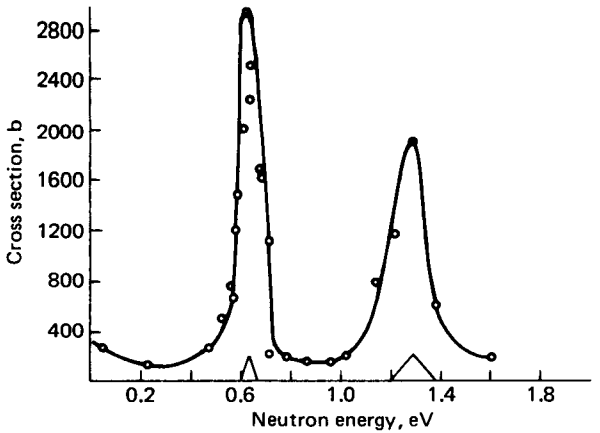


**Figure 14.20** The total neutron cross section of iridium (from Ref. 46).

well as its inverse (which is the energy resolution†), is shown in Fig. 14.21, assuming $d = 0.2$ nm, $\Delta\theta = 0.3°$, and $n = 1$. One can improve the resolution, as in the use of X-ray spectrometers, by decreasing $\Delta\theta$ and choosing a crystal with short interatomic distances. Using a beryllium crystal with $d = 0.0732$ nm and $\Delta\theta = 7.8$ min, a resolution of 2 percent at 1 eV has been achieved.[47]

The energy range over which the crystal spectrometer can be used is determined from the Bragg condition (Eq. 14.50) and the requirement that $0 < \sin\theta < 1$. Using Eqs. 14.49 and 14.50, one obtains for first-order reflection

$$\sin\theta_{\min} < \frac{0.028602}{2\sqrt{E\ (\text{eV})}\ d\ (\text{nm})} < 1 \tag{14.53}$$

which shows that the energy range is a function of the crystal (interplanar distance $d$) and the minimum observable angle $\theta_{\min}$. If one assumes $d = 0.2$ nm (LiF crystal) and $\theta_{\min} = 0.5°$, the energy range becomes $0.005\ \text{eV} < E < 67\ \text{eV}$. Both energy limits increase if a crystal with smaller interplanar distance $d$ is used. In practice, the upper limit is determined by the energy resolution that is acceptable for the experiment. As Fig. 14.21 shows, the resolution deteriorates rather rapidly as energy increases. Neutron crystal spectrometers are generally used for $E < 100$ eV. Crystals that have been used include LiF, calcite, mica, beryllium, and copper.

## 14.8 THE TIME-OF-FLIGHT METHOD

The time-of-flight (TOF) method determines the neutron energy with a resolution that is better than with any other detector. The principle of neutron TOF is

†Better resolution would be obtained with higher order reflections ($n > 1$), but unfortunately, the intensity is much lower.

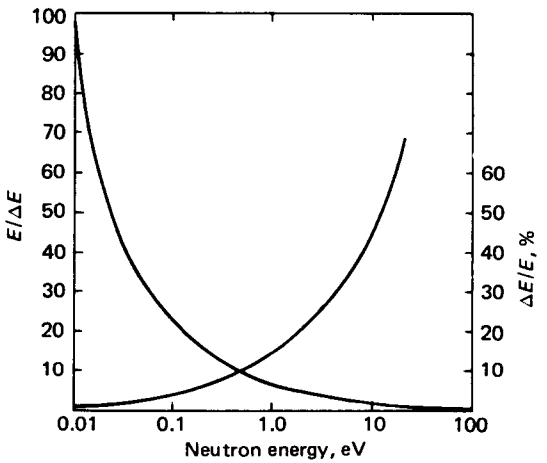


**Figure 14.21** Resolving power and energy resolution of a neutron crystal spectrometer ($n = 1$, $d = 0.2$ nm, $\Delta\theta = 0.3°$).

the same as for heavy ions (see Sec. 13.6). As was pointed out in Sec. 13.6, by using the TOF technique, the particle energy can be measured extremely accurately if the mass of the particle is known. The mass of the neutron is known (to within 3 keV), and energy resolution as good as 0.1 percent has been achieved.

In a TOF measurement, one determines the speed of the neutron $v$ from the time $t$ it takes to travel a flight path of length $L$. The kinetic energy of the neutron is given by

$$E = Mc^2\left(\frac{1}{\sqrt{1-\beta^2}} - 1\right) = Mc^2\left(\frac{1}{\sqrt{1 - L^2/c^2t^2}} - 1\right) \tag{14.54}$$

where

$$Mc^2 = 939.552 \text{ MeV} = \text{rest mass energy of the neutron}$$

The nonrelativistic equation is the familiar one,

$$E_{\text{NR}} = \frac{1}{2}Mv^2 = \frac{1}{2}M\frac{L^2}{t^2} \tag{14.55}$$

Which equation should be used depends on the energy range measured and the resolution of the experiment. At 1 MeV, the nonrelativistic equation, Eq. 14.55, introduces an error of 0.16 percent.

The energy resolution is, using Eqs. 14.54 and 14.55,

*Relativistic:*

$$\frac{\Delta E}{E} = \frac{E + Mc^2}{E}\frac{\beta^2}{1-\beta^2}\sqrt{\left(\frac{\Delta L}{L}\right)^2 + \left(\frac{\Delta t}{t}\right)^2} \tag{14.56}$$

*Nonrelativistic:*

$$\frac{\Delta E}{E} = 2\sqrt{\left(\frac{\Delta L}{L}\right)^2 + \left(\frac{\Delta t}{t}\right)^2} \tag{14.57}$$

In neutron TOF experiments, the neutron source is a burst of neutrons generated either by a velocity selector (chopper) or by an ion beam, as explained later in this section. The time-of-flight $t$ is the difference between the time of production of the neutron burst and the time of neutron detection.

The uncertainty $\Delta t$ consists of three parts.

1. $\Delta t_s$ is the uncertainty in the time of neutron emission; it is essentially equal to the width of the neutron burst and ranges from a few hundred nanoseconds to less than a hundred picoseconds.
2. $\Delta t_d$ is the uncertainty in the time of neutron detection; it depends on the pulse risetime, since it is the pulse risetime that signals the time of detection. Neutron detectors used today have a pulse risetime equal to 5 ns or less.[48]
3. $\Delta t_m$ is the uncertainty in neutron slowing-down time if the source is surrounded by a moderator.

The uncertainty $\Delta L$ is due to the finite thicknesses of the neutron-producing target and the neutron detector. The uncertainty in the measurement of $L$ itself can be made negligible. The longer the flight path is, the smaller the uncertainty $\Delta L/L$ becomes. As the length $L$ increases, however, the intensity of the source should increase, and by a greater factor, so that the counting rate in the detector stays the same.

It is customary to use the quantity $t/L$ as a *figure of merit* for TOF experiments. From Eqs. 14.54 and 14.55, one obtains

$$\left(\frac{t}{L}\right)_{\text{Rel}} = \frac{1}{c}\left[1 - \left(\frac{Mc^2}{E + Mc^2}\right)^2\right]^{-1/2} \tag{14.58}$$

$$\left(\frac{t}{L}\right)_{\text{NR}} = \frac{1}{c}\sqrt{\frac{Mc^2}{2E}} \tag{14.59}$$

Table 14.5 gives typical $t/L$ values.

The requirements for slow-neutron TOF experiments fall in the $\mu$s/m range, and those of fast neutrons in the ns/m range. Because of this large difference in timing requirements, it is impossible to span the whole neutron energy range (eV to MeV) with the same TOF spectrometer.

The change of resolution with neutron energy is the same for TOF and crystal spectrometers. In both systems, the energy spread $\Delta E$ changes, essen-

**Table 14.5 Typical Values of $t / L$ for Several Neutron Energies**

| $E$ (eV) | $t/L$ (μs/m) | $E$ (MeV) | $t/L$ (ns/m) |
|---|---|---|---|
| 0.01 | 722 | 0.1 | 228 |
| 0.1 | 228.5 | 1 | 72.3 |
| 1 | 72.2 | 2 | 51.2 |
| 10 | 22.8 | 5 | 32.4 |
| 100 | 7.2 | 10 | 23 |
| 1000 | 2.3 | 20 | 16 |

tially, as $E^{3/2}$ (compare Eqs. 14.52 and 14.57):

$$\Delta E = 2E\sqrt{\left(\frac{\Delta L}{L}\right)^2 + \left(\frac{\Delta t}{t}\right)^2} \approx 2E\frac{\Delta t}{t} = 2E\frac{L}{t}\frac{\Delta t}{L} \approx Ev \approx E^{3/2}$$

### 14.8.1 The Neutron Velocity Selector (Neutron Chopper)

The first velocity selector was designed by Fermi and his co-workers in the 1940s and is now known as the Fermi chopper.[49] The Fermi chopper consisted of a multiple sandwich of aluminum and cadmium foils that fit tightly into a steel cylinder about 38 mm (1.5 in) in diameter (Fig. 14.22). The cylinder was rotated at speeds of up to 15,000 r/min, thus allowing only bursts of neutrons to go through the aluminum channels. Based on the geometry of Fig. 14.22, no neutrons from a parallel beam would go through the channel when the chopper was more than $\Delta\theta/2$ degrees from its fully open position (Fig. 14.23), where $\Delta\theta$ = (width of channel)/(radius of cylinder). The spinning cylinder was viewed with two photocells, one giving a direct measure of the rotation and the other sending to the neutron detector a signal used for the measurement of the time-of-flight of the transmitted neutrons.

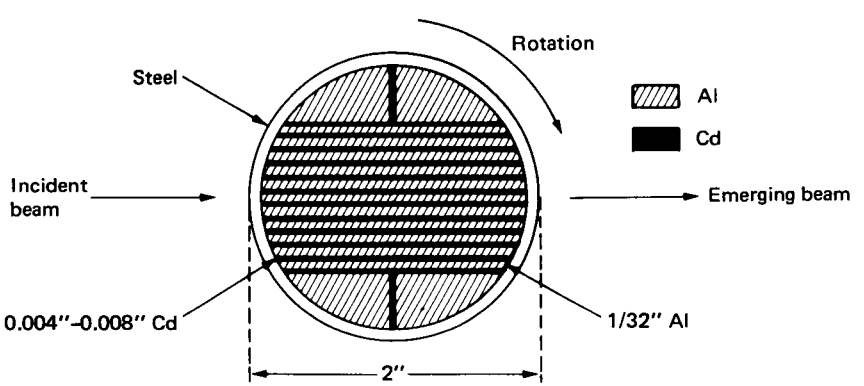


**Figure 14.22** The Fermi chopper.

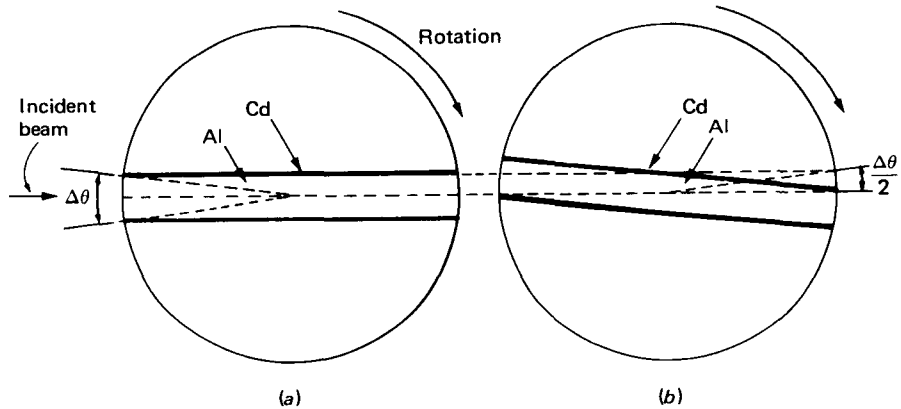


**Figure 14.23** (*a*) The channel is fully open. (*b*) The chopper has rotated by $\Delta\theta/2$, and the channel is closed.

Fermi's chopper was a "slow" chopper, the word slow referring to the speed of the neutrons, and was used for neutrons up to 1 eV. Fast choppers have also been developed for use with neutron energy up to the keV range,[50-52] with the rotating cylinders of the chopper having different design, depending on the requirements of the measurement.

The most important characteristic of any chopper is the width of the neutron burst. In all choppers, the shape of the pulse is essentially triangular with the base of the triangle being inversely proportional to the rotating speed of the shutter. The shape of the pulse changes slightly with the neutron speed and the shape of the channel. The width of the channel, which also affects the pulse, is a compromise between acceptable time resolution and adequate counting rate. Using choppers, neutron bursts with widths as low as 0.5 $\mu$s have been achieved.[48] The time resolution due to such a width is adequate for energies up to 10 keV. At higher energies, ion beams from accelerators are used to provide the neutron burst.

### 14.8.2 Pulsed-Ion Beams

Narrow and intense bursts of neutrons for TOF experiments are obtained by using ion beams. The ions are accelerated, strike a target, and produce neutrons through a (charged particle, $n$)-type reaction. Examples of such reactions are

$$^{2}\mathrm{H}(d,n), {}^{3}\mathrm{H}(p,n), {}^{7}\mathrm{Li}(p,n), {}^{9}\mathrm{Be}(p,n), {}^{9}\mathrm{Be}(\alpha,n), {}^{12}\mathrm{C}(d,n),$$
$$^{13}\mathrm{C}(\alpha,n), \mathrm{Ta}(\gamma,n), \mathrm{W}(p,n), \mathrm{W}(\gamma,n), \mathrm{Pb}(p,n), \mathrm{Pb}(\gamma,n), \mathrm{U}(p,n),$$
$$\mathrm{U}(\gamma,n)\ \mathrm{U}(\gamma,\mathrm{fission})$$

Neutrons produced by these reactions are in the MeV range.

The first accelerator to be used for neutron production was the cyclotron.[53] Since that time, other types of accelerators have been utilized in TOF experiments[54-57] such as electron linear accelerators; the Los Alamos Meson Physics Facility (LAMPF), which accelerates protons to 800 MeV[58,59]; and the ORELA facility at Oak Ridge, Tenn.[60] The width of neutron bursts produced by accelerators can be lower than 100 ps.[61,62] If the burst becomes as narrow as ~ 50 ps, the resolution is limited by the time response of the neutron detector.

## 14.9 COMPENSATED ION CHAMBERS

Neutron counters located close to a reactor core are subjected to both neutron and gamma bombardment. Although a neutron counter—e.g., a $^{10}B$ counter—is mainly sensitive to neutrons, it responds to gammas too. At low reactor power, when the neutron flux is small, the neutron signal is overshadowed by a signal due to gammas emitted from fission products that had been accumulated from earlier reactor operation. To eliminate the effect of the gammas, a *compensated ion chamber* is used.

Compensated ion chambers operate in such a way that the gamma signal is subtracted from the total $(n + \gamma)$ signal and the output is proportional to the neutron signal only. Figure 14.24 shows the basic principle of a compensated ion chamber. The counter consists of two compartments. One, coated with boron, is sensitive to both neutron and gammas and produces a signal proportional to the total radiation field. The other is sensitive to gammas only and produces a signal proportional to $\gamma$ radiation only. As Fig. 14.24 shows, the circuitry is such that the $\gamma$ signal is subtracted from the $(\gamma + n)$ signal, thus giving a signal proportional to the neutron field only. The signal, in the form of a current, is measured by a picoammeter.

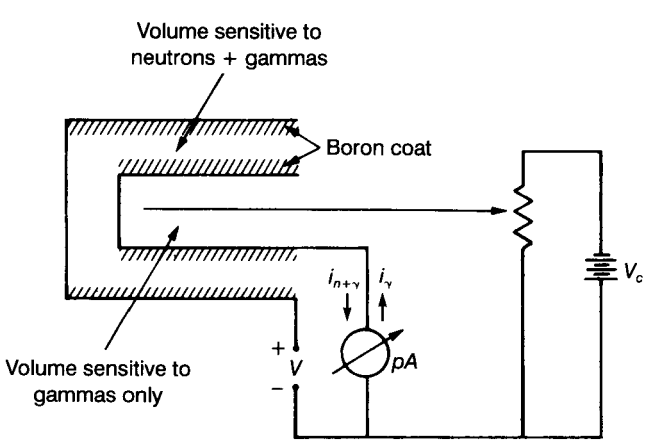


**Figure 14.24** A compensated ion chamber.

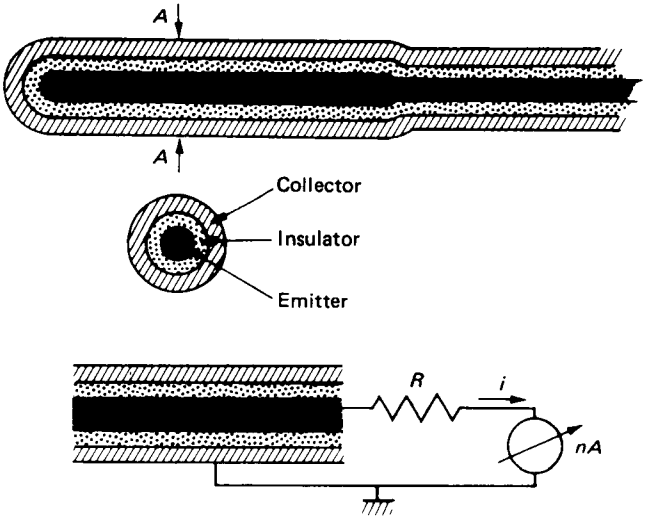


**Figure 14.25** Configuration of a self-powered detector.

Correct compensation is achieved when the signal is zero in a pure gamma field. This is accomplished by using the proper combination of volumes for the two compartments or by changing the voltages or by a combination of voltage and volume change. Typical compensation voltages ($V_c$) are of the order of $-25$ V; the positive voltage $V$ is of the order of $+800$ V. Without compensation, a detector of this type has a useful range from $2 \times 10^8$ to $2 \times 10^4$ neutrons/(m$^2$ ·s). With compensation, the useful range is extended downward by about two orders of magnitude. The sensitivity of compensated ion chambers is of the order of $10^{-18}$ A/[neutrons/(m$^2$ · s)].

## 14.10 SELF-POWERED NEUTRON DETECTORS (SPND)

Self-powered detectors, as their name implies, operate without an externally applied voltage. The incident radiation (neutrons or gammas or both) generates a signal in the form of a current proportional to the bombarding flux. The detectors are usually constructed in coaxial configuration (Fig. 14.25). The central conductor is called the *emitter* and is the material responsible for the generation of the signal. The outer conductor, called the *collector*, is separated from the emitter by an insulator. The collector is made of inconel alloy, and has the form of a metallic sheath encasing the insulator and the emitter.

The principle of signal generation in a self-powered detector is simple. As a result of bombardment by radiation, the emitter releases electrons (betas) that escape to the insulator and leave the emitter positively charged. If the emitter is connected to the collector through a resistor (Fig. 14.25), current flows, which

when measured, gives an estimate of the incident flux. Note that this is not an emitter-collector system: any beta particle escaping from the emitter contributes to the current, regardless of whether or not it reaches the collector.

Because self-powered detectors have been developed for use inside the core of power reactors, they are designed to have small size (a few millimeters in diameter), to be able to operate for rather long periods of time (years) in the intense radiation field of the reactor core without appreciable deterioration in performance, and finally, to operate without an external power supply.

The performance of a self-powered detector is given in terms of its sensitivity $S$, defined by the equation

$$S(t) = \frac{\Delta I(t)}{\Delta \phi} \tag{14.60}$$

where $I(t)$ = detector current after exposure to the flux $\phi$ for time $t$
$\phi$ = neutron flux

Thus, the sensitivity represents the change in detector current per unit change in the flux.

Many elements have been considered as emitters for self-powered detectors.[63-66] The ideal emitter should be such that the detector has

1. High sensitivity
2. Low burnup rate
3. Prompt response
4. Sensitivity to neutrons only

The material properties that determine these characteristics are discussed in Secs. 14.10.1 and 14.10.2, after the equations for the detector current and sensitivity are derived.

The properties of the insulator are also important. The insulator must have a resistance of about $10^{12}$ ohms at room temperature and $10^9$ ohms at reactor operating temperature. The two insulators commonly used are magnesium oxide (MgO) and aluminum oxide ($Al_2O_3$). Experiments have shown[67] that the resistance of MgO decreases with exposure to radiation, while that of $Al_2O_3$ does not change. For this reason, $Al_2O_3$ is gradually replacing MgO as an insulator for self-powered detectors.

The self-powered neutron detectors are divided into those with delayed response and those with prompt response. The characteristics of these types of self-powered detectors are presented in Secs. 14.10.1 and 14.10.2.

### 14.10.1 SPNDs with Delayed Response

Rhodium, vanadium, cobalt, and molybdenum have been used as emitters for SPNDs. Since rhodium SPNDs are the main in-core instruments for the determination of power distribution in pressurized-water reactors (PWR), they are discussed first and in greater detail than the others.

The signal of rhodium SPNDs is produced as a result of activation of the emitter ($^{103}$Rh) by the incident neutrons, and subsequent decay of the isotope $^{104}$Rh that is produced. The decay scheme of $^{104}$Rh is shown in Fig. 14.26. An isomeric state with a 4.4-min half-life is produced with a 12-b cross section. The ground state of $^{104}$Rh has a 43-s half-life and is formed with a cross section of 138 b (with thermal neutrons). It decays to $^{104}$Pd with a maximum $\beta^-$ energy of 2.5 MeV. This decay, which takes place 98.5 percent of the time, is primarily responsible for the signal of the rhodium detector. The isomeric state with the 4.4-min half-life contributes very little to the signal, but is responsible for a residual current after reactor shutdown.

To identify the factors that improve sensitivity of the detector and lengthen its life, one should look at the processes responsible for the generation of the detector signal. This is done below, and equations for current and sensitivity are derived for any emitter material.

Consider an emitter with an average neutron absorption cross section $\sigma$ exposed to a total neutron flux $\phi$, and upon absorption of a neutron becoming radioactive with a half-life $T$ [or decay constant $\lambda = (\ln 2)/T$]. The number of radioactive atoms $N(t)$ present after exposure for time $t$ is (see Eq. 14.16)

$$N(t) = \frac{s\sigma_e \phi N_0}{\lambda - \sigma_a \phi}(e^{-s\sigma_a \phi t} - e^{-\lambda t}) \tag{14.61}$$

where $N_0$ = number of emitter atoms at $t = 0$
$\sigma_a$ = absorption cross section of emitter
$\sigma_e$ = cross section that leads to the state that contributes to the signal
$s$ = self-shielding factor ($s < 1$)

The self-shielding factor $s$ corrects for the fact that the target (emitter) is thick, as a result of which the flux in the emitter is depressed. Thus, interior atoms are "shielded" from exposure to the full flux by the atoms close to the surface. The

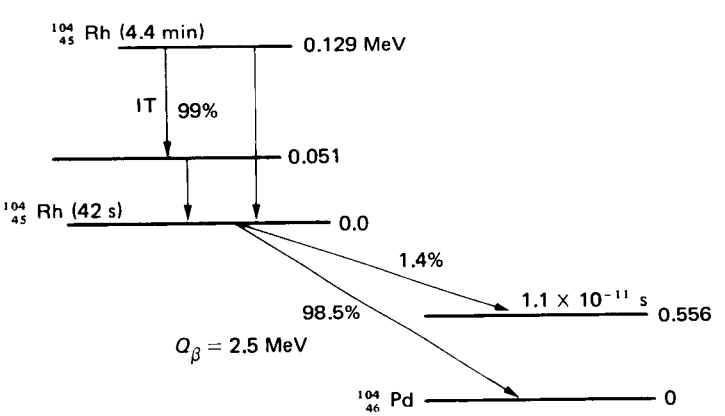


**Figure 14.26** The decay scheme of $^{104}$Rh.

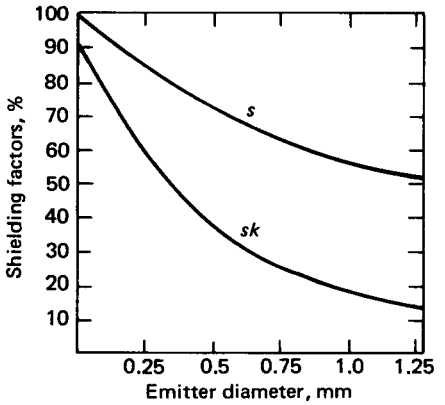


**Figure 14.27** The self-shielding factors for rhodium detectors with 10-mil (0.254-mm) thick MgO insulator (from Ref. 68).

shielding factor is less than 1 and decreases as the diameter of the emitter increases (see Fig. 14.27). If every decay of the radioisotope releases a particle with charge $q$, the current at time $t$ is equal to

$$I(t) = kqN(t)\lambda = kq\frac{s\sigma_e\phi N_0}{1 - \sigma_a\phi/\lambda}(e^{-s\sigma_a\phi t} - e^{-\lambda t}) \tag{14.62}$$

where $k$ is a constant that takes into account such effects as self-absorption of betas in the emitter or loss of betas in the insulator (see Fig. 14.27). The factor $\sigma_a\phi/\lambda$ in the denominator can be neglected because, for all emitters of interest, $\sigma_a\phi/\lambda \ll 1$. The exponential factors of Eq. 14.62 have the following meaning.

The factor $\exp(-\lambda t)$ gives the response of the detectors. If the flux undergoes a step increase, as shown in Fig. 14.28, the signal will rise exponentially to its saturated value. If the flux goes down suddenly, the signal will decay

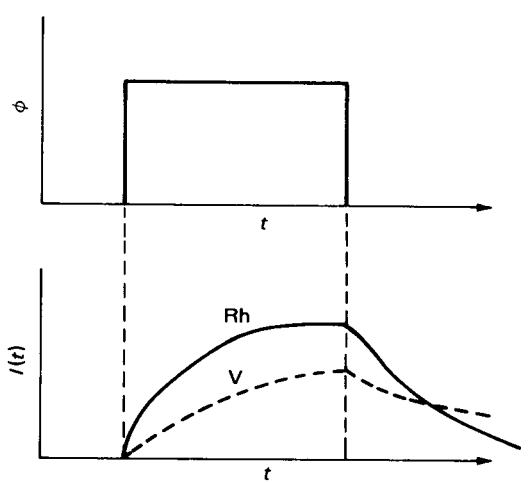


**Figure 14.28** The response of Rh and V SPNDs to a step change in neutron flux.

again exponentially. The speed of response is determined by the half-life of the isotope involved. Rhodium, with a half-life of 42 s, reaches saturation after about 5 min. Vanadium ($^{52}$V), with a half-life equal to 3.76 min, reaches saturation after about 25 min.

The factor $\exp(-s\sigma_a\phi t)$ gives the burnup rate of the emitter. It is the factor that determines the lifetime of the detector, because, as seen below, the decrease in sensitivity with time is essentially given by this same factor.

Assuming saturation, the sensitivity of the detector is given (using Eqs. 14.60 and 14.62) by

$$S(t) = \frac{\Delta I(t)}{\Delta\phi} = ks\sigma_e N_0 q(1 - s\sigma_a\phi t)e^{-s\sigma_a\phi t}\ \text{A/[neutrons/(m}^2\cdot\text{s)]} \quad (14.63)$$

If the emitter diameter is $D$, its length is $L$, its density is $\rho$, and its atomic weight is $A$, then the number of atoms is $N_0 = (\rho\pi D^2/4)(LN_A/A)$, where $N_A$ is Avogadro's number.

Substituting into Eq. 14.63, one obtains an equation for the sensitivity per unit length:

$$\frac{S(t)}{L} = ksq\sigma_e\rho\frac{\pi D^2}{4}\frac{N_A}{A}(1 - s\sigma_a\phi t)e^{-s\sigma_a\phi t}\ \text{(A/m)/[neutrons/(m}^2\cdot\text{s)]} \quad (14.64)$$

**Example 14.6** What is the sensitivity of Rh detectors 0.5 mm in diameter, per unit detector length under saturation conditions, for a new detector?

**Answer** For rhodium, $\sigma_e = 139$ b, $\sigma_a = 150$ b, $\rho = 12.4 \times 10^3$ kg/m$^3$, $A = 103$, and $q = 1.602 \times 10^{-19}$ C. At the beginning of life ($t = 0$),

$$\frac{S(0)}{L} = ks(1.602 \times 10^{-19}\ \text{C})(139 \times 10^{-28}\ \text{m}^2)(12.4 \times 10^3\ \text{kg/m}^3)$$
$$\times \pi\frac{(5 \times 10^{-4})^2\ \text{m}^2}{4}\left(\frac{6.022 \times 10^{26}}{103}\ \text{atoms/kg}\right)$$
$$= 3.17 \times 10^{-23}ks\ \text{(A/m)/[neutrons/(m}^2\cdot\text{s)]}$$

Typical values of $ks$ are about 0.4.[68] Since the flux in a large power reactor (1000 MWe) is about $10^{17}$ neutrons/(m$^2\cdot$s)[$10^{13}$neutrons/(cm$^2\cdot$s)] at full power, and the typical detector has a length of about 0.10 m, the expected current is of the order of

$$(0.8)(0.8 \times 10^{-23})\text{(A/m)/[neutrons/(m}^2\cdot\text{s)][}10^{17}\ \text{neutrons/(m}^2\cdot\text{s)](0.1 m)}$$
$$= 1.92 \times 10^{-7}\ \text{A} \approx 200\ \text{nA}$$

Equation 14.64 shows that to achieve high sensitivity, one should select an emitter with high cross section $\sigma_e$ and large diameter $D$. The diameter affects

the sensitivity through the factor $D^2$ and through the shielding factors $k$ and $s$, which decrease† as the diameter increases. The net result is that the sensitivity changes roughly as the first power of the diameter.[68]

A high cross section increases the sensitivity but also increases the rate at which the sensitivity decreases with time. Indeed, from Eq. 14.64, the ratio of the sensitivity after exposure for time $t$ to its value at time $t = 0$ is

$$\frac{S(t)}{S(0)} = (1 - s\sigma_a\phi t)e^{-s\sigma_a\phi t} \tag{14.65}$$

Table 14.6 gives the characteristics of several self-powered detectors. Rhodium detectors have the best sensitivity but also the largest burnup rate. Their change of sensitivity with time is important and necessitates a correction before the signal is used for the determination of power. The correction is not trivial because of changes in self-absorption effects in the emitter, and may introduce errors unless the detector is calibrated properly.

Despite the drawback of large burnup, rhodium SPNDs are used extensively in nuclear power plants, especially in PWRs for the determination of power distribution, fuel burnup, and other information related to the performance of the core. The detectors are inserted into a certain number of "instrumented" fuel assemblies through guide tubes. Every instrumented assembly has seven equally spaced SPNDs (a background detector and a thermocouple are also included in the package; see Fig. 14.29) for the measurement of the flux at seven axial locations. The outputs of the detectors, corrected for background, are transmitted to the plant computer, where after appropriate corrections are applied, the power, fuel burnup, plutonium production, etc., are calculated. Every PWR has a least 50 instrumented assemblies, which means that the flux is monitored at more than 350 locations.

†The factor $s$ is not constant over prolonged exposure. It tends to increase as the emitter burnup continues because a smaller number of emitter atoms is left for self-shielding.[65]

**Table 14.6 Characteristics of Self-Powered Detectors with 0.5-mm Emitter Diameter**[62,65]

| Emitter | Sensitivity (A/m)/[2 × $10^{17}$ neutrons/(m$^2$·s)] | Burnup†/year (%) for $\phi = 2 \times 10^{17}$ neutrons/(m$^2$·s) | Response |
|---|---|---|---|
| Rh | $2.4 \times 10^{-6}$ | 5 | Delayed |
| V | $1.5 \times 10^{-7}$ | 0.3 | Delayed |
| Co | $3.4 \times 10^{-8}$ | 2.3 | Prompt |
| Mo | $1.7 \times 10^{-8}$ | 0.9 | Prompt |
| Pt | $2.6 \times 10^{-7}$ | 0.2 | Prompt |

†Burnup $\approx 1 - \exp(\sigma_a\phi t)$.

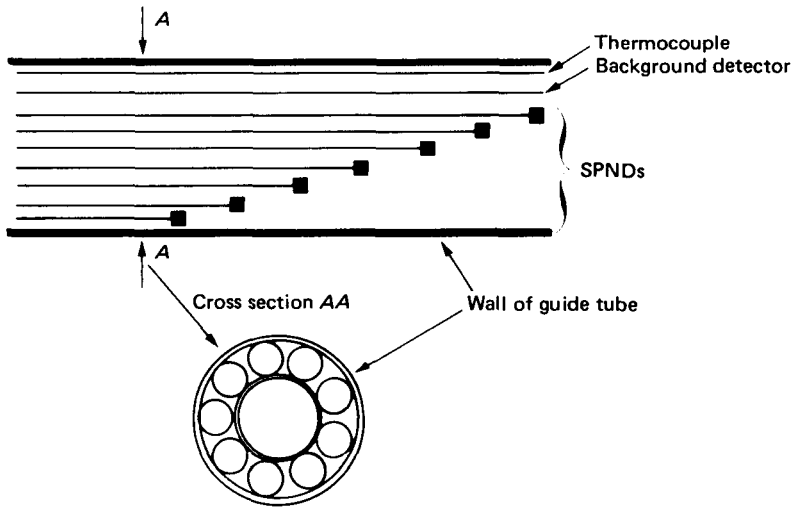


**Figure 14.29** Each detector tube contains seven SPNDs, one background detector, and one thermocouple.

### 14.10.2 SPNDs with Prompt Response

Neutron-sensitive self-powered detectors with prompt response operate on a different principle than rhodium and vanadium SPNDs. The emitter, in this case, absorbs a neutron and emits gammas at the time of capture. It is these capture gammas that are responsible for the signal, and since they are only emitted at the time of the neutron capture, the detector response is instanta-

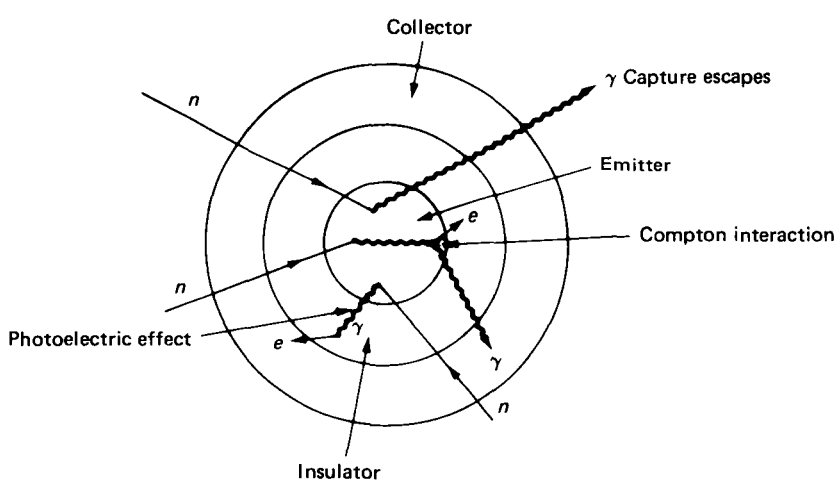


**Figure 14.30** Production of electrons by capture gammas from a Co emitter.

neous. Cobalt ($^{59}$Co) and molybdenum ($^{95}$Mo) are two elements seriously considered as emitters. The subsequent discussion is based on cobalt, but the processes involved in the signal generation are the same for molybdenum.

Consider, then, a cobalt SPND (Fig. 14.30). Most of the capture gammas traverse the emitter, the insulator, and the collector without an interaction. Those that do interact produce electrons through the photoelectric or Compton reactions. As these fast electrons travel, they produce an outward flow of charge that generates a current. Because relatively few gammas interact, the sensitivity of a cobalt detector is lower than that of either rhodium or vanadium detectors (see Table 14.6).

The Co detector has one undesirable characteristic due to the product of the neutron capture. That product is $^{60}$Co, a $\beta^-$ emitter with a 5.3-year half-life. The betas from $^{60}$Co produce a background signal that builds up with exposure. A way to suppress this background, using platinum shields, has been reported by Goldstein and Todt.[69]

## 14.11 CONCLUDING REMARKS

Neutron detection is, in general, more complicated and more difficult than detection of either charged particles or photons for two reasons. First, neutrons have no charge and can only be detected indirectly through photons or charged particles that they generate. Second, the neutron energy range spans at least 10 decades ($10^{-3}$ eV $< E <$ $10^8$ eV), over which the type and cross sections for

**Table 14.7 Summary of Neutron Detectors and Their Range of Application**

| Neutron energy | Measurement of number of neutrons only | Measurement of energy and number of neutrons |
|---|---|---|
| $0 < E < 1$ keV | $BF_3$, boron-coated, SPND, TLD,† $^6$Li, $^3$He<br>Foil activation<br>Fission track detectors† | Crystal spectrometer<br>Time-of-flight |
| 1 keV $< E \lesssim 2$ MeV | $BF_3$, $^6$Li (both with low efficiency)<br>Foil activation, SPND<br>Bonner ball † | Proton recoil (proportional counters, organic scintillators)<br>Time-of-flight<br>Threshold reactions |
| $E \gtrsim 1$ MeV | Foil activation | Organic scintillators<br>Threshold reactions<br>Time-of-flight |

† See Chap. 16.

neutron reactions change drastically. Table 14.7 gives a summary of all the methods for neutron detection and spectrometry.

## PROBLEMS

**14.1** Prove that for thermal neutrons, the kinetic energies of the alpha particle and the lithium in the $^{10}B(n, \alpha)^7Li$ reaction are given by

$$T_\alpha = \frac{M_{Li}}{M_\alpha + M_{Li}} Q \qquad T_{Li} = \frac{M_\alpha}{M_\alpha + M_{Li}} Q$$

**14.2** If the neutron energy is 1 MeV, what is the maximum energy of the proton in the $^3He(n, p)^3H$ reaction?

**14.3** Obtain the efficiency curve as a function of neutron energy for a 1-in-diameter proportional counter filled with $^3He$ at 10 atm. Assume $1/v$ cross section from 0.01 to 1000 eV. The neutron beam is perpendicular to the counter axis. Compare your result with that of Fig. 14.3.

**14.4** Show that the sensitivity of a neutron counter ($BF_3$ or boron-lined or fission counter) decreases with time as $\exp(-\sigma_a \phi t)$.

**14.5** What is the maximum thickness of $^{235}U$ coating inside a fission counter if it is required that a 60-MeV fission fragment lose no more than 10 percent of its energy as it goes through the uranium deposit? For the fission fragment, assume $Z = 45$, $A = 100$.

**14.6** How long should one irradiate an $^{115}In$ foil (100 $mm^2$ area, 1 mm thick) in a thermal neutron flux of $10^{14}$ neutrons/($m^2 \cdot s$) to obtain 1 mCi ($3.7 \times 10^7$ Bq) of activity? ($\sigma = 194$ b, $\rho = 7.3 \times 10^3$ $kg/m^3$, $T_{1/2} = 54$ min.)

**14.7** An aluminum foil is left in a reactor for 15 s in a flux of $10^{16}$ neutrons/($m^2 \cdot s$). What is the activity produced? ($\sigma = 0.23$ b, $T_{1/2} = 2.3$ min, $m = 10^{-6}$ kg.)

**14.8** The betas from the Al foil of Prob. 14.7 were counted in a $2\pi$ detection system with $\epsilon = 0.95$. Counting started 1 min after the end of the irradiation and stopped 2 min later. If the background is 20 counts/min, how many counts will the scaler record?

**14.9** Calculate the irradiation time needed to produce $^{198}Au$ in such a quantity that the gross counting rate is 1000 counts/min using a counter with $\Omega = 10^{-2}$, $\epsilon = 0.90$, and $F = 1$. The background is 100 counts/min. It takes 10 min to get the sample from the reactor, place it under the counter, and start counting. [$\phi = 10^{16}$ neutrons/($m^2 \cdot s$), $T_{1/2} = 2.7$ days, $\sigma = 99$ b, $m(^{197}Au) = 10^{-9}$ kg.]

**14.10** In a light-water reactor, how long will it take for the initial amount of $^{235}U$ to be reduced by 50 percent? ($\phi = 10^{17}$ neutrons/($m^2 \cdot s$), $\sigma_a = 670$ b.)

**14.11** Prove Eq. 14.24. Also show that the neutron and the proton directions after collision are 90° apart ($\theta + \phi = 90°$, Fig. 14.8).

**14.12** Calculate the measured neutron spectrum obtained by the proton recoil method if the detector response is a $\delta$-function and the source spectrum is the "square" function shown in the figure below. Assume $\sigma(n, p)$ is constant for the range $E_1 \le E \le E_2$.

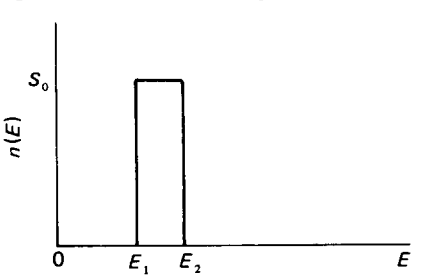

**14.13** Assuming that the threshold-reaction cross sections are ideal step functions, as shown in this figure, indicate how the neutron energy spectrum could be obtained. There are $N$ such cross sections with thresholds at $E_i|_{i=1,N}$ and $E_{i+1} - E_i = \Delta E =$ constant.

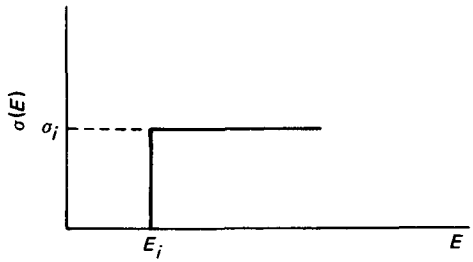


**14.14** Prove Eq. 14.49.

**14.15** Prove Eq. 14.56 and show that it takes the form of Eq. 14.57 in a nonrelativistic region.

**14.16** A neutron TOF experiment will be designed for the measurement of 1-MeV neutrons, with the requirement that the energy resolution is 0.1 percent. What should the length of the flight path be if $\Delta t = 1$ ns and $\Delta L/L$ is negligible?

**14.17** The original Fermi chopper consisted of a cylinder 1.5 in in diameter with a maximum rotational speed of 15,000 r/min. The open channels consisted of aluminum sheets $\frac{1}{32}$ inch thick.

(a) Calculate the angle during which the channel is fully open.

(b) Assuming the maximum rotational speed, what is the minimum neutron speed necessary for a neutron to make it through the channel?

**14.18** What is the burnup rate per month of an SPND using $^{235}U$ as the emitter and being exposed to a thermal flux of $2 \times 10^{17}$ neutrons/(m$^2 \cdot$ s)?

**14.19** How long will it take for the sensitivity of a rhodium SPND to decrease to 50 percent of its initial value? Assume a thermal flux of $10^{18}$ neutrons/(m$^2 \cdot$ s).

**14.20** Using semiquantitative arguments, show that the sensitivity of a Co detector increases as $D^m$, where $D$ is the emitter diameter and $2 < m < 3$.

## BIBLIOGRAPHY

"A Review of Radiation Energy Spectra Unfolding," Proceedings of a Seminar-Workshop, ORNL/RSIC-40 (1976).

Beckurts, K. H., and Wirtz, K., *Neutron Physics*, Springer-Verlag, Berlin, 1964.

Fleischer, R. L., Price, P. B., and Walker, R. M., *Nuclear Tracks in Solids*, University of California Press, Berkeley, Calif., 1975.

Knoll, G., *Radiation Detection and Measurement*, Wiley, New York, 1979.

## REFERENCES

1. Bishop, G. B., *Nucl. Instrum. Meth.* **62**:247 (1968).
2. Murray, R. B., *Nucl. Instrum. Meth.* **2**:237 (1958).
3. Ginther, R. J., and Schulman, J. H., *IRE Trans. Nucl. Sci.* **N.S-5**(3):92 (1958).
4. Voitovetskii, V. K., Tolmcheva, N. S., and Arsaev, M. I., *Atomn. Energ.* **6**:321 (1959).
5. Spowart, A. R., *Nucl. Instrum. Meth.* **135**:441 (1975).
6. Spowart, A. R., *Nucl. Instrum. Meth.* **140**:19 (1977).

7. Hill, N. W., Harvey, J. A., Slaughter, G. G., and St. James, A., 147, ORNL-4743 (1972).
8. Haacke, L. C., Hewett, J. S., and McNeill, K. S., *Nucl. Instrum. Meth.* **144**:507 (1977).
9. Benjamin, R. W., Ahlfeld, C. E., Harvey, J. A., and Hill, N. W., *Nucl. Sci. Eng.* **55**:440 (1974).
10. Bramblett, R. L., Ewing, R. L., and Bonner, T. W., *Nucl. Instrum. Meth.* **9**:1 (1960).
11. Bonner, T. W., *Nucl. Phys.* **23**:116 (1961).
12. Hanna, G. C., *Nucl. Sci. Eng.* **15**:325 (1963).
13. Brunfelter, B., Kockum, J., and Zetterstrom, H. O., *Nucl. Instrum. Meth.* **40**:84 (1966).
14. Bennett, E. F., *Nucl. Sci. Eng.* **27**:16 (1967).
15. Bennett, E. F., *Nucl. Sci. Eng.* **27**:28 (1967).
16. Bennett, E. F., Gold, R., and Olson, I. K., ANL-7394 (1968).
17. Bennett, E. F., and Yule, T. J., ANL-7763 (1971).
18. Johnson, R. H., ORNL/RSIC-40, p. 41 (1976).
19. Burrus, W. R., ORNL-3743 (June 1965).
20. Burrus, W. R., and Verbinski, V. V., *Nucl. Instrum. Meth.* **67**:181 (1969).
21. Burrus, W. R., ORNL/RSIC-40, p. 2 (1976).
22. Verbinski, V. V., Burrus, W. R., Love, T. A., Zobel, W., Hill, N. W., and Textor, R., *Nucl. Instrum. Meth.* **65**:8 (1968).
23. Kendrick, H., and Harris, L., Jr., GULF-RT-A10821 (1971).
24. Johnson, R. H., Wehring, B. W., and Dorning, J. J., *Nucl. Sci. Eng.* **73**:93 (1980).
25. "COOLC and FERDOR Spectra Unfolding Code," RSIC PSR-17, ORNL (19xx).
26. "FORIST Spectra Unfolding Code," RSIC PSR-92, ORNL (1975).
27. Bennett, E. F., and Yule, T. J., *Nucl. Sci. Eng.* **46**:236 (1971).
28. Verbinski, V. V., and Giovannini, R., *Nucl. Instrum. Meth.* **114**:205 (1974).
29. Snidow, N. L., and Warren, H. D., *Nucl. Instrum. Meth.* **51**:109 (1967).
30. Vehar, D. W., Clikeman, F. M., and Johnson, R. H., *ANS Trans.* **33**:697 (1979).
31. Brooks, F. D., *Nucl. Instrum. Meth.* **162**:477 (1979).
32. Nordell, B., *Nucl. Instrum. Meth.* **224**:547 (1984).
33. Furuta, Y., Kinbara, S., and Kaieda, K., *Nucl. Instrum. Meth.* **84**:269 (1970).
34. Ingersoll, D. T., and Wehring, B. W., *Nucl. Instrum. Meth.* **147**:551 (1977).
35. Harvey, J. A., and Hill, N. W., *Nucl. Instrum. Meth.* **162**:507 (1979).
36. Johnson, R. H., Ingersoll, D. T., Wehring, B. W., and Dorning, J. J., *Nucl. Instrum. Meth.* **145**:337 (1977).
37. Numata, S., Abe, T., and Shin, K., *Nucl. Instrum. Meth.* **269**:261 (1988).
38. Shin, K., and Hamamoto, M., *Nucl. Instrum. Meth.* **269**:272 (1988).
39. McElroy, W. N., Berg, S., and Crockett, T., AFWL-TR-67-41, vols. I-IV (1967).
40. Greer, C. R., and Walker, J. V., SC-DC-66-1512 (1966).
41. DiCola, G., and Rota, A., *Nucl. Sci. Eng.* **23**:344 (1965).
42. "LSL-M2 Least-Squares Logarithmic Adjustment of Neutron Spectra," PSR-233, RSIC/ORNL (July 1987).
43. Berg, S., BNWL-855 (1968).
44. Oster, C. A., Simons, R. L., Odette, G. R., McElroy, W. N., and Lippincott, E. P., ORNL/RSIC-40, p. 148 (1976).
45. Stallmann, F. W., NUREG/CR-2222, ORNL/TM-8976, USNRC (Dec. 1981).
46. Sawyer, R. B., Wollan, E. O., Bernstein, S., and Peterson, K. C., *Phys. Rev.* **72**:109 (1947).
47. Borst, L. B., and Sailor, V. L., *Rev. Sci. Instrum.* **24**:141 (1953).
48. Firk, F. W. K., *Nucl. Instrum. Meth.* **162**:539 (1979).
49. Fermi, E., and Marshall, L., *Phys. Rev.* **72**:193 (1947).
50. Selove, W., *Rev. of Sci. Instrum.* **23**:350 (1952).
51. Seidl, F. G. P., Hughes, D. J., Palevsky, H., Levin, J. S., Kato, W. Y., and Sjostrand, N. G., *Phys. Rev.* **95**:476 (1954).
52. Bollinger, L. M., Cote, R. E., and Thomas, G. E., *Proceedings of the 2nd Intern. Conference on Peaceful Uses of Atomic Energy*, **14**:239 (1958).
53. Alvarez, L. W., *Phys. Rev.* **54**:609 (1938).
54. Bareford, C. F., and Kelliker, M. G., *Phillips Technol. Rev.* **15**:1 (1953).

55. Firk, F. W. K., and Bowey, E. M., "Comptes Rendus du Congres Intern. de PHysique Nucleaire," P. Gugenberger (ed.), C.N.R.S., Paris, 1964.
56. Wasson, O. A., and Draper, J. E., *Nucl. Phys.* **73**:499 (1965).
57. Harvey, J. A., "Proc. Int. Conf. on Interactions of Neutrons with Nuclei," E. Sheldon (ed.), US ERDA Tech Info. Center, Oak Ridge, Tenn., p. 144.
58. Cokinos, D. M., and Van Tuyle, G. J., *ANS Transactions* **69**:423 (1993).
59. Bowman, C. D., Venneri, F., and Waters, L. S., *ANS Transactions* **69**:425 (1993).
60. Dickens, J. K., *ANS Transactions* **69**:424 (1993).
61. Norris, N. J., and Hanst, R. K., *Edgerton, Germeshausen and Grier, Prog. Rep. EGG*, 1183-2142 (1967).
62. Laszewski, R. M., Holt, R. J., and Jackson, H. E., *Phys. Rev. Lett.* **38**:813 (1977).
63. Hilborn, J. W., *Nucleonics* **22**(2):69 (1964).
64. Joslin, C. W., *Nucl. Eng. Intern.* (May 1972).
65. Kroon, J. C., Smith, F. M., and Taylor, R. I., *ANS Trans.* **23**:459 (1976).
66. Balcar, E., Bock, H., and Hahn, F., *Nucl. Instrum. Meth.* **153**:429 (1978).
67. Bozarth, D. P., and Warren, H. D., *ANS Trans.* **23**:517 (1976).
68. Hawer, J. M., and Beckerley, J. G., TID-25952-P1, vol. 1 (1973).
69. Goldstein, N. R., and Todt, W. H., *IEEE Trans.* **NS-26**:1 (1979).

CHAPTER
# FIFTEEN

# ACTIVATION ANALYSIS

## 15.1 INTRODUCTION

Activation analysis achieves a qualitative and quantitative analysis of an unknown sample by irradiating the sample and thus producing radioactive nuclides from stable or unstable isotopes present in the sample. The radioactive nuclides can then be identified from properties of the radiations they emit:

1. Type of radiation
2. Energy of radiation
3. Intensity of radiation
4. Half-life

The basic principle of activation analysis is not new. It was applied for the first time in 1936 by Hevesy and Levi,[1] who determined the amount of dysprosium in an yttrium sample. The dysprosium in the sample became radioative when bombarded with neutrons from a Ra-Be source. Two years later, Seaborg and Livingood[2] determined the gallium content in an iron sample by bombarding it with deuterons. The sensitivity of the method increased considerably with the availability of high neutron fluxes for nuclear reactors. Although charged particles, gamma rays, and 14-MeV neutrons may be used as the bombarding particles, thermal neutrons are, by far, the particles most frequently utilized for the irradiation of the sample.

Activation analysis has become, because of its extremely high sensitivity, an indispensable tool in a wide variety of fields[3] ranging from science and engineering[4] to industry,[5,6] minerals exploration,[7-14] medicine,[15-21] environmental monitoring,[12,22-28] and forensic science.[29-32] The purpose of this chapter is not to present all the aspects, details, and applications of this field, but to discuss the major steps that comprise the method, the interpretation of the results, the errors and sensitivity of the method, and certain representative applications. The reader will find many more details and an extensive list of applications in the bibliography and the references given at the end of the chapter.

The activation analysis method consists of the following major steps, to be discussed next:

1. Selection of the optimum nuclear reaction
2. Preparation of the sample for irradiation
3. Irradiation of the sample
4. Counting of the irradiated sample
5. Analysis of the counting results

## 15.2 SELECTION OF THE OPTIMUM NUCLEAR REACTION

The optimum nuclear reaction is chosen with these considerations in mind.

1. Production of large activity should occur within a reasonable irradiation time.
2. The radioisotope produced should have a reasonable half-life ($T >$ min).
3. The type and energy of the radiation emitted by the radioisotope should not present great counting difficulties.
4. A minimum number of interfering reactions should be involved.

If the sample is completely unknown, one starts with neutron irradiation because neutrons are absorbed by almost all isotopes. If the composition of the sample is known, then the best reaction for the identification of the isotope of interest should be chosen. Sometimes there is more than one reaction available for the same isotope. For example, aluminum bombarded with fast neutrons may be detected by three different reactions:

$$^{27}\mathrm{Al}(n, p)^{27}\mathrm{Mg}$$
$$^{27}\mathrm{Al}(n, \alpha)^{24}\mathrm{Na}$$
$$^{27}\mathrm{Al}(n, \gamma)^{28}\mathrm{Al}$$

The "optimum nuclear reaction" depends not only on the isotope and the bombarding particles but also on the composition of the sample that is analyzed. For example, the $^{27}\mathrm{Al}(n, \gamma)^{28}\mathrm{Al}$ reaction may be the best for detection of aluminum in a certain sample. However, if the sample contains silicon in

addition to aluminum, the reaction $^{28}Si(n, p)^{28}Al$ also produces $^{28}Al$, and thus causes an interference to the measurement. If silicon is present, it may be better to use the reaction $^{27}Al(n, p)^{27}Mg$ or $^{27}Al(n, \alpha)^{24}Na$. More details about interfering reactions are given in Sec. 15.9.

The most commonly used neutron reaction is the $(n, \gamma)$ reaction, which takes place with almost all isotopes (although with different probability) and has no threshold. In general, the $(n, \gamma)$ cross section is higher for thermal than for fast neutrons. Other neutron interactions are $(n, \alpha)$, $(n, p)$, and $(n, 2n)$ reactions; except for a few exothermic $(n, \alpha)$ reactions, the others have a threshold; therefore, they can occur with fast neutrons only. Table 15.1 lists neutron reactions for the identification of several elements. Details for many more elements and reactions can be found in the bibliography of this chapter.

**Table 15.1 Neutron Activation Reactions**

| Element | Symbol | Reaction | Threshold energy (MeV) | Half-life of product | Main radiation emitted and its energy (MeV) |
|---|---|---|---|---|---|
| Aluminum | Al | $^{27}Al(n, \gamma)^{28}Al$ | (–)† | 2.3 min | $\beta^-$ (2.85), $\gamma$ (1.78) |
| | | $^{27}Al(n, p)^{27}Mg$ | 1.9 | 9.46 min | $\beta^-$ (1.75), $\gamma$ (0.84, 1.013) |
| | | $^{27}Al(n, \alpha)^{24}Na$ | 3.27 | 15 h | $\beta^-$ (1.389), $\gamma$ (1.369, 2.754) |
| Arsenic | As | $^{75}As(n, \gamma)^{76}As$ | (–) | 26.4 h | $\beta^-$ (2.97), $\gamma$ (0.559) |
| | | $^{75}As(n, \alpha)^{72}Ga$ | (–) | 14.1 h | $\beta^-$ (3.15), $\gamma$ (0.835) |
| | | $^{75}As(n, 2n)^{74}As$ | 8.27 | 17.9 d | $\beta^-$ (3.15), $\gamma$ (0.835) |
| Cadmium | Cd | $^{110}Cd(n, \gamma)^{111m}Cd$ | (–) | 48.6 min | $e^-$, $\gamma$ (0.247) |
| | | $^{110}Cd(n, p)^{110m}Ag$ | 2.12 | 235 d | $\gamma$ (0.658) |
| Calcium | Ca | $^{48}Ca(n, \gamma)^{49}Ca$ | (–) | 8.8 min | $\gamma$ (3.07), $\beta$ (1.95) |
| Chlorine | Cl | $^{37}Cl(n, \gamma)^{38}Cl$ | (–) | 37.2 min | $\beta^-$ (4.91), $\gamma$ (1.6, 2.17) |
| | | $^{37}Cl(n, p)^{37}S$ | 3.6 | 5 min | $\beta^-$, $\gamma$ (3.09) |
| Copper | Cu | $^{63}Cu(n, 2n)^{62}Cu$ | 11.01 | 9.76 min | $\gamma$ (0.511) |
| Fluorine | F | $^{19}F(n, \alpha)^{16}N$ | 1.57 | 7.15 s | $\gamma$ (6.13) |
| Gold | Au | $^{197}Au(n, \gamma)^{198}Au$ | (–) | 2.7 d | $\beta^-$ (0.962), $\gamma$ (0.412) |
| | | $^{197}Au(n, 2n)^{196}Au$ | 7.36 | 6.18 d | $\beta^-$, $\gamma$ (0.356) |
| Iodine | I | $^{127}I(n, \gamma)^{128}I$ | (–) | 25 min | $\beta^-$ (2.12), $\gamma$ (0.441) |
| Iron | Fe | $^{58}Fe(n, \gamma)^{59}Fe$ | (–) | 45.5 d | $\beta^-$, $\gamma$ (1.095, 1.292) |
| | | $^{56}Fe(n, p)^{56}Mn$ | 2.98 | 2.57 d | $\beta^-$, $\gamma$ (0.847) |
| Lead | Pb | $^{208}Pb(n, 2n)^{207m}Pb$ | 7.45 | 0.885 s | $\gamma$ (0.570) |
| Mercury | Hg | $^{200}Hg(n, 2n)^{199m}Hg$ | 8.11 | 43 min | $\gamma$ (0.158) |
| | | $^{196}Hg(n, \gamma)^{197}Hg$ | (–) | 65 h | $\gamma$ (0.077) |
| | | $^{202}Hg(n, \gamma)^{203}Hg$ | (–) | 46.9 d | $\gamma$ (0.279) |
| Nickel | Ni | $^{58}N(n, 2n)^{57}Ni$ | 12.09 | 36 h | $\beta^+$, $\gamma$ (0.511, 1.37) |
| Nitrogen | N | $^{14}N(n, 2n)^{13}N$ | 11.31 | 10 min | $\gamma$ (0.511) |
| Oxygen | O | $^{16}O(n, p)^{16}N$ | 10.2 | 7.1 s | $\gamma$ (6.13) |
| Phosphorus | P | $^{31}P(n, \alpha)^{28}Al$ | 2 | 2.3 min | $\beta^-$, $\gamma$ (1.78) |
| Potassium | K | $^{39}K(n, 2n)^{38}K$ | 13.41 | 7.7 min | $\gamma$ (0.511, 2.17) |
| Silicon | Si | $^{28}Si(n, p)^{28}Al$ | 3.99 | 2.3 min | $\gamma$ (1.78) |
| Silver | Ag | $^{109}Ag(n, \gamma)^{110}Ag$ | (–) | 24 s | $\gamma$ (0.66) |

†(–) = No threshold.

Charged-particle reactions are also used in activation analysis. Their disadvantage over neutron reactions is that charged-particle reactions are mostly endothermic, i.e., they have a threshold. Table 15.2 gives several examples of such reactions.

Photon activation complements neutron and charged-particle activation. Photons are better than neutrons in certain cases. For example, photons are preferred if the product of the neutron activation is an isotope that has a very short half-life or emits only low-energy betas or low-energy X-rays. The cross sections for photonuclear reactions are generally smaller than those for neutrons and charged particles. Table 15.3 gives several photonuclear reactions that have been used in activation analysis.

## 15.3 PREPARATION OF THE SAMPLE FOR IRRADIATION

A sample should be prepared properly and then placed in a container before it is irradiated. The person who prepares the sample should be extremely careful not to contaminate it. Activation analysis is so sensitive that it can determine traces of elements undetectable by chemical methods. If the sample is left on a table for a certain period of time, it collects dust that acts as a contaminant. Touch by hand may transfer enough salt to cause the irradiated sample to show the presence of sodium and chlorine. To avoid contamination, samples should be handled in dry boxes or in clean rooms. The person who prepares the sample should use clean instruments (knife, file, tweezers, etc.) and also wear clean plastic gloves.

**Table 15.2 Charged-Particle Reactions**

| Element | Symbol | Reaction | Threshold energy (MeV) | Half-life of product | Main radiation emitted and its energy (MeV) |
|---|---|---|---|---|---|
| Boron | B | $^{10}B(\alpha, n)^{13}N$ | – | 10 min | $\beta^+, \gamma$ (0.511) |
| | | $^{10}B(p, \gamma)^{11}C$ | 0.4 | 20.4 min | $\beta^+, \gamma$ (0.511) |
| | | $^{11}B(p, n)^{11}C$ | 2.76 | | |
| Carbon | C | $^{12}C(p, n)^{12}N$ | 18.12 | 11 ms | |
| Nitrogen | N | $^{14}N(p, \alpha)^{11}C$ | 2.88 | 20.4 min | |
| Oxygen | O | $^{16}O(\alpha, d)^{18}F$ | 35 | 109.8 min | |
| Sodium | Na | $^{23}Na(\alpha, n)^{26m}Al$ | 4.62 | 6.7 s | $\beta^+, \gamma$ (0.511) |
| Aluminum | Al | $^{27}Al(\alpha, n)^{30}P$ | 3.38 | 2.55 min | $\beta^+, \gamma$ (0.511) |
| Copper | Cu | $^{63}Cu(\alpha, n)^{66}Ga$ | 7.69 | 9.45 h | |
| Phosphorus | P | $^{31}P(d, p)^{32}P$ | – | 14.3 d | $\beta^-$ ($E_{max} = 1.17$) |
| Iron | Fe | $^{54}Fe(d, n)^{55}Co$ | – | 18.2 h | $\beta^+, \gamma$ (0.511, 0.93) |

**Table 15.3 Photonuclear Reactions**

| Element | Symbol | Reaction | Threshold energy (MeV) | Half-life of product | Main radiation emitted and its energy (MeV) |
|---|---|---|---|---|---|
| Carbon | C | $^{12}C(\gamma, n)^{11}C$ | 18.7 | 20.4 min | $\beta^+$, $\gamma$ (0.511) |
| Fluorine | F | $^{19}F(\gamma, n)^{18}F$ | 10.5 | 109.8 min | $\beta^+$, $\gamma$ (0.511) |
| Nitrogen | N | $^{14}N(\gamma, n)^{13}N$ | 10.5 | 10 min | $\beta^+$, $\gamma$ (0.511) |
| Oxygen | O | $^{16}O(\gamma, n)^{15}O$ | 15.7 | 2.03 min | $\beta^+$, $\gamma$ (0.511) |
| Copper | Cu | $^{63}Cu(\gamma, n)^{62}Cu$ | 10.8 | 9.7 min | $\beta^+$, $\gamma$ (0.511) |
| | | $^{65}Cu(\gamma, n)^{64}Cu$ | 9.9 | 12.8 h | $\beta^+$, $\gamma$ (0.511) |
| Silver | Ag | $^{107}Ag(\gamma, n)^{106}Ag$ | 9.4 | 24 min | $\beta^+$, $\gamma$ (0.511) |
| Sodium | Na | $^{23}Na(\gamma, n)^{22}Na$ | 12.4 | 2.62 y | $\gamma$ (0.511) |
| Lead | Pb | $^{204}Pb(\gamma, n)^{203}Pb$ | 8.4 | 52.1 h | $\gamma$ (0.279) |

Solid samples should have their surfaces cleaned with a suitable cleaning fluid to remove any surface contamination. The weight of the sample should be determined after cleaning it. For maximum accuracy, the weight is determined again after irradiation and counting are completed.

Liquids and powders cannot be cleaned, so they are handled in clean containers, avoiding contamination from the container wall. For liquid samples, care should be exercised to avoid loss of fluid when the sample is transferred in and out of the container. In the case of powder (or powderized) samples, the observer should be certain that a truly representative sample has been prepared. This is especially important if the main sample under analysis is not homogeneous.

The packaging material or container should

1. Have high radiation and thermal resistance (i.e., it should not decompose, melt, or evaporate in the irradiation environment)
2. Have low content of elements that become radioactive
3. Be inexpensive and easy to handle

Materials that are used most frequently are polyethylene, silica, and aluminum foil. Polyethylene satisfies requirements 2 and 3 listed above, but it has low resistance to radiation and temperature. It becomes brittle after exposure to a fluence of $10^{21}$–$10^{22}$ neutrons/m$^2$. Polyethylene tubes of different diameters are routinely used in radiation laboratories. The tubes can be easily cleaned and sealed. Silica containers are not as useful as polyethylene because they are not as pure, they become radioactive, and sealing is more complicated. Aluminum foil is useful for packaging solids, but it becomes radioactive through $^{27}Al(n, \gamma)^{28}Al$ and $^{27}Al(n, \alpha)^{24}Na$ reactions. The second reaction is more troublesome than the first because the half-life of $^{24}Na$ is the 15 h, whereas the half-life of $^{28}Al$ is only 2.3 min.

## 15.4 SOURCES OF RADIATION

Intensities, energies, and special characteristics of the various radiation sources are briefly discussed in this section.

### 15.4.1 Sources of Neutrons

Neutron sources include nuclear reactors, accelerators, and isotopic sources. Nuclear reactors are, by far, the most frequently used irradiation facilities. They provide high fluxes [upper limit $10^{18}$ neutrons/(m$^2 \cdot$ s)] of mostly thermal neutrons ($E < 1$ eV). Fast neutrons in the keV range are also available, but at lower flux levels.

When short-lived isotopes are involved, a higher activity is produced by irradiating the sample in a reactor that can be pulsed (see Lenihan et al.). Such a reactor producing a high flux of about $10^{20}$ neutrons/(m$^2 \cdot$ s) for a short period of time (milliseconds) is the TRIGA reactor, marketed by General Atomic.

Accelerators produce fast neutrons as products of charged-particle reactions. The most popular device is the so-called neutron generator, which operates on the reaction

$$^{2}_{1}\mathrm{H} + ^{3}_{1}\mathrm{H} \rightarrow ^{1}_{0}n + ^{4}_{2}\mathrm{He} + 17.586\ \mathrm{MeV}$$

The cross section for this exothermic reaction peaks at a deuteron kinetic energy of about 120 keV with a value of about 5 b. The neutrons produced have an energy of about 14 MeV. (The neutron kinetic energy changes slightly with the direction of neutron emission.) The maximum neutron flux provided by a neutron generator is of the order of $10^{12}$ neutrons/(m$^2 \cdot$ s).

Neutrons with an average energy of about 2.5 MeV are produced by the $(d, d)$ reaction

$$^{2}_{1}\mathrm{H} + ^{2}_{1}\mathrm{H} \rightarrow ^{1}_{0}n + ^{3}_{2}\mathrm{H} + 3.266\ \mathrm{MeV}$$

The cross section for this reaction peaks at about 2-MeV bombarding deuteron energy with a value of about 100 mb. At acceleration voltages normally used in neutron generators ($\sim$ 150 kV), the cross section is about 30 mb. The $(d, d)$ reaction offers neutron fluxes of the order of $10^9$ neutrons/(m$^2 \cdot$ s). It is important to note that both the $(d, t)$ and the $(d, d)$ reactions produce essentially monoenergetic neutrons.

Isotopic neutron sources are based on $(\alpha, n)$ and $(\gamma, n)$ reactions, and on spontaneous fission ($^{252}$Cf). They all produce fast neutrons. The $(\alpha, n)$ and $(\gamma, n)$ sources produce the neutrons through the reactions

$$^{4}_{2}\mathrm{He} + ^{9}_{4}\mathrm{Be} \rightarrow ^{1}_{0}n + ^{12}_{6}\mathrm{C}$$

$$\gamma + ^{9}_{4}\mathrm{Be} \rightarrow ^{1}_{0}n + ^{8}_{4}\mathrm{Be}$$

The isotope $^{252}Cf$ is the only spontaneous fission (SF) source of neutrons easily available. It provides fission spectrum neutrons with an average of 2.3 MeV. The characteristics of isotopic neutron sources are given in Table 15.4.

### 15.4.2 Sources of Charged Particles

Apart from certain $\alpha$-emitting radioisotopes, accelerators are the only practical sources of charged particles. They can provide almost any charged particle or ion for bombardment of the target for a wide range of energies. The particles most commonly used as projectiles are protons, deuterons, alphas, tritons, and $^{3}He$ nuclei. The beam current of the accelerator is related to particles per second hitting the target by the equations[33]

$$I(\text{particles/s}) = 6.2 \times 10^{15} \frac{i(\text{mA})}{z} \tag{15.1}$$

where $i$ = the beam current in mA

$z$ = the charge of the accelerated particle in units of the electronic charge

Knowing the number of particles per second hitting the target and the cross section for the reaction, one can calculate the reaction rate.

### 15.4.3 Sources of Photons

The sources of photons include radioisotopes, nuclear reactions, and bremsstrahlung radiation.

There are many radioisotopes that emit gamma rays. The most useful ones are as follows:

1. $^{24}Na$ with a 15-h half-life emitting $\gamma$'s with energy 1.37 and 2.75 MeV
2. $^{60}Co$ with 5.3-year half-life emitting $\gamma$'s with energy 1.17 an 1.33 MeV
3. $^{124}Sb$ with a 60-d half-life emitting $\gamma$'s with energy 1.71, 2.1, and 2.3 MeV

**Table 15.4 Isotopic Neutron Sources†**

| Source | Reaction | Yield | Average neutron energy (MeV) | Half-life of isotope involved |
|---|---|---|---|---|
| $^{226}Ra$-Be | $(\alpha, n)$ | $7 \times 10^{5}$ neutrons/s·g (Ra) | ~4 | 1,600 y |
| $^{210}Po$-Be | $(\alpha, n)$ | $1 \times 10^{10}$ neutrons/s·g (Po) | ~4 | 138.4 d |
| $^{239}Pu$-Be | $(\alpha, n)$ | $1.0 \times 10^{5}$ neutrons/s·g (Pu) | ~4 | 24,131 y |
| $^{241}Am$-Be | $(\alpha, n)$ | $7 \times 10^{6}$ neutrons/s·g (Am) | ~4 | 432 y |
| $^{124}Sb$-Be | $(\gamma, n)$ | $1.0 \times 10^{10}$ neutrons/s·g | 0.024 | 60.2 d |
| $^{242}Cm$-$^{241}Am$-Be | $(\alpha, n)$ | $1 \times 10^{10}$ neutrons/s·g (Cm) | 4 | 162.8 d ($^{242}Cm$) |
| $^{252}Cf$ | (SF) | $2 \times 10^{12}$ neutrons/s·g | 2.3 | 2.646 y |

†From Lenihan, Thomson, and Guinn.

4. $^{22}$Na with a 2.6-y half-life emitting a gamma with energy 1.275 MeV ($^{22}$Na being a positron emitter is also a source of 0.511-MeV gamma rays)

Photons of extremely high energy may be produced by nuclear reactions. Examples are

$$^{3}\mathrm{H}(p,\gamma)^{4}\mathrm{He} \qquad E_\gamma = 19.8\ \mathrm{MeV}$$

$$^{7}\mathrm{Li}(p,\gamma)^{8}\mathrm{Be} \qquad E_\gamma = 14.8 \text{ and } 17.6\ \mathrm{MeV}$$

$$^{11}\mathrm{B}(p,\gamma)^{12}\mathrm{C} \qquad E_\gamma = 11.7 \text{ and } 16.1\ \mathrm{MeV}$$

Unfortunately, the gamma fluxes generated by these reactions are very small, relative to neutron fluxes produced by reactors.

Bremsstrahlung is produced with the help of electron accelerators. The electrons are accelerated to a certain energy and then are allowed to hit a solid target. The radiation produced has a continuous energy spectrum, extending from zero energy up to the maximum electron kinetic energy. Large photon fluxes are produced, and may be used for activation of rather large samples.

## 15.5 IRRADIATION OF THE SAMPLE

Depending on the selected reaction, irradiation of the sample may take place in a reactor, in an accelerator, or with an isotopic source. After the selection of an irradiation facility, the next step is a decision about the irradiation time. If the sample contains known isotopes at approximately known amounts, it is easy to estimate the proper irradiation time. If, on the other hand, the sample is completely unknown, one irradiates the sample for an arbitrary time, checks some of the isotopes present (from the emitted radiations), and then irradiates the sample again for a time that will provide enough activity for proper isotope identification with the desired accuracy.

Since neutrons are, by far, more frequently used for activation analysis than other particles, neutrons will be assumed to be the projectiles for the equations discussed next. However, it should be noted that the same equations apply when some other radiation is used as the bombarding particle.

The equation that gives the activity produced after irradiating the sample for time $t_0$ is (for derivation, see Sec. 14.4)

$$A(t_0) = a_i m \frac{N_A}{A_i} \sigma_i \phi (1 - e^{-\lambda_{i+1} t_0}) \tag{15.2}$$

where $m$ = mass of the element of interest in the sample
$a_i$ = weight fraction (abundance) of isotope with atomic mass $A_i$ ($A_i$ is an isotope of the element with mass $m$, the element of interest)
$\lambda_{i+1}$ = decay constant of the radioisotope produced

$\sigma_i$ = cross section for the reaction that makes the isotope with atomic weight $A_i$ radioactive
$\phi$ = particle flux [particles/(m$^2$ · s)]
$N_A$ = Avogadro's number

Equation 15.2 is valid if (see Sec. 14.4)

1. The number of target nuclei stays essentially constant, i.e., $\sigma_i \phi t \ll 1$.
2. The radioisotope produced has such a small reaction cross section that $\lambda_{i+1} \gg \phi \sigma_{i+1}$.
3. The flux is uniform throughout the target.

If the half-life of the radioisotope is much shorter than $t_0$ ($t_0 \gtrsim 6\tau_{1/2}$), saturation activity ($A_{\text{sat}}$) is obtained, given by

$$A_{\text{sat}} = a_i m \frac{N_A}{A_i} \sigma_i \phi \tag{15.3}$$

Equation 15.3 indicates that, for a particular isotope, the activity increases by irradiating a larger mass $m$ in a higher flux $\phi$.

The size of the sample (mass $m$) is dictated by four factors:

1. The maximum activity that can be safely handled under the conditions of the laboratory (i.e., shielding of source and detector, existence of remote control, automated remote handling of samples).
2. The size of the sample holder.
3. The self-absorption of the radiation emitted by the sample. This is particularly important if the radiation detected is betas or soft X-rays.
4. The size of the detector. Little, if anything, is gained by using a sample much larger than the detector size.

The flux $\phi$ is determined by the limitations of the irradiation facility. At the present time, the maximum flux is about $10^{18}$ neutrons/(m$^2$ · s) (thermal neutron flux).

## 15.6 COUNTING OF THE SAMPLE

After irradiation is completed, the sample is counted using an appropriate system. The qualitative and quantitative determination of an isotope is based on the analysis of the energy spectrum of the radiations emitted by the radioisotope of interest. Sometimes it may be necessary to use information about the half-life of the isotope(s). In such a case, counting may have to be repeated several times at specified time intervals.

The counting system depends on the radiation detected. Modern activation analysis systems depend on the detection of gamma rays and X-rays and very

seldom on detection of other particles. For this reason, the discussion in the rest of this chapter is based on the assumption that the irradiated sample emits photons.

A basic counting system for activation analysis consists of a detector [Ge or Si(Li)], electronics (i.e., preamplifier, amplifier), and a multichannel analyzer (MCA). Modern MCAs do much more than record the data. They are minicomputers or are connected to computers that store and analyze the recorded data. Examples are the ADCAM architecture offered by EG & G ORTEC and the Genie-ESP VAX-based Data Acquistion and Analysis System offered by Canberra.

## 15.7 ANALYSIS OF THE RESULTS

The analysis of an activation analysis spectrum is based on the procedures described in Sec. 12.7.3. It is performed either by the MCA itself, if that instrument has such capability, or by a digital computer. Several computer codes have been written for that purpose.[34-38]

Activation analysis may be qualitative or quantitative. In a qualitative measurement, only identification of the element is involved. This is accomplished, as shown in Sec. 12.7.3, from the energies and intensities of the peaks of the spectrum. In a quantitative measurement, on the other hand, in addition to identification, the amount of element in the sample is also determined. To illustrate how the mass is determined and what the errors and sensitivity of the method are, consider the energy spectrum of Fig. 15.1 as an example.

Assume that the mass of an element in the sample will be determined from the full-energy peak at $E_k$. Using the notation of Sec. 14.4, the mass $m$ is given by (see Eq. 14.22)

$$m = \frac{P_k A_i \lambda_{i+1}}{\epsilon(E_k) e_k a_i N_A \sigma_i \phi (1 - e^{-\lambda_{i+1} t_0})(e^{-\lambda_{i+1} t_1} - e^{-\lambda_{i+1} t_2})} \tag{15.4}$$

where $P_k$ = net number of counts under the peak (determined by one of the methods described in Sec. 12.7.3)

$\epsilon(E_k)^\dagger$ = absolute full-energy peak detector efficiency at energy $E_k$

$e_k$ = probability that a photon of energy $E_k$ is emitted per decay of the isotope (also known as intensity of this gamma)

$t_2 - t_1$ = counting time = $T$

The error in the value of $m$ depends on the errors of the quantities that comprise Eq. 15.4, such as $P_k$, $\lambda$, $\epsilon$, $\sigma_i$, and $\phi$. In the most general case, the standard derivation $\sigma_m$ is

$$\sigma_m = \sqrt{\left(\frac{\partial m}{\partial P_k}\right)^2 \sigma_{P_k}^2 + \left(\frac{\partial m}{\partial \phi}\right)^2 \sigma_\phi^2 + \left(\frac{\partial m}{\partial t}\right)^2 \sigma_t^2 + \cdots} \tag{15.5}$$

†In activation analysis, the efficiency is determined in such a way as to include the solid angle $\Omega$ and the other correction factors $F(E_k)$ discussed in Chap. 8.

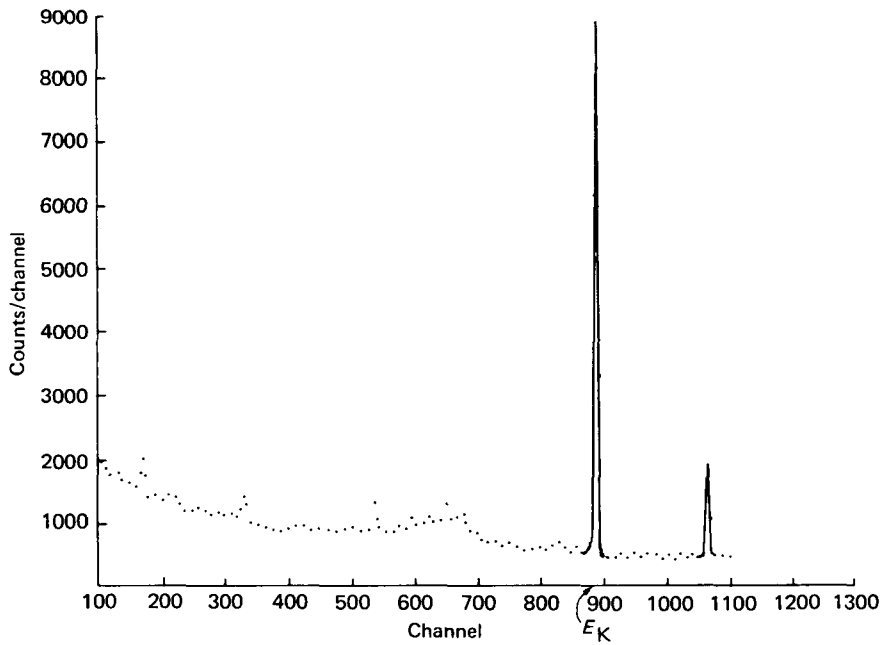


**Figure 15.1** A typical Ge(Li) energy spectrum. The element will be identified using the main peak at channel 888.

In practice, certain errors are always negligible when compared to others. The quantities $A_i$, $\lambda$, $e_k$, and $\sigma_i$ are known very accurately for most isotopes. Also, the flux $\phi$ and the efficiency $\epsilon$ can be determined with a known but small error. The error in the times $t_1$ and $t_2$ can be negligible. Thus, the major contribution to the error of $m$ comes from the error of $P_k$, i.e., the error of the area under the peak. Assuming that $\sigma_{P_k}$ is the only important error, the standard error of $m$ is

$$\sigma_m = \left(\frac{\partial m}{\partial P_k}\right)\sigma_{P_k} \tag{15.6}$$

or the relative error (using Eq. 15.4) is

$$\frac{\sigma_m}{m} = \frac{\sigma_{P_k}}{P_k} \tag{15.7}$$

Thus, the relative error of $m$ is equal to the relative error of $P_k$, in this case.

It should be emphasized that only one well-identified peak, and not the whole spectrum, is needed for quantitative determination of an element in the unknown sample. The other peaks, if used, should give results consistent with the one chosen for the analysis, and they should also be utilized as additional

check points to remove any doubts in the identification of the unknown. For example, if the $k$ peak leads to the identification of isotope X, other peaks in the spectrum should agree, in energy and intensity, with additional gammas emitted by isotope X.

In practice, the objective of the measurement is often to identify the mass of a particular trace element in the sample. Then the unknown mass is determined in a simpler way by irradiating, along with the unknown, a standard sample with a known mass of the trace element and counting both samples with the same counter. If $m_s$ is the mass of the standard and $m_x$ the mass of the unknown, using Eq. 15.4, one obtains

$$m_x = m_s \frac{(P_k)_x (e^{-\lambda_{i+1}t_1} - e^{-\lambda_{i+1}t_2})_s}{(P_k)_s (e^{-\lambda_{i+1}t_1} - e^{-\lambda_{i+1}t_2})_x} \tag{15.8}$$

where the times $t_1$ and $t_2$ are different for the standard and the unknown, but in both cases, $t_2 - t_1 = T$. Use of Eq. 15.8 constitutes a relative method, in contrast to the use of Eq. 15.4, which represents an absolute method.

## 15.8 SENSITIVITY OF ACTIVATION ANALYSIS

Sensitivity of the activation analysis method for a particular element refers to the minimum mass of that element that can be reliably detected. The minimum detectable mass is determined from Eq. 15.4 by assuming the most favorable conditions for the measurement and by setting an upper limit for the acceptable error of the result. The process is similar to the determination of the minimum detectable activity discussed in Sec. 2.20.

Assuming that the observer is willing to accept a maximum error $\sigma_m$ such that

$$\sigma_m \leq fm \tag{15.9}$$

($f < 1$) and that the only error in the determination of the mass comes from the error in the number of counts under the peak, a limiting counting rate can be defined as follows. If one defines a net counting rate $r_k$ as

$$r_k = \frac{G_k}{T} - b_k \tag{15.10}$$

where†

$$G_k = P_k + b_k T = r_k T + b_k T \tag{15.11}$$

then, using Eqs. 2.101, 15.7, and 15.11, one obtains for the minimum acceptable counting rate $r_k$,

$$r_k \geq \frac{1 + \sqrt{1 + 4f^2 T(b_k + T\sigma_b^2)}}{2f^2 T} \tag{15.12}$$

†Note that both $G_k$ and $b_k$ refer to gross counts and background of the peak $k$, and not the whole spectrum.

**Example 15.1** What is the minimum mass of gold that can be detected by neutron activation analysis under the conditions listed below?

$$\phi = 10^{16} \text{ neutrons}/(\text{m}^2 \cdot \text{s}) \qquad \epsilon = 0.30$$
$$t_0 = 2 \text{ h} \qquad t_1 = 5 \text{ min}$$
$$f = 0.50 \qquad t_2 = 125 \text{ min}$$
$$b = 20 \pm 0.2 \text{ counts/min}$$

For gold, $A = 197$, $a = 1$, $e_k = 1$, $\sigma = 99$ b, and $T_{1/2} = 2.7$ days.

**Answer** Using Eq. 15.12, the minimum acceptable counting rate is

$$r_k = \frac{1 + \sqrt{1 + 4(0.5)^2 20(120) + 4(0.5)^2(120)^2(0.2)^2}}{2(0.5)^2 120} = 0.93 \text{ counts/min}$$

Using Eqs. 15.10 and 15.11,

$$P_k = r_k T = 0.93(120) = 111.12 \text{ counts}$$

Since the half-life of $^{198}$Au is 2.7 days,

$$\lambda = \frac{\ln 2}{2.7 \text{ d}} = 2.971 \times 10^{-6} \text{ s}^{-1}$$

and the exponential factors in Eq. 15.4 become

$$\exp(-\lambda_{i+1} t_0) = \exp[(-2.971 \times 10^{-6})2(3600)] = 0.979$$
$$\exp(-\lambda_{i+1} t_1) = \exp[(-2.971 \times 10^{-6})300] = 0.999$$
$$\exp(-\lambda_{i+1} t_2) = \exp[(-2.971 \times 10^{-6})125(60)] = 0.978$$

Equation 15.4 gives

$$m = \frac{111.12(197 \times 10^{-3})(2.971 \times 10^{-6}) \text{ s}^{-1}}{0.30(6.022 \times 10^{23})(99 \times 10^{-28} \text{ m}^2)(10^{16} \text{ n/m}^2 \text{ s})(1 - 0.979)(0.999 - 0.978)}$$
$$= 8.24 \times 10^{-15} \text{ kg} = 8.24 \text{ pg}$$

**Example 15.2** What is the absolute minimum mass of an element that can be detected under the most favorable conditions?

**Answer** The absolute minimum mass will be determined if one assumes

Efficiency 100 percent ($\epsilon = 1$)

Intensity 100 percent ($e_k = 1$)

Saturation activity ($1 - e^{-\lambda t_0} = 1$)

Maximum thermal neutron flux [$\sim 10^{18}$ neutrons/(m$^2 \cdot$ s)]

Then Eq. 15.4 takes the form

$$m = \frac{P_k A_i \lambda_{i+1}}{a_i N_A \sigma_i \phi (e^{-\lambda_{i+1} t_1} - e^{-\lambda_{i+1} t_2})} \tag{15.13}$$

Factors that may further affect the result given by Eq. 15.13 depend on the background of the counting system and the maximum acceptable error (both background and acceptable error affect the minimum acceptable value of $P_k$).

## 15.9 INTERFERENCE REACTIONS

One source of error in activation analysis is interference reactions. These are reactions that produce the same isotope as the one being counted, through bombardment of a different isotope in the sample. As an example, assume that a sample is analyzed for magnesium by using fast-neutron activation. The reaction of interest is $^{24}Mg(n, p)^{24}Na$. Therefore, the activity of $^{24}Na$ will be recorded, and from that the amount of $^{24}Mg$ can be determined. If the sample contains $^{23}Na$ and $^{27}Al$, two other reactions may take place which also lead to $^{24}Na$. They are

$$^{23}Na(n, \gamma)^{24}Na$$
$$^{27}Al(n, \alpha)^{24}Na$$

If this is the case and the investigator does not consider these last two reactions, the mass of $^{24}Mg$ will be determined to be higher than it is.

Interference reactions are discussed in detail in many activation analysis books (see Rakovic, and Nargolwalla & Przybylowicz). A few representative examples are given below:

$^{68}Zn(n, \gamma)^{69m}Zn$ and $^{69}Ga(n, p)^{69m}Zn$ and $^{72}Ge(n, \alpha)^{69m}Zn$

$^{32}S(n, p)^{32}P$ and $^{31}P(n, \gamma)^{32}P$ and $^{35}Cl(n, \alpha)^{32}P$

$^{17}O(n, \alpha)^{14}C$ and $^{13}C(n, \gamma)^{14}C$ and $^{14}N(n, p)^{14}C$

$^{98}Tc(n, \gamma)^{99m}Tc$ and $^{98}Mo(n, \gamma)^{99}Mo \xrightarrow{\beta^-} {}^{99m}Tc$

$^{31}P(n, \gamma)^{32}P$ and $^{30}Si(n, \gamma)^{31}Si \xrightarrow{\beta^-} {}^{31}P(n, \gamma)^{32}P$

$^{55}Mn(n, \gamma)^{56}Mn$ and $^{54}Cr(n, \gamma)^{55}Cr \xrightarrow{\beta^-} {}^{55}Mn(n, \gamma)^{56}Mn$

$^{19}F(n, 2n)^{18}F$ and $^{17}O(p, \gamma)^{18}F$ and $^{18}O(p, n)^{18}F$

In the last two reactions, the proton is produced by the incident fast neutrons interacting with the target nuclei.

## 15.10 ADVANTAGES AND DISADVANTAGES OF THE ACTIVATION ANALYSIS METHOD

One of the greatest advantages of activation analysis is its ability to detect most of the isotopes with an extremely high sensitivity. Other advantages are that the method

1. Is nondestructive (in most cases)
2. Needs a sample with a very small mass
3. Can detect more than one element at a time
4. Identifies different isotopes of the same element
5. Provides results rapidly
6. Is not affected by the chemical form of the element of interest

The greatest disadvantage of the method is that it requires expensive equipment, and the analysis of the results is not trivial. Also, activation analysis does not provide information about the chemical compound in which the nuclide of interest belongs.

Overall, activation analysis is a very powerful technique, as demonstrated by its wide use in so many different fields—i.e., chemistry, biology, medicine, forensic medicine, industry, archaeology, and environmental research. For details regarding these special applications, the reader is referred to Refs. 3–33 and to the bibliography of this chapter, in particular, to the books by Nargolwalla and Przybylowicz, and by Rakovic.

## PROBLEMS

**15.1** Traces of manganese are suspected in an unknown sample that has been irradiated for 30 min in a flux of $10^{16}$ neutrons/(m$^2 \cdot$ s). Counting started 5 min after the irradiation ended. The 0.8-MeV gamma of $^{56}$Mn was detected by a counter with a 4 percent efficiency (F.$\epsilon$.$\Omega$). The sample gave 500 counts in 5 min, while the background was $30 \pm 1$ counts/min. Based on this information, calculate the mass of manganese in the sample and the standard error of this measurement. For $^{55}$Mn, $\sigma = 14$ b. For $^{56}$Mn, $T_{1/2} = 2.58$ h.

**15.2** What should the minimum activity of a sample be if it is required that in the worst case $\sigma_r = 0.8r$, and the sample is counted in a system for which $\epsilon = 0.50$, and the background is $100 \pm 5$ counts/min. The sample can only be counted for 1 min.

**15.3** In a neutron activation analysis experiment, a 10-percent-efficient Ge(Li) detector with $12 \pm 0.1$ counts/min background is used for the measurement of 0.6-MeV $\gamma$'s emitted by the sample. If the counting time is 5 min,

(a) What is the minimum acceptable counting rate if the maximum acceptable error is 60 percent?

(b) What is the minimum mass that can be detected if the isotope under investigation has $A = 75$, $\sigma = 0.21$ b, $T_{1/2}(^{76}X) = 20$ h, irradiation time = 8 h, and $\phi = 10^{16}$ neutrons/(m$^2 \cdot$ s)?

**15.4** Prove Eq. 15.12.

**15.5** What is the absolute minimum mass of phosphorus that can be detected using the reaction $(n, \alpha)$ under irradiation with 14-MeV neutrons? Assume $\phi = 10^{12}$ neutrons/(m$^2 \cdot$ s), $\sigma = 0.150$ b, counting system background = 15 ± 0.5 counts/min, counting time = 2 min, and maximum acceptable error is 30 percent.

## BIBLIOGRAPHY


Bowen, H. J. M., and Gibbons, D., *Radioactivation Analysis*, Oxford University Press, London, 1963.

Coomber, D. I. (ed.), *Radiochemical Methods in Analysis*, Plenum Press, New York, 1975.

Lederer, C. M., and Shirley, V. S. (eds.), *Table of Isotopes*, 7th ed., Wiley, New York, 1978.

Lenihan, M. M. A., Thomson, S. J., and Guinn, V. P., *Advances in Activation Analysis*, Academic, New York, 1972, vol. 2.

Lutz, G. J., Boreni, R. J., Maddock, R. S., and Wing, J. (eds.), "NBS Technical Note 467 Activation Analysis: A Bibliography Through 1971," National Bureau of Standards, 1972.

Lyon, W. S. (ed.), *Guide to Activation Analysis*, Van Nostrand, Princeton, N.J., 1964.

Nargolwalla, S. S., and Przybylowicz, E. P., *Activation Analysis with Neutron Generators*, Wiley, New York, 1973.

*Radiochemical Methods of Analysis*, Proceedings of a Symposium on Radiochemical Methods of Analysis, IAEA, Salzburg, Austria, 1964.

Rakovic, M., *Activation Analysis* (English translation), CRC Press, Cleveland, Ohio, 1970.


## REFERENCES


1. Hevesy, G., and Levi, H., *K. Danske Vidensk. Sels. Mat.-fys. Medd.* **14**:5 (1936).
2. Seaborg, G. T., and Livingood, J. J., *J. Am. Chem. Soc.* **60**:1784 (1938).
3. "International Nuclear and Atomic Activation Analysis Conference," October 1975, Gatlinburg, TN, Suppl. *L3 to ANS Trans.* **21**:1-45 (1975).
4. Ruf, H., and Fredrich, M., *Nucl. Technol.* **37**:79 (1978).
5. Wood, D. E., *Nucl. Instrum. Meth.* **92**:511 (1971).
6. Marsh, R. H., and Bechnell, D. E., *ANS Trans.* **14**:105 (1971).
7. Wogman, N. A., Rieck, H. G., Jr., Kosorok, J. R., and Perkins, R. W., BNWL-SA-4434 (1972).
8. Nargolwalla, S. S., *ANS Trans.* **21**:107 (1975).
9. Ruch, R. R., Cahil, R. A., Frost, J. K., Camp, L. R., and Gluskoter, H. J., *ANS Trans.* **21**:107 (1975).
10. Millard, H. T., and Swanson, V. E., *ANS Trans.* **21**:108 (1975).
11. Profio, A. E., and Pouraghabagher, A. R., *ANS Trans.* **21**:109 (1975).
12. Harrison, S. H., *ANS Trans.* **21**:110 (1975).
13. Rhodes, J. R., *ANS Trans.* **21**:113 (1976).
14. Darnley, A. G., *ANS Trans.* **21**:113 (1976).
15. Marshall, T. D., and Knight, A., *Nucl. Instrum. Meth.* **92**:595 (1971).
16. Battye, C. K., Knight, V., Marshall, T. O., Knight, A., and Godfrey, B. E., *Nucl. Instrum. Meth.* **92**:601 (1971).
17. Livingston, H. D., *ANS Trans.* **14**:98 (1971).
18. Podolsky, S., Cardarelli, J. A., and Burrows, B. A., *ANS Trans.* **14**:99 (1971).
19. McNeill, K. A., Cabeza, L., and Harrison, J. E., *ANS Trans.* **14**:100 (1971).
20. Comar, D., *ANS Trans.* **14**:101 (1971).
21. Bird, E. D., *ANS Trans.* **14**:102 (1971).
22. Friedman, M. H., and Tanner, J. T., *ANS Trans.* **21**:97 (1975).

23. Hankins, D. A., Babb, A. L., and Scribner, B. H., *ANS Trans.* **21**:98 (1975).
24. Ricci, E., *ANS Trans.* **21**:99 (1975).
25. Landsberger, S., and Wu, D., *ANS Transactions* **64**:10 (1991).
26. Spyrou, N., and Arshed, W., *ANS Transactions* **64**:11 (1991).
27. Lindstrom, R. M., and Norman, B. R., *ANS Transactions* **64**:12 (1991).
28. Becker, D. A., *ANS Transactions* **64**:12 (1991).
29. Ruch, R. R., Guinn, V. P., and Pinker, R. H., *Nucl. Sci. Eng.* **20**:381 (1964).
30. Guinn, V. P., and Rumos, J. C., *ANS Trans.* **14**:105 (1971).
31. Scheringer, H. L., and Lukens, H. R., *ANS Trans.* **14**:106 (1971).
32. Williamson, T. G., and Harrison, W. W., *ANS Trans.* **14**:107 (1971).
33. Ricci, E., "Charged Particle Activation Analysis," in J. M. A. Lenihan, S. J. Thomson, and V. P. Guinn (eds.), *Advances in Activation Analysis*, Academic, London, 1972, vol. 2.
34. Cline, J. E., Putnam, M. H., and Hermer, R. G., "GAUSS VI, A Computer Program for the Automatic Analysis of Gamma-Ray Spectra from Ge(Li) Spectrometers," ANCR-1113 (1973).
35. Heath, R. L., Helmer, R. G., Schmittroth, L. A., and Cazier, G. A., *Nucl. Instrum. Meth.* **47**:281 (1967).
36. Helmer, R. G., Heath, R. L., Schmittroth, L. A., Jayne, G. A., and Wagner, L. M., *Nucl. Instrum. Meth.* **47**:305 (1967).
37. Mariscotti, M. A., *Nucl. Instrum. Meth.* **50**:309 (1967).
38. Phillips, G. W., and Marlow, K. W., *Nucl. Instrum. Meth.* **137**:525 (1976).

CHAPTER
# SIXTEEN

# HEALTH PHYSICS FUNDAMENTALS

## 16.1 INTRODUCTION

Health physics is the discipline that consists of all the activities related to the protection of individuals and the general public from potentially harmful effects of ionizing radiation. Ionizing radiation comes from two sources:

1. Natural or background radiation which is radiation emitted by radioisotopes that exist on or inside the earth, in the air we breathe, in the water we drink, in the food we eat, and in our bodies, as well as radiation incident upon the earth from outer space (cosmic rays). Humans have been exposed to this natural radiation for as long as they have existed on this planet.
2. Man-made radiation which is radiation emitted by all the radioisotopes that have been produced through nuclear reactions (mainly fission), as well as radiation produced by machines used in medical installations (e.g., X-ray machines) or in scientific laboratories (e.g., accelerators).

Health physics is concerned with protection of people from radiation. Since the background radiation has been, is, and will always be on our planet at about the same level everywhere, there is not much a health physicist can do to protect individuals or populations from background radiation. Hence, health physics is concerned with protection of people from man-made radiation.

A health physicist performs many tasks. He or she, most importantly,

1. Is responsible for the detection and measurement of radiation in areas of work and in the environment

2. Is responsible for the proper operation and calibration of detection instruments
3. Inspects at regular intervals the facilities where radiation sources are used
4. Enforces federal and state regulations dealing with proper handling of radiation sources and establishment of acceptable levels of radiation fields at places of work
5. Keeps records of exposure for all individuals under his or her jurisdiction
6. Knows how to clean areas that have been contaminated with radioactive materials
7. Acts as the liaison representative between the regulatory agencies and his or her organization

Although the term health physics was coined after 1940, and a health physics society was established in 1955, the concern about the harmful effects of radiation had been born much earlier—but probably not early enough. The first recorded radiation damage case occurred in 1896, only a year after the discovery of X-rays, yet the first limits concerning X-ray exposure were set in the 1920s. Today, both national and international groups exist that act as advisory bodies[†] to the appropriate regulatory agencies.

Since improperly handled radiation may produce deleterious effects to humans, it is important that individuals who use radiation sources learn the fundamentals of dosimetry, definition of dose units, biological effects of radiation, standards for radiation protection, and operation of health physics instruments. This chapter briefly discusses all these items. If more detailed treatment of these topics is needed, consult the bibliography and references given at the end of the chapter.

## 16.2 UNITS OF EXPOSURE AND ABSORBED DOSE

Protection of individuals against radiation necessitates the completion of two tasks:

1. Development of safe radiation exposure limits
2. Construction of instruments that measure the intensity of radiation

Neither of these tasks can be accomplished without the means of quantitative description of radiation, i.e., without defining radiation units.

The radiation effect is measured in terms of exposure or dose. Exposure is defined as charge released per unit mass of air. Dose is defined as energy absorbed per unit mass of material. The first radiation unit to be defined was

[†]International Commission on Radiological Units and Measurements (ICRU); International Commission on Radiological Protection (ICRP); in the United States, the National Council on Radiation Protection and Measurements (NCRP).

the *roentgen* (symbol R):

1 R = exposure due to X-rays or gamma-rays of such intensity that the electrons produced by this radiation in 1 $cm^3$ of dry air, at standard temperature and pressure, generate along their tracks electron-ion pairs carrying a total charge of 1 esu of either sign

The SI unit of exposure is defined as 1 C/kg air, without any new name proposed for it. Numerically,

$$1\ \text{R} = 2.58 \times 10^{-4}\ \text{C/kg air}$$

The roentgen suffers from two limitations:

1. It was defined in terms of electromagnetic radiation only.
2. It was defined in terms of air only.

Radiation protection may involve other types of radiation, and media other than air. For this reason, another unit was defined called the *radiation absorbed dose* or *rad*, defined as

$$1\ \text{rad} = 100\ \text{erg/g}$$

The SI unit of absorbed dose is the *Gray* (Gy), defined as

$$1\ \text{Gy} = 1\ \text{J/kg} = 100\ \text{rad}$$

The rad (or the Gy) has a simple definition and is a unit independent of both type of radiation and material. But the measurement of absorbed dose in terms of rad (or Gy) is neither simple nor straightforward, because it is very difficult to measure energy deposited in a certain mass of tissue. Fortunately, one can bypass this difficulty by measuring energy deposited in air, which is proportional to the exposure, and then relate it to the absorbed dose.

The measurement of exposure is achieved by using ionization chambers, and the result is given in roentgens. Based on the definitions of the roentgen, the following relationship can be established between roentgens and rads.

$$\begin{aligned} 1\ \text{R} &= \frac{1\ \text{esu}}{1.293 \times 10^{-3}\ \text{g}}(2.082 \times 10^{9})\ \text{ion pairs/esu} \\ &\quad \times (34\ \text{eV/pair})1.602 \times 10^{-12}\ \text{ergs/eV} \\ &= 88\ \text{ergs/g} = 0.88\ \text{rad} = 8.8\ \text{mGy} \end{aligned}$$

If $D$ is the absorbed dose in air, and X is the exposure in air, the relationship between the two is

$$D = 0.88\text{X} \tag{16.1}$$

For media other than air, the relationship is obtained as follows. The absorbed dose rate in material $i$ is (in terms of energy deposited per unit mass per unit time)

$$\dot{\text{D}}_i = \phi\ [\text{part.}/(\text{cm}^2\ \text{s})]\ \mu_{a,i}\ (\text{m}^2/\text{kg})E\ (\text{J/part.}) \tag{16.2}$$

The absorbed dose rate in air is

$$\dot{D}_{air} = \phi\ [\text{part.}/(\text{cm}^2\ \text{s})]\ \mu_{a,\text{air}}\ (\text{m}^2/\text{kg})E\ (\text{J/part.}) \tag{16.3}$$

The ratio of Eq. 16.2 to Eq. 16.3 gives

$$\dot{D}_{a,i} = \frac{\mu_{a,i}}{\mu_{a,\text{air}}}\dot{D}_{a,\text{air}} = \frac{\mu_{a,i}}{\mu_{a,\text{air}}}(0.88)X_{\text{air}} \tag{16.4}$$

Equations 16.1 and 16.4 express the fact that the measurement of absorbed dose† is a two-step process:

1. Exposure (or exposure rate) is measured.
2. Absorbed dose (or dose rate) is calculated from the measured exposure using Eq. 16.4.

In practice, the instruments that measure radiation dose are, usually, properly calibrated to read rad or Gy.

## 16.3 THE RELATIVE BIOLOGICAL EFFECTIVENESS—THE DOSE EQUIVALENT

The units of absorbed dose defined in the previous section are quite adequate for the quantitative assessment of the effects of radiation to inanimate objects, like irradiated transistors or reactor fuel. For protection of people, however, the important thing is not the measurement of energy deposited—i.e., the absorbed dose—but the biological effects due to radiation exposure. Unfortunately, biological effects and absorbed dose do not always have one-to-one correspondence, and for this reason a new unit had to be defined: a unit that takes into account the biological effects of radiation.

The ideal unit for the measurement of biological effect should be such that a given dose, measured in that unit, produces a certain biological effect regardless of the *type and energy of radiation* and also regardless of the *biological effect* considered. Unfortunately, such a unit cannot be established because of the different modes by which radiation deposits energy in tissue, the intricate way by which the energy deposition is related to a given biological effect, and the complexity of biological organisms. An ideal unit may not exist, but some unit that "equalizes" biological effects had to be defined.

†Equations 16.2 and 16.3 give dose rate, not dose; the meaning of Eq. 16.4, however, is the same if one uses either dose or dose rate.

The first step toward that task was the introduction of a factor called the relative biological effectiveness (RBE), defined as

$$\mathrm{RBE}_i = \frac{\text{[absorbed dose from X-ray or gamma radiation (200–300 keV) producing a certain biological effect]}}{\text{[absorbed dose from radiation type } i \text{ producing the same biological effect]}} \tag{16.5}$$

In understanding the meaning of RBE, note the following:

1. RBE is defined in terms of photons; therefore, it follows that RBE = 1 for electromagnetic radiation. Also, although the definition of RBE specifies the energy of the photons to be 200–300 keV, RBE is taken as equal to 1 for photons of all energies.
2. A given type of radiation does not have a single RBE, because RBE values depend on the energy of the radiation, the cell, the biological effect being studied, the total dose, dose rate, and other factors.
3. It is a well-known fact that the biological damage increases as the energy deposited per unit distance, the *linear energy transfer* (LET), increases. Thus, heavier particles (alphas, heavy ions, fission fragments) are, for the same absorbed dose, more biologically damaging than photons, electrons, and positrons.

In 1963, the International Commission on Radiological Units and Measurements (ICRU) proposed the replacement of RBE by a new factor named the *quality factor* (QF). Here is an excerpt from their recommendation.

> In radiation protection it is necessary to provide a factor that denotes the modification of the effectiveness of a given absorbed dose by LET (Linear Energy Transfer). Unlike RBE, which is always experimentally determined, this factor *must* be *assigned* on the basis of a number of considerations and it is recommended that it be termed the *quality factor* (QF). Provisions for other factors are also made. Thus a *distribution factor* (DF) may be used to express the modification of biological effect due to nonuniform distribution of internally deposited radionuclides. The product of absorbed dose and modifying factors is termed the dose equivalent, ($H$).

In 1973 the ICRU[1] recommended dropping the "F" from QF, a suggestion that has now become practice. In 1977 the ICRP[2] recommended that the dose equivalent ($H$) at a point in tissue be written as

$$H = NQD \tag{16.6}$$

where $Q$ = quality factor
$D$ = absorbed dose
$N$ = product of all the modifying factors. The suggested value of $N$ is 1.

RBE is now used only in radiobiology, whereas $Q$ is used in radiation protection. A detailed discussion of similarities and differences between the two factors is given in Ref. 3. For the radiations and energy ranges considered in this book, RBE and $Q$ are practically the same, and from this point on, only the factor $Q$ will be mentioned. Table 16.1 gives $Q$ values for various radiations commonly encountered.

When the unit of absorbed dose is multiplied by the corresponding $Q$ value, the unit of dose equivalent ($H$) is obtained. The $H$ units are

$$1 \text{ rem} = Q \times 1 \text{ rad}$$

and the SI unit

$$1 \text{ Sievert (Sv)} = Q \times 1 \text{ Gy}$$

Thus

$$1 \text{ Sv} = 100 \text{ rem}$$

Because it is only the dose equivalent that equalizes biological effects from different types and energy of radiation, *only Sv (or rem) should be added*, never Gy (or rad).

**Example 16.1** At the open beam port of a research reactor, the absorbed dose rate consists of 10 mrad/h due to gammas, 10 mrad/h due to fast neutrons, and 6 mrad/h due to thermal neutrons. What is the total dose a person will receive by standing in front of the beam for 5 s?

**Answer** Calculate the dose equivalent $H$, as shown below:

| From | Abs. dose rate (mrad/h) | $Q$ | $\dot{H}$ (mrem/h) | $\dot{H}$ (mSv/h) |
|---|---|---|---|---|
| Gammas | 10 | 1 | 10 | 0.1 |
| Fast neutrons | 10 | 10 | 100 | 1.0 |
| Thermal neutrons | 6 | 2 | 12 | 0.12 |
| Total | | | 122 | 1.22 |

**Table 16.1 Quality Factors for Several Types of Radiation**[2, 4]

| Radiation type | $Q$ | Radiation type | $Q$ |
|---|---|---|---|
| Gamma-rays | 1 | Neutrons: | |
| X-rays | 1 | Thermal | 2 |
| Beta particles: | 1 | 0.005 MeV | 2 |
| Electrons | 1 | 0.02 MeV | 5 |
| Positrons | 1 | 0.10 MeV | 7.5 |
| Protons ($E < 14$ MeV) | 10 | 0.50 MeV | 11 |
| Alpha particles | | 1.00 MeV | 11 |
| ($E < 10$ MeV) | 20 | 5.0 MeV | 8 |
| Recoil nuclei ($A > 4$) | 20 | 10 MeV | 6.5 |

The total dose received by the individual is

$$H = 122 \text{ mrem/h} \left( \frac{5}{3600} \right) = 0.17 \text{ mrem} = 1.7 \times 10^{-6} \text{ Sv}$$

## 16.4 DOSIMETRY FOR RADIATION EXTERNAL TO THE BODY

The general dosimetry problem is defined as follows: Given the intensity of the radiation field at a certain point in space, calculate the dose rate received by an individual standing at that point. The radiation field, outside the body, is assumed to be known in terms of the type, energy, and number of particles involved. The calculation that follows disregards the possible perturbation of the field from the presence of the human body. The calculation is different for charged particles, photons, and neutrons.

### 16.4.1 Dose Due to Charged Particles

Consider a point in space where it is known that the charged-particle radiation field is given by

$\phi(E)\,dE$ = charged particles per $m^2$ s with kinetic energy between $E$ and $E + dE$

A person exposed to this field will receive a radiation dose because of energy deposited by these charged particles. The dose equivalent rate is given by

$$\dot{H} = \int_E dE\phi(E)\,[\text{part.}/(\text{m}^2\text{ s})]\,(dE/dx)\,(\text{MeV/m})Q(E)/\rho\,(\text{kg/m}^3) \quad (16.7)$$

where

$dE/dx$ = stopping power of tissue for particles of energy $E$

$\rho$ = density of tissue

$Q(E)$ = quality factor for particles of energy $E$

The units of Eq. 16.7 are MeV/(kg s). To obtain the result in Sv/s, one needs to transform MeV to J (1 MeV = $1.602 \times 10^{-13}$ J).

Most of the time in practice, the radiation field is computed not as an analytic function $\phi(E)$ but as an energy group distribution, where

$\phi_g = \int_{E_g}^{E_{g-1}} \phi(E)\,dE$ = number of particles per $m^2$ s with energy between $E_g$ and $E_{g-1}$ ($E_g < E_{g-1}$)

Using the multigroup structure, Eq. 16.7 takes the form

$$\dot{H} = \sum_{g=1}^{G} \phi_g (dE/dx)_g Q_g/\rho \text{ (Sv/s)} \quad (16.8)$$

where $G$ is the total number of energy groups and $Q_g$ is the average quality factor for group $g$. In principle, Eqs. 16.7 and 16.8 are valid for any charged-particle flux that hits a human body from the outside. In practice, for the particles and energies considered here, these equations are useful for electron and beta beams only, since alphas with $E < 10$ MeV do not penetrate the human skin. The dose from external beams of betas will be confined to a depth in tissue equal to the range of these particles.

The division between electrons and betas is necessary (although beta particles are electrons) because an electron beam consists of monoenergetic electrons; a beam of beta particles consists of electrons emitted by the beta decay of a nucleus. Therefore, as explained in Chap. 3, these particles have an energy spectrum with a maximum energy $E_{max}$ and an average energy $1/3E_{max}$.†

To calculate the dose rate from an electron or a beta beam, one can use Eq. 16.7 or Eq. 16.8 with $Q(E) = 1$. In practice, the actual calculation is shortened by using tables that provide flux-to-dose-rate conversion factors (Table 16.2). In terms of the flux-to-dose-rate conversion factors, the dose rate is written as

$$\dot{H} = \int_E C(E)\phi(E)\,dE \tag{16.9}$$

or, in terms of energy groups,

$$\dot{H} = \sum_{g=1}^{G} C_g \phi_g \tag{16.10}$$

†A more accurate equation for $E_{max}$ is given in Ref. 6.

**Table 16.2 Flux-to-Dose-Rate Conversion Factors for Electrons and Betas[5]**

| Electrons | | | Betas | | |
|---|---|---|---|---|---|
| $E_{max}$(MeV) | (Sv/s)/ [particles/(m² s)] | (mrem/h)/ [particles/(cm² s)] | $E$ (MeV)$_{max}$ | (Sv/s)/ [particles/(m² s)] | (mrem/h)/ [particles/(cm² s)] |
| 0.02 | 2.104 − 13† | 0.758 | 0.2 | 1.160 − 13 | 0.417 |
| 0.100 | 0.649 − 13 | 0.234 | 0.4 | 0.772 − 13 | 0.278 |
| 0.200 | 0.440 − 13 | 0.158 | 0.6 | 0.578 − 13 | 0.208 |
| 0.300 | 0.369 − 13 | 0.133 | 0.8 | 0.433 − 13 | 0.156 |
| 0.400 | 0.337 − 13 | 0.121 | 1 | 0.386 − 13 | 0.119 |
| 0.600 | 0.309 − 13 | 0.111 | 1.5 | 0.330 − 13 | 0.119 |
| 0.800 | 0.297 − 13 | 0.107 | 2 | 0.317 − 13 | 0.114 |
| 1 | 0.293 − 13 | 0.105 | 3 | 0.303 − 13 | 0.109 |
| 2 | 0.297 − 13 | 0.107 | | | |
| 3 | 0.303 − 13 | 0.109 | | | |
| 5 | 0.320 − 13 | 0.115 | | | |
| 7 | 0.324 − 13 | 0.118 | | | |
| 10 | 0.342 − 13 | 0.123 | | | |

†Read as $2.104 \times 10^{-13}$.

with the group conversion factor defined by

$$C_g = \frac{1}{E_{g-1} - E_g} \int_{E_g}^{E_{g-1}} C(E)\, dE \tag{16.11}$$

### 16.4.2 Dose Due to Photons

The dose rate due to a beam of photons is calculated based on an equation similar to Eq. 16.7:

$$\dot{H} = \int_0^\infty dE\, \phi(E) E \mu_a(E) \text{ (Sv/s)} \tag{16.12}$$

where $\mu_a(E)$ = energy absorption coefficient in tissue for a photon of energy $E(\text{m}^2/\text{kg})$.

Notice the two main differences between Eq. 16.7 and Eq. 16.12. For photons, $Q(E) = 1$ and $dE/dx$ is replaced by the product $E\mu_a(E)$. As with charged particles, the analytic form of $\phi(E)$ and $\mu_a(E)$ is seldom known. Instead, one has to work with a set of energy groups, and Eq. 16.12 takes the form

$$\dot{H} = \sum_g \phi_g E_g \mu_a^{\text{tiss}}(E_g) \text{ (Sv/s)} \tag{16.13}$$

where $\phi_g$ and $E_g$ have the same meaning as before.

As with charged particles, tables have been developed that provide a flux-to-dose-rate conversion factor as a function of photon energy (Table 16.3 and Fig. 16.1). Using the conversion factor $C(E)$, Eqs. 16.12 and 16.13 take the

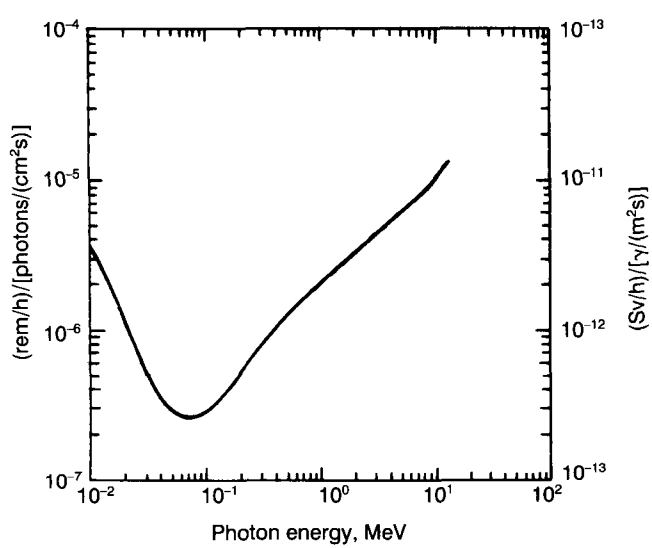


**Figure 16.1** Photon flux-to-dose rate factors for energies from $10^{-2}$ to 15 MeV (Ref. 7).

form

$$\dot{H} = \int_0^\infty dE\, \phi(E) C(E) \tag{16.14}$$

$$\dot{H} = \sum_g \phi_g C_g \tag{16.15}$$

**Example 16.2** What is the dose rate at 1 m away from $3.7 \times 10^{10}$ Bq (1 Ci) of $^{137}$Cs, if (a) the attenuating medium is water or (b) the attenuating medium is air? $^{137}$Cs emits a 0.662-MeV gamma 0.85 percent of the time.

**Answer** In both cases the dose rate is calculated by using Eq. 16.15 with a dose-to-flux conversion factor obtained from Table 16.3 for 0.662-MeV gammas. Using linear interpolation, that factor is $4.05 \times 10^{-16}$ (Sv/s)/[$\gamma$/(m$^2 \cdot$ s)].

The flux at $r$ meters from the source is given by $BSe^{-\mu r}/4\pi r^2$, where

$B$ = buildup factor (from App. E)

$S$ = source strength

$\mu$ = total attenuation coefficient for 0.662-MeV gammas in air or water

**Table 16.3 Gamma-Ray Flux-to-Dose-Rate Conversion Factors**[7]

| Photon energy (MeV) | (rem/h)/ [particles/(cm$^2$ s)] | (Sv/s)/ [particles/(m$^2$ s)] | Photon energy (MeV) | (rem/h)/ [particles/cm$^2$ s)] | (Sv/s)/ [particles/(m$^2$ s)] |
|---|---|---|---|---|---|
| 0.01 | 7.80 − 9 | 2.17 − 18 | 1.5 | 1.68 − 6 | 4.68 − 16 |
| 0.02 | 3.29 − 8 | 9.14 − 18 | 1.75 | 1.92 − 6 | 5.32 − 16 |
| 0.03 | 4.80 − 8 | 1.33 − 17 | 2.00 | 2.14 − 6 | 5.94 − 16 |
| 0.05 | 6.50 − 8 | 1.80 − 17 | 2.25 | 2.35 − 6 | 6.53 − 16 |
| 0.07 | 7.91 − 8 | 2.20 − 17 | 2.5 | 2.56 − 6 | 7.08 − 16 |
| 0.10 | 1.03 − 7 | 2.86 − 17 | 2.75 | 2.75 − 6 | 7.65 − 16 |
| 0.15 | 1.54 − 7 | 4.27 − 17 | 3.00 | 2.94 − 6 | 8.18 − 16 |
| 0.20 | 2.17 − 7 | 6.02 − 17 | 3.25 | 3.13 − 6 | 8.70 − 16 |
| 0.25 | 2.78 − 7 | 7.73 − 17 | 3.50 | 3.32 − 6 | 9.21 − 16 |
| 0.30 | 3.41 − 7 | 9.46 − 17 | 3.75 | 3.50 − 6 | 9.71 − 16 |
| 0.35 | 4.04 − 7 | 1.12 − 16 | 4.0 | 3.67 − 6 | 1.02 − 15 |
| 0.40 | 4.67 − 7 | 1.30 − 16 | 4.25 | 3.85 − 6 | 1.07 − 15 |
| 0.45 | 5.30 − 7 | 1.47 − 16 | 4.50 | 4.02 − 6 | 1.12 − 15 |
| 0.50 | 5.92 − 7 | 1.64 − 16 | 4.75 | 4.19 − 6 | 1.16 − 15 |
| 0.55 | 6.54 − 7 | 1.82 − 16 | 5.00 | 4.36 − 6 | 1.21 − 15 |
| 0.60 | 7.15 − 7 | 1.98 − 16 | 6.00 | 5.04 − 6 | 1.40 − 15 |
| 0.65 | 7.75 − 7 | 2.15 − 16 | 7.00 | 5.71 − 6 | 1.59 − 15 |
| 0.70 | 8.34 − 7 | 2.32 − 16 | 8.00 | 6.39 − 6 | 1.78 − 15 |
| 0.80 | 9.51 − 7 | 2.64 − 16 | 9.00 | 7.08 − 6 | 1.97 − 15 |
| 1.0 | 1.17 − 6 | 3.26 − 16 | 10.0 | 7.79 − 6 | 2.16 − 15 |

From App. E, the buildup factor is

$$B = 1 - a\mu r[\exp(b\mu r)]$$

where (using linear interpolation) $a = 1.96$ and $b = 0.054$.

(a) For water, the value of the total attenuation coefficient is (from App. D, using linear interpolation)

$$\mu = 0.00861 \text{ m}^2/\text{kg} = 0.0861 \text{ cm}^2/\text{g}$$

The number of mean free paths (mfp) in water is

$$\mu r = (0.00861 \text{ m}^2/\text{kg})(10^3 \text{ kg/m}^3)(1 \text{ m}) = 8.61 \text{ mfp}$$

Thus,

$$B \text{ (water)} = 1 + (1.96)(8.61)[\exp(8.61 \times 0.054)] = 27.86$$

The dose rate in water is

$$\dot{H} = \dot{D} = (27.86)(3.7 \times 10^{10})(\times 0.85)\left[\frac{e^{-8.61}}{4\pi(1^2)}\gamma/(\text{m}^2 \cdot \text{s})\right]$$
$$\times\{4.05 \times 10^{-16} \text{ (Sv/s)}/[\gamma/(\text{m}^2 \cdot \text{s})]\}$$
$$= 5.15 \times 10^{-9} \text{ Sv/s} = 1.85 \text{ mrem/h}$$

(b) For air, the value of the total attenuation coefficient is (from App. D, using linear interpolation)

$$\mu = 0.0082 \text{ m}^2/\text{kg} = 0.082 \text{ cm}^2/\text{g}$$
$$\mu r = (0.0082 \text{ m}^2/\text{kg})(1.29 \text{ kg/m}^3)(1 \text{ m}) = 0.01 \text{ mfp}$$

The buildup factor is

$$B \text{ (air)} = 1 + (1.96)(0.01)[\exp(0.01 \times 0.054)] = 1.02$$

The dose rate in air is

$$\dot{H} = \dot{D} = (1.02)(3.7 \times 10^{10})(\times 0.85)\left[\frac{e^{-0.01}}{4\pi(1)^2}\gamma/(\text{m}^2 \text{ s})\right]$$
$$\times\{4.05 \times 10^{-16} \text{ (Sv/s)}/[\gamma/(\text{m}^2 \text{ s})]\}$$
$$= 1.02 \times 10^{-6} \text{ Sv/s} = 0.368 \text{ rem/h}$$

As pointed out in Sec. 4.8.6, where buildup factors are defined and discussed in detail, the value of the buildup factor is significantly greater than 1 if the distance in mean free paths is significantly greater than 1. In Ex. 16.2 the distance in water is 8.61 mfp and $B = 27.86$, while in air the distance is 0.01 mfp and $B = 1.02$.

The buildup factor constants given in App. E apply to a point isotropic source in an infinite medium (Ex. 16.2 is such a case). The same constants can be used, however, in other geometries if no better values are available. For

example, one could use the constants given in App. E to calculate the dose rate from a point isotropic source in a semi-infinite medium or from a point isotropic source located behind a slab shield. In such cases, the use of the constants from App. E results in an overestimate of the buildup factor. Buildup factors for many different geometries are given in Ref. 5.

### 16.4.3 Dose Due to Neutrons

Neutrons hitting the human body deliver energy to it through elastic and inelastic collisions with nuclei, and through secondary radiation emitted by the radioisotopes produced after neutrons are captured.

If an individual is exposed to fast neutrons, most of the energy transfer takes place through elastic collisions with hydrogen ($\sim$ 90 percent) and, to a lesser extent, through collisions with oxygen and carbon nuclei. [The average neutron energy loss per collision with hydrogen (proton) is 50 percent of the incident neutron energy; the corresponding fractions for carbon and oxygen are 14 percent and 11 percent.] These "recoil" nuclei are charged particles, which lose their energy as they move and slow down in tissue. This is true for neutron energies down to about 20 keV. When the neutron energy reaches or becomes lower than a few keV, the importance of elastic collisions decreases, and the reaction $^{14}N(n, p)^{14}C$ produces more significant effects. As discussed in Chap. 14, this is an exothermic reaction producing protons with kinetic energy of 584 keV. Radioactive $^{14}C$ is also produced, emitting betas with a maximum energy of 156 keV. The biological damage comes mainly from the protons, not from the betas of $^{14}C$.

Thermal neutrons are absorbed in the body mainly through the reaction $^{1}H(n, \gamma)^{2}H$, which results in the emission of a 2.2-MeV gamma. A reaction of secondary importance is $^{23}Na(n, \gamma)^{24}Na$. The isotope $^{24}Na$ has a 15-h half-life and emits two energetic gammas with energy 1.37 and 2.75 MeV. Thus, when thermal neutrons are absorbed, damage is caused by the energetic gammas that are produced as a result of the neutron capture.

The general equation for the dose rate has the form

$$H(r, E) = \sum_{i=1}^{M} \phi(r, E)\left(\Sigma_s^i(E)\frac{2A_iE}{(A_i+1)^2} + \Sigma_\gamma^i f_\gamma^i E_\gamma^i + \Sigma_q^i Q_i + \cdots\right) Q(E) \text{ (Sv/s)} \tag{16.16}$$

where $\phi(r, E)$ = neutron flux $[n/(\text{m}^2\ \text{s})]$ at point $r$, of neutrons with energy $E$
$\Sigma^i(E)$ = macroscopic cross sections, for neutrons of energy $E$ for elastic scattering, capture, charged-particle-producing reactions, etc., for isotope $i$
$M$ = total number of isotopes present

**Table 16.4 Neutron Flux-to-Dose-Rate Conversion Factors**[4]

| Neutron energy (MeV) | (Sv/s)/[neutrons/(m² s)] | (rem/h)/[neutrons/(cm² s)] |
|---|---|---|
| 2.5 − 08† | 1.02 − 15 | 3.67 − 06 |
| 1.0 − 07 | 1.02 − 15 | 3.67 − 06 |
| 1.0 − 06 | 1.23 − 15 | 4.44 − 06 |
| 1.0 − 05 | 1.23 − 15 | 4.44 − 06 |
| 1.0 − 04 | 1.19 − 15 | 4.28 − 06 |
| 1.0 − 03 | 1.02 − 15 | 3.67 − 06 |
| 1.0 − 02 | 9.89 − 16 | 3.56 − 06 |
| 1.0 − 01 | 5.89 − 15 | 2.12 − 06 |
| 5.0 − 01 | 2.56 − 14 | 9.23 − 05 |
| 1.0 | 3.69 − 14 | 1.33 − 04 |
| 2.5 | 3.44 − 14 | 1.24 − 04 |
| 5.0 | 4.33 − 14 | 1.56 − 04 |
| 7.0 | 4.17 − 14 | 1.50 − 04 |
| 10.0 | 4.17 − 14 | 1.50 − 04 |
| 14.0 | 5.89 − 14 | 2.12 − 04 |
| 20.0 | 6.25 − 14 | 2.25 − 04 |

†Read as $2.5 \times 10^{-8}$.

$f_\gamma$ = fraction of gamma energy deposited at the capture site
$Q_i$ = the $Q$ value of the charged-particle reaction; all $Q_i$ are assumed to be deposited at site of the reaction
$Q(E)$ = quality factor for neutrons of energy $E$

Equation 16.16 neglects inelastic scattering, which is negligible for neutrons in tissue for the energies considered here. If neutrons of many energies are present, the calculation should be repeated for all energies, and the results summed to give the total dose rate. Flux-to-dose-rate conversion factors have been developed for neutrons as well (Table 16.4, Figs. 16.2 and 16.3). Using the conversion factor, Eq. 16.16 takes the form

$$\dot{H}(r, E) = \phi(r, E)C(E) \tag{16.17}$$

If the neutron spectrum is known in terms of energy groups, Eq. 16.16 becomes

$$\dot{H}(r) = \sum_g C_g \phi_g(r) \tag{16.18}$$

Although Eq. 16.16 is not normally used for everyday dose calculations, it is instructive to present it so that the reader may comprehend the various contributors to the neutron dose.

**Example 16.3** At the open beam port of a research reactor, the neutron flux at a certain power level consists of $1.6 \times 10^8$ neutrons/(m$^2$ · s) with energy 100

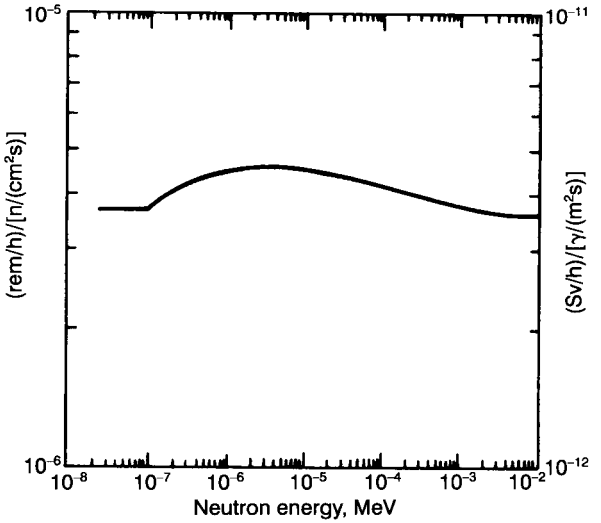


**Figure 16.2** Neutron flux-to-dose-rate factors for energies $10^{-8}$ to $10^{-2}$ MeV (Ref. 7).

keV, and $3.5 \times 10^9$ neutrons/(m$^2 \cdot$ s) with an average energy of 0.025 eV. What is the total dose rate at that point?

**Answer** Using Table 16.4, the dose rate is

$$\dot{H} = (1.6 \times 10^8)(5.89 \times 10^{-15}) + (3.5 \times 10^8)(1.02 \times 10^{-15})$$
$$= 1.30 \times 10^{-6} \text{ Sv/s} = 0.467 \text{ rem/h}$$

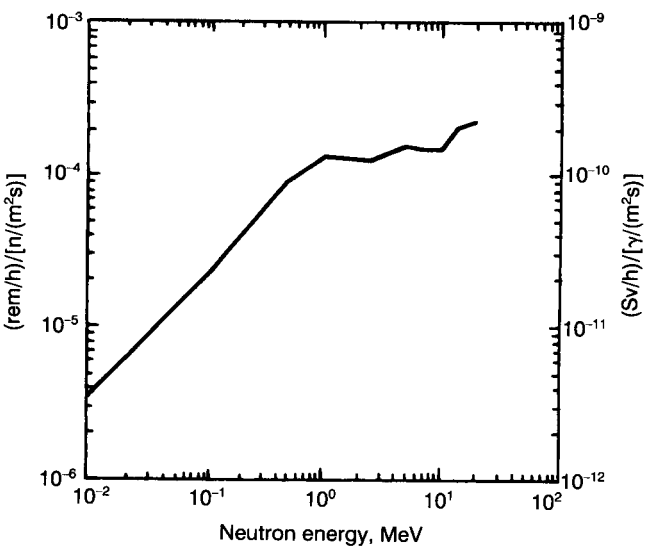


**Figure 16.3** Neutron flux-to-dose-rate factors for energies $10^{-2}$ to 20 MeV (Ref. 7).

## 16.5 DOSIMETRY FOR RADIATION INSIDE THE BODY

### 16.5.1 Dose from a Source of Charged Particles Inside the Body

If the charged particles ($e$, $p$, $\alpha$) are created or deposited inside the body, the calculation of the dose is easier because the range of the particles considered (energy less than 10 MeV) is millimeters or less and all the energy is deposited in a very small volume. (In the case of electrons, a fraction of the energy escapes as bremsstrahlung, but it represents a small correction; neglecting bremsstrahlung, one obtains a conservative answer.) The dose rate equivalent is given in this case by

$$H = \frac{\int_0^\infty E\,S(E)Q(E)\,dE}{\text{(mass in which the particle energy was deposited)}} \text{ (Sv/s)} \tag{16.19}$$

where $S(E)\,dE$ = number of particles emitted per second (activity) with energy between $E$ and $E + dE$.

If the particle spectrum is known in multigroup form, Eq. 16.19 becomes

$$H = \sum_g E_g S_g Q_g/\text{mass} \tag{16.20}$$

with

$$S_g = \int_{E_g} dE\,S(E)$$

If the charged-particle source is localized, i.e., it can be considered a point isotropic source, the mass in the denominator of Eq. 16.20 is equal to

$$\text{(Mass where energy was deposited)} = \tfrac{4}{3}\pi R^3 \rho$$

where $R$ = range of charged particle in tissue
$\rho$ = density of tissue

If the source is deposited in an organ, e.g., liver, thyroid, spleen, then the mass in the denominator of Eq. 16.20 is the mass of that organ, and the result of this calculation is the average dose rate for this organ. By using the mass of the organ, the tacit assumption is made that all the energy emitted by the radioactive source is absorbed in that volume. It is a conservative estimate, since some particles will be borne very close to the surface of the organ and escape from it after depositing only part of their energy there.

**Example 16.4** What is the dose rate from 1 pCi of an alpha source emitting 6-MeV alphas in tissue?

**Answer** The range of this alpha particle in tissue $4.7 \times 10^{-5}$ m. Thus,

$$\dot{H} = \frac{(3.7 \times 10^{-2}\alpha/\text{s})(6\ \text{MeV}/\alpha)(1.602 \times 10^{-13}\ \text{J/MeV})(20)}{(4/3)\pi(4.7 \times 10^{-5})^3(10^3\ \text{kg/m}^3)}$$
$$= 1.64 \times 10^{-3}\ \text{Sv/s} = 589\ \text{rem/h}$$

This is an extremely large dose rate, the result of the energy being deposited in a very small volume.

**Example 16.5** What is the dose rate due to the alphas of Ex. 16.4 if it is known that the source is uniformly distributed in the lungs?

**Answer** In this case, the mass affected is that of the lungs, which is (for a 70-kg person) about 1 kg. The dose rate is

$$\dot{H} = \frac{(3.7 \times 10^{-2})(6)(1.602 \times 10^{-13})(20)}{1}$$
$$= 7.11 \times 10^{-13}\ \text{Sv/s} = 2.56 \times 10^{-7}\ \text{rem/h}$$

**Example 16.6** What is the dose rate to the thyroid gland due to the betas emitted by 1 mCi of $^{131}$I?

**Answer** The isotope $^{131}$I emits two betas, one with $E_{\max}^{(1)} = 0.608$ MeV, 85 percent of the time, and a second with $E_{\max}^{(2)} = 0.315$ MeV, 15 percent of the time. The range of these betas in tissue is about 2 mm and 0.9 mm, respectively.

The thyroid gland has a mass of about 0.025 kg (i.e., a volume of about 25 cm$^3$); therefore, all the beta energy will be deposited in it.

The dose rate is obtained using Eq. 16.20:

$$\dot{H} = \frac{(3.7 \times 10^7)[0.85(0.608/3) + 0.15(0.315/3)](1.602 \times 10^{-13})}{25 \times 10^{-3}}$$
$$= 4.46 \times 10^{-5}\ \text{Sv/s} = 16.0\ \text{rem/h}$$

### 16.5.2 Dose from a Photon Source Inside the Body

Since photons have, essentially, an infinite range, the previous calculation for charged particles does not apply. A source of photons located anywhere in the body will deliver some dose to all the other parts of that body. The calculation of the dose rate proceeds as follows.

Consider an internal organ containing a uniform concentration of a radioisotope emitting a gamma with energy $E$ at the rate of $S_v[\gamma/(\text{s m}^3)]$ inside the volume $V_s$, called the source volume (Fig. 16.4). The dose rate received by

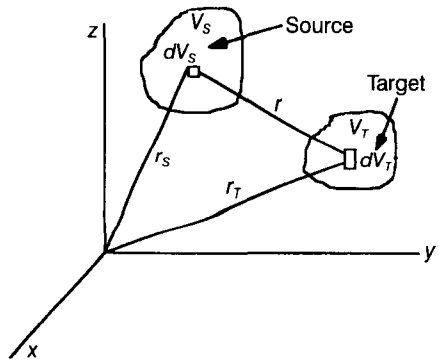


**Figure 16.4** The geometry used in the calculation of the dose to a target organ ($V_T$) from a radioisotope uniformly distributed in another volume ($V_S$).

another organ with volume $V_T$, called the target, is given by the expression

$$\dot{D} = \frac{\int_{V_S}\int_{V_T} (S_V\, dV_s/4\pi r^2)e^{-\mu r}[\gamma/(\mathrm{m}^2\,\mathrm{s})]E(\mathrm{MeV}/\gamma)\mu_a^{\mathrm{tiss}}(\mathrm{m}^2/\mathrm{kg})B(\mu r)\rho(\mathrm{kg}/\mathrm{m}^3)dV_T}{\rho(\mathrm{kg}/\mathrm{m}^3)V_T} \times 1.602 \times 10^{-13}\ \mathrm{J/MeV} \tag{16.21}$$

where $\mu$ = total linear attenuation coefficient in tissue for gammas of energy $E$
$\mu_a^{\mathrm{tiss}}$ = mass energy absorption coefficient in tissue for gammas of energy $E$
$B(\mu r) = B(\mu r, E)$ = buildup factor for gammas of energy $E$
$\rho$ = density of tissue

Or, pulling out of the integral the quantities that are constant in space, Eq. 16.21 becomes

$$\dot{D} = \dot{H} = \frac{S_V}{4\pi} E\mu_a^{\mathrm{tiss}} g \tag{16.22}$$

where the quantity

$$g = \frac{1}{V_T}\int_{V_T} dV_T \int_{V_S} dV_S \frac{e^{-\mu r}}{r^2} B(\mu r, E) \tag{16.23}$$

is called the geometry factor. Note that the factor $g$ has dimensions of length. Values of $g$ have been calculated and tabulated (e.g., Cember). The usefulness of $g$ stems from the fact that $g$ values can be calculated for a relatively small number of cases and then, by interpolation, other geometry factor values may be computed and used. Once $g$ is known, the dose rate to an organ can be calculated from Eq. 16.22, and such calculation will have an uncertainty mainly from the value of $g$. There is a certain similarity in the use of $g$ and the use of buildup factors. Buildup factors are also tabulated for a limited number of cases, and additional values are obtained by interpolation.

One common case utilizing the concept of the geometry factor is the calculation of the dose rate in an organ from a radioisotope deposited in that organ. For example, what is the dose rate to the thyroid from radioactive iodine given to a patient? If the organ is further assumed to be spherical, Eq. 16.23 takes the simple form

$$g = \int_0^R 4\pi r^2\, dr \frac{e^{-\mu r}}{r^2} = \frac{4\pi}{\mu}(1 - e^{-\mu R}) \tag{16.24}$$

Using this value of $g$ with Eq. 16.22 gives the dose rate at the center of the sphere. To obtain the average dose rate, an average value of $g$ should be used. For a sphere the average value of the geometry factor is (Cember)

$$\bar{g} = 0.75(g)_{\text{center}} \tag{16.25}$$

Average geometry factors for cylindrical bodies are given in Table 16.5. An example of using geometry factors is given in Sec. 16.6

The equations given above for the dose rate from photons are valid for monoenergetic sources. If the deposited radioisotope emits many discrete gammas or if a multigroup energy spectrum of the source is provided, the calculation should be repeated for all gammas (or groups) and the results added to obtain the total dose rate.

## 16.6 INTERNAL DOSE TIME DEPENDENCE—BIOLOGICAL HALF-LIFE

Radioisotopes may enter the body by inhalation, drinking, eating, injection, or through broken skin (wound). If the radiation source is inside the body, the exposure is internal and more damaging. No attenuation is provided by skin or

**Table 16.5 Average Geometry Factors for Cylindrical Organs Containing a Uniformly Distributed Photon Source**

| Cylinder height (cm) | Radius of cylinder (cm) | | | | | | | |
|---|---|---|---|---|---|---|---|---|
| | 3 | 5 | 10 | 15 | 20 | 25 | 30 | 35 |
| 2 | 17.5 | 22.1 | 30.3 | 34.0 | 36.2 | 37.5 | 38.6 | 39.3 |
| 5 | 22.3 | 31.8 | 47.7 | 56.4 | 61.6 | 65.2 | 67.9 | 70.5 |
| 10 | 25.1 | 38.1 | 61.3 | 76.1 | 86.5 | 93.4 | 98.4 | 103 |
| 20 | 25.7 | 40.5 | 68.9 | 89.8 | 105 | 117 | 126 | 133 |
| 30 | 25.9 | 41.0 | 71.3 | 94.6 | 112 | 126 | 137 | 146 |
| 40 | 25.9 | 41.3 | 72.4 | 96.5 | 116 | 131 | 143 | 153 |
| 60 | 26.0 | 41.6 | 73.0 | 97.8 | 118 | 134 | 148 | 159 |
| 80 | 26.0 | 41.6 | 73.3 | 98.4 | 119 | 135 | 150 | 161 |
| 100 | 26.0 | 41.6 | 73.3 | 98.5 | 119 | 136 | 150 | 162 |

From Hine & Brownell.

clothes, and the person cannot walk away from the source. The exposure continues until the radioisotope decays completely or is excreted by the body.

A radioisotope is rejected by the body at a rate that depends upon the chemical properties of the element. All isotopes of the same element are rejected at the same rate, whether they are stable or not. For most radioisotopes, the rate of rejection is proportional to the amount of the isotope in the body. This leads to an exponential elimination law as a result of the combination of decay and rejection.† Let

$N(t)$ = number of radioactive atoms at time $t$

$\lambda_R$ = radiological decay constant

$\lambda_B$ = biological decay constant

= probability of rejection (by the body) per atom per unit time

The rate of change of $N(t)$ is $dN(t)/dt = -\lambda_R N(t) - \lambda_B N(t)$, with solution

$$N(t) = N(0)e^{-(\lambda_R+\lambda_B)t} = N(0)e^{-\lambda_e t} \tag{16.26}$$

where $\lambda_e = \lambda_R + \lambda_B$ = effective decay constant.

A *biological half-life* is defined in terms of $\lambda_B$:

$$T_B = \frac{\ln 2}{\lambda_B} \tag{16.27}$$

and an *effective half-life* is defined by the equation

$$T_e = \frac{T_B T_R}{T_B + T_R} = \frac{\ln 2}{\lambda_e} \tag{16.28}$$

The biological excretion rate of an element from the human body is not necessarily the same for the whole body and for a particular organ. In fact, in most cases, the biological elimination rates are different for different organs and for the body as the whole. For example, the biological half-life of iodine is 138 days for rejection from the thyroid, 7 days for the kidneys, 14 days for the bones, and 138 days for the whole body. For this reason, a table of biological and effective half-lives ought to include the organ of reference. Table 16.6 gives radiological, biological, and effective half-lives for certain common isotopes. The reader should remember that the biological half-life is the same for all isotopes of the same element, but the effective half-life is not.

If $T_B \gg T_R$, the decay removes the material much faster than the body rejects it. An example of such a case is $^{131}$I, with $T_B$ = 138 days (thyroid), $T_R$ = 8 days, and $T_e$ = 7.6 days. If $T_B \ll T_R$, the biological elimination is mainly responsible for the removal of the isotope. An example of such a case is tritium, with $T_B$ = 12 days, $T_R$ = 12 years, and $T_e$ = 12 days.

†Other rejection laws have been proposed (see p. 35 of Ref. 8 and Ref. 9)

**Table 16.6 Radiological, Biological, and Effective Half-Lives of Certain Common Isotopes[8]**

| Isotope | Organ of reference | Radiological half-life | Biological half-life | Effective half-life |
|---|---|---|---|---|
| $^{3}H$ | Total body | 12.3 y | 12 d | 12 d |
| $^{14}C$ | Total body | 5,700 y | 10 d | 10 d |
| | Fat | | 12 d | 12 d |
| | Bone | | 40 d | 40 d |
| $^{32}P$ | Total body | 14.3 d | 257 d | 13.5 d |
| | Liver | | 18 d | 8 d |
| | Bone | | 1115 d | 14.1 d |
| | Brain | | 257 d | 13.5 d |
| $^{40}K$ | Total body | $1.28 \times 10^{9}$ y | 58 d | 58 d |
| $^{55}Fe$ | Total body | 1100 d | 800 d | 463 d |
| | Spleen | | 600 d | 388 d |
| | Lungs | | 3200 d | 819 d |
| | Liver | | 554 d | 368 d |
| | Bone | | 1680 d | 665 d |
| $^{57}Fe$ | Total body | 45.1 d | 800 d | 42.7 d |
| $^{99m}Tc$ | Total body | 0.25 d | 1 d | 0.2 d |
| | Kidneys | | 20 d | 0.25 d |
| | Lungs | | 5 d | 0.24 d |
| | Skin | | 10 d | 0.24 d |
| | Liver | | 30 d | 0.25 d |
| | Bone | | 25 d | 0.25 d |
| $^{129}I$ | Total body | $1.726 \times 10^{7}$ y | 138 d | 138 d |
| | Thyroid | | 138 d | 138 d |
| | Kidneys | | 7 d | 7 d |
| | Liver | | 7 d | 7 d |
| | Spleen | | 7 d | 7 d |
| | Testes | | 7 d | 7 d |
| | Bone | | 14 d | 14 d |
| $^{131}I$ | Thyroid | 8 d | 138 d | 7.6 d |
| $^{235}U$ | Total body | $7.12 \times 10^{8}$ y | 100 d | 100 d |
| | Kidneys | | 15 d | 15 d |
| | Bone | | 300 d | 300 d |
| $^{238}U$ | Total body | $4.66 \times 10^{9}$ y | 100 d | 100 d |
| $^{239}Pu$ | Total body | 24,000 | 175 y | 175 y |
| | Liver | | 82 y | 82 y |
| | Kidneys | | 87.7 y | 87.7 y |

As a result of the combined radioactive and biological elimination of a radioisotope from the whole body or from an organ, the dose rate to the body or the organ is not constant over time. Consider an amount of a certain radioisotope that delivers a dose rate equal to $\dot{H}(0)$ at the time the radioisotope entered the body. If the effective half life of the isotope is $T_e$, the total dose delivered

over a period of time $T$ is

$$H_T = \int_0^T \dot{H}(0)e^{-\lambda_e t}\,dt = \frac{\dot{H}(0)}{\lambda_e}(1 - e^{-\lambda_e T}) = \frac{\dot{H}(0)}{\ln 2}T_e(1 - e^{-\ln 2(T/T_e)}) \quad (16.29)$$

If $T \gg T_e$, then

$$H_T = \frac{\dot{H}(0)}{\ln 2}T_e \quad (16.30)$$

**Example 16.7** What is the total dose received by an individual who drank, accidentally, $10^{-7}$ kg of $^3H_2O$?

**Answer** Assuming that the $^3H_2O$ is uniformly distributed, the dose rate at the time of the accident ($t = 0$) is given by Eq. 16.20. Tritium is a beta emitter with $E_{max} = 18.6$ keV, $T_R = 12$ years, and $T_B = 12$ days. At $t = 0$, the source strength (i.e., the activity) is

$$S = N\lambda = (10^{-7}\text{ kg})(2\text{ at/molecule})\frac{6.022 \times 10^{23}\text{ molecules/mol}}{22 \times 10^{-3}\text{ kg/mol}}$$
$$\times\left[\frac{\ln 2}{12(3.15 \times 10^7)}\right] = 1.00 \times 10^{10}\text{ Bq} = 271\text{ mCi}$$

Considering an average-size person (70 kg), the dose rate at $t = 0$ is

$$\dot{H}(0) = \frac{[10^{10}(0.0186/3)\text{ MeV/s}](1.602 \times 10^{-13}\text{ J/MeV})(1)}{70\text{ kg}}$$
$$= 1.42 \times 10^{-7}\text{ Sv/s} = 51\text{ mrem/h}$$

The total dose is obtained by using Eq. 16.30 (with $T = 50y$):

$$H_T = \frac{1.42 \times 10^{-7}\text{ Sv/s}}{\ln 2}(12\text{ days})(86{,}400\text{ s/day})$$
$$= 0.212\text{ Sv} = 21.2\text{ rem}$$

**Example 16.8** A patient was given 10 $\mu$Ci of $^{131}I$ in an attempt to kill a thyroid tumor. Assuming that all the iodine is concentrated in the thyroid, calculate (a) the dose rate to the patient at the time of the injection and (b) the total dose received by this patient. Iodine emits 0.364-MeV gammas 82 percent of the time and 0.606-MeV betas 92 percent of the time. For $^{131}I$, $T_R = 8$ days, $T_B = 138$ days; mass of the thyroid is 0.020 kg. The radius of the thyroid, taken as a sphere, is $R = 16.8$ mm.

**Answer** a) The dose rate from the betas will be obtained with the assumption that all the beta energy is deposited in the thyroid. Thus,

$$\dot{D} = \dot{H} = \frac{\text{Energy/s}}{\text{mass}} = \frac{0.92(3.7 \times 10^5)(0.606/3)(1.602 \times 10^{-13})\ \text{J/s}}{20 \times 10^{-3}\ \text{kg}}$$

$$= 5.51 \times 10^{-7}\ \text{Sv/s} = 0.198\ \text{rem/h}$$

The dose rate from gammas is given by Eq. 16.22, and $g$ is calculated using Eqs. 16.24 and 16.25.

b) For 0.364-MeV gammas in tissue, $\mu = \mu_{\text{tot}} = 0.0101\ \text{m}^2/\text{kg} = 0.101\ \text{cm}^{-1}$, $\mu_a = 0.00325\ \text{m}^2/\text{kg}$. The volumetric gamma source strength needed for Eq. 16.22 is

$$S_V = (3.7E5)/V = 3.7E5/(20 \times 10^{-6}) = 1.85 \times 10^{10}\ \text{Bq/m}^3$$

$$\bar{g} = 0.75\frac{4\pi}{\mu}(1 - e^{-\mu r}) = 0.75 \times 19.3 = 14.5\ \text{cm} = 0.145\ \text{m}$$

$$\dot{H} = \frac{0.82(1.85 \times 10^{10}\gamma)/(\text{m}^3\ \text{s})}{4\pi} 0.364\ \text{MeV}(1.602 \times 10^{-13}\ \text{J/MeV})$$

$$\times (0.00325\ \text{m}^2/\text{kg})0.145\ \text{m} = 3.32 \times 10^{-8}\ \text{Sv/s} = 11.9\ \text{mrem/h}$$

The total dose (during 50 years after the intake) is given by Eq. 16.30, since

$$T_e = \frac{T_R T_B}{T_R + T_B} = \frac{8 \times 138}{8 + 138}\ \text{days} = 7.77\ \text{days} \ll T\ (= 50y)$$

$$H = \frac{\dot{H}(0)}{\ln 2} T_e = \frac{3.32 \times 10^{-8}\ \text{Sv/s}}{\ln 2} 7.77\ \text{days}(86{,}400\ \text{s/days})$$

$$= 0.032\ \text{Sv} = 3.2\ \text{rem}$$

## 16.7 BIOLOGICAL EFFECTS OF RADIATION

The study of the biological effects of radiation is a very complex and difficult task for two main reasons.

1. The human body is a very complicated entity with many organs of different sizes, functions, and sensitivities.
2. Pertinent experiments are practically impossible with humans. The existing human data on the biological effects of radiation come from accidents, through extrapolation from animal studies, and from experiments in vitro.

How and why does radiation produce damage to biological material? To answer the question, one should consider the constituents and the metabolism

of the human body. In terms of compounds, about 61 percent of the human body is water. Other compounds are proteins, nucleic acids, fats, and enzymes. In terms of chemical elemental composition, the human body is, by weight, about 10 percent H, 18 percent C, 3 percent N, 65 percent O, 1.5 percent Ca, 1 percent P, and other elements that contribute less than 1 percent each. To understand the basics of the metabolism, one needs to consider how the basic unit of every organism, which is the cell, functions.

### 16.7.1 Basic Description of the Human Cell

The cell, the basic unit of every living organism, consists of a semipermeable membrane enclosing an aqueous suspension of a liquid substance called the cytoplasm. The cell exchanges material with the rest of the organism through the membrane. A typical cell size is about $10^{-5}$ m (size of a typical atom is $10^{-10}$ m). At the center of the cell, there is another region called the nucleus, also enclosed by a semipermeable membrane. The nucleus is the most important part of the cell because it controls cell activities. Nucleic acids and chromosomes are the cell's most significant contents.

The two nucleic acids found in the nucleus of a cell are ribonucleic acid (RNA) and deoxyribonucleic acid (DNA). The RNA controls the synthesis of proteins. The DNA contains the genetic code of the species. The structure of the DNA has been determined to be a double helix, or staircase with the stairsteps consisting of paired molecules of four bases: adenine (A), guanine (G), cytosine (C), and thymine (T). It is the combination of these four compounds, A, G, C, and T, that makes the genes (a gene is a segment of DNA) that contain the instructions for the metabolism of the cell. The DNA molecules have a molecular weight of about $10^9$. They are usually coiled inside the cell, but when extended like a string, the width of the double-stranded helix of the DNA is about 2 nm.

The chromosomes are threadlike assemblies that are extremely important because they contain the genes that transmit the hereditary information. Every species has a definite number of chromosomes. The human species has 23 pairs, one chromosome of each pair being contributed by each parent. Every cell has 23 pairs of chromosomes with the exception of the egg and the sperm, which have 23 chromosomes each. When fertilization occurs, the first cell of the new organism contains 23 pairs of chromosomes, equally contributed by each parent.

Cells multiply by a dividing process called mitosis. Just before mitosis is to take place, each chromosome of the cell splits in two. Thus, each of the two new cells has exactly the same number of chromosomes as the parent cell. There are some human cells that do not divide, such as the blood cells and the nerve cells. The blood cells are regenerated by the blood-forming organs, primarily by the bone marrow. The nerve cells, when destroyed, are not supplied again.

Radiation may damage the cell when it delivers extra energy to it because that energy may be used to destroy parts or functions of the cell. For example, as a result of irradiation, chromosomes or DNA molecules may break. The

break may occur either by direct collision with an incoming fast particle (e.g., fast neutron) or as the result of chemical activity initiated by the radiation. It has been determined experimentally that the energy imparted by the radiation may be used to break chemical bonds and create free radicals, which are always chemically active and which may produce new chemical compounds unhealthy for the organism. For example, a water molecule may break into two radicals that, in turn, may form hydrogen peroxide ($H_2O_2$)[†]:

$$H_2O^{\cdot} \rightarrow HO^{\cdot} + H^{\cdot}$$
$$HO^{\cdot} + HO^{\cdot} \rightarrow H_2O_2$$

A damaged cell may react in different ways. It may recover, or die, or grow out of control if the radiation has damaged the RNA and DNA molecules that provide the instructions to feed and divide the cell. Obviously, the net result of the damage to the organism depends on many factors, such as the number and the type of cells destroyed. Another effect of irradiation may be damage to the DNA of the germ cells, the sperm and the egg, that carry the genetic code of the new organism. This type of damage (called genetic; see Sec. 16.7.2) will appear in the offspring of the irradiated cell or organism.

### 16.7.2 Stochastic and Nonstochastic Effects

As explained in the previous section, radiation imparts energy to the cell, which may trigger mechanisms that result in biological damage. This "damage," which starts at the microscopic (cell) level, may, in some cases, manifest itself as a macroscopic observable biological effect.

The biological effects of radiation are divided into different categories, depending upon the objective of the discussion. Examples are somatic (effects appearing on the individual being irradiated), genetic (appearing in the offspring of the irradiated person), short-term effects, long-term effects, etc. The division to be used here is stochastic and nonstochastic effects because it is this characterization that leads to a better understanding of the dose-effect relationship.

Examples of nonstochastic (or deterministic) effects are erythema, nausea, loss of hair, cataracts, sterility, etc. Stochastic (or probabilistic) effects are cancer and genetic defects (birth defects) (Table 16.7). Genetic effects are abnormalities that may appear in the offspring of persons exposed to radiation, one or many generations after the exposure.

An important difference between stochastic and nonstochastic effects is that nonstochastic effects have a threshold; stochastic effects do not. The "threshold" is a minimum radiation dose that has to be received in a relatively short time period for the effect to appear (Fig. 16.5). A dose below the threshold will not

[†]Chemical poisoning by $H_2O_2$ shows many of the radiation sickness symptoms.

**Table 16.7 Biological Effects of Radiation**

| | Stochastic (probabilistic) | Nonstochastic (deterministic) |
|---|---|---|
| Somatic | Cancer | Erythema<br>Loss of Hair<br>Nausea<br>Sterility<br>Cataracts<br>Fever<br>Death<br>etc. |
| Genetic | Birth defects | |

produce nonstochastic effect. A dose above the threshold will definitely cause the effect. The threshold line in Fig. 16.5*a* is shaded to emphasize the point that the threshold dose is not a single one but a range of doses that depends on the effect considered and on the individual receiving the dose. Different effects have different threshold doses. For example, the threshold dose for erythema is much less than that for death. For stochastic effects, it is believed today that there is no threshold. All one can say is that there is a probability that the effect *may* appear (some time later, probably years) after any amount of radiation exposure above zero. It is also accepted today that the probability that the effect will appear increases with dose received. There is no scientific proof that a threshold *does not* exist. Also there is no concrete scientific proof that all radiation effects are detrimental. However, in the absence of proof that a threshold does exist and that radiation may, at certain dose levels, be beneficial, the conservative approach is taken, which is no threshold and any radiation dose is damaging. Notice, however, the word *may*. It is not certain that the effect will appear; all one can say is that there is a probability that it may happen.

An example of stochastic versus nonstochastic effects can be made using alcohol. If a person drinks 20 glasses of wine in a short period of time, it is

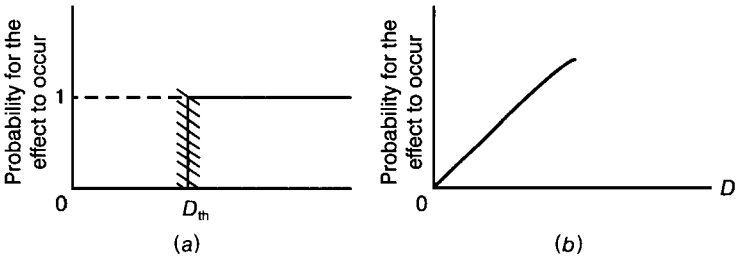


**Figure 16.5** (*a*) The probability for a nonstochastic effect to occur versus dose *D*. (*b*) The probability for a stochastic effect to occur versus dose *D*.

certain that the individual will get drunk. Drunkenness is a nonstochastic effect caused by alcohol (the "threshold" is not 20 glasses for everybody, it depends on the individual, on the rate of wine consumption, etc.). Examples of stochastic effects caused by alcohol are cirrhosis of the liver and birth defects to a child whose mother was drinking during pregnancy. One glass of wine, just once in a lifetime, or one glass per day may cause cirrhosis or produce a child with birth defects; on the other hand, it may cause neither.

Nonstochastic effects appear after relatively high doses in the Sv (rem) range. The first measurable effect of a whole-body irradiation appears after a dose of 0.25–0.50 Sv (25–50 rem). The individual exposed to this dose will feel nothing, and clinical tests will not show any symptoms of illness or injury. Depending on the person, a clinical test may show changes in the blood. A dose of 4–5 Sv (400–500 rem) is indicated as LD-50, meaning that it is lethal to about 50 percent of the persons so exposed (death will occur in months). A dose of 10 Sv (1000 rem) or more to the whole body is considered lethal (death will occur in days), no matter what treatment may be applied. In the range of about 1–10 Sv (100–1000 rem), symptoms that may appear are nausea, vomiting, fever, diarrhea, loss of hair, inability of the body to fight infection, etc. These symptoms have been observed in victims of accidents and in patients undergoing radiation treatment.

The incidence of stochastic effects can only be treated in a probabilistic manner. Consider cancer first. In the United States the normal incidence of cancer (not necessarily fatal) in the adult population is 25 percent. The estimate for radiation-induced cancer is[9,10] $(1.5–4.5) \times 10^{-2}$ per manSv [$(1.5–4.5) \times 10^{-4}$ per manrem]. To understand this estimate better, consider an example. In a group of 10,000 adult Americans, about 2500 cases of cancer will be detected (not necessarily fatal). If this group of 10,000 persons receives 0.01 Sv (1 rem) of radiation collectively, the estimated number of cancers due to this radiation dose is 1.5–4.5. Therefore, the total number of cancers expected to be detected will be between 2501.5 and 2504.5. The incidence of fatal cancer in the United States is 16.4 percent. The risk of deadly cancer from radiation is estimated to be $(0.7–2.26) \times 10^{-2}$ per manSv [$(0.7–2.26) \times 10^{-4}$ per manrem].

Genetic effects are those related to the transmission of harmful hereditary information from one generation to the next. It is known today that the carriers of the hereditary code are the genes, which are parts of DNA molecules and are contained in the chromosomes. The gene is an extremely stable entity. Its structure is transmitted from generation to generation without any changes, which means that it transmits identical information from generation to generation. But sometimes a gene may change and become a *mutation*. The mutated gene may be transmitted through many generations without any further change, or it may change again to its original form or to a new third form. It is generally believed by geneticists that most mutations are harmful; therefore, conditions that increase the rate of mutations should be avoided.

The current incidence of human genetic disorders is 107,000 per $10^6$ births, or about 0.11 per birth. These effects constitute the so-called spontaneous

mutation rate. The genetic risk from radiation is expressed in terms of the ratio

$$\frac{m_r}{m_s} = \frac{\text{(radiation-induced mutations)}}{\text{(spontaneous mutations)}}$$

This ratio is equal to (2–0.4)/Sv [(0.02–0.004)/rem]. One quantity that is always reported along with this risk is the "doubling dose," i.e., the dose that if inflicted to a population over many generations will eventually result in doubling the rate of spontaneous mutations. From the ratio given above, the doubling dose is 0.5–2.5 Sv (50–250 rem).

Is radiation the only agent that causes mutations? Definitely not. Known mutagenic agents include certain chemicals, certain drugs, elevated temperature, and ionizing radiation. It is quite possible that many other mutagenic substances or environments may exist but are still unknown. Humans have been exposed to ionizing radiation since first appearing on this planet. The level of this background radiation is not constant at every point on the surface of the earth, but at sea level it is about 1.5–3 mSv/y (150–300 mrem/y). Every individual receives this exposure every year of his life. There is no doubt that genetic effects have been caused as a result of this exposure. Yet it should be pointed out that (a) there is no proof that radiation causes *only* detrimental genetic effects, and (b) despite the continuous exposure during thousands of years, there is no evidence of genetic deterioration of the human race.

## 16.8 RADIATION PROTECTION GUIDES AND EXPOSURE LIMITS

All regulations relevant to the protection of humans can be found in Title 10, Chapter 1, Part 20 *Code of Federal Regulations* (10CFR20). The 10CFR20 that is in force today,[4] which became effective January 1, 1994, is based on the recommendations of the International Commission on Radiological Protection (ICRP),[2] published in 1977 as ICRP Publication 26. The general principles upon which the new 10CFR20 radiation protection guides have been established are as follows.

1. No person should be exposed to any man-made radiation unless some benefit is derived from the exposure.
2. Radiation exposure limits are set at such levels that nonstochastic biological effects do not occur.
3. Radiation exposure limits are set at such levels that stochastic effects are minimized and become acceptable in view of the benefits derived from the exposure.
4. In every activity that may involve radiation exposure, it is not enough to keep exposure limits below the maximum allowed. Instead, every effort should be made to keep the exposure as low as reasonably achievable (ALARA).

The ALARA principle is strictly enforced by the U. S. Nuclear Regulatory Commission (NRC).

Since nonstochastic effects have a threshold, all that is needed to satisfy requirement 2 is to set the exposure limits below that threshold. For nonstochastic effects, the maximum allowed dose is set at 0.5 Sv (50 rem) for any tissue, except for the lens of the eye, for which the limit is set at 0.15 Sv (15 rem). For stochastic effects the limits are set at an acceptable level of risk. Ideally, the limit should be zero, since any exposure is supposed to increase the probability for stochastic effects to occur. Obviously, a zero limit is not practical. For stochastic effects the 10CFR20 sets the limiting exposure on the basis that the risk should be equal regardless of whether the whole body is irradiated uniformly or different tissues receive different doses. Recognizing the fact that different tissues have different sensitivities and, therefore, the proportionality constant between dose and effect is not the same for all tissues, the limit is expressed in terms of the "effective dose equivalent" ($H_E$), defined as

$$H_E = \sum_T w_T H_T \tag{16.31}$$

where $H_T$ is the dose equivalent to tissue or organ $T$ and $w_T$ is a weighting factor for tissue $T$. The values of $w_T$ are presented in Table 16.8.

The interpretation of the weighting factors is as follows. Consider the factor $w_T = 0.25$ for the gonads. This means that irradiation of the gonads alone would present about one-fourth the risk for stochastic effects expected to appear after uniform irradiation of the whole body at the same dose level. The risk per Sv due to irradiation of the gonads is derived from

$$\begin{aligned}(\text{Risk/Sv-gonads}) &= (\text{Risk/Sv-whole body})w_T \\ &= 1.65 \times 10^{-2}(0.25) = 4.1 \times 10^{-3}\end{aligned}$$

(or 1 in 250). Table 16.9 presents various maximum exposure limits. For

**Table 16.8 Organ Dose Weighting Factors**

| Organ or tissue | $w_T$ | Risk coefficient (Sv) | Probability (Sv) |
|---|---|---|---|
| Gonads | 0.25 | $4.14 \times 10^{-3}$ | 1 in 250 |
| Breast | 0.15 | $2.5 \times 10^{-3}$ | 1 in 400 |
| Red bone marrow | 0.12 | $2 \times 10^{-3}$ | 1 in 500 |
| Lung | 0.12 | $2 \times 10^{-3}$ | 1 in 500 |
| Thyroid | 0.03 | $5 \times 10^{-4}$ | 1 in 2000 |
| Bone surface | 0.03 | $5 \times 10^{-4}$ | 1 in 2000 |
| Remainder† | 0.30 | $5 \times 10^{-3}$ | 1 in 200 |
| Total (whole body) | 1.0 | $1.65 \times 10^{-2}$ | 1 in 60 |

†The remainder is 0.06 for each of five remaining organs, excluding the skin and the lens of the eye, which receive the highest doses.

**Table 16.9 Various Maximum Exposure Limits**

| | Old 10CFR20 | 10CFR20 effective Jan. 1, 1994 | ICRP 60 (1990) |
|---|---|---|---|
| Whole body | 5 rem/yr | 50 mSv/yr (stochastic) (5 rem/yr) 500 mSv/yr (nonstochastic) (50 rem/yr) | 20 mSv/yr, averaged over 5 yr, less than 50 mSv in any single year |
| Lens of eye | 1.25/quarter, 5.0 rem/yr | 15 mSv/yr (15 rem) | 15 mSv/yr |
| Extremities | 18.75 rem/ quarter, 75 rem/yr | 500 mSv/yr (50 rem/yr) | 500 mSv/yr |
| Thyroid-skin | 7.5 rem/ quarter, 30 rem/yr | 50 mSv/yr (stochastic) (5 rem/yr) 500 mSv/yr (nonstochastic) (50 rem/yr) | — |
| Lifetime dose | less than 5(N-18) | — | — |
| Dose to minors | | 10 percent of adult limit | 10 percent of adult limit |
| Public | 0.5 rem/yr | 1 mSv/yr (100 mrem) | 1 mSv/yr |
| Dose to fetus | — | 5 mSv (500 mrem) | 2 mSv (200 mrem) |
| ALARA program | recommended | required | required |

comparison, limits of the old 10CFR20 are given as well as limits recommended by the ICRP in 1990.[11] Judging from past experience, it is likely that the 1990 ICRP recommendations will be adopted in the not too distant future.

For the dose from radioisotopes inhaled or ingested by the body, several other doses have been defined, as follows.

*Committed dose equivalent* ($H_{50,T}$): the dose equivalent to organs or tissues that will be received from an intake of radioactive material by an individual, during a 50-year period following the intake.

*Committed effective dose equivalent* ($H_{E,50}$): the sum, over all relevant tissues or organs, of the product of the factor $w_T$ times the corresponding committed dose equivalent:

$$H_{E,50} = \sum_T w_T H_{50,T} \tag{16.32}$$

*Deep dose equivalent*: It applies to external whole body exposure and is the dose equivalent at a depth of tissue of 1 cm (1000 mg/cm$^2$).

*Total effective dose equivalent* (TEDE): the sum of the deep dose equivalent (for external exposure) and the committed effective dose equivalent (for internal exposure)

$$\text{TEDE} = H_d + H_{E,50} \tag{16.33}$$

The annual limit for radiation workers is the more limiting of the following two: a) TEDE being equal to 50 mSv (5 rem); or b) the sum of the deep dose equivalent and the committed dose equivalent to any individual organ or tissue other than the lens of the eye being equal to 0.5 Sv (50 rem).

*Annual limit of intake* (ALI): the amount of a radioactive material taken into the body of an adult worker in one year, by inhalation or ingestion, that would result in an effective committed dose equivalent of 0.05 Sv (5 rem) or a committed dose equivalent of 0.5 Sv (50 rem) to any single tissue or organ.

*Derived air concentration* (DAC): the concentration for a given radioisotope is that concentration in air that, if breathed by an adult for a working year of 2000 hours under conditions of light activity (inhalation rate $2.0E^4$ mL/min), would result in total intake of 1 ALI. Values of ALI and DAC for several radioisotopes are given in App. B of 10CFR20.[4]

For radon (Rn) and its daughters the radiation limits are given in terms of the working level (WL) and working level month (WLM), where 1 WL is the amount, in 1 $l$ of air, of any combination of Rn and its daughters that results in the release of $1.3 \times 10^5$ MeV of alpha-particle energy. This number is approximately the energy released by the short-lived daughters in equilibrium with 100 pCi and Rn. One WLM is equal to exposure to 1 WL for 170 h (170 = 2000/12). As an example, if a worker is exposed to 1 WL for 50 h, the exposure is $(50/170) \times 1 = 0.294$ WLM.

In addition to exposure from man-made radiation, humans are exposed to natural radiation. The components of the natural or background radiation are shown in Table 16.10.

## 16.9 HEALTH PHYSICS INSTRUMENTS

A health physics instrument is a device that can provide information about the dose rate or dose at the location where the instrument is placed. Health physics instruments are detectors like those discussed in Chaps. 5–7. They have to

**Table 16.10 Sources of Background Radiation in the United States**

| | | | Bone | | |
|---|---|---|---|---|---|
| Source | Gonads | Lung | Surface | Marrow | GI tract |
| Cosmic radiation[+] | 28 | 28 | 28 | 28 | 28 |
| Cosmogenic nuclides | 0.7 | 0.7 | 0.8 | 0.7 | 0.7 |
| External terrestrial | 26 | 26 | 26 | 26 | 26 |
| Inhaled nuclides | — | 100–450 | — | — | — |
| Radionuclides in body[‡] | 27 | 24 | 60 | 24 | 24 |
| Total (rounded) | 80 | 180–350 | 115 | 80 | 80 |

All values are in units of mrem/yr.

[+]The cosmic-ray component is given at sea level; it increases with altitude.

[‡]Radionuclides in the body are, primarily, $^{14}C$ and $^{40}K$.

satisfy some unique requirements, however, because their purpose is to measure dose equivalent, which is the absorbed dose in tissue times a quality factor. Radiation detectors provide a signal that, in general, depends on the energy deposited in the material of which the detector is made; that material does not necessarily have the same response as tissue to the radiation field being investigated. Even if the detector material responds to the radiation exactly like tissue, the problem still exists of getting dose equivalent from absorbed dose (which the detector signal provides). Thus, the dose measurement involves three steps.

1. Measurement of energy deposition in the detector (a quantity proportional to $D$ in the detector material)
2. Determination of $D_{\text{tissue}}$ by comparing the response to the incident radiation of tissue versus the response of the material of which the detector is made
3. Computation of dose equivalent $H$, from $D_{\text{tissue}}$ by incorporating the appropriate quality factor

In practice, the instruments are properly calibrated to read directly Sv (or rem), or Gy (or rad). For some neutron detection instruments, the neutron flux is recorded. Then the dose equivalent is obtained after multiplying the flux by the conversion factor given in Table 16.4. Since different detectors do not have the same efficiency or sensitivity for all types of radiation and for all energies, there is no single instrument that can be used for all particles ($\alpha$, $\beta$, $\gamma$, $n$) and all energies.

Health physics instruments are divided into two general groups according to the way they are used:

1. Survey instruments—portable and nonportable
2. Personnel monitoring instruments (dosimeters)

The rest of this section discusses the most commonly used devices. Survey instruments are described in Sec. 16.9.1. Dosimeters are described in Secs. 16.9.2–16.9.8.

### 16.9.1 Survey Instruments

The portable survey instruments are detectors like those described in detail in Chaps. 5–7. The most commonly used are GM counters and the so-called "cutie pie" meter. Many commercial GM counters offer a fixed thin window that will allow betas and photons to traverse it and be counted, and one or more movable windows that will stop the betas and allow only the gammas to enter the counter. In a mixed $\beta$-$\gamma$ field, such an instrument will provide information for $\beta$ and $\gamma$ separately. The cutie pie is an ionization counter that can be used to detect X-rays, alphas, and some high-energy betas.

The nonportable instruments are set at fixed locations to detect the radiation field; they are usually equipped with an alarm that will provide an audio and/or visual signal when the field intensity exceeds a preset limit. Examples are continuous air monitors and personnel monitors (e.g., hand, foot, and whole body). A list of several health physics instruments and their characteristics is given in Table 16.11.

### 16.9.2 Thermoluminescent Dosimeters

Thermoluminescent dosimeters (TLDs) are based on the property of thermoluminescence, which can be understood if one refers to the electronic energy-band diagram of crystals (see also Chap. 7). When ionizing radiation bombards a crystal, the energy given to the electrons may bring about several results (Fig. 16.6). The electron may acquire enough energy to move from the valence to the conduction band, in which case the event is called ionization. Or the electron acquires enough energy to move to an excited state (to the exciton band) and form an exciton. An exciton, consisting of an electron and a hole bound electrostatically, can migrate through the crystal. Electrons, holes, and excitons may be caught in many "traps" that exist in the solid. Traps are formed in a variety of ways. Foreign atoms (impurities), interstitial atoms, dislocations, vacancies, and imperfections may act as traps. The trapped carriers remain in place for long periods of time if the temperature of the crystal stays constant or decreases. If the temperature is raised, however, the probability of escape increases. As electrons and holes are freed and return to the ground state, they emit light (Fig. 16.7). The emission of this light is called thermoluminescence and is the property upon which the operation of TLDs is based.

A TLD is essentially a piece of a thermoluminescent material, exposed to the radiation being measured. After irradiation stops, the TLD is heated under controlled conditions (Fig. 16.8), and the light intensity is measured either as a function of temperature or as a function of the time during which the temperature is raised. The result of such a measurement is a graph called the *glow curve* (Fig. 16.9). Glow curves have more than one peak, corresponding to traps at various energy levels. The amplitudes of the peaks are proportional to the number of carriers trapped in the corresponding energy traps. The absorbed dose may be measured either from the total light emitted by the glow curve or from the height of one or more peaks of the glow curve. The TLD is annealed—i.e., it returns to its original condition—and is ready to be used again after being heated long enough that all the traps have been emptied; then it is left to cool down to room temperature. Measurement of the light from the glow curve, and subsequent annealing, are performed by instruments generally called *readers*, which are available commercially (e.g., from Harshaw Co.).

There are many thermoluminescent materials, but those useful for dosimetry should have the following characteristics.

1. Retention of trapped carriers for long periods of time at temperatures encountered during the exposure

**Table 16.11 A List of Common Health Physics Instruments**

| Instrument | Detector | Radiation detected | Range (nominal) | Remarks |
|---|---|---|---|---|
| | | Portable | | |
| Film badge | Photographic emulsions | $\gamma, \beta, n_f, n_{th}$ | 0.1–1,000 rad of mixed radiations | Measurement of integrated dose |
| Pocket chamber (direct reading) | Ionization chamber (air) | $\gamma$ | 5–200 mR; available with higher ranges | Visual check on gamma exposure |
| Personnel radiation monitor | G-M tube | $\gamma$, X-ray, high-level $\beta$ | Maximum audible warning at $\sim$ 0.5 R/h | Audible warning of radiation field |
| Cutie-pie survey meter | Ionization chamber (air) | $\gamma$, X-ray, high-energy $\beta$ | 5–10,000 mrad/h | Dose-rate meter for $\gamma$ and X-rays (0.008–2 MeV within 10 percent) |
| PIC-6 | Proportional gas-filled counter | $\gamma$ | 1 mR/h to 1000 R/h | Measures $\gamma$ dose rate |
| PAC-4G | Proportional gas-filled counter | $\alpha$ | | |
| Rem ball | Bonner sphere with $BF_3$ or LiI as the detector | $n$ | | Measures neutron dose equivalent |
| | | Nonportable | | |
| Continuous $\beta$–$\gamma$ particulate air monitor | GM tube (shielded) | $\beta, \gamma$ | 0–5,000 cpm | Light and audible alarms for preset levels |
| Continuous $\alpha$ particulate air monitor | ZnS(Ag) for $\alpha$ | $\alpha, \beta$ | 0–1,000 cpm | Light and audible alarms for preset levels |
| Hand and foot monitor | Halogen-quenched GM tube | $\beta, \gamma$ | Low-level | Simultaneous detection of $\beta$ and $\gamma$ contamination of hands and shoes |

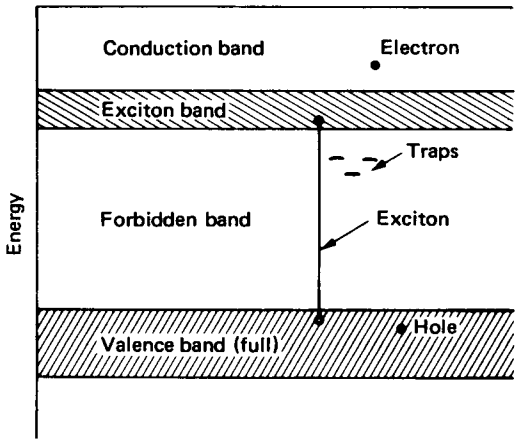


**Figure 16.6** Energy-band diagram of a crystal.

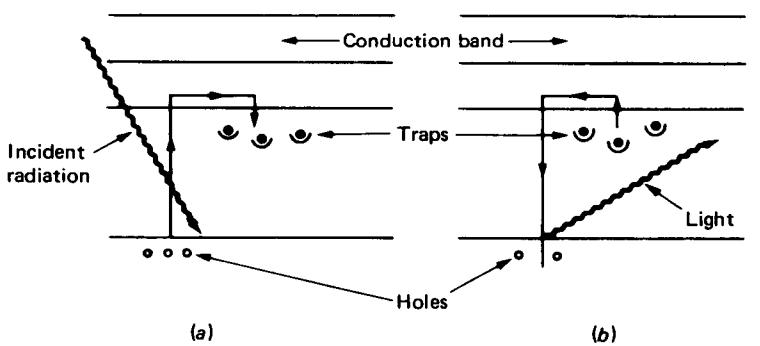


**Figure 16.7** (*a*) As a result of irradiation, some carriers fall into traps. (*b*) Upon heating, the carriers are given enough energy to escape from the traps and return to the valence band, with the emission of light.

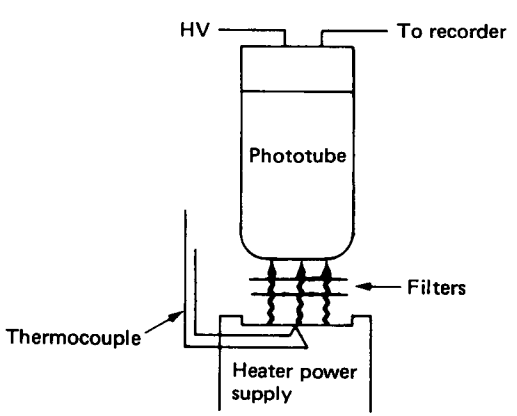


**Figure 16.8** A setup used to read a TLD.

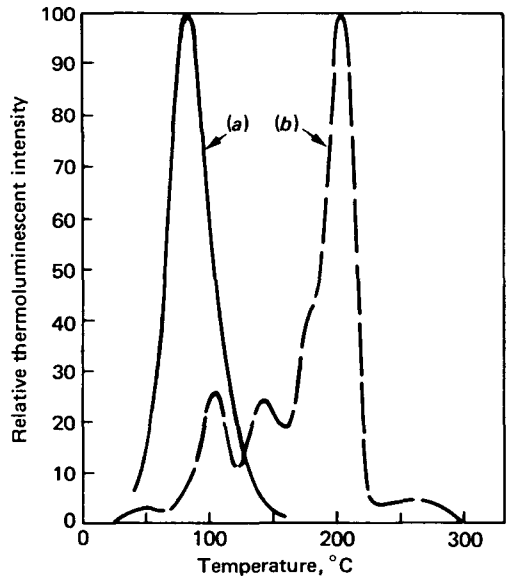


**Figure 16.9** Typical thermoluminescent glow curves. (*a*) Glow curve of $CaSO_4$: Mn heated at 6° C/min. (*b*) LiF (TLD-100) exposed to $10^4$ R and heated at 20° C/min (from Ref. 12).

2. Large amount of light output
3. Linear response over a large dose range
4. Perfect annealing to enable repetitive use

Materials commercially available that satisfy most of these requirements are $CaSO_4$: Mn, $CaF_2$ (natural), $CaF_2$: Mn, $Li_2B_4O_7$: Mn, and LiF. $CaSO_4$ and $CaF_2$ are used for gammas only. Other materials that have been studied are $CaSO_4$: Dy, BeO, and $Al_2O_3$. A commercial dosimetry package, based on a combination of $CaSO_4$ and $Li_2B_4O_7$, and known as Panasonic UD-802 or UD-854 is used in nuclear power plants. The main features of some of these materials are given in Table 16.12. Various uses are described in Refs. 13–19. The book by Shani (see

**Table 16.12 Properties of Certain TLDs†**

| Material | Radiation to which it responds | $Z_{eff}$ | Range |
|---|---|---|---|
| $CaSO_4$ (Mn) | $\gamma$ | 15.3 | $\mu$R–$10^3$ R |
| $CaF_2$ (Natural) | $\gamma$ | 16.3 | mR–$10^3$ R |
| $CaF_2$ (Mn) | $\gamma$, *n* (thermal, low response) | 16.3 | mR–$10^5$ R |
| LiF (TLD-100)‡ | $\gamma$, *n* (thermal), $\beta$ | 8.2 | mR–$10^4$ R |
| LiF (TLD-600) | $\gamma$, *n* (thermal), p | 8.2 | mR–$10^5$ R |
| LiF (TLD-700) | $\gamma$, $\alpha$ | 8.2 | mR–$10^5$ R |

†From Ref. 12.
‡TLD-100, TLD-600, TLD-700 are products of the Harshaw Chemical Company.

bibliography) gives many details for the construction, use, and performance characteristics of all TLD materials studied.

The three LiF TLDs listed in Table 16.12 have found wide use for measurements in mixed neutron-gamma fields. The TLD-100 containing natural lithium (92.6 percent $^7$Li, 7.4 percent $^6$Li) responds to gamma and thermal neutrons. Thermal neutrons are detected through the $(n, \alpha)$ reaction with $^6$Li, which has a cross section equal to 950 b for thermal energies. If a TLD-100 is exposed to about $3 \times 10^{11}$ neutrons/m$^2$ (thermal), its light output is equivalent to that from 1 R of gamma radiation. The TLD-600, containing lithium enriched to 95.62 percent in $^6$Li, is extremely sensitive to thermal neutrons and also to gammas. The TLD-700, containing 99.993 percent $^7$Li, is sensitive to gammas only, because the neutron cross section for $^7$Li is very small (about 0.033 b for thermal neutrons). In a mixed neutron-gamma field, one can achieve $\gamma$–$n$ discrimination by exposing to the radiation a TLD-100 plus a TLD-700, or a TLD-600 plus a TLD-700. The difference in response between the two dosimeters of either pair gives the dose due to the neutrons only. A very sensitive LiF TLD has been reported by Nakajima et al.[19] It consists of LiF with three dopants: Mg, Cu, and P. Its sensitivity is supposed to be 23 times that of TLD-600.

### 16.9.3 Solid-State Track Recorders (SSTRs)

The technique of measuring the number of particles by observing their tracks in certain organic and inorganic materials has been used for the study of phenomena in such diverse fields as geology, archeology, astrophysics, nuclear physics, and dosimetry. The book by Fleischer et al. is an excellent review of materials used as SSTRs, of the theories for track formation, and of the techniques used for track etching. In the field of radiation measurements, SSTRs are used for fission rate measurements[20,21] and as alpha[22] and neutron dosimeters.[23–25]

The SSTR technique is based on the damage created in a solid along the path of a heavily ionizing particle such as an alpha particle or a fission fragment. The damage along the path, called a track, may become visible under an ordinary optical microscope after etching with suitable chemicals. The visible tracks are counted either by direct observation by a human or with the help of automated instruments.[26–28]

Many theories have been proposed for the production of tracks by ionizing particles in solids, but none explains all the phenomena involved for both organic and inorganic materials. The basic mechanisms of energy loss are known (see Chap. 4). A fast-moving charged particle loses energy by excitation and ionization. Ionization creates charge centers in any solid. The ejected electrons, also called $\delta$-rays, can produce further excitation and ionization. In organic materials, such as polymers, the deexcitation may break the long molecular chains and produce free radicals. As the ion slows down, it starts picking up electrons, and thus its charge decreases. Close to the end of its path, atomic rather than electronic collisions are the dominant mode of energy loss. The

result of atomic collisions is atom displacement and creation of a vacancy. Pictorially, the formation of the track in a crystal and a polymer is believed to be taking place as shown in Fig. 16.10.

The best means of observing the tracks is by etching the SSTR material with a chemical that preferentially attacks the damaged material and enlarges the original track. It is believed that the damaged region is preferentially attacked because it becomes more active chemically than the surrounding undamaged region. This is a result of the free energy associated with the disorders created along the trajectory of the particle. After etching, the track is enlarged because the chemical attacks the surface of the SSTR and the interior surface of the original track and creates a conical hole as shown in Fig. 16.11. Thus, tracks that originally intersected the surface will appear as circles or ellipses under the microscope. If the etching continues further, some tracks may be "etched away"; therefore the level of etching is important, especially in absolute measurements.

As dosimeters, the SSTRs are used for neutron dose measurements. The SSTR is formed by placing a uniform deposit of a fissionable isotope on a

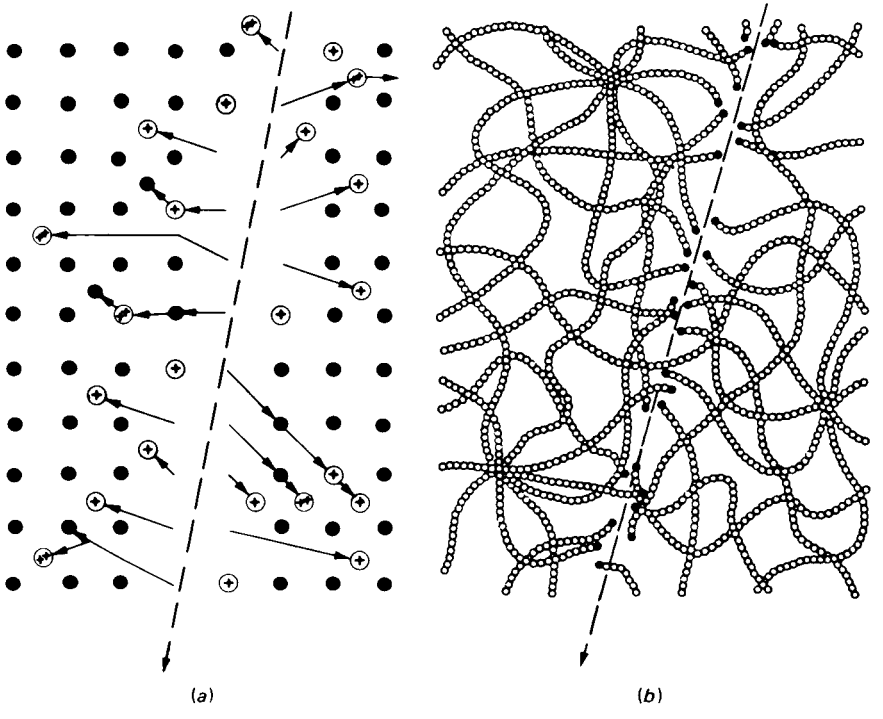


**Figure 16.10** The formation of a particle track in (*a*) a crystal and (*b*) a polymer (from Fleischer et al.).

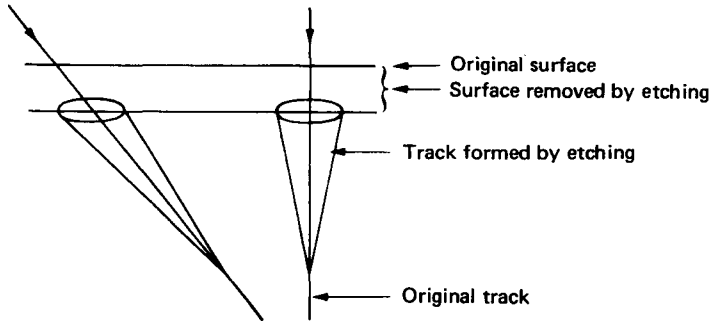


**Figure 16.11** Enlargement of a track by etching.

material such as mica or lexan.† When the SSTR is exposed to neutrons, fissions take place, and the fission fragments are imbedded into the SSTR material and produce the tracks. For absolute measurement of fission rate, the observer should be certain that all the fission fragments enter the SSTR and create visible tracks; or, if some fragments are lost, a correction should be applied to the observed fission rate. Some fission fragments will not escape no matter how thin the fissionable deposit is (Fig. 16.12). As Fig. 16.12 shows, a fission fragment emitted toward the SSTR will not reach it unless it is emitted within a cone defined by the angle $2\theta = 2\arccos(x/R)$, where $x$ is the depth at which the fission took place and $R$ is the range of that fragment. If $t < R$, where $t$ is the thickness of the deposit, the fraction of fragments reaching the SSTR is equal to $1 - t/2R$. If one places a second SSTR on the other side of the deposit, the fraction of escaping fission fragments is doubled. As the thickness $t$ decreases, a greater fraction of fragments escape, but at the same time a smaller number of fissions takes place and a smaller number of tracks is formed.

In addition to fission-fragment track measurements, thermal neutrons can also be detected by alpha tracks from $(n, \alpha)$ reactions with $^6$Li or $^{10}$B. Finally,

†Lexan is a polymer developed by General Electric, with atomic composition $C_{16}H_{14}O_3$.

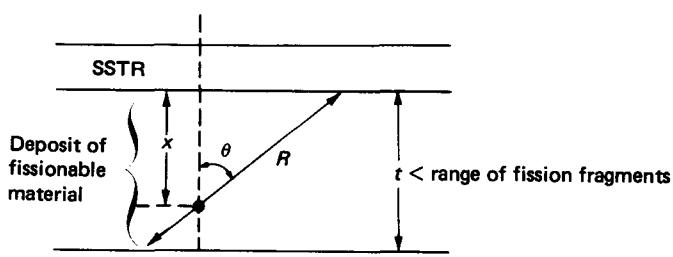


**Figure 16.12** A fission fragment emitted at an angle greater than $\theta$ ($\theta = \arccos x/R$) will not reach SSTR.

SSTRs have been used as monitors of alphas particles,[22] especially alphas emitted by radon and its daughters.

### 16.9.4 The Bonner Sphere (the Rem Ball)

The Bonner sphere,[29] named after one of the first people to study its features and use it, is a neutron detector. It consists of a polyethylene sphere, at the center of which a neutron detector is placed (LiI scintillator or $BF_3$ or $^3He$ counter). With any one of these materials, the neutrons are detected through the reactions

$$^6Li(n,\alpha)^3H \qquad ^{10}B(n,\alpha)^7Li \qquad ^3He(n,p)^3H$$

The polyethylene serves as the moderating material. The Bonner sphere has been found to be very useful for neutron dose measurements because the response of a 0.25- to 0.30-m (10–12 in) diameter sphere has an energy dependence very close to the dose equivalent delivered by neutrons (Figs. 16.13 and 16.14). The line indicated as RPG in these two figures is the dose rate $\dot{H}$ per unit neutron flux. The similarity between detector response and dose equivalent $H$ is just a coincidence. This coincidence is utilized, in practice, for the determination of neutron dose rate $\dot{H}$ in a neutron field of unknown energy. Note from Fig. 16.13 that the sensitivity (efficiency) of the Bonner sphere is high for high-energy neutrons (with high $Q$ value) and lower for low-energy neutrons (low $Q$ value). For this reason, the number of counts recorded by the sphere

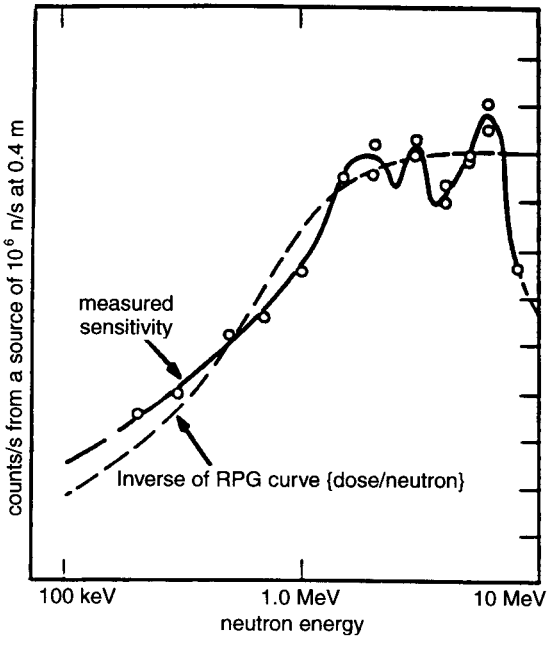


**Figure 16.13** Sensitivity of a 10-in (0.254 m) diameter Bonner sphere surrounding a 4 mm × 4 mm LiI scintillator. For comparison, the inverse of the response function RPG is also shown. The RPG gives dose rate, $\dot{H}$, per unit neutron flux (Ref. 30).

placed in an unknown spectrum $\phi(E)$ automatically includes a weighting factor for all energies.

The match between response and neutron dose rate is not perfect, as Fig. 16.14 clearly shows, particularly for energy less than 100 keV. If the unknown spectrum contains many neutrons in the energy range of discrepancy between the two curves, then the dose rate will be overestimated for the following reason. Consider $E = 10$ keV. The calculated response is about 1.7; the RPG is about 0.3. The inverse of RPG is about 3.3, which means that the detector will record 3.3 when the response ought to be close 1.7; hence, dose rate is overestimated. Another point to mention is the underresponse at $E > 10$ MeV (Fig. 16.13); luckily, this energy is not important for neutron fields encountered at nuclear power plants.

Another advantage of the Bonner sphere, in addition to its convenient response function, is its complete insensitivity to gammas. This is the result of relying for neutron detection on charged-particle reactions with high $Q$ value, thus making possible the complete rejection of pulses due to gammas with the use of a proper discriminator level.

In the nuclear industry the Bonner sphere is known as the rem ball or rem meter.

### 16.9.5 The Neutron Bubble Detector

The neutron bubble detector (trade name BD-100R) is a reusable, passive integrating dosimeter that allows instant, visible detection of neutron dose. The bubble detector consists of a glass tube filled with thousands of superheated liquid drops in a stabilizing matrix. When exposed to neutrons, these droplets vaporize, forming visible permanent bubbles in an elastic polymer. The total number of bubbles formed is proportional to the neutron dose equivalent $H$. The bubbles can be counted manually or by a machine. Figure 16.15 shows the response of the bubble detector as a function of neutron energy.

The bubble dosimeter is reusable; it is insensitive to gammas (the formation of the bubbles is based on the stopping power of the recoil nuclei produced by collisions with neutrons); it responds to a neutron energy range from 200 keV to

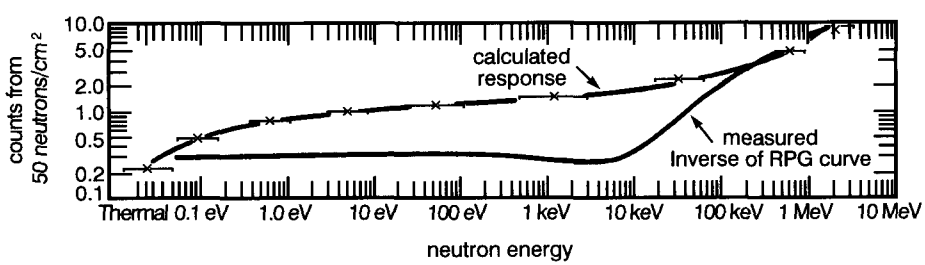


**Figure 16.14** Calculated sensitivity of a 10-in (0.254 m) diameter Bonner sphere compared with the measured response (Ref. 30).

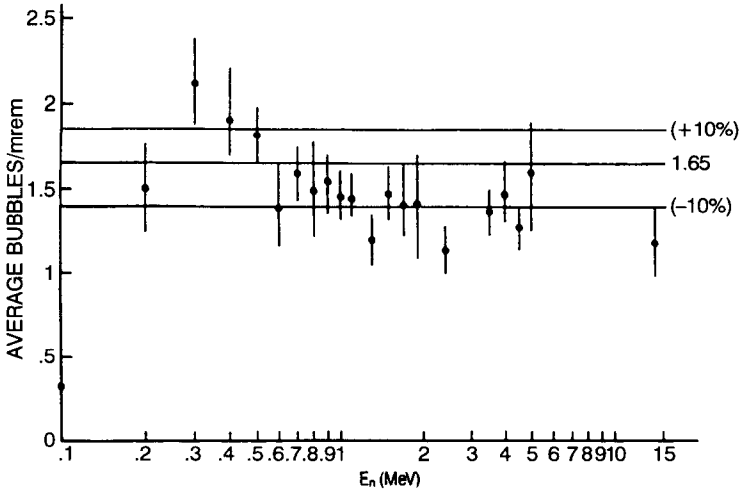


**Figure 16.15** The response of the neutron bubble dosimeter as a function of neutron energy (Siemens, 1993).

about 14 MeV. The dose range extends from less than 1 mrem to 1 rem; its useful life is 3 months, if recycled; its shelf life is 1 year.

### 16.9.6 The Electronic Personal Dosimeter

The electronic personal dosimeter (EPD) was developed by England's National Radiological Protection Board and is now marketed by Siemens.[31] The EPD, having the size and weight of a small pocket pager, uses the latest in integrated circuitry technology. It is a solid-state device based on silicon diodes. Complete details of the design are proprietary.

The objective of the EPD project was to produce a dosimeter that is accurate over a wide energy and dose range, rugged, and can communicate with a computer for data storage and subsequent analysis. All indications are that the EPD satisfies these requirements. It is small and rugged and the energy range is from 20 keV to 7 MeV for gammas and 250 keV to 1.5 MeV (average energy) for betas. In terms of dose, the dosimeter can display doses from 1 $\mu$Sv to 1 Sv (0.1 mrem to 100 rem) and dose rates from 1 $\mu$Sv/h to 10 Sv/h and is equipped with audible and visual alarms that can be set only by authorized persons.

The EPD uses infrared links to interface with a computer, thus providing the data to authorized persons who can read the dose received, add up previous exposures, and establish dose-alarm threshold settings. A custom lithium battery that lasts for a year powers the EPD. Each unit will be issued to a radiation worker for a full year.

### 16.9.7 Foil Activation Used for Neutron Dosimetry

Neutron dosimetry by foil activation is not used so much to record doses received by personnel as it is to record doses to materials, instruments, or other components that may suffer radiation damage as a result of neutron bombardment. The principle of this method was presented in Secs. 14.4 and 14.6. A target, in the form of a thin small foil, is exposed to the neutron field and becomes radioactive. The relationship between activity and neutron flux is

$$A(t) = N\sigma\phi(1 - e^{-\lambda t}) \tag{16.34}$$

where $N$ = number of targets
$\sigma$ = neutron absorption cross section
$\phi$ = neutron flux
$\lambda$ = decay constant of the radioisotope produced

After irradiation, the activity $A(t)$ is counted and the flux is determined from Eq. 16.34. Depending on the foil used (reaction involved), information about the neutron energy spectrum may also be obtained. Information about the neutron spectrum $\phi(E)$ is necessary for the determination of the neutron dose equivalent $H$.

## 16.10 PROPER USE OF RADIATION

Since radiation may be hazardous, it is important that individuals who handle ionizing radiation follow certain rules to avoid accidents. The official rules to be followed by all persons licensed to handle radioactive materials have been studied and proposed by such bodies as the ICRP and the National Research Council (NRC), which is an arm of the National Academy of Sciences. The proposed standards are adopted and enforced by federal agencies such as the U.S. NRC and the Environment Protection Agency (EPA). The NRC and EPA standards for protection against radiation are contained in *Code of Federal Regulations*.[32] The exposure limits, based on these guidelines, were discussed in Sec. 16.8.

To protect personnel, areas where radiation sources are used are marked with certain signs. The definitions of "radiation areas" and the corresponding signs are as follows.[4]

> "Restricted area" means any area access to which is controlled by the licensee for purposes of protection of individuals from exposure to radiation and radioactive materials. "Restricted area" shall not include any areas used as residential quarters, although a separate room or rooms in a residential building may be set apart as a restricted area.

> "Radiation area" means an area, accessible to individuals, in which radiation levels could result in an individual's receiving a dose equivalent in excess of 0.050 mSv (5 mrem) in 1 hour at 0.30 m from the radiation source or from any surface that the radiation penetrates.

> "High radiation area" means an area, accessible to individuals, in which radiation levels could result in an individual's receiving a dose equivalent in excess of 1 mSv (100 mrem) in 1 hour at 0.30 m from the radiation source or from any surface that the radiation penetrates.

Radiation areas should be marked with the radiation symbol shown in Fig. 16.16 and with cautionary signs. If necessary, the radiation area should be roped off or, if it is a room, should be locked to keep people out.

People who work in radiation areas or use radioisotopes should keep in mind the following simple principle:

> Radiation exposure should be avoided, if at all possible. If exposure is necessary, the risk from the exposure should be balanced against the expected benefit. The exposure is justified if the benefit outweighs the risk.

If exposure is justified, the employer and the employee should obey the ALARA principle (Sec. 16.8). Satisfying ALARA means not just keeping exposure below the maximum allowed limits; it means taking all possible "reasonably achievable" measures to minimize the dose received in any task that has to be performed. The best assurance against violating ALARA is constant education and training of the radiation workers. Given below are some commonsense rules that have proved helpful in reducing exposure.

1. Try to avoid internal exposure. Substances enter the body by mouth (eating, drinking), by breathing, through wounds, and by injection. Therefore, in places where radioactive materials are handled, do not eat, do not drink, and

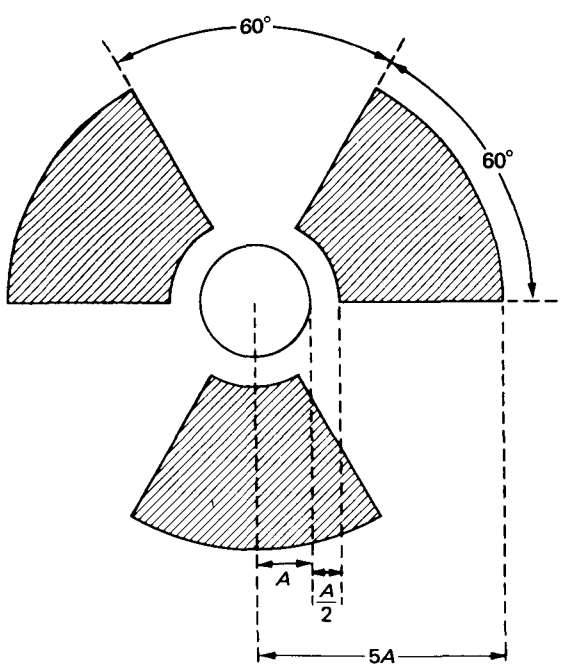


**Figure 16.16** The standard radiation symbol with dimensions as shown has a yellow background, with the hatched area being magenta or purple.

cover all wounds. If the air is contaminated, wear a mask. Hands should be washed after the operation is over, especially if no protective gloves were used.
2. Stay close to the source of radiation for as short a time interval as possible.
3. Use protective covers, if this is the suggestion of the health physicist.
4. Place the source behind a shield or in a proper container.
5. If practical, wait for the radiation to decay to a safer level before handling it. The exponential decay law is a helpful ally.
6. Stay as far away from the source as practical. The flux of a point isotropic source decreases as $1/r^2$ ($r$ = distance away from the source).

The shielding medium that should be used is not the same for all types of radiation. Here are simple suggestions for the three types of radiation considered in this book.

**Charged particles.** Charged particles have a definite range. Therefore, to stop them completely, a shielding material with thickness at least equal to the range (in that material) of the most penetrating particle should be placed between the source and the worker. A few millimeters of metal will definitely stop all charged particles emitted by radioisotopic sources. Some bremsstrahlung may get through, though.

**Gammas.** A beam of gammas going through a material of thickness $t$ is attenuated by a factor $\exp(-\mu t)$, where $\mu$ is the total linear attenuation coefficient of the gamma in that medium. The higher the value of $\mu$ is, the smaller the thickness $t$ that reduces the intensity of the beam by a desired factor. In theory, the beam cannot be attenuated to zero level. In practice, the attenuation is considered complete if the radiation level equals the background.

The attenuation coefficient $\mu$ increases with the atomic number of the material. The most useful practical element for gamma shielding is lead ($Z = 82$). Lead is relatively inexpensive, and it is easy to melt it and make shields with it having the desired shape, size, and thickness.

**Neutrons.** Shielding against neutrons is more difficult than shielding either against charged particles or photons. If the source emits fast neutrons, the first step is to provide a material that will thermalize the neutrons. Such materials are water, wax, or paraffin.

Thermalized neutrons are easily absorbed by many isotopes. Examples are $^{115}$In, $^{113}$Cd, and $^{10}$B. Of these, the most practical to use is boron. It can be used in powder form or be dissolved in water or liquid wax. A very simple but effective shield for a source of fast neutrons is 0.15–0.30 m of wax or paraffin to which boron has been added. The thickness of this borated material may change, depending on the strength of the source and the amount of boron

added. Cadmium is very useful in sheet form. A cadmium sheet 3–6 mm ($\frac{1}{8}$ – $\frac{1}{4}$ in) will stop a thermal neutron beam almost completely. Finally, shields have been manufactured that are flexible, like rubber, yet are excellent neutron attenuators.[33]

## PROBLEMS

**16.1** What is the total dose received by an individual standing in front of the open beam port of a research reactor for 10 s under the radiation levels listed in the figure below?

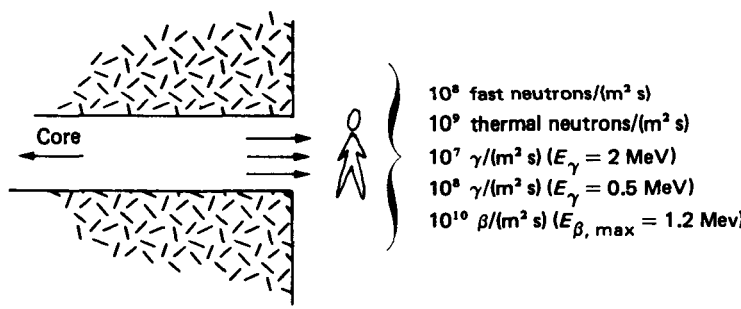


**16.2** What is the dose rate per curie of $^{24}$Na if it is shielded by 0.025 m of lead as shown below?

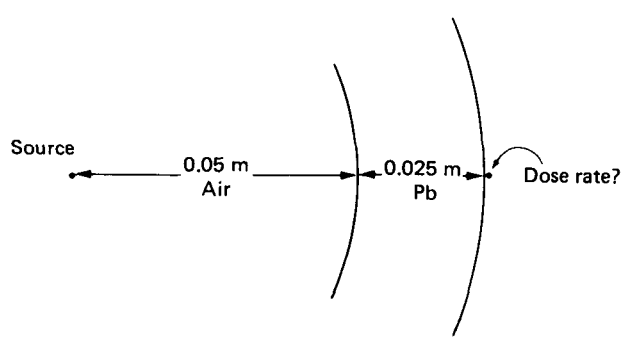


$^{24}$Na emits a 1.37-MeV gamma and a 2.75-MeV gamma 100 percent of the time, betas with $E_{max}$ = 4.17 MeV 0.003 percent of the time, and betas with $E_{max}$ = 1.389 MeV 100 percent of the time.

**16.3** As a result of carelessness, a worker inhaled 1 $\mu$g of $^{241}$Am. Considering alpha particles only and assuming that the americium is spread uniformly in the bones, (a) what is the dose rate at the time of the accident and (b) what is the total dose to that individual? For $^{241}$Am, $T_R$ = 433 years and $T_B$ = 200 years, mass of bones = 10 kg.

**16.4** What is the dose rate 0.30 m away from 1 Ci of $^{60}$Co if (a) the attenuating medium is air, and (b) if the source is shielded by 0.01 m of aluminum?

**16.5** What is the thickness of a lead container that will result in a dose rate at its surface of 2.5

mrem/h = $2.5 \times 10^{-5}$ Sv/h, if it is used to store 1 Ci of $^{124}$Sb? $^{124}$Sb emits the following gammas:

| Energy (MeV) | Intensity (%) | Energy (MeV) | Intensity (%) | Energy (MeV) | Intensity (%) |
|---|---|---|---|---|---|
| 0.603 | 97 | 0.967 | 2.4 | 1.37 | 5 |
| 0.644 | 7 | 1.048 | 2.4 | 1.45 | 2 |
| 0.720 | 14 | 1.31 | 3 | 1.692 | 50 |
| | | | | 2.089 | 7 |

**16.6** What is the dose rate due to the $^{124}$Sb of Prob. 16.5 at a distance equal to the thickness of the container, if the attenuating medium is air?

**16.7** A 1-Ci sample of $^{60}$Co is stored behind a concrete and lead shield as shown below. What is the dose rate at point $P$?

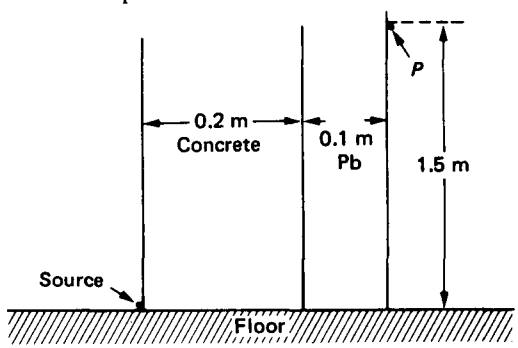


**16.8** The isotope $^{99m}$Tc is used *in vivo* for diagnostic purposes in humans. It emits X-rays with energy 140 keV and betas with $E_{max}$ = 0.119 MeV. If a person is injected with 1 $\mu$Ci of this isotope, what is the total dose to the brain, assuming that all the isotope is uniformly distributed there? (Mass of the brain = 1.5 kg.)

**16.9** If all the water in the human body were suddenly changed to $T_2O$($T = {}^3H$), what would be the total dose to that individual? Assume 61 percent of the body is water.

**16.10** If 1 pCi of $^{239}$Pu is inhaled by breathing and gets into the lungs, what is going to be the total dose to that individual? ($T_R$ = 24,000 years, $T_B$ = 200 years, mass of lungs = 1 kg.)

**16.11** Calculate the total dose rate at the center of a spherical submarine submerged in contaminated water with activity 1 Ci/m$^3$ of $^{137}$Cs. The submarine is made of steel 0.025 m thick. Its radius is 1.5 m and it is filled with air at 1 atm.

**16.12** What is the annual dose to a person due to the $^{40}$K found in every human body? The isotopic abundance of $^{40}$K in potassium is 0.0119 percent. The human body contains $1.7 \times 10^{-3}$ kg of potassium per kg. $^{40}$K emits the following radiations:

| Particle | Energy (MeV) | Intensity (%) |
|---|---|---|
| $\beta^-$ | 1.31 | 89 |
| $\beta^+$ | 0.49 | $10^{-3}$ |
| $\gamma$ | 1.46 | 11 |
| $\gamma$ | 0.511 | $2 \times 10^{-3}$ |

**16.13** A "hot particle" (a tiny speck of radioactive material) was lodged on the palm of a radiation worker, from where it was removed after 10 min of scrubbing. What is the estimated total dose

received by the tissue exposed to this radiation if it was determined that the radioactivity came from a beta emitter with $E_{max} = 1.7$ MeV, half-life equal to 2 days, and initial estimated activity equal to 1.3 mCi?

**16.14** Show that the doubling dose for radiation-induced mutations is between 0.5 and 2.5 Sv (50–250 rem) if the probability to induce a mutation by irradiation is 2–0.4 per Sv.

**16.15** Prove that the probability that a fission fragment will escape from one side of a fissile deposit is $\frac{1}{2}(1 - x/R)$, where $R$ is the average range of fission fragments and $x$ is the depth in the deposit where the fission took place.

**16.16** Prove that the total number of fission fragments escaping from one side of a fissile deposit of thickness $t$ ($t <$ range) is equal to $F(t - t^2/2R)$, where $F$ is the number of fissions per unit volume.

## BIBLIOGRAPHY


Attix, F. H., *Introduction to Radiological Physics and Radiation Dosimetry*, Wiley, 1986.

Attix, F. H., and Tochilin, E., (eds.), *Radiation Dosimetry* I, II, III, Academic, New York, 1969.

Cember, H., *Introduction to Health Physics*, Pergamon, 1969.

Fitzgerald, J. J., Brownell, G. L., and Mahoney, F. J., *Mathematical Theory of Radiation Dosimetry*, Gordon and Breach, 1967.

Fleischer, R. L., Price, P. B., and Walker, R. M., *Nuclear Tracks in Solids*, University of California Press, Berkeley, Calif., 1975.

Hine, G. J., and Brownell, G., *Radiation Dosimetry*, Academic, New York, 1956.

Miller, K. L., *Handbook of Management of Radiation Protection Programs*, 2nd ed., CRC Press, Boca Raton, Fla., 1992.

Morgan, K. Z., and Turner, J. E., (eds.), *Principles of Radiation Protection*, Wiley, 1967.

Prasad, K. N., *Handbook of Radiobiology*, CRC Press, Boca Raton, Fla., 1984.

Shani, G., *Radiation Dosimetry Instrumentation and Methods*, CRC Press, Boca Raton, Fla., 1991.


## REFERENCES


1. Dose Equivalent ICRU Report 19 (suppl.), Washington, D.C. (1973).
2. *1977 Recommendations of the International Commission on Radiological Protection* (ICRP Publication 26), Pergamon, 1977.
3. Report of the RBE Committee to ICRU, *Health Phys.* **9**:357 (1963).
4. Standards for Protection against Radiation, *Code of Federal Regulations*, Title 10, Part 20, Dec. 1992, chap. 1.
5. *Engineering Compendium on Radiation Shielding*, vol. 1: *Shielding Fundamentals and Methods*, Springer-Verlag, 1968.
6. Stamatelatos, M. G., and England, T. R., *Nuclear Sci. Eng.* **63**:204 (1977).
7. Neutron and Gamma-ray Flux-to-Dose Rate Factors, American National Standard, ANSI/ANS-6.1.1-1991.
8. Report of the ICRP Committee II on Permissible Dose for Internal Radiation (1959). *Health Phys.* **3**:146 (June 1960).
9. The Effects on Populations of Exposure to Low Levels of Ionizing Radiation: 1980 (the BEIR-III report), National Academy Press, Washington, D.C., 1980.
10. Health Effects of Exposure to Low Levels of Ionizing Radiation (the BEIR-V report), National Academy Press, Washington, D.C., 1990.
11. *1990 Recommendations of the International Commission on Radiological Protection* (ICRP Publication 60), Pergamon, 1991.
12. Dudley, R. A., in F. H. Attix and W. C. Roesch (eds.), *Radiation Dosimetry*, II, Academic Press, New York, 1966.

13. Charalambous, S., and Petridou, C., *Nucl. Instrum. Meth.* **137**:441 (1976).
14. Simons, G. G., and Emmons, L. L., *Nucl. Instrum. Meth.* **160**:79 (1979).
15. Ohno, A., and Matsuura, S., *Nucl. Tech. Meth.* **47**:485 (1980).
16. Bacci, C., Calicchia, A., Pugliani, L., Salvadori, P., and Furetta, C., *Health Phys.* **38**:21 (1980).
17. Vohra, K. G., Bhatt, R. C., Chandra, B., Pradhan, A. S., Lakshmanan, A. R., and Shastry, S. S., *Health Phys.* **38**:113 (1980).
18. Liu, N. H., Gilliam, J. D., and Anderson, D. W., *Health Phys.* **38**:359 (1980).
19. Nakajima, T., Murayama, Y., Matsuzawa, T., and Kayano, A., *Nucl. Instrum. Meth.* **157**:155 (1978).
20. Draper, E. L., Jr., *Nucl. Sci. Eng.* **46**:31 (1971).
21. Gilliam, D. M., Dudey, N. D., and Popek, R. J., *Nucl. Technol.* **25**:237 (1975).
22. Lovett, D. B., *Health Phys.* **16**:623 (1969).
23. Seitz, M. G., Walker, R. M., and Carpenter, B. S., *J. Appl. Phys.* **44**:510 (1973).
24. Gomaa, M. A., and Hamdan, M. A., *Nucl. Instrum. Meth.* **146**:527 (1977).
25. Aframian, A., *Nucl. Technol.* **42**:343 (1979).
26. Paretti, C., and Ricci, A., *Nucl. Instrum. Meth.* **122**:389 (1974).
27. Cohn, C. E., and Gold, R., *Rev. Sci. Instrum.* **43**:13 (1972).
28. Chou, H. P., Johnson, R. H., and Clikeman, F. M., *Proceedings Int. Conf. on Nucl. Cross Sections for Technol.*, Knoxville, Tenn., Oct. 1979.
29. Bonner, T. W., *Nucl. Phys.* **23**:116 (1961).
30. Hankins, D. E., LA-2717 (1962).
31. Marshall, T. O., Bartlett, D. T., Burgess, P. H., Cranston, D. J., Higginbottom, D. J., and Sutton, K. W., Occupational Radiation Exposure, BNES Paper 44, London (1991), p. 129.
32. Standards for Protection against Radiation, *Code of Federal Regulations*, Title 40, Part 190–192, Dec. 1992.
33. Reactor Experiments, Inc., Sunnyvale, Calif. (1990).

APPENDIX

# A

# USEFUL CONSTANTS AND CONVERSION FACTORS

**Table A1 Useful Constants**

| Constant | Symbol or definition | Value 0.6022169 |
|---|---|---|
| Avogadro's number | $N_A$ | $0.6022045 \times 10^{24}$ at/mol |
| Elementary charge | $e$ | $1.6021917 \times 10^{-19}$ C $= 4.803250 \times 10^{-10}$ esu |
| Atomic mass unit | u | $1.66040 \times 10^{-27}$ kg = 931.481 MeV |
| Atomic mass unit | $\frac{1}{12}$ of mass ${}^{12}_{6}C$ | |
| Electron rest mass | $m$ | $9.109558 \times 10^{-31}$ kg = 0.511 MeV |
| Proton rest mass | $M_p$ | $1.672622 \times 10^{-27}$ kg = 938.258 MeV |
| Neutron rest mass | $M_n$ | $1.674928 \times 10^{-27}$ kg = 939.552 MeV |
| Planck constant | $h$ | $6.626196 \times 10^{-34}$ J·s |
| Boltzmann constant | $k$ | $1.380622 \times 10^{-23}$ J/K |
| Standard atmosphere | | 101,325 Pa = 14.696 lb/in$^2$ |
| Fine-structure constant | $\alpha = e^2/(\hbar \cdot c)$ | 1/137.14 |
| Classical electron radius | $r_0 = e^2/(m \cdot c^2)$ | $2.818042 \times 10^{-15}$ m |
| Bohr radius | $\hbar^2/(m \cdot e^2)$ | $0.529177 \times 10^{-10}$ m |
| Compton wavelength | $h/(m \cdot c)$ | $2.424631 \times 10^{-12}$ m |

**Table A2 Conversion Table**

| To convert | Multiply by | To obtain (symbol) |
|---|---|---|
| MeV | $1.602 \times 10^{-13}$ | Joules (J) |
| Pounds (lb) | 0.4536 | Kilograms (kg) |
| Inches | $2.54 \times 10^{-2}$ | Meters (m) |
| Lb/in$^2$ | $6.8946 \times 10^3$ | Pascal (Pa) |
| Btu/h | 0.29307 | Watts (W) |
| Pounds force | 4.4482 | Newtons (N) |
| Flux [particles/(cm$^2$ s)] | $10^4$ | Flux (particles/m$^2$·s) |
| Density (g/cm$^3$) | $10^3$ | Density (kg/m$^3$) |
| $\mu$ (cm$^2$/g) | $10^{-1}$ | $\mu$ (m$^2$/kg) |
| $\mu$ (cm$^{-1}$) | 100 | $\mu$ (m$^{-1}$) |
| $\Sigma$ (cm$^{-1}$) | 100 | $\Sigma$ (m$^{-1}$) |
| Range (g/cm$^2$) | 10 | Range (kg/m$^2$) |
| Curies | $3.7 \times 10^{10}$ | Becquerels (Bq) |
| Rad | $10^{-2}$ | Grays (Gy) |
| Rem | $10^{-2}$ | Sieverts (Sv) |

**Table A3 Prefix and SI Symbols of Multiplication Factors**

| | |
|---|---|
| $10^{12}$ tera (T) | $10^{-6}$ micro ($\mu$) |
| $10^{9}$ giga (G) | $10^{-9}$ nano (n) |
| $10^{6}$ mega (M) | $10^{-12}$ pico (p) |
| $10^{3}$ kilo (k) | $10^{-15}$ femto (f) |
| $10^{-3}$ milli (m) | $10^{-18}$ atto (a) |

APPENDIX
# B

# ATOMIC MASSES AND OTHER PROPERTIES OF ISOTOPES

| Name | Symbol | $Z$ | $A$ | Isotopic mass (u)† | Natural abundance (%) | Density of element (in $10^3$ kg/m$^3$) | $\sigma_a$ (b) for $(n, \gamma)$ (0.0253-eV neutrons) |
|---|---|---|---|---|---|---|---|
| Aluminum | Al | 13 | 27 | 26.98153 | 100 | 2.7‡ | 0.235 |
| Antimony | Sb | 51 | 121 | 120.9038 | 57.25 | 6.62 | 5.9 |
| | | | 123 | 122.9041 | 42.75 | | 4.1 |
| Argon | Ar | 18 | 36 | 35.96755 | 0.337 | Gas | 6.0 |
| | | | 38 | 37.96272 | 0.063 | | 0.8 |
| | | | 40 | 39.96238 | 99.60 | | 0.61 |
| Arsenic | As | 33 | 75 | 74.9216 | 100 | 5.73 | 4.5 |
| Beryllium | Be | 4 | 9 | 9.01218 | 100 | 1.85 | 0.0095 |
| Bismuth | Bi | 83 | 209 | 208.9804 | 100 | 9.8 | 0.034 |
| Boron | B | 5 | 10 | 10.01294 | 19.78 | 2.3 | 3,837 |
| | | | 11 | 11.00931 | 80.22 | | 0.04 |
| Cadmium | Cd | 48 | 106 | 105.9070 | 1.22 | 8.65 | 2,450.0 |
| | | | 108 | 107.9040 | 0.88 | | 2.0 |
| | | | 110 | 109.9039 | 12.39 | | 0.1 |
| | | | 111 | 110.9042 | 12.75 | | – |
| | | | 112 | 111.9028 | 24.07 | | 0.03 |
| | | | 113 | 112.9046 | 12.26 | | 20,000.0 |
| | | | 114 | 113.9036 | 28.86 | | 0.14 |
| | | | 116 | 115.9050 | 7.58 | | 1.4 |
| Carbon | C | 6 | 12 | 12.0000 | 98.89 | 1.60 | 0.0034 |
| | | | 13 | 13.00335 | 1.11 | | 0.0009 |
| Cesium | Cs | 55 | 133 | 132.9051 | 100 | 1.9 | 29.0 |
| Cobalt | Co | 27 | 59 | 59.93344 | 100 | 8.8 | 37.2 |
| Copper | Cu | 29 | 63 | 62.9298 | 60.09 | 8.96 | 4.5 |
| | | | 65 | 64.9278 | 30.91 | | 2.2 |
| Gadolinium | Gd | 64 | 152 | 151.9195 | 0.20 | 7.95 | < 180 |
| | | | 154 | 153.9207 | 2.15 | | 100.0 |
| | | | 155 | 154.9226 | 14.73 | | 61,000.0 |
| | | | 156 | 155.9221 | 20.47 | | 11.5 |
| | | | 157 | 156.9339 | 15.68 | | 254,000.0 |
| | | | 158 | 157.9241 | 24.87 | | 3.5 |

| Name | Symbol | $Z$ | $A$ | Isotopic mass (u)† | Natural abundance (%) | Density of element (in $10^3$ kg/m$^3$) | $\sigma_a$ (b) for $(n, \gamma)$ (0.0253-eV neutrons) |
|---|---|---|---|---|---|---|---|
| Germanium | Ge | 32 | 70 | 69.9243 | 20.52 | 5.36 | 3.68 |
| | | | 72 | 71.9217 | 27.43 | | 0.98 |
| | | | 73 | 72.9234 | 7.76 | | 14.0 |
| | | | 74 | 73.9212 | 36.54 | | 0.45 |
| | | | 76 | 75.9214 | 7.76 | | 0.2 |
| Gold | Au | 79 | 197 | 196.9666 | 100 | 19.32 | 98.8 |
| Helium | He | 2 | 3 | 3.01603 | 0.00013 | Gas | 5,327.0 |
| | | | 4 | 4.00260 | 99.99987 | | – |
| Hydrogen | H | 1 | 1 | 1.007825 | 99.985 | Gas | 0.332 |
| | | | 2 | 2.01410 | 0.015 | | 0.0005 |
| Indium | In | 49 | 113 | 112.9043 | 4.28 | 7.31 | 11.1 |
| | | | 115 | 114.9041 | 95.72 | | 193.2 |
| Iodine | I | 53 | 127 | 126.9044 | 100 | 4.93 | 6.2 |
| Iron | Fe | 26 | 54 | 53.9396 | 5.82 | 7.87 | 2.3 |
| | | | 56 | 55.9349 | 91.66 | | 2.7 |
| | | | 57 | 56.9354 | 2.19 | | 2.5 |
| | | | 58 | 57.9333 | 0.33 | | 1.2 |
| Lead | Pb | 82 | 204 | 203.9730 | 1.48 | 11.34 | 0.17 |
| | | | 206 | 205.9745 | 23.6 | | 0.0305 |
| | | | 207 | 206.9759 | 22.6 | | 0.709 |
| | | | 208 | 207.9766 | 52.3 | | < 0.03 |
| Lithium | Li | 3 | 6 | 6.01512 | 7.42 | 0.53 | 245 $(n, \alpha)$ |
| | | | 7 | 7.01600 | 92.58 | | 0.037 |
| Mercury | Hg | 80 | 196 | 195.9650 | 0.146 | 13.55 | 3,100.0 |
| | | | 198 | 197.9668 | 10.02 | | 0.018 |
| | | | 199 | 198.9683 | 16.84 | | 2,500.0 |
| | | | 200 | 199.9683 | 23.13 | | 50.0 |
| | | | 201 | 200.9703 | 13.22 | | 50.0 |
| | | | 202 | 201.9706 | 29.80 | | 4.5 |
| | | | 204 | 203.9735 | 6.85 | | 0.4 |
| Nickel | Ni | 28 | 58 | 57.9353 | 67.88 | 8.90 | 4.4 |
| | | | 60 | 59.9308 | 26.23 | | 2.6 |
| | | | 61 | 60.9310 | 1.19 | | 2.0 |
| | | | 62 | 61.9283 | 3.66 | | 14.2 |
| | | | 64 | 63.9280 | 1.08 | | 1.5 |
| Nitrogen | N | 7 | 14 | 14.00307 | 99.63 | Gas | 1.81 |
| | | | 15 | 15.00011 | 0.37 | | 0.00004 |
| Oxygen | O | 8 | 16 | 15.99491 | 99.759 | Gas | 0.000178 |
| | | | 17 | 16.99914 | 0.037 | | 0.04 |
| | | | 18 | 17.99915 | 0.204 | | 0.00016 |
| Phosphorus | P | 15 | 31 | 30.97376 | 100 | 1.82 | 0.19 |
| Platinum | Pt | 78 | 190 | 189.9600 | 0.0127 | 21.45 | 150.0 |
| | | | 192 | 191.9614 | 0.78 | | 8.0 |
| | | | 194 | 193.9628 | 32.19 | | 1.2 |
| | | | 195 | 194.9648 | 33.8 | | 27.0 |
| | | | 196 | 195.9650 | 25.3 | | 1.0 |

| Name | Symbol | $Z$ | $A$ | Isotopic mass (u)† | Natural abundance (%) | Density of element (in $10^3$ kg/m$^3$) | $\sigma_a$ (b) for $(n, \gamma)$ (0.0253-eV neutrons) |
|---|---|---|---|---|---|---|---|
| | | | 198 | 197.9675 | 7.21 | | 4.0 |
| Rhodium | Rh | 45 | 103 | 102.9048 | 100 | 12.41 | 150.0 |
| Silicon | Si | 14 | 28 | 27.97693 | 92.21 | 2.33 | 0.080 |
| | | | 29 | 28.97649 | 4.70 | | 0.28 |
| | | | 30 | 29.97376 | 3.09 | | 0.40 |
| Silver | Ag | 47 | 107 | 106.9041 | 51.82 | 10.49 | 37.0 |
| | | | 109 | 108.9047 | 45.18 | | 92.0 |
| Sodium | Na | 11 | 23 | 22.98977 | 100 | 0.97 | 0.534 |
| Uranium | U | 92 | 234 | 234.0409 | 0.0057 | 19.1 | 95.0 |
| | | | 235 | 235.0439 | 0.710 | | 678.0 |
| | | | 238 | 238.0508 | 99.284 | | 2.73 |

†Isotopic masses from *Nuclear Heat Transfer* by M. M. El-Wakil, International Textbook Co., N.Y. (1971).

‡Same number gives density in g/cm$^3$ or $10^3$ kg/m$^3$.

APPENDIX
# C

# ALPHA, BETA, AND GAMMA SOURCES COMMONLY USED

**Table C1 Alpha Sources**

| Isotope | Half-life | Alpha energy (MeV) | Relative intensity† (%) |
|---|---|---|---|
| $^{210}$Po | 138.38 d | 5.304 | 100 |
| $^{234}$U | $2.446 \times 10^5$ y | 4.774 | 72 |
| | | 4.723 | 28 |
| $^{235}$U | $7.038 \times 10^8$ y | 4.397 | 57 |
| | | 4.367 | 18 |
| $^{238}$U | $4.468 \times 10^9$ y | 4.196 | 77 |
| | | 4.149 | 23 |
| $^{239}$Pu | $2.413 \times 10^4$ y | 5.155 | 73.3 |
| | | 5.143 | 15.1 |
| | | 5.105 | 11.5 |
| $^{241}$Am | 432.02 y | 5.486 | 86 |
| | | 5.443 | 12.7 |
| $^{252}$Cf | 2.646 y | 6.118 | 84 |
| | | 6.076 | 15.8 |

†Only intensities greater than 10 percent are listed.

**Table C2 Electron and Beta Sources**

| Isotope | Half-life | Type of particle | Energy (MeV) |
|---|---|---|---|
| $^{3}$H | 12.33 y | $\beta^-$ | 0.0186 |
| $^{14}$C | 5730 y | $\beta^-$ | 0.1565 |
| $^{32}$P | 14.28 d | $\beta^-$ | 1.7104 |
| $^{35}$S | 87.4 d | $\beta^-$ | 0.1675 |
| $^{36}$Cl | $3.0 \times 10^5$ y | $\beta^-$ | 0.7095 |
| $^{89}$Sr | 50.55 d | $\beta^-$ | 1.463 |
| $^{90}$Y | 64 h | $\beta^-$ | 2.282 |
| $^{99}$Tc | $2.14 \times 10^5$ y | $\beta^-$ | 0.292 |
| $^{63}$Ni | 100 y | $\beta^-$ | 0.0659 |
| $^{113}$Sn | 115.1 d | IC electron | $E_K = 0.3625$ |
| | | | $E_L = 0.3875$ |
| $^{137}$Cs† | 30.17 y | IC electron | $E_K = 0.626$ |
| | | | $E_L = 0.656$ |
| $^{207}$Bi | 38 y | IC electron | $E_K = 0.4816, 0.5558$ |
| | | | $E_L = 0.9754, 1.0496$ |
| | | | $E_M = 1.060$ |

†$^{137}$Cs is also a $\beta^-$ emitter.

## Table C3 Gamma Rays Used as Reference Standards for Energy Calibration†

| Parent nuclide | Gamma-ray energy (keV) | Parent nuclide | Gamma-ray energy (keV) | Parent nuclide | Gamma-ray energy (keV) | Parent nuclide | Gamma-ray energy (keV) |
|---|---|---|---|---|---|---|---|
| $^{183}$Ta | 52.596 ± 0.001 | $^{183}$Ta | 264.072 ± 0.006 | $^{94}$Nb | 702.627 ± 0.019 | $^{56}$Co | 1238.256 ± 0.027 |
| $^{241}$Am | 59.537 ± 0.001 | $^{75}$Se | 264.651 ± 0.008 | $^{110m}$Ag | 706.669 ± 0.020 | $^{182}$Ta | 1257.390 ± 0.028 |
| $^{75}$Se | 66.055 ± 0.009 | $^{133}$Ba | 276.397 ± 0.012 | $^{124}$Sb | 713.761 ± 0.018 | $^{160}$Tb | 1271.850 ± 0.026 |
| $^{182}$Ta | 67.750 ± 0.001 | $^{203}$Hg | 279.188 ± 0.006 | $^{185}$Os | 717.424 ± 0.018 | $^{182}$Ta | 1273.703 ± 0.028 |
| $^{153}$Gd | 69.676 ± 0.002 | $^{203}$Pb | 279.188 ± 0.006 | $^{124}$Sb | 722.767 ± 0.018 | $^{22}$Na | 1274.511 ± 0.028 |
| $^{133}$Ba | 80.998 ± 0.008 | $^{75}$Se | 279.528 ± 0.008 | $^{95}$Zr-$^{95}$Nb | 724.184 ± 0.018 | $^{182}$Ta | 1289.126 ± 0.029 |
| $^{183}$Ta | 82.919 ± 0.001 | $^{183}$Ta | 291.724 ± 0.006 | $^{110m}$Ag | 744.254 ± 0.020 | $^{58}$Fe | 1291.564 ± 0.028 |
| $^{170}$Tm | 84.254 ± 0.003 | $^{192}$Ir | 295.949 ± 0.006 | $^{95}$Zr-$^{95}$Nb | 756.715 ± 0.019 | $^{82}$Br | 1317.440 ± 0.027 |
| $^{182}$Ta | 84.680 ± 0.002 | $^{160}$Tb | 298.572 ± 0.006 | $^{110m}$Ag | 763.928 ± 0.019 | $^{132}$Cs | 1317.890 ± 0.028 |
| $^{183}$Ta | 84.712 ± 0.002 | $^{133}$Ba | 302.851 ± 0.015 | $^{95}$Zr-$^{95}$Nb | 765.786 ± 0.019 | $^{124}$Sb | 1325.478 ± 0.029 |
| $^{160}$Tb | 86.786 ± 0.002 | $^{75}$Se | 303.913 ± 0.007 | $^{82}$Br | 776.502 ± 0.016 | $^{60}$Co | 1332.464 ± 0.028 |
| $^{109}$Cd | 88.037 ± 0.005 | $^{192}$Ir | 308.445 ± 0.007 | $^{95m}$Tc | 786.184 ± 0.017 | $^{56}$Co | 1360.175 ± 0.029 |
| $^{160}$Tb | 93.917 ± 0.006 | $^{192}$Ir | 316.497 ± 0.007 | $^{58}$Co | 810.757 ± 0.021 | $^{124}$Sb | 1368.130 ± 0.029 |
| $^{75}$Se | 96.733 ± 0.002 | $^{51}$Cr | 320.078 ± 0.008 | $^{110m}$Ag | 818.018 ± 0.022 | $^{24}$Na | 1368.599 ± 0.029 |
| $^{153}$Gd | 97.432 ± 0.003 | $^{183}$Ta | 353.999 ± 0.004 | $^{95m}$Tc | 820.608 ± 0.019 | $^{182}$Ta | 1373.807 ± 0.030 |
| $^{183}$Ta | 99.080 ± 0.002 | $^{133}$Ba | 356.005 ± 0.017 | $^{82}$Br | 827.809 ± 0.019 | $^{110m}$Ag | 1384.267 ± 0.029 |
| $^{182}$Ta | 100.105 ± 0.001 | $^{183}$Ta | 365.615 ± 0.007 | $^{54}$Mn | 834.827 ± 0.021 | $^{182}$Ta | 1387.376 ± 0.030 |
| $^{153}$Gd | 103.180 ± 0.002 | $^{133}$Ba | 383.851 ± 0.020 | $^{95m}$Tc | 835.132 ± 0.018 | $^{82}$Br | 1474.853 ± 0.030 |
| $^{183}$Ta | 107.932 ± 0.002 | $^{113}$Sn | 391.688 ± 0.010 | $^{56}$Co | 846.751 ± 0.019 | $^{110m}$Ag | 1475.757 ± 0.034 |
| $^{177}$Lu | 112.954 ± 0.003 | $^{75}$Se | 400.646 ± 0.009 | $^{58}$Co | 863.935 ± 0.018 | $^{144}$Ce | 1489.124 ± 0.032 |
| $^{182}$Ta | 113.673 ± 0.002 | $^{203}$Pb | 401.315 ± 0.013 | $^{94}$Nb | 871.099 ± 0.018 | $^{110m}$Ag | 1505.006 ± 0.032 |
| $^{182}$Ta | 116.418 ± 0.002 | $^{183}$Ta | 406.589 ± 0.006 | $^{185}$Os | 874.814 ± 0.019 | $^{110m}$Ag | 1562.264 ± 0.033 |
| $^{75}$Se | 121.115 ± 0.003 | $^{198}$Au | 411.794 ± 0.008 | $^{160}$Tb | 879.364 ± 0.018 | $^{82}$Br | 1650.296 ± 0.034 |
| $^{57}$Co | 122.063 ± 0.004 | $^{110m}$Ag | 446.791 ± 0.010 | $^{185}$Os | 880.272 ± 0.019 | $^{58}$Co | 1674.679 ± 0.036 |
| $^{185}$Os | 125.358 ± 0.004 | $^{192}$Ir | 468.062 ± 0.010 | $^{84}$Rb | 881.595 ± 0.018 | $^{124}$Sb | 1690.942 ± 0.036 |
| $^{75}$Se | 136.000 ± 0.005 | $^{7}$Be | 477.593 ± 0.012 | $^{192}$Ir | 884.523 ± 0.018 | $^{207}$Bi | 1770.188 ± 0.037 |
| $^{57}$Co | 136.473 ± 0.004 | $^{192}$Ir | 484.570 ± 0.011 | $^{110m}$Ag | 884.667 ± 0.018 | $^{56}$Co | 1771.303 ± 0.037 |
| $^{59}$Fe | 142.648 ± 0.004 | $^{85}$Sr | 513.996 ± 0.016 | $^{46}$Sc | 889.258 ± 0.018 | $^{125}$Sn | 1806.652 ± 0.038 |
| $^{183}$Ta | 144.127 ± 0.002 | $^{82}$Br | 554.334 ± 0.012 | $^{88}$Y | 898.021 ± 0.019 | $^{56}$Co | 1810.672 ± 0.039 |
| $^{141}$Ce | 145.440 ± 0.003 | $^{207}$Bi | 569.689 ± 0.013 | $^{110m}$Ag | 937.483 ± 0.020 | $^{88}$Y | 1836.014 ± 0.037 |

| | | | | | | | |
|---|---|---|---|---|---|---|---|
| $^{182}$Ta | 152.434 ± 0.002 | $^{95m}$Tc | 582.068 ± 0.013 | $^{160}$Tb | 962.295 ± 0.020 | $^{125}$Sn | 1889.844 ± 0.039 |
| $^{182}$Ta | 156.387 ± 0.002 | $^{228}$Th | 583.174 ± 0.013 | $^{160}$Tb | 966.151 ± 0.020 | $^{84}$Rb | 1897.727 ± 0.038 |
| $^{199}$Au | 158.370 ± 0.003 | $^{192}$Ir | 588.572 ± 0.012 | $^{124}$Sb | 968.188 ± 0.022 | $^{56}$Co | 1963.669 ± 0.040 |
| $^{185}$Os | 162.854 ± 0.008 | $^{185}$Os | 592.066 ± 0.014 | $^{84}$Rb | 1016.143 ± 0.021 | $^{132}$Cs | 1985.581 ± 0.041 |
| $^{139}$Ce | 165.853 ± 0.007 | $^{124}$Sb | 602.715 ± 0.013 | $^{56}$Co | 1037.815 ± 0.022 | $^{125}$Sn | 2002.089 ± 0.043 |
| $^{182}$Ta | 179.393 ± 0.003 | $^{192}$Ir | 604.401 ± 0.012 | $^{95m}$Tc | 1039.247 ± 0.022 | $^{56}$Co | 2015.133 ± 0.040 |
| $^{59}$Fe | 192.344 ± 0.006 | $^{192}$Ir | 612.450 ± 0.013 | $^{82}$Br | 1043.973 ± 0.022 | $^{56}$Co | 2034.706 ± 0.041 |
| $^{183}$Ta | 192.646 ± 0.005 | $^{82}$Br | 619.088 ± 0.013 | $^{124}$Sb | 1045.106 ± 0.022 | $^{124}$Sb | 2090.889 ± 0.044 |
| $^{160}$Tb | 197.030 ± 0.004 | $^{110m}$Ag | 620.342 ± 0.016 | $^{207}$Bi | 1063.635 ± 0.024 | $^{56}$Co | 2113.049 ± 0.045 |
| $^{182}$Ta | 198.356 ± 0.004 | $^{124}$Sb | 645.835 ± 0.017 | $^{198}$Au | 1087.633 ± 0.024 | $^{144}$Ce | 2185.608 ± 0.046 |
| $^{75}$Se | 198.596 ± 0.007 | $^{185}$Os | 646.111 ± 0.017 | $^{59}$Fe | 1099.224 ± 0.025 | $^{125}$Sn | 2200.965 ± 0.047 |
| $^{95m}$Tc | 204.117 ± 0.005 | $^{110m}$Ag | 657.744 ± 0.017 | $^{65}$Zn | 1115.518 ± 0.025 | $^{56}$Co | 2212.862 ± 0.049 |
| $^{199}$Au | 208.196 ± 0.005 | $^{137}$Cs | 661.638 ± 0.019 | $^{46}$Sc | 1120.516 ± 0.025 | $^{125}$Sn | 2275.710 ± 0.048 |
| $^{177}$Lu | 208.362 ± 0.010 | $^{132}$Cs | 667.698 ± 0.017 | $^{182}$Ta | 1121.272 ± 0.026 | $^{56}$Co | 2598.400 ± 0.053 |
| $^{160}$Tb | 215.641 ± 0.004 | $^{198}$Au | 675.871 ± 0.018 | $^{60}$Co | 1173.208 ± 0.025 | $^{228}$Th | 2614.471 ± 0.054 |
| $^{82}$Br | 221.476 ± 0.005 | $^{110m}$Ag | 677.601 ± 0.018 | $^{56}$Co | 1175.067 ± 0.026 | $^{24}$Na | 2753.965 ± 0.056 |
| $^{182}$Ta | 222.110 ± 0.003 | $^{203}$Pb | 680.495 ± 0.017 | $^{160}$Tb | 1177.934 ± 0.024 | $^{56}$Co | 3201.878 ± 0.064 |
| $^{182}$Ta | 229.322 ± 0.006 | $^{110m}$Ag | 686.998 ± 0.019 | $^{182}$Ta | 1189.022 ± 0.027 | $^{56}$Co | 3253.341 ± 0.065 |
| $^{185}$Os | 234.158 ± 0.010 | $^{144}$Ce | 696.492 ± 0.019 | $^{182}$Ta | 1221.376 ± 0.027 | $^{56}$Co | 3272.912 ± 0.065 |
| $^{95m}$Tc | 253.066 ± 0.006 | $^{82}$Br | 698.358 ± 0.016 | $^{182}$Ta | 1230.989 ± 0.028 | $^{56}$Co | 3451.064 ± 0.069 |

†From R. L. Heath, "Gamma Ray Spectrum Catalogue, Ge(Li) and Si(Li) Spectrometry Vol. 2," Aerojet Nuclear Co. Report ANCR-1000-2, USAEC (1974).

APPENDIX

# D

# TABLES OF PHOTON ATTENUATION COEFFICIENTS

**Table D1 Total Mass Attenuation Coefficients in $cm^2 / g^{\dagger}$ for Gamma Rays$^{\ddagger}$**

| Photon energy (MeV) | H | Be | C | N | O | Na |
|---|---|---|---|---|---|---|
| 1.00 − 02[§] | 3.85 − 01 | 5.36 − 01 | 2.17 + 00 | 3.57 + 00 | 5.58 + 00 | 1.51 + 01 |
| 1.50 − 02 | 3.76 − 01 | 2.68 − 01 | 7.22 − 01 | 1.09 + 00 | 1.62 + 00 | 4.37 + 00 |
| 2.00 − 02 | 3.69 − 01 | 2.06 − 01 | 3.88 − 01 | 5.41 − 01 | 7.54 − 01 | 1.88 + 00 |
| 3.00 − 02 | 3.57 − 01 | 1.71 − 01 | 2.30 − 01 | 2.76 − 01 | 3.35 − 01 | 6.39 − 01 |
| 4.00 − 02 | 3.46 − 01 | 1.59 − 01 | 1.93 − 01 | 2.12 − 01 | 2.36 − 01 | 3.55 − 01 |
| 5.00 − 02 | 3.35 − 01 | 1.52 − 01 | 1.79 − 01 | 1.87 − 01 | 1.99 − 01 | 2.54 − 01 |
| 6.00 − 02 | 3.26 − 01 | 1.47 − 01 | 1.70 − 01 | 1.74 − 01 | 1.81 − 01 | 2.09 − 01 |
| 8.00 − 02 | 3.09 − 01 | 1.39 − 01 | 1.58 − 01 | 1.60 − 01 | 1.62 − 01 | 1.70 − 01 |
| 1.00 − 01 | 2.94 − 01 | 1.32 − 01 | 1.50 − 01 | 1.50 − 01 | 1.52 − 01 | 1.52 − 01 |
| 1.50 − 01 | 2.65 − 01 | 1.19 − 01 | 1.34 − 01 | 1.34 − 01 | 1.34 − 01 | 1.31 − 01 |
| 2.00 − 01 | 2.43 − 01 | 1.09 − 01 | 1.23 − 01 | 1.23 − 01 | 1.23 − 01 | 1.18 − 01 |
| 3.00 − 01 | 2.11 − 01 | 9.45 − 02 | 1.07 − 01 | 1.06 − 01 | 1.07 − 01 | 1.02 − 01 |
| 4.00 − 01 | 1.89 − 01 | 8.47 − 02 | 9.55 − 02 | 9.54 − 02 | 9.54 − 02 | 9.14 − 02 |
| 5.00 − 01 | 1.73 − 01 | 7.73 − 02 | 8.72 − 02 | 8.71 − 02 | 8.71 − 02 | 8.34 − 02 |
| 6.00 − 01 | 1.60 − 01 | 7.15 − 02 | 8.07 − 02 | 8.05 − 02 | 8.06 − 02 | 7.72 − 02 |
| 8.00 − 01 | 1.40 − 01 | 6.29 − 02 | 7.09 − 02 | 7.08 − 02 | 7.08 − 02 | 6.78 − 02 |
| 1.00 + 00 | 1.26 − 01 | 5.65 − 02 | 6.37 − 02 | 6.36 − 02 | 6.37 − 02 | 6.09 − 02 |
| 1.50 + 00 | 1.03 − 01 | 4.60 − 02 | 5.19 − 02 | 5.18 − 02 | 5.18 − 02 | 4.97 − 02 |
| 2.00 + 00 | 8.75 − 02 | 3.94 − 02 | 4.45 − 02 | 4.45 − 02 | 4.46 − 02 | 4.28 − 02 |
| 3.00 + 00 | 6.91 − 02 | 3.14 − 02 | 3.57 − 02 | 3.58 − 02 | 3.60 − 02 | 3.49 − 02 |
| 4.00 + 00 | 5.81 − 02 | 2.66 − 02 | 3.05 − 02 | 3.07 − 02 | 3.10 − 02 | 3.04 − 02 |
| 5.00 + 00 | 5.05 − 02 | 2.35 − 02 | 2.71 − 02 | 2.74 − 02 | 2.78 − 02 | 2.76 − 02 |
| 6.00 + 00 | 4.50 − 02 | 2.12 − 02 | 2.47 − 02 | 2.51 − 02 | 2.55 − 02 | 2.56 − 02 |
| 8.00 + 00 | 3.75 − 02 | 1.82 − 02 | 2.16 − 02 | 2.21 − 02 | 2.26 − 02 | 2.32 − 02 |
| 1.00 + 01 | 3.25 − 02 | 1.63 − 02 | 1.96 − 02 | 2.02 − 02 | 2.09 − 02 | 2.18 − 02 |

| | Al | Si | Fe | Cu | Pb | NaI |
|---|---|---|---|---|---|---|
| 1.00 − 02 | 2.58 + 01 | 3.36 + 01 | 1.72 + 02 | 2.23 + 02 | 1.28 + 02 | 1.36 + 02 |
| 1.50 − 02 | 7.66 + 00 | 9.97 + 00 | 5.57 + 01 | 7.33 + 01 | 1.12 + 02 | 4.59 + 01 |
| 2.00 − 02 | 3.24 + 00 | 4.19 + 00 | 2.51 + 01 | 3.30 + 01 | 8.34 + 01 | 2.12 + 01 |
| 3.00 − 02 | 1.03 + 00 | 1.31 + 00 | 7.88 + 00 | 1.06 + 01 | 2.84 + 01 | 6.86 + 00 |

**Table D1 Total Mass Attenuation Coefficients in $cm^2$ / g† for Gamma Rays‡** (Continued)

| Photon energy (MeV) | Al | Si | Fe | Cu | Pb | NaI |
|---|---|---|---|---|---|---|
| 4.00 − 02 | 5.14 − 01 | 6.35 − 01 | 3.46 + 00 | 4.71 + 00 | 1.31 + 01 | 1.89 + 01 |
| 5.00 − 02 | 3.34 − 01 | 3.96 − 01 | 1.84 + 00 | 2.50 + 00 | 7.22 + 00 | 1.05 + 01 |
| 6.00 − 02 | 2.55 − 01 | 2.92 − 01 | 1.13 + 00 | 1.52 + 00 | 4.43 + 00 | 6.42 + 00 |
| 8.00 − 02 | 1.89 − 01 | 2.07 − 01 | 5.50 − 01 | 7.18 − 01 | 2.07 + 00 | 3.00 + 00 |
| 1.00 − 01 | 1.62 − 01 | 1.73 − 01 | 3.42 − 01 | 4.27 − 01 | 5.23 + 00 | 1.64 + 00 |
| 1.50 − 01 | 1.34 − 01 | 1.40 − 01 | 1.84 − 01 | 2.08 − 01 | 1.89 + 00 | 5.90 − 01 |
| 2.00 − 01 | 1.20 − 01 | 1.25 − 01 | 1.39 − 01 | 1.48 − 01 | 9.45 − 01 | 3.14 − 01 |
| 3.00 − 01 | 1.03 − 01 | 1.07 − 01 | 1.07 − 01 | 1.08 − 01 | 3.83 − 01 | 1.58 − 01 |
| 4.00 − 01 | 9.22 − 02 | 9.54 − 02 | 9.21 − 02 | 9.19 − 02 | 2.20 − 01 | 1.12 − 01 |
| 5.00 − 01 | 8.41 − 02 | 8.70 − 02 | 8.29 − 02 | 8.22 − 02 | 1.54 − 01 | 9.21 − 02 |
| 6.00 − 01 | 7.77 − 02 | 8.05 − 02 | 7.62 − 02 | 7.52 − 02 | 1.20 − 01 | 8.02 − 02 |
| 8.00 − 01 | 6.83 − 02 | 7.06 − 02 | 6.65 − 02 | 6.55 − 02 | 8.56 − 02 | 6.63 − 02 |
| 1.00 + 00 | 6.14 − 02 | 6.35 − 02 | 5.96 − 02 | 5.86 − 02 | 6.90 − 02 | 5.80 − 02 |
| 1.50 + 00 | 5.00 − 02 | 5.18 − 02 | 4.87 − 02 | 4.79 − 02 | 5.10 − 02 | 4.66 − 02 |
| 2.00 + 00 | 4.32 − 02 | 4.48 − 02 | 4.25 − 02 | 4.19 − 02 | 4.50 − 02 | 4.12 − 02 |
| 3.00 + 00 | 3.54 − 02 | 3.68 − 02 | 3.62 − 02 | 3.59 − 02 | 4.16 − 02 | 3.66 − 02 |
| 4.00 + 00 | 3.11 − 02 | 3.24 − 02 | 3.31 − 02 | 3.32 − 02 | 4.14 − 02 | 3.50 − 02 |
| 5.00 + 00 | 2.84 − 02 | 2.97 − 02 | 3.14 − 02 | 3.18 − 02 | 4.24 − 02 | 3.46 − 02 |
| 6.00 + 00 | 2.66 − 02 | 2.79 − 02 | 3.05 − 02 | 3.10 − 02 | 4.34 − 02 | 3.47 − 02 |
| 8.00 + 00 | 2.44 − 02 | 2.57 − 02 | 2.98 − 02 | 3.06 − 02 | 4.59 − 02 | 3.55 − 02 |
| 1.00 + 01 | 2.31 − 02 | 2.46 − 02 | 2.98 − 02 | 3.08 − 02 | 4.84 − 02 | 3.68 − 02 |

| | Air | $H_2O$ | Compact bone | Muscle, striated | concrete | Pyrex glass | Lucite $(C_5H_8O_2)_n$ |
|---|---|---|---|---|---|---|---|
| 1.00 − 02 | 4.82 + 00 | 4.99 + 00 | 2.00 + 01 | 5.09 + 00 | 2.65 + 01 | 1.67 + 01 | 3.11 + 00 |
| 1.50 − 02 | 1.45 + 00 | 1.48 + 00 | 6.15 + 00 | 1.53 + 00 | 8.01 + 00 | 4.95 + 00 | 9.82 − 01 |
| 2.00 − 02 | 6.91 − 01 | 7.11 − 01 | 2.68 + 00 | 7.31 − 01 | 3.45 + 00 | 2.13 + 00 | 5.03 − 01 |
| 3.00 − 02 | 3.18 − 01 | 3.38 − 01 | 9.07 − 01 | 3.42 − 01 | 1.12 + 00 | 7.24 − 01 | 2.74 − 01 |
| 4.00 − 02 | 2.29 − 01 | 2.48 − 01 | 4.78 − 01 | 2.49 − 01 | 5.59 − 01 | 3.94 − 01 | 2.19 − 01 |
| 5.00 − 02 | 1.96 − 01 | 2.14 − 01 | 3.27 − 01 | 2.14 − 01 | 3.61 − 01 | 2.77 − 01 | 1.98 − 01 |
| 6.00 − 02 | 1.79 − 01 | 1.97 − 01 | 2.58 − 01 | 1.97 − 01 | 2.73 − 01 | 2.25 − 01 | 1.86 − 01 |
| 8.00 − 02 | 1.62 − 01 | 1.79 − 01 | 2.00 − 01 | 1.78 − 01 | 2.00 − 01 | 1.80 − 01 | 1.72 − 01 |
| 1.00 − 01 | 1.51 − 01 | 1.68 − 01 | 1.74 − 01 | 1.66 − 01 | 1.70 − 01 | 1.60 − 01 | 1.62 − 01 |
| 1.50 − 01 | 1.34 − 01 | 1.49 − 01 | 1.47 − 01 | 1.48 − 01 | 1.40 − 01 | 1.36 − 01 | 1.45 − 01 |
| 2.00 − 01 | 1.23 − 01 | 1.36 − 01 | 1.32 − 01 | 1.35 − 01 | 1.25 − 01 | 1.23 − 01 | 1.32 − 01 |
| 3.00 − 01 | 1.06 − 01 | 1.18 − 01 | 1.14 − 01 | 1.17 − 01 | 1.07 − 01 | 1.06 − 01 | 1.15 − 01 |
| 4.00 − 01 | 9.53 − 02 | 1.06 − 01 | 1.01 − 01 | 1.05 − 01 | 9.58 − 02 | 9.50 − 02 | 1.03 − 01 |
| 5.00 − 01 | 8.70 − 02 | 9.67 − 02 | 9.25 − 02 | 9.59 − 02 | 8.73 − 02 | 8.67 − 02 | 9.41 − 02 |
| 6.00 − 01 | 8.05 − 02 | 8.95 − 02 | 8.56 − 02 | 8.87 − 02 | 8.07 − 02 | 8.02 − 02 | 8.70 − 02 |
| 8.00 − 01 | 7.07 − 02 | 7.86 − 02 | 7.51 − 02 | 7.79 − 02 | 7.09 − 02 | 7.04 − 02 | 7.65 − 02 |

**Table D1 Total Mass Attenuation Coefficients in $cm^2$ / g† for Gamma Rays‡** (Continued)

| Photon energy (MeV) | Air | $H_2O$ | Compact bone | Muscle, striated | concrete | Pyrex glass | Lucite $(C_5H_8O_2)_n$ |
|---|---|---|---|---|---|---|---|
| 1.00 + 00 | 6.36 − 02 | 7.07 − 02 | 6.75 − 02 | 7.00 − 02 | 6.37 − 02 | 6.33 − 02 | 6.87 − 02 |
| 1.50 + 00 | 5.18 − 02 | 5.75 − 02 | 5.50 − 02 | 5.70 − 02 | 5.19 − 02 | 5.16 − 02 | 5.59 − 02 |
| 2.00 + 00 | 4.45 − 02 | 4.94 − 02 | 4.73 − 02 | 4.89 − 02 | 4.48 − 02 | 4.44 − 02 | 4.80 − 02 |
| 3.00 + 00 | 3.58 − 02 | 3.97 − 02 | 3.83 − 02 | 3.93 − 02 | 3.65 − 02 | 3.61 − 02 | 3.85 − 02 |
| 4.00 + 00 | 3.08 − 02 | 3.40 − 02 | 3.31 − 02 | 3.37 − 02 | 3.19 − 02 | 3.14 − 02 | 3.29 − 02 |
| 5.00 + 00 | 2.75 − 02 | 3.03 − 02 | 2.97 − 02 | 3.00 − 02 | 2.90 − 02 | 2.84 − 02 | 2.92 − 02 |
| 6.00 + 00 | 2.52 − 02 | 2.77 − 02 | 2.74 − 02 | 2.74 − 02 | 2.70 − 02 | 2.63 − 02 | 2.66 − 02 |
| 8.00 + 00 | 2.23 − 02 | 2.43 − 02 | 2.44 − 02 | 2.40 − 02 | 2.45 − 02 | 2.37 − 02 | 2.32 − 02 |
| 1.00 + 01 | 2.04 − 02 | 2.22 − 02 | 2.26 − 02 | 2.19 − 02 | 2.31 − 02 | 2.22 − 02 | 2.11 − 02 |

†Multiply by $10^{-1}$ to obtain $m^2$/kg.
‡From J. H. Hubbell, "Photon Cross Sections, Attenuation Coefficients, and Energy Absorption Coefficients from 10 keV to 100 GeV," NSRDS-NBS 29 C (1969).
§Read × $10^{-2}$

**Table D2 Mass Energy Absorption Coefficients in $cm^2$ / g† for Gamma Rays‡**

| Photon energy (MeV) | H | Be | C | N | O | Na |
|---|---|---|---|---|---|---|
| 0.01 | 0.00986 | 0.368 | 1.97 | 3.38 | 5.39 | 14.9 |
| 0.015 | 0.0110 | 0.104 | 0.536 | 0.908 | 1.44 | 4.20 |
| 0.02 | 0.0135 | 0.0469 | 0.208 | 0.362 | 0.575 | 1.70 |
| 0.03 | 0.0185 | 0.0195 | 0.0594 | 0.105 | 0.165 | 0.475 |
| 0.04 | 0.0231 | 0.0146 | 0.0306 | 0.0493 | 0.0733 | 0.199 |
| 0.05 | 0.0271 | 0.0142 | 0.0233 | 0.0319 | 0.0437 | 0.106 |
| 0.06 | 0.0306 | 0.0147 | 0.0211 | 0.0256 | 0.0322 | 0.0668 |
| 0.08 | 0.0362 | 0.0166 | 0.0205 | 0.0223 | 0.0249 | 0.0382 |
| 0.10 | 0.0406 | 0.0184 | 0.0215 | 0.0224 | 0.0237 | 0.0297 |
| 0.15 | 0.0481 | 0.0216 | 0.0245 | 0.0247 | 0.0251 | 0.0260 |
| 0.2 | 0.0525 | 0.0235 | 0.0265 | 0.0267 | 0.0268 | 0.0264 |
| 0.3 | 0.0569 | 0.0255 | 0.0287 | 0.0287 | 0.0288 | 0.0277 |
| 0.4 | 0.0586 | 0.0262 | 0.0295 | 0.0295 | 0.0295 | 0.0284 |
| 0.5 | 0.0593 | 0.0265 | 0.0297 | 0.0296 | 0.0297 | 0.0285 |
| 0.6 | 0.0587 | 0.0263 | 0.0295 | 0.0295 | 0.0296 | 0.0284 |
| 0.8 | 0.0574 | 0.0256 | 0.0288 | 0.0289 | 0.0289 | 0.0275 |
| 1.0 | 0.0555 | 0.0248 | 0.0279 | 0.0279 | 0.0278 | 0.0266 |
| 1.5 | 0.0507 | 0.0227 | 0.0255 | 0.0255 | 0.0254 | 0.0243 |
| 2 | 0.0464 | 0.0208 | 0.0234 | 0.0234 | 0.0234 | 0.0225 |
| 3 | 0.0398 | 0.0180 | 0.0204 | 0.0205 | 0.0206 | 0.0199 |

**Table D2 Mass Energy Absorption Coefficients in $cm^2 / g^{\dagger}$ for Gamma Rays$^{\ddagger}$** (Continued)

| Photon energy (MeV) | H | Be | C | N | O | Na |
|---|---|---|---|---|---|---|
| 4 | 0.0352 | 0.0161 | 0.0185 | 0.0186 | 0.0188 | 0.0184 |
| 5 | 0.0317 | 0.0148 | 0.0171 | 0.0173 | 0.0175 | 0.0174 |
| 6 | 0.0290 | 0.0138 | 0.0161 | 0.0163 | 0.0166 | 0.0161 |
| 8 | 0.0252 | 0.0123 | 0.0147 | 0.0151 | 0.0155 | 0.0159 |
| 10 | 0.0225 | 0.0114 | 0.0138 | 0.0143 | 0.0148 | 0.0155 |

| | Al | Si | Fe | Cu | Pb | Air |
|---|---|---|---|---|---|---|
| 0.01 | 25.5 | 33.3 | 142 | 160 | 127 | 4.61 |
| 0.015 | 7.47 | 9.75 | 49.3 | 59.4 | 91.7 | 1.27 |
| 0.02 | 3.06 | 4.01 | 22.8 | 28.2 | 69.1 | 0.511 |
| 0.03 | 0.868 | 1.14 | 7.28 | 9.50 | 24.6 | 0.148 |
| 0.04 | 0.357 | 0.472 | 3.17 | 4.24 | 11.8 | 0.0668 |
| 0.05 | 0.184 | 0.241 | 1.64 | 2.22 | 6.54 | 0.0406 |
| 0.06 | 0.111 | 0.144 | 0.961 | 1.32 | 4.08 | 0.0305 |
| 0.08 | 0.0562 | 0.0700 | 0.414 | 0.573 | 1.86 | 0.0243 |
| 0.10 | 0.0386 | 0.0459 | 0.219 | 0.302 | 2.28 | 0.0234 |
| 0.15 | 0.0285 | 0.0312 | 0.0814 | 0.106 | 1.15 | 0.0250 |
| 0.2 | 0.0276 | 0.0292 | 0.0495 | 0.0597 | 0.629 | 0.0268 |
| 0.3 | 0.0282 | 0.0294 | 0.0335 | 0.0370 | 0.259 | 0.0287 |
| 0.4 | 0.0287 | 0.0298 | 0.0308 | 0.0318 | 0.143 | 0.0295 |
| 0.5 | 0.0286 | 0.0298 | 0.0295 | 0.0298 | 0.0951 | 0.0296 |
| 0.6 | 0.0286 | 0.0295 | 0.0286 | 0.0286 | 0.0710 | 0.0295 |
| 0.8 | 0.0277 | 0.0288 | 0.0273 | 0.0271 | 0.0481 | 0.0289 |
| 1.0 | 0.0269 | 0.0277 | 0.0262 | 0.0258 | 0.0377 | 0.0278 |
| 1.5 | 0.0245 | 0.0253 | 0.0237 | 0.0233 | 0.0271 | 0.0254 |
| 2 | 0.0226 | 0.0234 | 0.0220 | 0.0217 | 0.0240 | 0.0234 |
| 3 | 0.0202 | 0.0210 | 0.0204 | 0.0202 | 0.0234 | 0.0205 |
| 4 | 0.0188 | 0.0196 | 0.0199 | 0.0200 | 0.0245 | 0.0186 |
| 5 | 0.0179 | 0.0187 | 0.0198 | 0.0200 | 0.0259 | 0.0174 |
| 6 | 0.0172 | 0.0182 | 0.0199 | 0.0202 | 0.0272 | 0.0164 |
| 8 | 0.0168 | 0.0177 | 0.0204 | 0.0209 | 0.0294 | 0.0152 |
| 10 | 0.0165 | 0.0175 | 0.0209 | 0.0215 | 0.0310 | 0.0145 |

| | $H_2O$ | Compact bone | Muscle, striated | Concrete | Pyrex glass | Lucite $(C_5H_8O_2)_n$ |
|---|---|---|---|---|---|---|
| 0.01 | 4.79 | 19.2 | 4.87 | 25.5 | 16.5 | 2.91 |
| 0.015 | 1.28 | 5.84 | 1.32 | 7.66 | 4.75 | 0.783 |
| 0.02 | 0.512 | 2.46 | 0.533 | 3.22 | 1.94 | 0.310 |
| 0.03 | 0.149 | 0.720 | 0.154 | 0.936 | 0.554 | 0.0899 |

**Table D2 Mass Energy Absorption Coefficients in $cm^2 / g^{\dagger}$ for Gamma Rays‡** (Continued)

| Photon energy (MeV) | $H_2O$ | Compact bone | Muscle, striated | Concrete | Pyrex glass | Lucite $(C_5H_8O_2)_n$ |
|---|---|---|---|---|---|---|
| 0.04 | 0.0677 | 0.304 | 0.0701 | 0.393 | 0.232 | 0.0437 |
| 0.05 | 0.0418 | 0.161 | 0.0431 | 0.204 | 0.122 | 0.0301 |
| 0.06 | 0.0320 | 0.0998 | 0.0328 | 0.124 | 0.0768 | 0.0254 |
| 0.08 | 0.0262 | 0.0537 | 0.0264 | 0.0625 | 0.0428 | 0.0232 |
| 0.10 | 0.0256 | 0.0387 | 0.0256 | 0.0424 | 0.0325 | 0.0238 |
| 0.15 | 0.0277 | 0.0305 | 0.0275 | 0.0290 | 0.0274 | 0.0266 |
| 0.2 | 0.0297 | 0.0301 | 0.0294 | 0.0290 | 0.0276 | 0.0287 |
| 0.3 | 0.0319 | 0.0310 | 0.0317 | 0.0295 | 0.0289 | 0.0310 |
| 0.4 | 0.0328 | 0.0315 | 0.0325 | 0.0298 | 0.0295 | 0.0318 |
| 0.5 | 0.0330 | 0.0317 | 0.0328 | 0.0300 | 0.0297 | 0.0322 |
| 0.6 | 0.0329 | 0.0314 | 0.0325 | 0.0297 | 0.0294 | 0.0319 |
| 0.8 | 0.0321 | 0.0306 | 0.0318 | 0.0289 | 0.0287 | 0.0311 |
| 1.0 | 0.0309 | 0.0295 | 0.0306 | 0.0279 | 0.0277 | 0.0301 |
| 1.5 | 0.0282 | 0.0270 | 0.0280 | 0.0254 | 0.0252 | 0.0275 |
| 2 | 0.0260 | 0.0249 | 0.0257 | 0.0235 | 0.0233 | 0.0253 |
| 3 | 0.0227 | 0.0219 | 0.0225 | 0.0209 | 0.0207 | 0.0220 |
| 4 | 0.0206 | 0.0200 | 0.0204 | 0.0193 | 0.0190 | 0.0199 |
| 5 | 0.0191 | 0.0187 | 0.0189 | 0.0182 | 0.0179 | 0.0184 |
| 6 | 0.0180 | 0.0178 | 0.0178 | 0.0176 | 0.0171 | 0.0173 |
| 8 | 0.0166 | 0.0167 | 0.0164 | 0.0168 | 0.0163 | 0.0158 |
| 10 | 0.0157 | 0.0159 | 0.0155 | 0.0163 | 0.0157 | 0.0148 |

†Multiply by $10^{-1}$ to obtain $m^2/kg$.

‡From J. H. Hubbell, "Photon Cross Sections, Attenuation Coefficients, and Energy Absorption Coefficients from 10 keV to 100 GeV," NSRDS-NBS 29 C (1969).

APPENDIX
# E

# TABLE OF BUILDUP FACTOR CONSTANTS

**Coefficients of the Berger Equation for Dose Buildup Factors**
$B = 1 + a\mu r \exp(b\mu r)$†

| | Concrete‡ | | Air§ | | Water§ | |
|---|---|---|---|---|---|---|
| $E$ (MeV) | $a$ | $b$ | $a$ | $b$ | $a$ | $b$ |
| 0.015 | 0.01 | 0.029 | 0.08 | −0.034 | 0.09 | −0.036 |
| 0.02 | 0.03 | 0.041 | 0.23 | −0.032 | 0.26 | −0.032 |
| 0.03 | 0.10 | −0.036 | 0.93 | −0.009 | 1.01 | −0.006 |
| 0.04 | 0.26 | 0.035 | 2.40 | 0.018 | 2.58 | 0.024 |
| 0.05 | 0.52 | −0.026 | 4.05 | 0.050 | 4.36 | 0.057 |
| 0.06 | 0.78 | −0.008 | 5.27 | 0.075 | 5.59 | 0.082 |
| 0.08 | 1.42 | 0.007 | 6.11 | 0.102 | 6.47 | 0.108 |
| 0.1 | 1.83 | 0.028 | 5.93 | 0.113 | 6.11 | 0.120 |
| 0.15 | 2.19 | 0.054 | 4.70 | 0.121 | 4.88 | 0.125 |
| 0.2 | 2.20 | 0.065 | 3.94 | 0.113 | 4.13 | 0.118 |
| 0.3 | 2.03 | 0.067 | 3.10 | 0.094 | 3.18 | 0.096 |
| 0.4 | 1.87 | 0.061 | 2.61 | 0.079 | 2.67 | 0.080 |
| 0.5 | 1.73 | 0.055 | 2.29 | 0.067 | 2.32 | 0.068 |
| 0.6 | 1.60 | 0.049 | 2.05 | 0.058 | 2.07 | 0.059 |
| 0.8 | 1.41 | 0.040 | 1.71 | 0.045 | 1.74 | 0.045 |
| 1 | 1.27 | 0.032 | 1.50 | 0.035 | 1.50 | 0.036 |
| 1.5 | 1.02 | 0.021 | 1.16 | 0.021 | 1.16 | 0.021 |
| 2 | 0.89 | 0.014 | 0.97 | 0.013 | 0.97 | 0.013 |
| 3 | 0.71 | 0.007 | 0.75 | 0.005 | 0.74 | 0.005 |
| 4 | 0.59 | 0.004 | 0.61 | 0.001 | 0.62 | 0.000 |
| 5 | 0.49 | 0.004 | 0.53 | −0.002 | 0.52 | −0.002 |
| 6 | 0.45 | 0.002 | 0.47 | −0.004 | 0.47 | −0.005 |
| 8 | 0.36 | 0.001 | 0.37 | −0.004 | 0.38 | −0.006 |
| 10 | 0.30 | 0.003 | 0.31 | −0.004 | 0.31 | −0.005 |
| 15 | 0.21 | 0.004 | 0.23 | −0.006 | 0.23 | −0.008 |

†Good up to 40 mean free paths, for point isotropic source in infinite medium.
‡From A. B. Chilton, *Nuc. Sci. Eng.* **69**:436 (1979).
§From A. B. Chilton, C. M. Eisenhauer, and G. L. Simmons, *Nuc. Sci. Eng.* **73**:97 (1980).

# INDEX


Absorption coefficients (*see* Attenuation coefficients)
Accuracy, 3, 5
Activation analysis:
  charged particle reactions, 526
  counting the sample, 531
  interference reactions, 536
  neutron reactions, 525
  neutron sources, 529
  photon sources, 529
  photonuclear reactions, 527
  sample irradiation, 530
  sample preparation, 526
  sensitivity, 534
  standard error, 532
Activation equation, 481
Activator, 212
Activity, 105
  minimum detectable, 71
  specific, 105
ALARA, 567, 583
Alpha, 90
  detector, long-range, 204
  range, 134
$\alpha$ particle (*see* Alpha)
Amplifier, 14, 343
  coarse gain, 16
  fine gain, 16
  nonlinearity, 343, 344
Analog-to-digital converter (ADC), 308, 345, 348
  nonlinearity, 346, 347
Annihilation, 102
  gammas, 157
Annual limit of intake (ALI), 569
Anticoincidence, 331
Antineutrino, 86, 98
Antiparticle, 102
Arithmetic mean, 31, 33
  standard error, 50
Atomic mass unit, 87
Atomic number, 86
  effective, 131, 139, 147
Atoms, 83
  radius, 83
  energy levels, 84
Attenuation coefficient:
  beta, 142
  gamma, 158, 159
  gamma, for compounds, 160
Average, 31
  binding energy per nucleon, 90
  cross section, 173
  lifetime of nucleus, 105
  of a function, 31

Background radiation, 541, 570
Barn, definition, 167
Bateman equation, 107
Beta particle, 98, 99
  average energy, 100
  mass absorption coefficient, 142
$BF_3$ counter, 469
$BF_3$ sensitivity, 472
Binding energy, 87
  of proton, 89
  of neutron, 89
  of alpha, 90
  average per nucleon, 90

Binomial distribution, 35
  mean, 36
  standard deviation, 37
  variance, 37
Biological effects, 562
Biological half life, 559
Bonner sphere, 579
Bragg condition, 421
Bragg-Kleeman rule, 134, 135
Bremsstrahlung, 123, 129, 150
Buildup factors, 162, 164
  Berger formula, 165
  dose, 164
  energy deposition, 164
  geometric progression (GP), 165
  number, 164
  Taylor formula, 165

$CaF_2$(Eu), 217
Capacitance, 318
Carrier, mobility, 243
CDF, 29
CdTe detector, 419
Cell, 563
Central limit theorem, 45
Cerenkov, detector, 122
Channel electron multiplier (CEM), 454
Charged particles, 121
Chauvenet criterion, 61
$\chi^2$ criterion, 59, 60
Chromosome, 563
Circuit:
  differentiating, 321
  integrating, 324
  LR, 319
  RC, 319
Coincidence, 331
  accidental, 335
  figure of merit, 336
  resolving time, 333
  width, 333
Committed dose equivalent, 569
Committed effective dose equivalent, 569
Compensated ion chambers, 510
Compton coefficient, 156
  (*See also* Cross section)
Compton, cross section, 156
Compton edge, 387
Compton, effect, 154
Compton scattering, 154
Compton-suppression spectrometer, 388
Conduction band, 212
Conductors, 236, 238
Confidence limits, 52, 53
Corrections of measurements (*see* Measurement)
Correlation, 33
Correlation coefficient, 34
Coulomb interactions, 122
Counter (*see* Detector)
Counter, gas-flow, 201
Counter, internal gas, 205
Counting rate, 287
  background, 65
  combining of, 67
  gross, 65
  net, 65
  true, 74
  true net, 75
Covariance 33, 34
Cross section:
  average, 173
  Compton, 156
  macroscopic, 169
  microscopic, 167, 169
  pair production, 157
  photoelectric, 153
Crystal spectrometer, neutron, 503
Crystal spectrometer, X-ray, 421
CsI (Na), 217
CsI (Tl), 217
Cumulative distribution function (CDF), 29
Current chamber, 177
Current-type system, 7
Curve fitting, 354
  exponential, 355
  linear, 355
  power, 355
Cutie pie, 573

DAC, 569
Data smoothing, 373
Dead time, 73
  MCA, 346
  measurement, 75
Decay:
  alpha, 96
  beta, 98
  $\beta^+$, 100
  $\beta^-$, 98
  constant, 103
  gamma, 94
  law, 104
  nuclear, 92
  statistical nature of, 5
Deep dose equivalent, 569

Delay line, 325, 334
Delayed gammas, 115
Delta function, 364
δ-rays, 123
Derived air concentration (DAC), 569
Detector, 7
  $BF_3$, 469
  boron-lined, 473
  CdTe, 259, 419
  compensated ion chamber, 510
  dead time of, 8
  diffused junction, 252
  $E(dE/dx)$, 455
  energy resolution, 8
  fission chamber, 477
  gas-filled, 177
    geometry, 207
    pressure, 208
    window, 208
  gas-flow, 201
  Ge, 258
  Ge(Li), 258
  GM, 199
  $^3$He, 475
  $HgI_2$, 259, 419
  ionization, 181, 183
  $^6$Li, 474
  MWPC, 461
  phoswich, 232
  position-sensitive, 459
  proportional 189
  scintillation (*see* Scintillators)
  semiconductor, 235
  Si(Li), 254
  SPND, 511, 512, 517
  surface barrier, 252
Detector efficiency, 8, 283, 285
  absolute total, 390
  $BF_3$, 471
  double escape peak, 390, 391
  effect of density, 284
  effect of particle energy, 284
  Freeman-Jenkin equation, 409
  full-energy peak, 390
  intrinsic total, 390
  McNelles-Campbell equation, 410
  Mowatt equation, 409
  NaI(Tl), 392, 394
  relative, 391
  single-escape peak, 391
Detector pulse height, 8
Detector response, 364
Differentiating circuit, 321
Discharge, electric, 180
Discriminator, 17, 18
Dispersion indexes, 33
Distributions, 28
  binomial, 35
  Fermi, 237
  Gaussian, 39
  Lorentzian, 46
  mean of, 31
  median of, 31
  mode of, 30
  Poisson, 37
  standard normal, 43
DNA, 563
Dose:
  absorbed, 543
  equivalent (H), 546
  from charged particles, 547, 555
  from neutrons, 552
  from photons, 549
    geometry factor, 557
Dosimeter:
  activated foils, 582
  Bonner sphere, 579
  bubble detector, 580
  EPD, 581
  SSTR, 576
  TLD, 572, 575
Doubling dose, 567
Drift velocity:
  electrons, 184
  ions, 184

$E(dE/dx)$ detectors, 455
Effective:
  atomic number, 131, 139
  charge, 147
  dose equivalent, 568
  half-life, 559
  molecular weight, 134
Efficiency (*see* Detector efficiency)
Electron:
  backscattering, 439
  capture (EC), 101
  electron-hole pair, 240
  electron-ion pair, 177
    average energy for production, 189
  range, 138
Electronic noise, 303
Electronic personal dosimeter (EPD), 581
Electrostatic spectrometer, 458
Energy, binding, 87
  (*See also* Binding energy)
Energy calibration, Schmitt method, 450

Energy levels:
atomic, 84,
nuclear, 91
Energy loss, mechanisms, 122
Energy loss, 124
(*See also* Stopping power)
Energy resolution, 300, 305
crystal spectrometer, 421, 504
electron detectors, 441
Ge detector, 411
Energy spectrum, 293
area under the peak, 415
differential, 293, 296
integral, 294, 295
measured, 299
source, 299
Energy states (*see* Energy levels)
Energy straggling, 433, 434, 437
EPD, 581
Error:
definition, 3
determinate, 5
probable, 49
propagation, 55, 56
radiation measurements, 62
random, 5, 6
reduction, 68
relative importance, 70
standard, 49, 56
standard, of single measurement, 51
statistical, 5, 6
systematic, 5
type I, 71
type II, 71
types, 5
Error function, 42, 44
Event, 23, 25
Excitation, 85, 123
Exciton, 213
Expectation value (*see* Average)
Exposure, 543

Fano factor, 301, 411
Flux-to-dose rate conversion factor:
betas and electrons, 548
neutrons, 553
photons, 550, 556
Fermi distribution, 237
FET, 341
Field-effect-transistor (*see* FET)
Fission, 113
betas, 115
chamber, 477
foil preparation, 452
fragments, 115
neutrinos, 116
neutrons, 116
yield, 116
Fluorescent radiation, 102
Folding, 363, 365
Frequency function, 29
Full width at half maximum (FWHM), 42, 300

Gamma:
absorption coefficient, 161
attenuation (*see* Attenuation coefficients)
backscatter peak, 387
buildup factors, 162, 164
double escape peak, 387
energy deposition, 382, 385
full energy peak, 387
gammas, total, 158
Ge detector, 400
interactions, 150
mean free path, 160
NE, 213, 398
single escape peak, 387
Gamma detection with:
Ge detector, 400
NaI(Tl) scintillator, 392
NE-213 scintillator, 398
Gaussian distribution (*see* Normal distribution)
Ge:
properties, 249
resistivity, 247
Ge detector, 258, 400
efficiency, 401, 405, 406, 407, 408
energy resolution, 411
energy spectra, 413
escape peaks, 415
Geiger-Muller (GM) counter, 181
external quenching, 199
plateau, 195
pulse, 200
quenching, 199
self-quenching, 199
Geiger-Muller (GM) region, 180
Ge(Li) detector, 258
Gene, 563
Genetic effects, 566
doubling dose, 567
Geometry factor (*see* Solid angle)
Goodness of data, 58
Gray (Gy), 543

Half-life:
biological, 559
effective, 559
of nucleus, 105
partial, 106
Health physics, 541
Health physics instruments, 573
Heavy ion, calibration sources, 452
$HgI_2$ detector, 259, 419
High pass filter, 323
High-voltage:
plateau, 195
slope, 197
Hole, 240
HVPS, 9

IC electron spectrum, 443
Impedance, 321
Indexes:
dispersion, 33
location, 30
Inductance, 318
Insulators, 236, 238
Integrating chamber, 177
Integrating circuit, 324
Internal conversion (IC), 94, 96
Interpolation, 355
Lagrange formula, 356
error, 356
Ion beams, pulsed, 509
Ionization, 85, 123
chamber, 181, 183
potential, 85, 86
potential, mean, 126
primary, 178
region, 179
secondary, 178
Ionization chamber:
current, 187
pulse, 183
Isobar, 86
Isomer, 87
Isotone, 87
Isotope, 87

Kurie plot, 443

Lagrange formula, 356
Least-squares fit, 359
general functions, 361
linear, 359
nonlinear, 359
straight line, 360
Light pipe, 228
LiI(Eu), 217
Low pass filter, 325
LR circuit, 320
LRAD, 204

Macroscopic cross section, 169
((*See also* Cross section)
Magnetic rigidity, 456
Magnetic spectrometer, 456
Mean, 31
(*See also* Average)
Mean free path:
gamma, 160
neutron, 170
Measurement:
absolute, 265
accuracy of, 3
anticoincidence, 331
coincidence, 331
detector effects, 282
efficiency, 283
window, 282
error of, 3
geometry effects, 267
outcome, 25
precision of, 3
relative, 265
solid angle, 268
source effects, 277
backscattering factor, 279
self-absorption, 277
Median, 31
Microscopic cross section, 167, 169
(*See also* Cross section)
Minimum detectable activity (MDA), 71, 73
Mobility of carriers, 243
Multichannel analyzer (MCA), 21, 307
calibration, 310
dead time, 346
multichannel scaling (MCS), 307
pulse-height analysis, 307
Multiparameter analyzer, 347
Multiplication factor, gas, 179
Multiwire proportional counter (MWPC), 461

NaI(Tl), 216
NE-213, 398
Neutrino, 100

Neutron, 89
absorption, 166
Bonner sphere, 579
bubble detector, 580
chopper, 508
cross section, average, 173
cross sections, 167
crystal spectrometer, 503
detection by exothermic reactions, 468
detection by organic scintillator, 494
detection by proton recoil, 467
detection by threshold reactions, 496
foil activation, 478, 482, 582
interactions, 166, 525
reaction rate, 171, 172
scattering, 166
sources, 528, 529
time-of-flight method, 505
Neutron detection with:
$BF_3$ counter, 469
boron-lined counter, 473
Bonner ball, 475, 579
crystal spectrometer, 503
$^3$He counter, 475
$^6$LiF, 474
(n, $\alpha$) reaction, 469
(n, $\gamma$) reaction, 478
(n, p) reaction, 484, 489
proportional counter, 489
proton recoil, 484
scintillators, 474, 494
self-powered neutron detectors, 511, 512, 517
SSTR, 576
threshold reactions, 496
time-of-flight, 505
TLD, 576
Nuclear instrument module (NIM), 9
Noise, electronic, 8, 303
Nonstochastic effects, 564
Normal distribution, 39
CDF, 41
mean, 41
standard, 43
standard deviation, 41
variance, 41
Nuclear:
decay, 92
(*See also* Decay)
mass, 87
radius, 87
reactions, 107
kinematics, 109
threshold, 113
Nuclei, 86
Nucleic acids, 563
Nucleus, compound, 108

Oscilloscope, 16

Pair:
electron-hole, 240
production, 157, 386
Pair production coefficient, 157
(*See also* Cross section)
PDF, 29
Peak-to-Compton ratio, 404
Peak-to-total ratio, 390
Phoswich detector, 232
Photoelectric effect, 153
Photoelectric:
coefficient, 153
(*See also* Cross section)
cross section, 153
Photomultiplier tube, 211, 224
dark current, 226
electron multiplication, 227
$\mu$-metal, 227
photocathode, 225
Photon, interactions, 150
Phototube, 211
(*See also* Photomultiplier tube)
*p-n* junction, 246, 250
capacitance, 251
reverse bias, 249
Poisson distribution, 37
mean, 39
standard deviation, 39
variance, 39
Positron, 100
Preamplifier, 11, 339
Precision, 3, 5
Primary ionization, 178
Probability:
addition law, 26
definition, 23
density function (PDF), 29
distributions, 28
multiplication law, 26
theorems, 25
Prompt gammas, 115
Proportional counter, 181
for neutron detection, 489
for X-ray detection, 399
gas multiplication, 189, 192
multiwire (MWPC), 461
pulse, 194
Proportional region, 180

Proton recoil method, 467, 484
Pulse height defect, 433, 447
Pulse shape discrimination, 337
Pulse shaping, 326, 327
Pulse timing, 328, 418
  constant fraction, 331
  jitter, 329
  leading edge, 329
  walk, 329
  zero-crossing, 330
Pulse-type system, 7, 8

Quality factor (Q), 545

Rad, 543
Radiation, 1
  biological effects of, 562
    nonstochastic, 564
    stochastic, 564, 566
  cancer incidence, 566
  exposure limits, 569
  fluorescent, 102
  ionizing, 1
  nonionizing, 1
  protection guides, 567
  statistical nature of, 2
Radiation area, 582
Random variable, 34
  continuous, 28, 29
  discrete, 28, 29
Range, 132
  alpha, 134
  $\alpha$, $p$, $d$, $t$, 133
  electrons, 138
  extrapolated, 134
  heavy ions, 149
  mean, 134
  protons, 137
  straggling, 438
Rate meter, 206
RC circuit, 319
Reaction rate, 171, 172
Reactions, 107
  (*See also* Nuclear reactions)
Recombination region, 179
Rejection of data, 61
Relative biological effectiveness (RBE), 545
Relativistic kinematics, 80
  kinetic energy, 81
  momentum, 81
Relativity postulates, 80
Rem, 546
Rem ball, 579
Resistance, 318
Resolving power, crystal spectrometer, 504
Response function, 304
  alpha detector, 446
  Ge detector, 413
  NaI(Tl), 396
Restricted area, 582
RNA, 563
Roentgen (R), 543

Saturation activity, 480, 531
Scaler, 20
Scattered beam, 163
Scintillation counter:
  background, 231
  dead time, 230
  organic for neutron detection, 494
Scintillation process, 218
Scintillators, 211
  Anthracene, 220
  $CaF_2$(Eu), 217
  crystal, 212, 215
  CsI(Na), 217
  CsI(Tl), 217
  gaseous, 222
  inorganic, response, 222
  LiI(Eu), 217
  NaI(Tl), 216
  organic, 218, 219, 220
  organic liquid, 220
    response, 223
  photon emission rate, 215
  plastic, 221
  trans-stilbene, 220
Secondary ionization, 178
Self-powered neutron detectors (SPND), 511, 512, 517
Semiconductor detectors, 235
  radiation damage, 260
Semiconductors, 236, 239
  acceptor states, 245
  conductivity, 243
  donor states, 245
  doping, 245
  energy gap, 241
  extrinsic, 245
  intrinsic, 245
  $n$-type, 245
  $p$-$n$ junction, 246
  $p$-type, 245
Si:
  properties, 249
  resistivity, 248
Sievert (Sv), 546

Signal-to-noise ratio, 327
Si(Li) detector, 254
  FWHM, 420
  X-ray, 420
Single-channel analyzer (SCA), 17, 20
Smoothing of data, 373
Solid angle, 268, 269, 273, 274, 276
Solid-state track recorders (SSTR), 576
Source backscattering factor, 279, 280, 281
Spectrometer:
  calibration, 422
  Compton suppression, 388
  crystal, neutron, 503
  crystal, X-ray, 421
  electrostatic, 458
  magnetic, 456
Spectrum (*see* Energy spectrum)
Standard error, 48
  of average, 63
  of counting rates, 64
Standard normal distribution, 43
Stochastic effects, 564
Stopping power, 124
  $\alpha$, $p$, $d$, $t$, 125
  compounds, 131
  density effect, 127
  electrons, 125
  heavy ions, 144
  positrons, 125
Surface barrier detector, 252

TAC, 336
Thermoluminescent dosimeters (*see* TLD)
Threshold reactions, 496, 499
Time-of-flight, 505
  figure of merit, 507
  spectrometer, 453
Time-to-amplitude converter (*see* TAC)
Timer, 21
TLD, 572, 575
Total effective dose equivalent (TEDE), 569–570

Unfolding, 305, 364, 368, 371, 372
  FERDOR method, 488
  LSL-M2 method, 503
  proton recoil spectra, 487
  RDMM method, 502
  SAND-II method, 501
  SPECTRA method, 502
Unscattered beam, 162

Valence band, 212
Variance, 33

Weighting factors ($w_T$), 568
Working level (WL), 570
Working level month (WLM), 570

X-ray crystal spectrometer, 421
  Bragg condition 421
  energy resolution, 428, 429
  fluorescent, 427
  Johanson type, 427
  rocking curve, 425, 426
X-ray detection with:
  crystal spectrometer, 421
  proportional counter, 399
  scintillators, 392
  Si(Li) detector, 420
X-rays, 1, 150
X-rays, energy, 84